Science and engineering of short fibre reinforced polymer composites

Related titles:

Ageing of composites
(ISBN 978-1-84569-352-7)
This important book addresses the highly topical subject of composite ageing. An increasing proportion of composites are being used in structural applications in industries such as transport, oil and gas, chemical processing, marine and civil engineering. These composites are replacing traditional materials, particularly metals, and many have been developed only relatively recently. Consequently, there are uncertainties about the long-term performance of these composites and how they will age under various conditions. The book examines the processes that cause premature ageing of composites, modelling and prediction of ageing and actual case studies.

Delamination behaviour of composites
(ISBN 978-1-84569-244-5)
Delamination is a phenomenon that is of critical importance to the composites industry. It involves a breakdown in the bond between the reinforcement and the matrix material of the composite. With growing use of composites in aerospace and other sectors, understanding delamination behaviour is essential for preventing catastrophic failures. In this important book reviewing the phenomenon of delamination in composites, Part I focuses on delamination as a mode of failure, Part II covers testing of delamination resistance, while Part III analyses detection and characterisation. Further parts cover analysis of delamination behaviour from tests, modelling delamination, analysis of structural performance under delamination and prevention and mitigation of delamination.

Composites forming technologies
(ISBN 978-1-84569-033-5)
When forming composite materials with textiles there is always a degree of error when draping a fabric over the mould and adding the resin. The fabric can deform or shift in the mould before the resin is added or whilst it is being poured in. Such problems can cause weaknesses in the composite leading to failure or even rendering the composite useless. In order to counteract this it is necessary to be able to model the draping of different textiles to fully understand the issues that may arise and how to prevent them from occurring in the future. *Composites forming technologies* brings together the research of leading experts to give a comprehensive understanding of modelling and simulation within composite forming and design.

Details of these and other Woodhead Publishing materials books can be obtained by:

- visiting our web site at www.woodheadpublishing.com
- contacting Customer Services (e-mail: sales@woodheadpublishing.com; fax: +44 (0) 1223 893694; tel.: +44 (0) 1223 891358 ext. 130; address: Woodhead Publishing Limited, Abington Hall, Granta Park, Great Abington, Cambridge CB21 6AH, UK)

If you would like to receive information on forthcoming titles, please send your address details to: Francis Dodds (address, tel. and fax as above; e-mail: francis.dodds@woodheadpublishing.com). Please confirm which subject areas you are interested in.

Science and engineering of short fibre reinforced polymer composites

Shao-Yun Fu, Bernd Lauke
and Yiu-Wing Mai

CRC Press
Boca Raton Boston New York Washington, DC

WOODHEAD PUBLISHING LIMITED
Oxford Cambridge New Delhi

Published by Woodhead Publishing Limited, Abington Hall, Granta Park, Great Abington, Cambridge CB21 6AH, UK
www.woodheadpublishing.com

Woodhead Publishing India Private Limited, G-2, Vardaan House, 7/28 Ansari Road, Daryaganj, New Delhi – 110002, India

Published in North America by CRC Press LLC, 6000 Broken Sound Parkway, NW, Suite 300, Boca Raton, FL 33487, USA

First published 2009, Woodhead Publishing Limited and CRC Press LLC

British Library Cataloguing in Publication Data
A catalogue record for this book is available from the British Library.

Library of Congress Cataloging in Publication Data
A catalog record for this book is available from the Library of Congress.

Woodhead Publishing ISBN 978-1-84569-269-8 (book)
Woodhead Publishing ISBN 978-1-84569-649-8 (e-book)
CRC Press ISBN 978-1-4398-1099-6
CRC Press order number: N10096

The publishers' policy is to use permanent paper from mills that operate a sustainable forestry policy, and which has been manufactured from pulp which is processed using acid-free and elemental chlorine-free practices. Furthermore, the publishers ensure that the text paper and cover board used have met acceptable environmental accreditation standards.

Typeset by SNP Best-set Typesetter Ltd., Hong Kong
Printed by TJ International Limited, Padstow, Cornwall, UK

To Our Families

Contents

Notation

a	size parameter for fibre length probability density function
A	crack area (area of crack plane, $A = B \cdot c$), in the limit specimen cross section
A_{m1}	matrix area between two neighbouring fibres
b	shape parameter for fibre length probability density function; also beam width
B	specimen thickness; also axial distance between two neighbouring flights in a screw
c	crack length or subscript for expressing 'composite'
c_0	initial crack length, in Sections 10.10.5 and 10.11, normalised by the fibre length l.
$\tilde{c}$	critical crack length at the instability point, in Sections 10.10.5 and 10.11, normalised by the fibre length l.
Δc	change in crack length, $\Delta c = c - c_0$, in Sections 10.6.5 and 10.6.6. normalised by the fibre length l.
C	compliance (tensor)
C^*_{ijkl}	effective stiffness constants
C_0	thickness of core layer
d	fibre diameter = $2r_f$
D	fibre to fibre spacing in the multi-fibre model; also internal diameter of a cylindrical barrel in a screw
E	elastic modulus
E_c	composite modulus
E_{cy}	transverse composite modulus
E_f	axial fibre modulus
E_{flex}	flexural composite modulus
E_{fy}	transverse fibre modulus
E_m	matrix modulus
E_{ph}	interphase modulus
E_{ij}	engineering stiffness constants in the directions i, j

$\bar{E}$	effective modulus of continuous-fibre reinforced composite
E^{T}	Eshelby's tensor
E_{c}^{0}	longitudinal composite modulus for the undamaged system
E_{cy}	transverse composite modulus
E^{*}	complex modulus
f	subscript and superscript for expressing 'fibre'
$f(l)$	probability density function of fibre length
f_{θ}	fibre orientation coefficient
F	external force
$F(l)$	cumulative probability function of fibre length
F_{c}	critical external force
F_{Q}	5% offset load
$g(\theta)$, $g(\phi)$, $g(\theta, \phi)$	probability density functions of fibre orientation
G	energy release rate (energy per crack plane) used in Chapter 10
$\bar{G}$	effective shear modulus used in Chapter 4
G_{12}, G_{13}	axial shear modulus of the composite, $j = 1, 2$
G_{23}	plane strain shear modulus of the composite
G_{c}	critical energy release rate of the composite, also composite fracture toughness
$G_{\mathrm{c,m}}$	critical energy release rate of the matrix, also matrix fracture toughness
G_{f}	shear modulus of fibre
G_{m}	shear modulus of matrix
$G(\theta)$	cumulative probability of fibre orientation
h	thickness of composite plate; also characteristic length of representative element
h_{c}	thickness of core layer
h_{f}	characteristic length of fibre
h_{k}	thickness fraction of the kth ply
h_{m}	characteristic length of matrix
h_{p}	half length of plastically deformed matrix bridges between neighbouring fibres
J	J-integral
k	serial index of ply
k_{ij}	stress concentration factor
K	stress intensity factor
K_0	relaxation constant
K_{i}	stress intensity factor for mode i = I, II, III
K_{c}	critical stress intensity factor of the composite; also composite fracture toughness

K_c	composite thermal conductivity
$K_{c,m}$	critical stress intensity factor of the matrix, also matrix fracture toughness
$K_{c,core}$	critical stress intensity factor of the core layer, also fracture toughness of core
$K_{c,skin}$	critical stress intensity factor of the skin layer, also fracture toughness of skin
$K_{c,d}$	critical dynamic (impact) stress intensity, also impact toughness
$K^{c}_{c,d}$	critical dynamic (impact) stress intensity of the composite, also composite impact toughness
$K^{m}_{c,d}$	critical dynamic (impact) stress intensity of the matrix, also matrix impact toughness
K_{1c}	critical stress intensity of material 1
K_{2c}	critical stress intensity of material 2
K_{23}	plane strain bulk modulus
K_Q	stress intensity for the 5% offset force
K_1	thermal conductivity parallel to the fibre direction for a unidirectional composite
K_2	thermal conductivity perpendicular to the fibre direction for a unidirectional composite
K_{f1}	fibre thermal conductivity in the axis direction
K_{f2}	fibre thermal conductivity in the direction transverse to the fibre axis
K_m	thermal conductivity of the matrix
l	fibre length
l_c	critical fibre length for axial loading
l_{cb}	critical length of a branched fibre
$l_{c\theta,c\delta}$	critical fibre length for inclined (θ or δ) loading
l_{min}	minimum fibre length
l_{max}	maximum fibre length
l_{mean}	mean fibre length (number average fibre length)
l^{w}_{mean}	weight average fibre length
l_{mod}	most probable fibre length
l_d	debonding length on one side of the fibre
l_s	sliding length on one side of the fibre
l_s	length of the shorter embedded fibre segment
L	ligament length (un-notched region of a specimen in front of the notch; also span length in three-point testing)
$L_{A,B}$	lengths of two edges of photographs for fibre length measurement
L_e	embedded fibre length

m	subscript and superscript for expressing 'matrix'
m	$= \cos\theta$
M	microstructural efficiency factor
M_i	bending and twisting moments per unit width, $i = 1, 2, 6$
$M_{m,c}(t)$	creep compliance of matrix and composite, respectively
$M^u_{m,c}$	unrelaxed compliance of matrix and composite, respectively
$M^r_{m,c}$	relaxed compliance of matrix and composite, respectively
n	number of length intervals and $n = l_{max}/\Delta l$
n	$= \sin\theta$
n	number of fibres contributing to energy dissipation per crack plane ($n = N_A/A$)
$n_i(\theta, l)$	number of fibres with an angle θ and a length $l < l_c$
$n_j(\theta, l)$	number of fibres with an angle θ and a length $l > l_c$
$\tilde{n}$	number of fibres contributing to energy dissipation per volume ($\tilde{n} = N_V/(A \cdot 2 \cdot r^i_D)$
N	total number of fibres
$N_{A,V}$	number of active fibres in the cross section or volume respectively
N_i	total number of fibres with a length of l to $l + dl$
N_{int}	number of fibres with a length of l to $l + dl$ intersecting photographs for fibre length measurement
N_v	total fibre number in the composite with a volume V
N_{wit}	number of fibres with a length of l to $l + dl$ within photographs for fibre length measurement
p	shape parameter for fibre orientation distribution
P	weight
q	shape parameter for fibre orientation distribution
Q	energy necessary for crack propagation
Q_{ij}	stiffness matrix of the composite
Q^{-1}	inverse quality factor of an oscillating system
r	coordinate perpendicular to the fibre axis; also distance from the crack tip
r_b	radius of branched fibre
r_f	fibre radius
r_p	radius of the plastic zone
r^i_D	radius of dissipation zone of the mechanisms i
R	crack resistance (energy per crack plane); also mean separation of fibres normal to their lengths

R^0	crack resistance (energy per crack plane), constant with changing crack length
R_0	radius of the representative element
s	displacement perpendicular to the crack plane
s_c	crack opening displacement
S	thickness of half skin layer; also axial distance of one full turn of a screw
S	stiffness tensor
S_1	strain-concentration tensor
S_2	stress-concentration tensor
t	time
t	interphase thickness; also fibre aspect ratio l/d
T	specimen width
T	temperature
T_1, T_2	strain concentration tensors
u	displacement in the fibre axial direction
$u_F(z)$	cross-sectional average of the fibre displacement
$u_M(z)$	cross-sectional average of the matrix displacement
$u_f(z)$	fibre displacment at the interface (at $r = r_f$)
$u_m(r,z)$, $u_m(r,x)$	matrix displacment
$u_m(z)$	matrix displacment at the interface (at $r = r_f$)
U_e	elastic strain energy
U_p	potential energy of the loading system
U_{pot}	total potential energy
U_t	total energy
U_{pl}	plastic energy (under the force–displacement curve)
ΔU	dissipation energy per cycle of loading
v	fibre volume fraction
v_c	critical fibre volume fraction
v^{crit}	critical (minimun) fibre volume fraction for improving composite strength
v_i	fibre volume sub-fraction
v_m	matrix volume fraction, $v_m = 1 - v$
v_{max}	maximum packing fraction for randomly oriented short fibres
v_p	particle or porosity volume fraction
V	volume
V_p	volume of the plastic zone
w	specific work of fracture (energy per crack plane) in static and impact loading of notched specimen
w_e	specific essential work of fracture (energy per crack plane)
w_i	specific work of fracture (energy per crack plane) of the dissipation mechanism $i = d, s, fi, po, m$ with d: fibre/

	matrix debonding, *s*: fibre/matrix sliding, *fi*: fibre fracture, *po*: fibre pull-out, *m*: matrix fracture
$w_{m,y}$	specific work of fracture (energy per crack plane) of ductile matrix fracture
w_m^0	specific work of fracture (energy per crack plane) of brittle matrix fracture
w_{init}	specific crack initiation energy (energy per crack plane, which is equal to specimen cross section)
w_{un}	impact energy of unnotched specimen (energy per crack plane, which is equal to specimen cross section)
W	energy released on the crack surfaces
W_d^I	fibre/matrix debonding energy for mode I loading
W_d^{II}	fibre/matrix debonding energy for mode II loading
W_e	essential work of fracture
W_f	work of fracture
W_i	work of fracture of the dissipation mechanism $i = d, s, fi, po$ with *d*: fibre/matrix debonding, *s*: fibre/matrix sliding, *fi*: fibre fracture, *po*: fibre pull-out, *m*: matrix yielding
W_p	non-essential work of fracture
W_{po}^{Δ}	restricted pull-out energy of one fibre (pull-out over the distance Δ)
x_i	Cartesian coordinates ($i = 1, 2, 3$)
x, y, z	Cartesian coordinates
Y_i	calibration factors, $i = 1, 2, a$
r, φ, θ	radial and angular coordinates with the origin at the crack tip
I, II, II	index for mode I, mode II and mode III for the fracture mechanical parameters
α	fraction of the brittle fracture area of the crack plane; also percentage of sub-critical fibres
$\alpha_1, \alpha_2, \alpha_c$	composite thermal expansion coefficient
α_i	weighting fraction of the mechanisms (i)
β	shape factor of the volume of plastic zone
χ	fibre reinforcing coefficient for composite strength
χ_1	fibre orientation factor for composite strength
χ_2	fibre length factor for composite strength
δ	phase angle
δ	fibre spacing
δ	interfibre spacing (Chapter 6)
$\delta(z)$	boundary of plastic zone in the multi-fibre model
Δ	relaxation strength (Chapter 9)
Δ	pull-out distance (Chapter 10); also in Sections 10.10.5 and 10.11, normalised by the fibre length l

ε	strain
$\varepsilon_{C,F,M}$	average strain of the composite, fibre, and matrix, respectively
$\overline{\varepsilon}_{F,M}$	axial mean strain of fibre and matrix, respectively
ε_{fy}	transverse fibre strain
$\overline{\varepsilon}_{fy}$	mean transverse fibre strain
ε_d	failure strain for debonding at the fibre–matrix interface
ε^A	applied strain on composite
ε^C	strain within the ellipsoidal inclusion in Eshelby model
ε^T	transformation or eigen strain
ε_F^u	ultimate deformation of the fibre
ε_M^u	ultimate deformation of the matrix
$\tilde{\varepsilon}_M$	matrix strain for stabilised necking
$\Delta\varepsilon$	difference in ultimate deformations of the matrix, ε_M^u, and fibre, ε_F^u
γ	specific fracture surface energy (energy per unit area of crack surface)
γ_d^{II}	specific fracture surface energy of fibre–matrix interface under mode II loading
γ_d^I	specific fracture surface energy of fibre–matrix interface under mode I loading
γ_m^0	specific fracture surface energy of brittle matrix under mode I loading
$\gamma_{m,y}$	specific fracture surface energy of ductile matrix
γ_{fi}	specific fracture surface energy of fibre
γ_{12}	shear strain of the composite
γ_f, γ_m	shear strain of fibre and matrix, respectively
η, η_2	shear lag parameter or decay parameters of fibre stress
η_i	energy density of the dissipation mechanism i, $i = d$ for fibre–matrix debonding, $i = s$ for fibre/matrix sliding, $i = p$ for plastic matrix deformation (energy per volume)
η_e	elastic energy density (energy per volume)
η_c	elastic energy density of the composite until creation (initiation) of crack propagation (energy per volume)
η_l	fibre length factor for composite flexural modulus
η_θ	fibre orientation factor for composite flexural modulus
$\tilde{\eta}_{el}$	geometry coefficients for elastic energy (dimension: one over area)
$\tilde{\eta}_{pl}$	geometry coefficients for plastic energy (dimension: one over area)
λ	a parameter for characterising fibre orientation distribution

$\lambda, \lambda_1, \lambda_2$	fibre reinforcing coefficient for composite modulus
μ	fibre–matrix friction coefficient; also snubbing friction coefficient in Chapter 9
ν_i	Poisson ratio of component i, $i = f, m$
ν_{ij}	directional Poisson ratio
θ	fibre orientation angle
θ_{min}	minimum fibre orientation angle
θ_{max}	maximum fibre orientation angle
(Θ, Φ)	applied loading direction with respect to fibre axis
ϕ	fibre orientation angle
φ	angle between two branches of a branched fibre
ρ	matter density
σ	stress
σ_A	applied stress in general
σ_c	applied stress of composite
σ_c^d	composite stress for fibre–matrix debonding
σ_c^s	composite stress for fibre–matrix sliding
σ_c^u	composite strength
σ_f	stress at a point in the fibre
σ_{fy}	transverse fibre stress
$\sigma_{F,M}$	cross-sectional mean stress of fibre and matrix, respectively; they are mean stresses in fibre (Chapter 5) and matrix (Chapters 3 and 5) at the failure of the composite
σ_F^b	average stress of a branched fibre
σ_F^u	ultimate fibre strength
$\sigma_{F\theta,F\theta\phi}, \sigma_{F\delta,F\delta\phi}$	mean stress of an oblique fibre
$\sigma_{F\theta}^u$	fracture stress of an oblique fibre
σ_{ij}	stress component, i-direction of force, j-direction of surface normal
σ_m	stress at a point in the matrix
σ_{my}	transverse matrix stress
$\sigma_{M,y}$	matrix yield stress
σ_M^u	matrix strength
σ_n^T	thermal stress at the fibre–matrix interface
σ_0	amplitude of the external stress σ_c
σ_y	yield stress
σ_y	applied stress in y-direction (Chapter 6)
τ	shear stress at the interface
τ'	physical-chemical interaction shear stress at the interface
τ_y	matrix yield shear stress
τ_d	debonding shear strength at the fibre–matrix interface

τ_f	shear stress at the fibre surface
τ_m	shear stress at the matrix surface to the fibre
τ_p	pull-out shear stress between fibre and matrix
$\overline{\tau}$	mean shear stress along the fibre axis
$\overline{\tau}^{(s)}$	mean shear stress in the sliding zone (l_s) along the fibre axis
$\hat{\tau}$	relaxation time
ω	frequency
ω_c	crack creation (initiation) energy per volume of the composite
ω_m	plastic deformation energy per volume of the matrix
ω_f	plastic deformation energy per volume of the fibre
Ω	volume per sample cross section of crack initiation processes
Ψ	solid angle

Foreword

Some time ago, the publisher asked me whether I would like to prepare a foreword to a book on short fibre reinforced polymer composites (SFRP). When I recognized the authors, I could not say no. I have been in close contact with each of them during many years of research activity, and I know many of their scientific contributions. It is therefore a pleasure for me to write this foreword.

I met Yiu-Wing Mai for first time in the 1980s. In 2006–2007 I worked with him during an international professorial fellowship at the University of Sydney. He is an outstanding researcher in the field of fracture mechanics, providing a fundamental understanding of cracks in fibre reinforced composite materials.

I visited Bernd Lauke at his invitation, based on our common interests in the fracture behaviour of short fibre composites, at the Institute for Technology of Polymers, Dresden, in East Germany in 1987. Soon after the German reunification, i.e. in 1991, I invited him to work in my group at the Institute for Composite Materials in Kaiserslautern. Shao-Yun Fu worked with Bernd Lauke as a Humboldt Fellow during 1995–1996 and they visited me several times. Both scientists have contributed a lot to the understanding of the action of fibres in composites. Their major working activities have been focused on stiffness, strength and toughness, both from the experimental and from the modelling side.

There are a huge number of journal publications related to the topic of this book, but only a few books have summarized the state of the art in this field. The last one dates back to 1998. After more than 10 years, it is the right time to renew the extent of our knowledge of SFRP through a new book. Knowing the authors' work in this field, it will be worth the wait.

This book is not a collection of chapters from different contributors but is wholly written by the authors. This is a big advantage. All definitions and main symbols are valid from the first to the last page. The contents provide a systematic coverage, ranging from the introduction to the components of these composites to the description of the production technologies involved and the experimental determination and modelling of their mechanical

properties. It is well balanced between experimental findings and micromechanical modelling, including analytical as well as numerical techniques.

The book provides a huge survey and evaluation of relevant publications concerning the subjects raised within the various chapters. But more than this, the authors provide their own contributions to the different subjects which they have developed over recent years. For me it is a special pleasure to recognize that the scientific findings of my previous research groups in this subject are acknowledged.

Readers of the book will benefit not only from basic knowledge about SFRPs but they will also extend their knowledge of future developments. In this way, they will find new starting points for their own research activities in this field.

I would like to thank the authors for a very interesting book and wish them well for their continuing research in this important field. Last, but not least, I also hope the publisher will have a great success with this new book.

Klaus Friedrich
Kaiserslautern

Preface

Composites reinforced with discontinuous fibres are classified as short fibre composites. A short fibre reinforced polymer (SFRP) composite usually consists of relatively short, variable length and imperfectly aligned fibres distributed in a continuous polymer matrix. Although short fibres, such as whiskers, have been employed to reinforce metals, the majority of short fibre composites are based on polymer matrices. Short fibre reinforced polymers (SFRPs) have versatile properties and are comparatively inexpensive to make. The concern of rapid consumption of world resources in metals has contributed to great interest in composite materials. Short fibre reinforced polymers constitute a major proportion of composites used in automotive, marine, building, construction, aerospace and household applications, amongst others. The fibres are mostly glass, although carbon, graphite, Kevlar, and natural fibres are also used.

Extrusion compounding and injection moulding techniques are conventional methods of manufacturing thermoplastics. When these thermoplastics are filled with chopped strands of short fibres, compounds can also be used with conventional extrusion and injection moulding techniques, producing a range of new materials having properties that are intermediate between parent thermoplastics and their corresponding continuous fibre composites. The shear forces of screws and rams during extrusion compounding and injection moulding often break down the fibres, resulting in a fibre length distribution (FLD). For SFRP composites, fibre length or aspect ratio plays a critical role in determining the composite mechanical and physical properties. Fibre orientation is another crucial microstructural parameter that influences the mechanical behaviour of SFRP composites. The orientation of the short fibres depends on the processing conditions employed and may vary from random to nearly perfectly aligned. In general, there is a fibre orientation distribution (FOD) in the final injection moulded SFRP composite parts. It is hence imperative to include the effects of fibre orientation and fibre aspect ratio on composite mechanical properties. In the last three decades, injection moulded short fibre reinforced polymers (SFRP) have become a very common construction material since these

composites are commercially very attractive. Even though they do not have as high a level of stiffness and strength as continuous fibre reinforced counterparts, they have the advantages of low cost, better surface quality; and injection moulding processes also allow intricately shaped parts to be made.

To the best of our knowledge, three books (Folkes, 1985; De and White, 1996; Jones, 1998) have been published on short fibre reinforced polymers. Folkes (1985) wrote the first book with a similar title and his book described some of the concepts on which short fibre reinforcements are based and which can be used to develop products having specified properties. De and White (1996) edited a book on short fibre-polymer composites. Research work on various systems that they and other researchers had studied previously was summarized. A special feature of their book is that it includes significant discussions on rubber-matrix fibre composites. The third book, more like a brochure, was edited by Jones in 1998. Components including fillers, additives and polymers that are often used for manufacturing short fibre reinforced plastics were presented. Brief introductions on the selection of raw materials, testing and evaluation of short fibre reinforced polymers were also given.

Since about two decades ago, there has been much research and development activity into short fibre reinforced thermoplastics. The present book summarizes the advances and developments in this area, and serves as a key reference for readers who are interested in entering this exciting field. It focuses on the basic science and engineering aspects which govern the mechanical and physical properties, such as modulus, strength, fracture toughness, thermal conductivity and expansion of short fibre reinforced polymers. The book is aimed at design engineers and plastics technologists who are working with SFRP composites and are seeking further insight into their manufacture and material behaviours. It is also hoped that the topics covered will provide technical information and guidance to graduate students, educators and researchers in this field.

Finally, Shao-Yun Fu wishes to thank the following: the Leibniz-Institut für Polymerforschung Dresden, e.V., Germany; Nanyang Technological University, Singapore; the Centre for Advanced Materials and Technology, Sydney University, Australia; City University of Hong Kong, Hong Kong SAR, China; and the Technical Institute of Physics and Chemistry, Chinese Academy of Sciences, Beijing, China for the opportunity to work on this subject. Financial support from an Alexander von Humboldt Fellowship, the National Science Foundation of China, the Chinese Academy of Sciences, and the Australian Research Council (ARC) is greatly appreciated.

Bernd Lauke also thanks the Leibniz-Institut für Polymerforschung Dresden e.V., Germany for the opportunity to work on this book. In particular, he would like to thank his former colleagues, Professor Bernd

Schultrich and Professor Wolfgang Pompe, for their long-time cooperation and valuable contributions to this subject. Yiu-Wing Mai acknowledges the continuous financial support of the Australian Research Council for his research projects on fibre composites in the past two decades. He is also grateful to Professor Jian Lu, Hong Kong Polytechnic University, for the time to finalize the book when he was Visiting Chair Professor in the Department of Mechanical Engineering.

Shao-Yun Fu
Bernd Lauke
Yiu-Wing Mai

Beijing, Dresden and Sydney

References

De S K and White J R (1996), *Short fibre-polymer composites*, Woodhead, Cambridge.

Folkes M J (1985). *Short fibre reinforced thermoplastics*, John Wiley & Sons, Chichester.

Jones R F (1998), *Guide to short fibre reinforced plastics*, Carl Hanser Verlag, Munich.

1

Introduction to short fibre reinforced polymer composites

1.1 Introduction

In this book, when fibres in a composite are discontinuous and are shorter than a few millimetres, the composite is called 'short fibre reinforced composite'. That is, short fibre reinforced composites contain discontinuous fibres with a length less than a few millimetres. In most cases, polymers are used as matrices for discontinuous fibre reinforced composites.

Short fibre reinforced polymer (SFRP) composites have found extensive applications in automobiles, business machines, durable consumer items, sporting goods and electrical industries, etc., owing to their low cost, easy processing and their superior mechanical properties over the parent polymers. Extrusion compounding and injection moulding processes are frequently employed to make SFRP composites. The use of these conventional fabrication techniques to produce large-scale SFRP composite parts makes manufacturing of these composites efficient and inexpensive compared to manufacturing of continuous-fibre reinforced polymer composites, which are fabricated by time-consuming processes, rendering them unsuitable for high volume production. At present, SFRP composites are only one class within a variety of composite materials with a high growth rate due to their extensive applications and comparatively simple manufacturing techniques.

1.2 Mechanical and physical properties

The mechanical and physical properties of SFRP composites have been the subject of much attention and are influenced to a great degree by the type, amount and morphology of the reinforcing fibres, and the interfacial bonding efficiency between the fibres and polymer matrix. Variables such as fibre content, orientation, aspect ratio and interfacial strength are of prime importance to the final balance of properties exhibited by injection-moulded polymer composites. The addition of short fibres to thermoplastics

Table 1.1 Strength and Young's modulus of some SFRP composites and matrices respectively*

Materials	Fibre content (%)	σ_M^u (MPa)	σ_c^u (MPa)	E_m (GPa)	E_c (GPa)	References
ABS/SGF	15 vol.	42.8	68.0	2.39	8.33	Fu and Lauke (1998b)
ABS/SGF	30 wt.	43.4	68.0–84.0	2.24	5.12–6.47	Ozkoc *et al.* (2005)
ABS/PA6(70:30)/SGF	30 wt.	43.4	93.0	2.24	8.82	Ozkoc *et al.* (2005)
PA 6,6/SEBS-g-MA(80:20)/SGF	30 wt.	39.0	65.0	0.83	4.07	Tjong *et al.* (2002)
PA6,6/SGF	50 wt.	~78.0	~250.0	—	—	Thomason (2008)
PEEK/SGF	10 wt.	91.4	108.9	3.10	4.70	Sarasua *et al.* (1995)
PEEK/SCF	10 wt.	91.4	135.6	3.10	6.37	Sarasua *et al.* (1995)
PP/SCF	25 vol.	31.6	60.1	1.30	14.9	Fu *et al.* (2000a)
PP/SGF	25 vol.	31.6	51.5	1.30	8.75	Fu *et al.* (2000a)
PC/SGF	30 wt.	40.3	67.2	1.33	8.74	Ho *et al.* (1996)

Note: volume fraction (vol.); weight fraction (wt.); short (or discontinuous) glass fibre (SGF); short (or discontinuous) carbon fibre (SCF); acrylonitrile-butadiene-styrene (ABS); polypropylene (PP); polycarbonate (PC); polyamide 6,6 (PA6,6); polyamide 6 (PA6); maleated styrene-ethylene butylenes-styrene (SEBS-g-MA).

leads to composites that show significant improvements in mechanical properties, such as strength and elastic stiffness as shown in Table 1.1. However, fracture toughness may be reduced for certain fibre-matrix systems. For example, if a tough thermoplastic matrix like polycarbonate (Din and Hashemi, 1997) or polyamide (Fu *et al.*, 2006) is reinforced by short glass fibres, the strength and elastic stiffness can be improved but the fracture toughness is reduced. Nonetheless, for relatively brittle polymer matrices, this problem may not exist and incorporation of short fibres can

increase the fracture toughness. The mechanical and physical properties of short fibre reinforced polymer composites have been shown to depend mainly on the following factors (Lauke *et al.*, 1990; Fu and Lauke, 1996, 1997, 1998a,b; Fu and Mai, 2003):

- properties of components
- fibre-matrix interface strength
- fibre volume fraction
- fibre orientation distribution (FOD) and
- fibre length distribution (FLD).

Theoretical interpretations of strength, stiffness and fracture toughness of SFRP composites are given in terms of these factors.

In a short fibre reinforced polymer composite, the deformation of the matrix transfers stresses by means of the fibre-matrix interface traction to the embedded fibres. The mechanical properties of a short fibre composite are therefore critically dependent on the efficiency of stress transfer from the matrix to the fibres. Many theories have been developed to predict the stress transfer in short fibre composites (Cox, 1952; Piggott, 1980; Lauke and Schultrich, 1983; Lauke, 1992; Rosen, 1965; Fu *et al.*, 2000b). Since the problem of stress transfer in single short fibre composites is relatively simple, existing theories start with these composites. Because the stress transfer takes place between the only fibre and surrounding matrix, these models do not include the effect of neighbouring fibres on the stress transfer. In real multi-short fibre composites, the neighbouring fibres affect the stress transfer from the matrix to the fibres. Hence, the stress transfer behaviour in multi-short fibre composites is of practical importance for real short fibre composites. The stress transfer is critical to achieving high strength and high fracture toughness, etc., of SFRP composites.

When polymeric materials are used in electronic packaging applications, where highly thermally conductive materials are required, polymers are often incorporated with inorganic fillers, like short glass or short carbon fibres, with a high thermal conductivity to fabricate the composites to meet the high thermal conductivity criterion. The effective thermal conductivity of a SFRP composite depends on the thermal conductivities of its components. Besides, the composite thermal conductivity is critically dependent on the FLD and FOD in the SFRP composite. Further, dimensional stability is also important for polymers that are used in areas where temperature varies. Polymers usually have high thermal expansion which can be effectively decreased by adding inorganic short fibres to increase the dimensional stability for applications where temperature often changes. The thermal expansion of SFRP composites also depends on fibre length and fibre orientation distributions.

1.3 Organisation of the book

This book is arranged as follows. Because extrusion compounding and injection moulding processes are most often employed to make short fibre reinforced thermoplastic composites, in Chapter 2, a brief introduction of these processes and the influence of the processing parameters on the microstructures (FLD and FOD) and morphology (layered structure, etc) are given. Chapter 3 describes the major factors influencing the mechanical and physical properties of short fibre reinforced thermoplastics polymers. Some of the factors, namely, FOD and FLD, are dependent on processing conditions. Thus, the effect of processing conditions on these factors is discussed. Chapter 4 concerns the stress transfer in short fibre reinforced polymer composites. Chapters 5 and 6, respectively, discuss the dependence of composite tensile strength and Young's modulus on these major factors. Owing to the partial fibre orientation, short fibre reinforced thermoplastics polymers show anisotropic mechanical properties. Hence, the anisotropies of strength and modulus are also discussed in Chapters 5 and 6. The flexural modulus of SFRP composites, which is highly influenced by the layered structure of SFRP composites or the fibre orientation, is considered in Chapter 7. Chapter 8 covers the thermal properties (e.g., thermal conductivity and linear thermal expansion) of SFRP composites. In Chapter 9, the non-linear stress–strain behaviour and, in Chapter 10, fracture mechanics of SFRP composites are discussed in detail. Fracture toughness of SFRP composites is controlled by fibre-related and matrix-related failure mechanisms, methods for evaluation of fracture toughness are therefore presented in Chapter 10.

1.4 References

Cox H L (1952), 'The elasticity and strength of paper and other fibrous materials', *Brit J Appl Phys*, 3, 72–79.

Din K J and Hashemi S (1997), 'Influence of short-fibre reinforcement on the mechanical and fracture behaviour of polycarbonate/acylonitrile butadiene styrene polymer blend', *J Mater Sci*, 32 (2), 375–387.

Fu S Y and Lauke B (1996), 'Effects of fibre length and orientation distributions on the tensile strength of short-fibre-reinforced polymers', *Compos Sci Technol*, 56 (10), 1179–1190.

Fu S Y and Lauke B (1997), Fibre pull-out energy of misaligned short fibre composites. *J Mater Sci*, 32 (8), 1985–1993.

Fu S Y and Lauke B (1998a), 'The elastic modulus of misaligned short fibre reinforced polymers', *Compos Sci Technol*, 58 (3–4), 389–400.

Fu S Y and Lauke B (1998b), 'Characterization of tensile behaviour of hybrid short glass fibre/calcite particle/ABS composites', *Compos Part A – Appl Sci Manu,* 29 (5–6), 575–583.

Fu S Y and Mai Y-W (2003), 'Thermal conductivity of misaligned short-fiber-reinforced polymer composites', *J Appl Polym Sci*, 88 (6), 1495–1505.

Fu S Y, Lauke B, Maeder E, Yue C Y and Hu X (2000a), 'Tensile properties of short-glass-fiber- and short-carbon-fiber-reinforced polypropylene composites', *Compos Part A – Appl Sci Manu*, 31 (10), 1117–1125.

Fu S Y, Yue C Y, Hu X and Mai Y-W (2000b), 'On the elastic stress transfer and longitudinal modulus of unidirectional multi-short-fiber composites', *Compos Sci Technol*, 60 (16), 3001–3012.

Fu S Y, Lauke B, Li R K Y and Mai Y-W (2006), 'Effects of PA6,6/PP ratio on the mechanical properties of short glass fiber reinforced and rubber-toughened polyamide 6,6/polypropylene blends', *Compos Part B – Eng*, 37 (2–3), 182–190.

Ho K C, Hwang J R and Doong J L (1996), 'Tensile properties of short glass fibre reinforced polycarbonate', *Polym Polym Compos*, 4 (8), 563–575.

Lauke B (1992), 'Theoretical considerations on deformation and toughness of short-fiber reinforced polymers', *J Polym Eng,* 11, 103–151.

Lauke B and Schultrich B (1983), 'Deformation behavior of short-fiber reinforced materials with debonding interfaces', *Compos Sci Technol*, 19 (2), 111–126.

Lauke B, Schultrich B and Pompe W (1990), 'Theoretical considerations of toughness of short-fibre reinforced thermoplastics', *Polymer – Plastics Technology and Engineering,* 29 (7–8), 607–832.

Ozkoc G, Bayram G and Bayramli E (2005), 'Short glass fiber reinforced ABS and ABS/PA6 composites', *Polym Composite*, 26 (6), 745–755.

Piggott M R (1980), *Load-bearing fibre composites*, Pergamon Press Ltd., Oxford, pp. 83–85.

Rosen B W (1965), *Mechanics of composite strengthening*, Fibre Composite Materials, Amer. Soc. for Metals, Metals Park, Ohio, 1965, pp. 37–75.

Sarasua J R, Remiro P M and Pouyet J (1995), 'The mechanical behavior of PEEK short fibre composites', *J Mater Sci*, 30 (13), 3501–3508.

Thomason J L (2008), 'The influence of fibre length, diameter and concentration on the strength and strain to failure of glass-fibre reinforced Polyamide 6,6', *Compos Part A – Appl Sci Manu*, 39 (10), 1618–1624.

Tjong S C, Xu S A, Li R K Y and Mai Y-W (2002), 'Short glass fiber-reinforced polyamide 6,6 composites toughened with maleated SEBS', *Compos Sci Technol*, 62 (15), 2017–2027.

2

Extrusion compounding and injection moulding

Abstract: This chapter gives a brief introduction of extrusion compounding and injection moulding processes since they are most often used to manufacture short fibre reinforced thermoplastic composites. The influences of various processing parameters including holding pressure, back pressure, screw speed, melt temperature and barrel temperature profile, etc., on the microstructures (fibre length distribution and fibre orientation distribution) and morphology (layered structure, etc.) are discussed.

Key words: extrusion compounding, injection moulding, processing parameters, microstructure, morphology.

2.1 Introduction

Short fibre reinforced polymer (SFRP) composites are very attractive because of their versatile properties and mass production. Extrusion compounding and injection moulding are conventional techniques for fast manufacturing of thermoplastics. When thermoplastics are compounded with chopped strands of short fibres, like short glass fibres or short carbon fibres, etc., these compounds can be used in conventional extrusion compounding and injection moulding methods to produce a range of new materials possessing properties that are intermediate between the parent thermoplastics and their corresponding continuous fibre composites. In the past two decades, injection moulded SFRP composites have become a very common construction material because they are commercially very attractive. Though they do not have as high a level of stiffness and strength as their continuous fibre reinforced counterparts, they have the advantages of low cost and better surface quality. In addition, the injection moulding process also allows intricately shaped parts to be easily manufactured.

It is well known that some processing steps in the two techniques of extrusion compounding and injection moulding may reduce significantly the fibre length through breakage. For example, Kamal *et al.* (1986) reported a decrease from 0.71 mm to 0.27 mm during injection moulding of short fibre reinforced thermoplastics. Reduction in fibre length will

lead to decrease in composite strength, modulus and fracture toughness (Fu and Lauke, 1996, 1997, 1998). In the following sections, an introduction to the extrusion compounding and injection moulding processes is given; and an understanding of the fibre degradation mechanisms which are important to achieve high fibre aspect ratios in SFRP composites is provided.

2.2 Extrusion compounding

2.2.1 Processing of extrusion compounding

Before injection moulding of a SFRP, extrusion compounding can be made using an extruder for the corresponding compound containing a few components. Extrusion compounding employs a screw as a transport mechanism due to the ability of the screw geometry to perform all the elementary steps of polymer processing: feeding, pumping, melting, and mixing. Individual extruder screws that have been employed in processing of polymer and SFRP compounding are briefly introduced below.

Figure 2.1(a) shows the geometry of a single-flighted extruder screw (White, 1990). The screw fits inside a cylindrical barrel with an internal diameter D. The radial clearance between the crest of the screw flight and the inner barrel surface is δ_r. The distance between the screw root and the internal barrel surface is H. The axial distance of one full turn of the screw is S. The axial distance between two neighbouring flights is B. The perpendicular distance between two flights along the helical path of the screw is W. The angle of the helix is ϕ and the width of the flights is e. The quantities defined above are not necessarily constant along the screw. The distance W may increase with increasing altitude of the flight. ϕ and e may also vary not only with the screw radius from the screw root to the barrel but along the length of the screw. More generally, extruder screws are multi-flighted. Namely, melted compounding will simultaneously travel along two or more parallel flights. A double-flighted extruder screw and a triple-flighted extruder screw are shown in Figs 2.1(b) and 2.1(c), respectively. Screw elements may be forward or backward pumping and are often described as right-handed and left-handed when rotation is in a clockwise direction as shown in Fig. 2.2.

The main advantages of screw plasticising include the relatively large quantity of compound material, the homogeneity of the melt and the relative ease of temperature control of the melt compared to plunger equipment of similar size. A good compound melt must have a uniform temperature throughout to ensure uniform quality of the end product. The screw rotates within the barrel in the extruder and the screw is driven by an electric or hydraulic motor. The screw flights are so shaped that the

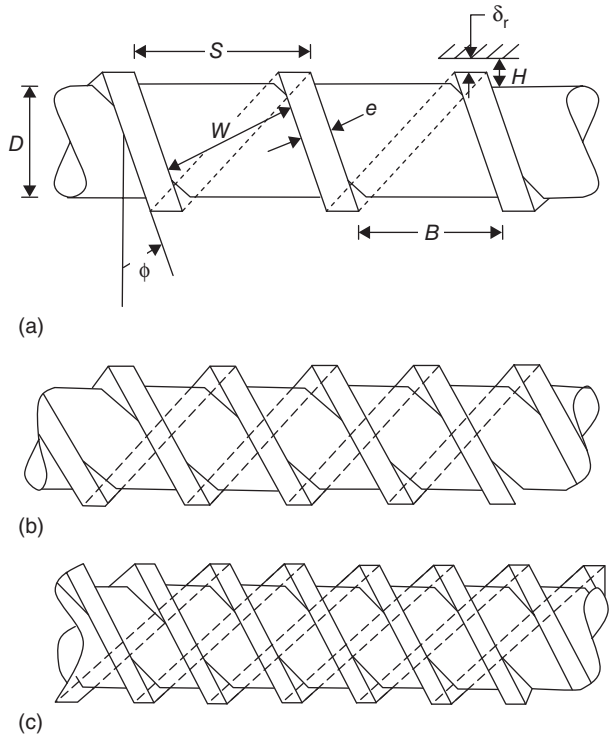

2.1 (a) Single-flighted extruder screw, (b) double-flighted extruder screw, and (c) triple-flighted extruder screw. Adapted from White (1990).

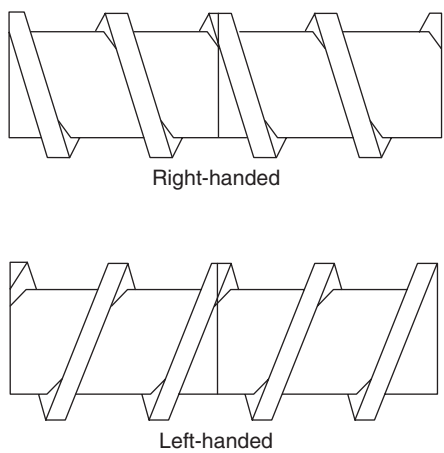

2.2 Forward (right-handed) and backward (left-handed) pumping screws. Adapted from White (1990).

compound is forced against the heated inside wall of the cylinder as the screw rotates. The polymer or SFRP compound is then transported towards the other end of the cylinder.

We will consider only the area of extrusion technology that is important for injection moulding of SFRP composites. In the extrusion process, the forward pressure is sufficient to drive the melted material through the extrusion die. The extruded material can have various desired shapes such as sheets, flats, films or profiles, etc. After leaving the die, the shaped material is cooled, normally using water, and then cut to length. The polymer material in the compound melts gradually as it travels along the barrel from its feeding end to the other end due to the heat generated by friction between the contacting surfaces of the screw and the barrel and by friction between the compound materials themselves. When the compound material reaches the end of the barrel, the polymer material in the compound should be melted and inorganic fillers such as short glass fibres, short carbon fibres and glass beads, etc., should be well mixed with the polymer matrix.

Among the various extrusion technologies, twin screw compounding is a popular method for short fibre reinforced polymers since it is economically attractive. Twin screw extruders are of co-rotating or counter-rotating type with separated, intermeshing or tangential screws. As an example, compounding of short glass fibre (SGF) and glass bead (GB) reinforced polyoxymethylene (POM) composites is described below (Hashemi *et al.*, 1997). First, formulations of composite compounds are determined and mixed. The mixtures are then passed through an extruder (Brabender 330 twin screw extruder) in an attempt to produce a homogeneous dispersion of fibres and beads throughout the POM matrix. The melt temperature is kept constant at 200 °C and the screw speed is set at 4 rpm. As composite compounds emerge from the die exit, the extrudates are passed along a conveyor belt for cooling purposes to allow formation of continuous rods of composite materials. The rods are finally fed through a granulator to make composite pellets for injection moulding.

A co-rotating twin screw extruder, Werner Pfleiderer (screw diameter = 40 mm and screw length = 500 mm) with a fully intermeshing screw design as shown in Fig. 2.3 (Ramani *et al.*, 1995), is used in preparing syndiotatic polystyrene (SPS) pellets reinforced by 40% by weight of glass fibres. The glass fibres are added to the melted polymer using a weight loss feeder with a screw to convey the fibres into the barrel and meanwhile vacuum is applied after the mixing section to remove volatiles. The screw configuration after the melting section consists of the mixing section. The mixing section can be altered during the experiments to investigate the effect of screw section design on fibre length degradation. The extrudates are pulled out through an eight strand die, then a water bath and finally pelletised. The pellets will then be used in injection moulding to obtain SFRP parts.

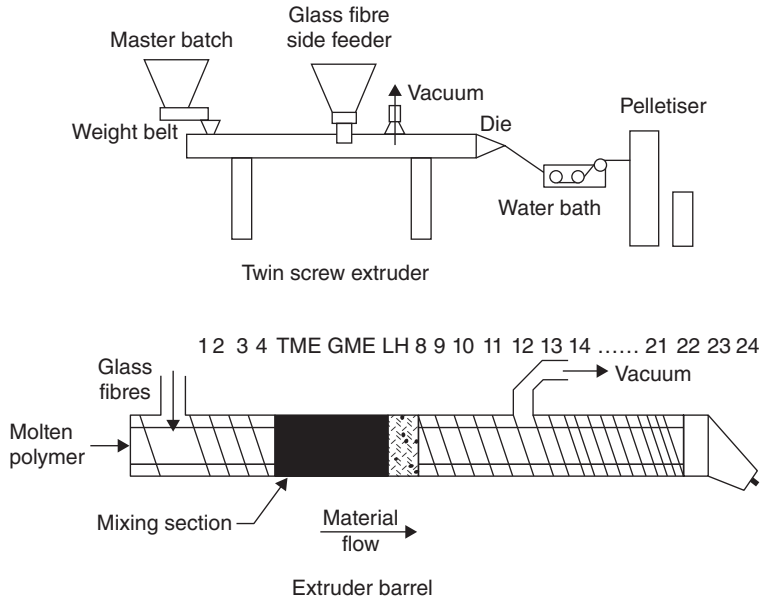

2.3 Schematic of a typical twin screw extruder and the extruder barrel. Adapted from Ramani *et al.* (1995).

Screw sections can be designed in various forms for compounding and three different designs are shown in Fig. 2.4 (Ramani *et al.*, 1995). The three mixing sections are combined with two toothed turbine mixing elements (gear mixing elements, GME) and a left-handed element (LHE) to give different intensities of mixing and residence times in the mixing section. LHE has a very large backup effect on the flow through the screw and increases the residence time in the toothed elements. GME produces primarily distributive mixing that is necessary for mixing discontinuous fibres with high viscosity polymer matrices. Screw design #1 has two right-handed GME and a LHE and would correspond to the longest residence time in the mixing section and produce the highest intensity of mixing among the three screw designs. Screw design #2 has two right-handed GME and the LHE is replaced by a right-handed element of the same pitch, which would reduce the backup effect and produce a lower residence time but keep the same intensity of mixing in the mixing section. Screw design #3 has one right-handed GME and a LHE. Removal of one GME provides a lower intensity of mixing than screw design #2 but retains the high residence time due to the backup effect of the LHE.

The screw section geometry has an effect on the final fibre length. The number average fibre lengths for the 40 wt% glass-SPS for three different screw designs (Ramani *et al.*, 1995) are shown in Fig. 2.5. The fibre lengths

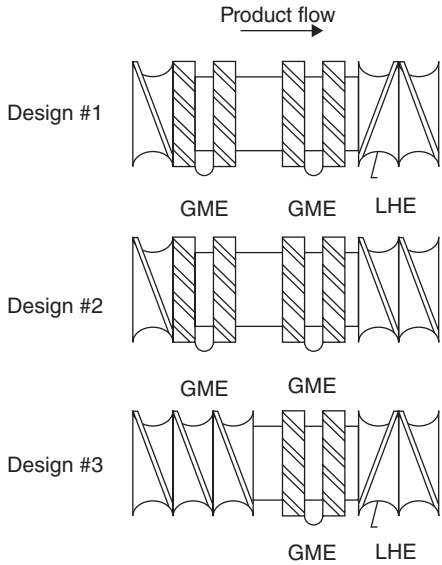

2.4 Three different mixing sections used. GME: Gear mixing element; LHS: Left-handed screw. Adapted from Ramani *et al.* (1995).

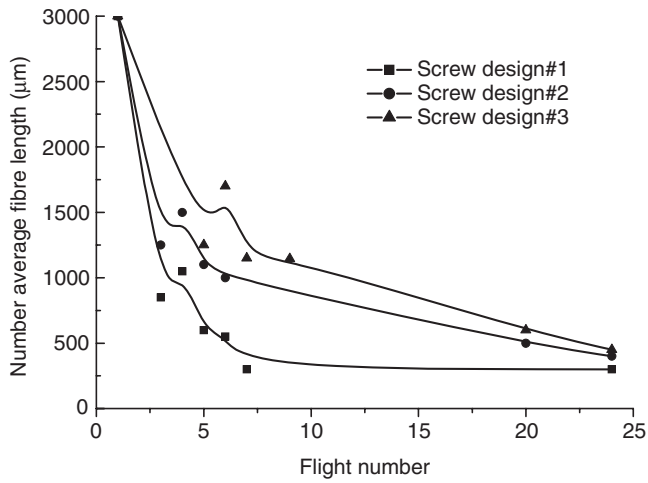

2.5 Number average fibre lengths along the screw for 40 wt% glass-SPS. Adapted from Ramani *et al.* (1995).

show the deepest decline in the portion before the mixing section; and the fibre bundles are broken and filamentised. The fibre length reduction is larger in the mixing section than in the rest of the screw after the mixing section. Moreover, screw design #1 corresponds to the most severe fibre damage while screw design #3 shows the least fibre degradation.

2.2.2 Fibre attrition and retention during compounding

When chopped strands of fibres are mixed in the thermoplastic using conventional extrusion technique, the composite pellets produced can be used for injection moulded SFRP parts. One of the deficiencies in producing composite pellets is the length degradation of reinforcing fibres. The fibre length is reduced by an order of magnitude or even more from the original length. The length reduction decreases the reinforcement efficiency of the fibres, most notably affecting the mechanical strength, modulus and fracture toughness. It is necessary to understand the damage mechanisms of fibres during processing in order to maintain longer fibres.

The length reduction of fibres during extrusion compounding as a consequence of their incorporation into a resin is well documented. There are three likely major reasons for fibre damage (von Turkovich and Erwin, 1983; Fu *et al.*, 1999):

1. Fibre-fibre interaction – abrasion of fibre surfaces reduces strength by inducing stress concentration, leading to direct or subsequent fracture. Fibre breakage may also occur due to bending stresses caused by fibre overlap.
2. Fibre contact with equipment surfaces – evident due to the wear of compounding equipment.
3. Fibre interaction with polymer matrix – viscous forces imparted by the polymer matrix may cause fibre fracture.

A procedure is described below for assessing the extent of fibre damage individually in the compression, melting, and mixing zones along the screw as shown in Fig. 2.6 (von Turkovich and Erwin, 1983). The extrusion process is interrupted with the barrel full of the compound melt containing fibre and resin materials. The melt is allowed to cool down on the screw shaft. The internal threads in the screw tip are used to fit a device by which the screw can be pulled out of the barrel. The composite compound is in the

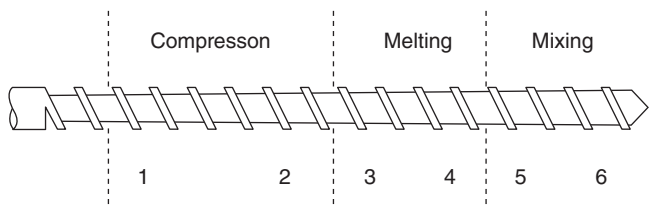

2.6 Location of the screw for analysis of fibre length distribution. Adapted from von Turkovich and Erwin (1983) (*Polymer Engineering and Science,* Vol. 23, No. 13, 1983, p. 745. Copyright, 1983, John Wiley & Sons Inc. Reprinted with permission of John Wiley & Sons Inc.).

form of a helical ribbon with the thickness varying upon the screw section from which it can be obtained. The compound samples are taken from the compression, melting and mixing zones for analysis. Most fibres in zone 1 of Fig. 2.6 maintain their original length, indicating that during this stage fibre bending by solid polymer powder–fibre interaction and inter-fibre abrasion do not play much of a role in fibre fracture. In zone 2, long fibres still predominate but a significant number of short fibres appear. Examination of the material in the channel section shows that some melting begins to take place. The presence of short fibres is due to the mechanism of fibre fracture responsible for damage in the melting zone. In the melting zone (zones 3 and 4), a rapid reduction of fibre length takes place. In the mixing zone (zones 5 and 6), the fibres and especially longer fibres found in the melting zone are further reduced and length reduction in this area is assumed to take place due to the viscous force of fibres by the polymer in shear flow.

Some examples are given below to help readers to understand what factors influence the fibre reduction during extrusion compounding. Fisa (1985) dealt with the mechanical degradation of glass fibres during extrusion compounding with polypropylene. Effects of the parameters, which include resin viscosity and fibre concentration, etc., on fibre length and dispersion, were studied using an automatic particle size analyser. It was noted that the length degradation is most severe during the very first stage of the process, namely when fibre bundles are being filamentised. The resin viscosity also affects the fibre length significantly and a higher resin viscosity generally leads to a lower average fibre length. Fibre length attrition depends on fibre concentration, suggesting that the fibre degradation results from fibre–fibre and fibre–melt interactions. Bader and Bowyer (1973) observed that only 20% of fibres with a diameter of 12 μm in short glass fibre reinforced nylon 66 exceeded the critical length ($l_c \sim 270$ μm) after extrusion compounding though the initial fibre length was much larger. Experimental work (Lunt and Shortall, 1979, 1980) shows that variation in glass content and processing conditions during extrusion compounding of short glass reinforced nylon 66 can lead to significant differences in the fibre length distribution of the resultant extrudates; and incorporation of glass fibres into an already molten resin as opposed to processing of glass fibre resin dry blends may give better results in fibre retention.

In a dilute suspension of short fibres, the fibre–fibre interaction can be ignored. This assumption holds true for a small number of thin and rigid rods in shear flow. However, concentrated suspensions show somewhat different behaviour. In a densely populated flow of fibres, it is very likely that there is fibre–fibre interaction since most commercially interesting suspensions exceed the maximum packing volume fraction of high aspect ratios rods (Milewski, 1974). The maximum volume fraction of randomly oriented

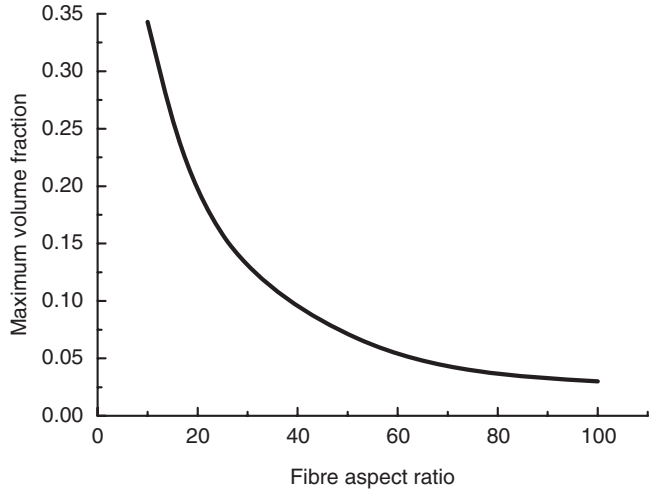

2.7 Maximum fibre volume fraction as a function of average fibre aspect ratio. Adapted from von Turkovich and Erwin (1983) and Milewski (1974) (*Polymer Engineering and Science*, Vol. 23, No. 13, 1983, p. 744. Copyright, 1983, John Wiley & Sons Inc. Reprinted with permission of John Wiley & Sons Inc.).

fibres is shown in Fig. 2.7 as a function of average fibre aspect ratio in a composite (von Turkovich and Erwin, 1983; Milewski, 1974). Fibres are bent, broken or even aligned when fibre volume fraction exceeds the maximum value.

Since processing of fibre compounds in single screw plasticating units inevitably causes fibre fracture, fibre attrition mechanisms are studied and some suggestions are made by Wolf (1994) for prevention of fibre attrition. The reduction of initial fibre length starts before the polymer becomes molten in screw compounding with the incorporation of fibres into a polymer matrix. During compounding in screw machines where a dry blend of chopped fibres and the polymer is extrusion compounded and then granulated, the fibres are usually considerably shortened in the process of coating fibres with polymer. Variation in processing conditions has a considerable effect on the resulting fibre length distributions. Consequently, it becomes possible to substantially minimise the reduction of fibre length by proper selection of processing conditions. It is accepted that pultruded granules containing perfectly wetted fibres offer the most favourable conditions with regard to a well processable compound of large residual fibre lengths. Granule length should thus be increased until the process of feeding is obstructed. To achieve good fibre dispersion and large average fibre lengths, the temperature profile of the barrel and residence time must be set according to the geometry. A gentle conversion and a minimum resi-

dence time in the melt are conveyed to preserve fibre bundles to a great extent. Moreover, granule preheating is a helpful measure to reduce the dissipation of conductive heating. As a guideline, the screw length should not exceed 18*D* (where *D* is internal diameter) and the melting zone should not be longer than 3*D*. To ensure high residual fibre length, the stress in the molten material has to be reduced by choice of a slight compression ratio, e.g., 1:18 over a length of 10*D*–12*D*.

The classical route, namely extrusion compounding for preparing fibre filled polymer pellets, has a practical processing limit on the maximum fibre content in the range of 40–45 wt% of fibres. The composite applications for these materials cannot be too demanding. When the stiffness and strength criteria can be met with fibre volume fraction of 0.2 or less, an extrusion compounding technique is applicable. However, this is low compared to 'high performance' applications where volume fractions of 0.5 or greater of aligned continuous fibres can be used, usually at the cost of accepting a lower level of processing efficiency. Therefore, long (discontinuous, greater than 1 mm or so) fibre reinforced polymers have received great attention. Long fibre reinforced polymers can be made by wire coating, cross-head extrusion or thermoplastic pultrusion techniques (Hamada *et al.*, 2000; Huang *et al.*, 1999; Karger-Kocsis, 2000; Lee and Jang, 1999, 2000; Lin, 2003; Long *et al.*, 2001; Neves *et al.*, 2002; Thomason, 2002, 2005, 2008; Thomason and Vlug, 1996, 1997; Waschitschek *et al.*, 2002; Zebarjad, 2003). The long fibre reinforced composite pellets for injection moulding can give composites with many significantly enhanced properties in comparison with conventional short fibre compounds (Thomason, 2002, 2005).

2.3 Injection moulding

2.3.1 Processing of injection moulding

Although many fabricating processes are available for producing non-reinforced plastic products, injection moulding (IM) is used to produce at least 50% by weight of short fibre reinforced polymers. Moulded parts manufactured by IM have the advantages of economy, vast quantity and no post-moulding finishing operations. IM is principally a mass-production method and the best return is realised when it is so used (Rosato, 1995, 1998).

A screw plasticising system is normally used in the injection moulding equipment. The typical reciprocating screw will melt and mix the compound through compression and shear. As the screw moves to the rear of the cylinder, the melt accumulates in front of the screw. When the desired amount of melt is attained for shot, the screw stops rotating and acts as a ram to push the melt into the mould. In a typical plasticising screw extruder, the compound is fed from a hopper into the side of a long heated cylinder

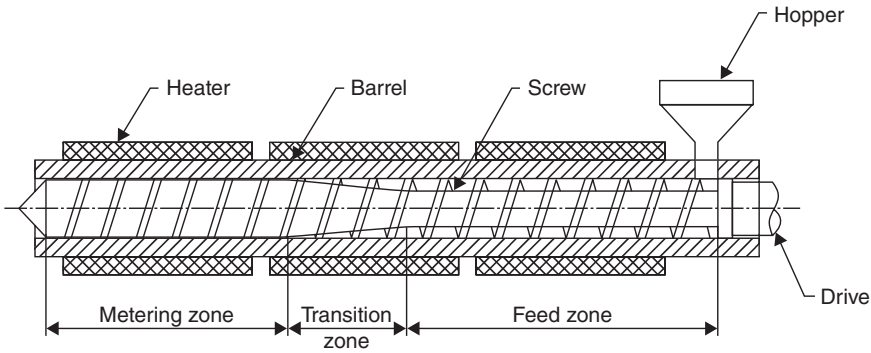

2.8 A typical plasticising screw extruder showing zone locations. Adapted from Rees (1994).

or barrel near its end (Fig. 2.8) (Rees, 1994). The typical screw consists of three basic zones: feed, transition (melting) and metering. The first zone is the feed zone where the compound material is fed from the hopper into the heated barrel. The section of the screw in this zone acts like an auger and is designed to be an efficient conveyor for conveying away the compound material from the hopper. The second zone is the transition or compression zone which starts at the end of the feed zone, in which the compound material is melted and homogenised. The section of the screw in this zone is designed to enhance the friction and contact of the compound material with the barrel, which is different from the feed zone. Finally, the third zone is the metering zone. This zone is designed to act as a pump by generating pressure in the homogeneously molten material and to meter accurately by supplying a quantity of molten compound material under pressure, which is consistent for each operation. The design of the screw is important for obtaining the desired mixing and melt properties, output rate and temperature control. One important design factor is the compression ratio defined as the ratio of the screw flight depth in the feed zone to that in the metering zone. Thermoplastics generally require compression ratios between 1.5 to 1 and 4.5 to 1. However, there is no universal screw for all compounds. It is particularly important to choose a screw design for short fibre reinforced polymers so that no excessive attrition of fibres will take place by an overly high compression ratio.

In the IM process, the composite compound is first introduced into a heated chamber where the compound melts (technically softens for amorphous or melts for semi-crystalline materials, but the term ‘melt’ is used hereafter for convenience), then the melted compound is injected under pressure into a metal-machined mould cavity. Afterwards, the part solidifies into the intended shape. Finally, the part is ejected from the mould. The three basic mechanical units, including melting and injection unit, mould

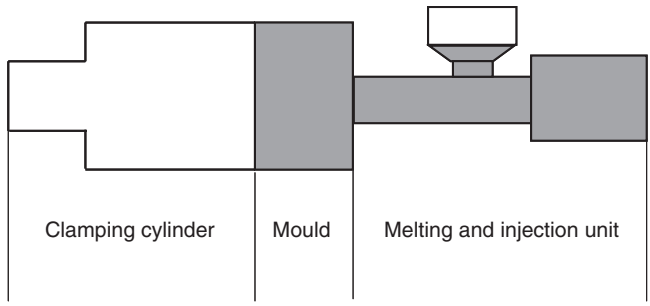

2.9 Three basic mechanical units of the injection molding process. Adapted from Rosato (1998).

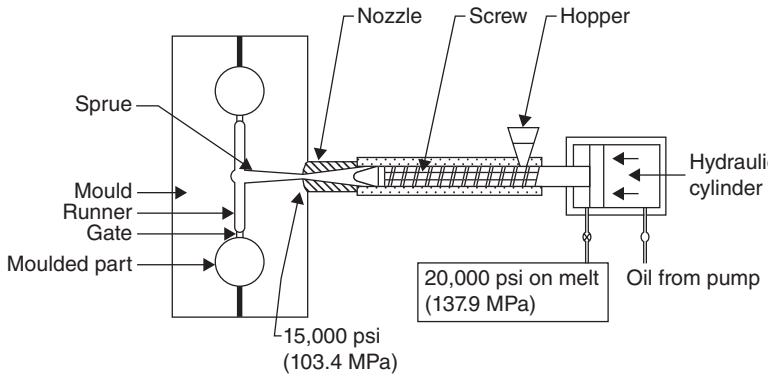

2.10 Schematic showing pressure loading on the melted compound going from the injection unit to the mould cavities (right to left). Adapted from Rosato (1998).

and clamping cylinder as shown in Fig. 2.9 (Rosato, 1998), are combined to perform injection moulding. The metal-machined mould may have a single cavity with a sprue that channels the flow of the compound melt from the heating and injection chamber to the mould cavity. The mould may have multiple cavities that are connected to the flow channels (runners) that direct the melt flow from the sprue to the cavities as shown in Fig. 2.10 (Rosato, 1998).

Basically, there are two different types of moulds, namely 'cold runner' and 'hot runner' moulds, as shown in Fig. 2.11 (Rosato, 1998). The cold runner mould requires that the sprue and runners solidify as the part does, then the sprue and runners are removed when the part is ejected. This mould contains water lines that cool both the part and the runner, hence the name 'cold runner' mould. When the mould is kept hot around the sprue and runner, and water cooling lines are used around the cavity, only the compound in the cavity solidifies, thus the name 'hot runner' mould. It is

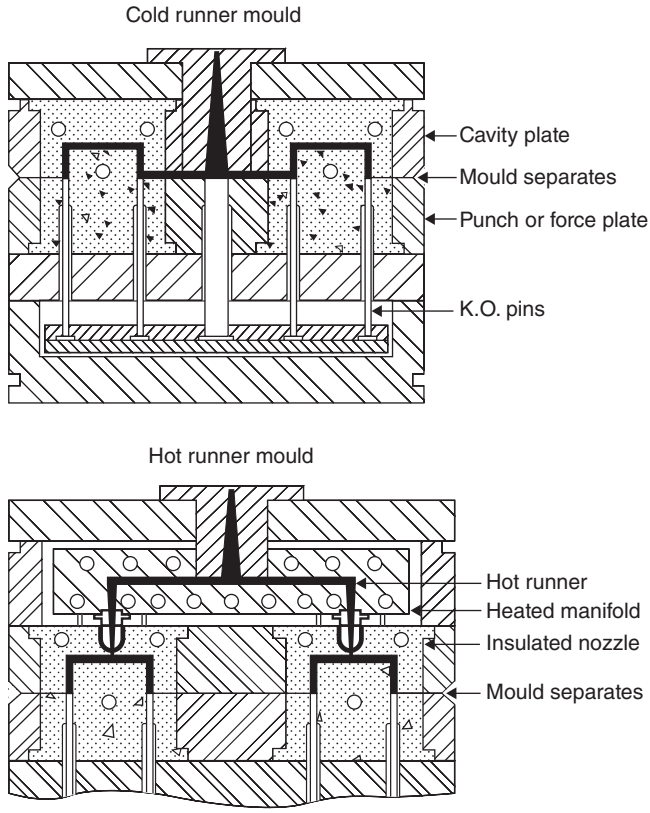

2.11 Schematic diagrams for the cold and hot runner moulds. Adapted from Rosato (1998).

more difficult but more efficient to operate the hot runner mould than the cold runner mould. In addition to these two basic types of moulds, there are many others that are derived from them, including three plate models, insulated runner moulds, hot manifold moulds and stacked moulds. For details, readers can refer to Rosato (1998).

When the compound melt is injected into the mould, both the fibre reinforcements and the polymer molecules disengage from each other and orient themselves parallel to the flow direction of the melt. When high-speed flow occurs through a narrow gate as well as a thin and confined wall section, a high degree of orientation is most pronounced. Otherwise, the degree of orientation will be reduced at least in the centre of the injection moulded part. That may result in the skin–core–skin structure in the final parts as shown in Fig. 2.12 (Xia *et al.*, 1995). Two surface (skin) layers are oriented in the main flow direction while the central (core) layer contains fibres transversely aligned to the main flow direction. The portion of the

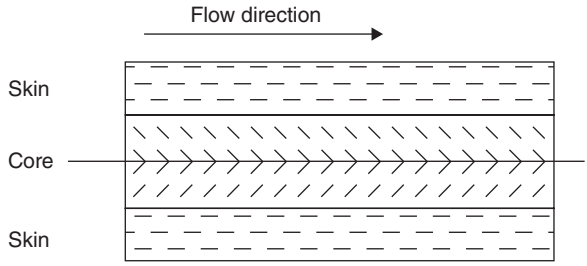

2.12 Schematic diagram of an injection moulded SFRP along the main flow direction.

melt in contact with the cold mould surface solidifies first with the preferred orientation in the flow direction as it flows into the mould cavity.

The SFRP composite with partially aligned fibre orientation shows anisotropic physical and mechanical properties. Namely, the physical and mechanical properties of the SFRP are strongly directionally dependent. To reduce the degree of misalignment of fibres in the SFRP, proper formulations can be selected to contain glass beads or other particulate fillers. The preferred orientation of the fibres in the flow direction increases properties such as strength, elastic modulus, toughness and thermal conductivity, etc., when measured in the flow direction. When fibre orientation is undesirable, increase in the mould temperature and reduction in the filling rate will help. Increase in the gate diameter and the wall thickness of the part will also assist by reducing the shear rate.

In some situations, weld lines may be formed. For example, when the flow of the melt is obstructed by any core used in the design of the part, the melt splits as it surrounds the core and reunites on the other side and continues flowing until the cavity is filled, finally the rejoining of the split melt forms a weld line. Multiple gating may also cause the formation of weld lines. Since short fibres tend to be oriented in the direction of resin flow, in the weld line where flow fronts meet, the short fibres are preferentially aligned perpendicular to the major flow direction (normally the loading direction). Hence, the weld lines reduce composite strength, stiffness and toughness and hence should be avoided whenever possible. When weld lines cannot be avoided, the weld line strength may be optimised by increasing injection moulding time during processing. It is particularly difficult to use long discontinuous fibres in injection moulded parts that unavoidably involve weld lines. In contrast, short fibres may be preferable for such design in practical applications.

Short glass fibre (SGF) reinforced polyoxymethylene (POM) specimens prepared using injection moulding containing weld lines fracture in a brittle manner at the weld line (Hashemi *et al.*, 1997). The critical influence of the

Table 2.1 Tensile strength of POM and SGF/POM composites

Fibre volume fraction	0%	6%	9%	12%	18%
Strength without weldline (MPa)	56.87 ± 0.17	75.00 ± 0.21	82.60 ± 0.13	92.00 ± 0.14	106.60 ± 0.17
Weldline strength (MPa)	56.55 ± 0.21	64.01 ± 0.18	66.72 ± 0.25	70.80 ± 0.16	74.90 ± 0.22

Adapted from Hashemi *et al.* (1997).

weld line on the tensile strength of SGF/POM composites is illustrated in Table 2.1. The strength values of the composites containing weld lines are considerably lower than those composites containing no weld lines. The main cause of the weakness across the weld line is due to preferential alignment of short fibres along the weld line and thus normal to the applied loading direction. Nonetheless, the weld line strength for these composites is still higher than that of the weld-free POM matrix, indicating that short glass fibres are beneficial as reinforcing fillers even in the presence of weld lines.

2.3.2 Fibre attrition and retention during injection moulding

Short fibres and particulate fillers significantly influence moulding characteristics and, in turn, filler dispersion state, fibre orientation and length are affected markedly by processing parameters. The fibrous and particular fillers in the polymer matrix increase apparent viscosity and impede melt flow. This effect increases with increasing filler contents and proper processing of filled polymers requires higher temperatures and pressures accordingly. In some situations, the effects of gating and moulding conditions can be substantial. Moreover, the processing conditions have significant influence on the final fibre length in injection moulded composite parts (Barbosa and Kenny, 1999; Lafranche *et al.*, 2005; Tjong *et al.*, 2003; Ozkoc *et al.*, 2005; Vu-Khanh *et al.*, 1991). Hence, different properties of SFRP composites can be obtained by varying gating geometry, temperature, pressure and time, etc. Attrition of fibres can occur during processing and, in general, low screw speed and low back pressure are desirable to avoid excessive fibre attrition. It is important to choose the right moulding conditions in addition to the right combination of fibres and polymer matrix to obtain high performance SFRP composites.

Significant fibre breakage occurs during the injection moulding process; number average fibre length can be reduced by an order or more. Fibres may be damaged at a number of key stages during injection moulding: in the screw pre-plasticisation zone, in passing through the die, in the gate region of the mould, and interim convergences and divergences in the mould itself (Bailey and Kraft, 1987).

The mechanical properties of short fibre reinforced polymers depend on the retention of fibre length in the finished part. Consequently, optimisation of the injection moulding process is required to achieve better composite mechanical performance. The injection moulding conditions for long glass fibre reinforced poly(butylene terephthalate)/poly(ethylene terephthalate) blends prepared using a standard Hengel injection moulding press of 70 tons with a general-purpose screw having a compression ratio of 22:1 are optimised through controlling the six main moulding variables (Vu-Khanh *et al.*, 1991): peak cavity pressure, holding pressure, back pressure, screw speed, melt temperature and barrel temperature profile. In general, these moulding parameters and their interactions have significant effects on fibre attrition. Table 2.2 shows the results for fibre lengths of SFRP composites prepared under different injection moulding conditions. Besides the effects of the processing parameters, the polymer matrix also has a significant influence on fibre length in the final injection moulded composites such as those found in short glass fibre reinforced polyamide 6,6/polypropylene (PA 6,6/PP) blends toughened by rubber (Fu *et al.*, 2005). The level of glass fibre attrition in long fibre reinforced polypropylene composites is consistently less than that for nylon-based composites (Bailey and Kraft, 1987).

Fibre attrition is also studied in short glass fibre reinforced polypropylene/polystyrene (PP/PS = 70/30) blend composites with special attention to long glass fibre reinforcement (Inberg *et al.*, 1999). Specimens are produced in three different ways: by dry blending (direct injection moulding), mild compounding with a single screw extruder, and intensive compounding with a twin screw extruder. Thus, three different series of injection moulded specimens are made. The first is compounded with the twin screw extruder, the second with the angle screw extruder, and the third is dry blended. The single screw compounding conditions are set at 230 °C and a screw speed of 30 rpm (Brabender 30/25*D*, 3 mm die, screw diameter = 30 mm, with constant screw channel depth). The twin screw compounding conditions are set at 230 °C and 120 rpm (Berstorff, co-rotating, L/D = 33, 3 mm die, and screw diameter = 25 mm). The dry blend series is produced directly using the pre-specified fibre content. For the extrusion compounded materials, extrudates containing 30 wt% are first obtained and are then mixed with the original PP and PS to obtain the 10 and 20 wt% series. The extrudates are chopped into granules of 9 mm. Subsequently, tensile and impact samples are made using injection moulding (Arburg Allrounder

Table 2.2 Effects of injection moulding conditions on fibre attrition

Peak cavity pressure (GPa)	Holding pressure (GPa)	Back pressure (kPa)	Screw speed (rpm)	Melt temperature (°C)	Barrel temperature profile	Number average fibre length (mm)
14	1	0	50	260	Decreasing	1.06
70	1	0	50	260	Increasing	0.85
70	7	0	50	260	Decreasing	0.83
14	1	700	100	260	Decreasing	0.74
70	1	700	100	260	Increasing	0.89
14	7	0	100	260	Decreasing	0.79
70	7	0	100	260	Increasing	0.99
14	7	700	50	260	Increasing	0.79
70	7	700	50	260	Decreasing	0.82
14	1	0	100	260	Increasing	0.95
70	1	0	100	260	Decreasing	0.81
14	7	700	50	290	Decreasing	0.91
14	1	0	100	290	Decreasing	1.23
70	1	0	100	290	Increasing	0.97
70	1	0	50	290	Decreasing	1.45
14	1	700	50	290	Increasing	0.91
70	1	700	100	290	Decreasing	1.12
14	7	0	50	290	Increasing	1.03
70	7	0	100	290	Decreasing	1.00
14	7	700	100	290	Increasing	0.89
70	7	700	50	290	Increasing	0.71
70	7	700	100	260	Decreasing	0.74

Adapted from Vu-Khanh *et al.* (1991).

221-55-250, screw diameter = 30 mm). The fibre lengths before and after injection moulding are measured; the results are given in Table 2.3 (Inberg *et al.*, 1999). Before injection moulding, the fibre length depends on the compounding method. Fibre lengths in twin screw granules are much shorter than those in single screw granules, indicating considerable fibre attrition has taken place with twin screw compounding. For the dry blend, the fibre length before injection moulding is as-received 4.5 mm. The injection moulding of the dry blends and the compounds causes further fibre attrition. The fibre reduction worsens as the fibre content increases for the single screw extruded compound and the dry blend. This decreasing trend of fibre length with increasing fibre content is a common phenomenon (Fu *et al.*, 2000, 2001; Thomason, 2005). Moreover, when hybrid composites are produced simultaneously using two types of fibres (e.g. glass and carbon fibres) at a fixed total fibre content, the average fibre length of the rela-

Table 2.3 Glass fibre lengths before and after injection moulding

	Fibre content (wt %)	Number average fibre length l_{mean} (mm)	Weight average fibre length l^{w}_{mean} (mm)
Before injection moulding			
Single screw granules	30	1.33	2.52
Twin screw granules	30	0.35	0.46
After injection moulding			
Dry blend	10	2.21	3.43
Dry blend	20	1.48	2.72
Dry blend	30	1.09	2.25
Single screw	10	1.11	1.96
Single screw	20	0.92	1.55
Single screw	30	0.72	1.06
Twin screw	10	0.35	0.46
Twin screw	20	0.36	0.49
Twin screw	30	0.33	0.46

Adapted from Inberg *et al.* (1999). (*Polymer Engineering and Science,* Vol. 39, No. 2, 1999, p. 341. Copyright 1999 John Wiley & Sons Inc. Reprinted with permission of John Wiley & Sons Inc.).

tively less brittle glass fibre increases as its content increases while a different trend is true for the more brittle carbon fibre (Fu *et al.*, 2001). The order of fibre attrition after injection moulding for these three series is: twin screw extruded compound > single screw extruded compound > dry blend. Therefore, for injection moulded SFRP composites, on the one hand, there is a variable fibre alignment over the composite part; on the other hand, the process of injection moulding filamentises the fibres causing a wide distribution of fibre lengths. This must be kept in mind when developing a mathematical model to predict the composite strength (Templeton, 1990).

In the past three decades, the growth in using structural composites has resulted in the need for higher performance SFRP composites. High performance levels can only be achieved from a composite part containing fibres of high aspect ratio and high fibre concentration. However, the demands of mass production are often in conflict with the retention of high aspect ratios and the use of high fibre concentrations (Thomason and Vlug, 1996). This has provided the impetus for the development of techniques to produce long fibre reinforced polymer composites. Although the fibre volume fraction is easy to control, this is not the case for fibre length in a SFRP composite, principally because most thermoplastic composite prepa-

ration routes lead to significant uncontrollable degradation of fibre length (Bailey and Kraft, 1987; Fisa, 1985; Franzen *et al.*, 1989; Harmia and Friedrich, 1995; Vu-Khanh *et al.*, 1991; Yu *et al.*, 1994). Thus, it is important to set appropriate targets for the desired fibre concentration and fibre aspect ratio in a composite part. Moreover, fibre length is an important factor in determining fibre concentration at which fibre packing problems manifest themselves (Thomason and Vlug, 1996).

Pultrusion is often used for producing long fibre pellets which are then used for making relatively 'long' fibre reinforced polymers using injection moulding (Truckenmueller and Fritz, 1992; Wolf, 1994). Here 'long' denotes that discontinuous fibres have a length of ~1 mm or longer. Strictly speaking, composites based on polymers reinforced with these 'long' fibres are still SFRP composites. Alternatively, the direct incorporation of continuous fibres (DIF) as a relatively inexpensive method is also used to substitute the relatively expensive pultrusion process to produce long fibre pellets (Truckenmueller, 1993). Nonetheless, good fibre dispersion and high fibre length are often mutually exclusive in DIF injection moulded SFRP composites. Truckenmueller (1993) studied direct processing of continuous fibres in injection moulding machines to improve fibre dispersion with minimum fibre breakage. The schematic of the DIF process (Truckenmueller, 1993) is shown in Fig. 2.13. The roving strands that are normally provided in spools of several kilograms are guided into the specially designed vent of the devolatilising unit and fed into the melt by the

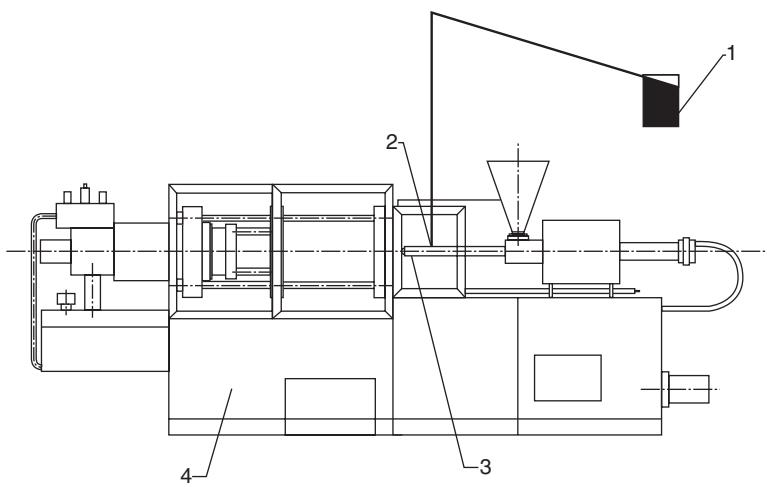

2.13 Schematic illustration of the DIF-technology: (1) spools of roving strands, (2) specially designed vent opening, (3) devolatilising unit, and (4) standard injection moulding machine. Adapted from Truckenmueller (1993).

shearing motion of the screw. To achieve good fibre dispersion and minimum fibre breakage, mixing elements are introduced to provide good distributive mixing performance. Conversely, the dispersive mixing action should be as low as possible to avoid fibre breakage. Large fibre length is achieved and fibre length distribution in DIF injection moulded discs is close to that in composites based on long fibre pellets (Truckenmueller and Fritz, 1992).

In summary, short fibre reinforced polymers are extrusion pre-compounded, resulting in a fibre length distribution even before the injection moulding process takes place. It is well accepted that discontinuous fibre reinforced polymer composites should be moulded with a degree of care to preserve the fibre aspect ratio in the final moulded articles. The use of low back pressure, generous gate and runner dimensions can lead to minimised fibre length reductions (Folkes, 1982; Bailey and Kraft, 1987). Back pressure has a more dramatic effect on the fibre length than does injection speed or injection pressure. A large gate will be associated with lower shearing forces which will damage fibres to a lesser degree. Also, matrix type and fibre content are two important factors on fibre attrition.

2.4 References

Bader M G and Bowyer W H (1973), 'Improved method of production for high strength fibre-reinforced thermoplastics', *Composites*, 4 (4), 150–156.

Bailey R and Kraft H (1987), 'A study of fibre attrition in the processing of long fibre reinforced thermoplastics', *Int Polym Proc*, 2 (2), 94–101.

Barbosa S E and Kenny J M (1999), 'Processing of short fiber reinforced polypropylene. II: Statistical study of the effects of processing conditions on the impact strength', *Polym Eng Sci*, 39 (10), 1880–1890.

Fisa B (1985), 'Mechanical degradation of glass fibres during compounding with polypropylene', *Polym Composite*, 6 (4), 232–241.

Folkes M J (1982), *Short fibre reinforced thermoplastics*, Research Studies Press, J. Wiley & Sons, New York.

Franzen B, Kalson C, Kubat J and Kitano T (1989), 'Fibre degradation during processing of short fibre reinforced thermoplastics', *Composites*, 20 (1), 65–76.

Fu S Y and Lauke B (1996), 'Effects of fibre length and orientation distributions on the tensile strength of short fibre reinforced polymers', *Compos Sci Technol*, 56 (10), 1179–1190.

Fu S Y and Lauke B (1997), 'The fibre pull-out energy of misaligned short fibre composites', *J Mater Sci*, 32 (8), 1985–1993.

Fu S Y and Lauke B (1998), 'The elastic modulus of misaligned short fibre reinforced polymers', *Compos Sci Technol*, 58 (3–4), 389–400.

Fu S Y, Hu X and Yue C Y (1999), 'Effects of fibre length and orientation distributions on the mechanical properties of short-fibre-reinforced polymers – a review', *Mater Sci Res Int*, 5 (2), 74–83.

Fu S Y, Lauke B, Maeder E, Yue C Y and Hu X (2000), 'Tensile properties of short-glass-fibre- and short-carbon-fibre-reinforced polypropylene composites', *Compos Part A – Appl Sci Manu*, 31 (10), 1117–1125.

Fu S Y, Lauke B, Maeder E, Yue C Y, Hu X and Mai Y-W (2001), 'Hybrid effects on tensile properties of hybrid short-glass-fibre- and short-carbon-fibre reinforced polypropylene composites', *J Mater Sci*, 36 (5), 1243–1251.

Fu S Y, Lauke B, Zhang Y H, Mai Y-W (2005), 'On the post-mortem fracture surface morphology of short fibre reinforced thermoplastics', *Compos Part A – Appl Sci Manu*, 36 (7), 987–994.

Hamada H, Fujihara K and Harada A (2000), 'The influence of sizing conditions on bending properties of continuous glass fibre reinforced polypropylene composites', *Compos Part A – Appl Sci Manu*, 31 (9), 979–990.

Harmia T and Friedrich K (1995), 'Mechanical and thermomechanical properties of discontinuous long glass fibre reinforced PA66/PP blends', *Plastics, Rubber Compos Proces Applic*, 23 (2), 63–69.

Hashemi S, Elmes P and Sandford S (1997), 'Hybrid effects on mechanical properties of polyoxymethylene', *Polym Eng Sci*, 37 (1), 45–58.

Huang C, Li R K Y, Wu C M L and Duan Z P (1999), 'Stiffness behavior of injection moulded short glass fibre/impact modifier/polypropylene hybrid composites', *J Mater Process Tech*, 96 (1–3), 48–52.

Inberg J P F, Hunse P H and Gaymans R J (1999), 'Long fibre reinforcement of polypropylene/polystyrene blends', *Polym Eng Sci*, 39 (2), 340–346.

Kamal M R, Song L and Singh P (1986), 'Measurement of fibre and matrix orientations in fibre reinforced composites', *Polym Composite*, 7 (5), 323–329.

Karger-Kocsis J (2000), 'Swirl mat- and long discontinuous fibre mat-reinforced polypropylene composites – status and future trends', *Polym Composite*, 21 (4), 514–522.

Lafranche E, Patricia K, Ciolczyk J P and Maugey J (2005), 'Injection moulding of long glass fibre reinforced polyamide 66: processing conditions/microstructure/flexural properties relationship', *Adv Polym Tech*, 24 (2), 114–131.

Lee N J and Jang J (1999), 'Effect of fibre content on the mechanical properties of glass fibre mat/polypropylene composites', *Compos Part A – Appl Sci Manu*, 30 (6), 815–822.

Lee N J and Jang J (2000), 'Effect of fibre content gradient on the mechanical properties of glass-fibre-mat/polypropylene composites', *Compos Sci Technol*, 60 (2), 209–217.

Lin J S (2003), 'Effect of heat treatment on the tensile strength of glass fibre reinforced polypropylene', *Polym Polym Compos*, 11 (5), 369–381.

Long A C, Wilks C E and Rudd C D (2001), 'Experimental characterisation of the consolidation of a commingled glass/polypropylene composite', *Compos Sci Technol*, 61 (11), 1591–1603.

Lunt J M and Shortall J B (1979), 'The effect of extrusion compounding on fibre degradation and strength properties in short glass-fibre reinforced nylon 66', *Plast Rubber Process*, 4 (4), 108–114.

Lunt J M and Shortall J B (1980), 'Extrusion compounding of short-glass-fibre-filled nylon 6.6 bends', *Plast Rubber Process*, 5 (2), 37–44.

Milewski J (1974), 'Study of the packing of milled fibreglass and glass beads', *Polym Plast Technol Eng*, 3, 101–120.

Neves N M, Pontes A J, Velosa J C, Faria A R and Pouzada A S (2002), 'Glass fibre content of PP plates and their properties. II. Tensile mechanical properties', *Key Eng Mater*, 230–232, 48–51.

Ozkoc G, Bayram G and Bayramli E (2005), 'Short glass fibre reinforced ABS and ABS/PA6 composites: processing and characterization', *Polym Composite*, 26 (6), 745–755.

Ramani K, Bank D and Kraemer N (1995), 'Effect of screw design on fibre damage in extrusion compounding and composite properties', *Polym Composite*, 16 (3), 258–266.

Rees H (1994), *Injection molding technology*, Carl Hanser Verlag, Munich, p.15.

Rosato D V (1995), *Injection molding handbook*, 2nd edn, Chapman & Hall, New York.

Rosato D V (1998), 'Injection molding' in *Guide to short fibre reinforced plastics*, ed. Jones R F, Carl Hanser Verlag, Munich, pp. 104–137.

Templeton P A (1990), 'Strength predictions of injection molding compounds', *J Reinf Plast Comp*, 9 (2), 210–225.

Thomason J L (2002), 'The influence of fibre length and concentration on the properties of glass fibre reinforced polypropylene. 5. Injection moulded long and short fibre PP', *Compos Part A – Appl Sci Manu*, 33 (12), 1641–1652.

Thomason J L (2005), 'The influence of fibre length and concentration on the properties of glass fibre reinforced polypropylene. 6. The properties of injection moulded long fibre PP at high fibre content', *Compos Part A – Appl Sci Manu*, 36 (7), 995–1003.

Thomason J L (2008), 'The influence of fibre length, diameter and concentration on the strength and strain to failure of glass-fibre reinforced polyamide 6,6', *Compos Part A – Appl Sci Manu*, 39 (10), 1618–1624.

Thomason J L and Vlug M A (1996), 'Influence of fibre length and concentration on the properties of glass fibre-reinforced polypropylene: 1. Tensile and flexural modulus', *Compos Part A – Appl Sci Manu*, 27 (6), 477–484.

Thomason J L and Vlug M A (1997), 'The influence of fibre length and concentration on the properties of glass fibre-reinforced polypropylene. 4. Impact properties', *Compos Part A – Appl Sci Manu*, 28 (3), 277–288.

Tjong S C, Xu S A and Mai Y-W (2003), 'Process–structure–property relationship in ternary short-glass-fibre/elastomer/polypropylene composites', *J Appl Polym Sci*, 88 (5), 1384–1392.

Truckenmueller F M (1993), 'Direct processing of continuous fibres onto injection molding machines', *J Reinf Plast Comp*, 12 (6), 624–632.

Truckenmueller F M and Fritz H G (1992), 'Direktverarbeitung von Endlosfasern auf Spritzgiessmaschinen', *Kunststoffe*, 82 (2), 98–101.

von Turkovich R and Erwin L (1983), 'Fiber fracture in reinforced thermoplastic processing', *Polym Eng Sci*, 23 (13), 743–749.

Vu-Khanh T, Denault J, Habib P and Low A (1991), 'The effects of injection molding on the mechanical behavior of long-fibre reinforced PBT/PET blends', *Compos Sci Technol*, 40 (4), 423–435.

Waschitschek K, Kech A and Christiansen J C (2002), 'Influence of push-pull injection moulding on fibres and matrix of fibre reinforced polypropylene', *Compos Part A – Appl Sci Manu*, 33 (5), 735–744.

White J L (1990), *Twin screw extrusion: technology and principles*, Carl Hanser Verlag, Munich, pp. 4–9.

Wolf H J (1994), 'Screw plasticating of discontinuous fibre filled thermoplastics: mechanisms and prevention of fibre attrition', *Polym Composite*, 15 (5), 375–383.

Xia M, Hamada H and Maekawa Z (1995), 'Flexural stiffness of injection molded glass fiber reinforced thermoplastics', *Intern Polym Proc*, 10 (1), 74–81.

Yu Z, Brisson J and Ait-Kadi A (1994), 'Prediction of mechanical properties of short Kevlar fibre-nylon-6,6 composites', *Polym Composite*, 15 (1), 64–73.

Zebarjad S M (2003), 'The influence of glass fibre on fracture behavior of isotactic polypropylene', *Mater Des*, 24 (7), 531–535.

3

Major factors affecting the performance of short fibre reinforced polymers

Abstract: There are a few major factors that play critical roles in determining the mechanical performance of SFRP composites. These major factors include fibre and matrix properties, fibre–matrix interface characteristics, fibre length distribution, fibre orientation distribution and fibre volume fraction. This chapter describes these major factors. Some of the factors, for example, fibre length distribution (FLD) and fibre orientation distribution (FOD), are dependent on processing conditions. Consequently, measuring methods and definitions of FLD and FOD are given in this chapter.

Key words: fibre length distribution, fibre orientation distribution, fibre and matrix properties, interface characteristics, fibre volume fraction.

3.1 Introduction

The disadvantages of pure polymers for structural or semi-structural applications are their relatively low stiffness and strength. The incorporation of high stiffness and high strength short fibres into the polymer matrices is aimed mainly at improving these mechanical properties. An additional advantage is that extrusion compounding and injection moulding techniques that were developed originally for un-reinforced polymers can be adopted to produce short fibre reinforced polymer (SFRP) composites. The extrusion compounding and injection moulding processes are easy, rapid manufacturing techniques that have made possible the fabrication of SFRP products much faster compared with that of continuous fibre composites using time-consuming techniques. SFRP composites are being used increasingly in automobiles, business machines, durable consumer items, sporting goods and electrical industries, etc., owing to their superior mechanical properties over corresponding parent polymers and their low cost and easy processing. To develop high performance SFRP composites, researchers need to know the major factors that play critical roles in determining the mechanical performance of SFRP composites. The major factors include fibre and matrix properties, fibre-matrix interface characteristics, fibre length distribution, fibre orientation distribution and fibre volume fraction. In this chapter an introduction to these major

factors is given. Discussion of the mechanical and physical properties which depend on these major factors will be given in detail in corresponding sections.

3.2 Modified rule of mixtures

Before discussing these major factors, the modified rule of mixtures for the strength and modulus of SFRP composites is first introduced. This knowledge is helpful to understand why fibre and matrix properties, interface characteristics, fibre length distribution, fibre orientation distribution and fibre volume fraction are the major factors. The strength (σ_c^u) of SFRP composites can be estimated by assuming that the load is carried mainly by the fibres and matrix at the instance of fracture. This leads to a modified rule of mixtures equation as below:

$$\sigma_c^u = \lambda \sigma_F^u v + \sigma_M v_m, \tag{3.1}$$

where v and v_m are, respectively, fibre and matrix volume fraction; σ_F^u and σ_M are, respectively, ultimate strength of fibre and the stress level of the matrix at failure of the composite. λ is fibre reinforcing coefficient for composite strength and is a function of fibre aspect ratio (the ratio of fibre length over diameter as a measurement of fibre relative length), fibre orientation and fibre–matrix interfacial adhesion. The value of λ is less than 1.0 for SFRP composites and is equal to 1.0 for unidirectional continuous fibre composites. It is obvious that the composite strength is proportional to the strength of the fibre and the stress level of the matrix at failure of the composite. The stress level of the matrix at failure of the composites is proportional to the matrix stiffness and is a product of matrix stiffness and composite failure strain if the matrix is still in the elastic range. The fibre generally plays a dominant role in determining the strength of SFRP composite because the strength of the fibre is often much higher than that of the polymer matrix.

Similarly, an expression for the composite modulus can be written as:

$$E_c = \chi E_f v + E_m v_m, \tag{3.2}$$

where χ is fibre reinforcing coefficient for composite modulus and is a function of fibre aspect ratio and fibre orientation; it is not strongly dependent on the interfacial adhesion strength because modulus is a material property at low strain. E_f and E_m are, respectively, the modulus of the fibre and the matrix. Equation [3.2] is an approximate expression for the composite modulus. Detailed discussion will be given in Chapter 6 on elastic modulus.

3.3 Fibres

The fibres usually used to reinforce polymers have diameters of the order of 10 μm. The most commonly used reinforcement is glass fibre. However, to meet various demands from industries on composite strength and modulus, various fibres are applied. Advanced reinforcement materials include but are not limited to glass, carbon, boron, silicon carbide, aramid and polyethylene fibres. A survey of the mechanical and physical properties of some selected reinforcing fibres is summarised in Table 3.1, in which the properties of high carbon steel are also provided for comparison. These data show that carbon, boron, SiC and Kevlar-49 fibres have a much higher Young's modulus than glass fibres, but their prices are also much higher. Sometimes, hybridisation of two or more different types of fibres is used to reinforce polymers to achieve a balance of properties and cost. A brief introduction of some selected reinforcing fibres is given below. Detailed discussion on these fibres has already been given by Jang (1994) and Weeton *et al.* (1990).

Glass fibres comprise well over ~90% of the fibres used in SFRP composites as they are inexpensive to produce and possess high strength, high stiffness (relative to parent plastics), low specific gravity, superior chemical resistance and good insulating characteristics. There are also some disadvantages including relatively low modulus, self-abrasiveness, low fatigue resistance and poor adhesion to polymer matrix resins. Several chemicals

Table 3.1 Typical physical and mechanical properties of some selected reinforcing fibres[a]

Fibre materials	Specific density (g/cm^3)	Fibre diameter (μm)	Young's modulus (GPa)	Tensile strength (GPa)
Carbon (PAN HM)	1.80	7–10	400	2.0–2.8
Carbon (PAN HT)	1.7	7–10	200	3.0–3.5
Carbon (PAN A)	1.9	7–10	220	3.2
Carbon (mesophase)	2.02	7–10	380	2.0–2.4
Boron	2.6	130	400	3.4
SiC (whisker)	3.2	1–50	480	up to 7.0
E-glass	2.50–2.54	10–14	70–72.4	1.5–3.5
S-glass	2.48–2.60	10–14	85.5–90	4.6
Kevlar-29	1.44	12	60	2.8
Kevlar-49	1.45	12	130	2.8–3.6
Polyethylene	0.97	12	117	2.6
High carbon steel	7.8	250	210	2.8

[a] After Agarwal and Broutman (1990), Harris (1986), Jang (1994), Jones (1994) and Pilato and Michno (1994).

can be added to silica/sand to prepare for glassmaking; different combinations give rise to different types of glass, including A-glass, C-glass, E-glass and S-glass fibres. A-glass is a high-alkali glass. The important alkalis in A-glass are soda and lime, which make up ~25% of A-glass by weight. A-glass has very good resistance to chemicals. But, its high alkali content lowers its electrical properties. C-glass (chemical-glass) is a special mixture with extremely high resistance to chemicals. It is intended for use in situations where high chemical resistance is required. E-glass is named for its electrical properties. With low alkali content, it offers much better electrical insulation than A-glass. As a fibre, it has good all-around strength, and it can strongly resist attack by water. S-glass is a high strength glass fibre and its tensile strength can be much higher than that of E-glass fibre. It also holds its strength better at high temperatures and resists fatigue well. Some typical physical and mechanical properties of E-glass and S-glass fibres are given in Table 3.1.

High strength and high modulus carbon fibres are manufactured by treating organic fibres (precursors) with heat and tension, leading to a highly ordered carbon structure. The most commonly used precursors are rayon-based filaments, polyacrylonitrile and pitch. Rayon carbon filaments are stretched in a series of steps in an inert atmosphere at ~2700 °C. Tension at high temperatures causes the graphite layer planes to align with the fibre axis, imparting high strength and high modulus to the fibres. Polyacrylonitrile is a long-chain linear polymer composing of a carbon backbone with attached carbonitrile groups. The conversion of polyacrylonitrile fibres into carbon fibres involves treatment of the fibres in an oxidising atmosphere at temperatures typically in the range of 200–300 °C while under tension to avoid shrinkage. Pitch, a by-product of the coal gasification and petrochemical industries, has long been considered as an attractive, inexpensive precursor for production of carbon fibres. The pitch precursor is melt spun and the spun precursor is extruded through a capillary spinneret and is then drawn and wound onto a rotating bobbin to produce fibres. The fibres are generally carbonised by rapidly heating to a temperature in the range of 1500–2800 °C. A few types of carbon fibres are available in a wide range of modulus and strength. Some typical physical and mechanical properties of representative classes of carbon fibres are listed in Table 3.1 (Harris, 1986; Agarwal and Broutman, 1990; Jang, 1994; Jones, 1994).

Aramid fibre is a generic term for aromatic polyamide fibres. As an example, Kevlar® fibres, developed by Du Pont, consist of poly(1,4-phenylene-terephthalamide) (Takayanagi *et al.*, 1982). The fibres are produced as Kevlar®-29, Kevlar®-49, the latter having a higher modulus is more commonly used in composite structures. Other types of aramid fibres have also been developed. For details, readers should consult the books by Jang

(1994) and Weeton *et al.* (1990). Some specific physical and mechanical properties of Kevlar-29 and Kevlar-49 fibres are given in Table 3.1.

The name 'boron fibres' is not strictly accurate because these fibres are actually composites. Boron filament is manufactured by chemical vapour deposition (CVD) and the metal boron is coated on a thin filament of another substance called a substrate. Substrates are usually tungsten (W) or carbon. Boron fibres have been used for many years for polymer matrices. The elastic modulus of boron fibre is extremely high, offering good stiffness to reinforced composites. Some specific physical and mechanical properties of boron fibres are given in Table 3.1.

Silicon-carbide filaments are also produced by CVD. β-SiC is obtained by the reaction of silane and hydrogen gases with the carbon filament being the substrate for deposition. SiC fibres have physical and mechanical properties comparable to those of boron fibres. SiC fibre is less expensive than boron fibre when available in production quantities. Typical mechanical and physical properties of SiC and polyethylene fibres are given in Table 3.1.

3.4 Polymer matrices

While the reinforcing fibres play a very important role in determining the stiffness and strength of SFRP composites, the ability of the matrix to support the fibres and transfer the applied stress to the fibres is also very important. Most polymers are relatively high molecular weight materials, in which no further chemical reaction occurs. By taking advantage of the inherent nature of polymer molecules to undergo thermally-induced flow, various shaped SFRP products can be fabricated at elevated temperatures by easy and fast processing techniques, such as extrusion compounding and injection moulding processes.

Matrix materials in SFRP composites are extensive, such as polypropylene (PP), polyamides (PA6 and PA6,6), polystyrene (PS), acrylonitrile butadiene styrene (ABS) terpolymer, polyethylene (PE), polybutylene terephthalate (PBT), polycarbonate (PC) and poly (ether ether ketone) (PEEK), etc. The property requirements for matrix materials are different from those for short fibres. Since the fibres must serve as the principal load-bearing members in a composite, they must be of high strength and stiffness. Reinforcement fibres usually have low ductility; but in contrast, polymer matrix materials usually have relatively high ductility. The matrix serves to bind the fibres and protect the rigid and brittle fibres from abrasion and corrosion. The matrix transmits the applied stress in and out of composites and in some cases the matrix carries some (especially transverse) load. The mechanical properties of some selected polymers that are most often used in SFRP composites are given in Table 3.2. It must be recognised that the values given in the table represent only the range of these mechanical

Table 3.2 Typical physical and mechanical properties of selected polymer matrices[a]

Materials	Specific density (g/cm^3)	Young's modulus (GPa)	Tensile strength (MPa)
Polypropylene (PP)	0.9	1.1–1.6	30–40
Nylon 6	—	3.0	80
Nylon 6,6	1.14	2.5–3.8	50–90
Polystyrene (PS)	1.05	2.37–3.0	40–49.6
Rubber	0.85–0.90	0.001	—
Poly-2,6-dimethyl-1,4-phenylene oxide (PPO)	1.07	1.65	68.9
Acrylonitrile butadiene styrene (ABS)	—	2.2	45
Polycarbonate (PC)	1.06–1.2	2.2	65
Polybutylene terephthalate (PBT)	—	2.6	60
Poly ether ether ketone (PEEK)	1.32	3.1–4.5	90–103
Poly ether sulphone (PES)	1.37	2.4–2.6	80–84
Polyethylene terephthalate (PET)	1.21	2.7–4.0	50–70
Poly (phenylene sulfide) (PPS)	—	3.5–4.4	74–80

[a] After Berglund (1998), Berthelot (1999), De and White (1996), Tekkanat and Gibala (1991), Jones (1994) and Pilato and Michno (1994).

properties because they depend on testing and environmental conditions, breakdown of molecular chains and chemical reaction during thermal treatment (that is, melting and cooling).

3.5 Interface and interphase

The mechanical properties like strength and toughness, etc., of SFRP composites depend critically on the properties of the interface or interphase between the fibre and matrix. An 'interface' is a boundary demarcating distinct phases such as fibre, matrix and coating layer. An 'interphase' may be a diffusion zone, a nucleation zone, a chemical reaction zone, a thin layer of fibre coating or any combination of the above. Sizing materials are normally coated on the surface of fibres immediately after forming as protection from mechanical damage. The coating material of the fibres involves different agents. It contains in general a film-forming agent for protection, lubricants for reduction of wear during handling and coupling agents for

enhancement of the fibre-matrix interfacial adhesion. For glass reinforcement used in SFRP composites, the sizing usually contains a coupling agent to bridge the fibre surface with the polymer resin matrix used in the SFRP composites. The coating of the fibres leads to an interlayer between the two components.

The interface plays a decisive role in stress transfer from polymer matrix to short fibres and controls the mechanical properties of the SFRP composites, thus, sufficiently high stress transfer ability must be guaranteed to achieve high strength of the composite. Therefore, appropriate coupling agents are often used to improve the quality of bonding between fibres and polymer matrix, since the interfacial shear stress τ between them is important to stress transfer. τ can be used to evaluate the critical fibre length, l_c, at which the fibre stress at its ends transferred from the matrix reaches the maximum stress, that is, the fibre failure stress:

$$l_c = r_f \cdot \sigma_F^u / \tau, \tag{3.3}$$

where r_f is fibre radius. Undoubtedly, the interface or interphase between polymer matrix and short fibres is one key factor to understand composite performance. The effects of the interface on the mechanical properties of SFRP composites are explored in the following chapter. But a detailed study of the mechanisms by which the interface works lies outside the scope of this book. Further discussions of the coating materials and the mechanics of interface and interphase can be found in Jang (1994), Kim and Mai (1998) and Watts (1980).

3.6 Fibre length

3.6.1 Fibre length in SFRP composites

Short fibre reinforced polymer (SFRP) composites are often produced by rapid, low-cost extrusion compounding and injection moulding processes. In the course of these processes, the shear stresses exerted by the screw or ram will break the fibres and result finally in a fibre length distribution with an asymmetric character with a tail at the long fibre end. The fibre length is governed by a number of factors including fibre content and processing conditions, etc. (see Fu *et al.*, 1999a and references therein). The viscosity of the matrix affects the final fibre length distribution in the SFRP composite, which in turn controls the composite mechanical properties. A higher matrix viscosity leads to a lower mean fibre length, and thus a lower fibre reinforcing efficiency for the composite strength and modulus.

Fibre breakage in processing of reinforced polymers is often caused by fibre–fibre interaction, fibre–matrix interaction and fibre contact with the surfaces of equipment. The fibre damage is related not only to the equip-

ment type used and the processing conditions but also to the fibre content and the resin type. It is generally observed that when the fibre content increases, the fibre–fibre interaction will cause more damage to fibre length so that the final mean fibre length decreases with increasing fibre content. That is, the mean fibre length is inversely proportional to fibre content (Fu *et al.*, 2000).

3.6.2 Measurement of fibre length

Mechanical properties, such as strength, elastic modulus and fracture toughness, of SFRP composites are critically dependent on the fibre length distribution (FLD). To study the relationships between mechanical properties and FLD, the latter parameter must be measured. The most common method used for fibre length measurement is direct measurement of fibre lengths after resin burnout (Arroyo and Avalos, 1989; Chin *et al.*, 1988; Fu *et al.*, 2002; von Turkovich and Erwin, 1983).

Conventional fibre length measurement is simple and rapid. Fibre samples are collected by burning off resin matrix in a muffle furnace or removing resin matrix using solvent extraction. The fibres are cast onto glass slides and dispersed in an aqueous solution like saline/lubricant solution or natural water. The fibre dispersion is then dried, leaving an even fibre distribution on the glass slides. The fibre samples are then used for measurement of fibre length as shown in Fig. 3.1. First, optical photos can be taken for fibre samples. Fibre lengths are then measured using a slide projector (von Turkovich and Erwin, 1983) or with computer software SemAfore 4.0 (Fu *et al.*, 2002). When using a slide projector, the light source projects the image of the fibres onto the digitising tablet as shown in Fig. 3.2. Magnetisation of the fibre image is controlled by adjusting the focal length of the projection. The operator uses a magnetic pen to locate the end-points of each fibre to obtain the fibre length. When using the computer software SemAfore 4.0, the optical micrographs of short fibres stored in a computer are used for

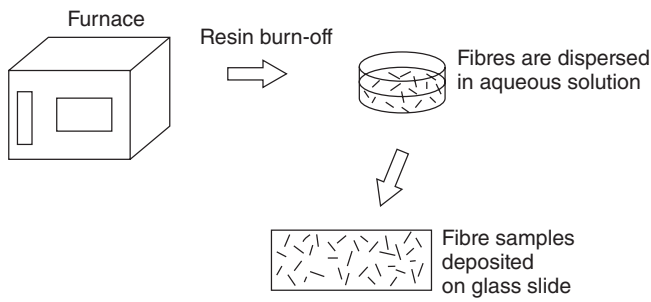

3.1 Preparation of fibre sample for fibre length measurement.

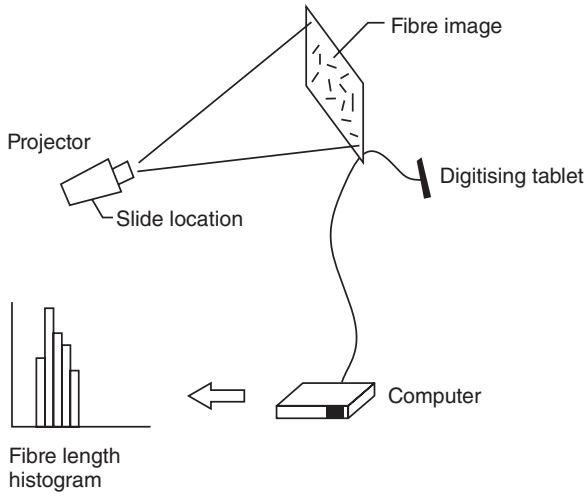

3.2 Fibre length measurement using a slide projector (von Turkovich and Erwin, 1983). (*Polymer Engineering and Science*, Vol. 23, No. 13, 1983, p. 745. Copyright, 1983, John Wiley & Sons Inc. Reprinted with permission of John Wiley & Sons Inc.).

measurement of fibre lengths and fibre length measurements can be easily carried out by semi-automatically locating the two ends of short fibres in the micrographs to evaluate values of fibre lengths.

Figure 3.3(a) shows a schematic of the full view of fibres to be photographed and PIC 1–4 therein will be used for measurement of fibre length (Fu *et al.*, 2002). It can be seen that the fibres crossing the edges of the pictures cannot be measured because the parts beyond the picture edges of the crossing fibres are not visible. The crossing fibres usually have longer fibre length than the un-crossing fibres near the edges and as a result the average fibre length would be underestimated since the crossing fibres could not be properly counted. In the photomicrograph technique, fibres are normally cast onto the surface of glass slides or the like and the fibres are then photographed using an optical microscope. Fibre length can be measured using computer software or a scale on photographs of extracted short fibres from the samples. However, the photographs cannot be unlimitedly large as shown in Fig. 3.3(a). So, there will be many fibres intersecting the edges of the pictures as shown in Fig. 3.3(b).

To obtain the correct average fibre length, all the fibres within the photographs and across the edges of the photographs have to be considered. The lengths of the fibres within the photographs can be easily measured. Normally, 600–1000 fibres in total are needed for measurement of short fibres. Assume the number of the fibres with a length of l to $l + \mathrm{d}l$ is N_{wit}

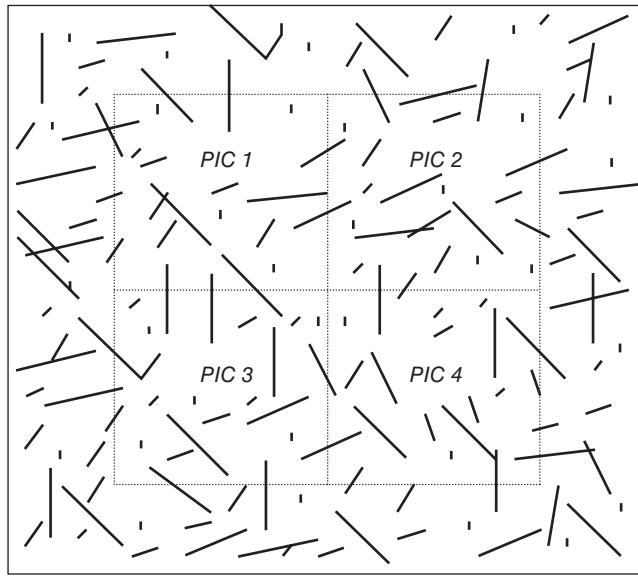

(a)

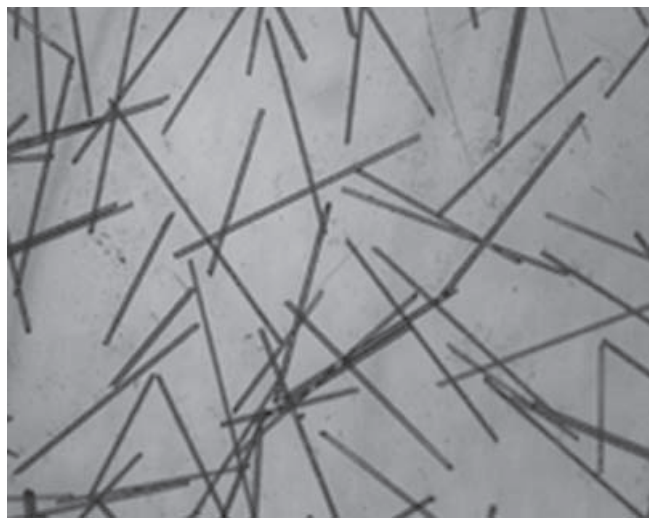

(b)

3.3 (a) Schematic showing the full view of the fibres to be photographed and used for measurement of fibre lengths, (b) optical photograph of short fibres in which the length of fibres only within the photograph can be measured. Adapted from Fu *et al.* (2002).

within the photographs, which are simply counted. Then, the number (N_{int}) of fibres with the same length range intersecting the photographs can be obtained from Fu *et al.* (2002):

$$N_{int} = \frac{1.2732l(L_A + L_B)N_{wit}}{L_A L_B - 0.6366l(L_A + L_B) + 0.3183l^2}, \quad 3.4$$

where L_A and L_B are the lengths of the two edges of the photographs. When L_A, $L_B >> l$, $N_{int} << N_{wit}$. For example, $L_A = L_B = 100l$, then $N_{int} = 0.025\ N_{wit}$. Otherwise, N_{int} has to be counted in the total number of fibres for evaluation of fibre length. For example, $L_A = L_B = 10l$, then $N_{int} = 0.29\ N_{wit}$. This means more long fibres than short fibres would intersect the edges of the photographs that are used for measurement of fibre length. As a result, the total number (N_i) of fibres with a length of l to $l + dl$ is $N_{wit} + N_{int}$. Finally, the (number) average fibre length can be obtained by counting all the fibres within and across the photographs:

$$l_{mean} = \frac{\sum(l + \Delta l/2)N_i}{\sum N_i}. \quad 3.5$$

Sometimes, the weight average fibre length is also evaluated and is defined by:

$$l^w_{mean} = \frac{\sum(l + \Delta l/2)^2 N_i}{\sum(l + \Delta l/2)N_i}. \quad 3.6$$

3.6.3 Definition and characterisation of fibre length distribution (FLD)

To predict the physical and mechanical properties of SFRP composites, the fibre length distribution should be properly defined. The length distribution of fibres in a short fibre reinforced polymer composite can be described with a probability density function. The fibre length probability density function $f(l)$ can be defined such that $f(l)dl$ and $F(l)$ are the probability density that the fibre length is between l and $l + dl$ and the probability that the fibre length is less than or equal to l, respectively. Thus, the relation of $f(l)$ and $F(l)$ is given by (Fu and Lauke, 1996, 1997a, 1998a, b, Lauke and Fu, 1999):

$$F(l) = \int_0^l f(x)dx \quad 3.7$$

and

$$\int_{l_{min}}^{l_{max}} f(x)dx = 1, \quad 3.8$$

where l_{min} and l_{max} are, respectively, minimum and maximum fibre length. A reasonable fibre length probability density function that allows the description of the experimental results is given by:

$$f(l) = abl^{b-1}\exp\left(-al^{b}\right) \quad \text{for} \quad l > 0, \tag{3.9}$$

where a and b are size and shape parameters, respectively. Therefore, the cumulative distribution function, $F(l)$, is given by combination of eqns [3.7] and [3.9] so that:

$$F(l) = 1 - \exp\left(-al^{b}\right) \quad \text{for} \quad l > 0. \tag{3.10}$$

From eqn [3.9] the mean fibre length (i.e., the number average fibre length) becomes:

$$l_{mean} = \int_{0}^{\infty} lf(l)\,\mathrm{d}l = a^{-1/b}\Gamma(1/b+1), \tag{3.11}$$

where $\Gamma(x)$ is the gamma function. To fulfill the normalisation condition of eqn [3.8] the limiting case of l_{min} close to zero and l_{max} close to infinity is assumed. The most probable length (mode length), l_{mod}, where the probability density function has a peak value, is obtained by differentiating eqn [3.9] and putting the resultant equation equal to zero, which gives:

$$l_{mod} = \left[1/a - 1/(ab)\right]^{1/b}. \tag{3.12}$$

An indirect two-section experimental method is also proposed for estimating the average fibre length in layered composites by using data generated from two parallel, closely spaced sections of a specimen (Zak *et al.*, 2000). The average fibre length is estimated from the ratio of matched fibres appearing in both cross sections to the total number observed in a single cross section. The results obtained by this indirect method are consistent with the most commonly used matrix burnout method. However, it should be noted that this indirect method can only provide the data of average fibre length (Zak *et al.*, 2000).

Assume the fibre length (l) varies from zero to l_{max} in a short fibre reinforced polymer composite. The fibre length l_{max} can be divided into n intervals and each fibre length interval equals Δl, then,

$$n = \frac{l_{max}}{\Delta l}. \tag{3.13}$$

It is obvious that n decreases with increasing Δl. Assume that N fibres are collected in total and the number of fibres with a length within the ith interval ($i = 1, 2, \ldots n$) is N_i as done in measurement of fibre length. The total number of fibres within all the intervals is:

$$N = \sum_{i=1}^{n} N_i. \tag{3.14}$$

Naturally, N does not depend on Δl. The number fraction relative frequency $h(l)$ of the fibres within the ith interval is defined by:

$$h(l) = \frac{N_i}{N}, \qquad 3.15$$

where l is the fibre length at the beginning of the ith interval. Equation [3.15] is often used to characterise the fibre length distribution in SFRP composites. But the number fraction of the fibres depends on the size of the fibre length interval Δl and increases with Δl. Hence, the fibre length distribution obtained according to eqn [3.15] is not constant.

It is more reasonable to characterise the fibre length distribution (FLD) by the fibre length probability density:

$$f(l) = \frac{N_i/N}{\Delta l}. \qquad 3.16$$

Equation [3.16] has been shown to describe the FLD well (Fu *et al.*, 2001a). In principle, when Δl is infinitely small, the fibre length probability density could be independent of the fibre length interval Δl. However, this is impractical because very tedious experimental work in measuring fibre length is then required. In practice, the fibre length probability density still depends on the fibre length interval. As an example, Fig. 3.4 shows the fibre length probability density $f(l)$ as a function of fibre length using experimental data

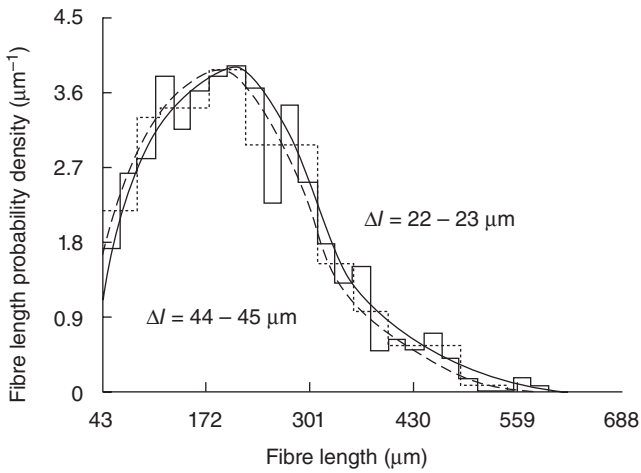

3.4 Fibre length probability density versus fibre length for a 30 wt% short glass fibre reinforced polybutylene terepthalate (PBT) composite. Adapted from Fu *et al.* (2001a).

given by Sarasua *et al.* (1995). It is clear that $f(l)$ depends on the fibre length interval Δl. The FLD curve moves horizontally by an amount about $[(\Delta l)_1 - (\Delta l)_2]/2$ when the fibre length interval changes from $(\Delta l)_1$ to $(\Delta l)_2$, where $(\Delta l)_1 = 22–23\ \mu$m and $(\Delta l)_2 = 44–45\ \mu$m (Fu *et al.*, 2001a).

In contrast, the cumulative fraction of fibres with a length from 0 to l does not depend on the fibre length interval Δl. The cumulative fraction of fibres is given by:

$$F(l) = \sum_{l_i=0}^{l} N_i / N. \tag{3.17}$$

The same cumulative fibre length distribution can be obtained by changing the fibre length interval Δl. This is because the cumulative number of fibres with a length less than a certain value is constant for all fibre length intervals and thus does not depend on fibre length interval.

The cumulative fibre length distribution can be described with the cumulative distribution function, $F(l)$, expressed by eqn [3.10]. If the values of $F(l)$ at l_1 and l_2 are known, then a and b can be evaluated from eqns [3.18] and [3.19]:

$$F(l_1) = 1 - \exp\left(-a l_1^b\right) \tag{3.18}$$

$$F(l_2) = 1 - \exp\left(-a l_2^b\right). \tag{3.19}$$

Combination of eqns [3.18] and [3.19] gives the solutions of a and b as:

$$b = \frac{\ln\left\{\ln\left[1 - F(l_1)\right] / \ln\left[1 - F(l_2)\right]\right\}}{\ln\left(l_1 / l_2\right)} \tag{3.20}$$

$$a = -\frac{\ln\left[1 - F(l_1)\right]}{l_1^b}. \tag{3.21}$$

Since the cumulative fibre length distribution $F(l)$ does not depend on the fibre length interval, the parameters a and b can be determined according to eqns [3.20] and [3.21].

Alternatively, the parameters a and b can also be obtained from eqns [3.11] and [3.12] provided the mean fibre length (l_{mean}) and mode fibre length (l_{mod}) are given experimentally, in which l_{mean} is obtained in terms of eqn [3.5] while l_{mod} can be obtained from the measured fibre length profile:

$$(1 - 1/b)^{1/b} / (1/b + 1) = l_{mod} / l_{mean} \tag{3.22}$$

$$a = (1 - 1/b) l_{mod}^b \tag{3.23}$$

The number average fibre length and the weight average fibre length can be evaluated from the measured fibre lengths and are given by eqns [3.5] and [3.6].

3.7 Fibre orientation

3.7.1 Fibre orientation in SFRP composites

SFRP composites are very attractive because of their ease of fabrication, economy and superior mechanical properties. Conventional injection moulding is often used to make SFRP composites (Bader and Collins, 1983; Bijsterbosch and Gaymans, 1995; Biolzi *et al.*, 1994; Curtis *et al.*, 1978; Denault *et al.*, 1989; Doshi and Charrier, 1989; Friedrich, 1985; Fu and Lauke, 1997b, 1998c,d; Fu *et al.*, 1999b, 2000, 2005, 2006; Hine *et al.*, 1993a; Ho *et al.*, 1996; Joshi *et al.*, 1994). In the final SFRP composites prepared using this technique, the fibres will show certain orientation distribution. Several studies (Bay and Tucker, 1992; Fu *et al.*, 2002; Gupta and Wang, 1993; Silva *et al.*, 2006) revealed that injection-moulded SFRP composites have quite complex fibre orientation distributions which vary both through the thickness and at different positions along the composite mouldings (Barbosa and Kenny, 1999). Mechanical properties of SFRP composites are normally orthotropic due to partial fibre misalignment in moulded parts. The fibre orientation pattern is the dominant structural feature of injection moulded short fibre reinforced polymer composites. The composite is stiffer and stronger in the direction of the major orientation while much weaker in the transverse direction. Fibre orientation can be strongly influenced by processing condition and mould geometry.

Fibre orientation is dependent on mould geometry and hence specimen geometry. For large samples like injection moulded plaques, the composite moulding has a typical skin–core–skin structure with two skin layers where the fibres are highly oriented in the flow direction and a core layer where fibres are mainly aligned transversely to the flow direction (Bay and Tucker, 1992; Darlington and McGinley, 1975; Fu *et al.*, 2002; Friedrich, 1998; Solomon *et al.*, 2005; Tjong *et al.*, 2002; Xia *et al.*, 1995). An example is given in Fig. 3.5 for a 45 wt% short-glass-fibre (SGF)/polyethyleneterephthalate (PET) composite (Friedrich, 1998), in which the skin–core–skin structure in the sample cut from an injection moulded plaque is clearly demonstrated. In the centre section away from the surfaces, the fibres are distributed more transversely to the mould flow direction. In contrast, for small specimens with narrow cross sections used for tensile testing, the fibres will be aligned preferentially along the mould flow direction. Figure 3.6 shows SEM micrographs of the fracture surfaces of a short glass fibre (SGF)/polypropylene (PP) composite in three different positions across the specimen thickness from one side to the middle, and to the other side (Fig. 3.6a–c). It can be seen that the short fibres are aligned preferentially along the flow direction in the whole specimen thickness. This observation agrees with previous studies from fractured surfaces (Fu and Lauke, 1998c; Ramsteiner and

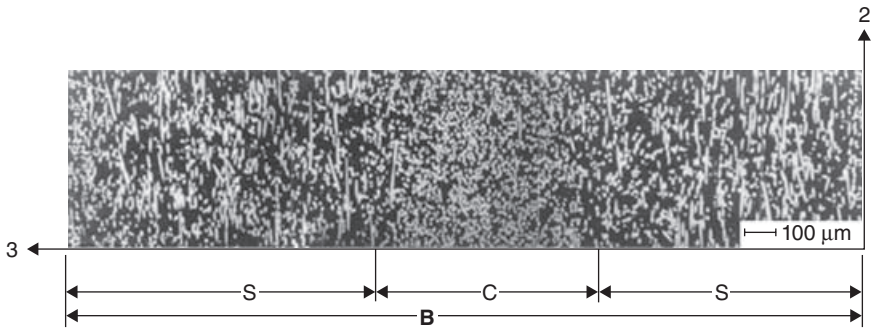

3.5 SEM micrograph of the layer structure in the 2–3 plane (cross-section) of a 45 wt% SGF/PET composite. 'C' and 'S' are respectively the core and skin layer size while 'B' is the specimen thickness. Adapted from Friedrich (1998).

Theysohn, 1979) and polished surfaces (Takahashi and Choi, 1991) of tensile samples with narrow cross sections. Moreover, when short glass and short carbon reinforced polypropylene composite specimens were injection moulded into dumbbell-shaped tensile bars (Fu *et al.*, 2001b), in which an end gated mould was used according to DIN 53455, the fibres in the tensile bars were preferentially oriented in the flow direction as shown in Fig. 3.7. Here, it should be pointed out that 'preferentially oriented' does not mean perfect alignment and there should be a fibre orientation distribution with a small average angle of the fibres with the flow direction. Further, as the specimen thickness increases, fibre orientation also changes. The fibre orientation or orientation distribution can be measured using the image analyser technique discussed below.

3.7.2 Measurement of fibre orientation

Fibre orientation can be measured using an image analyser system (Clarke *et al.*, 1990, 1993; Hine *et al.*, 1996; Lee *et al.*, 2003). The system works by imaging directly from a polished and etched section taken from the SFRP composite, in which each fibre image appears as an ellipse. The reflection microscopy of a polished composite section easily lends itself to automation allowing a large number of fibre images to be processed in a short time at the order of 10,000 images in 20 minutes. The analysis method allows three-dimensional (3D) fibre orientation distribution functions to be determined. The two Euler angles (θ ϕ) which specify the 3D orientation of a fibre can be calculated by the analysis system for every fibre image with no need to make any assumptions about the symmetry of the fibre orientation distribution (e.g. transverse isotropy).

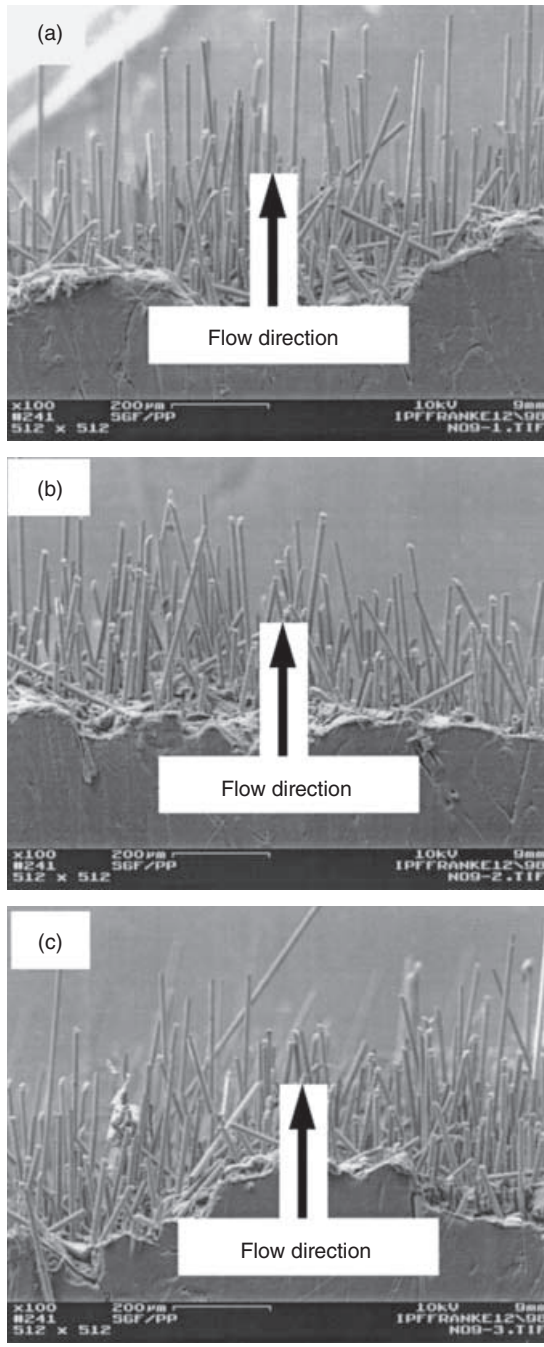

3.6 SEM micrographs of tensile fracture surfaces of an SGF/PP composite with an 8 vol% glass fibres: (a) one side, (b) middle, (c) another side. Adapted from Fu *et al.* (2000).

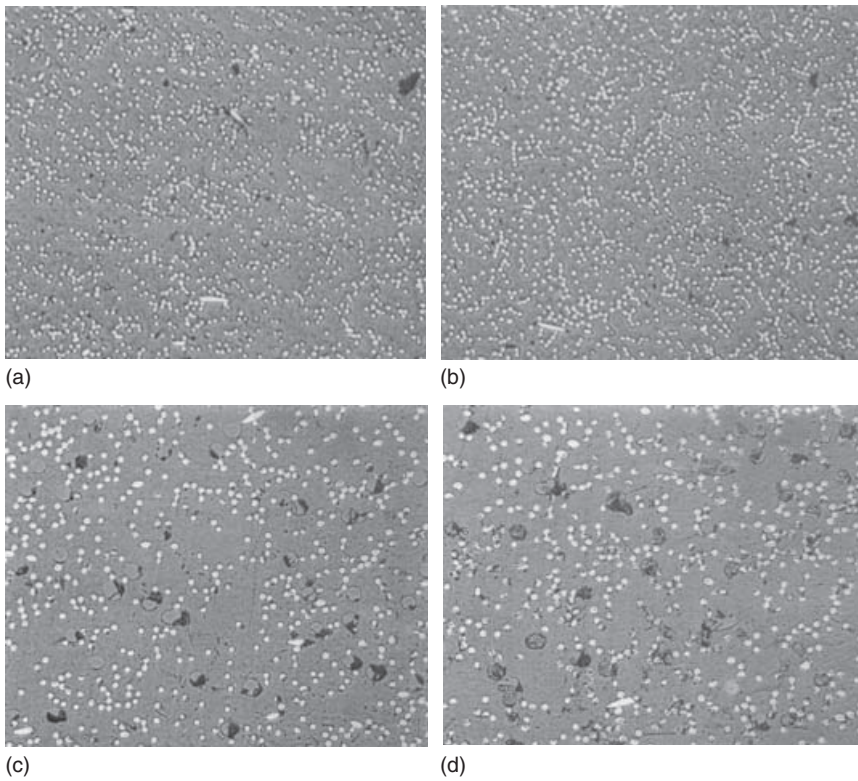

3.7 Orientation of fibres in specimens taken from: (a) the side and (b) the central area of the short carbon fibre (SCF)/PP composite with *v*(carbon) = 25%, (c) the side and (d) the central area of the hybrid SGF/SCF/PP composite with *v*(carbon) = 18.75% and *v*(glass) = 6.25%. Adapted from Fu *et al.* (2001b).

The spatial position of a fibre can be defined by the two Euler angles θ and ϕ as shown in Fig. 3.8. θ is defined as the angle that the fibre makes with the injection direction 1 or the normal direction of a plane on which the fibre orientation will be measured. ϕ is the angle that the fibre makes with the 2-axes when projected onto the 2–3 plane, that is, the one whose normal is parallel to the 1-axis direction. θ is determined by the inverse cosine of the ratio of the semi-minor to semi-major axis of the ellipse, while ϕ is determined from the orientation of the semi-major axis of the ellipse to the 2-axis. The image analysis system for measuring fibre orientation takes each image frame, and fits an ellipse to every fibre image and then determines θ and ϕ (Hine *et al.*, 1996). For further details on the use of the image analysis system and a more detailed discussion, please see Clarke *et al.* (1990, 1993) and Hine *et al.* (1996).

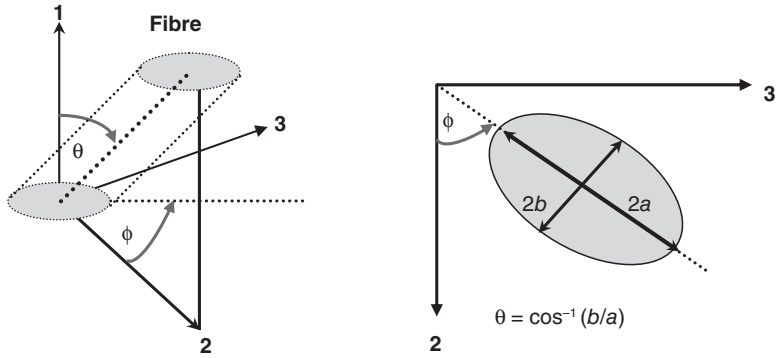

3.8 Definition and determination of the fibre orientation angles θ and ϕ. Adapted from Hine *et al.* (1996). (*Polymer Composites*, Vol. 17, No. 3, 1996, p. 402. Copyright, 1996, John Wiley & Sons Inc. Reprinted with permission of John Wiley & Sons Inc.).

The measurement of fibre orientation by the image analysis technique requires the preparation of a cross section at a prescribed location in the finished SFRP component. The preparation method depends on the technique, e.g., scanning electron microscopy (SEM) or reflected light microscopy used to image the polished cross section of the specimen. The cost of a light microscope is considerably less than that of a SEM and is thus the preferred choice. The preparation of a specimen for inspection by reflected light microscopy requires high contrast between fibre and matrix. A major increase in contrast can be achieved if the specimen is etched with oxygen ions (Mlekusch *et al.*, 1999). The matrix is roughened resulting in greater light scattering and images with contrast comparable to those obtained by SEM (Mlekusch *et al.*, 1999).

It is recognised when a polished section is taken through an SFRP composite the fibres appear as circular or elliptical images. Measurement of the elliptical parameters of these images allows the fibre orientation distributions to be measured. Methods to obtain the elliptical parameters include direct measurements of photographs (Yurgatis, 1987; Fakirov and Fakirova, 1985) and use of commercially developed image analysers (Fischer and Eyerer, 1988; Fischer *et al.*, 1990). A polished composite section must be prepared for image analysis. Figure 3.9 shows a typical sectioned surface whose axes are defined as X, Y′ and Z′ (Hine *et al.*, 1993b). In theory, this section could be made at any angle α to the Z-axis. Although the transverse section (X–Y plane) is taken traditionally, this can cause problems with well-aligned fibres. For well-aligned fibre reinforced composites, it is beneficial to prepare the section at a small angle to the Z-axis, making the majority of the fibre images elliptical with a large ellipticity.

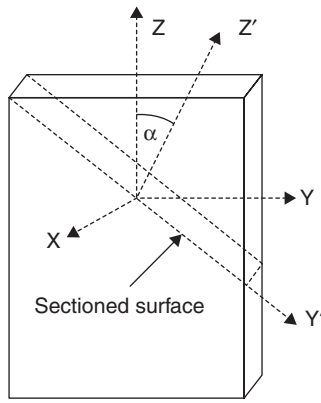

3.9 Definition of the section angle (Hine *et al.,* 1993b).

Elliptical fibre images measured on this sectioned plane are defined by the angles θ and ϕ. θ is the angle the fibre makes with the Z′-axis, while ϕ is the angle between the projection of the fibre image in the X–Y plane and X-axis. $\theta = \cos^{-1}(b/a)$, where a and b are major and minor axes of the ellipse, respectively. For a near circular image ($\theta \approx 0$), a 1% error can lead to an uncertainty of 8° in θ. However, when the section is taken at an angle to the Z-axis for the aligned fibre composite, this makes all the images elliptical. Then, a 1% change in b/a gives a 0.5° error in θ. Therefore, it is recommended that the cross section to be used for measurement of fibre orientation in aligned SFRP composites should be selected at an angle to the Z-axis so that the measuring error can be very small.

The above approach uses destructive techniques for determining fibre orientation. As stated above, destructive techniques generally consist of cutting a material sample by a microtome, polishing the surface and analysing the elliptical footprints left by fibres cut by the sectioning plane by means of image analysis software. In contrast, non-destructive techniques consisting of using X-rays are also used to obtain an image projection of the fibres on a plane perpendicular to irradiation direction (Kim *et al.*, 2001; Bernasconi *et al.*, 2008). Using non-destructive techniques, the planar fibre orientation distribution can be obtained, but fibre orientations along the thickness of the sample cannot be captured. To obtain a complete spatial distribution description, computed microtomography (μCT) is required. The X-rays produced by the source hit the sample, which is placed on a rotating table, travel through the structures and are collected on the detector plane located downstream. In this way, a large number of radiographs (projections) of the sample are taken at small angular increments over a 180/360° rotation. From these projections it is possible to reconstruct the

internal 3D microstructure of the sample using well-known mathematical algorithms.

3.7.3 Definition and characterisation of fibre orientation distribution (FOD)

To describe the fibre orientation distribution (FOD) in a short fibre reinforced polymer composite, a spatial curvilinear coordinate system is adopted as shown in Fig. 3.10. Provided θ is the angle that one end of a fibre makes with the 1-axis, then $(\pi - \theta)$ is the angle at the other end of the fibre with the 1-axis. ϕ and $(\pi + \phi)$ are the two angles of the projection of the two fibre ends onto the 2–3 plane with the 2-axis, respectively.

A two-parameter exponential function is used to describe the fibre orientation distribution $g(\theta)$ as follows:

$$g(\theta) = \frac{\sin\theta^{2p-1}\cos\theta^{2q-1}}{\int_{\theta_{min}}^{\theta_{max}} \sin\theta^{2p-1}\cos\theta^{2q-1}\mathrm{d}\theta} \quad \text{for} \quad 0 \le \theta_{min} \le \theta \le \theta_{max} \le \pi/2, \quad 3.24$$

where p and q are the shape parameters that can be employed to determine the shape of the distribution curve, and $p \geq 1/2$ and $q \geq 1/2$. $g(\theta)\,\mathrm{d}\theta$ is the probability that the fibre orientation is between θ and $\theta + \mathrm{d}\theta$. Equation [3.24] has been verified to be a suitable probability density function to describe the fibre orientation distribution $g(\theta)$ in injection moulded short-fibre reinforced polymer composites (Fu and Lauke, 1996,

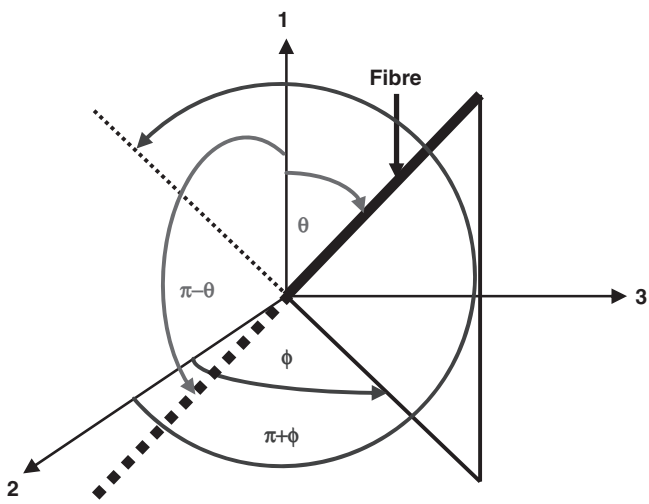

3.10 Definition of the fibre orientation angles: θ, $\pi - \theta$, ϕ and $\pi + \phi$.

1998,a,b). The mean fibre orientation angle (θ_{mean}) can be obtained from eqn [3.24] by:

$$\theta_{mean} = \int_{\theta_{min}}^{\theta_{max}} \theta g(\theta) d\theta. \quad 3.25$$

Let the resultant equation after differentiating eqn [3.24] be zero, then we have:

$$\theta_{mod} = \arctan\left\{\left[(2p-1)/(2q-1)\right]^{1/2}\right\}. \quad 3.26$$

Equation [3.26] represents the most probable fibre orientation angle, namely, mode fibre angle at which the fibre probability density is the highest. When $p = q = 1$, then $\theta_{mod} = \pi/4$; when $p = 1$ and $q > 1$, $\theta_{mod} < \pi/4$; when $p > 1$ and $q = 1$, $\theta_{mod} > \pi/4$; when $p = 1/2$, $\theta_{mod} = 0$; when $q = 1/2$, $\theta_{mod} = \pi/2$; when $p = q = 1/2$, there will be no θ_{mod} and the fibres are randomly distributed in the SFRP composite; the corresponding fibre orientation distribution curves are shown in Fig. 3.11. Moreover, when $p = 1/2$, large q (e.g. 100 or larger) indicates that fibres are preferentially aligned parallel to the $\theta_{mod} = 0$ direction; when $q = 1/2$, large p (e.g. 100 or larger) means fibres have a major preferential orientation normal to the $\theta_{mod} = 0$ direction. So, all the cases of fibre orientation distribution in SFRP composites can be included in eqn [3.24]. The fibre orientation coefficient, f_θ, can then be defined below:

$$f_\theta = 2\int_{\theta_{min}}^{\theta_{max}} g(\theta)\cos^2\theta d\theta - 1. \quad 3.27$$

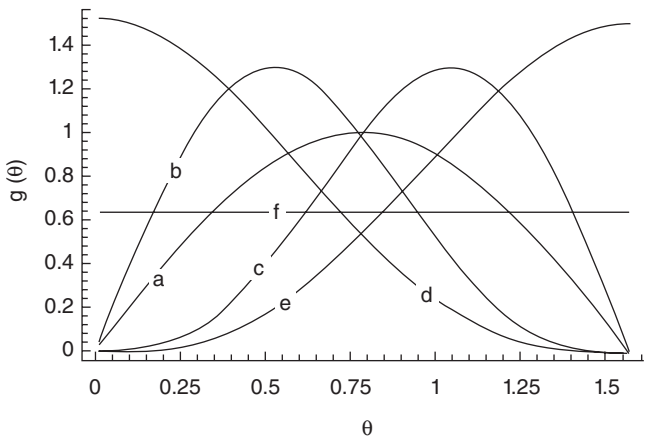

3.11 Fibre orientation distribution curves for (a) $p = q = 1$; (b) $p = 1$, $q = 2$; (c) $p = 2$, $q = 1$; (d) $p = 1/2$, $q = 2$; (e) $p = 2$, $q = 1/2$; (f) $p = q = 1/2$. Adapted from Fu and Lauke (1996).

For $f_\theta = 1$, all fibres are aligned parallel to the 1-axis direction. $f_\theta = 0$ corresponds to a two-dimensional (2D) random distribution or a symmetric distribution about the direction angle of $\pi/4$. For $f_\theta = -1$, all fibres lie perpendicular to the 1-axis direction.

The cumulative distribution function of fibre orientation (θ) is hence given by:

$$G(\theta) = \int_{\theta_{\min}}^{\theta} g(\theta)\,\mathrm{d}\theta = \frac{\int_{\theta_{\min}}^{\theta} \sin\theta^{2p-1}\cos\theta^{2q-1} d\theta}{\int_{\theta_{\min}}^{\theta_{\max}} \sin\theta^{2p-1}\cos\theta^{2q-1}\,\mathrm{d}\theta}. \qquad 3.28$$

$G(\theta)$ is the cumulative percentage of the fibres whose orientation varies from $\theta_{\min}$ to θ.

Equation [3.24] is the fibre orientation distribution function for θ in the range of 0 to $\pi/2$. Thus, the equivalent to eqn [3.24] in the range of 0 to π can be obtained by replacing $\cos\theta$ with $|\cos\theta|$, where $\|$ denotes the absolute value sign since the value of $\cos\theta$ would be negative when θ is greater than $\pi/2$. Similar to the definition of $g(\theta)$, we can define an orientation probability density function $g(\phi)$ for the fibre orientation angle ϕ in the range of 0 to 2π by:

$$g(\phi) = \frac{|\sin\phi|^{2s-1}|\cos\phi|^{2t-1}}{\int_{\phi_{\min}}^{\phi_{\max}} |\sin\phi|^{2s-1}|\cos\phi|^{2t-1}\,\mathrm{d}\phi} \quad \text{for} \quad 0 \le \phi_{\min} \le \phi \le \phi_{\max} \le 2\pi, \qquad 3.29$$

where s and t are shape parameters that determine the shape of the $g(\phi)$ curve. $g(\phi)\mathrm{d}\phi$ is the probability density that the orientation of fibres lies between ϕ to $\phi + \mathrm{d}\phi$.

The probability function for a pair of orientation angles (θ, ϕ), also known as the orientation distribution function $g(\theta, \phi)$, is defined such that the probability of the fibres lying in the infinitesimal ranges of θ to $\theta + \mathrm{d}\theta$ and ϕ to $\phi + \mathrm{d}\phi$ is given by $g(\theta, \phi)\mathrm{d}\Psi$, where $\mathrm{d}\Psi$ is the infinitesimal solid angle:

$$d\Psi = \sin\theta \mathrm{d}\theta \mathrm{d}\phi. \qquad 3.30$$

The probability density distribution must meet two physical conditions. The first condition is that one end of the fibre is indistinguishable from the other end, so θ and ϕ must be periodic:

$$g(\theta, \phi) = g(\pi - \theta, \phi + \pi). \qquad 3.31$$

The second condition is that every fibre must have a pair of orientation angles θ and ϕ so that the integral over all possible directions or the orientation space must equal unity:

$$\int_{\phi_{\min}}^{\phi_{\max}} \int_{\theta_{\min}}^{\theta_{\max}} g(\theta,\phi)\sin(\theta)\,\mathrm{d}\theta\,\mathrm{d}\phi = 1, \qquad 3.32$$

where $0 \le \theta_{\min} \le \theta \le \theta_{\max} \le \pi$ and $0 \le \phi_{\min} \le \phi \le \phi_{\max} \le 2\pi$.

Since the probability of finding a fibre in the infinitesimal ranges of angles between θ and $\theta + \mathrm{d}\theta$ and between ϕ and $\phi + \mathrm{d}\phi$ is either equal to $g(\theta, \phi)\,\mathrm{d}\Psi$ or equal to $g(\theta)g(\phi)\mathrm{d}\theta\,\mathrm{d}\phi$, then we have:

$$g(\theta,\phi) = g(\theta)\,g(\phi)/\sin\theta. \qquad 3.33$$

Finally, $g(\theta, \phi)$ can be derived from $g(\theta)$ and $g(\phi)$. It can be easily verified that the orientation distribution function $g(\theta, \phi)$ satisfies its periodic condition (eqn [3.31]) and its normalization condition (eqn [3.32]). Thus, $g(\theta, \phi)$ is a proper probability density function for a pair of orientation angles (θ, ϕ).

Fibre orientation distribution is also described using the modified Kacir *et al.* (1975, 1977) exponential function to satisfy the requirement that $G(\pi/2) = 1$ (Chin *et al.*, 1988). The modified density and cumulative distribution functions are:

$$g(\theta) = \frac{\lambda e^{-\lambda\theta}}{1 - e^{-\frac{\pi}{2}\lambda}}$$

$$G(\theta) = \frac{1 - e^{-\lambda\theta}}{1 - e^{-\frac{\pi}{2}\lambda}}.$$

Large λ indicates that fibres have a major preferential alignment. Some 90% of fibres are oriented within 10° of each other at λ greater than 10°. In contrast, as λ decreases, fibre orientation becomes more random. Thus, the variation of the shape parameter λ indicates a change of material type from unidirectional to quasi-isotropic.

3.8 Fibre volume fraction

Consider a SFRP composite with a volume V_c comprising a volume V_f of short fibres and a volume V_m of polymer matrix. The volume fraction v of short fibres is:

$$v = \frac{V_f}{V_c}. \qquad 3.34$$

And the volume fraction of the matrix is:

$$v_m = \frac{V_m}{V_c}. \qquad 3.35$$

As $V_f + V_m = V_c$, then we have $v + v_m = 1$.

Since fibre weight fraction is often used in practice, it is necessary to convert the weight fraction to volume fraction by the following equation:

$$v = \frac{P_f/\rho_f}{P_f/\rho_f + P_m/\rho_m}, \tag{3.36}$$

where P represents weight and ρ denotes density for fibre (f) and matrix (m). When there are more components in a SFRP composite, the denominator of the above equation is the volume sum of all components.

For a two-component SFRP composite, the density ρ_c of the SFRP composite can be evaluated from:

$$\frac{P_c}{\rho_c} = \frac{P_f}{\rho_f} + \frac{P_m}{\rho_m}, \tag{3.37}$$

and the composite density is given by:

$$\rho_c = \frac{P_c}{P_f/\rho_f + P_m/\rho_m}. \tag{3.38}$$

It may occur that the density measured experimentally does not agree with that estimated by eqn [3.38]. In the case where the deviation exceeds the experimental errors, it can be attributed to the existence of porosity. The difference between the theoretical density ρ_{ct} and the experimental density ρ_{ce} allows the porosity volume fraction v_p to be estiamted by:

$$v_p = \frac{\rho_{ct} - \rho_{ce}}{\rho_{ct}}. \tag{3.39}$$

The presence of porosity in a SFRP composite may cause a decrease in its mechanical properties. Thus, preparation of high quality SFRP composites is of great importance.

Further, there exists a critical fibre volume fraction below which the composite strength cannot be improved by addition of short fibres. For reinforcement, we must have (Piggott, 1980):

$$\sigma_c^u > \sigma_M^u, \tag{3.40}$$

where σ_M^u is ultimate tensile strength of matrix. At $\sigma_c^u = \sigma_M^u$, there is a critical volume fraction for composite strength. Thus, combination of the above equation and eqn [3.1] gives the critical fibre volume fraction as:

$$v^{crit} = \frac{\sigma_M^u - \sigma_M\left(\varepsilon_C^u\right)}{\lambda\sigma_F^u - \sigma_M\left(\varepsilon_C^u\right)} \tag{3.41}$$

where $\sigma_M(\varepsilon_c^u)$ is matrix stress at composite failure and equals $E_m \cdot \varepsilon_C^u$ if the failure strain ε_C^u is in the elastic range of the matrix. It now becomes possible to evaluate the critical volume fraction for composite strength. For example, for $\lambda = 0.5$, $\sigma_M(\varepsilon_C^u) = 40$ MPa, $\sigma_M^u = 60$ MPa and $\sigma_F^u = 2000$ MPa, then $v^{crit} = 2\%$. Thus, only when the fibre volume fraction is higher than 2%, can the composite strength be improved by incorporation of short fibres.

Otherwise, the composite strength cannot be enhanced or even lowered by the addition of short fibres. Eqn [3.41] gives the minimum fibre volume fraction above which inclusion of short fibres can be effective in improving the composite strength.

Evans and Gibson (1986) discussed the maximum packing fraction achievable for a random array of short fibres. As the maximum possible packing density is approached, the available free volume for fibres decreases. The point at which maximum packing of fibres is reached is defined as that at which the short fibres, whilst remaining randomly oriented, no longer have any rotational freedom, being constrained by the neighbouring fibres. An expression has been proposed for the maximum packing fraction for randomly oriented short fibres, which is:

$$v_{\max} = kd/l, \tag{3.42}$$

where k is a constant with a value of 4 for the three-dimensional random fibre composite. In short fibre reinforced polymer composites where random orientation is imposed during some part of the fabrication process, it is expected that the form of eqn [3.42] provides a fundamental limitation to the amount of short fibre reinforcement which can be added to the polymer matrix. However, eqn [3.42] obviously fails to hold for small aspect ratios of short fibres. A slightly improved expression is given by:

$$v_{\max} = \frac{4d}{l}\left(\frac{1}{1+d/l}\right). \tag{3.43}$$

The inaccuracy at low aspect ratios is unimportant since most short fibre reinforcements of practical interest have rather high aspect ratios.

The mechanical and physical properties of SFRP composites depend strongly on fibre volume fraction. For injection moulded short fibre reinforced polymer composites, the composite performance cannot be simply linearly related to fibre volume fraction as expressed in eqns [3.1] and [3.2] as fibre damage is related to fibre content. In general, fibre–fibre interaction causes more damage to fibre length as the fibre content increases. Hence, final mean fibre length decreases with increasing fibre volume fraction. The mean fibre length l_{mean} as a function of fibre volume fraction v can be described by a fitting exponential function with an offset (Fu *et al.*, 2000):

$$l_{mean} = C_1 \cdot \exp(C_2 v) + C_3, \tag{3.44}$$

where the absolute value of C_1 is magnification of the exponential function $[\exp(C_2 v)]$. $(C_1 + C_3)$ is the extrapolated fibre length at $v = 0$, C_2 and C_3 are constants for a given fibre–matrix system. Since mean fibre length in practice decreases with increasing fibre content, then $C_1 < 0$ while $C_2 > 0$ and $C_3 > 0$ holds true.

References

Agarwal B D and Broutman L J (1990), *Analysis and performance of fiber composites*, 2nd ed., New York, Wiley Interscience.

Arroyo M and Avalos F (1989), 'Polypropylene/low density polyethylene blend matrices and short glass fibers based composites. I. Mechanical degradation of fibers as a function of processing method', *Polym Composite*, 16 (5), 363–369.

Bader M G and Collins J F (1983), 'The effect of fibre-interface and processing variables on the mechanical properties of glass-fibre filled nylon 6', *Fibre Sci Technol*, 18 (3), 217–231.

Barbosa S E and Kenny J M (1999), 'Analysis of the relationship between processing conditions – fiber orientation – final properties in short fiber reinforced polypropylene', *J Reinf Plast Comp*, 18 (5), 413–420.

Bay R S and Tucker III C L (1992), 'Fiber orientation in simple injection moldings. Part II: Experimental results', *Polym Composite*, 13 (4), 332–341.

Berglund L A (1998), 'Thermoplastic resins', in Peters S T, *Handbook of composites,* Cambridge, Chapman & Hall, pp. 115–130.

Bernasconi A, Cosmi F and Dreossi D (2008), 'Local anisotropy analysis of injection moulded fibre reinforced polymer composites', *Compos Sci Technol*, 68 (12), 2574–2581.

Berthelot J M (1999), *Composite materials: mechanical behavior and structural analysis*, Springer-Verlag, New York.

Bijsterbosch H and Gaymans R J (1995), 'Polyamide 6-long glass fiber injection moldings', *Polym Composite*, 16 (5), 363–369.

Biolzi L, Castellani L and Pitacco I (1994), 'On the mechanical response of short fibre reinforced polymer composites', *J Mater Sci*, 29 (9), 2507–2512.

Chin W, Liu H and Lee Y (1988), 'Effects of fibre length and orientation distribution on the elastic modulus of short fibre reinforced thermoplastics', *Polym Composite*, 9 (1), 27–35.

Clarke A R, Davidson N and Archenhold G (1990), 'Image analyser of carbon fibre orientations in composite materials', International Conference on Applications of Transputers, Southampton, IOS Press, p. 248.

Clarke A R, Archenhold G, Davidson N and Williamson N J (1993), '3D fibre orientation measurements with the confocal laser scanning microscope', *Metal Matrix Composites*, 5, 201.

Curtis P T, Bader M G and Bailey J E (1978), 'The stiffness and strength of a polyamide thermoplastic reinforced with glass and carbon fibres', *J Mater Sci*, 13 (2), 377–390.

Darlington M W and McGinley P L (1975), 'Fibre orientation distribution in short fibre reinforced plastics', *J Mater Sci*, 10 (5), 906–910.

De S K and White J R (1996), *Short fibre-polymer composites*, Cambridge, Woodhead.

Denault J, Vu-Khanh T and Foster B (1989), 'Tensile properties of injection molded long fiber thermoplastic composites', *Polym Composite*, 10 (5), 313–321.

Doshi S R and Charrier J M (1989), 'A simple illustration of structure-properties relationships for short fiber-reinforced thermoplastics', *Polym Composite*, 10 (1), 28–38.

Evans K E and Gibson A G (1986), 'Prediction of the maximum packing fraction achievable in randomly oriented short-fibre composites', *Compos Sci Technol*, 25 (2), 149–162.

Fakirov S and Fakirova C (1985), 'Direct determination of the orientation of short glass fibres in injection moulded PET', *Polym Composite*, 6 (1), 41–46.

Fischer G and Eyerer P (1988), 'Measuring spatial orientation of short fibre reinforced thermoplastics by image analysis', *Polym Composite,* 9, 297–304.

Fischer G, Schwarz P, Mueller U and Fritz U (1990), 'Measuring spatial fibre orientation – a method for quality control of fibre reinforced plastics', *Adv Polym Tech*, 10, 135–141.

Friedrich K (1985), 'Microstructural efficiency and fracture toughness of short fiber/thermoplastic matrix composites', *Compos Sci Technol*, 22 (1), 43–74.

Friedrich K (1998), 'Mesoscopic aspects of polymer composites: processing, structure and properties', *J Mater Sci*, 33 (23), 5535–5556.

Fu S Y and Lauke B (1996), 'Effects of fibre length and orientation distributions on the tensile strength of short fibre reinforced polymers', *Compos Sci Technol*, 56 (10), 1179–1190.

Fu S Y and Lauke B (1997a) 'The fibre pull-out energy of misaligned short fibre reinforced polymers', *J Maker Sci*, 32 (8), 1985–1993.

Fu S Y and Lauke B (1997b), 'Analysis of mechanical properties of ABS terpolymer reinforced with short glass fibers and calcite particles', *J Mater Sci Technol*, 13 (5), 389–396.

Fu S Y and Lauke B (1998a), 'The elastic modulus of misaligned short fibre reinforced polymers', *Compos Sci Technol*, 58 (3–4), 389–400.

Fu S Y and Lauke B (1998b), 'An analytical characterization of the anisotropy of the elastic modulus of misaligned short-fiber-reinforced polymers', *Compos Sci Technol*, 58 (12), 1961–1972.

Fu S Y and Lauke B (1998c), 'Characterization of tensile behavior of hybrid short glass-fiber/calcite-particle/ABS composites', *Compos Part A – Appl Sci Manu*, 29 (5–6), 575–583.

Fu S Y and Lauke B (1998d), 'Fracture resistance of unfilled and calcite-particle filled ABS composites reinforced by short glass fiber (SGF) under impact load', *Compos Part A – Appl Sci Manu*, 29 (5–6), 631–641.

Fu S Y, Hu X and Yue C Y (1999a), 'Effects of fiber length and orientation distributions on the mechanical properties of short-fiber-reinforced polymers – a review', *Mater Sci Res Int*, 5 (2), 74–83.

Fu S Y, Lauke B, Maeder E, Hu X and Yue C Y (1999b), 'Fracture resistance of short-glass-fiber-reinforced and short-carbon-fiber-reinforced polypropylene under Charpy impact load and its dependence on processing', *J Mater Process Tech*, 89–90, 501–507.

Fu S Y, Lauke B, Maeder E, Yue C Y and Hu X (2000), 'Tensile properties of short-glass-fiber- and short-carbon-fiber-reinforced polypropylene composites', *Compos Part A – Appl Sci Manu*, 31 (10), 1117–1125.

Fu S Y, Yue CY, Hu X and Mai Y-W (2001a), 'Characterization of fiber length distribution of short-fiber reinforced thermoplastics', *J Mater Sci Lett*, 20 (1), 31–33.

Fu S Y, Lauke B, Maeder E, Yue C Y, Hu X and Mai Y-W (2001b), 'Hybrid effects on tensile properties of hybrid short-glass-fiber- and short-carbon-fiber reinforced polypropylene composites', *J Mater Sci*, 36 (5), 1243–1251.

Fu S Y, Mai Y-W, Ching E C Y and Li R K Y (2002), 'Correction of the measurement of fiber length of short fiber reinforced thermoplastics', *Compos Part A – Appl Sci Manu,* 33 (11), 1549–1555.

Fu S Y, Lauke B, Zhang Y H and Mai Y-W (2005), 'On the post-mortem fracture surface morphology of short fiber reinforced thermoplastics', *Compos Part A – Appl Sci Manu*, 36 (7), 987–994.

Fu S Y, Lauke B, Li R K Y and Mai Y-W (2006), 'Effects of PA6,6/PP ratio on the mechanical properties of short glass fiber reinforced and rubber-toughened polyamide 6,6/polypropylene blends', *Compos Part B – Eng*, 37 (2–3), 182–190.

Gupta M and Wang K K (1993), 'Fiber orientation and mechanical properties of short-fiber-reinforced injection-molding composites: simulated and experimental results', *Polym Composite*, 14 (5), 367–382.

Harris B (1986), *Engineering composite materials*, London, The Institute of Metals.

Hine P J, Duckett R A and Ward I M (1993a), 'The fracture behavior of short glass fiber-reinforced polyoxymethylene', *Composites*, 24 (8), 643–649.

Hine P J, Duckett R A, Davidson N and Clarke A R (1993b), 'Modelling of the elastic properties of fiber reinforced composites. I: Orientation measurement', *Compos Sci Technol*, 47 (1), 65–73.

Hine P J, Duckett R A, Ward I M, Allan P S and Bevis M J (1996), 'Polypropylene plates made by conventional injection molding and using shear controlled injection molding', *Polym Composite*, 17 (3), 400–407.

Ho K C, Hwang J R and Doong J L (1996), 'Tensile properties of short glass fibre reinforced polycarbonate', *Polym Polym Compos*, 4 (8), 563–575.

Jang B Z (1994), *Advanced polymer composites: principles and applications*, Materials Park, OH, ASM International.

Jones F R (1994), *Handbook of polymer-fibre composites*, Harlow, Longman Scientific & Technical.

Joshi M, Maiti S N and Misra A (1994), 'Influence of fiber length, fiber orientation, and interfacial adhesion on poly(butylene terephthalate)/polyethylene alloys reinforced with short glass fibers', *Polym Composite*, 15 (5), 349–358.

Kacir L, Narkis M and Ishai O (1975), 'Oriented short glass-fiber composites. 1. Preparation and statistical-analysis of aligned fiber mats', *Polym Eng Sci*, 15 (7), 525–531.

Kacir L, Narkis M and Ishai O (1977), 'Oriented short glass-fiber composites. 3. Structure and mechanical-properties of molded sheets', *Polym Eng Sci*, 17 (4), 234–241.

Kim E G, Park J K and Jo S H (2001), 'A study on fiber orientation during the injection molding of fiber-reinforced polymeric composites (Comparison between image processing results and numerical simulation)', *J Mater Process Tech*, 111, 225–232.

Kim J K and Mai Y-W (1998), *Engineered interfaces in fibre reinforced composites*, Oxford, Elsevier.

Lauke B and Fu S Y (1999), 'The strength anisotropy of misaligned short-fiber-reinforced polymers', *Compos Sci Technol*, 59 (5), 699–708.

Lee K S, Lee S W, Chung K, Kang T J and Youn J R (2003), 'Measurement and numerical simulation of three-dimensional fiber orientation states in injection-molded short-fiber-reinforced plastics', *J Appl Polym Sci*, 88 (2), 500–509.

Mlekusch B, Lehner E A, Geymayer W (1999), 'Fibre orientation in short-fibre-reinforced thermoplastics I. Contrast enhancement for image analysis', *Compos Sci Technol*, 59 (4), 543–545.

Piggott M R (1980), *Load bearing fibre composites*, Oxford, Pergamon.

Pilato L A and Michno M J (1994), *Advanced composite materials*, Berlin, Springer-Verlag.

Ramsteiner F and Theysohn R (1979), 'Tensile and impact strengths of unidirectional, short fiber-reinforced thermoplastics', *Composites*, 10 (2), 111–119.

Sarasua J R, Remiro P and Pouyet J (1995), 'Mechanical behaviour of PEEK short fibre composites', *J Mater Sci*, 30 (13), 3501–3508.

Silva C A, Viana J L, van Hattum F W J, Cunha A M (2006), 'Fiber orientation in divergent/convergent flows in expansion and compression injection molding', *Polym Composite*, 27 (5), 539–551.

Solomon S, Bakar A A, Ishak Z A M, Ishiaku U S and Hamada H (2005), 'Microstructure and fracture behavior of (Co) injection-molded polyamide 6 composites with short glass/carbon fiber hybrid reinforcement', *J Appl Polym Sci*, 97 (3), 957–967.

Takahashi K and Choi N S (1991), 'Influence of fibre weight fraction on the failure mechanisms of poly(ethylene terephthalate) reinforced by short-glass fibres', *J Mater Sci*, 26 (17), 4648–4656.

Takayanagi M, Kajiyama T and Katayose T (1982), 'Surface-modified kevlar fiber-reinforced polyethylene and ionomer', *J Appl Polym Sci*, 27 (10), 3903–3917.

Tekkanat B and Gibala R (1991), 'Short fiber reinforced thermoplastics. Prediction of stiffness in injection molded PS-PPO blends', *J Thermoplast Compos Mater*, 4 (2), 190–204.

Tjong S C, Xu S A, Li R K Y and Mai Y-W (2002), 'Mechanical behavior and fracture toughness evaluation of maleic anhydride compatibilized short glass fiber/SEBS/polypropylene hybrid composites', *Compos Sci Technol*, 62 (6), 831–840.

von Turkovich R and Erwin L (1983), 'Fiber fracture in reinforced thermoplastic processing', *Polym Eng Sci*, 23 (13), 743–749.

Watts A (1980), *Commercial opportunities for advanced composites*, Philadelphia, STP 704, ASTM.

Weeton J W, Peters D M and Thomas K L (1990), *Engineers' guide to composite materials*, Metals Park, OH, American Society for Metals.

Xia M, Hamada H and Maekawa Z (1995), 'Flexural stiffness of injection molded glass fiber reinforced thermoplastics', *Int Polym Proc*, 10 (1), 74–81.

Yurgartis S W (1987), 'Measurement of small angle fibre misalignments in continuous fibre composites', *Compos Sci Technol*, 30 (4), 279–293.

Zak G, Haberer M, Park C B and Benhabib B (2000), 'Estimation of average fibre length in short-fibre composites by a two-section method', *Compos Sci Technol*, 60 (9), 1763–1772.

4

Stress transfer in short fibre reinforced polymers

Abstract: The knowledge of stress distribution around an embedded fibre within a matrix material is crucial for the understanding of the reinforcing action of fibres in composite materials. This chapter provides the basic analytical expressions for the stresses on the fibre, at the interface and within the matrix. After a review of models, both single- and multi-fibre arrangements are considered. The chapter also includes a discussion of the effect of an interphase between the fibres and matrix on the stress distribution. Finite element calculations are summarised.

Key words: interface shear stress, single fibre, multi-fibre arrangement, interphase, finite element analysis.

4.1 Model review

Fibre reinforced composites show their improved properties mainly by tension along the fibre axis. The structure preferred in application is just that which can easily be dealt with theoretically, for the symmetry of stress coincides with the symmetry of geometry. Hence, the largest amount of theoretical and experimental work concerning the mechanical properties of fibre reinforced materials deals with unidirectional tension in the direction of the fibre axis. Thus, here, considerations are first restricted to this loading condition. By doing so we neglect all such effects, which result from fibre curvature or fibre orientation distribution (this effect is discussed in Chapters 3, 5–8 and 10). The fibres are considered to be straight and aligned. The central problem with the load-bearing properties of short fibre composites is the load transfer from the surrounding matrix to the reinforcing fibres. The general picture of stress variation along the fibre axis is sketched in Fig. 4.1(a) for the ideal case of elastic components and bonded interface, where it is assumed that no stress is transmitted over the end face of the fibre. Near the fibre end region, the fibre axial stress will be small, less than or equal to the matrix stress. The higher fibre stiffness has lead to deviations in the mean displacements and caused shear stresses along the interface. Thus, the load is transferred from the surrounding region to the fibre until the fibre stress reaches its 'equilibrium' value corresponding to a composite with continuous fibres. The stress distribution in Fig. 4.1(b) is characteristic

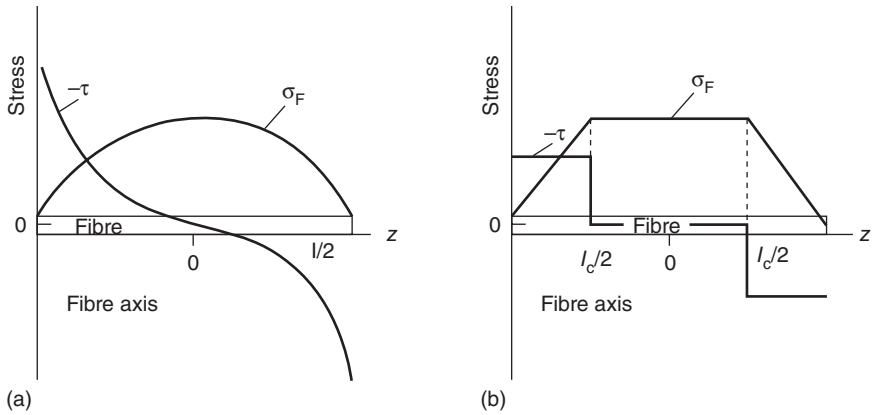

4.1 Tensile and shear stress distribution along the fibre: (a) elastic matrix, and (b) plastic matrix; l_c-critical fibre length.

of short fibre composites with an elastic-plastic matrix. The increment of fibre stress is determined by the constant shear stress of the matrix in the plastic state. In any case, a part of the fibres is not fully loaded. This fact is responsible for the reduced reinforcing efficiency of short fibres compared to continuous fibres. The importance of length effects can be estimated by comparison with the 'critical fibre length' concept which describes the length necessary to build up a certain stress level in the fibre. The critical stress may be determined by: (a) a certain fraction of the stress of an infinitely long fibre ($\sigma_F = \varepsilon_F E_f$); (b) the fibre actual stress ($\sigma_F = \alpha\sigma_c E_f/\bar{E}$, where $\bar{E}$ is effective modulus of continuous fibre reinforced composite), and (c) the fibre strength ($\sigma_F = \sigma_F^u$). For sufficiently long fibres ($l \geq l_c$) the fibre strength σ_F^u would be exceeded and the fibres would fracture, thus reducing their length (may even become shorter than the critical length). The stress field around and along the fibres has been calculated in many studies, especially for the case of perfect bonding and elastic behaviour of the components.

Three different approaches corresponding to different levels of approximation are used:

1. analytical transformation to integral equations for the elastic fields along the interface and their numerical evaluation (analytical-numerical methods);
2. approximation of ordinary partial differential equations and their analytical solution (analytical method, shear-lag analysis); and
3. finite element analysis of partial differential equations of elasticity (numerical methods).

In the case of analytical-numerical methods the basic equations are partially solved by using Green's function of the elastic problem in an infinite

medium and according to the Fredholm–Gebbia formula, and determination of the stress field can be reduced to the stress distribution along the fibre–matrix interface. Such calculations were performed, e.g., by Tolf (1983) who integrated Navier's equations. He assumed perfect bonding at the fibre–matrix interface and elastic behaviour of the components.

The main objective of a theoretical consideration is the derivation of qualitative or quantitative statements concerning the influence of several parameters (e.g., fibre length and fibre volume fraction), and deformation or failure processes on the general behaviour of composites. This allows suppression of undesirable damage and optimisation of composite parameters. To solve this task, analytical methods are most appropriate. With this approach, the displacement field is modelled by few characteristic displacements. Thus, it is a relatively crude approximation, but it yields analytical results containing all the parameters of interest and allows a lucid discussion. A main advantage of the analytical methods lies in the fact that they reveal how different deformation mechanisms act. Many analytical (such as shear-lag) calculations are based on single-fibre models. Early works have been reviewed, for example, by Holister and Thomas (1966) and Pegoraro *et al.* (1977).

The simplest and most widely used models of this kind, following Cox (1952), start from a characteristic composite element containing one fibre only. It is embedded in a corresponding amount of matrix, which is regarded as showing all the essential properties of the whole composite. Cox (1952) studied an elastic matrix reinforced by elastic fibres with intact interfaces. Kelly and Tyson (1965), however, proposed a model with plastic behaviour around the fibres by assuming constant shear stress along the interface. Another non-elastic aspect was considered by Outwater and Murphy (1969), who studied debonding along the fibre–matrix interface. The shear stress within the debonded zone was described by frictional forces between matrix and fibre surface. This leads formally to the same result of a constant shear stress. Such a statement of a constant shear stress implies that these interfaces carry their maximum shear stress already at low applied loads. However, for polymer composites, this will hold true only for composite loads that nearly achieve the composite strength. Hence, this model is well suited for the case of high loads and hence for strength considerations. In contrast, Cox's model is more suitable at low loads where interface failure can be neglected. There are many extensions of these models in the literature. The extensions concern the stress transfer across the fibre end faces by Fukuda and Chou (1981) and Clyne (1989); the incorporation of axial matrix loads by Takao (1983); the consideration of more complicated loading conditions like tension non-parallel to the fibre direction by Chou and Sun (1980); and the fibre–fibre interaction which will be discussed in Section 4.4. Takao (1985, 1987) examined the effect of shear resistance at

the fibre ends on damage propagation. He used the critical load to calculate a modified shear-lag model.

Aspden (1994) presented a method based on a rigorous solution of the equations of elasticity in cylindrical coordinates developed by Filon (1902). Solutions for the stress and strain fields within the fibre are derived for given stress distributions at the surface of the fibre. The application of the finite element (FE) method for stress calculations in SFRP is discussed briefly in Section 4.5.

In the next section, an analytical model is given which is general enough to include interface and fracture problems, and simple enough to allow mathematical handling and physical transparency.

4.2 Single-fibre model

The model assumes aligned discontinuous fibres embedded in a matrix loaded in the direction of fibres. At this stage, no restrictions are imposed on the material properties of fibre, matrix and interface. Radial stresses and strains are neglected. The single-fibre models are based on a representative composite element consisting of one fibre (radius r_f, length l) embedded in a cylindrical piece of matrix (radius R_0) (cf. Fig. 4.2). The two radii determine the volume fraction of fibres: $v = (r_f/R_0)^2$.

Hence, the spatial variation is simplified to a rotation symmetry problem with displacement in the loading direction: $u(z, r)$, where r is the radial coordinate perpendicular to the fibre axis. The basic idea of the model is a further reduction of variables by replacing the displacement field, $u(z, r)$, by the functions $u_F(z)$, $u_M(z)$, $u_f(z)$, $u_m(z)$, describing the cross-sectional averages (index F, M) and the interface displacements (index f, m) of fibre and matrix, respectively:

$$\varepsilon_F = \frac{\partial u_F}{\partial z} \quad \varepsilon_M = \frac{\partial u_M}{\partial z} \qquad \gamma_f = \frac{u_f - u_F}{h_f} \quad \gamma_m = \frac{u_M - u_m}{h_m}. \tag{4.1}$$

For shear deformation at the interface, the radial derivative is approximated by the difference quotient, where h_f and h_m, denote characteristic

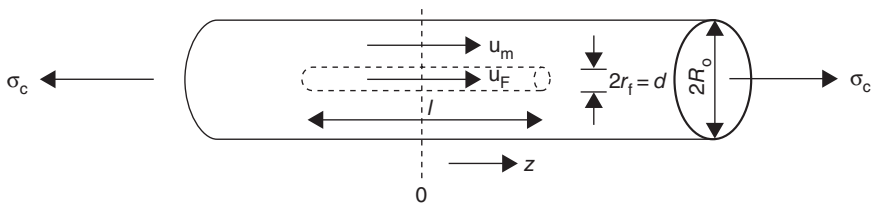

4.2 Characteristic volume element of composite.

lengths comparable with r_f and R_0. Various expressions for h_f and h_m have been given in the literature. For instance, the estimations (see Schultrich *et al.*, 1978):

$$h_m = \frac{r_f}{2}\left(\frac{l\ln(1/v)}{1-v} - 1\right)$$

for cubic fibre arrangement; and

$$h_m = \frac{r_f}{2} l\ln\left(\frac{2\pi}{\sqrt{3v}}\right)$$

for a hexagonal fibre package deviating by nearly one order of magnitude (v = 0.5: h_m = 0.99r_f, h_m = 0.19r_f, respectively). Here, the approximately derived expressions from an elastic calculation by Schultrich *et al.* (1978) are used. From the deformation, we obtain the stresses by means of the material laws:

$$\sigma_F[\varepsilon_F], \quad \tau_F[\gamma_F], \quad \sigma_M[\varepsilon_M], \quad \tau_m[\gamma_m], \quad \tau[u_m - u_f], \tag{4.2}$$

with τ as the shear stress at the interface. The condition of force equilibrium for a narrow slice of the fibre yields:

$$\frac{\partial\sigma_F}{\partial z} = -\frac{2}{r}\tau; \quad \frac{\partial\sigma_M}{\partial z} = \frac{2r_f}{R_0^2 - r_f^2}\tau = \frac{2}{r_f}\frac{v}{1-v}\tau. \tag{4.3}$$

For loading in fibre direction the external load is transferred completely within the considered composite element; that is, the mean stress averaged over the section is constant:

$$\sigma_c = v\sigma_F(z) + (1-v)\sigma_M. \tag{4.4}$$

This rule of mixtures connects the fibre and matrix stresses. Also, assumptions concerning the load transfer across the fibre ends are necessary. In general, it is assumed that the end faces of the fibre are free of stress; that is, applied stress is acting on the matrix only:

$$\sigma_F(\pm l/2) = 0. \tag{4.5}$$

This makes sense because in real composites the fibre end faces are often debonded on account of stress concentrations and not being covered by a coating.

In the case of elastic behaviour of matrix and fibre, stresses and deformations are connected by linear material equations:

$$\sigma_F = E_f\varepsilon_F \quad \tau_f = G_f\gamma_f \quad \sigma_M = E_m\varepsilon_M \quad \tau_m = G_m\gamma_m. \tag{4.6}$$

Because of the continuity of shear stresses at the fibre–matrix interface, $\tau_f = \tau_m = \tau$ holds. With this, the shear stress relations can be transformed into:

$$\tau = \frac{\bar{G}}{h}\left(u_{\mathrm{M}} - u_{\mathrm{F}} - \Delta u\right), \quad \frac{\bar{G}}{h} = \frac{G_{\mathrm{f}} G_{\mathrm{m}}}{G_{\mathrm{f}} h_{\mathrm{m}} + G_{\mathrm{m}} h_{\mathrm{f}}}, \tag{4.7}$$

where $\Delta u = (u_{\mathrm{m}} - u_{\mathrm{f}})$ describes a discontinuity in the displacements due to possible interface sliding and h is a characteristic length of the representative composite element over which shear deformations act. With $h_{\mathrm{f}} = d/2 = r_{\mathrm{f}}$ and $h_{\mathrm{m}} = D/2$ (D is fibre-to-fibre distance), $\bar{G}/h$ is reduced to:

$$\frac{\bar{G}}{h} = \frac{1}{r_{\mathrm{f}}} \frac{v\, G_{\mathrm{m}} G_{\mathrm{f}}}{(1-v) G_{\mathrm{f}} + v G_{\mathrm{m}}}. \tag{4.8}$$

Equations [4.1] to [4.4] permit the derivation of the basic differential equation for the fibre stress:

$$\frac{\mathrm{d}^2}{\mathrm{d}z^2}\sigma_{\mathrm{F}} - \eta^2 \sigma_{\mathrm{F}} + \frac{E_{\mathrm{f}}}{\bar{E}} \eta^2 \sigma_{\mathrm{c}} - \frac{E_{\mathrm{f}} E_{\mathrm{m}} (1-v)}{\bar{E}} \eta^2 \frac{\mathrm{d}}{\mathrm{d}z} \Delta u = 0, \tag{4.9}$$

where $\bar{E} = vE_{\mathrm{f}} + (1 - v)\, E_{\mathrm{m}}$ denotes the elastic modulus for a unidirectional composite with continuous fibres, and the characteristic length $1/\eta$ is defined by:

$$\eta^2 = \frac{\bar{G}}{h} \frac{2\bar{E}}{r_{\mathrm{f}} (1-v) E_{\mathrm{m}} E_{\mathrm{f}}}. \tag{4.10}$$

This length $1/\eta$ is, in any case, comparable to r_{f}, thus agreeing with St Venant's principle.

4.3 Multi-fibre model

The single-fibre model takes into account the load redistribution only between fibre and matrix. It is obvious, however, that the matrix should be able to transfer load from one fibre to another. Rosen (1965) tried to take into consideration this interaction with the neighbourhood as a lump by putting the composite element into a homogeneous medium having the effective material properties of the composite. However, the formalism presented in (Rosen, 1965) is inconsistent, for it ascribes to the matrix the ability of carrying tensile load by assuming: $\bar{E} = vE_{\mathrm{f}} + (1 - v)\, E_{\mathrm{m}}$, but neglects this ability within the composite element. If the material laws of the components are nonlinear, such an embedding in an effective material leads to difficulties, because in that case the effective material law is not uniquely defined, without any additional assumptions. Further, the local stress enhancement from neighbouring fibre ends is not effective in such a crude consideration of the surrounding. This is why Schultrich *et al.* (1978) and Lauke *et al.* (1990) preferred to follow the approach proposed by Hedgepeth and van Dyke (1967). To this end, an arrangement of plates embedded in a matrix, as shown in Figs 4.3(a) and 4.3(b), was applied, which may be regarded as a two-dimensional fibrous composite. The deformation field is simplified again by some characteristic

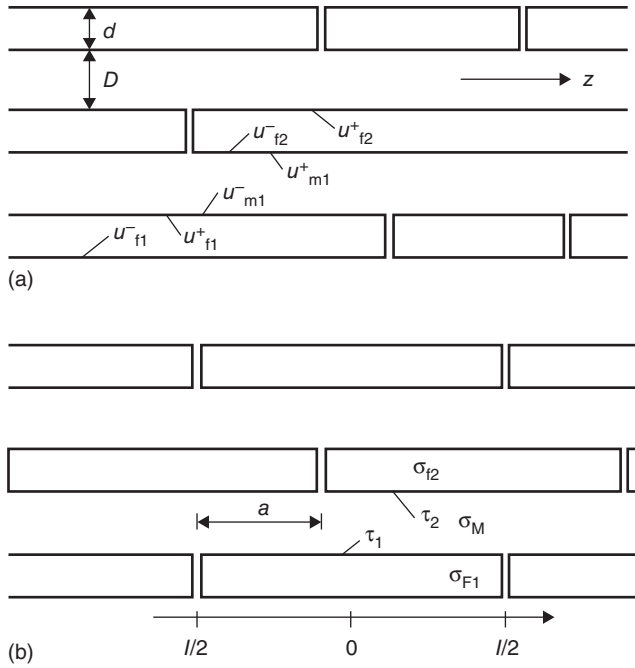

4.3 Arrays of fibres: (a) fibre discontinuities irregularly distributed, and (b) regular array of fibres of length *l*.

displacement functions of fibre and matrix (transverse displacements are not considered). Due to the lack of symmetry we need three such functions for every layer: two for the upper and the lower side labelled by + and −, and one cross-sectional average: u_f^+, u_f^-, u_F, u_m^+, u_m^-, u_M. The displacement may be discontinuous at the interface. Analogous to eqn [4.1], we obtain for the longitudinal tensile strain, $\varepsilon_z = \partial u/\partial z$ and for the shear strains:

$$\gamma_m^+ = \frac{u_m^+ - u_M}{h_m} \quad \gamma_m^- = \frac{u_M - u_m^-}{h_m}$$

$$\gamma_f^+ = \frac{u_f^+ - u_F}{h_f} \quad \gamma_f^- = \frac{u_f - u_f^-}{h_f}. \qquad 4.11$$

These deformations are related to stresses via the material laws of fibre, matrix and interface. The condition of equilibrium takes the form:

$$\frac{\partial}{\partial z}\sigma_F = -\frac{\tau_f^+ - \tau_f^-}{d} \quad \frac{\partial}{\partial z}\sigma_M = -\frac{\tau_m^+ - \tau_m^-}{D}, \qquad 4.12$$

with d and D denoting the thickness of fibre and matrix, respectively. The total balance of forces and the condition of stress-free fibre ends provide the boundary conditions given by eqns [4.4] and [4.5].

In a composite of high modulus ratio and sufficiently long fibres, where the matrix tensile stress can be neglected, this model converges to that of Hedgepeth and van Dyke (1967). That is, $\sigma_M = 0$ leads to:

$$\tau_m^- = \tau_m^+ = G_m \frac{u_m^+ - u_m^-}{2h_m} = G_m \frac{u_{f2}^+ - u_{f1}^-}{2h_m}. \quad 4.13$$

In the special array of fibres, where all the fibre ends lie in the same plane, there is no load transfer between parallel fibres for reasons of symmetry, and the single-fibre model described above is adequate.

Another approximation to analyse the stress transfer for multi-fibre composites was carried out in Fu *et al.* (2000). The material is treated as a three-cylinder composite, where a fibre is located at the centre of a coaxial shell of the matrix which, in turn, is surrounded by a trans-isotropic composite medium. This outer material has the properties of the composite, thus it is a self-consistent approximation. The shear stresses in the radial direction (perpendicular to the loading direction) are approximated by a Lamé form consisting of a term proportional to r^{-1} and another term proportional to r. This form of solution is obtained by solving the axi-symmetrical elastic problem. Together with all boundary and equilibrium conditions the stress distributions within the fibre and matrix were calculated.

4.4 Local stress distribution

We start with a discussion of the stress distribution within the framework of the single-fibre composites model with a perfectly bonded interface.

For sufficiently small applied stresses below a critical limit, $\sigma_c \le \sigma_c^d$ (σ_c^d is composite stress where debonding starts), ideal bonding is assumed, that is, $u_f = u_m$, or $\Delta u = 0$. The differential eqn [4.9] and boundary conditions eqn [4.5] provide solutions of the well-known hyperbolic-function type:

$$\sigma_F = \sigma_c \frac{E_f}{\bar{E}}\left(1 - \frac{\cosh(\eta z)}{\cosh(\eta l/2)}\right), \quad \tau = \frac{r_f \eta E_c}{2\bar{E}} \sigma_c \frac{\sinh \eta z}{\cosh(\eta l/2)}. \quad 4.14$$

In sufficiently long fibres, the tensile stress has the value of $\sigma_c E_f/\bar{E}$ along nearly all of their length, except for a distance $1/\eta$ from the ends where it falls to zero. Hence, the shear stress as its derivative (see eqn [4.3]) vanishes nearly everywhere, except for the end regions where it reaches its maximum value of:

$$\tau_{max} = \frac{\eta r_f}{2} \sigma_c \frac{E_f}{\bar{E}} \tanh(\eta l/2) \cong \frac{\eta r_f}{2} \sigma_{F,max}. \quad 4.15$$

The distribution of fibre tensile and shear stresses is shown in Fig. 4.4 as the dashed curves. To consider the reduced load-bearing capability at the fibre ends, the critical fibre length l_c can be introduced. Hence, at this fibre

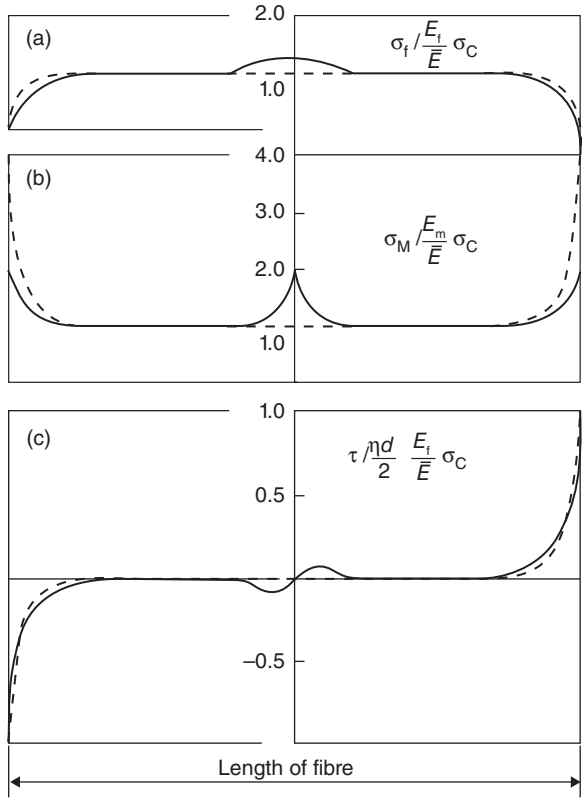

4.4 Stress along the fibre axis, dashed lines representing the single-fibre model: (a) mean axial fibre tensile stress; (b) mean axial matrix tensile stress; and (c) interfacial shear stress.

length, the fibre stress reaches a fraction α of the fibre stress $\sigma_c E_f/\bar{E}$ of a continuous-fibre reinforced composite. Thus from eqn [4.14], we have:

$$l_c = -\frac{2}{\eta} l \ln\left(\frac{1-\alpha}{2}\right) \qquad 4.16$$

Because the fibre tensile stress increases over the length of about $1/\eta$ from the fibre end twice that value provides an approximation for the critical fibre length: $l_c \approx 2/\eta$. Using eqn [4.10] it is obtained that:

$$l_c/d = \left[\left((1-v)E_f(1+\nu_m) + vE_m(1+\nu_f)\right)\frac{1-v}{v\bar{E}}\right]^{1/2}. \qquad 4.17$$

Rosen (1965) derived an expression:

$$l_c/d = 1.15\frac{\left(1-v^{1/2}\right)}{v^{1/2}}\left(E_f/G_m\right)^{1/2}, \qquad 4.18$$

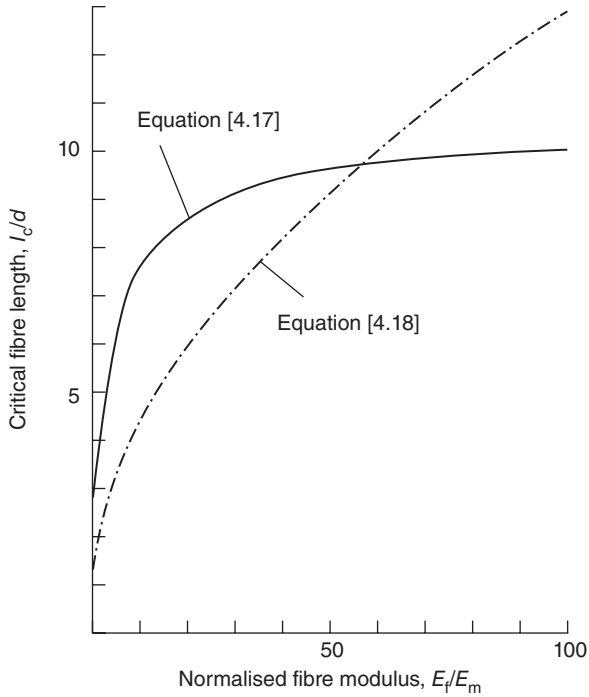

4.5 Critical fibre length *versus* fibre modulus.

which provides a $l_c \approx E_f^{1/2}$ dependence. In Fig. 4.5 both solutions are compared. Equation [4.17] gives a nearly linear increase for $E_f/E_m < 10$. Performing finite element calculations, Termonia (1987b) succeeded in confirming the $l_c \approx E_f$ proportionality in the $E_f/E_m < 50$ range. Another way to introduce a critical fibre length is based on fibre failure (see Chapter 9, Section 9.1.3 later).

The effect of fibre interaction can be discussed in a lucid manner by means of a regular version of the multi-fibre model (see Fig. 4.3). Only one additional parameter is needed which describes the overlap of fibre ends. The overlap parameter, a, may assume values between 1/2 and 0; the case $a = 0$ corresponds to the single-fibre model without load transfer between the fibres.

The stress distribution based on exponential functions is similar to that given by eqn [4.14] but more complicated (Schultrich *et al.*, 1978). The stresses represent a superposition of two kinds of exponentials with different decay lengths:

$$1/\eta' = \left(\frac{r_f h}{\bar{G}} \frac{(1-\nu) E_m E_f}{\bar{E}} \right)^{1/2} \quad 1/k = \left(\frac{r_f h}{\bar{G}} E_f \right)^{1/2}. \qquad 4.19$$

The first describes the stress transfer between the fibre and its matrix environment; the second concerns the effect of neighbouring fibres due to the surrounding matrix. (Comparison with the equivalent expression for $1/\eta$ given in eqn [4.10] shows that the fibre radius r_f is replaced by the fibre diameter d.)

The modification of stress variation along the fibres is illustrated in Fig. 4.4. If the overlap, a, (see Fig. 4.3) is somewhat larger than $1/\eta'$, fibre stress peaks arise due to the discontinuities of neighbouring fibres. If $a \leq 1/\eta'$ no additional stress peaks arise. Then, the results agree with those of the single-fibre model. The fibre overlap, as a typical composite parameter, becomes more important, the more 'composite-like' the material is, that is, the more fibre and matrix differ in their properties. Thus, large discrepancies in the results of this more sophisticated model and the simple single-fibre model may arise in cases of high modulus ratio, provided the overlap, a, is not too small. A finite overlap usually exists because of the statistical nature of fibre arrangement and the purpose of effective load transfer between fibres as reinforcing elements. But also in such composites, a situation similar to the simple case ($a = 0$) may develop during the fracture process when the adjacent fibres break successively under the influence of stress concentration from the previously broken fibre.

4.4.1 Influence of an interphase on stress distribution

During manufacture or as a result of special fibre coating, a certain interlayer may exist between fibre and matrix (cf. Chapter 3, Section 3.5). The coating of fibres may lead to an interlayer between the components. The question, however, is whether this coating remains on the fibre surface during processing or is being dispersed within the matrix. Yet, even if the coating does not remain at the fibre surface, the region where fibre and matrix meet shows a complex chemical and physical structure. Hence, the reduction of the boundary layer to an interface will even have an approximate character.

The load from the matrix is mainly transferred across the interface. Thus, a sufficient stress transfer ability (though not generally proven, it is most often characterised by the adhesion strength) must be guaranteed to obtain high strength values of the composite. To achieve this aim, coupling agents are used. They improve the bonding quality between different molecular structures of the constituents. Phenomena of adhesion cannot be described by the interaction forces only. The failure behaviour of the adhesive joint is decisively affected by imperfections (flaws) and abnormalities. With these facts, it is necessary to treat the interface as a finite region with a special structure.

The concept of an interphase has been quite comprehensively discussed by Theocaris (1987). A model is developed to calculate the thermomechani-

cal behaviour of composites on the basis of a mesophase situated entirely on the side of the polymer matrix. The mesophase material is treated as inhomogeneous, the properties of which depend on the distance from the fibres. A major aspect of the model is the fact that it allows the assessment of adhesion quality of the fibre–matrix interface.

Because of special fibre coating a certain interlayer may exist between fibre and matrix. The influence of such an interphase on the stress distribution was considered by several authors (Theocaris and Papanicolau, 1979; Piggott, 1987; Shih and Ebert, 1987) on the basis of shear lag models. The representative volume element consists of three components: fibre, interphase and matrix. If such a model is considered we have only minor changes in the equations derived above. With the assumption that the interphase deformation, ε_{ph}, is equal to that of the matrix, ε_M, the continuity conditions of shear stresses at the fibre–interphase and interphase–matrix interfaces provide the following changes:

$$\eta \to \eta_{ph} = \frac{2}{r_f}\left(\frac{\bar{G}}{h}\right)_{ph} \frac{\bar{E}}{v_m E_m E_f}, \quad \frac{\bar{G}}{h} \to \left(\frac{\bar{G}}{h}\right)_{ph} = \left[\frac{r_f}{v}\left(\frac{v}{G_f} + \frac{v_m}{G_m} + \frac{v_{ph}}{G_{ph}}\right)\right]^{-1}$$

$$E_m \to E'_m = E_m + \left(v_{ph}/v_m\right)E_{ph} \qquad 4.20$$

with $v + v_{ph} + v_m = 1$, $v_{ph} = (2t/d)$ (t: interphase thickness), and $\bar{E} = vE_f + v_m E'_m$. Consequently, the solution for the stress distribution is still valid but with the above given replacements.

The relation $(\bar{G}/h)_{ph}$ shows that the change of fibre stress (cf. eqn [4.14]) is negligible if v_{ph} is small compared to v (or $t << r_f$). In polymer composites reinforced with short glass fibres, the silane interphase was determined to be in the range of 1 to 10 nm in thickness. In composites with untreated fibres, this interphase is reduced to an even smaller phase, which is reduced in most models to the fibre–matrix interface. However, Hayes *et al.* (2001) showed that even a very thin interphase could significantly affect the load transfer between fibre and matrix.

The influence of the interphase properties on composite stiffness is given in Chapter 6, Section 6.8.

Kroh and Bohse (1986) examined the change of the stress field within the matrix due to the presence of an interlayer. They calculated the fibre and matrix normal stresses on the basis of a hybrid element program by reducing their multi-fibre model to a single-fibre model. Some of their results are shown in Fig. 4.6. Their calculations clearly show that the stress concentration of short fibre composites shifts to the fibre centre with an increasing interlayer modulus (E_{ph}), whereas a decrease of the interlayer thickness results in the opposite behaviour for $E_{ph} < E_m$ (see Fig. 4.6).

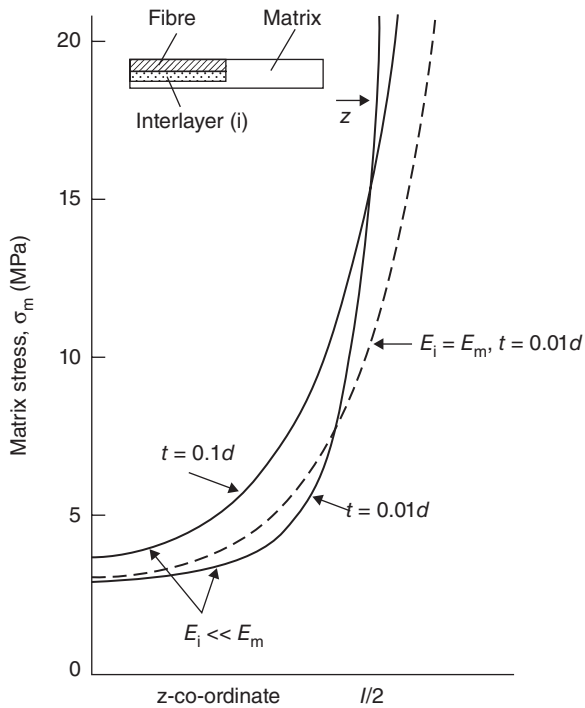

4.6 Influence of an interlayer between fibre and matrix on matrix stress. Adapted from Kroh and Bohse (1986).

4.5 Finite element analysis

Analytical solutions of differential equations of mechanical problems, whether elastic or non-elastic, very often result in difficult mathematical manipulations. For example, the simple problem of a particle within an elastic matrix under an applied tensile load can be solved analytically (Goodier, 1933). However, if the matrix shows plastic behaviour it will require numerical solution procedures such as the minimum energy principle (Lee and Mear, 1999).

Another approach to solve such problems is to apply numerical methods for solving the differential equations of the considered material under load. The governing equations will be discretised before solving on a digital computer. Discretisation means the approximation of a derivative by an algebraic expression. There are several different techniques to do this: finite difference, finite volume and finite element (FE). For advantages and disadvantages of these techniques please refer to textbooks, such as Zienkiewicz (1984) and Bathe (1990).

The numerical approach provides more or less exact solutions of the stress fields for special sets of parameters. The information available from such calculations is limited, of course, due to the special geometry and the special elastic properties. However, their results are very useful to evaluate and to check the solutions of cruder approximations.

For the problem of short fibres in matrix there are some early publications by Carrara and McGarry (1968), Barker and MacLaughlin (1971) and Larder and Beadle (1976) which used the finite element technique. Barker and MacLaughlin (1971) calculated stress concentrations near the fibre ends for different sets of parameters such as fibre gap size, volume fraction and modulus ratio. The stress distribution of aligned and oriented fibres were examined by Sun and Wu (1983) using the FE method. They considered the influence of different geometrical shapes of the fibre ends, such as rectangular, semi-circular or V-shaped.

Termonia (1987a) used the finite difference technique, at that time more appropriate because of the more efficient numerical algorithms available, compared to that of the finite element technique. He showed that the load transfer from the matrix across the fibre end is of marked influence if the front faces are ideally bonded to the matrix. One of the major results is shown in Fig. 4.7. It reveals that the assumption in eqn [4.5] of the analytical treatment is not correct. Over the fibre end surface there are stresses trans-

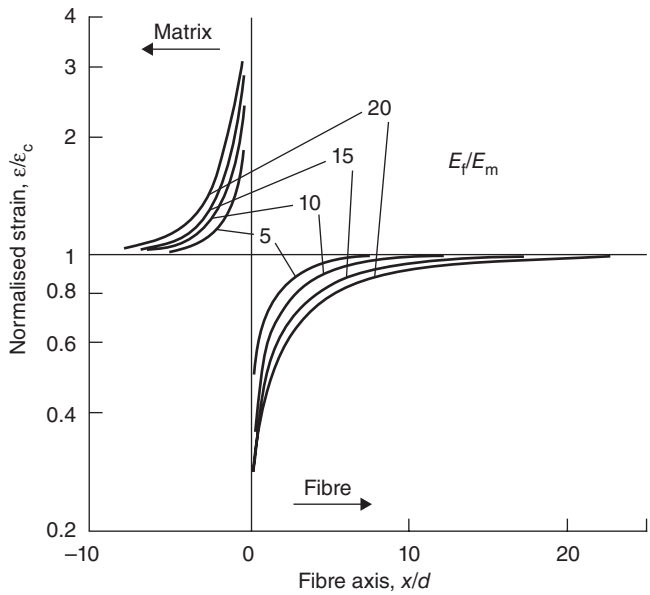

4.7 Tensile strain in fibre centre and in matrix near a fibre end. Strain is normalised to the composite strain; *d* is fibre diameter in lattice units. Adapted from Termonia (1987a).

mitted from the matrix to the fibre which are of the order of 25% of the fibre overall stress.

Kroh and Bohse (1986) took into account the influence of a finite interlayer between fibre and matrix. The assumption of linear-elastic matrix materials and ideal bonding between the components restricts the discussion to the initial stage of deformation or to special systems with a brittle polymer matrix, such as polymethylmetacrylate (PMMA). However, many thermoplastics show high strain capabilities and debonding effects may occur at the interface of the constituents. The problem of elastic-plastic finite element analysis was discussed by Agarwal *et al.* (1974). They calculated the local stress distribution and the stress–strain curve of an aligned short fibre composite with an elastic-plastic matrix subjected to axial load.

Also, shear stress distribution provided by shear lag analysis is approximate as comparisons between analytical and finite element results reveal. On the basis of FE calculations, Marotzke (1993) provided the variation of stresses along the fibre within a matrix for the fibre pull-out problem. In this case the fibre is embedded over the length L_e in a matrix cylinder and the fibre is loaded along its axis. This is a special micromechanical test to determine fibre–matrix interface properties, but not the typical loading situation within a SFRP. But it reveals some important features of the local stress distribution near the fibre ends. Figure 4.8 shows the normalised shear stress along the fibre axis for carbon fibres within a polycarbonate matrix. It reveals that the shear-lag approaches underestimate the stress concentration. A typical finite element mesh for this pull-out geometry is shown in Fig. 4.9; it was developed by Beckert and Lauke (1995) for stress calcula-

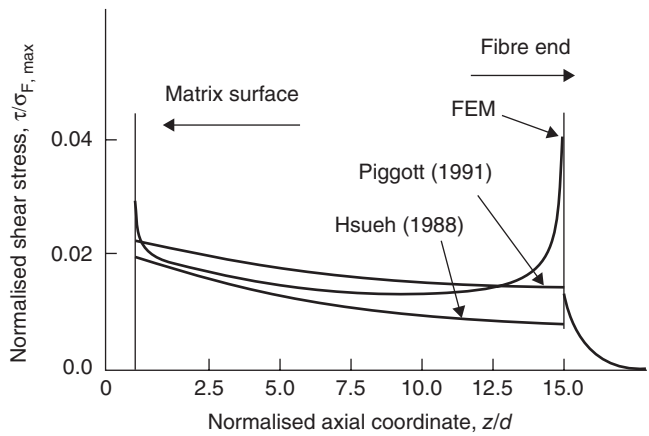

4.8 Shear stress along the embedded fibre–matrix interface, normalised by the maximum fibre stress. Comparison of shear lag analysis and FE results for carbon fibres (aspect ratio, $l/d = 15$). Adapted from Marotzke (1993).

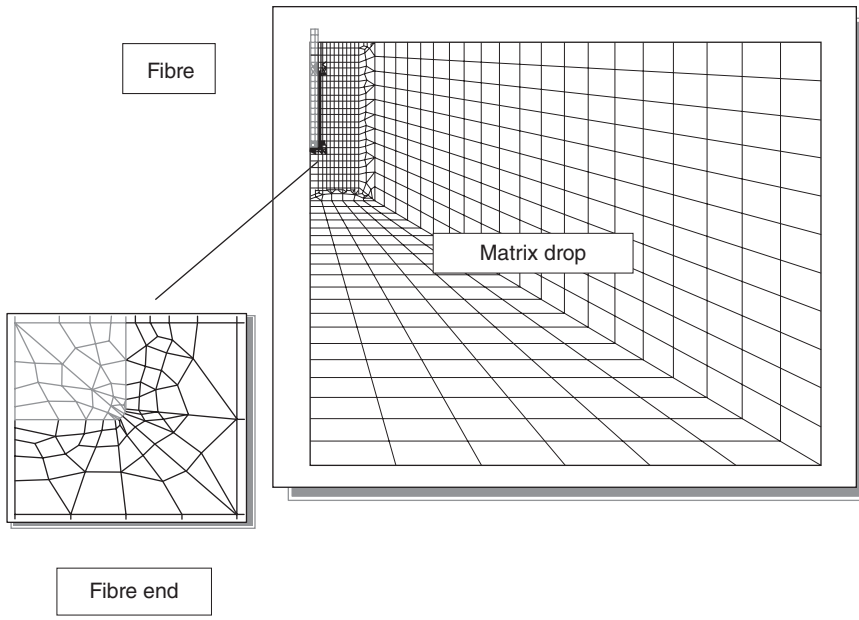

4.9 Finite element model of the single-fibre pull-out geometry. Adapted from Beckert and Lauke (1995).

tions and comparison of analytical and finite element results. On the basis of this finite element model, Singletary *et al.* (1997) calculated the shear stress along the interface, which is given for different embedded lengths in Fig. 4.10. Only for rather long L_e does the shear-lag analysis describe the real situation over a broad region, except the entrance and fibre end regions. However, for short L_e there is a huge discrepancy. Therefore, analytical shear lag results are appropriate for higher aspect ratios of fibres and describe the mean values reasonably. But great caution must be taken if these results are intended to be used for the initiation of failure mechanisms. The highest stresses appear at the fibre ends, exactly where the analytical results are wrong. Consequently, the values of shear stresses should not be used. Conversely, linear elastic finite element results provide infinite values at the fibre end leading to singularities of stresses. However, sometimes it is not shown in diagrams for it is dependent on the element size used. For smaller and smaller element sizes the stresses increase to infinity. In real materials this is also not the case because the material will show matrix yielding or some failure processes will be initiated. More realistic results can only be obtained by the application of non-linear finite element modelling.

Chen *et al.* (1996) and Tripathi *et al*., (1996) analysed the effect of matrix yielding on interfacial stress transfer in a fragmentation specimen. This is

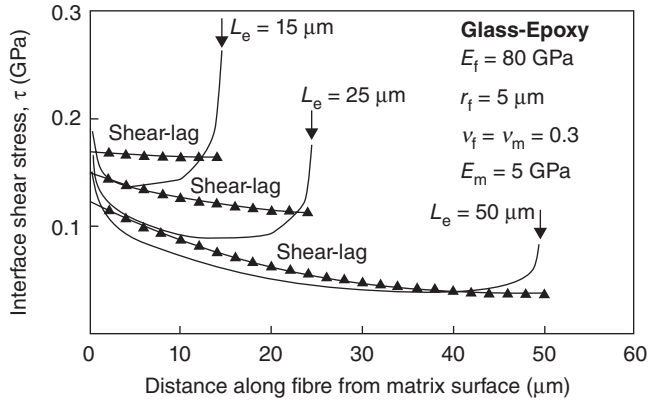

4.10 Predicted interfacial shear stress along length of embedded fibre. Predictions are from FE model and shear lag model of Greszczuk (1969). Results are given for different embedded lengths L_e. Adapted from Singletary *et al.* (1997).

another micromechanical specimen to determine interfacial properties at the fibre–matix interface. Calculations have shown that the shear stress development at the interface is limited by the yielding of the matrix material.

The fibre–fibre interaction for elasto-plastic properties of a metal matrix material was considered by Yang and Qin (2001), however, the method can be transferred to polymer matrix materials. To do so, a different elasto-plastic material law must be applied. For FE modelling they used a micro-structure similar to that of Fig. 4.3 and extracted a unit cell with two overlapping fibres. Results for the local stress fields and the effective properties were given (see Chapter 9, Section 9.2.3). The variation of stress–strain curves with fibre aspect ratio is similar to that of analytical calculations described in Chapter 9, Section 9.1 (see Fig. 9.5).

Similar considerations, however, for a single fibre embedded in a matrix cylinder have been published by Ding *et al.* (2002). Matrix plasticity was formulated by the J_2 flow theory and a large strain axisymmetric model together with the rule of mixtures for stress and strain was used to study the stress–strain curves as functions of material parameters.

All the above-quoted papers deal with a 2D approximation of the complex structure of SFRP. The symmetry conditions used for polymers with continuous fibres, for example, transversely isotropic arrangement, cannot be expected here. Hence, 3D models with special representative elements (unit cells) are necessary.

Weissenbeck (1994) used a 3D unit cell for short fibres, as shown in Fig. 4.11. This staggered arrangement of fibres is relatively restricted in geom-

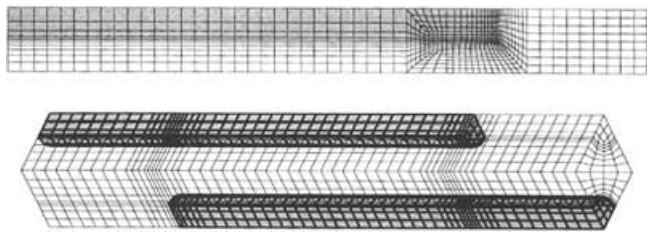

4.11 Finite element mesh for 3D staggered configuration. Adapted from Weissenbek (1994).

etry and is computationally time consuming. Axisymmetric models are more appropriate to describe the axial behaviour of SFRC.

Hayes *et al.* (2001) used true stress–true strain relations for the matrix and interphase for the FE implementation. The modelling was carried out for the fragmentation geometry, i.e., a fibre embedded within a block of resin. Because debonding cannot be seen, the maximum axial strain is the key quantity for elastic and plastic stress transfer. An important conclusion from the obtained results is that the ultimate composite properties can be engineered by controlling the interphase behaviour.

A 3D finite element analysis for fibre composites with a plastic interphase and plastic matrix was performed by Lane *et al.* (2001). At higher levels of applied strain the lower yield strength limits the stress transfer ability. A plastic interphase leads to a reduction of strain concentration in the neighbourhood of a broken fibre compared to the same situation without an interphase.

Non-aligned fibre arrangements are much more difficult to model by the FE method and especially random arrangements are most problematic. Böhm *et al.* (2002) proposed unit cell models for describing elasto-plastic behaviour of such metal matrix reinforced composites. Additional to the effective properties, micromechanical values such as von Mises equivalent stresses for the components were calculated.

A recent review with further literature on finite element modelling of stress transfer was given by Goh *et al.* (2004). Finite element modelling was also used for calculation of the stress–strain behaviour and the effective properties of SFRP. These topics are considered in Chapters 6 and 9, respectively.

In closing this chapter, it should be pointed out that the stress transfer problems considering interface/interphases using 2- or 3-cylinder models, mechanics and characterisations of fibre–matrix interfaces using single-fibre pullout and single-fibre fragmentation tests, and design of high toughness and high strength composites with tailored interfaces, etc., are also extensively covered in a recent research monograph (Kim and Mai, 1998).

Instead of the stress approach advocated in this chapter, an alternative new approach based on fracture mechanics principles is used to solve these problems. Interested readers may refer to this monograph and the appropriate references cited therein.

4.6 References

Agarwal B D, Lifshitz J M and Broutman L J (1974), 'Elastic-plastic finite element analysis of short fibre composites', *Fibre Sci Technol*, 7 (1), 45–62.

Aspden R M (1994), 'Fibre stress and strain in fibre-reinforced composites', *J Mater Sci*, 29 (5), 1310–1318.

Barker R M and MacLaughlin T F (1971), 'Stress concentrations near a discontinuity in fibrous composites', *J Compos Mater*, 5 (10), 492–503.

Bathe K J (1990), *Finite-Element-Methoden*, Berlin, Springer-Verlag.

Beckert W and Lauke B (1995), 'Fracture mechanics finite-element analysis of debonding crack extension for a single fibre pull-out specimen', *J Mater Sci Lett*, 14 (5), 333–336.

Böhm H J, Eckschlager A and Han W (2002), 'Multi-inclusion unit cell models for metal matrix composites with randomly oriented discontinuous reinforcements', *Comput Mater Sci*, 25 (1–2), 42–53.

Carrara A S and McGarry (1968), 'Matrix and interface stresses in a discontinuous fiber composite model', *J Compos Mater*, 2 (2), 222–243.

Chen F, Tripathi D and Jones F R (1996), 'Determination of the interfacial shear strength of glass-fibre-reinforced phenolic composites by a bimatrix fragmentation technique', *Compos Sci Technol*, 56 (6), 609–622.

Chou C T and Sun T W (1980), 'Stress distribution along a short fibre in fibre reinforced plastics', *J Mater Sci*, 15 (4), 931–938.

Clyne T W (1989), 'A simple development of the shear lag theory appropriate for composites with a relatively small modulus mismatch', *Mat Sci Eng A–Struct*, 122 (2), 183–192.

Cox H L (1952), 'The elasticity and strength of paper and other fibrous materials', *Brit J Appl Phys*, 3 (3), 72–79.

Ding X D, Jiang Z H, Sun J, Lian J S and Xiao L (2002), 'Stress–strain behavior in initial yield stage of short-fiber reinforced metal matrix composite', *Compos Sci Technol*, 62 (6), 841–850.

Filon L N G (1902), 'On the elastic equilibrium of circular cylinders under certain practical systems of load', *Phil Trans R Soc Lond*, A198, 147–234.

Fu S Y, Yue C Y, Hu X and Mai Y-W (2000), 'Analyses of the micromechanics of the stress transfer in single- and multi-fiber pull-out tests', *Compos Sci Technol*, 60 (4) 569–579.

Fukuda H and Chou T W (1981), 'An advanced shear-lag model applicable to discontinuous fibre composites', *J Compos Mater*, 15 (1), 79–91.

Goh K L, Aspen R M and Hukins D W L (2004), 'Review: finite element analysis of stress transfer in short-fibre composite materials', *Compos Sci Technol*, 64 (9), 1091–110.

Goodier J N (1933) 'Concentration of stress around spherical and cylindrical inclusions and flaws'. *J Appl Mech*, 55(7), 39–44.

Greszczuk L B (1969), 'Theoretical studies of the mechanics of fiber–matrix interface in composites', in *Interfaces in Composites*, ASTM 452, Philadelphia, 42–58.

Hayes S A, Lane R and Jones F R (2001), 'Fibre/matrix stress transfer through a discrete interphase. Part 1: Single-fibre model composite', *Compos Part A – Appl Sci Manu*, 32 (3–4), 379–389.

Hedgepeth J M and van Dyke P (1967), 'Local stress concentrations in imperfect filamentary composite materials', *J Compos Mater*, 1 (3), 294–309.

Holister G S and Thomas C (1966), *Fibre reinforced materials*, Amsterdam, Elsevier.

Hsueh C H (1988), 'Elastic load transfer from partially embedded axially loaded fibre to matrix', *J Mater Sci Lett*, 7(5), 497–500.

Kelly A and Tyson W R (1965), 'Tensile properties of fibre-reinforced metals: copper/tungsten and copper/molybdenum', *J Mech Phys Solids*, 13 (6), 329–338.

Kim J K and Mai Y-W (1998), *Engineered interfaces in fibre reinforced composites*, Oxford, Elsevier.

Kroh G and Bohse J (1986), 'Analyse des lokalen Spannungs-Deformations-Zustands in kurzfaserverstärkten Polymerverbunden', *Plaste und Kautschuk*, 33 (3), 110–113.

Lane R, Hayes S A and Jones F R (2001), 'Fibre/matrix stress transfer through a discrete interphase: 2. High volume fraction systems', *Compos Sci Technol*, 61 (4), 565–578.

Larder R A and Beadle C W (1976), 'The stochastic finite element simulation of parallel fiber composites', *J Compos Mater*, 10 (1), 21–31.

Lauke B, Schultrich B and Pompe W (1990), 'Theoretical considerations of toughness of short-fibre reinforced thermoplastics', *Polymer – Plastics Technology and Engineering*, 29 (7–8), 607–832.

Lee B L and Mear M E (1999), 'Stress concentration induced by an elastic spheroidal particle in a plastically deforming solid', *J Mech Phys Solids*, 47 (6), 1301–1336.

Marotzke Ch (1993), 'Influence of the fiber length on the stress transfer from glass and carbon fibers into a thermoplastic matrix in the pull-out test', *Compos Interface*, 1 (2), 153–166.

Outwater J and Murphy M C (1969), 'On the fracture energy of uni-directional laminates', 24th Annual Tech. Conf. Reinforced Plastics/Composites Div. of SPI, Paper 11C, Section 11-C, pp. 1–8.

Pegoraro M, Pagani G, Clerici P and Penati A (1977), 'Interaction between short sub-critical length fibres and polymer matrix, an approximate adhesion evaluation', *Fibre Sci Technol*, 10 (4), 263–272.

Piggott M R (1987), 'The effect of the interface/interphase on fiber composite properties', *Polym Composite*, 8 (5), 291–297.

Piggott M R (1991), 'Failure processes in the fibre-polymer interphase', *Compos Sci Technol*, 42 (1–3), 57–76.

Rosen B W (1965), 'Mechanics of composite strengthening', *Fibre Composite Materials*, Metals Park, OH, American Society of Metals, pp. 37–75.

Schultrich B, Pompe W and Weiss H-J (1978), 'The influence of fibre discontinuities on the stress–strain behaviour of composites', *Fibre Sci Technol*, 11 (1), 1–18.

Shih G C and Ebert L J (1987), 'Theoretical modelling of the effect of the interfacial shear strength on the longitudinal tensile strength of unidirectional composites', *J Compos Mater*, 21 (3), 207–224.

Singletary J, Lauke B, Beckert W and Friedrich K (1997), 'Examination of fundamental assumptions of analytical modelling of fiber pullout test', *Mech Compos Mater Struct*, 4 (2), 95–112.

Sun C T and Wu J K (1983), 'Stress distribution of aligned short-fiber composites under axial load', *J Reinf Plast Comp*, 3 (2), 130–144.
Takao Y (1983), 'Microscopic damage criteria in the vicinity of short (broken) fiber ends in composite materials', *Trans JSCM*, 9 (2), 56–62.
Takao Y (1985), 'Development of microscopic damage around short (broken) fiber ends in composite materials', *Proceedings ICCM-V*, San Diego, pp. 67–84.
Takao Y (1987), 'The effects of shear resistance at fiber ends of the damage propagation', *Proceedings of ICCM* & 6th *ECCM*, London, pp. 3136–3145.
Termonia Y (1987a), 'Theoretical study of the stress transfer in single fibre composites', *J Mater Sci*, 22 (2), 504–508.
Termonia Y (1987b), 'Computer model for the elastic properties of short fibre and particulate filled polymers', *J Mater Sci*, 22 (5), 1733–1736.
Theocaris P S (1987), *The mesophase concept in composites*, Berlin, Springer.
Theocaris P S and Papanicolau G C (1979), 'The effect of the boundary interphase on the thermomechanical behaviour of composites reinforced with short fibres', *Fibre Sci Technol*, 12 (6), 421–433.
Tolf G (1983), 'Mechanical behavior of a short fiber composite', *Mechanical Behavior of Materials–IV: Proceedings of the Fourth Int Conf*, Stockholm, Aug. 15–19, Sweden, Oxford, Pergamon Press, pp. 587–593.
Tripathi D, Chen F and Jones F (1996), 'The effect of matrix plasticity on the stress field in a single filament composite and the value of interfacial shear strength obtained from the fragmentation test', *Proc R Soc Lond A*, 452 (3), 621–653.
Weissenbek E (1994), 'Finite element modelling of discontinuously reinforced metal matrix composites', *Fortschrittsberichte*, 18 (164), Düsseldorf, VDI-Verlag.
Yang Q S and Qin Q H (2001), 'Fibre interactions and effective elasto-plastic properties of short-fiber composites', *Compos Struct*, 54 (4), 523–528.
Zienkiewicz O C (1984), *Methode der finiten Elemente*, Munich, Carl Hanser.

5

Strength of short fibre reinforced polymers

Abstract: Theoretical models for the longitudinal strength of unidirectionally aligned short fibre reinforced polymers are first discussed in Chapter 5 before the theoretical model for the strength of partially aligned short fibre reinforced polymers is presented. The chapter then reviews the theoretical models for the tensile strength anisotropy of SFRP composites, strength of randomly aligned SFRPs and strength of hybrid SFRP composites. Finally, dependence of the tensile strength of SFRP composites on those major factors described in Chapter 3 is discussed.

Key words: longitudinal strength, strength anisotropy, partial alignment, random alignment, hybrid SFRP composites.

5.1 Introduction

Short fibre reinforced polymer (SFRP) composites have many applications as a class of structural materials because of their ease of fabrication, relatively low cost, and superior mechanical properties to those of the parent polymers. Extrusion compounding and injection moulding techniques are often used to make SFRP composites (Ramsteiner and Theysohn, 1985; Fu and Lauke 1997a, 1998c, 1998d; Fu *et al.*, 1999a, 2000, 2001, 2002a; Sarasua *et al.*, 1995; Shiao *et al.*, 1994; Zhou *et al.*, 1997; Ranganathan, 1990). Fibres are damaged due to processing and the resulting short fibres are misaligned in the products. Hence, in the final composites, there exist a fibre length distribution (FLD) and a fibre orientation distribution (FOD). Studies on the mechanical properties of SFRP composites have shown that both the FLD and the FOD play very important roles in determining their mechanical properties (Fu and Lauke, 1996, 1997b, 1998a, 1998b; Lauke and Fu, 1999; Fu *et al.*, 1999b; Piggott, 1994).

Tensile strength is among the most important properties of engineering materials. One of the basic motivations for using composites as a class of engineering materials is their high tensile strength that can be achieved by introducing high strength fibres into polymer matrices since these fibres can carry most of the applied load. The term ‘macroscopic strength’ represents the ability of an engineering material to withstand stresses before failure. Strength even in isotropic materials would not simply be expressed by a value but by a closed surface in three dimensions set up by

the principal stresses, because stress is a tensor that can be described by three principal stresses and three orientations. Since it is much more convenient to have simple values instead of surfaces in abstract space for characterising a material, one readily sacrifices rigour while trying to find a simple approach under the guidance of physical reasons. It is assumed that cracks in a material tend to propagate along a plane normal to the direction of the largest tensile stress, that is, the largest principal stress. Thus, conventionally, strength is defined as the maximum tensile stress existing within the material body at fracture load. The failure initiation and fracture process of SFRP composite depend to a large extent on the fibre volume fraction, orientation angle and aspect ratio, fibre–matrix interfacial properties and fibre to matrix failure strain ratio.

It is important to be able to predict the mechanical properties of a SFRP composite given the component properties, their geometric size and arrangement. In this chapter we will consider the strength of SFRP composites. Based on the fibre orientation, SFRP composites can be divided into three categories:

1. unidirectionally aligned (longitudinal),
2. partially aligned, and
3. randomly aligned.

In the following, the strength of short fibre composites is discussed first for the case of unidirectionally aligned fibres. Then, the case of partially aligned fibres is considered and the anisotropy of the strength of short fibre composites is discussed. Finally, the cases of two-dimensional (2D) and three-dimensional (3D) randomly aligned fibres are considred.

5.2 Longitudinal strength of unidirectionally aligned short fibre reinforced polymers (SFRP)

The pioneering research of Cox (1952) on the strength of paper and other fibrous materials serves as the foundation of two slightly divergent approaches: paper physics and mechanics for the strength of short fibre reinforced composites. The Cox model and other improved theories (Jayaraman and Kortschot, 1996; Fukuda and Chou, 1982) are based on calculation of the force sustained by the fibres crossing a scan line, i.e., an arbitary line perpendicular to the applied load in a rectangular specimen.

The paper physics approach (Cox, 1952; Kallmes *et al.*, 1977; Jayaraman and Kortschot, 1996) involves:

1. calculating the number of fibres of length l and θ that cross the scan line of the specimen,
2. finding the axial force in a fibre of length l and θ,

3. obtaining the load-direction component of the axial force in a fibre of length l and θ,
4. multiplying the number of fibres that cross the scan line by the load-direction component of the axial force in a fibre of length l and θ, and
5. integrating the above quantity over fibre length and fibre orientation distributions to find the total force sustained by all the fibres across the scan line of the investigated specimen.

In contrast, the composite mechanics approach (Fukuda and Kawata, 1974; Fukuda and Chou, 1982) involves:

1. calculating the number of fibres of length l and θ that cross the scan line,
2. finding the axial force in a fibre of length l and θ,
3. obtaining the load-direction component of the axial force in a fibre of length l and θ,
4. averaging the load-direction component of the axial force in all the fibres in the specimen, and
5. multiplying the number of fibres that cross the scan line by the average load-direction component of the force in all fibres in the specimen to find the total force that is sustained by all the fibres crossing the scan line.

Jayaraman and Kortschot (1996) pointed out that the composite mechanics approach (Fukuda and Kawata, 1974; Fukuda and Chou, 1982) underpredicted the force sustained by the fibres crossing the scan line since the average load-direction component of the axial force is obtained by averaging all the fibres in the specimen rather than over the fibres that cross the scan line.

To achieve high strength SFRP composites, short fibres are designed to be perfectly aligned along the loading direction. The tensile strength of unidirectionally aligned SFRP composites is first studied for the cases of (1) plain fibres and (2) branched fibres.

5.2.1 Plain fibres

For plain fibres, the variation of fibre axial stress with fibre length is shown in Fig. 5.1 for the three cases of $l < l_c$, $l = l_c$ and $l > l_c$, in which the profile of linear stress variation from two fibre ends results from the assumption of a constant interfacial shear stress. The critical fibre length (l_c) is defined as the minimum fibre length necessary to build up the axial fibre stress to the ultimate strength of the fibre (σ_F^u) at the fibre ends:

$$l_c = r_f \sigma_F^u / \tau, \qquad 5.1$$

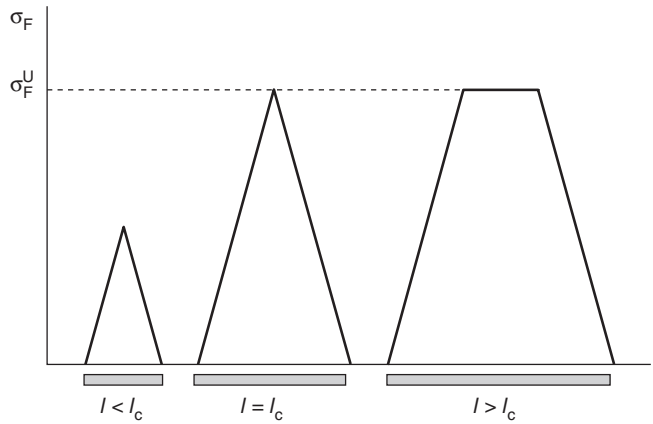

5.1 Variation of fibre axial stress with fibre length.

where τ is interfacial shear stress between fibre and matrix and r_f is fibre radius. Critical fibre length is an important factor for strength of SFRP composites and can be determined by measuring the lengths of the longest filaments which protrude from the fracture surface of an injection moulded composite (Fu *et al.*, 2006; Templeton, 1990). By definition, this length is just less than one-half of the critical fibre length because the other part of the fibre is assumed to be still embedded in the polymer matrix. The average length of the longest fibres multiplied by 2 can then be taken as the critical fibre length as an approximation. This method is simple and easy in determining the critical length.

The fibre stress at a distance x from the fibre end is given by:

$$\sigma_F = 2\tau x / r_f. \tag{5.2}$$

The composite strength for a plain short fibre reinforced polymer composite can be evaluated by:

$$\sigma_c^u = v\sigma_F + v_m\sigma_M, \tag{5.3}$$

where σ_c^u is ultimate composite strength; v and v_m are volume fraction of fibre and matrix, respectively; σ_F and σ_M are mean cross sectional stresses in fibre and matrix at composite failure. The mean axial stress of the fibre in the SFRP composite can be obtained by (Kelly and Tyson, 1965; Mittal and Gupta, 1982; Taya and Arsenault, 1989):

$$\sigma_F = \frac{2}{l}\int_0^{l/2} \frac{2\tau x}{r_f}\,dx \quad \text{for} \quad l < l_c. \tag{5.4}$$

Then,

$$\sigma_F = \frac{\tau l}{2r_f} = \sigma_F^u \cdot \frac{l}{2l_c} \quad \text{for} \quad l < l_c \tag{5.5}$$

and

$$\sigma_F = \frac{2}{l}\left(\int_0^{l_c/2} \frac{2\tau x}{r_f} dx + \int_{l_c/2}^{l/2} \frac{2\tau l_c}{r_f} dx \right) \quad \text{for} \quad l \geq l_c. \tag{5.6}$$

Thus, we have:

$$\sigma_F = \sigma_F^u (1 - l_c/2l) \quad \text{for} \quad l \geq l_c. \tag{5.7}$$

When fibres have a uniform length l, the modified rule of mixtures (MROM) for predicting the tensile strength of a SFRP composite is given by:

$$\sigma_c^u = \chi \sigma_F^u v + \sigma_M v_m, \tag{5.8}$$

where χ is fibre length factor for composite strength and can be expressed for $l < l_c$ and $l \geq l_c$ as:

$$\chi = l/(2l_c) \qquad \text{for} \quad l < l_c \tag{5.9}$$

$$\chi = 1 - l_c/(2l) \quad \text{for} \quad l \geq l_c. \tag{5.10}$$

It is clear that the shorter the critical fibre length, the higher is the fibre length factor and thus the composite strength.

If the fibre length is not uniform, eqns [5.9] and [5.10] must be modified. Kelly and Tyson (1965) put forward a model considering the effect of fibres with sub- and super-critical fibre length, namely, shorter and longer than the critical fibre length. This model gives:

$$\sigma_c^u = \sum_{l_i = l_{min}}^{l_c} l_i/(2l_c)\sigma_F^u v_i + \sum_{l_j = l_c}^{l_{max}} \left[1 - l_c/(2l_j)\right]\sigma_F^u v_j + \sigma_M v_m. \tag{5.11}$$

The first and second terms are contributions from fibres with sub-critical length shorter than l_c and fibres with super-critical length longer than l_c, respectively. If the fibre length changes continuously, there will be a fibre length distribution function, then the fibre efficiency factor for the composite strength is given by Fu and Lauke (1996) as:

$$\chi = \int_{l_{min}}^{l_c} \left[l^2/(2l_c l_{mean})\right] f(l) dl + \int_{l_c}^{l_{max}} (l/l_{mean})\left[1 - l_c/(2l)\right] f(l) dl, \tag{5.12}$$

where l_{mean} is the mean fibre length and $f(l)$ is the fibre length probability density, namely, fibre length distribution function which was defined in Chapter 3. Finally, the composite strength can be evaluated using eqn [5.8].

5.2.2 Branched fibres

The case of plain fibres has been discussed above for longitudinal strength of aligned SFRP composites. The case of branched fibres and hence the effect of fibre structure on composite strength is discussed below. When a polymer is reinforced by short fibres with branched structures at their two ends as shown in Fig. 5.2, the composite strength can still be evaluated using eqn [5.8]. However, the average stress of the branched fibre is increasesd over that of the corresponding plain fibre at composite failure. It is assumed that the cross-sectional area of the main stem of the branched fibre with a radius r_f is equal to the sum of those of the two branches with spherical circumference having the same radius, r_b, and the branching points of the fibre are so strong that they cannot fracture before the composite fails. Then, we assume:

$$r_f = \sqrt{2} r_b . \qquad 5.13$$

If the fibre length is l, then half of the main stem or each branch of the branched fibre is $l/4$. Further, the relationship between the fibre fracture stress σ_F^u and the critical length l_{cb} of the branched fibre can be obtained from (Fu *et al.*, 1993):

$$\sigma_F^u = \tau l_{cb} / (2r_f) + \sqrt{2}\tau l_{cb} \exp(\mu\varphi)/2r_f , \qquad 5.14$$

where 2φ is the angle between the two branches of the branched fibre as shown in Fig. 5.2. μ is defined hereafter in this chapter as the snubbing friction coefficient between the fibre and matrix at the fibre branching points and has a value between 0 and 1. Due to the snubbing friction effect at fibre branching points, $l_{cb} < l_c$ (this can be seen from comparing eqn [5.14] with [5.1]). The average stress of the branched fibre can be evaluated for different fibre lengths. When $l < l_{cb}$, the average stress σ_F^b of the branched fibre can be evaluated by:

$$\sigma_F^b = \frac{2}{l}\left(\int_{0.}^{l/4} \sigma_{f1} dx + \int_{l/4}^{l/2} \sigma_{f2} dx \right), \qquad 5.15$$

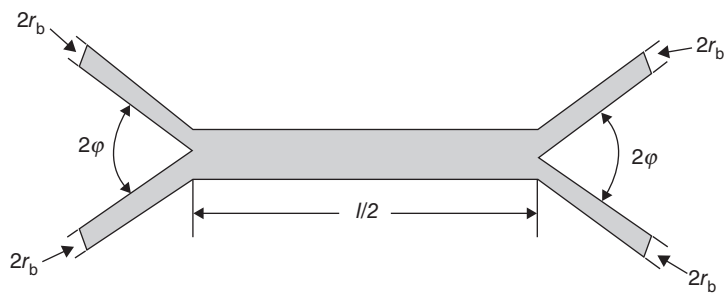

5.2 Schematic drawing of a branched short fibre.

where

$$\sigma_{f1} = 2\sqrt{2}x\tau\exp(\mu\varphi)/r_f \quad 5.16$$

$$\sigma_{f2} = \sqrt{2}l\tau\exp(\mu\varphi)/(2r_f) + 2(x - l/4)\tau/r_f. \quad 5.17$$

Thus, we have

$$\sigma_F^b = \frac{\tau l}{2r_f}\left[1.06\exp(\mu\varphi) + \frac{1}{4}\right]. \quad 5.18$$

It is clear that the average stress (eqn [5.18]) of the branched fibre is greater than that (eqn [5.5]) of the plain fibre.

When $l_{cb} < l < 2l_{cb}$, the average stress σ_F^b of the branched fibre can be obtained from:

$$\sigma_F^b = \frac{2}{l}\left(\int_0^{l/4}\sigma_{f1}dx + \int_{l/4}^{l_{cb}/2}\sigma_{f2}dx + \int_{l_{cb}/2}^{l/2}\sigma_F^u dx\right). \quad 5.19$$

For the plain fibre with length $l > l_c$, eqn [5.6] for the average fibre stress can be rewritten as:

$$\sigma_F = \frac{2}{l}\left(\int_0^{l_c/2}\sigma_{f3}dx + \int_{l_c/2}^{l/2}\sigma_F^u dx\right), \quad 5.20$$

where

$$\sigma_{f3} = 2\tau x/r_f. \quad 5.21$$

Since σ_{f1} (eqn [5.16]) and σ_{f2} (eqn [5.17]) are greater than σ_{f3} (eqn [5.21]) and $l_{cb} < l_c$, then $\sigma_F^b > \sigma_F$.

When $l > 2l_{cb}$, the average stress of the branched fibre is given by:

$$\sigma_F^b = \frac{2}{l}\left(\int_0^{l_{cb}/2}\sigma_{f1}dx + \int_{l_{cb}/2}^{l/2}\sigma_F^u dx\right). \quad 5.22$$

It can be seen that σ_F^b (eqn [5.22]) is greater than σ_F (eqn [5.20]).

Since the composite strength is contributed by all the fibres with sub-critical and super-critical lengths in the SFRP composite and is estimated based on eqn [5.8], it is clear that the strength of the composite reinforced with branched short fibres would be greater than that of the SFRP composite with the same matrix reinforced with the corresponding plain fibres. This concept can be extended to bone-shaped short fibres and the corresponding composite strength should also be higher than that of the plain short fibre reinforced composite. The composite strength increase is derived from the effective stress transfer from the matrix to the fibres via mechanical interlocking at the enlarged fibre ends (Zhu *et al.*, 1999; Jiang *et al.*, 2000; Zhu and Beyerlein, 2002).

5.3 Strength of partially aligned short fibre reinforced polymers (SFRP)

To achieve high stiffness and high strength of SFRP composites in the fibre direction, it is desirable to orient the fibres along the applied load direction. However, it is often difficult to achieve perfect alignment of short fibres in a SFRP composite. Partial alignment of short fibres is typical in injection moulded SFRP composites. It will be shown here that fibre orientation plays a crucial role in determining the composite strength.

5.3.1 Fibre bridging stress

When an applied load is exerted on a short fibre reinforced polymer composite, the interfacial shear stress between fibres and matrix will increase with increasing applied load. To estimate the stress required to break the SFRP composite at some random cross section, the average bridging stress of the short fibres across the failure plane needs to be evaluated. The bridging stress of a single short fibre will be first evaluated below.

When a fibre intersects the crack plane and the fibre orientates parallel to the applied load, F, or the normal of the crack plane as shown in Fig. 5.3(a), then the bridging stress σ_F of the fibre across the crack is given by:

$$\sigma_F = l_S 2\pi r_f \tau / \left(\pi r_f^2\right) = 2 l_S \tau / r_f \quad \text{for} \quad l_S < l_c/2 \tag{5.23}$$

$$\sigma_F = \sigma_F^u \quad \text{for} \quad l_S \geq l_c/2, \tag{5.24}$$

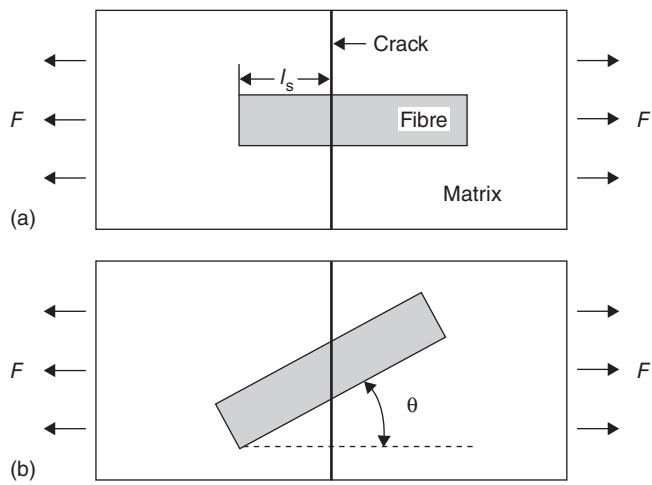

5.3 Schematic drawing of a fibre across a crack plane. (a) A fibre parallel to the crack plane normal; and (b) a fibre crossing obliquely with the crack plane.

where l_S is the length of the shorter embedded fibre segment. However, when the fibre crosses obliquely at an angle θ with the crack plane (see Fig. 5.3(b)), the fibre bridging stress $\sigma_{F\theta}$ can be given by (Fu *et al.*, 1993):

$$\sigma_{F\theta} = 2l_S(\tau/r_f)\exp(\mu\theta) \quad \text{for} \quad l_S < l_{c\theta}/2, \tag{5.25}$$

where θ is the angle between the fibre and the crack plane normal; μ is the snubbing friction coefficient between fibre and matrix at the crossing point (Fu *et al.*, 1993; Li *et al.*, 1990; Jain and Wetherhold, 1992; Wetherhold and Jain, 1992); $l_{c\theta}$ denotes the critical length of the fibre crossing obliquely (θ) with the crack plane. When $l_s \geq l_{c\theta}/2$, the bridging stress of the oblique fibre is (Piggott, 1974, 1994)):

$$\sigma_{F\theta} = \sigma^u_{F\theta} \quad \text{for} \quad l_S \geq l_{c\theta}/2, \tag{5.26}$$

where $\sigma^u_{F\theta}$ is the fracture stress of the oblique fibres, i.e., the inclined fibre tensile strength (Bartos and Duris, 1994). Since the flexural stresses exerted on the oblique fibres during loading of the composite cause an apparent loss of fibre strength, the fracture strength for the oblique fibres is then reduced. The pull-out test of the oblique steel fibres also indicated that the inclined tensile strength of the oblique steel fibres is significantly reduced and decreases with increasing inclination angle (Piggott, 1974, 1994). This is because the flexural stresses in the steel fibres caused an apparent loss of fibre strength when the fibres crossed obliquely at an angle to the crack plane normal. Hence, the introduction of the inclined fibre tensile strength can undoubtedly help predict better strength of the SFRP composites with partially aligned short fibres. If the fibres (e.g., glass fibres or carbon fibres, etc.) are brittle, $\sigma^u_{F\theta}$ can be expressed by (Piggott, 1974, 1994):

$$\sigma^u_{F\theta} = \sigma^u_F\left[1 - A_f \tan(\theta)\right], \tag{5.27}$$

where A_f is a constant for a given fibre–matrix system and equals 0.083 for the carbon/epoxy system (Piggott, 1994). From eqn [5.27] it is clear that there is a maximum fibre orientation angle for $\sigma^u_{F\theta} \geq 0$ which is given by:

$$\theta_{max} = \arctan(1/A_f). \tag{5.28}$$

For oblique fibres with $\theta \geq \theta_{max}$: $\sigma^u_{F\theta} = 0$. Consequently, taking into consideration both the snubbing friction and flexural effects, the critical length of the oblique fibres can be derived from eqns [5.25] to [5.27]. That is,

$$l_{c\theta} = l_c\left[1 - A_f \tan(\theta)\right]/\exp(\mu\theta). \tag{5.29}$$

Because of the snubbing friction and flexural effects, $l_{c\theta}$ is generally smaller than l_c. If the snubbing friction effect is neglected, i.e., $\mu = 0$, then eqn [5.29] becomes:

$$l_{c\theta} = l_c\left[1 - A_f \tan(\theta)\right]. \tag{5.30}$$

Equation [5.30] is the same as that of Piggott (1994). If the fibre flexural effect is neglected, i.e., $A_f = 0$, eqn [5.29] becomes:

$$l_{c\theta} = l_c / \exp(\mu\theta). \tag{5.31}$$

Equation [5.31] is the same as that of Wetherhold and Jain (1992). If both the snubbing friction effect and the fibre flexural effect are neglected, i.e. $\mu = 0$ and $A_f = 0$, eqn [5.29] is:

$$l_{c\theta} = l_c. \tag{5.32}$$

This is the same as the critical fibre length of normal plain fibres aligned along the applied loading direction when both the snubbing friction effect and the fibre flexural effect are not considered.

5.3.2 Average fibre stress in an aligned composite

It is assumed that all the fibres are uniformly distributed in a SFRP composite and the fibres have the same length l and diameter d, and are perfectly aligned in the direction of the applied load, F. The stress required to break the composite is estimated at some random cross section. The fibre across the crack plane is divided by the crack plane as shown in Fig. 5.3(a) into two segments. The shorter segment length of the fibre across the crack plane ranges from 0 to $l/2$. When the shorter segment length is less than $l_c/2$, the fibre will debond fully and pull out from the matrix against the shear stress τ at the failure of the SFRP composite. Otherwise, the fibre will break at the crack plane.

When the fibre length l is less than l_c, the fibre will be pulled out as the length of the shorter segment is less than $l_c/2$. Since the length of the shorter segment in the matrix crossing the crack plane varies from 0 to $l/2$, its average length across the crack plane is $l/4$ due to the assumption that the fibres are uniformly distributed in the matrix. Thus, the average bridging stress of the fibres across the crack plane in the aligned SFRP composite is given by:

$$\sigma_F = (l/4)2\pi r_f \tau / \left(\pi r_f^2\right) = l\tau/d, \tag{5.33}$$

then the average bridging fibre stress is:

$$\sigma_F = \sigma_F^u \, l/(2l_c). \tag{5.34}$$

On the contrary, when fibre length l is greater than l_c, the shorter fibre segment will be either less than or greater than $l_c/2$. The shorter segment of the fibre will be pulled out if it is less than $l_c/2$. And the shorter segment length will vary from 0 to $l_c/2$. Thus, the average length of the shorter

segments of the fibres is $l_c/4$ and the corresponding fraction of the fibres is l_c/l. If the shorter segment length is greater than $l_c/2$, then the fibres will not be pulled out but will be broken at composite failure and the fraction of the fibres is $(1 - l_c/l)$. Thus, the average bridging stress of the fibres with a length greater than l_C is given by:

$$\sigma_F = \left[(l_c/l)(l_c/4)\cdot 2\pi r_f \tau + (1-l_c/l)\pi r_f^2 \sigma_F^u\right] \Big/ \left(\pi r_f^2\right) = \sigma_F^u\left(1-l_c/(2l)\right). \qquad 5.35$$

For simplicity, the above derivation has neglected the effect of crack diversion for very short embedded segments and the stresses across fibre ends that were considered by Piggott (1994).

We now consider a composite with fibres oriented obliquely at an angle θ with the crack plane (see Fig. 5.3(b)). Similar to the above derivation, the average bridging stress of the fibres crossing the crack plane is obtained from:

$$\sigma_{F\theta} = (l/4)2\pi r_f \tau \exp(\mu\theta) \Big/ \left(\pi r_f^2\right) = \sigma_F^u l \exp(\mu\theta)/2l_c \qquad \text{for} \quad l < l_{c\theta}, \qquad 5.36$$

$$\sigma_{F\theta} = \left\{\frac{l_{c\theta}^2}{4l} 2\pi r_f \tau \exp(\mu\theta) + \left(1-\frac{l_{c\theta}}{l}\right)\sigma_{F\theta}^u r_f^2\right\} \Big/ \left(\pi r_f^2\right) = \sigma_{F\theta}^u\left(1-\frac{l_{c\theta}}{2l}\right) \quad \text{for} \quad l \geq l_{c\theta}. \qquad 5.37$$

When θ is equal to zero, $l_{c\theta}$ would become l_c and eqns [5.36] and [5.37] naturally become the same as eqns [5.34] and [5.35].

5.3.3 Strength of SFRP composite with partial fibre alignment

Based on the above discussion it is possible to derive the strength of the SFRP composite with partial fibre alignment (Fu and Lauke, 1996). Consider the case that the fibres are uniformly distributed in the SFRP composite, then the failure strength of any cross section of the SFRP composite can represent the composite strength. Assume the total fibre number is N_V in the composite, and N_i is the number of fibres with a length from l to $l + dl$ and the orientation angle from θ to $\theta + d\theta$. Moreover, $f(l)$ and $g(\theta)$ are, respectively, the fibre length distribution function and the fibre orientation distribution function as defined in Chapter 3. Thus, we have:

$$N_i/N_V = f(l)g(\theta)dld\theta. \qquad 5.38$$

Then, the volume sub-fraction v_i of the fibres with a length from l to $l + dl$ and an orientation angle from θ to $\theta + d\theta$ can be obtained by:

$$v_i = v\left[(N_i l\pi)/(N_v l_{mean}\pi)\right] = v\frac{N_i l}{N_v l_{mean}}, \qquad 5.39$$

where v is the fibre volume fraction and l_{mean} is the mean fibre length in the SFRP composite. All the fibres with length from l_{min} to l_{max} and orientation angle from θ_{min} to θ_{max} and matrix contribute to the tensile strength of the composite:

$$\sigma_c^u = \sum_{\theta=\theta_{min}}^{\theta_{max}} \sum_{l=l_{min}}^{l_{max}} \sigma_{F\theta} v_i + \sigma_M v_m. \tag{5.40}$$

Combining eqns [5.38]–[5.40] and replacing the summation by the integral gives:

$$\sigma_c^u = v \int_{\theta_{min}}^{\theta_{max}} \int_{l_{min}}^{l_{max}} f(l) g(\theta) (l/l_{mean}) \sigma_{F\theta} \mathrm{d}l\mathrm{d}\theta + \sigma_M v_m. \tag{5.41}$$

The strength of the SFRP composite can be obtained by substituting eqns [5.27], [5.29], [5.36] and [5.37] into [5.41]. Thus, we have:

$$\begin{aligned}\sigma_c^u = v \Bigg[& \int_{\theta_{min}}^{\theta_{max}} \int_{l_{min}}^{l_{c\theta}} f(l) g(\theta) (l/l_{mean}) \sigma_F^u \left(l/(2l_C)\right) \exp(\mu\theta) \mathrm{d}l\mathrm{d}\theta \\ & + \int_{\theta_{min}}^{\theta_{max}} \int_{l_{c\theta}}^{l_{max}} f(l) g(\theta) (l/l_{mean}) \sigma_F^u \left(1 - A_f \tan(\theta)\right) \\ & \times \left(1 - l_c \left(1 - A_f \tan(\theta)\right)/2l \exp(\mu\theta)\right) \mathrm{d}l\mathrm{d}\theta \Bigg] + \sigma_M v_m. \end{aligned} \tag{5.42}$$

Equation [5.42] can be rewritten as the modified rule of mixtures:

$$\sigma_c^u = \chi_1 \chi_2 \sigma_F^u v + \sigma_M v_m, \tag{5.43}$$

where

$$\begin{aligned}\chi_1 \chi_2 = & \int_{\theta_{min}}^{\theta_{max}} \int_{l_{min}}^{l_{c\theta}} f(l) g(\theta) (l/l_{mean}) \left(l/(2l_C)\right) \exp(\mu\theta) \mathrm{d}l\mathrm{d}\theta \\ & + \int_{\theta_{min}}^{\theta_{max}} \int_{l_{c\theta}}^{l_{max}} f(l) g(\theta) (l/l_{mean}) \left(1 - A_f \tan(\theta)\right) \\ & \times \left(1 - l_c \left(1 - A_f \tan(\theta)\right)/\left(2l \exp(\mu\theta)\right)\right) \mathrm{d}l\mathrm{d}\theta, \end{aligned} \tag{5.44}$$

where χ_1 is fibre orientation factor while χ_2 is fibre length factor for the composite strength. In general χ_1 and χ_2 are not independent of each other since the critical length of an oblique fibre is dependent on the fibre orientation angle. So, the product of $\chi_1\chi_2$ can be used to predict the composite strength. The larger the product value of $\chi_1\chi_2$, the higher is the composite strength. For the special case of $\theta = 0$, χ_1 is equal to 1 and this is the case of unidirectionally aligned short fibre composites. Then, the fibre length factor can be obtained as:

$$\chi_2 = \int_{l_{min}}^{l_c} \left(l^2/(2l_c l_{mean})\right) f(l) \mathrm{d}l + \int_{l_c}^{l_{max}} (l/l_{mean}) \left[1 - l_c/(2l)\right] f(l) \mathrm{d}l. \tag{5.45}$$

In SFRP composites, both super-critical and sub-critical fibres of lengths greater than and less than the critical fibre length will contribute to the composite strength. The percentage α of the sub-critical fibres can be evaluated from fibre length density distribution function $f(l)$:

$$\alpha = 1 - \exp\left(-al_c^b\right). \tag{5.46}$$

The value of the fibre length factor χ_2 can be estimated according to eqn [5.45] if l_{min}, l_{max}, l_c and $f(l)$ are known. Then, the composite strength can be evaluated using eqn [5.43] for unidirectionally aligned short fibre composites.

Assuming l_{mod} = 0.2 mm and the parameter b is given, then we obtain values of the parameter a from eqn [3.12], the mean fibre length l_{mean} from eqn [3.11], and the probability density function $f(l)$ from eqn [3.9], respectively. The percentage α of the fibres with a length less than l_c can be evaluated with eqn [5.46]. Moreover, we can assume l_{min} and l_{max} to be, respectively, 0 and ∞ mm, and l_c 0.2, 0.4 and 0.8 mm, then the calculated results for the percentage α and the fibre length factor χ_2 are shown in Figs 5.4 and 5.5, respectively, for the case of unidirectional SFRP composites. Figure 5.4 shows that the percentage α decreases dramatically with increasing mean fibre length at small mean fibre lengths and gradually reaches a plateau level as the mean fibre length increases. In contrast, the percentage α decreases with decreasing critical fibre length at the same

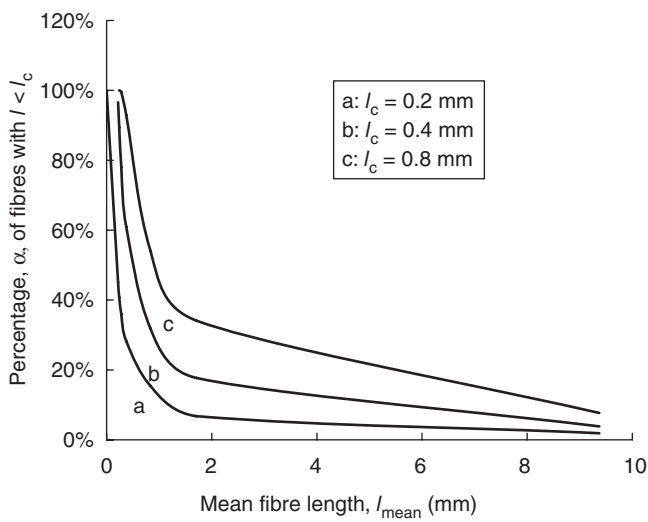

5.4 Variation of the percentage, α, of fibres with $l < l_c$ as mean fibre length, l_{mean}, varies for the cases of different l_c, where l_{mod} = 0.2 mm, l_{min} = 0 mm and l_{max} = ∞ mm. Adapted from Fu and Lauke (1996).

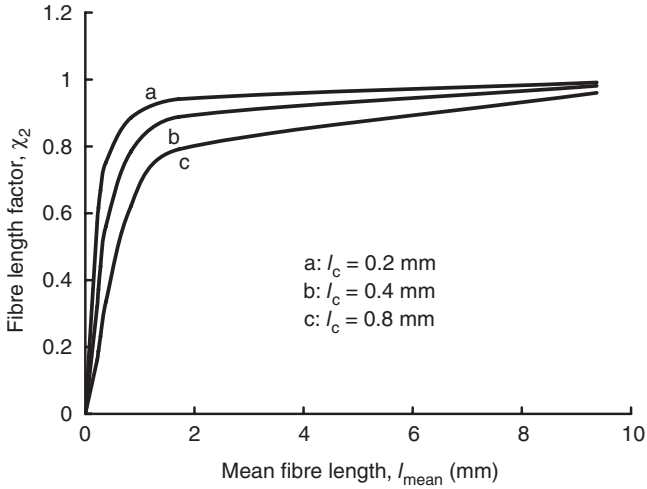

5.5 Effects of mean fibre length, l_{mean} and critical fibre length, l_c, on fibre length factor, χ_2, for the case of unidirectional composites, where l_{mod} = 0.2 mm, l_{min} = 0 mm and $l_{max} = \infty$ mm. Adapted from Fu and Lauke (1996).

mean fibre length. Since the super-critical fibres with lengths greater than l_c would make a larger contribution to the composite strength than that of sub-critical fibres with lengths less than l_c, the value of χ_2 increases rapidly with the increase of mean fibre length l_{mean} at small mean fibre lengths and approaches gradually a plateau level at large mean fibre lengths (see Fig. 5.5). Therefore, the tensile strength of unidirectionally aligned short fibre composites increases rapidly as the mean fibre length l_{mean} increases for the case of small mean fibre lengths and approaches a plateau level as l_{mean} increases for the case of large mean fibre lengths. This is consistent with existing experimental results (Thomason and Vlug, 1995). Furthermore, the strength of SFRP increases as the fibre content increases if all other parameters are the same as indicated in eqn [5.43]. An increase in fibre content leads to a reduction in mean fibre length (Thomason, 2007). As a result, the combined effect of increasing fibre content and decreasing mean fibre length brings about an up-and-down tendency of composite strength as fibre content increases (Thomason, 2007).

The percentage α of fibres with $l < l_c$ is shown in Fig. 5.6 as a function of critical fibre length l_c. Smaller critical fibre length corresponds to lower content of sub-critical fibres (see Fig. 5.6) and hence higher value of χ_2 (see Fig. 5.7). Thus, a smaller critical fibre length will bring about a higher composite strength. This is consistent with experimental results (Yu *et al.*, 1994) and the concept of critical fibre length has been used to explain the effect of PA6,6 to PP ratio on the strength of injection-moulded rubber-toughened

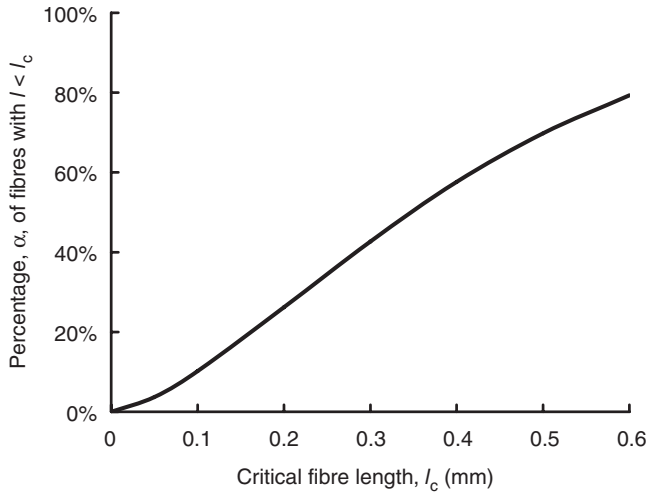

5.6 Percentage α of fibres with $l < l_C$ as a function of critical fibre length l_C, where $l_{mean} = 0.4$ mm, $l_{mod} = 0.213$ mm, $l_{min} = 0$ mm and $l_{max} = \infty$ mm. Adapted from Fu and Lauke (1996).

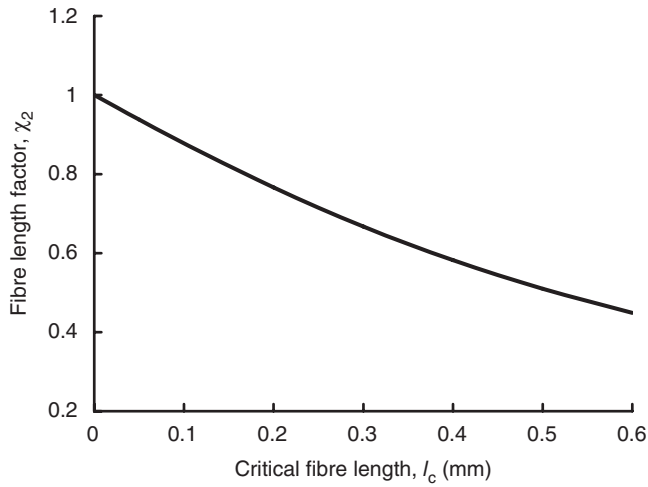

5.7 Effect of critical fibre length l_c on fibre length factor, χ_2, for the case of unidirectional composites, where $l_{mean} = 0.4$ mm, $l_{mod} = 0.213$ mm, $l_{min} = 0$ mm and $l_{max} = \infty$ mm. Adapted from Fu and Lauke (1996).

PA6,6/PP blends reinforced with short glass fibres (SGF) (Fu *et al.*, 2006). Since the critical fibre length l_c is inversely propotional to the interfacial adhesion strength τ_i, i.e., $l_c = r_f\sigma_f^u/\tau_i$, thus the strength of a SFRP composite increases with increasing interfacial adhesion strength. This has also been verified by experiments (Ozkoc *et al.*, 2004).

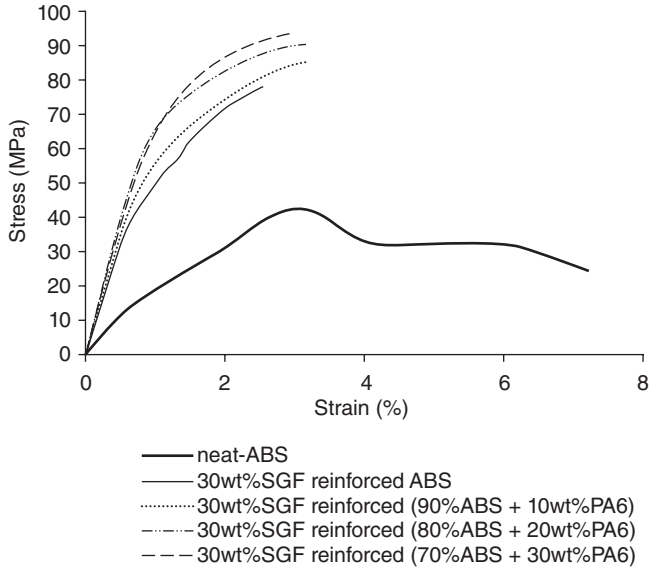

5.8 Tensile stress–strain curves of SGF reinforced ABS and ABS/PA6 blends. Adapted from Ozkoc *et al.* (2004).

Table 5.1 Ultimate strength of SGF reinforced ABS-PA6 composites (Ozkoc *et al.*, 2004)

Material	Tensile strength (MPa)
Neat ABS	44.0 ± 6.0
30% SGF reinforced ABS (with 0 wt% PA6)	78.0 ± 2.5
30% SGF reinforced (90 wt% ABS + 10 wt% PA6) blend	85.0 ± 3.0
30% SGF reinforced (80 wt% ABS + 20 wt% PA6) blend	91.0 ± 1.1
30% SGF reinforced (70 wt% ABS + 30 wt% PA6) blend	93.0 ± 1.8

The tensile stress–strain curves for 30 wt% short glass fibre reinforced acrylonitrile-butadiene-styrene (ABS) blended with various amounts of polyamide 6 (PA6) are shown in Fig. 5.8 (Ozkoc *et al.*, 2004). The results for strength are presented in Table 5.1. The composite tensile strength increases with increasing relative ratio of PA6 in the polymer blend matrix. The strength of composites is a direct indicator of the strength of interfacial bonds since the applied stress is more efficiently transferred through the interface (Yue and Cheung, 1992). The result for the tensile strength can be attributed to the increasing extent of acid–base

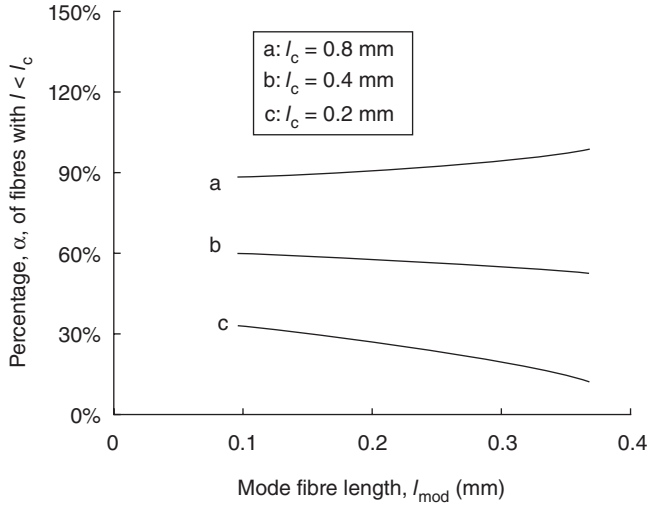

5.9 Variation of percentage, α, of fibres with $l < l_c$ as mode fibre length, l_{mod}, varies for different l_c (l_{mean} = 0.4 mm, l_{min} = 0 mm and $l_{max} = \infty$ mm). Adapted from Fu and Lauke (1996).

reaction between acidic end group of PA6 chains and aminopropyl functional group of coupling agent used on the glass fibre surface as the amount of PA6 in the matrix increases. A similar observation has also been reported for short glass fibre reinforced polyamide 66 (PA 6,6)/polypropylene (PP) blends (Fu *et al.*, 2006). When the relative PA 6,6 ratio in the blend increases, the fibre–matrix interfacial strength increases, leading to higher composite tensile strength.

Assuming l_{min}, l_{max} and l_{mean} to be 0, ∞ and 0.4 mm, and l_c: 0.2, 0.4 and 0.8 mm, respectively, the calculated percentage α of fibres with sub-critical lengths and the fibre length factor χ_2 are shown in Figs 5.9 and 5.10, respectively. Figure 5.9 shows that the content of the fibres with sub-critical fibre length decreases with increasing mode fibre length l_{mod} (as discussed in Chapter 3) for smaller critical fibre length, i.e., l_c = 0.2 and 0.4 mm. The content of fibres with sub-critical fibre length increases with increasing mode fibre length l_{mod} for larger critical fibre length, i.e., l_c = 0.8 mm. Figure 5.10 illustrates that χ_2 decreases with increasing l_{mod}, thus the tensile strength of aligned short fibre composites decreases with mode fibre length. However, the effect of mode fibre length on tensile strength is relatively small compared to the effects of mean fibre length and critical fibre length as shown in Figs 5.5 and 5.7. Especially for the case of $l_c < l_{mean}$, e.g., l_c = 0.2 mm < l_{mean} = 0.4 mm, this effect is very small (see Fig. 5.10). Therefore, in practice as an approximation, the effect of mode fibre length can be neglected on the strength of injected moulded SFRP composites for the

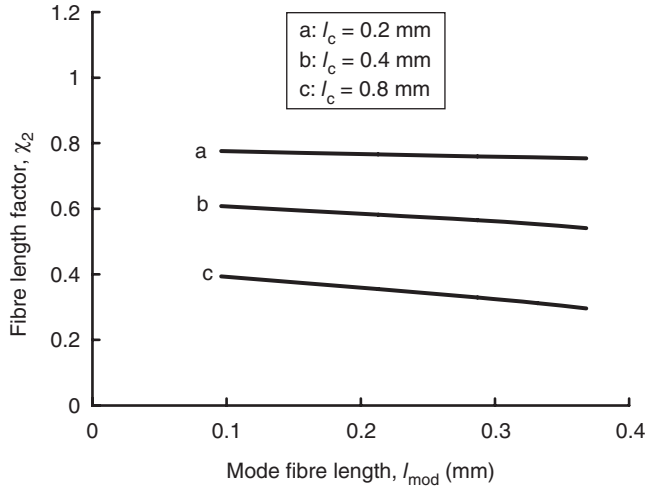

5.10 Effects of mode fibre length l_{mod} and critical fibre length l_c on fibre length factor, χ_2, for the case of unidirectional composites (l_{mean} = 0.4 mm, l_{min} = 0 mm and l_{max} = ∞ mm). Adapted from Fu and Lauke (1996).

purpose of simplicity while the mean fibre length and critical fibre length (hence interfacial adhesion strength) should be given priority over the mode fibre length in considering the influencing factors for the strength of SFRP composites.

Tables 5.2 and 5.3 show the effect of fibre orientation distribution (FOD) on the fibre efficiency factor $\chi_1\chi_2$ for the composite strength, where $\mu = 0.1$, $A = 0.4$, $l_{min} = 0$, $l_{max} = \infty$, $l_{mean} = 0.4$ mm, $l_{mod} = 0.213$ mm and $l_c = 0.2$ mm. Table 5.2 shows that the value of $\chi_1\chi_2$ and hence the composite strength increases with decreasing mean fibre orientation angle and with increasing fibre orientation coefficient f_θ. Table 5.3 shows that for the same fibre orientation coefficient f_θ (for definition, see eqn [3.27]), the variance of $\chi_1\chi_2$ with the mean fibre orientation angle is dependent on the sign (positive or negative) of f_θ; when $f_\theta > 0$, the value of $\chi_1\chi_2$ increases with increasing mean fibre orientation angle; in contrast, when $f_\theta < 0$, the value of $\chi_1\chi_2$ decreases with the increase in mean fibre orientation angle. When $f_\theta = 0$, there is almost no change in the mean fibre orientation angle and hence the value of $\chi_1\chi_2$. Moreover, no direct relationship is found between the value of $\chi_1\chi_2$ and the most probable fibre orientation angle, θ_{mod}. In summary, amongst the influencing factors studied above, the mean fibre orientation angle plays the most important role while the mode fibre orientation angle the least role in determining the strength of injection moulded SFRP composites.

The effect of the snubbing friction coefficient μ on $\chi_1\chi_2$ is given in Fig. 5.11, where $A_f = 0.4$, $l_{min} = 0$, $l_{max} = \infty$, $l_{mean} = 0.4$ mm, $l_c = 0.2$ mm and

Table 5.2 Effect of FOD on the tensile strength of SFRP composites. Adapted from Fu and Lauke, 1996*

p	q	θ_{mean}	θ_{mod}	f_θ	$\chi_1\chi_2$
100	0.5	1.514	$\pi/2$	–0.99	0
16	1	1.351	1.393	–0.88	0.013
8	1	1.262	1.318	–0.78	0.068
4	1	1.141	1.209	–0.6	0.174
2	1	0.982	1.047	–0.33	0.308
0.5	0.5	0.785	no	0	0.417
0.5	1	0.571	0.0	0.33	0.549
1	4	0.430	0.361	0.6	0.652
1	8	0.308	0.253	0.78	0.693
1	16	0.220	0.178	0.88	0.717
0.5	10	0.179	0.0	0.91	0.726
0.5	100	0.056	0.0	0.99	0.755

* p and q are parameters for fibre orientation distribution as shown in eqn [3.24] of Chapter 3; f_θ is fibre orientation coefficient defined in eqn [3.27] of Chapter 3.

Table 5.3 Effect of FOD on the tensile strength of SFRP composites. Adapted from Fu and Lauke, 1996

p	q	θ_{mean}	θ_{mod}	f_θ	$\chi_1\chi_2$
0.5	1	0.571	0.0	0.33	0.549
1	2	0.589	0.524	0.33	0.569
2	4	0.601	0.580	0.33	0.588
4	8	0.608	0.599	0.33	0.595
0.5	0.5	0.785	no	0	0.417
1	1	0.785	0.785	0	0.416
2	2	0.785	0.785	0	0.415
4	4	0.785	0.785	0	0.414
8	4	0.962	0.972	–0.33	0.351
4	2	0.970	0.991	–0.33	0.330
2	1	0.982	1.047	–0.33	0.308
1	0.5	0.999	1.57	–0.33	0.290

$l_{mod} = 0.213$ mm, and $p = 0.5$ and $q = 10$ for the fibre orientation distribution function, respectively. It is obvious that the value of $\chi_1\chi_2$ increases slightly with increasing snubbing friction coefficient, suggesting that snubbing friction has only a small effect on the strength of SFRP composites.

Figure 5.12 shows the effect of the constant A_f on the value of $\chi_1\chi_2$. It is clear that the fibre efficiency factor $\chi_1\chi_2$ decreases with increasing A_f. This means that if the fibre flexural effect on the fracture strength of oblique

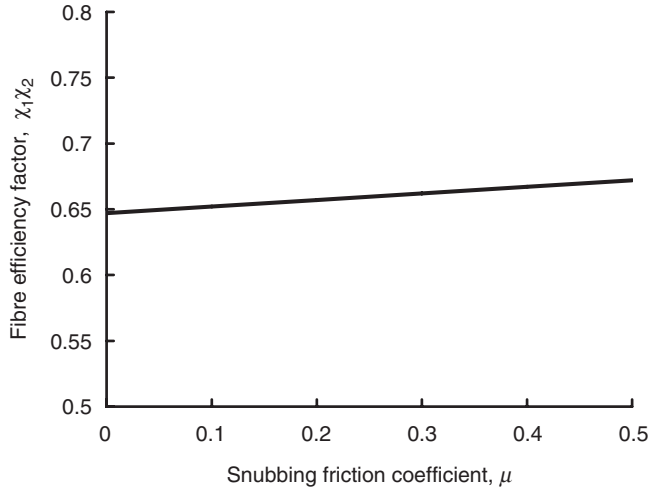

5.11 Effect of snubbing friction coefficient, μ, on fibre efficiency factor $\chi_1\chi_2$ for the composite strength. Adapted from Fu and Lauke (1996).

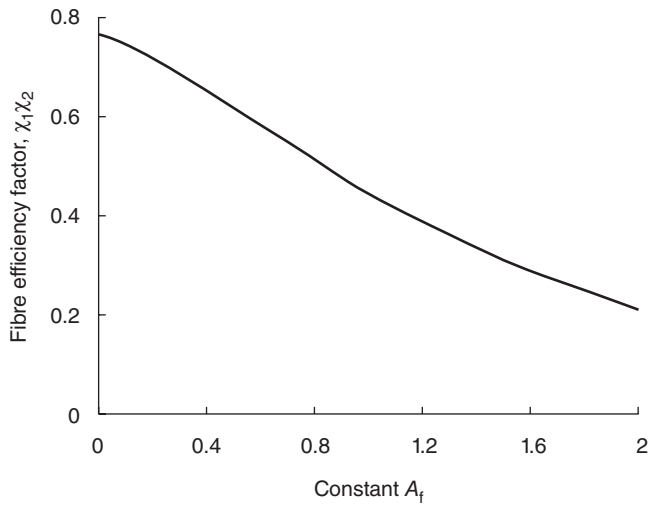

5.12 Effect of the constant A_f on fibre efficiency factor $\chi_1\chi_2$ for the composite strength. Adapted from Fu and Lauke (1996).

fibres is small, the composite strength would be high. Otherwise, the composite strength would be relatively low. Hence, the inclined fibre tensile strength is a very useful parameter for the development of high strength misaligned SFRP composites.

Theoretical models are developed to explain observed data and predict future results. They are as good as can be verified with published

experiments. Equations [5.43] and [5.44] are applied to the experimental results of Templeton (1990). Since the composite strength, the fibre volume fraction and the matrix strength have all been obtained, then the experimental values of $(\chi_1\chi_2)_e$ can be estimated with eqn [5.43] as shown in Table 5.4. Also, the mean fibre length is given, then with eqn [3.11] the parameter a can be obtained by setting arbitrarily, $b = 1.2$. This arbitrary value will not result in a large error since different values of b may result in different mode fibre lengths, but as shown in Fig. 5.10, the effect of mode fibre length on the tensile strength of SFRP is very small. The parameter q can be evaluated from eqn [3.27] by setting arbitrarily, $p = 1$ because the fibre orientation coefficient is given (Templeton, 1990). This arbitrary value may bring about only a small error for a given fibre orientation coefficient as shown in

Table 5.4 Comparison of the theory (eqns [5.43] and [5.44]) (Fu and Lauke, 1996) with experimental results (Templeton, 1990)*

ID	Glass fibre strength (MPa)	Matrix strength (MPa)	Fibre volume fraction	Critical fibre length (mm)	Mean fibre length (mm)	Fibre orientation coefficient (f_θ)	Composite strength (MPa)
Nylon-1	2758	74.6	0.176	0.5613	0.8814	0.4333	201.5
Nylon-2	2758	74.6	0.186	0.5994	1.1862	0.3461	191.0
Nylon-3	2758	74.6	0.186	0.5994	0.8712	0.4095	195.8
PP-1	2758	31.1	0.100	1.4554	2.4714	0.2359	61.5
PP-2	2758	31.1	0.100	1.3995	2.4841	0.2029	58.1
PP-3	2758	31.1	0.100	1.3995	2.4866	0.2985	75.1
PBT-1	2758	34.2	0.181	0.6807	0.9144	0.3673	142.0
PBT-2	2758	34.2	0.181	0.8407	0.9931	0.3407	137.8
PBT-3	2758	34.2	0.181	0.6807	1.0007	0.3472	140.7

ID	a	b	p	q	μ	A	$(\chi_1\chi_2)_e$	$(\chi_1\chi_2)_t$
Nylon-1	1.0813	1.2	1	2.5294	0.1	1.2	0.2884	0.2826
Nylon-2	0.7571	1.2	1	2.0586	0.1	1.2	0.2539	0.2550
Nylon-3	1.0964	1.2	1	2.3870	0.1	1.2	0.2633	0.2682
PP-1	0.3138	1.2	1	1.6175	0.1	1.7	0.1215	0.1262
PP-2	0.3118	1.2	1	1.5091	0.1	1.7	0.1090	0.1197
PP-3	0.3115	1.2	1	1.8510	0.1	1.7	0.1707	0.1425
PBT-1	1.0346	1.2	1	2.1611	0.1	1.3	0.2284	0.2237
PBT-2	0.9370	1.2	1	2.0335	0.1	1.3	0.2199	0.2082
PBT-3	0.9284	1.2	1	2.0637	0.1	1.3	0.2258	0.2202

* PP: polypropylene and PBT: polybutylene terephthalate; a, b, p and q are parameters respectively for determining fibre length distribution and fibre orientation distribution, given in Chapter 3.

Table 5.3. The snubbing friction coefficient μ can be arbitrarily assumed as 0.1 because μ has only a very small effect on the value of $\chi_1\chi_2$ as indicated in Fig. 5.11. And the constant A_f can be adjusted. Consequently, the theoretical values of $(\chi_1\chi_2)_t$ can be evaluated and the final results are listed in Table 5.4. The comparison shows that the theoretical results agree well with the experimental data, indicating that the theory (eqns [5.43] and [5.44]) can give good predictions of the strength of SFRP composites.

5.4 Anisotropy of tensile strength of short fibre reinforced polymer (SFRP) composites

It is well documented that the mechanical properties, such as tensile strength, of short fibre reinforced polymer (SFRP) composites depend on the fibre length distribution (FLD) and the fibre orientation distribution (FOD) in final composite parts (Chin *et al.*, 1988; Chou and Nomura, 1981; Choy *et al.*, 1992; Fu and Lauke, 1996; Lauke and Fu, 1999; Hine *et al.*, 1995; Xia *et al.*, 1995). Owing to the partial fibre orientation in the final parts, SFRP composites show anisotropy or direction dependence of their mechanical properties. The anisotropy of the strength of SFRP composites will be discussed below.

5.4.1 Bridging stress of fibres

To study the direction dependence of the strength of a SFRP composite, it is assumed that a force F is applied in the (Θ, Φ) direction on the SFRP composite (see Fig. 5.13). To estimate the stress in the (Θ, Φ) direction required to break the composite, it is necessary to estimate the average bridging stress of the fibres across the corresponding failure plane. The single fibre bridging case will be first considered as follows.

When a fibre intersecting the crack plane orients normally to the crack plane, the bridging stress σ_F of the fibre across the crack plane can be estimated by eqn [5.23] (Fu and Lauke, 1996). In contrast, when a fibre obliquely crosses the crack plane, the bridging stress $\sigma_{F\delta}$ is given by Fu *et al.* (1993), Jain and Wetherhold (1992) and Li *et al.* (1990):

$$\sigma_{F\delta} = 2l_S(\tau/r_f)\exp(\mu\delta) \quad \text{for} \quad l_S < l_{c\delta}/2, \tag{5.47}$$

where l_s is the embedded length (shown in Fig. 5.3 but θ should be replaced by δ), $l_{c\delta}$ denotes the critical fibre length for an obliquely crossed fibre (Li *et al.*, 1990; Fu *et al.*, 1993); δ is the angle between the fibre axial direction (θ, ϕ) and the crack plane normal or the applied loading direction (Θ, Φ) (see Fig. 5.13), we have:

$$\cos\delta = \cos\Theta\cos\theta + \sin\Theta\sin\theta\cos(\phi - \Phi). \tag{5.48}$$

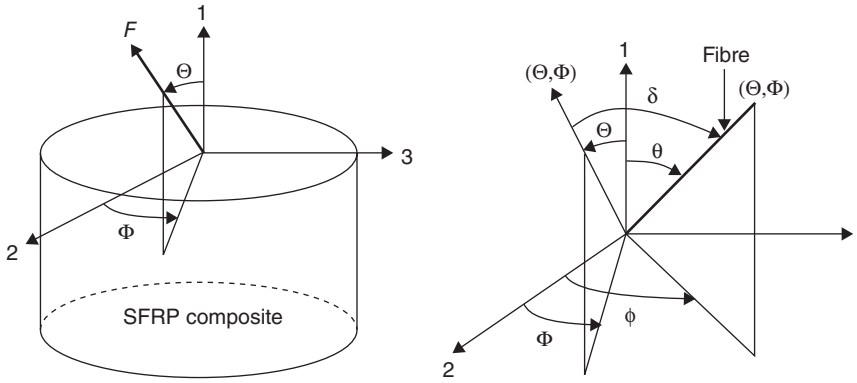

5.13 Definition of loading direction angles Θ and Φ.

Assume $\delta \leqq 90°$, then the right-hand side of eqn [5.48] should have an absolute value. If l_S is not less than $l_{c\delta}/2$, the bridging stress of the oblique fibre is given by:

$$\sigma_{F\theta} = \sigma_{F\delta}^{u} \quad \text{for} \quad l_S \geq l_{c\delta}/2, \tag{5.49}$$

where $\sigma_{F\delta}^{u}$ denotes the fracture stress (namely, inclined tensile strength) of the oblique fibres due to the fibre flexural effect (Bartos and Duris, 1994). Since the flexural stresses for the oblique fibre cause an apparent loss of fibre strength during loading, the fracture strength for the oblique fibre would be reduced (Piggott, 1974, 1994). If the fibres are brittle (e.g., glass or carbon fibres, etc.), $\sigma_{F\delta}^{u}$ can be estimated using eqn [5.27] (Piggott, 1974, 1994). Obviously, there will be a maximum fibre orientation angle for $\sigma_{F\delta}^{u} \geq 0$:

$$\delta_{max} = \arctan(1/A_f). \tag{5.50}$$

The above equation is the same as eqn [5.28]. When $\delta \geq \delta_{max}$, $\sigma_{F\delta}^{u} = 0$. Taking into account the fibre snubbing friction and flexural effects, the expression for the critical length of the oblique fibre is the same as eqn [5.29] by replacing θ with δ.

5.4.2 Average fibre stress in aligned SFRP composites

To estimate the stress in the applied loading (Θ, Φ) direction required to break the composite, the average bridging stress of the fibres is evaluated below. Consider an aligned SFRP composite with uniformly distributed short fibres having the same length l, the fibres are aligned perfectly along the (Θ, Φ) direction. When l is less than l_c, the average fibre bridging stress is estimated by eqn [5.5]. When $l \geq l_c$, the average bridging stress of the fibres

is expressed by eqn [5.7]. Conversely, for a composite with short fibres that are oriented obliquely at an angle δ with the (Θ, Φ) direction, the average bridging stress of the fibres crossing the crack plane is, respectively, expressed by eqns [5.36] and [5.37] by replacing θ with δ (Fu and Lauke, 1996).

5.4.3 Anisotropy of strength of SFRP composite

The anisotropy on the mechanical properties including strength of SFRP composites is dominated by the fibre orientation (Hine *et al.*, 1996). The strength anisotropy of a SFRP composite is the dependence of the composite strength on the applied loading direction (Θ, Φ). Let N_v be the total fibre number in the composite, and N_i the number of fibres with a length from l to $l + dl$ and a pair of orientation angles from θ to $\theta + d\theta$ and from ϕ to $\phi + d\phi$. Then, we have:

$$N_i/N_v = f(l)g(\theta)g(\phi)dl d\theta d\phi. \qquad 5.51$$

The volume subfraction v_i of the fibres with a length from l to $l + dl$ and a pair of orientation angles from θ to $\theta + d\theta$ and from ϕ to $\phi + d\phi$ can be otained from:

$$v_i = v\left[\left(N_i l\pi r_f^2\right)/\left(N_v l_{mean}\pi r_f^2\right)\right] = v\left[\left(N_i l\right)/\left(N_v l_{mean}\right)\right]. \qquad 5.52$$

The composite strength is contributed by all the fibres in the composite. Thus, similar to the derivation of eqn [5.42], the composite strength for loading in the (Θ, Φ) direction is given by:

$$\sigma_c^u(\Theta,\Phi) = \sum_{\phi=\phi_{min}}^{\phi_{max}} \sum_{\theta=\theta_{min}}^{\theta_{max}} \sum_{l=l_{min}}^{l_{max}} \sigma_{F\theta\phi} v + \sigma_M v_m, \qquad 5.53$$

where $\sigma_{F\theta\phi} = \sigma_{F\delta}$ and θ, ϕ and δ satisfy eqn [5.48]. Combining eqns [5.51]–[5.53] and replacing the summation by the integral, we have:

$$\sigma_c^u(\Theta,\Phi) = v\int_{\phi_{min}}^{\phi_{max}} \int_{\theta_{min}}^{\theta_{max}} \int_{l_{min}}^{l_{max}} f(l)g(\theta)g(\phi)(l/l_{mean})\sigma_{F\delta} dl d\theta d\phi + \sigma_M v_m. \qquad 5.54$$

Thus, the strength of SFRP composite in the (Θ, Φ) direction becomes:

$$\begin{aligned}\sigma_c^u(\Theta,\Phi) = v\Bigg[&\int_{\phi_{min}}^{\phi_{max}} \int_{\theta_{min}}^{\theta_{max}} \int_{l_{min}}^{l_{c\delta}} f(l)g(\theta)g(\phi)(l/l_{mean})\sigma_F^u\left(l/(2l_c)\right)\exp(\mu\delta)dl d\theta d\phi \\ &+ \int_{\phi_{min}}^{\phi_{max}} \int_{\theta_{min}}^{\theta_{max}} \int_{l_{c\delta}}^{l_{max}} f(l)g(\theta)g(\phi)(l/l_{mean})\sigma_F^u\left(1-A_f\tan(\delta)\right) \\ &\times\left(1-l_C\left(1-A_f\tan(\delta)\right)/\left(2l\exp(\mu\delta)\right)\right)dl d\theta d\phi\Bigg] + \sigma_M v_m. \end{aligned} \qquad 5.55$$

Equation [5.55] can be rewritten in the following form:

$$\sigma_c^u(\Theta,\Phi) = \chi\sigma_F^u v + \sigma_M v_m, \qquad 5.56$$

where

$$\chi = \int_{\phi_{\min}}^{\phi_{\max}} \int_{\theta_{\min}}^{\theta_{\max}} \int_{l_{\min}}^{l_{c\delta}} f(l)g(\theta)g(\phi)(l/l_{\text{mean}})\left(l/(2l_{\text{C}})\right)\exp(\mu\delta)\mathrm{d}l\mathrm{d}\theta d\phi + \int_{\phi_{\min}}^{\phi_{\max}} \int_{\theta_{\min}}^{\theta_{\max}} \int_{l_{c\delta}}^{l_{\max}} f(l)g(\theta)g(\phi)(l/l_{\text{mean}})\left(1-A_{\text{f}}\tan(\delta)\right) \times \left(1-l_{\text{c}}\left(1-A_{\text{f}}\tan(\delta)\right)/\left(2l\exp(\mu\delta)\right)\right)\mathrm{d}l\mathrm{d}\theta\mathrm{d}\phi. \quad 5.57$$

The parameter χ is defined as the fibre reinforcing efficiency factor containing both the fibre length and orientation effects for the strength of the SFRP composite in the (Θ, Φ) direction. The larger the value of χ, the higher is the composite strength in the (Θ, Φ) direction. The dependence of the composite strength on the loading direction (Θ, Φ), namely, the anisotropy of the composite strength, can be investigated using eqns [5.56] and [5.57]. In the case of transverse loading ($\Theta = 90°$, $\Phi = 0°$) and the fibres aligned along the $\theta = 0°$ direction, the fibre contribution to the composite strength is ignored (namely, $\sigma_{\text{F}\delta}^{\text{u}} = 0$) and the failure of the SFRP composite is matrix- and/or interface-controlled.

For a unidirectional short fibre composite, the strength anisotropy is obtained from eqns [5.56] and [5.57]. Here, $\theta = 0$, and $\delta = \Theta$ according to eqn [5.48] and Fig. 5.13. The angle ϕ is independent of other angles and fibre length, its integration is unity in eqn [5.57]. Hence, the parameter χ for the strength anisotropy $\sigma_{\text{c}}^{\text{u}}(\Theta, \Phi)$ of a unidirectional fibre composite can be derived from eqn [5.57]. That is,

$$\chi = \int_{l_{\min}}^{l_{c\Theta}} f(l)\cdot\frac{l}{l_{\text{mean}}}\cdot\frac{l}{2l_{\text{c}}}\cdot\exp(\mu\Theta)\mathrm{d}l + \int_{l_{c\Theta}}^{l_{\max}} f(l)\cdot\frac{l}{l_{\text{mean}}}\cdot(1-A_{\text{f}}\tan\Theta)\cdot\left(1-\frac{l_{\text{c}}(1-A_{\text{f}}\tan\Theta)}{2l\exp(\mu\Theta)}\right)\mathrm{d}l. \quad 5.58$$

Equation [5.58] can be further simplified for a unidirectional short fibre composite with a constant length l.

$$\chi = \cdot\frac{l}{2l_{\text{c}}}\cdot\exp(\mu\Theta) \quad \text{for} \quad l < l_{\text{c}} \quad 5.59$$

$$\chi = \cdot(1-A_{\text{f}}\tan\Theta)\cdot\left(1-\frac{l_{\text{c}}(1-A_{\text{f}}\tan\Theta)}{2l\exp(\mu\Theta)}\right) \quad \text{for} \quad l \geq l_{\text{c}}. \quad 5.60$$

Equations [5.59] and [5.60] are the expressions for the fibre length factor (also the fibre reinforcing efficiency factor since the fibre orientation factor equals 1) for the strength of a unidirectional short fibre composite loaded at the (Θ, Φ) direction and the composite strength can be estimated by: $\sigma_{\text{c}}^{\text{u}}(\Theta, \Phi) = \chi\sigma_{\text{F}}^{\text{u}}v + \sigma_{\text{M}}v_{\text{m.}}$ When $\Theta = 0$, eqns [5.59] and [5.60] naturally become the same as eqns [5.9] and [5.10], respectively.

The following parametric values are used in the calculation: $A_f = 0.4$, $\mu = 0.1$, $l_c = 0.2$ mm, $l_{mean} = 3.198$ mm ($a = 0.15$ and $b = 1.5$) and $\theta_{mean} = 12.95°$ ($p = 0.6$ and $q = 8$). For simplicity and without loss of generality, one important case, namely, the planar fibre orientation distribution (Chin *et al.*, 1988; Xia *et al.*, 1995; Kwok *et al.*, 1997), in which $s = 0.5$ and $t = \infty$ for $g(\phi)$ (see eqn [3.29]), will be considered. Also, $g(\theta)$ is reasonably assumed to be symmetrical about $\theta = 0°$, which is the mould flow direction.

Figure 5.14 shows the fibre efficiency factor χ plotted as a function of the direction angle Θ and the mean fibre length. It is clearly seen that χ increases with increasing mean fibre length at small Θ while it is insensitive to (Fig. 5.14(a)) or independent of (Fig. 5.14(b)) the mean fibre length at large Θ ($\geq 70°$). Moreover, χ decreases generally with increasing angle Θ at both $\Phi = 0°$ and 90° while it becomes insensitive to angle Θ when $\Theta = \sim 70°$ at

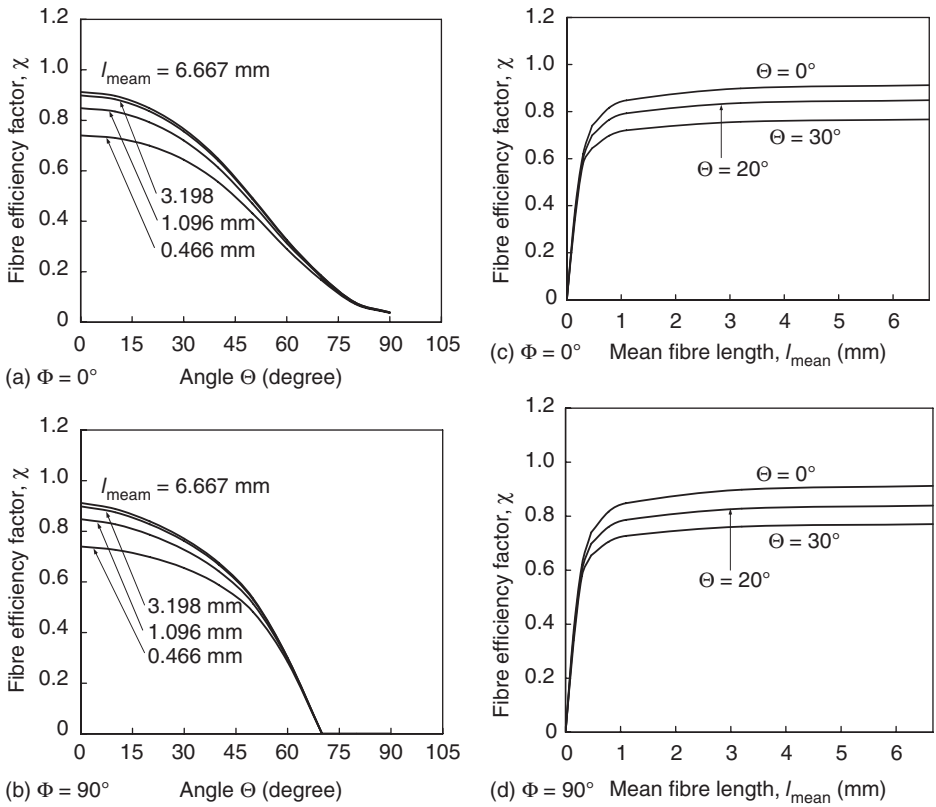

5.14 Variation of fibre efficiency factor, χ, for strength of SFRP composites with direction angle Θ for various mean fibre lengths at (a) $\Phi = 0°$ and (b) $\Phi = 90°$ and with mean fibre length for various Θ at (c) $\Phi = 0°$ and (d) $\Phi = 90°$. Adapted from Lauke and Fu (1999).

$\Phi = 90°$. Further, from Fig. 5.14(c)–(d) it is obvious that the fibre efficiency factor χ increases dramatically with increasing mean fibre length when it is small while it increases slowly with increasing mean fibre length when it is large at various loading directions.

The fibre efficiency factor χ for the composite strength at $\Phi = 0°$ and 90° is shown in Fig. 5.15 as a function of the direction angle Θ for various critical fibre lengths. It can be seen that a smaller critical fibre length (or a larger

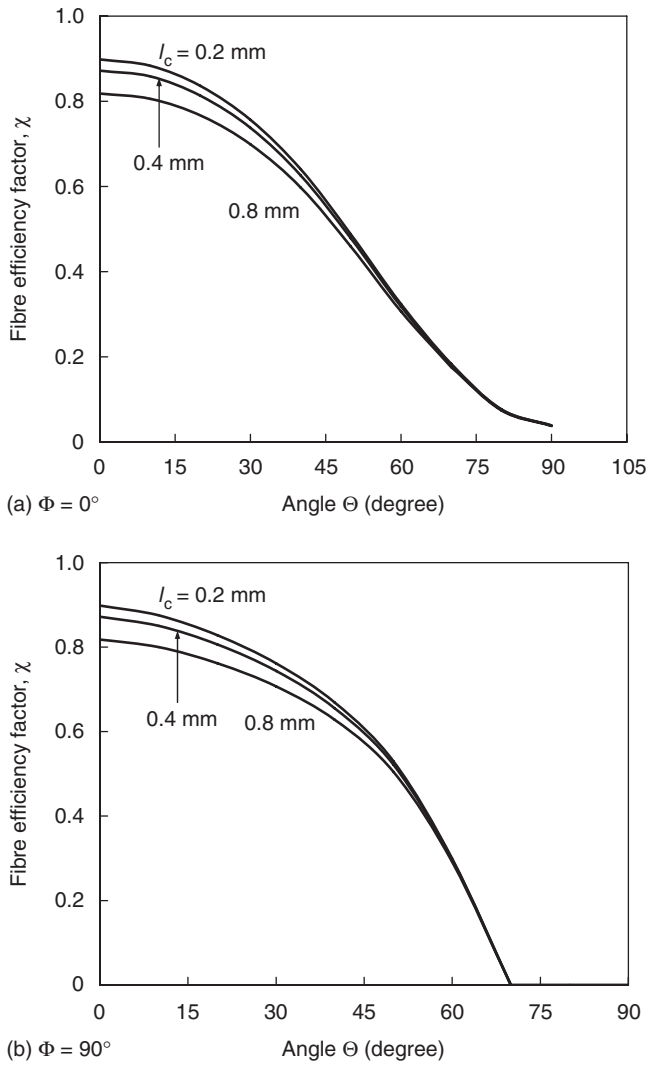

5.15 Variation of fibre efficiency factor, χ, for composite strength with direction angle Φ for various critical fibre lengths at (a) $\Phi = 0°$ and (b) $\Phi = 90°$. Adapted from Lauke and Fu (1999).

interfacial adhesion strength, since $l_c = r_f\sigma_F^u/\tau_i$) generally leads to a higher fibre efficiency factor when Θ is not large (<~70°) while the fibre efficiency factor becomes insensitive to (Φ = 0°, Fig. 5.15(a)) or independent of (Φ = 90°, Fig. 5.15(b)) the critical fibre length when Θ is larger than a certain value (here ≥ ~70° for $A_f = 0.4$). Note that the critical value of Θ is dependent on the constant A_f which determines the critical angle of δ_{max} (eqn [5.50]) and then the critical angle of θ_{max} (eqn [5.48]) and finally the critical value of Θ.

Figure 5.16 displays the effect of mode fibre length on the fibre efficiency factor for the strength of SFRP composites with the direction angle Θ at Φ = 0° and 90°. It is shown that the mode fibre length has only a small influence on the fibre efficiency factor for the two cases of small and large mean fibre lengths at various loading directions.

The anisotropy of the composite strength definitely and strongly depends on the fibre orientation distribution in the SFRP composite. The effect of the mean fibre orientation angle on the fibre efficiency factor for composite strength as a function of the direction angle Θ is shown in Fig. 5.17. It reveals that at Φ = 0° the fibre efficiency factor decreases with increasing mean fibre orientation angle θ_{mean} when Θ is small (e.g., ≤45°) but it increases with increasing mean fibre orientation angle when Θ is large (≥50°). For the two-dimensional (2D) random fibre alignment case with a 45° mean fibre orientation angle, the fibre efficiency factor is constant with changing Θ. At Φ = 90°, the fibre efficiency factor decreases monotonically with increasing mean fibre orientation angle when Θ is small (<~70°) and then becomes zero when Θ is large (≥~70°).

Figure 5.18 shows the effects of mode fibre orientation angle and fibre orientation coefficient on the fibre efficiency factor as a function of the direction angle Θ. At Φ = 0° (Fig. 5.18(a)) a smaller mode fibre orientation angle or a smaller fibre orientation coefficient corresponds to a higher fibre efficiency factor when Θ is small (≤~25°) while a larger mean fibre orientation angle or a larger fibre orientation coefficient corresponds to a higher fibre efficiency factor when Θ is medium (about 25° ≤ Θ ≤ ~80°). Figure 5.18(b) shows that at Φ = 90°, a smaller mode fibre orientation angle (or a smaller fibre orientation coefficient) corresponds in general to a higher fibre efficiency factor when Θ is not large (<~50°) while the fibre efficiency factor becomes insensitive to Θ when Θ is large or is even equal to zero when Θ ≥ ~70°.

Therefore, an SFRP composite with partial fibre alignment obviously shows direction dependence of its strength and its strength anisotropy is controlled by the fibre length and fibre orientation distributions. The fibre efficiency factor and hence the composite strength decreases generally with increasing loading direction angle Θ as shown in Figs 5.14–5.18. Comparatively, the mean fibre length at a small value less than 1 mm has

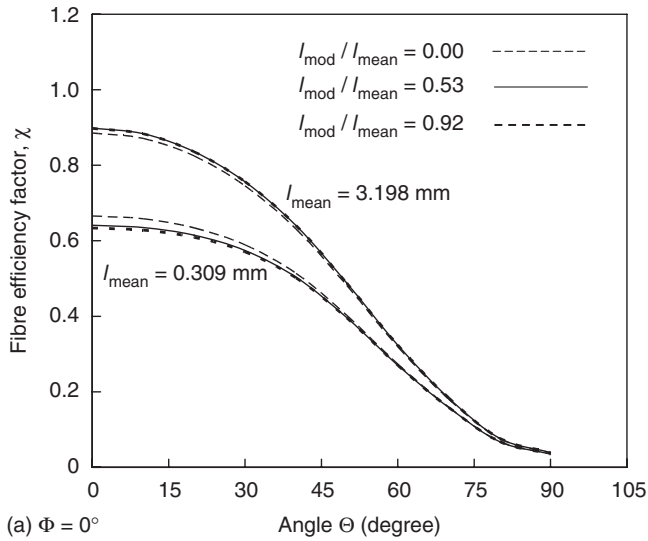

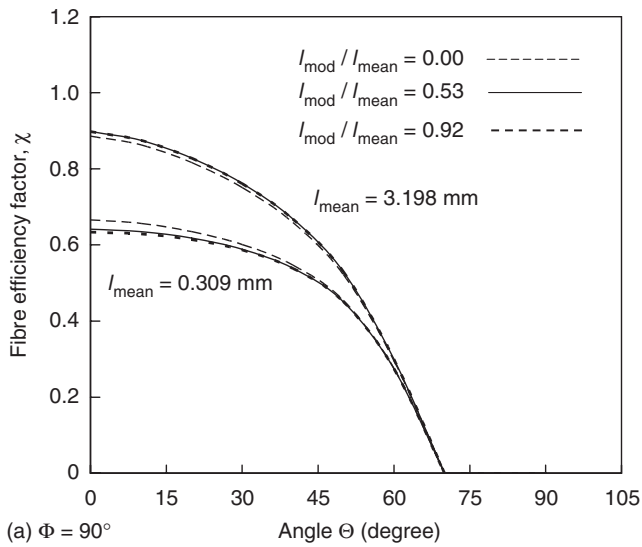

5.16 Effect of mode fibre length on fibre efficiency factor, χ, for strength of SFRP composites as a function of direction angle Θ at (a) $\Phi = 0°$ and (b) $\Phi = 90°$. Adapted from Lauke and Fu (1999).

a significant effect and the critical fibre length has a moderate effect while the mode fibre length has little effect on the strength anisotropy of the SFRP composite. Moreover, mean fibre orientation angle has a significant influence while mode fibre orientation and fibre orientation coefficient have a moderate influence on the strength anisotropy. In practice, injection

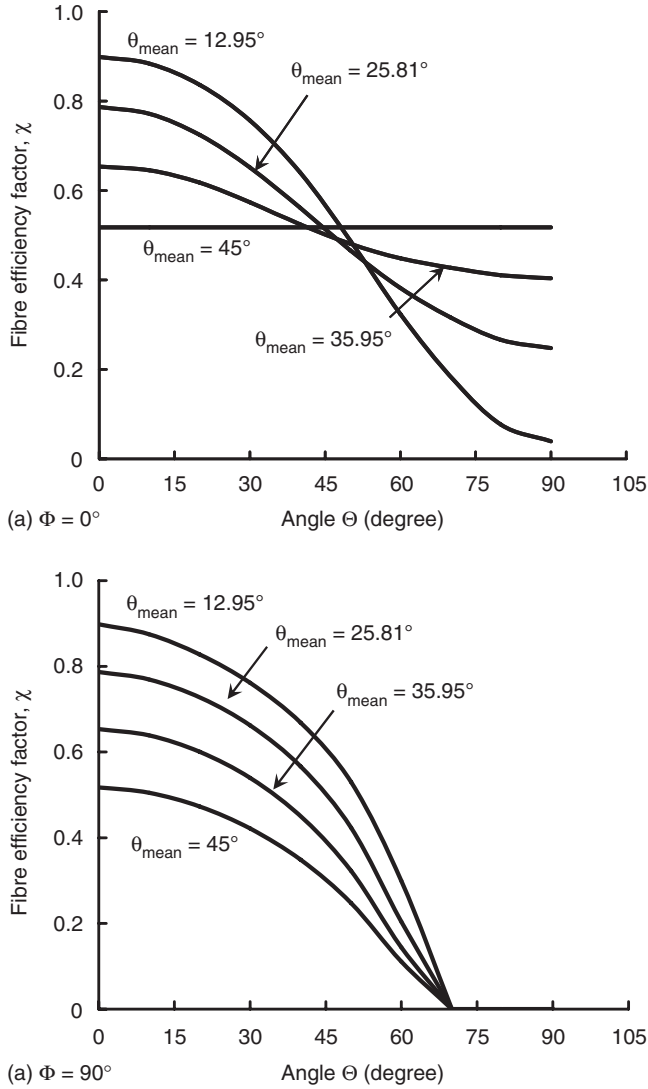

5.17 Effect of mean fibre orientation angle on fibre efficiency factor, χ, for strength of SFRP composites as a function of direction angle Θ at (a) $\Phi = 0°$ and (b) $\Phi = 90°$. Adapted from Lauke and Fu (1999).

moulded SFRP composite parts often show anisotropic mechanical properties owing to the flow-induced partial fibre orientation (Liang and Stokes, 2005). Thus, mechanical properties of short glass fibre filled poly(butylene terephthalate) composite plaques are strongly thickness dependent. The thinnest plaques display the largest differences between the flow and crossflow tensile strengths and moduli. These differences decrease with

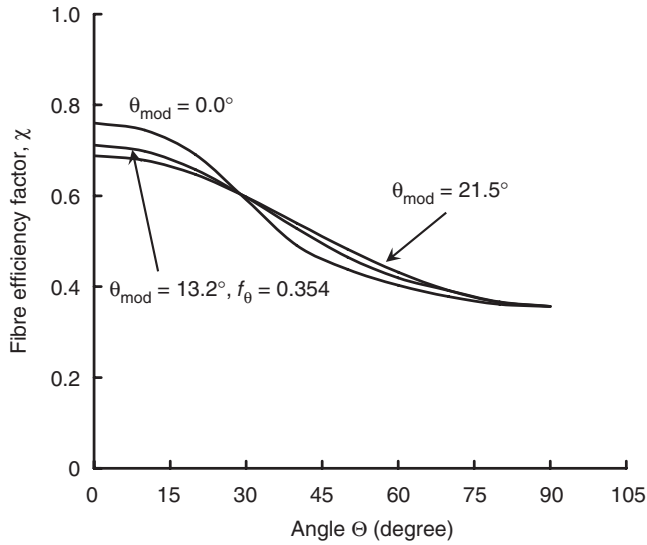

(a) $\Phi = 0°$, $\theta_{mean} = 32.7°$

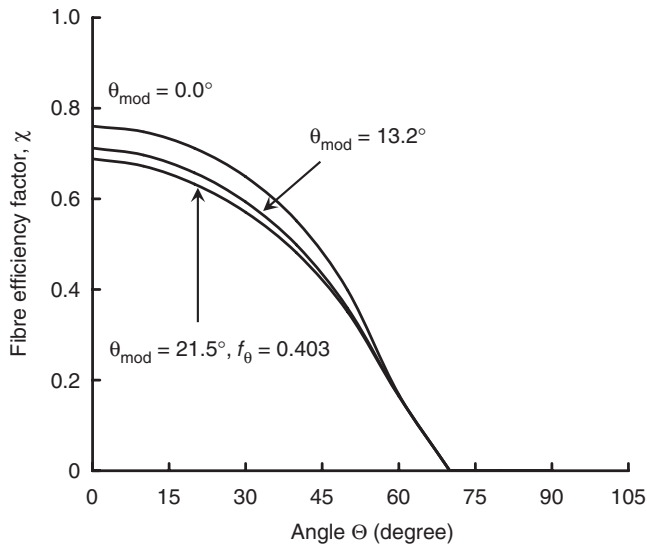

(b) $\Phi = 90°$, $\theta_{mean} = 32.7°$

5.18 Effect of mode fibre orientation angle and fibre orientation coefficient on fibre efficiency factor, χ, for strength of SFRP composites as a function of direction angle Θ at (a) $\Phi = 0°$ and (b) $\Phi = 90°$. Adapted from Lauke and Fu (1999).

increasing plaque thickness. Hence, thinner plaques have higher in-plane anisotropic mechanical properties than thicker plaques.

5.5 Strength of randomly aligned short fibre reinforced polymers (SFRP)

Now we consider two-dimensional (2D) and three-dimensional (3D) random fibre distribution cases. A two-dimensional (2D) random fibre composite is defined as that in which all the fibres are randomly distributed in a plane (namely a two-dimensional space) while a three-dimensional (3D) fibre composite is defined as that in which all the fibres are randomly distributed in a three-dimensional space. The strength is discussed below for the 2D and 3D random cases.

5.5.1 Two-dimensional random fibre distribution

If a short fibre reinforced polymer composite is assumed to be of the form of a sheet thinner than the average fibre length, the composite can be modelled as a quasi-isotropic laminate. In principle, the laminate can be established by stacking up laminae of unidirectional fibres in all directions in the plane of the laminate. Hahn (1975) replaced the two-dimensional (2D) random fibre composite by a laminate consisting of unidirectional fibres in all directions in the laminate plane and applied a rule of mixtures to evaluate the 2D random fibre laminate strength such that:

$$\sigma_{\mathrm{c-2Dr}}^{\mathrm{u}} = \frac{2}{\pi}\int_{0}^{\pi/2} \sigma_{\mathrm{c},\theta}^{\mathrm{u}}\,\mathrm{d}\theta, \qquad 5.61$$

where $\sigma_{\mathrm{c},\theta}^{\mathrm{u}}$ is the strength of a unidirectional laminate with a fibre orientation angle θ. Using the maximum stress theory for failure, Hahn (1975) derived the strength of the 2D random fibre composite as:

$$\sigma_{\mathrm{c-2Dr}}^{\mathrm{u}} = \frac{4}{\pi}\left(\sigma_{\mathrm{c}}^{\mathrm{L,u}}\sigma_{\mathrm{c}}^{\mathrm{T,u}}\right)^{1/2}, \qquad 5.62$$

where $\sigma_{\mathrm{c}}^{\mathrm{L,u}}$ and $\sigma_{\mathrm{c}}^{\mathrm{T,u}}$ represent, respectively, the longitudinal and transverse strength of a unidirectional fibre laminate with the same fibre volume fraction as the 2D random fibre composite.

An alternative approach for predicting the strength of a two-dimensional random fibre composite is the method of laminate analogy. Equations [5.43] and [5.44] can be used for prediction of the strength of a two-dimensional (2D) random case, in which $g(\theta)$ must be constant for the angle θ in the whole range of 0 to $\pi/2$, then $g(\theta) = 2/\pi$. Also, we have $\sigma_{\mathrm{c-2Dr}}^{\mathrm{u}} = \chi\sigma_{\mathrm{F}}^{\mathrm{u}}v + \sigma_{\mathrm{M}}v_{\mathrm{m}}$, where χ is the fibre reinforcing coefficient for the 2D random fibre composite and can be determined by:

$$\chi = \int_0^{\pi/2}\int_{l_{\min}}^{l_{c\theta}} \frac{2}{\pi}\cdot f(l)\cdot\frac{l^2}{2l_{\text{mean}}l_c}\cdot\exp(\mu\theta)\,\mathrm{d}l\,\mathrm{d}\theta + \int_0^{\pi/2}\int_{l_{c\theta}}^{l_{\max}} \frac{2}{\pi}\cdot f(l)\cdot\frac{l}{l_{\text{mean}}}\cdot(1-A_f\tan\theta)\cdot\left(1-\frac{l_c(1-A_f\tan\theta)}{2l\exp(\mu\theta)}\right)\mathrm{d}l\,\mathrm{d}\theta. \quad 5.63$$

When the fibre length is constant in the 2D random fibre composite, then we obtain:

$$\chi = \int_0^{\pi/2}\frac{2}{\pi}\cdot\frac{l}{2l_c}\cdot\exp(\mu\theta)\,\mathrm{d}\theta \quad \text{for} \quad l < l_{c\theta} \quad 5.64$$

$$\chi = \int_0^{\pi/2}\frac{2}{\pi}\cdot(1-A_f\tan\theta)\cdot\left(1-\frac{l_c(1-A_f\tan\theta)}{2l\exp(\mu\theta)}\right)\mathrm{d}\theta \quad \text{for} \quad l \ge l_{c\theta}. \quad 5.65$$

The strength of a 2D random SFRP composite with a constant length l is obtained by Miwa *et al.* (1979, 1980; Miwa and Horiba 1994) dependent on the interfacial shear strength τ_d and is written as follows:

$$\sigma^u_{c-2Dr} = \frac{2\tau_d}{\pi}\left\{2+\ln\left[\frac{(1-l_c/2l)\sigma^u_F\sigma^u_M v+\sigma_M\sigma'_M v_m}{\tau_d^2}\right]\right\}-[\sigma_r]_T \quad \text{for} \quad l \ge l_c \quad 5.66$$

$$\sigma^u_{c-2Dr} = \frac{2\tau_d}{\pi}\left\{2+\ln\left[\frac{\tau_d(l/d_f)\sigma^u_M v+\sigma^2_M v_m}{\tau^2}\right]\right\}-[\sigma_r]_T \quad \text{for} \quad l < l_c, \quad 5.67$$

where σ'_M is the matrix stress at the breaking strain of the fibre, σ_M is the mean stress in the matrix at the failure of the composite, $[\sigma_r]_T$ is the thermal stress produced during moulding of the composite due to the difference of the thermal expansion coefficients between fibres and polymer matrix, and is given by:

$$[\sigma_r]_T = \frac{2(\alpha_m-\alpha_f)E_m\Delta T}{(1+\upsilon_m)+(1+\upsilon_f)(E_m/E_f)},$$

where α_f and α_m are, respectively, the thermal expansion coefficient of the fibres and matrix, and ΔT is the temperature difference from the moulding temperature to room temperature.

5.5.2 Three-dimensional random fibre distribution

For a three-dimensional (3D) random fibre composite, $g(\theta)$ must be constant for the angle θ in the whole range of 0 to $\pi/2$, then $g(\theta) = 2/\pi$; while $g(\phi)$ must also be constant for the angle ϕ in the whole range of 0 to π, then $g(\phi) = 1/\pi$. For a 3D random short fibre composite, the composite strength does not change with the applied loading direction. Namely, a 3D random short fibre composite shows isotropic characteristics in its strength and the composite strength in the ($\Theta = 0$, Φ) direction can be evaluated.

Equations [5.56] and [5.57] will be used to predict the strength of the 3D random short fibre composite and $\sigma^{u}_{c-3Dr} = \chi\sigma^{u}_{F}v + \sigma_{M}v_{m}$, where χ is the fibre reinforcing coefficient for the 3D random fibre composite. From eqn [5.48], we have $\delta = \theta$ since Θ is assumed to be zero. Then, we can obtain χ from eqn [5.57] as:

$$\chi = \int_{0}^{\pi/2}\int_{l_{min}}^{l_{c\theta}} \frac{2}{\pi}\cdot f(l)\cdot\frac{l^2}{2l_{mean}l_c}\exp(\mu\theta)\mathrm{d}l\mathrm{d}\theta + \int_{0}^{\pi/2}\int_{l_{c\theta}}^{l_{max}} \frac{2}{\pi}\cdot f(l)\cdot\frac{l}{l_{mean}}\cdot(1-A_f\tan\theta)\cdot\left(1-\frac{l_c(1-A_f\tan\theta)}{2l\exp(\mu\theta)}\right)\mathrm{d}l\mathrm{d}\theta. \quad 5.68$$

The above equation is the same as eqn [5.63]. This indicates that the strength of a 3D random fibre composite is independent of the angle ϕ, and then the composite strength for both the 2D and 3D random cases will be the same if they have the same fibre length distribution for a given fibre–matrix system. If both the snubbing friction effect and the fibre flexural effect are neglected, i.e. $\mu = 0$ and $A_f = 0$, eqn [5.68] or [5.63] becomes:

$$\chi = \int_{l_{min}}^{l_c} f(l)\cdot\frac{l^2}{2l_{mean}l_c}\mathrm{d}l + \int_{l_c}^{l_{max}} f(l)\cdot\frac{l}{l_{mean}}\cdot\left(1-\frac{l_c}{2l}\right)\mathrm{d}l. \quad 5.69$$

If the fibre length is constant, eqn [5.69] can be further simplified to:

$$\chi = l/(2l_c) \quad \text{for} \quad l < l_c \quad 5.70$$

$$\chi = 1 - l_c/(2l) \quad \text{for} \quad l \geq l_c. \quad 5.71$$

The above equations are the same as eqns [5.9] and [5.10] for the unidirectional SFRP composites. This shows that it is possible to obtain the composite strength of random composites in the same way as for unidirectional SFRP composites when the snubbing friction effect and the fibre flexural effect are neglected. This information may be useful in designing high performance SFRP composites or similar composites since random composites have the same strength at all directions in 2D plane (2D random case) or 3D space (3D random case).

5.6 Strength of hybrid short fibre reinforced polymer (SFRP) composites

When two different types of short fibres are simulataneously used to reinforce a polymer matrix, the strength $[\sigma^{u}_{c}]_H$ of the hybrid short fibre composite can be estimated using the following rule-of-hybrid mixtures (RoHM) equation (Hashemi *et al.*, 1997; Fu *et al.*, 2002b)

$$\left[\sigma^{u}_{c}\right]_H = \left[\sigma^{u}_{c}\right]_1[v]_1 + \left[\sigma^{u}_{c}\right]_2[v]_2, \quad 5.72$$

where $[v]_1$ and $[v]_2$ are, respectively, hybrid volume fraction of the two types of short fibres and $[v]_1 + [v]_2 = 1$. $[\sigma_c^u]_1$ and $[\sigma_c^u]_2$ are strengths of the composites reinforced, respectively, by these two types of fibres at the same volume fraction as the total fibre volume fraction. $[\sigma_c^u]_1$ and $[\sigma_c^u]_2$ can be evaluated using all of the above theoretical equations when appropriate. For example, when the short fibres are unidirectionally aligned along the loading direction with lengths smaller than their critical lengths, eqn [5.5] can be used to predict the composite strength for each SFRP composite. Equation [5.72] can be extended for hybrid composites containing three or more types of short fibres and the right-hand term should include contributions from three or more types of short fibres.

Hybrid equations such as eqn [5.72] are often used to estimate composite mechanical properties including strength and toughness. If the experimentally obtained composite mechanical properties are higher than those estimated using the hybrid equations, it is then regarded that the SFRP composite shows a positive or 'synergistic' effect on the mechanical properties (Fu *et al.*, 2001, 2002a,b). The effect of the relative carbon fibre volume fraction on the tensile strength of injection moulded polypropylene (PP) composites reinforced with hybrids of short glass and carbon fibres is presented in Fig. 5.19 (Fu *et al.*, 2001), where the total glass and carbon volume fraction is fixed at 25%. Figure 5.19 shows that the experimental values of the ultimate strength of the hybrid fibre composites lie above the RoHM prediction. This indicates that the strength exhibits a positive deviation from the mixtures rule and hence shows a synergistic hybrid effect for the composite strength.

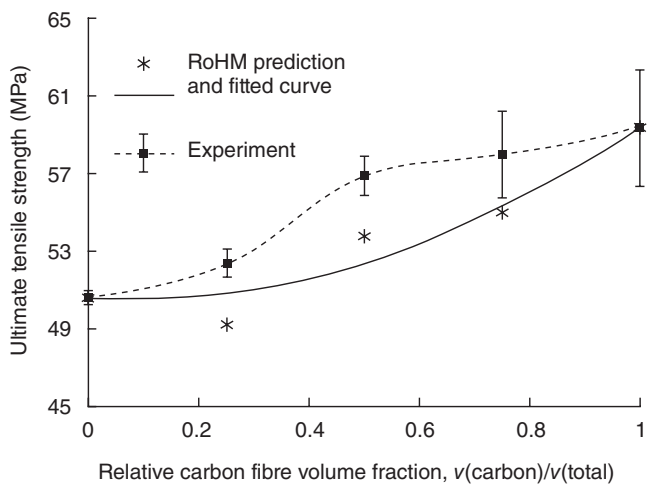

5.19 Tensile strength *versus* relative carbon fibre volume fraction for hybrid SGF/SCF/PP composites with *v*(total) = *v*(carbon) + *v*(glass) = 0.2 s. Adapted from Fu *et al.* (2001).

5.7 References

Bartos P J M and Duris M (1994), 'Inclined tensile strength of steel fibres in a cement-based composite', *Composites*, 25 (10), 945–952.

Chin W K, Liu H T and Lee Y D (1988), 'Effects of fibre length and orientation distribution on the elastic modulus of short fibre reinforced thermoplastics', *Polym Composite*, 9 (1), 27–35.

Chou T S and Nomura S (1981), 'Fibre orientation effects of the thermoplastic properties of short-fibre composites', *Fibre Compos Technol,* 14 (4), 279–291.

Choy C L, Leung W P, Kowk K W and Lau F P (1992), 'Elastic modulus and thermal conductivity of injection-molded short-fibre-reinforced thermoplastics', *Polym Composite*, 13 (1), 69–80.

Cox H L (1952), 'The elasticity and strength of paper and other fibrous materials'. *Brit J Appl Phys,* 3 (1), 72–79.

Fu S Y and Lauke B (1996), 'Effects of fibre length and orientation distributions on the tensile strength of short-fibre-reinforced polymers', *Compos Sci Technol*, 56 (10), 1179–1190.

Fu S Y and Lauke B (1997a), 'Analysis of mechanical properties of injection molded short glass fibre (SGF)/calcite/ABS composites', *J Mater Sci Technol*, 13 (5), 389–396.

Fu S Y and Lauke B (1997b), 'Fibre pull-out energy of misaligned short fibre composites', *J Mater Sci*, 32 (8), 1985–1993.

Fu S Y and Lauke B (1998a), 'The elastic modulus of misaligned short fibre reinforced polymers', *Compos Sci Technol*, 58 (3–4), 389–400.

Fu S Y and Lauke B (1998b), 'An analytical characterization of the elastic modulus of misaligned short fibre reinforced polymers', *Compos Sci Technol*, 58 (12), 1961–1972.

Fu S Y and Lauke B (1998c), 'Characterization of tensile behaviour of hybrid short glass fibre/calcite particle/ABS composites', *Compos Part A – Appl Sci Manu,* 29 (5–6), 575–583.

Fu S Y and Lauke B (1998d), 'Fracture resistance of unfilled and calcite-particle-filled ABS composites reinforced by short glass fibers (SGF) under impact load', *Compos Part A – Appl Sci Manu*, 29 (5–6), 631–642.

Fu S Y, Zhou B L and Lung C W (1993), 'On the pull-out of fibres with a branched structure and the inference of strength and fracture toughness of composites', *Compos Sci Technol*, 47 (3), 245–250.

Fu S Y, Lauke B, Maeder E, Hu X and Yue C Y (1999a), 'Fracture resistance of short-glass-fiber-reinforced and short-carbon-fiber-reinforced polypropylene under Charpy impact load and its dependence on processing', *J Mater Process Tech*, 89–90 (May), 501–507.

Fu S Y, Hu X and Yue C Y (1999b), 'The flexural modulus of misaligned short-fiber-reinforced polymers', *Compos Sci Technol*, 59 (10), 1533–1542.

Fu S Y, Lauke B, Maeder E, Yue C Y and Hu X (2000), 'Tensile properties of short-glass-fiber- and short-carbon-fiber-reinforced polypropylene composites', *Compos Part A – Appl Sci Manu*, 31 (10), 1117–1125.

Fu S Y, Lauke B, Maeder E, Yue C Y, Hu X and Mai Y-W (2001), 'Hybrid effects on tensile properties of hybrid short-glass-fiber- and short-carbon-fiber-reinforced polypropylene composites', *J Mater Sci*, 36 (5), 1243–1250.

Fu S Y, Mai Y-W, Lauke B and Yue C Y (2002a), 'Synergistic effect on the fracture toughness of hybrid short glass fibre and short carbon fibre reinforced polypropylene composites', *Mat Sci Eng A – Struct*, 323 (1–2), 326–335.

Fu S Y, Xu G S and Mai Y-W (2002b), 'On the elastic modulus of hybrid particle/short-fibre/polymer composites', *Compos Part B – Eng*, 33 (4), 291–299.

Fu S Y, Lauke B, Li R K Y and Mai Y-W (2006), 'Effects of PA6,6/PP ratio on the mechanical properties of short glass fiber reinforced and rubber-toughened polyamide 6,6/polypropylene blends', *Compos Part B – Eng*, 37 (2–3), 182–190.

Fukuda H and Chou T W (1982), 'Probabilistic theory of the strength of short fibre composites with variable fibre length and orientation', *J Mater Sci*, 17 (4), 1003–1011.

Fukuda H and Kawata K (1974), 'On Young's modulus of short fibre composites', *Fibre Sci Technol*, 7 (3), 207–222.

Hahn H T (1975), 'On approximations for strength of random fiber composites', *J Compos Mater*, 9 (4), 316–326.

Hashemi S, Elmes P and Sandford S (1997), 'Hybrid effects on mechanical properties of polyoxymethylene', *Polym Eng S*ci, 37 (1), 45–58.

Hine P J, Davidson N, Duckett R A and Ward I M (1995), 'Measuring the fibre orientation and modelling the elastic properties of injection-molded long-fibre-reinforced nylon', *Compos Sci Technol*, 53 (2), 125–131.

Hine P J, Duckett R A, Ward I M, Allan P S and Bevis M J (1996), 'Comparison of short glass fiber reinforced polypropylene plates made by conventional injection molding and using shear controlled injection molding', *Polym Composite*, 17 (3), 400–407.

Jain L K and Wetherhold R C (1992), 'Effect of fiber orientation on the fracture toughness of brittle matrix composites', *Acta Metall et Materialia*, 40 (6), 1135–1143.

Jayaraman K and Kortschot M T (1996), 'Correction to the Fukuda–Kawata Young's modulus and the Fukuda–Chou strength theory for short fibre-reinforced composite materials', *J Mater Sci*, 31 (8), 2059–2064.

Jiang H, Valdez J A, Zhu Y T, Beyerlein I J and Lowe T C (2000), 'The strength and toughness of cement reinforced with bone-shaped steel wires', *Compos Sci Technol*, 60 (9), 1753–1761.

Kallmes O J, Bernier G A and Perez M (1977), 'Mechanistic theory of the load-elongation properties of paper – 1. Uniform stain theory for paper', *Paper Technol Ind*, 18 (7), 222, 224–226.

Kelly A and Tyson W R (1965), 'Tensile properties of fibre-reinforced metals: copper/tungsten and copper/molybdenum', *J Mech Phys Solids*, 13 (2), 329–350.

Kwok K W, Choy C L and Lau F P (1997), 'Elastic modulus of injection-molded short-glass-fiber-reinforced poly(ethylene terephthalate)', *J Reinf Plast Comp*, 16, 290–305.

Lauke B and Fu S Y (1999), 'Strength anisotropy of misaligned short-fibre-reinforced polymers', *Compos Sci Technol*, 59 (5), 699–708.

Li V C, Wang Y and Backer S (1990), 'Effect of inclining angle, bundling, and surface treatments on synthetic fiber pull-out from a cement matrix', *Composites*, 21 (2), 132–139.

Liang E W and Stokes V K (2005), 'Mechanical properties of injection-molded short-fiber thermoplastic composites. Part 1. The elastic moduli and strengths of glass-filled poly(butylene terephthalate)', *Polym Composite*, 26 (4), 428–447.

Mittal R K and Gupta V B (1982), 'The strength of the fibre-polymer interface in short glass fibre-reinforced polypropylene', *J Mater Sci*, 17 (11), 3179–3188.

Miwa M and Horiba N (1994), 'Effects of fibre length on tensile strength of carbon/glass fibre hybrid composites', *J Mater Sci*, 29 (4), 973–977.

Miwa M, Nakayama A, Ohsawa T and Hasegawa A (1979), 'Temperature dependence of the tensile strength of glass fiber-epoxy and glass fiber-unsaturated polyester composites', *J Appl Polym Sci*, 23 (10), 2957–2966.

Miwa M, Ohsawa T and Tahara K (1980), 'Effects of fiber length on the tensile strength of epoxy/glass fiber and polyester/glass fiber composites', *J Appl Polym Sci*, 25 (5), 795–807.

Ozkoc G, Bayram G and Bayramli E (2004), 'Effects of polyamide 6 incorporation to the short glass fiber reinforced ABS composites: an interfacial approach', *Polymer*, 45 (26), 8957–8966.

Piggott M R (1974), 'Toughness in obliquely-stressed fibrous composites', *J Mech Phys Solids*, 22 (6), 457–468.

Piggott M R (1994), 'Short fibre polymer composites: a fracture-based theory of fibre reinforced', *J Compos Mater*, 28 (7), 588–606.

Ramsteiner F and Theysohn R (1985), 'Influence of fibre diameter on the tensile behavior of short-glass-fibre reinforced polymers', *Compos Sci Technol*, 24 (3), 231–240.

Ranganathan S (1990), 'Characterization of orientation clustering in short-fiber composites', *J Polym Sci Part B Polym Phys*, 28 (13), 2651–2672.

Sarasua J R, Remiro P M and Pouyet J (1995), 'Mechanical behaviour of PEEK short fibre composites', *J Mater Sci*, 30 (13), 3501–3508.

Shiao M L, Nair S V, Garrett P D and Pollard R E (1994), 'Effect of glass-fibre reinforcement and annealing on microstructure and mechanical behaviour of nylon 6,6 – Part I microstructure and morphology', *J Mater Sci*, 29 (7), 1973–1981.

Taya M and Arsenault R J (1989), *Metal matrix composites*, Oxford, Pergamon, pp. 63–101.

Templeton P A (1990), 'Strength predictions of injection molding compounds', *J Reinf Plast Comp*, 9 (May), 210–225.

Thomason J L (2007), 'The influence of fibre length and concentration on the properties of glass fibre reinforced polypropylene: 7. Interface strength and fibre strain in injection moulded long fibre PP at high fibre content', *Compos A*, 38 (1), 210–216.

Thomason J L and Vlug M A (1995), 'The influence of fibre length and concentration on the properties of glass fibre reinforced polypropylene', 3rd Int. Conf on Deformation and Fracture of Composites, Section 1. University of Surrey, Guildford, UK, 27–29 March 1995, pp. 47–55.

Wetherhold R C and Jain L K (1992), 'The toughness of brittle matrix composites reinforced with discontinuous fibers', *Mater Sci Eng A – Struct*, 151 (2), 169–177.

Xia M, Hamada H and Maekawa Z (1995), 'Flexural stiffness of injection molded glass fibre reinforced thermoplastics', *Int Polym Proc*, 10 (1), 74–81.

Yu Z, Brisson J and Ait-Kadi A (1994), 'Prediction of mechanical properties of short Kevlar fiber-nylon-6,6 composites, *Polym Composite*, 15 (1), 64–73.

Yue C Y and Cheung W L (1992), 'Interfacial properties of fibre-reinforced composites', *J Mater Sci*, 27(14), 3843–3855.

Zhou J, Li G, Li B and He T (1997), 'Flexural fatigue behavior of injection-molded composites based on poly(phenylene ether ketone)', *J Appl Polym Sci*, 65 (10), 1857–1864.

Zhu Y T and Beyerlein I J (2002), 'Bone-shaped short fiber composites – an overview', *Mater Sci Eng A – Struct*, 326 (3–4), 208–227.

Zhu Y T, Valdez J A, Beyerlein I J, Zhou S J, Liu C, Stout M G, Butt D P and Lowe T C (1999), 'Mechanical properties of bone-shaped-short-fiber reinforced composites', *Acta Materialia*, 47 (6), 1767–1781.

6

Elastic modulus of short fibre reinforced polymers

Abstract: Chapter 6 begins by reviewing different theoretical models for longitudinal modulus of unidirectionally aligned short fibre reinforced polymers before discussing the theoretical model for the elastic modulus of partially aligned short fibre reinforced polymers. Theoretical models for elastic modulus anisotropy, modulus of randomly aligned and hybrid SFRP composites are then discussed. Also, numerical methods for elastic modulus of SFRP composites and effect of interphase properties on composite modulus are presented.

Key words: Young's modulus, modulus anisotropy, analytical approaches, numerical methods, interphase effect.

6.1 Introduction

Fibre reinforced polymer composites are practical and useful, but there is always a problem with understanding how they work. Even the elastic modulus of aligned continuous fibre reinforced composites has been the subject of a great deal of study, in which the strains in the fibres and the polymer matrix are assumed to be the same. Thus, so long as neither matrix nor fibres have yielded, the rule of mixtures (RoM) can be used to predict the elastic modulus:

$$E_c = E_f v + E_m v_m \tag{6.1}$$

Just as in continuous fibre reinforced composites, the study of elastic modulus of short fibre reinforced polymer (SFRP) composites has been the most active among all mechanical and physical properties. It is convenient to subdivide short fibre reinforced polymer composites into three categories in terms of fibre orientation: (a) aligned short fibres, (b) partially aligned short fibres, and (c) random short fibres. The elastic modulus in this chapter refers to the initial modulus at infinitesimal strains. For SFRP composites, the elastic modulus depends significantly on both fibre length distribution (FLD) and fibre orientation distribution (FOD). It also depends on the loading direction, that is, SFRP composites show modulus anisotropy. The elastic modulus of SFRP composites and its anisotropy will be discussed in detail in this chapter.

6.2 Elastic modulus of unidirectional short fibre reinforced polymer composites

In practice, injection-moulded SFRP composites have misoriented fibres of highly variable length but aligned SFRP properties with a constant fibre length are always calculated as a prelude to model the more realistic situations. Here, models that predict the elastic moduli of SFRP composites having aligned short fibres with uniform length and properties are first given. Modelling of more realistic SFRP composites with distributions of fibre orientation and length are then discussed.

6.2.1 Cox shear lag model

The Cox shear lag model (1952) is the pioneering work on the longitudinal elasticity of paper and fibrous materials containing aligned discontinuous fibres. Detailed derivation of Cox's model is given below. A unidirectional short fibre composite shown in Fig. 6.1 is subjected to an applied strain and a typical composite element is selected in which $2R$ is the diameter of the element and R is mean centre to centre separation of fibres normal to their lengths (Cox, 1952; Piggott, 1980). r_f is fibre radius and l is embedded fibre length. It is

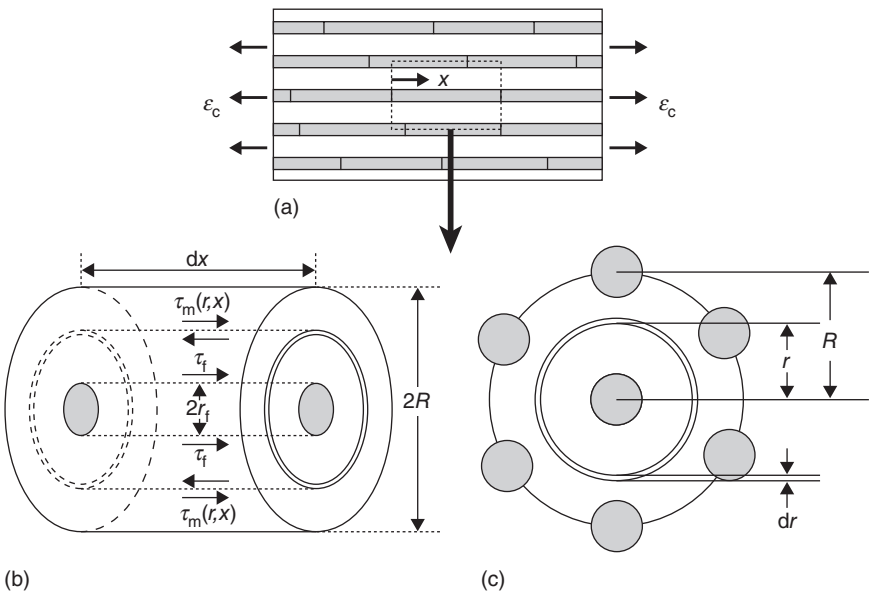

6.1 Schematic drawing of (a) a multi-discontinuous-fibre composite with no fibre end gap, (b) short length of fibre and surrounding matrix, (c) fibre with nearest neighbouring fibres, hexagonally packed.

assumed that perfect bonding exists between fibre and matrix and lateral contraction of fibre and matrix is equal (Cox, 1952).

Equating the shear stress $\tau_m(r, x)$ at distance r with that $\tau_f(x)$ at the fibre surface ($r = r_f$) in the composite element, we have (Piggott, 1980):

$$2\pi r\tau_m(r, x)\,dx = 2\pi r_f \tau_f(x)\,dx \qquad 6.2$$

or

$$\tau_m(r, x) = r_f \tau_f(x)/r.$$

The ratio, $\tau_m(r, x)$, to shear strain, $du_m(r, x)/dr$, is equal to the matrix shear modulus G_m, so that

$$\frac{\tau_m(r, x)}{G_m} = \frac{du_m(r, x)}{dr} = \frac{\tau_f(x) r_f}{G_m r}. \qquad 6.3$$

This equation is integrated between r_f and R to give:

$$\tau_f(x) = \frac{G_m}{r_f \ln(R/r_f)}\left[u_m(R, x) - u_m(r_f, x)\right]. \qquad 6.4$$

$\tau_f(x)$ transfers stress to the fibres. Equilibrium of the fibre–matrix interface shear stress $\tau_f(x)$ and the axial fibre stress $\sigma_F(x)$ requires:

$$\frac{d\sigma_F(x)}{dx} = -\frac{2}{r_f}\tau_f(x). \qquad 6.5$$

Substitution of $\tau_f(x)$ (eqn [6.4]) into eqn [6.5] yields:

$$\frac{d\sigma_F(x)}{dx} = -\frac{2G_m}{r_f^2 \ln(R/r_f)}\left[u_m(R, x) - u_m(r_f, x)\right]. \qquad 6.6$$

By using the continuity condition of displacements at the interface: $u_m(r_f, x) = u_m(x) = u_f(r_f, x)$ and the assumption that the interface displacement is equal to the mean displacement of the fibre cross section: $u_f(r_f, x) = u_F$, then differentiation of eqn [6.6] about x gives:

$$\frac{d^2\sigma_F(x)}{dx^2} = -\frac{2G_m}{r_f^2 \ln(R/r_f)}\left[\frac{du_m(R, x)}{dx} - \frac{du_F(x)}{dx}\right]. \qquad 6.7$$

The fibre displacement, $u_F(x)$, can be calculated from the fibre stress, since the fibre strain is $\varepsilon_F = du_F(x)/dx$. Thus, $du_F(x)/dx = \sigma_F(x)/E_f$. At $r = R$, the strain is assumed equal to the overall strain (far field strain), that is,

$$du_m(R, x)/dx = \varepsilon_c = \text{constant}. \qquad 6.8$$

Thus, eqn [6.7] becomes:

$$\frac{d^2\sigma_F(x)}{dx^2} = -\frac{2G_m}{r_f^2 \ln(R/r_f)}\left[\varepsilon_c - \frac{\sigma_F(x)}{E_f}\right]. \qquad 6.9$$

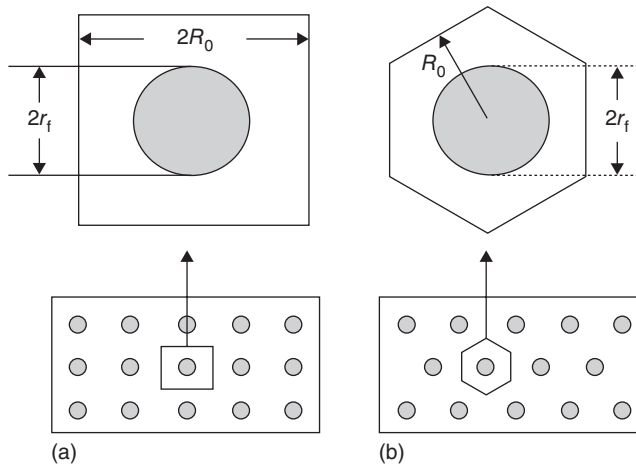

6.2 Schematic drawing of (a) the square packing of fibres and (b) the hexagonal packing of fibres.

Then, the solution of eqn [6.9] is given by:

$$\sigma_F(x) = E_f\varepsilon_c + A\sinh\eta x + B\cosh\eta x, \qquad 6.10$$

where A and B are constants that can be determined by the boundary conditions at the fibres when stress transfer is intended to be studied. The shear lag parameter η is given by:

$$\eta = \sqrt{\frac{2G_m}{r_f^2 E_f \ln(R/r_f)}}. \qquad 6.11$$

For square packing of fibres (see Fig. 6.2(a)), the fibre volume fraction is:

$$v = \frac{\pi r_f^2}{R^2} = \frac{\pi r_f^2}{4R_0^2} \qquad 6.12$$

or

$$\ln(2R_0/r_f) = \frac{1}{2}\ln(\pi/v). \qquad 6.13$$

Similarly, for hexagonal packing (see Fig. 6.2(b)), we obtain:

$$v = \frac{2\pi r_f^2}{\sqrt{3}R^2} = \frac{\pi r_f^2}{2\sqrt{3}R_0^2} \qquad 6.14$$

or

$$\ln(2R_0/r_f) = \frac{1}{2}\ln(2\pi/\sqrt{3}v). \qquad 6.15$$

By taking into account the boundary conditions, $\sigma_F(x) = 0$ at $x = 0$ and at $x = l$, the axial fibre stress is finally given as:

$$\sigma_F(x) = E_f \varepsilon_c \left[1 - \frac{\cosh \eta (l/2 - x)}{\cosh \eta l/2} \right] \quad 6.16$$

or

$$\frac{\sigma_F(x)}{\sigma_c} = \frac{E_f}{E_c} \left[1 - \frac{\cosh \eta (l/2 - x)}{\cosh \eta l/2} \right], \quad 6.17$$

where σ_c is applied stress on the composite and is equal to $E_c\varepsilon_c$ in which E_c is composite modulus. From eqn [6.16], the mean stress in the fibre is obtained as:

$$\sigma_F = E_f \varepsilon_c \left[1 - \frac{\tanh \eta l/2}{\eta l/2} \right]. \quad 6.18$$

The longitudinal modulus of the composite can then be obtained by the equilibrium of forces for the composite element and can be expressed using a modified rule of mixtures (MRoM) equation by introducing a fibre length factor λ: $E_c\varepsilon_c = \lambda E_f v\varepsilon_c + E_m(1 - v)\varepsilon_c$. Hence by eliminating ε_c on both sides, we have

$$E_c = \lambda E_f v + E_m (1 - v), \quad 6.19$$

where λ can be written as:

$$\lambda = 1 - \frac{\tanh \eta l/2}{\eta l/2}. \quad 6.20$$

The composite modulus is thus diminished by the reduced fibre stress by λ. This approach is very similar to that given in Section 9.2.1.

6.2.2 Semi-empirical equation

Semi-empirical approaches are used to derive the elastic constants of unidirectional fibre composites. A well-known example is the Halpin–Tsai equation (Halpin and Tsai, 1967), which is obtained by reducing Hermans' solution (1967) to a simpler analytical form. For unidirectional short fibre composites, the elastic properties such as elastic modulus, Poisson's ratio, and shear modulus are predicted by the following Halpin–Tsai equations (Halpin and Tsai, 1967; Tsai and Hahn, 1980):

$$E_c = E_{11} = \frac{1 + 2(l/d)\eta_L v}{1 - \eta_L v} E_m \quad 6.21$$

$$E_{22} = \frac{1 + 2\eta_T v}{1 - \eta_T v} E_m \quad 6.22$$

$$\nu_{12} = \nu_f v + \nu_m v_m \tag{6.23}$$

$$\nu_{21} = \frac{E_{22}}{E_{11}} \nu_{12} \tag{6.24}$$

$$G_{12} = \frac{1+\eta_G v}{1-\eta_G v} G_m, \tag{6.25}$$

where

$$\eta_L = \frac{E_f/E_m - 1}{E_f/E_m + 2(l/d)} \tag{6.26}$$

$$\eta_T = \frac{E_f/E_m - 1}{E_f/E_m + 2} \tag{6.27}$$

$$\eta_G = \frac{G_f/G_m - 1}{G_f/G_m + 1} \tag{6.28}$$

and l/d = fibre aspect ratio. In theory, as l/d becomes large, the modulus of a SFRP composite attains a plateau representing the continuous fibre result. The critical value of l/d at which the plateau is reached is strongly dependent on the ratio of E_f/E_m. For glass fibres, the critical value of l/d is approximately equal to 100 (Fu and Lauke, 1998c, 1998d).

Equation [6.21] indicates that the longitudinal elastic modulus of a unidirectional SFRP composite depends not only on the fibre volume fraction and the fibre–matrix modulus ratio, but also on the fibre aspect ratio l/d. For a high aspect ratio SFRP composite, the longitudinal elastic modulus approaches a limiting value that is the same as that for a unidirectional continuous fibre composite given by the rule-of-mixtures equation.

Since the composite elastic modulus is not a linear function of fibre length, the predicted elastic modulus using the mean fibre length by the Halpin–Tsai equation is not the same as the mean elastic modulus using the fibre length distribution density function $f(l)$. The mean Young's modulus is defined as (Chin *et al.*, 1988; Fu and Lauke, 1998c):

$$E_c = \frac{\int_{l_{min}}^{l_{max}} E_{11}(l) f(l) \mathrm{d}l}{\int_{l_{min}}^{l_{max}} f(l) \mathrm{d}l}. \tag{6.29}$$

The difference between the elastic modulus calculated using eqn [6.21] and the above equation is:

$$E\% = \left| \frac{E_{11} - E_c}{E_c} \right| * 100\%.$$

This difference is generally non-zero since the fibre length distribution at a fixed mean fibre length but different mode fibre length has an effect on the composite Young's modulus to be shown later.

6.2.3 Self-consistent method

In the self-consistent method, it is assumed that the fibre and matrix are isotropic, homogeneous, and linearly elastic and the aligned fibre composite is macroscopically homogeneous and transversely isotropic. There exist two basic variants of the self-consistent approach, namely, the method used by Hill (1965a, 1965b) and that used by Kilchinskii (1965, 1966) and Hermans (1967). Chou *et al.* (1980) used Hill's approach to study the stiffness of SFRP composites by simulating short fibres as ellipsoidal inclusions and obtained stiffness solutions for multi-component systems. In the self-consistent model, a single inclusion is assumed to be embedded in a continuous and homogeneous medium. The inclusion has the same elastic properties as that of the short fibres while the surrounding material has the properties of the composite, which is the unknown composite elastic property to be determined. The short fibres are represented by ellipsoidal inclusions that are aligned and uniformly distributed in the short fibre reinforced composite. The constitutive equations of the unidirectional short fibre composite are expressed in terms of five independent stiffness constants (Hashin and Rosen, 1964). Thus, we have,

$$\langle \sigma_{11} \rangle = C^*_{1111} \langle \varepsilon_{11} \rangle + C^*_{1122} \langle \varepsilon_{22} + \varepsilon_{33} \rangle \tag{6.30}$$

$$\langle \sigma_{22} \rangle = C^*_{1122} \langle \varepsilon_{11} \rangle + C^*_{2222} \langle \varepsilon_{22} \rangle + C^*_{2233} \langle \varepsilon_{33} \rangle \tag{6.31}$$

$$\langle \sigma_{33} \rangle = C^*_{1122} \langle \varepsilon_{11} \rangle + C^*_{2233} \langle \varepsilon_{22} \rangle + C^*_{2222} \langle \varepsilon_{33} \rangle \tag{6.32}$$

$$\langle \sigma_{12} \rangle = 2C^*_{1212} \langle \varepsilon_{12} \rangle \tag{6.33}$$

$$\langle \sigma_{23} \rangle = (C^*_{2222} - C^*_{2233}) \langle \varepsilon_{23} \rangle, \tag{6.34}$$

where '1' direction is along the fibre axis. Following Hashin and Rosen (1964), the effective stiffness constants C^*_{ijkl} can be expressed in terms of the familiar engineering constants: longitudinal Young's modulus E_{11}, plane strain bulk modulus K_{23}, plane strain shear modulus G_{23}, axial shear modulus G_{13} and major Poisson's ratio υ_{21} (= υ_{31}). Thus, we obtain:

$$C^*_{1111} = E_{11} + 4K_{23}\upsilon_{21}^2 \tag{6.35}$$

$$C^*_{2222} = K_{23} + G_{23} \tag{6.36}$$

$$C^*_{1212} = G_{12} \tag{6.37}$$

$$C^*_{2233} = K_{23} - G_{23} \tag{6.38}$$

$$C^*_{1122} = 2K_{23}\upsilon_{21}. \tag{6.39}$$

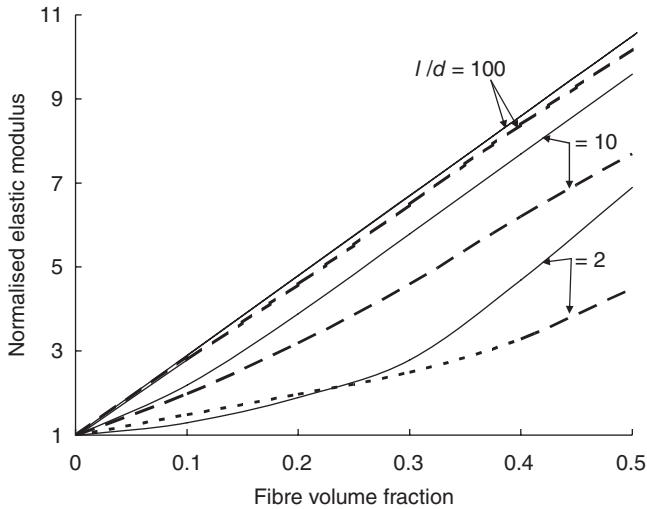

6.3 Variation of normalised longitudinal modulus (E_c/E_m) of short glass fibre reinforced epoxy composites with fibre volume fraction v at three different fibre aspect ratios (l/d). Solid line: self-consistent model; dashed line: Halpin–Tsai equation. Adapted from Chou *et al.* (1980).

From the above equations, the expressions for the elastic stiffness constants of the SFRP composite can be established. The solutions of the self-consistent model are obtained by the iteration method. Convergence will occur and the iteration process will then terminate. Prediction of the elastic modulus of short fibre composites was performed for the special case of a binary system of a matrix and one type of fibre. Figure 6.3 shows the variation of normalised longitudinal modulus (E_c/E_m) of short glass fibre reinforced epoxy composites with fibre volume fraction v at three different fibre aspect ratios (l/d). For $l/d = 100$, the self-consistent model predicts that the short fibres behave like continuous fibres and the rule-of-mixtures is approximately valid. This is because the Young's modulus of SFRP composites would approach a plateau level as the fibre aspect ratio increases for the case of $l/d \geq 100$ (Fu and Lauke, 1998c). The predictions of the semi-empirical relation of Halpin–Tsai equation are also presented in Fig. 6.3 for the composite modulus. The discrepancy between the self-consistent model and the Halpin–Tsai equation is most pronounced at intermediate values of aspect ratio.

6.2.4 Dilute model

The purpose of the micromechanics models is to predict the average elastic modulus of the SFRP composites. Subject a representative volume to

surface displacements consistent with a uniform strain, the average stiffness of the composite is the tensor S that maps this uniform strain to the average stress:

$$\sigma_c = S\varepsilon_C. \tag{6.40}$$

The average compliance C is defined in a similar way:

$$\varepsilon_C = C\sigma_c. \tag{6.41}$$

It is clear that $C = S^{-1}$. An important related concept first introduced by Hill (1963) is the idea of strain and stress concentration tensors T_1 and T_2. They are essentially the ratios between the average fibre strain (or stress) and the corresponding average in the composite:

$$\varepsilon_F = T_1\varepsilon_C \tag{6.42}$$

$$\sigma_F = T_2\sigma_c. \tag{6.43}$$

T_1 and T_2 are fourth-order tensors and they must be found from a solution of the microscopic stress or strain fields. The average composite stiffness can be cast in terms of the strain concentration tensor T_1 and the fibre and matrix properties (Hill, 1963; Tucker III and Liang, 1999):

$$S = S^m + v\left(S^f - S^m\right)T_1. \tag{6.44}$$

The dual equation for the compliance is:

$$C = C^m + v\left(C^f - C^m\right)T_2. \tag{6.45}$$

Eshelby solved the problem for the elastic stress field in and around an ellipsoidal particle in an infinite matrix (Eshelby, 1957, 1961). By letting the particle be a prolate ellipsoid of revolution, Eshelby's result can be used to model the stress and strain fields around a cylinder fibre. Consider an infinite solid body with stiffness S^m that is initially stress-free. A particular small region of the body is called the inclusion and the rest of the body is called the matrix as shown in Fig. 6.4. Suppose the inclusion undergoes some type of transformation which would acquire a uniform strain ε^T (called the transformation strain or the eigen-strain) with no surface traction or stress. The inclusion is bonded to the matrix, so when the transformation occurs, the whole body develops some complicated strain field $\varepsilon^C(x)$ relative to its shape. The stress within the matrix is simply the stiffness times this strain:

$$\sigma^m(x) = S^m\varepsilon^C(x). \tag{6.46}$$

But the transformation strain within the inclusion does not contribute to the stress, so the inclusion stress can be expressed by:

$$\sigma^I = S^m(\varepsilon^C - \varepsilon^T). \tag{6.47}$$

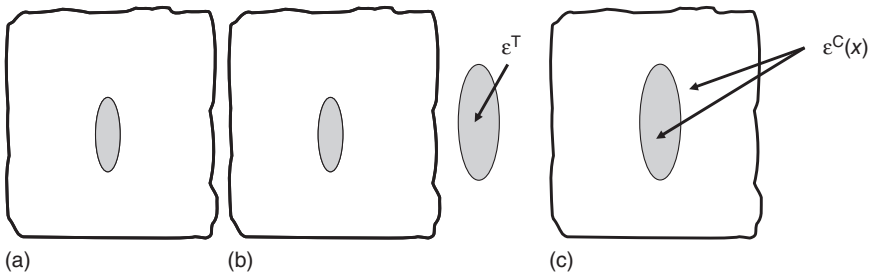

6.4 Eshelby's inclusion problem. Starting from the stress-free state (a), the inclusion undergoes a stress-free transformation strain ε^{T}(b). Fitting the inclusion and matrix back together (c) produces the strain $\varepsilon^{C}(x)$ in both the inclusion and the matrix. Adapted from Tucker III and Liang (1999).

The strain within the ellipsoidal inclusion is uniform and is related to the transformation strain by:

$$\varepsilon^{C} = E^{T}\varepsilon^{T}. \tag{6.48}$$

E^{T} is called Eshelby's tensor and depends only on the inclusion aspect ratio and the matrix elastic constants.

Recall from eqn [6.44], to obtain the stiffness we only have to find the strain concentration tensor T_1. For a dilute composite the average strain is identical to the applied strain:

$$\varepsilon_{C} = \varepsilon^{A}. \tag{6.49}$$

From Eshelby, the fibre strain is uniform and is given by the following equation:

$$\varepsilon_{F} = \varepsilon^{A} + \varepsilon^{C}. \tag{6.50}$$

Finally, the following equation is obtained:

$$\left[\mathbf{I} + E^{T}C^{m}\left(S^{f} - S^{m}\right)\right]\varepsilon_{F} = \varepsilon_{C}, \tag{6.51}$$

where the symbol $\mathbf{I}$ represents the fourth-order unit tensor. Comparing this to eqn [6.42] shows that the strain concentration tensor for Eshelby's equivalent inclusion is:

$$T^{1}_{\text{Eshelby}} = \left[\mathbf{I} + E^{T}C^{m}\left(S^{f} - S^{m}\right)\right]^{-1}. \tag{6.52}$$

This can be used in eqn [6.44] to predict the modulus of unidirectional SFRP composites. Calculations using the dilute Eshelby model to explore the effect of filler aspect ratio on stiffness are presented by Chow (1977). Modulus predictions based on eqs [6.44] and [6.52] should be accurate only at low volume fractions, say up to v = 1%. Therefore, the dilute Eshelby

model is not very practical since in many applications, fibre content much higher than 1% is usually employed.

6.2.5 Model for transverse modulus

A model to determine the transverse modulus (E_{cy}) of SFRP composites was developed by Fu *et al.* (1998) and is provided below.

The case of continuous fibres will be studied first. Consider a rectangular specimen with lengths c_1, c_2 and c_3 and the c_3 axis is parallel to the fibre axis or the x-axis, as shown in Fig. 6.5 (Fu *et al.*, 1998). It is further assumed that the fibres in the unidirectional fibre composite are distributed uniformly in the matrix and the fibre–matrix interfacial adhesion is perfect. As long as the fibre–matrix interfacial adhesion is good enough, the interfacial adhesion has little influence on the transverse composite modulus since E_{cy} is a property of material at low strain.

For both square and hexagonal arrangements of fibres, a representative volume element can be chosen as shown in Fig. 6.5, which can be divided into three regions: I, II and III along the x-z plane. In regions I and III, the matrix alone bears the load and hence the mean matrix strain ε_{My} is approximately equal to:

$$\varepsilon_{My} = \sigma_y / E_m, \tag{6.53}$$

where σ_y is the applied stress in the y-direction.

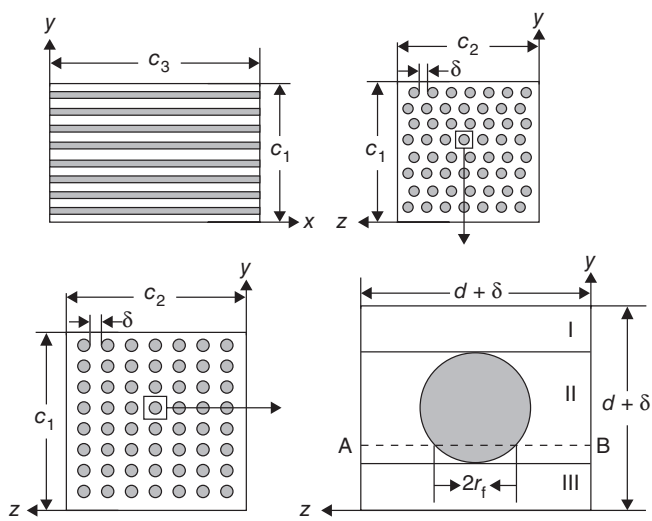

6.5 Schematic drawing of a continuous fibre composite and a corresponding simple representative volume element. A perfect bond is assumed between fibres and matrix. Adapted from Fu *et al.* (1998).

In any given cross section ABB′A′ of region II parallel to the *x*-*z* plane (where the line A′B′ not shown in Fig. 6.5 is parallel with the line AB), the stress equilibrium condition can be written as:

$$\frac{2r_{\mathrm{fi}}}{d+\delta}\sigma_{\mathrm{fy}}+\frac{d+\delta-2r_{\mathrm{fi}}}{d+\delta}\sigma_{\mathrm{my}}=\sigma_{\mathrm{y}}, \tag{6.54}$$

where σ_{fy} and σ_{my} are the transverse fibre stress and the transverse matrix stress, respectively, δ the inter-fibre spacing and $2r_{\mathrm{fi}}$ the string length of the fibre cross section intersecting with the cross section ABB′A′.

In region II, the matrix and fibre bear the applied load. In the given cross section ABB′A′, the matrix strain must be identical to the fibre strain since the fibre–matrix interface is assumed to be perfect, i.e., the fibre is completely bonded with the matrix. Thus, eqn [6.54] becomes:

$$\frac{2r_{\mathrm{fi}}}{d+\delta}E_{\mathrm{fy}}\varepsilon_{\mathrm{fy}}+\frac{d+\delta-2r_{\mathrm{fi}}}{d+\delta}E_{\mathrm{m}}\varepsilon_{\mathrm{fy}}=\sigma_{\mathrm{y}}, \tag{6.55}$$

where E_{fy} is the transverse fibre modulus, $\varepsilon_{\mathrm{fy}}$ and $\varepsilon_{\mathrm{my}}$ are the transverse fibre and matrix strain, respectively.

Now we can estimate the mean transverse fibre strain $\varepsilon_{\mathrm{Fy}}$. The mean value ($\overline{r}_{\mathrm{fi}}$) of r_{fi} is first evaluated by assuming that the fibre diameter is uniformly divided into n segments and n is very large, the length of each segment is then equal to $2r_{\mathrm{f}}/n$. Thus, we have,

$$\frac{2r_{\mathrm{f}}}{n}\sum_{i=1}^{n}2r_{\mathrm{fi}}=\pi r_{\mathrm{f}}^{2} \tag{6.56}$$

and

$$\overline{r}_{\mathrm{fi}}=\frac{\sum_{i=1}^{n}r_{\mathrm{fi}}}{n}=\frac{\pi}{4}r_{\mathrm{f}}. \tag{6.57}$$

Replacing r_{fi} with $\overline{r}_{\mathrm{fi}}$ and $\varepsilon_{\mathrm{fy}}$ with $\varepsilon_{\mathrm{Fy}}$ in eqn [6.55] gives:

$$\frac{2\overline{r}_{\mathrm{fi}}}{d+\delta}E_{\mathrm{fy}}\varepsilon_{\mathrm{Fy}}+\frac{d+\delta-2\overline{r}_{\mathrm{fi}}}{d+\delta}E_{\mathrm{m}}\varepsilon_{\mathrm{Fy}}=\sigma_{\mathrm{y}}. \tag{6.58}$$

In addition, it is imagined that $c_1 = m_1(d + \delta)$ and $c_2 = m_2(d + \delta)$, where m_1 and m_2 are integers. Thus, there are $m_1 \times m_2$ representative volume elements in the composite. The fibre volume fraction can be obtained as:

$$v=\frac{\pi r_{\mathrm{f}}^{2}}{(d+\delta)^{2}}. \tag{6.59}$$

Equations [6.57–6.59] can be combined to give the mean transverse fibre strain:

$$\varepsilon_{\mathrm{Fy}} = \frac{\sigma_{\mathrm{y}}}{\sqrt{\frac{\pi v}{4}}E_{\mathrm{fy}} + \left(1 - \sqrt{\frac{\pi v}{4}}\right)E_{\mathrm{m}}}. \tag{6.60}$$

Therefore, the composite strain $\varepsilon_{\mathrm{cy}}$ is given by:

$$\begin{aligned}\varepsilon_{\mathrm{cy}} &= v_{\mathrm{II}}\varepsilon_{\mathrm{Fy}} + \left(v_{\mathrm{I}} + v_{\mathrm{III}}\right)\varepsilon_{\mathrm{My}} \\ &= \frac{d}{d+\delta}\varepsilon_{\mathrm{Fy}} + \frac{\delta}{d+\delta}\varepsilon_{\mathrm{My}},\end{aligned} \tag{6.61}$$

where v_{I}, v_{II} and v_{III} are the volume fractions of regions I, II and III in the whole representative element, respectively. Consequently, by inserting eqns [6.53], [6.59] and [6.60] into eqn [6.61], we can obtain:

$$\varepsilon_{\mathrm{cy}} = \sqrt{\frac{4v}{\pi}}\frac{\sigma_{\mathrm{y}}}{\sqrt{\frac{\pi v}{4}}E_{\mathrm{fy}} + \left(1 - \sqrt{\frac{\pi v}{4}}\right)E_{\mathrm{m}}} + \left(1 - \sqrt{\frac{4v}{\pi}}\right)\frac{\sigma_{\mathrm{y}}}{E_{\mathrm{m}}}. \tag{6.62}$$

Since $\varepsilon_{\mathrm{cy}} = \sigma_{\mathrm{y}}/E_{\mathrm{cy}}$, the transverse composite modulus E_{cy} follows immediately from eqn [6.62]:

$$\frac{1}{E_{\mathrm{cy}}} = \frac{\sqrt{4v/\pi}}{\sqrt{\pi v/4}E_{\mathrm{fy}} + \left(1 - \sqrt{\pi v/4}\right)E_{\mathrm{m}}} + \frac{\left(1 - \sqrt{4v/\pi}\right)}{E_{\mathrm{m}}}. \tag{6.63}$$

Equation [6.63] gives the transverse modulus of unidirectional continuous fibre composites. An expression for the transverse modulus of discontinuous fibre composites can now be developed in the following.

Assume that short fibres of a length l are distributed uniformly in the SFRP composite, and the inter-fibre spacing is δ and the gap between two fibre ends is l_1. A representative volume element is arbitrarily chosen as shown in Fig. 6.6. The fibre volume fraction is then given by:

$$v = \frac{\pi r_{\mathrm{f}}^2 l}{\left(2r_{\mathrm{f}} + \delta\right)^2\left(l + l_1\right)} = \frac{\pi}{4\left(1 + \delta/d\right)^2\left(1 + l_1/l\right)}. \tag{6.64}$$

Using the same treatment as for the case of continuous fibres, we divide the cross section of the element into three regions parallel to the x-z plane as shown in Fig. 6.6. In regions I and III, the matrix bears the load alone, then the mean matrix strain is the same as that in eqn [6.53].

In region II, both the fibre and the matrix bear the load and their strains in this region should be approximately the same. The stress equilibrium equation in the cross section parallel to the x-z plane denoted by the dotted line can be written as follows:

$$\frac{2r_{\mathrm{fi}}l}{(d+\delta)(l+l_1)}E_{\mathrm{fy}}\varepsilon_{\mathrm{fy}} + \left[1 - \frac{2r_{\mathrm{fi}}l}{(d+\delta)(l+l_1)}\right]E_{\mathrm{m}}\varepsilon_{\mathrm{fy}} = \sigma_{\mathrm{y}}. \tag{6.65}$$

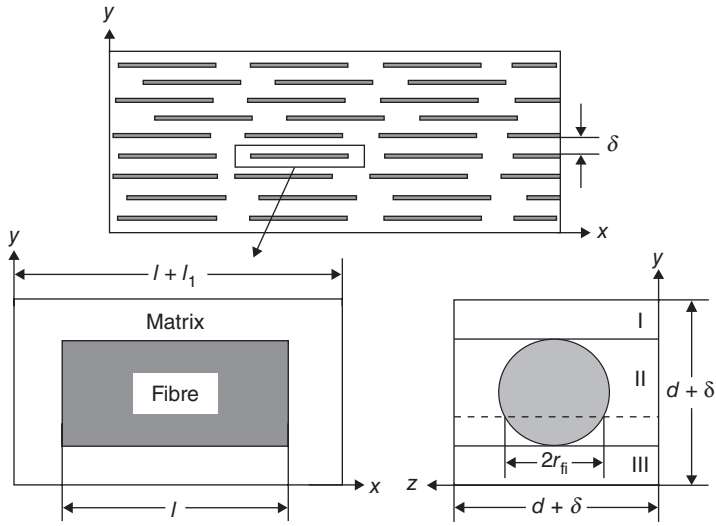

6.6 Schematic drawing of an aligned discontinuous fibre composite and a corresponding simple representative volume element. A perfect bond is assumed between fibres and matrix. Adapted from Fu *et al.* (1998).

By replacing $2r_{\mathrm{fi}}$ with $2\bar{r}_{\mathrm{fi}}$ and $\varepsilon_{\mathrm{fy}}$ with $\bar{\varepsilon}_{\mathrm{fy}}$ in eqn [6.65] and combining with eqn [6.64], then the mean transverse fibre strain is obtained as:

$$\varepsilon_{\mathrm{Fy}} = \frac{\sigma_y}{\sqrt{\frac{\pi v}{4(1+l_1/l)}}E_{\mathrm{fy}} + \left(1-\sqrt{\frac{\pi v}{4(1+l_1/l)}}\right)E_{\mathrm{m}}}. \qquad 6.66$$

The composite strain is then given by:

$$\varepsilon_{\mathrm{cy}} = \frac{d}{d+\delta}\varepsilon_{\mathrm{Fy}} + \frac{\delta}{d+\delta}\varepsilon_{\mathrm{My}}. \qquad 6.67$$

By inserting eqns [6.53], [6.64] and [6.66] into eqn [6.67] and using the relationship: $\varepsilon_{\mathrm{cy}} = \sigma_{\mathrm{y}}/E_{\mathrm{cy}}$, we have:

$$\frac{1}{E_{\mathrm{cy}}} = \frac{\sqrt{4v(1+l_1/l)/\pi}}{\sqrt{\pi v/\left[4(1+l_1/l)\right]}E_{\mathrm{fy}} + \left(1-\sqrt{\pi v/\left[4(1+l_1/l)\right]}\right)E_{\mathrm{m}}} + \frac{\left(1-\sqrt{4v(1+l_1/l)/\pi}\right)}{E_{\mathrm{m}}}. \qquad 6.68$$

Equation [6.68] can be used for the prediction of the transverse modulus of SFRP composites. In the limit of $l_1/l = 0$, the transverse modulus of discontinuous fibre composites becomes independent of the fibre length (or

fibre aspect ratio) and eqn [6.68] reduces to eqn [6.63] for a continuous fibre reinforced composite. In practice, short fibres are randomly distributed in SFRP composites and the limiting case will not appear. And l_1 can be obtained from eqn [6.64] as a function of fibre volume fraction, fibre length and diameter if δ is known or vice versa.

6.2.6 The rule of mixtures equations for the transverse modulus

The rule of mixtures (RoM) (see eqn [6.1]) has been proposed for the prediction of the longitudinal Young's modulus of unidirectional continuous fibre reinforced polymers. In parallel, the inverse rule of mixtures (iRoM) equation has also been developed for approximate prediction of the transverse modulus of unidirectional continuous fibre composites and is given by (Tsai and Hahn, 1980; Piggott, 1980):

$$\frac{1}{E_{cy}} = \frac{v}{E_{fy}} + \frac{v_m}{E_m}. \tag{6.69}$$

In addition, the modified RoM equation (eqn [6.19]: $E_c = \lambda E_f v + E_m(1 - v)$) has also been proposed for prediction of the longitudinal Young's modulus of unidirectional SFRP composites. Similarly, the modified iRoM (miRoM) equation below has also been used to predict the transverse modulus of unidirectional short fibre composites (Tsai and Hahn, 1980):

$$\frac{1}{E_{cy}} = \frac{v}{E_{fy}} + \frac{v_m}{E_m} - vv_m \frac{v^2 E_m / E_{fy} + v_m^2 E_{fy} / E_m - 2vv_m}{vE_{fy} + v_m E_m}. \tag{6.70}$$

In eqns [6.69] and [6.70], the subscript y is used to denote the transverse modulus of fibres in case the fibre is transversely isotropic.

We now compare predictions using the Halpin–Tsai equation, iROM equation, miRoM and Fu *et al.* model with known experimental results in Table 6.1. For the case of short fibres, $l_1/l = 0.02$ is used. The theoretical values of the transverse modulus (assuming $l_1 = \delta$ and $l = d = 10\,\mu$m) are also given in order to compare the model with experiments for particulate composites. Table 6.1 shows that the theoretical results agree well with experimental data for the two cases of continuous and discontinuous fibres. For the particulate composite, predicted values of transverse modulus are also fairly close to the test data. Results predicted with Halpin–Tsai's equation [6.22] are consistent with but lower than the experimental data. However, iRoM and miRoM (eqns [6.69] and [6.70]) give much lower predicted values of the transverse composite modulus than experiments.

Table 6.1 Comparisons of different models and experimental results for transverse moduli of some glass/epoxy composites (Kardos, 1991)

Material	E_m (GPa)	v	Transverse modulus, E_{cy} (GPa)				
			Experimental results	Halpin–Tsai equation	iRoM equation	miRoM equation	Fu *et al.* model
Glass bead/ epoxy	2.1	0.5	10.3	—	—	—	11.56
	2.8	0.5	11.7	—	—	—	14.33
Short glass fibre/ epoxy	2.1	0.5	9.6	7.44	4.08	4.59	9.09
Continuous glass fibre/ epoxy	2.1	0.6	12.4	9.82	5.03	5.66	12.95
	2.8	0.6	14.5	12.48	6.62	7.41	16.07

6.3 Elastic modulus of partially aligned short fibre reinforced composites

In SFRP composites, it is desirable to orientate the fibres for enhanced mechanical properties such as strength and modulus. However, it is usually difficult, if not impossible, to perfectly align short fibres in an injection moulded SFRP composite. Partial short fibre alignment is typical in injection moulded SFRP composites. Several approaches have been adopted for the prediction of elastic modulus of partially aligned SFRP composites.

6.3.1 The laminate analogy approach

In general, the laminate analogy approach (LAA) is considered to be applicable to the evaluation of elastic modulus of SFRP composites with planar fibre orientation distributions because such short fibre composites can be simulated as a sequential stack of various laminae with different planar fibre orientation and different fibre length. However, in practice, there usually exist spatial fibre orientation distributions in the final injection moulded SFRP composites (Xia *et al.*, 1995; Toll and Andersson, 1991; Haddout and Villoutreix, 1994; McGrath and Wille, 1995; Fu and Lauke, 1997a,b). Therefore, a spatial fibre orientation distribution should be considered for injection moulded SFRP composites. Consequently, it appears to be inappropriate to use the laminate analogy approach to evaluate the

elastic modulus of SFRP composites with a 3D spatial fibre orientation distribution, since the requirement of planar fibre orientation distribution for the laminate analogy approach cannot be satisfied. Conversely, it is noticed from the paper physics approach (Jayaraman and Kortschot, 1996) that the elastic modulus of SFRP composites is only dependent on the angle θ fibres make with the direction in which the composite elastic modulus is to be evaluated as shown in Fig. 6.7 (the modulus in the '1' direction is to be evaluated). That is, the composite elastic modulus for the case of a spatial fibre orientation distribution $g(\theta, \phi)$ [$g(\theta, \phi) = g(\theta)g(\phi)/\sin(\theta)$, where $g(\phi)$ is defined as the fibre orientation probability density function for the angle ϕ] is the same as that for the case of a planar orientation distribution $g(\theta)$, when $g(\theta)$ is the same for the two cases and no matter how the fibre

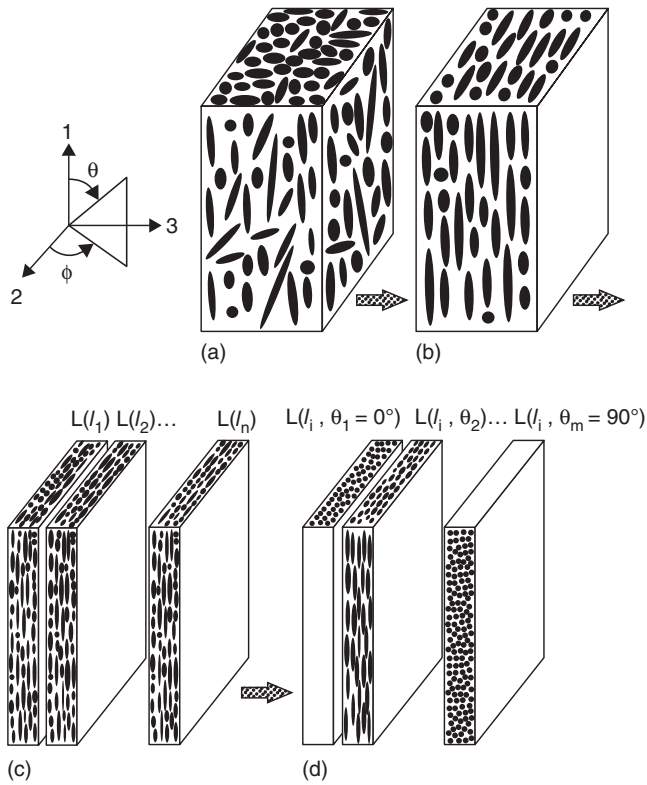

6.7 Simulated progress of the laminated plate model of a 3D misaligned SFRP composite: (a) the real 3D SFRP, (b) the imagined SFRP composite, (c) the imagined SFRP composite is considered as a combination of laminates, each laminate having the same fibre length and (d) each laminate is treated as a stacked sequence of laminae, each lamina having the same fibre length and the same fibre orientation. Adapted from Fu and Lauke (1998c).

orientation distribution $g(\phi)$ is (Fu and Lauke, 1998c). This is a very useful idea since we can replace the real SFRP composite with a spatial fibre orientation distribution $g(\theta, \phi)$ by an imagined short fibre composite with only a planar fibre orientation distribution $g(\theta)$ in order to evaluate the elastic modulus of the real SFRP composite.

The simulated progress of a laminated plate model of a 3D misaligned SFRP composite is shown in Fig. 6.7. A SFRP composite with a 3D spatial fibre orientation distribution function $g(\theta, \phi)$ [$= g(\theta)g(\phi)/\sin\theta$] having fibre end cross sections in the three visible planes (see Fig. 6.7(a)) is first replaced by an imagined SFRP composite with the same $g(\theta)$ but $\phi = 0$ having no fibre end cross sections in the 1-2 plane or having no fibres of out-of-planar direction (the 3-axis direction is out-of-planar) (see Fig. 6.7(b)). Hence, according to fibre length distributions, the imagined SFRP composite is regarded as a combination of laminates, each laminate is comprised of fibres having the same fibre length (see Fig. 6.7(c)). In Fig. 6.7(c), '$\mathrm{L}(l_i)$, $i = 1, 2, \ldots n$' denotes the ith laminate containing fibres of the same length l_i. Each laminate with the same fibre length is then treated as a stacked sequence of the laminae, each lamina consists of fibres having the same fibre length and the same fibre orientation (see Fig. 6.7(d)). In Fig. 6.7(d), '$\mathrm{L}(l_i, \theta_j)$, $j = 1, 2, \ldots m$' denotes the jth lamina containing the fibres having the same length l_i and the same angle θ_j. The elastic modulus of the imagined SFRP composite will be evaluated first, the elastic modulus of the real SFRP can then be obtained as stated above.

Now, the imagined SFRP composite is considered which only has a planar fibre orientation distribution $g(\theta)$ (ϕ = constant, for example 0), and which is assumed as a stack of plies. The fibres of length between l and $l + \mathrm{d}l$ and orientation between θ and $\theta + \mathrm{d}\theta$ are imagined to be included in the same ply. First, the stiffness constants for each ply are given by the laminate theory. Second, the stiffness constants for each ply are integrated through the thickness of the laminate to obtain the overall stiffness constants of the simulated laminate. Third, the elastic modulus of the imagined composite can be obtained from the relation between the stiffness constants and the elastic modulus. Finally, the elastic modulus of the real SFRP composite with a spatial fibre orientation distribution can be obtained directly from the elastic modulus of the imagined SFRP composite. The laminate analogy approach is sometimes called the 'Fu–Lauke model' (Thomason, 2008).

For unidirectional short fibre composites, the longitudinal elastic modulus can be obtained from the Cox shear lag model (eqn [6.19]: $E_c = \lambda E_f v + E_m(1 - v)$). The transverse modulus and the in-plane shear modulus, E_{22} and G_{12}, are almost independent of fibre aspect ratio and can be evaluated using Halpin–Tsai equations [6.22] and [6.25]. The longitudinal Poisson's ratio, ν_{12}, which is not sensitive to fibre length, can be estimated using the rule-of-mixtures equation [6.23]. The transverse Poisson's ratio, ν_{21}, is given

by eqn [6.24]. Then, we can calculate the components of the stiffness matrix Q_{ij} that relates the stress to the strain for the uniaxial ply when the principal stress directions are aligned with the principal fibre directions. That is,

$$\begin{Bmatrix}\sigma_1\\ \sigma_2\\ \tau_{12}\end{Bmatrix}=\begin{Bmatrix}Q_{11} & Q_{12} & Q_{16}\\ Q_{12} & Q_{22} & Q_{26}\\ Q_{16} & Q_{26} & Q_{66}\end{Bmatrix}\begin{Bmatrix}\varepsilon_1\\ \varepsilon_2\\ \gamma_{12}\end{Bmatrix}, \tag{6.71}$$

where

$$Q_{11}=E_{11}/(1-\nu_{12}\nu_{21}) \tag{6.72}$$

$$Q_{12}=\nu_{21}Q_{11} \tag{6.73}$$

$$Q_{16}=0 \tag{6.74}$$

$$Q_{22}=E_{22}/(1-\nu_{12}\nu_{21}) \tag{6.75}$$

$$Q_{26}=0 \tag{6.76}$$

$$Q_{66}=G_{12}. \tag{6.77}$$

The stress–strain relation in the off-axis system is given by:

$$\begin{Bmatrix}\sigma_1'\\ \sigma_2'\\ \tau_{12}'\end{Bmatrix}=\begin{Bmatrix}Q_{11}' & Q_{12}' & Q_{16}'\\ Q_{12}' & Q_{22}' & Q_{26}'\\ Q_{16}' & Q_{26}' & Q_{66}'\end{Bmatrix}\begin{Bmatrix}\varepsilon_1'\\ \varepsilon_2'\\ \gamma_{12}'\end{Bmatrix}. \tag{6.78}$$

The transformation equation between the components of stiffness matrix in the on-axis system and that in the off-axis system is:

$$\begin{Bmatrix}Q_{11}'\\ Q_{22}'\\ Q_{12}'\\ Q_{66}'\\ Q_{16}'\\ Q_{26}'\end{Bmatrix}=\begin{Bmatrix}m^4 & n^4 & 2m^2n^2 & 4m^2n^2\\ n^4 & m^4 & 2m^2n^2 & 4m^2n^2\\ m^2n^2 & m^2n^2 & m^4+n^4 & -4m^2n^2\\ m^2n^2 & m^2n^2 & -2m^2n^2 & (m^2-n^2)^2\\ m^3n & -mn^3 & mn^3-m^3n & 2(mn^3-m^3n)\\ mn^3 & -m^3n & m^3n-mn^3 & 2(m^3n-mn^3)\end{Bmatrix}\begin{Bmatrix}Q_{11}\\ Q_{22}\\ Q_{12}\\ Q_{66}\end{Bmatrix}, \tag{6.79}$$

where $m=\cos\theta$ and $n=\sin\theta$.

The transformed stiffness constants, Q_{ij}', are integrated through the thickness of the laminate to obtain the overall laminate stiffness matrix, $\bar{A}_{ij}$:

$$\bar{A}_{ij}=\sum_{k=1}^{M}Q_{ij}'h_k, \tag{6.80}$$

where M represents the number of plies in the laminate; k is the serial index of the ply in the laminate; and h_k is thickness fraction of the kth ply. Since the imagined SFRP composite has a continuous fibre orientation

distribution and a continuous fibre length distribution, then, as described above, the kth ply can be considered to contain fibres of length between l and $l + \mathrm{d}l$ and orientation between θ and $\theta + \mathrm{d}\theta$. Thus, the summation in eqn [6.80] must be replaced by the corresponding integral:

$$\bar{A}_{ij} = \int_{l_{min}}^{l_{max}} \int_{\theta min}^{\theta_{max}} Q'_{ij} f(l) g(\theta) \mathrm{d}l \mathrm{d}\theta, \qquad 6.81$$

where $0 \leq l_{min} \leq l \leq l_{max} < \infty$ and $0 \leq \theta_{min} \leq \theta \leq \theta_{max} \leq \pi/2$. The engineering tensile stiffness is obtained from the laminate stiffness components:

$$\bar{E}_{11} = \frac{\bar{A}_{11}\bar{A}_{22} - \bar{A}_{12}^2}{\bar{A}_{22}} \qquad 6.82$$

$$\bar{E}_{22} = \frac{\bar{A}_{11}\bar{A}_{22} - \bar{A}_{12}^2}{\bar{A}_{11}} \qquad 6.83$$

$$\bar{G}_{12} = \bar{A}_{66} \qquad 6.84$$

$$\bar{v}_{12} = \bar{E}_{11} \frac{\bar{A}_{12}}{\bar{A}_{11}\bar{A}_{22} - \bar{A}_{12}^2} = \frac{\bar{A}_{12}}{\bar{A}_{22}}. \qquad 6.85$$

$\bar{E}_{11}$ in eqn [6.82] is not only the elastic modulus of the imagined SFRP composite with a planar fibre orientation distribution $g(\theta)$, but also that of the real SFRP composite with a 3D spatial fibre orientation distribution $g(\theta, \phi)$ and $g(\theta)$ is the same as that of the imagined SFRP composite, while other expressions for $\bar{E}_{22}$, $\bar{G}_{12}$ and $\bar{v}_{12}$ hold true only for the imagined SFRP composite with a planar fibre orientation distribution.

Xia *et al.* (1995) used the laminate analogy approach to derive the expression for the elastic modulus of SFRP composites by considering a spatial fibre orientation distribution; however, the length of the fibres in the core layer was projected onto one plane so that the fibre length is reduced by the projection, hence the elastic modulus of SFRP is underestimated. Also, other researchers (Chin *et al.*, 1988; Choy *et al.*, 1992; Sirkis *et al.*, 1994; Yu *et al.*, 1994) used the laminate analogy approach to derive the elastic modulus of SFRP composites but only considered the case of planar fibre orientation distribution which is rarely true in reality for the injection moulded SFRP composites. Moreover, none of them presented a detailed study on the effects of the fibre length distribution and fibre orientation distribution on the elastic modulus of SFRP composites. Equation [6.82], suitable for cases of both 2D and 3D fibre orientation distributions, and eqns [6.83]–[6.85], suitable for the case of 2D fibre orientation distribution, can be used to evaluate engineering stiffness taking into account effects of fibre length and orientation distributions.

The elastic modulus of SFRP composites with a fibre length distribution $f(l)$ and a fibre orientation distribution $g(\theta)$ can be discussed in terms of

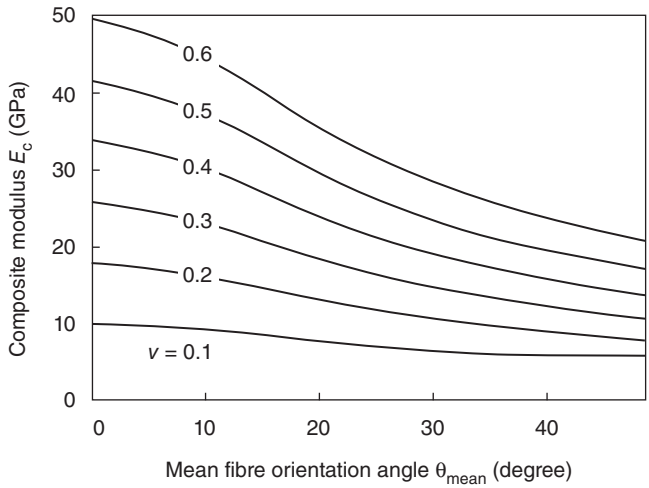

6.8 The elastic modulus of the SFRP composites predicted by the Fu and Lauke model for different fibre orientation distributions and various fibre volume fractions. Adapted from Fu and Lauke (1998c).

eqn [6.82]. The following parametric data are used: E_f = 82.7 GPa, G_f = 27.6 GPa, ν_f = 0.22, E_m = 2.18 GPa, G_m = 1.03 GPa, ν_m = 0.35, d = 10 μm, v = 0.3, l = 3.198 mm (a = 0.15 and b = 1.5). The predicted results of the elastic modulus of SFRP composites as a function of mean fibre orientation angle are shown in Fig. 6.8 for various v. The fibre orientation distributions are given by setting p = 0.6 and various q. Figure 6.8 shows that both the fibre volume fraction and mean fibre orientation angle have a significant effect on the longitudinal elastic modulus of SFRP composites. A higher fibre volume fraction corresponds to a higher elastic modulus. The composite elastic modulus decreases slowly with increasing mean fibre orientation angle when the fibre volume fraction is small (e.g., v = 10%); but it decreases dramatically with the increase of mean fibre orientation angle when the fibre volume fraction is large (e.g., v = 50%).

Figure 6.9 shows the effect of mean aspect ratio on the elastic modulus of SFRP composites, where other parameters except the mean fibre orientation angle which equals 9.46° are the same as in Fig. 6.8. When the mean fibre aspect ratio is small (e.g., <90), the composite elastic modulus increases with the mean fibre length or aspect ratio. However, when the mean fibre length is large (e.g., >1.0 mm and the corresponding aspect ratio is >100), the mean fibre length or aspect ratio has nearly no influence on the elastic modulus of SFRP composites (Fu and Lauke, 1998c). It is necessary to clarify that the composite modulus is dependent on aspect ratio but independent of fibre diameter if the aspect ratio is the same. This has been verified by experiments (Ramsteiner and Theysohn, 1985).

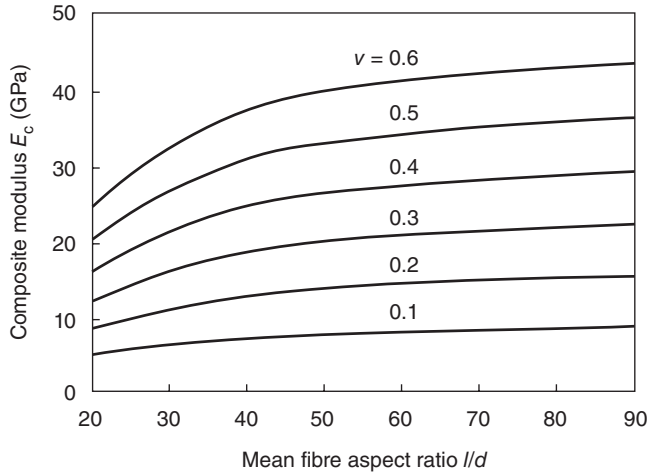

6.9 Effect of mean fibre aspect ratio (a = 5 and various b, see eqn [3.9]) on the elastic modulus of SFRP composites. Adapted from Fu and Lauke (1998c).

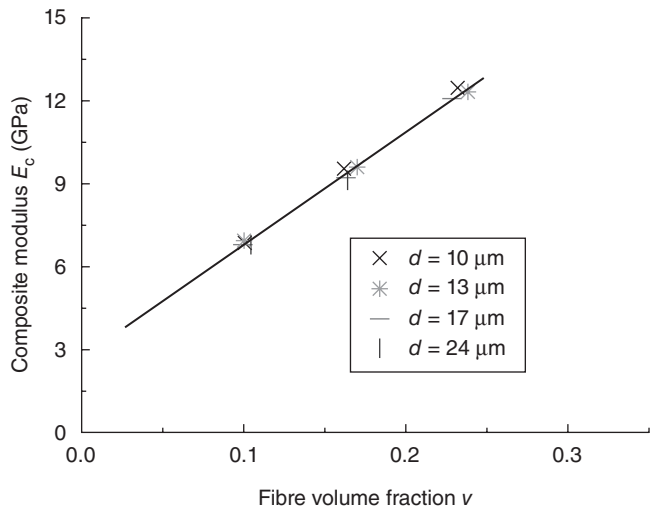

6.10 Young's modulus of short glass fibre reinforced polyamide (d = fibre diameter). Adapted from Ramsteiner and Theysohn (1985).

The Young's modulus of short glass fibre reinforced polyamide composites as a function of fibre volume fraction for different fibre diameters is shown in Fig. 6.10 (Ramsteiner and Theysohn, 1985). Clearly, the diameter of the fibres does not play an important role in determining the Young's modulus as long as the fibre aspect ratio is not too much different. The results for the aspect ratios of fibres with four different diameters show that

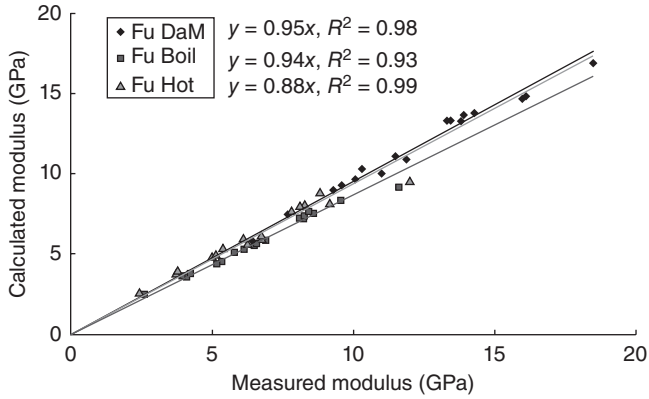

6.11 Comparison of Fu–Lauke model predictions against experimental values (Thomason, 2008).

with increasing fibre content, the fibres become shorter as a consequence of the enhanced mutual attrition of the fibres during processing. The aspect ratios for the four fibre diameters exhibit similar values at a specific fibre content. This indicates that the Young's modulus of SFRP composites is determined mainly by the fibre aspect ratio rather than the fibre diameter. This is consistent with the predictions by the models stated above.

Results for prediction of composite modulus using Fu–Lauke's model are compared with experimental data in Fig. 6.11 (Thomason, 2008). It can be seen that this model gives predicted values that show good linear correlation with experimental data. It is noted that in all cases the model appears to underestimate the measured composite modulus; however, the differences are within the range of experimental errors on various input values (Thomason, 2008). Thus, the Fu–Lauke approach is a most robust model for the prediction of elastic modulus of SFRP composites.

Further, the effect of fibre packing arrangement on the elastic modulus of SFRP composites is also investigated and the results show that the fibre packing arrangement (see eqns [6.13] and [6.15]) has nearly no influence on the composite elastic modulus (Fu and Lauke, 1998c).

6.3.2 Paper physics approach

The paper physics approach (PPA) (Jayaraman and Kortschot, 1996) has also been developed for prediction of the elastic modulus of SFRP composites. The PPA analysis is based on the elasticity solution of load transfer between fibre and matrix in a single short fibre model and the assumption of negligible interactions between neighbouring fibres. In the PPA analysis, the plane stress condition is adopted. According to the PPA, the elastic

modulus of short fibre composites can be expressed in the modified rule of mixtures:

$$\bar{E}_{11} = \lambda_1 \lambda_2 E_f v + E_m v_m, \tag{6.86}$$

where λ_1 and λ_2 are respectively the fibre length and orientation factors for the composite elastic modulus and their expressions are given as follows:

$$\lambda_1 = \frac{1}{l_{mean}} \int_{l_{min}}^{l_{max}} \left[1 - \frac{\tanh(\eta l/2)}{\eta l/2} \right] l f(l) \, dl \tag{6.87}$$

$$\lambda_2 = \int_{\theta_{min}}^{\theta_{max}} \left[(\cos\theta)^2 - v_{12} (\sin\theta)^2 \right] (\cos\theta)^2 \, g(\theta) \, d\theta, \tag{6.88}$$

where $0 \le l_{min} \le l \le l_{max} < \infty$ and $0 \le \theta_{min} \le \theta \le \theta_{max} \le \pi/2$.

Comparison of theoretical results of elastic moduli of SFRP composites using the laminate analogy approach (LAA) (Fu and Lauke, 1998c) and paper physics approach (PPA) (Jayaraman and Kortschot, 1996) is given in Fig. 6.12 for cases of mean fibre orientation angle varying from 0 to 48.5°, where the values of the parameters are the same as those in Fig. 6.8. The elastic moduli predicted by the PPA are slightly higher than those by the LAA and the difference depends on the fibre volume fraction when the mean fibre orientation angle is small (see Fig. 6.12). At intermediate mean fibre orientation angles the results predicted by the two approaches are very

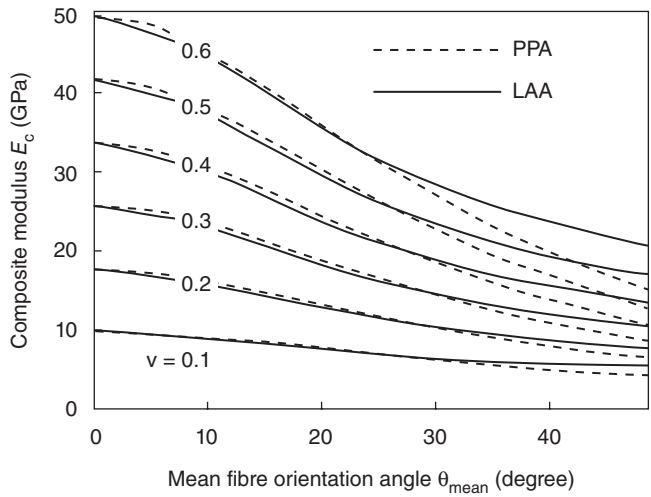

6.12 Comparison of the theoretical results of the elastic modulus of SFRP composites for different fibre orientation (θ) distributions and various fibre volume fractions predicted by the laminate analogy approach (LAA) by the Fu and Lauke model (solid lines) and the paper physics approach (PPA) (broken lines). Adapted from Fu and Lauke (1998c).

close. When the mean fibre orientation angle is large, the results predicted by the PPA are lower than those by the LAA model. This is because for the PPA the angle θ must be less than some critical angle θ_c ($\theta_c = \arcsin\{[1/(1+\nu_{12})]^{1/2}\}$), otherwise the fibres of an orientation angle θ greater than θ_c would make a negative contribution to the stiffness of short fibre composites (see eqn [6.88]). However, the experimental results (Kardos, 1991) show that the transverse stiffness of unidirectional short and long glass fibre reinforced epoxy composites is higher than that of pure epoxy matrix, it can then be concluded that the fibres of $\theta = \pi/2$ should make a positive contribution to the composite elastic modulus since they constrain the deformation of composites. So the argument in the PPA that the fibres of an angle with the applied strain direction greater than θ_c make a negative contribution to the composite elastic modulus is incorrect. And this is also inconsistent with the fact that the off-axis modulus of unidirectional composites is higher than the matrix modulus (Kardos, 1991). Thus, it can be concluded that the contribution of the fibres of any angle with the applied strain direction to the composite modulus is positive. Therefore, the contribution of the fibres of a large angle with the applied strain direction to the composite elastic modulus will be underestimated by the PPA, and hence in cases where the fibre orientation angle between fibre axis direction and the applied strain direction is comparatively large, the paper physics approach would be invalid in predicting the elastic modulus of SFRP composites.

6.4 Anisotropy of modulus of short fibre reinforced polymer (SFRP) composites

Consider a single misaligned fibre of a length l and a pair of orientation angles (θ, ϕ) as defined in Fig. 6.13. For a given direction (Θ, Φ) (see Fig. 6.13), which may be the loading direction in which the elastic modulus of a SFRP is to be measured, we can obtain the angle δ between the fibre axial direction (θ, ϕ) and the given direction (Θ, Φ) from the following equation:

$$\cos\delta = \cos\Theta\cos\theta + \sin\Theta\sin\theta\cos(\phi - \Phi). \qquad 6.89$$

Similar to the derivation for the composite elastic modulus in the mould flow direction ($\Theta = 0, \Phi$) (namely, the 1-axis direction in Fig. 6.13) (Fu and Lauke, 1998c), we can easily derive an expression for the composite elastic modulus in any desired direction (Θ, Φ). The SFRP composite is simulated by a laminate and is assumed as a stack of plies as was done in deriving the expression for the elastic modulus of SFRP composites in the direction ($\Theta = 0, \Phi$) (Fu and Lauke, 1998c). The fibres of length between l and $l + dl$ and a pair of orientation angles between θ and $\theta + d\theta$ and between ϕ

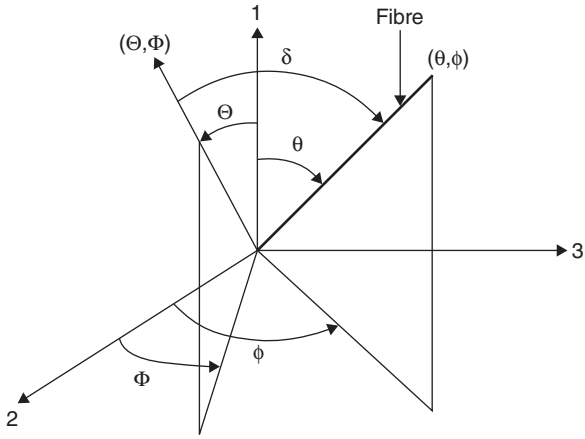

6.13 Definitions of the fibre orientation angles (θ, ϕ) and the loading direction angles (Θ, Φ) in which the composite elastic modulus is measured.

and $\phi + d\phi$ are imagined to be included in the same ply. First, the stiffness constants for each ply are given by the laminate theory. Second, the stiffness constants for each ply are integrated through the thickness of the laminate to obtain the overall stiffness constants of the simulated laminate. Finally, the elastic modulus of SFRP composites is obtained from the relation between the stiffness constants and the elastic modulus of the laminate.

The transformation equation for a uniaxial ply between the components of stiffness matrix in the on-axis system and that in the off-axis system is given by (Tsai and Hahn, 1980):

$$\begin{Bmatrix} Q'_{11} \\ Q'_{22} \\ Q'_{12} \\ Q'_{66} \\ Q'_{16} \\ Q'_{26} \end{Bmatrix} = \begin{Bmatrix} m^4 & n^4 & 2m^2n^2 & 4m^2n^2 \\ n^4 & m^4 & 2m^2n^2 & 4m^2n^2 \\ m^2n^2 & m^2n^2 & m^4+n^4 & -4m^2n^2 \\ m^2n^2 & m^2n^2 & -2m^2n^2 & \left(m^2-n^2\right)^2 \\ m^3n & -mn^3 & mn^3-m^3n & 2\left(mn^3-m^3n\right) \\ mn^3 & -m^3n & m^3n-mn^3 & 2\left(m^3n-mn^3\right) \end{Bmatrix} \begin{Bmatrix} Q_{11} \\ Q_{22} \\ Q_{12} \\ Q_{66} \end{Bmatrix}, \quad 6.90$$

where $m = \cos\delta$ and $n = \sin\delta$. Note that here the definitions of m and n are different from those ($m = \cos\theta$ and $n = \sin\theta$) in the direction ($\Theta = 0$, Φ) (Fu and Lauke, 1998c), because the angle between the fibre axial direction (θ, ϕ) and the direction (Θ, Φ) is now equal to δ. $\{Q_{ij}\}$ ($i, j = 1, 2, 6$) is the stiffness matrix in the on-axis system and Q_{ij} have been defined in eqns [6.72]–[6.77]. $\{Q'_{ij}\}$ ($i, j = 1, 2, 6$) is the stiffness matrix in the off-axis system.

The transformed stiffness constants, Q'_{ij}, are integrated through the thickness of the laminate to obtain the overall laminate stiffness matrix, $\bar{A}_{ij}$:

$$\bar{A}_{ij} = \sum_{k=1}^{M} Q'_{ij} h_k, \tag{6.91}$$

where M represents the number of plies in the laminate; k is the serial index of the ply in the laminate; and h_k is the thickness fraction of the kth ply. Since the SFRP composite has a continuous fibre orientation distribution and a continuous fibre length distribution, then, as described above, the kth ply can be considered to contain the fibres of length between l and $l + dl$ and a pair of orientation angles between θ and $\theta + d\theta$ and between ϕ and $\phi + d\phi$, thus the summation in eqn [6.91] must be replaced by the corresponding integral:

$$\bar{A}_{ij} = \int_{l_{min}}^{l_{max}} \int_{\theta_{min}}^{\theta_{max}} \int_{\phi_{min}}^{\phi_{max}} Q'_{ij} f(l) g(\theta) g(\phi) dl d\theta d\phi. \tag{6.92}$$

Here, $m(= \cos\delta)$ and $n(= \sin\delta)$ in eqn [6.90] can be transformed with eqn [6.89] in the functions containing θ and ϕ. Finally, we can obtain the elastic modulus of SFRP composites in any direction (Θ, Φ) by:

$$E_c(\Theta, \Phi) = \frac{\bar{A}_{11}\bar{A}_{22} - \bar{A}_{12}^2}{\bar{A}_{22}}. \tag{6.93}$$

The variation of the elastic modulus $E_c(\Theta, \Phi)$ of SFRP composites with the direction (Θ, Φ) (namely, the anisotropy of the composite elastic modulus) can be discussed in terms of eqn [6.93] by taking into consideration both the effects of the FLD and FOD.

The following values of the parameters are used: E_f = 82.7 GPa, G_f = 27.6 GPa, ν_f = 0.22, E_m = 2.18 GPa, G_m = 1.03 GPa, ν_m = 0.35, v = 0.20, d = 10 μm, l = 3.198 mm (a = 0.15 and b = 1.5, see eqn [3.9]) and θ_{mean} = 9.46° (p = 0.6 and q = 15). Also, $g(\phi) = 1/(2\pi)$ (namely, $s = t = 0.5$ for the angle distribution function described in Chapter 3, $0 \le \phi \le 2\pi$) is considered at first. The predicted elastic modulus of SFRP composites as a function of both the direction angle Θ and the fibre volume fraction v is shown in Fig. 6.14 for the unidirectional short fibre alignment case (i.e. $p = 0.5$, $q = \infty$ and $\theta_{mean} = 0°$), where the direction angle Φ is of any value. Figure 6.14 shows that the elastic modulus of SFRP composites varies with the direction angle Θ and the fibre volume fraction v. The elastic modulus of SFRP composites possesses the maximum value at $\Theta = 0°$, decreases with increase of Θ and approaches an approximate plateau for $\Theta \ge$ ~50°. Nonetheless, the data in Fig. 6.14 demonstrate that there is a minimum in the modulus at Θ = ~80° for v = 0.1, at Θ = ~70° for v = 0.2 and 0.3 and at Θ = ~60° for v = 0.4 and 0.5 (very slightly lower than that at $\Theta = 90°$). This phenomenon was also observed by Warner and Stobbs (1989). Obviously, higher v values in the

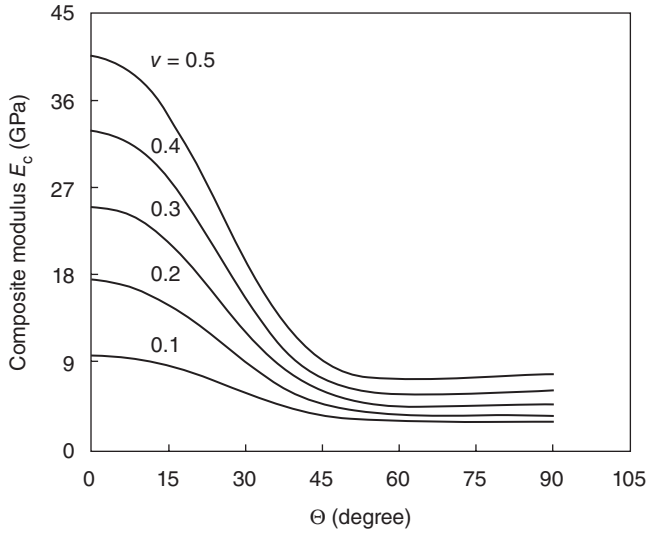

6.14 The composite elastic modulus versus the direction angle Θ for various fibre volume fractions and any value of Φ. Adapted from Fu and Lauke (1998d).

composite will result in greater composite modulus. In addition, since the results in Fig. 6.14 are obtained for any value Φ, the modulus is unrelated to the direction angle Φ.

The variation of the elastic modulus of SFRP composites with the direction (Θ, Φ) is shown in Fig. 6.15 for various θ_{mean}, namely, (a) $\theta_{mean} = 0°$ ($p = 0.5$ and $q = \infty$), (b) $\theta_{mean} = 12.95°$ ($p = 0.6$ and $q = 8$), (c) $\theta_{mean} = 35.95°$ ($p = 0.6$ and $q = 1$), and (d) $\theta_{mean} = 45°$ ($p = 0.5$ and $q = 0.5$)); other parameters are the same as in Fig. 6.14. The curves show that the mean fibre orientation angle θ_{mean} significantly influences the variation of the elastic modulus of SFRP composites with the direction (Θ, Φ). Comparison of Fig. 6.15(a)–(d) reveals that when the direction angle Θ is small, the elastic modulus increases with decreasing mean fibre orientation angle θ_{mean}; but when the direction angle Θ is large, the modulus decreases to some extent with decreasing mean fibre orientation angle θ_{mean}. At Θ = 90°, for the cases of small mean fibre orientation angle θ_{mean} the composite modulus hardly varies with Φ (see Fig. 6.15(a) and (b)) while for the cases of large mean fibre orientation angle the modulus decreases with Φ to its minimum at Φ = 90° and afterwards increases with Φ to its maximum at Φ = 180°. Moreover, for the cases of $\theta_{mean} \neq 0$ it can be seen from Fig. 6.15(b)–(d) that when Φ is small (e.g., as shown in Fig. 6.15(c), $0° \leq \Phi \leq \sim 70°$) or large (e.g., in Fig. 6.15(c), $\sim 110° \leq \Phi \leq 180°$), the composite modulus increases with Θ to a peak value and then decreases with Θ to the minimum value at Θ = 90°. Further, Fig. 6.15 shows that the variation of the elastic modulus of SFRP

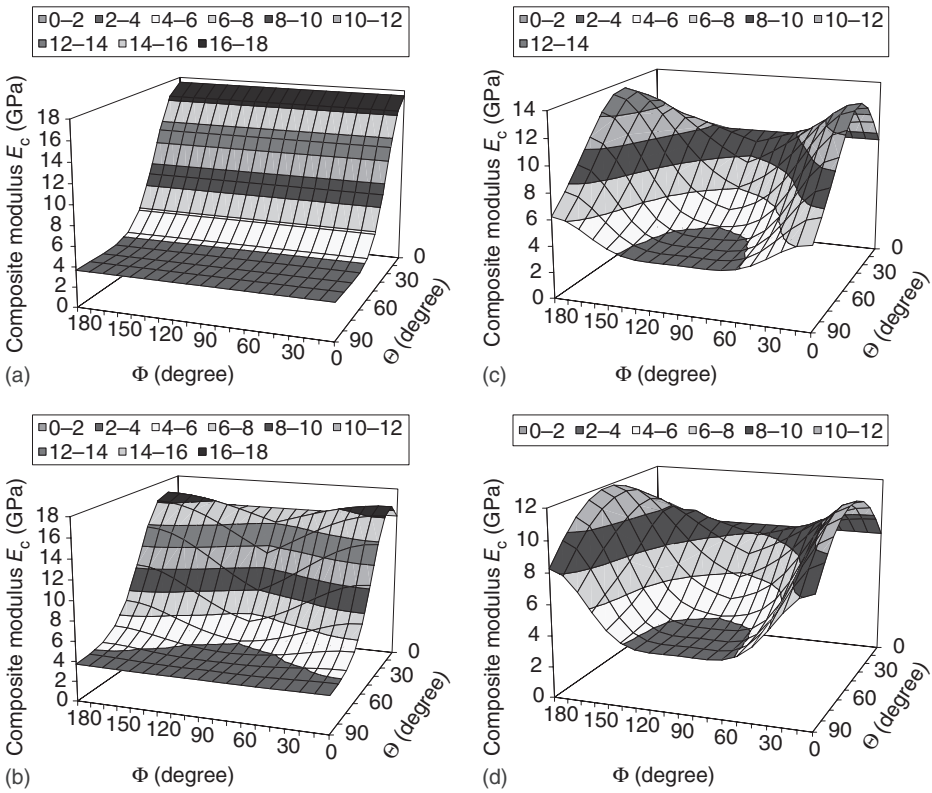

6.15 The composite elastic modulus versus the direction (Θ, Φ) for various mean fibre orientation angle θ_{mean}: (a) $\theta_{mean} = 0°$, (b) $\theta_{mean} = 12.95°$, (c) $\theta_{mean} = 35.95°$ and (d) $\theta_{mean} = 45°$. Adapted from Fu and Lauke (1998d).

composites with the direction (Θ, Φ) is symmetric about the direction angle $\Phi = 90°$.

Equation [6.93] is used to predict the composite modulus in the direction $\Theta = 0$ and $\pi/2$ for the unidirectional fibre alignment case and compared with experimental results (Kardos, 1991) as shown in Table 6.2. Two mean fibre lengths [$l_{mean} = 0.466$ mm ($a = 5$ and $b = 2.5$) and $l_{mean} = 3.198$ mm ($a = 0.15$ and $b = 1.5$)] and $d = 10$ μm are assumed and $E_f = 72.4$ GPa, $G_f = 29.6$ GPa, $\nu_f = 0.22$, $E_m = 2.8$ GPa, $G_m = 1.17$ GPa, $\nu_m = 0.35$ and $\nu = 0.50$ (Kardos, 1991). Table 6.2 shows that the results of the composite modulus for $\Theta = 0$ (longitudinal to short fibres) and $\Theta = \pi/2$ (transverse to short fibres) predicted by eqn [6.93] agree well with the experimental data, and when $l_{mean} = 0.466$ mm is used, the theoretical value for the elastic modulus in the direction ($\Theta = 0$, Φ) is closer to the experimental result than that when $l_{mean} = 3.198$ mm is used. Thus, it can be speculated that the aspect ratio of $l/d = 46.6$ (0.466 mm/10 μm) may be closer to the real aspect ratio

Table 6.2 Comparison of theoretical and experimental results of longitudinal and transverse modulus of unidirectional short-glass-fibre epoxy composites

Stiffness (GPa)				
Stress direction	Equation [6.93]		Equation [6.94]	Experimental results (Kardos, 1991)
	l_{mean} = 0.466 mm	l_{mean} = 3.198 mm		
Longitudinal to short fibres	31.93	36.21	—	31.0
Transverse to short fibres	9.58	9.58	5.39	9.6

value. Also, a simple model for the transverse modulus (i.e., the transverse modulus theory) (Bader and Hill, 1993; Piggott, 1980):

$$E_c(\Theta = 90°, \Phi) = E_f E_m / \left(vE_m + (1-v)E_f\right) \tag{6.94}$$

is applied to existing experimental results. However, the modulus value evaluated with this transverse modulus theory is much lower. Hence, eqn [6.93] is more precise to predict the transverse modulus of SFRP for unidirectional aligned fibre composites than eqn [6.94].

6.5 Random short fibre reinforced polymer (SFRP) composites

An approximate averaging technique to generate a rule-of-thumb expression is used for estimation of the modulus of a structure with a 2D random fibre orientation (Lavengood and Goettler, 1971; Kardos, 1991):

$$E_c = \bar{E}_{11} = \frac{3}{8}E_{11} + \frac{5}{8}E_{22}. \tag{6.95}$$

The shear modulus G_c of the 2D random short fibre composite is given by:

$$G_c = \frac{1}{8}E_{11} + \frac{1}{4}E_{22}, \tag{6.96}$$

where E_{11} and E_{22} can be calculated using the Halpin–Tsai equations [6.21] and [6.22], respectively.

For a 3D random short fibre composite, a slightly different equation for Young's modulus is given by (Lavengood and Goettler, 1971):

$$E_c = \frac{1}{5}E_{11} + \frac{4}{5}E_{22}. \tag{6.97}$$

The Poisson's ratio of a random short fibre composite is calculated from the following equation which is valid for isotropic materials:

$$\nu_c = \frac{E_c}{2G_c} - 1. \qquad 6.98$$

The PAA (Fu and Lauke, 1998c) (eqn [6.82]) for the elastic modulus of partially misaligned SFRP composites is applicable to the prediction of the modulus of SFRP composites with any fibre orientation distribution and thus is also suitable for 2D and 3D random fibre distribution cases. The paper physics approach (PPA) [eqn 6.86] is, in principle, also suitable for the 2D and 3D random fibre distribution cases.

The PPA and LAA approaches and the rule-of-thumb expressions are used to predict the composite modulus of 2D ($p = 0.5$ and $q = 0.5$ with $g(\theta) = \pi/2$ and $\theta_{mean} = 45°$) random short fibre composites (Fig. 6.16), and compared with the experimental results (Thomason and Vlug, 1996), where $E_f = 75$ GPa, $G_f = 30$ GPa, $\nu_f = 0.25$, $E_m = 1.6$ GPa, $G_m = 0.59$ GPa, $\nu_m = 0.35$ and $d = 13$ μm. Obviously, the results predicted by the LAA (eqn [6.82]) are closer than the PPA and the rule-of-thumb expressions to the experimental data, showing that the LAA method is more appropriate in predicting the modulus SFRP composites. Moreover, this further indicates that the PPA underestimates the composite modulus for the case of large fibre orientation angle while the laminate analogy approach (LAA) is suitable for prediction of elastic modulus of SFRP composites.

6.6 Hybrid short fibre reinforced polymer (SFRP) composites

The simultaneous use (hybridisation) of inorganic particles and short fibres in polymers leads to the development of hybrid particle/short fibre/polymer composites (Fu and Lauke, 1997a, 1998a,b; Rueda *et al.*, 1988; Yilmazer, 1992; Hargarter *et al.*, 1993). Particles and short fibres can be simply incorporated into polymers by extrusion compounding and injection moulding processes. The rule of hybrid mixtures and the laminate analogy approach are used to predict the Young's modulus of hybrid particle/short fibre/polymer composites.

It is assumed, in a hybrid particle/short fibre/polymer composite, that particles and short fibres are separated, respectively, in the corresponding particulate and short fibre composites as shown in Fig. 6.17. There is no interaction between particles and short fibres since particles and short fibres are separated completely. Iso-strain condition is applied to the two single systems, namely $\varepsilon_c = \varepsilon_{c1} = \varepsilon_{c2}$, where ε_c, ε_{c1} and ε_{c2} are, respectively, the strain

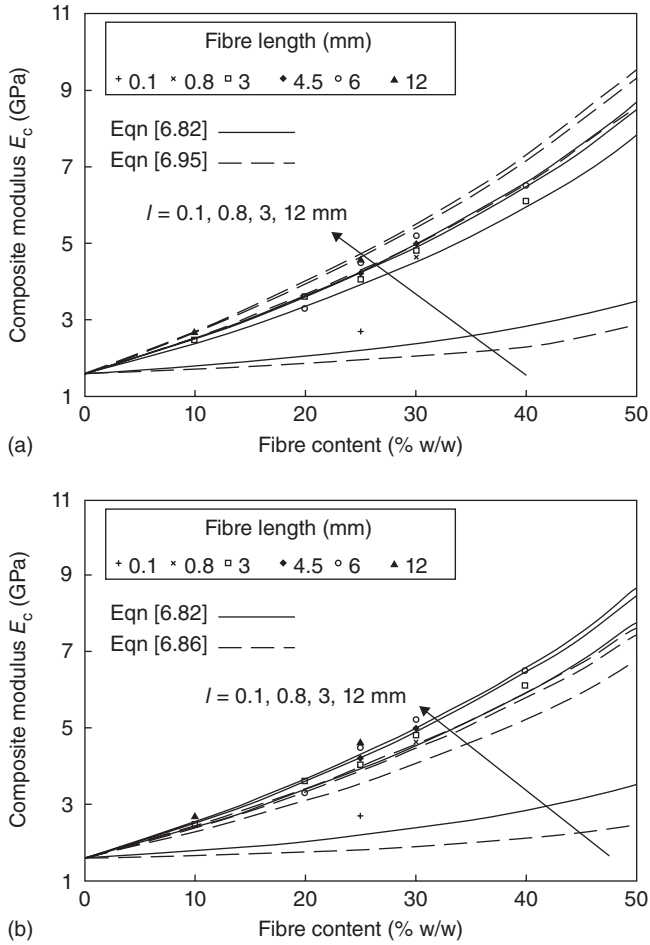

6.16 Comparison of predicted composite modulus of 2D random SFRP composites by eqn [6.82] (Fu and Lauke, 1998c), and (a) existing rule-of-thumb expression [6.95] (Lavengood and Goettler, 1971; Kardos, 1991), and (b) eqn [6.86] (Jayaraman and Kortschot, 1996) with the experimental results (Thomason and Vlug, 1996). Adapted from Fu and Lauke (1998d).

of the hybrid composite, the particulate composite and the short fibre composite. Force equilibrium requires that:

$$E_c\varepsilon_c = E_{c1}\varepsilon_{c1}v_{c1} + E_{c2}\varepsilon_{c2}v_{c2}, \qquad 6.99$$

where E_c is the Young's modulus of the hybrid composite, E_{c1} and E_{c2} are, respectively, the elastic modulus of the particulate composite and the short fibre composite, v_{c1} and v_{c2} are, respectively, the relative volume fraction of the particle/polymer system and the short fibre/polymer system, and v_{c1} +

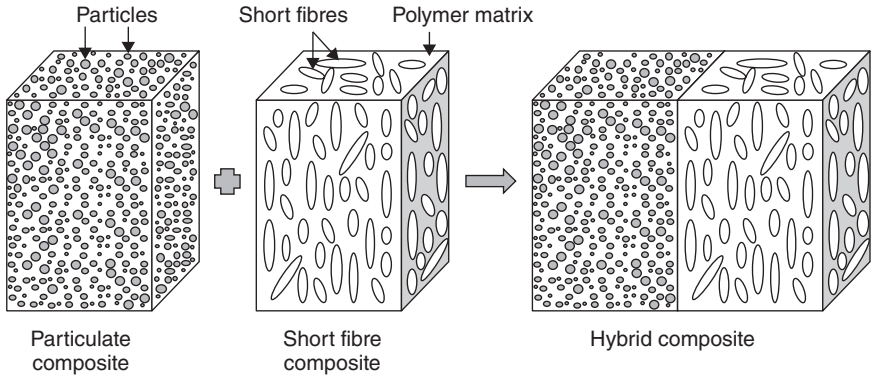

6.17 Simulated progress of a hybrid particle/short fibre/polymer composite for prediction of the elastic modulus of the hybrid composite using the rule of the hybrid mixture. Particles and short fibres are separated respectively in the corresponding particulate and short fibre composites. Adapted from Fu *et al.* (2002).

$v_{c2} = 1$, $v_{c1} = v_p/v_t$ and $v_{c2} = v_f/v_t$, where v_t is the total reinforcement volume fraction and equals $v_p + v_f$. The Young's modulus of the hybrid composite is then evaluated from the rule of hybrid mixtures (RoHM) by neglecting the interaction between particles and short fibres:

$$E_c = E_{c1}v_{c1} + E_{c2}v_{c2}. \qquad 6.100$$

A positive or negative hybrid effect is defined as a positive or negative deviation from the Young's modulus of the hybrid composite from the RoHM.

In the RoHM, the particles and the short fibres are assumed to be separated in two different systems. So, no interaction between particles and short fibres is considered. In reality, particles and short fibres are evenly and stochastically distributed in the polymer matrix. Therefore, the laminate analogy approach (LAA) is used for prediction of the elastic modulus of the hybrid particle/short fibre/polymer composite. In this approach, particle-filled polymer is regarded as a new, effective matrix to be reinforced by short fibres as shown in Fig. 6.18. Particles and short fibres are uniformly and stochastically distributed in the pure polymer matrix. In this case, the elastic modulus and Poisson's ratio of the particle-filled polymer are first evaluated and are taken as E_m and ν_m for short fibre reinforced effective matrix composite. The elastic modulus of the effective matrix can be estimated using the corresponding models for particulate composites (Callister, 1999; Fu *et al.*, 2002). The Poisson's ratio (ν_{cp}) for the particulate composite can be estimated using the law of the mixtures such that (Theocaris, 1987):

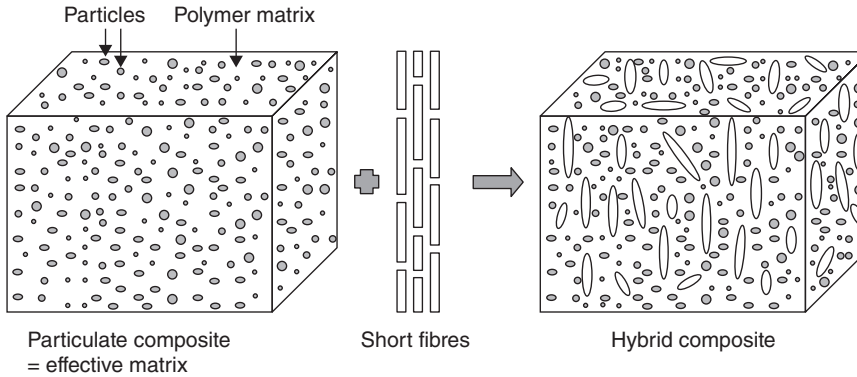

6.18 Simulated progress of a hybrid particle/short fibre/polymer composite for prediction of the elastic modulus of the hybrid composite using the laminate analogy approach. Particles and short fibres are evenly and stochastically distributed in the pure polymer matrix or, say, short fibres are uniformly distributed in the particulate composite (as the effective matrix). Adapted from Fu *et al.* (2002).

$$\nu_{cp} = \frac{\nu_m \nu_p}{\nu_p \nu_m + \nu_m \nu_p}, \qquad 6.101$$

where ν_p and ν_m are particle and polymer matrix Poisson's ratio; and v_p and v_m are particle and matrix volume fraction. The interaction between particles and short fibres is then incarnated in a manner that short fibres are added to the effective matrix containing particles. Prediction of elastic modulus of the hybrid particle/short fibre/polymer composite can be done using the LAA similar to that for short fibre reinforced pure polymer composites (eqn [6.82]) (Fu and Lauke, 1998c).

The predicted results for the Young's modulus of hybrid particle/short fibre/polymer composites using RoHM and LAA are shown in Fig. 6.19 as a function of relative fibre volume fraction for various fibre elastic moduli (Fu *et al.*, 2002). The elastic modulus of the hybrid composites increases as fibre elastic modulus and relative fibre volume fraction increases (see Fig. 6.18). The predicted values for the hybrid composite modulus by the RoHM are somewhat lower than those by LAA. Moreover, the relative difference increases as the fibre elastic modulus increases. Both the RoHM and the LAA are applied to calcite particle/short glass fibre/ABS composites (Fu *et al.*, 2002). It is found that the RoHM gives somewhat lower (about 5%) prediction of the elastic modulus of the hybrid composites while the predicted results by the LAA are in good agreement with the experimental results (Fu and Lauke, 1998a). This indicates that the LAA is more suitable for the prediction of the hybrid particle/short fibre/polymer composites.

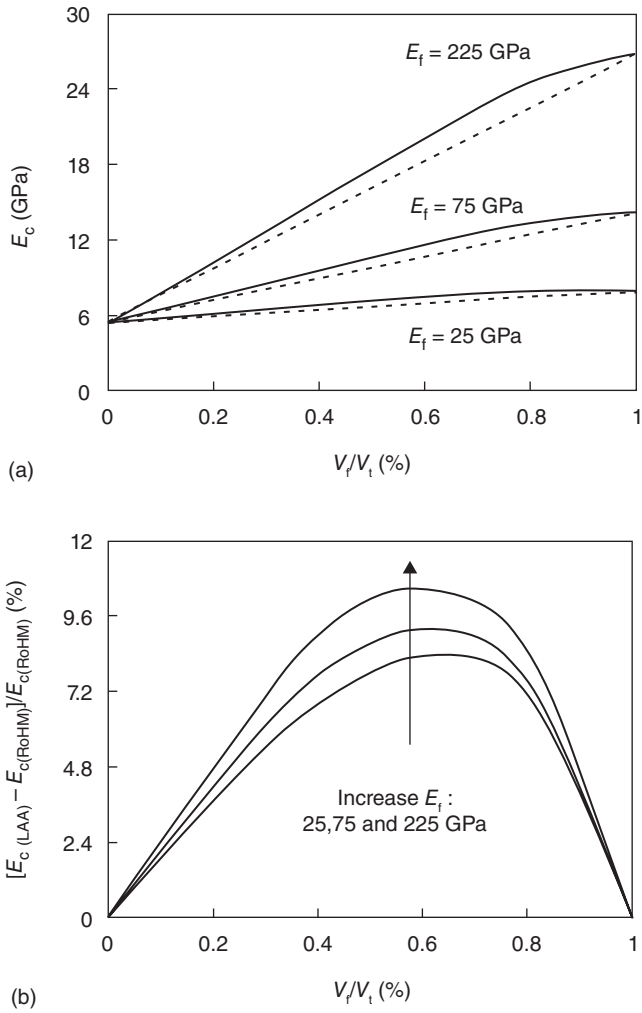

6.19 (a) Comparison of the results for the elastic modulus of the hybrid particle/short fibre/polymer composite predicted by the RoHM (broken lines) and the LAA (solid lines) and (b) relative difference as a function of relative fibre volume fraction for various fibre elastic moduli. Adapted from Fu *et al.* (2002).

6.7 Numerical methods

Until now we have discussed the evaluation of elastic properties on the basis of analytical modelling or semi-empirical equations. Numerical methods have also been applied to determine the effective elastic properties. Comprehensive contributions to modelling the elastic properties of

SFRP composites on the basis of finite element (FE) computations are provided by a number of researchers: Gusev *et al.* (2002), Hine *et al.* (2002, 2004), Lusti *et al.* (2002), Price *et al.* (2006), among others. Some matrices (e.g., liquid crystalline polymers) and fibres (e.g., carbon) possess anisotropic properties. FE modeling was conducted based on these published studies.

In FE models, the fibres are represented by sphero-cylinders (Lusti *et al.*, 2002). Namely, they are a combination of a cylindrical body and two hemispheric caps at both ends to avoid the presence of cylinder edges during mesh generation. To apply FE models to experimental results, short glass fibre reinforced polypropylene dumbbells of 80 mm length with a gauge length of 25 mm and a gauge diameter of 5 mm are prepared by conventional and shear controlled orientation injection moulding (SCORIM) processes using a mould gated at both ends. The Young's modulus and Poisson's ratio for polypropylene and glass fibres are (1.57 GPa, 0.335) and (72.5 GPa, 0.2), respectively. The average length is 448 μm for the conventionally moulded sample whereas it is slightly smaller with 427 μm for the SCORIM sample. The diameter of glass fibres is 12 μm in both samples and the fibre volume fraction is 8%. The orientation of each fibre is determined individually by sampling the fibre orientation distribution (see Fig. 6.20) with a Monte Carlo algorithm. The measured frequency distribution of the angle θ is transformed into the cumulative probability density function with 150 random numbers so that to any number in the interval [0,1] a unique angle θ is assigned. Moreover, the angle ϕ is assumed to be homogeneously distributed in the interval [0°,360°] and another 150 random numbers are necessary to randomly determine the second angle ϕ. After the length, diameter and orientation of all 150 fibres are given, they are then successively positioned in the periodic box. The fibres are inserted at random positions into this box and a subroutine is checked for overlaps with already positioned fibres. If overlaps occur, the position is rejected and the algorithm repeats the procedure until the fibre is placed without overlaps and all fibres are placed in the periodic box.

In Fig. 6.21, examples of the FE models are shown together with cuts through the finite element meshes. The effective elastic properties are numerically calculated from the response to an applied perturbation in the form of a constant strain. By averaging the individual orientation distributions of the FE models, the measured distributions are approximated more accurately (see Fig. 6.20). An iterative conjugate-gradient solver with a diagonal pre-conditioner is used for the finite element analysis (Gusev, 1997). At the energy minimum the local strains are known and allow us to assemble the effective stress. The effective elastic constants can then be calculated from the linear-elastic response equation. Six independent minimisation runs with six different effective strains are necessary to determine all 21 independent components of the stiffness matrix.

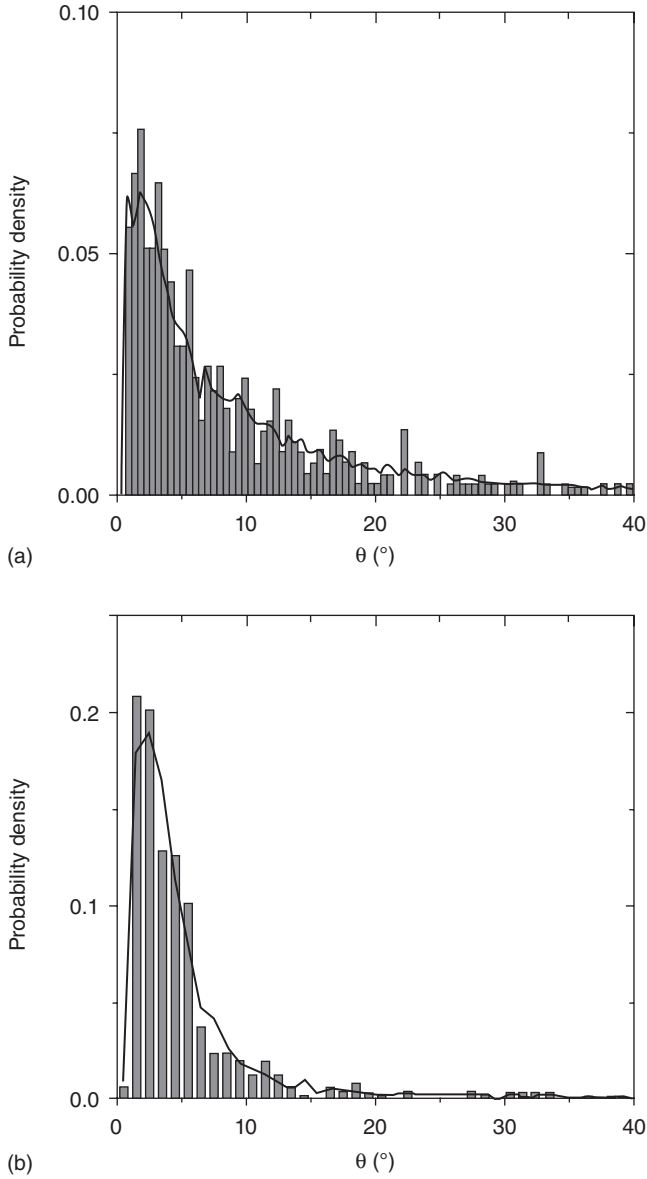

6.20 The θ distributions of the fibres in computer models by sampling the measured θ distribution during a Monte Carlo run for the conventionally moulded composite (a) and for the SCORIM moulded composite (b). Adapted from Lusti *et al.* (2002).

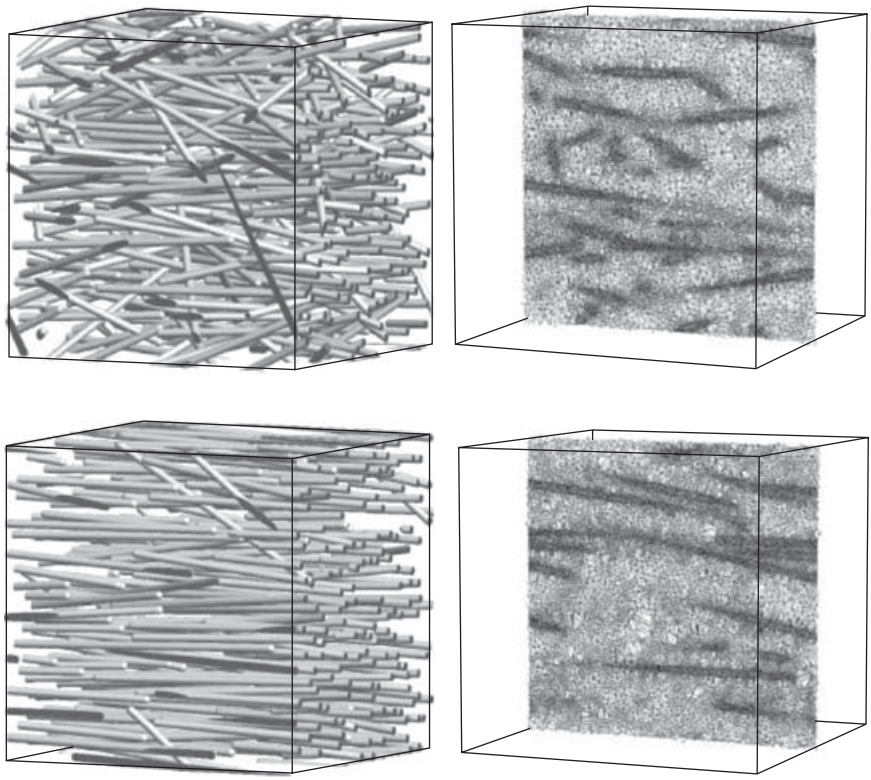

6.21 On the left-hand side, snapshots of the 3D multi-fibre computer models for both the conventionally (top) and the SCORIM (bottom) moulded composites; on the right-hand side, the corresponding longitudinal cuts through the finite element mesh of both computer models. Adapted from Lusti *et al.* (2002).

Both experimental and numerical results of the Young's modulus in the longitudinal direction of the glass-fibre/polypropylene dumbbell are listed in Table 6.3. The numerically calculated Young's modulus is slightly higher than the measured value for both conventional and SCORIM samples and is well inside the error range of the measurements. Both the experimental and numerical results lie much closer to the upper bound predictions of the micromechanical model (Tandon and Weng, 1984), confirming that a state of constant strain is the most appropriate for well-aligned glass fibre reinforced polymers. Tandon and Weng's model (1984) combined with Ward's approach (1962) give an upper and a lower bound for aggregate properties. The upper bound is close to the measured values for both conventionally and SCORIM moulded samples, while the lower bound is significantly lower.

Table 6.3 Longitudinal Young's modulus of both conventionally and SCORIM injection moulded glass fibre/polypropylene dumbbell composites (Lusti *et al.*, 2002)

	Young's modulus (GPa)	
	Conventional	SCORIM
Measured	5.09 ± 0.25	5.99 ± 0.31
Numerical	5.14 ± 0.1	6.04 ± 0.02
Tandon-Weng/Aggregate (1984)		
Upper bound	5.01	5.90
Lower bound	3.78	5.48

In analytical modelling, three steps were used, whereby subsequently all the collected knowledge of previous research was considered. The first step consists in providing the properties of the unit of structure with aligned fibre orientation. The second step is to find the orientation function of the distributed fibres and the third step applies appropriate averaging procedures to determine the aggregate properties. These researchers made detailed mechanical measurements as well as analytical and numerical calculations. On that basis, it could be concluded (among others) that the analytical model by Qiu and Weng (1990) for the unit structure with the number average of fibre length is most appropriate to determine the elastic properties of the unit cell. Another group of researchers (Kari *et al.*, 2007; Berger *et al.*, 2007) also considered the calculation of effective properties of randomly oriented short fibre composites. On the basis of a representative volume element that is statistically representative and is sufficiently large relative to the fibre size to ensure the results to be independent of the boundary conditions, the effective elastic properties of materials are evaluated.

A numerical homogenisation technique based on the finite element method (FEM) is employed to evaluate the effective elastic modulus of SFRP composites with periodic boundary conditions (Kari *et al.*, 2007). The common approach to model the macroscopic properties of fibre reinforced composites is to create a representative volume element (RVE) or a unit cell that captures the major features of the underlying microstructure. A modified random sequential adsorption algorithm (RSA) is applied to generate the three-dimensional unit cell models of randomly distributed short cylindrical fibre composites. Figure 6.22 shows the general procedure of homogenisation for car parts made of randomly distributed short fibre reinforced polymer composites.

A randomly distributed short fibre (RDSF) reinforced composite is now considered to evaluate the effective elastic properties by carrying out the

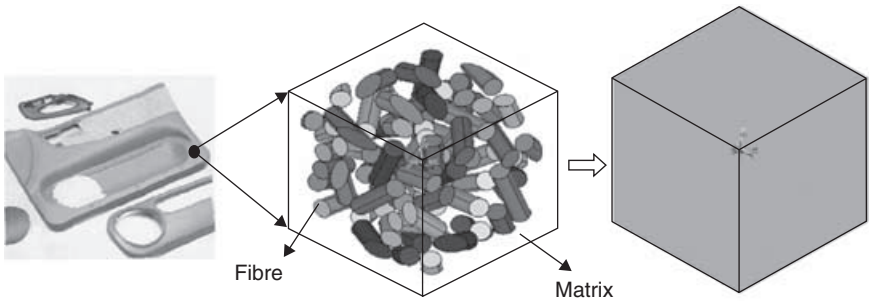

6.22 Procedure of homogenisation for car parts made of randomly distributed short fibre reinforced polymer composites. Adapted from Kari *et al.* (2007).

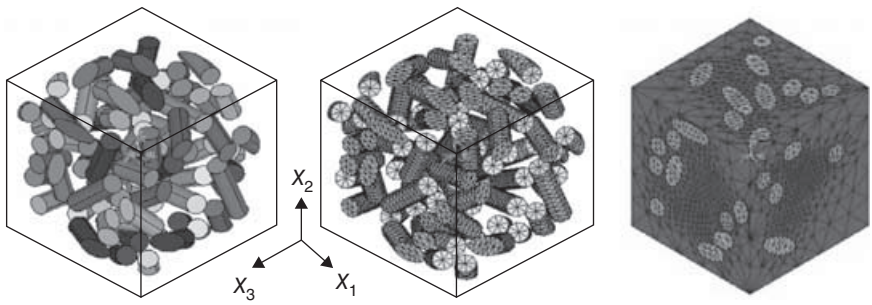

6.23 The RVE of randomly distributed short fibre (RDSF) composites and its FE mesh. Adapted from Kari *et al.* (2007).

parametric (volume fraction and aspect ratio) study of fibres. Figure 2.23 shows the RVE model and the corresponding FE mesh of the RDSF composite and all finite element evaluations are conducted using the commercial FE package ANSYS. The matrix and the fibres are meshed with ten node tetrahedron elements with full integration. To obtain the effective elastic modulus of short fibre composites, periodic boundary conditions are applied to the RVE by coupling opposite nodes on the opposite boundary surfaces. Homogenisation techniques and boundary conditions (Berger *et al.*, 2005, 2006) are applied to evaluate the effective elastic properties. The ANSYS Parametric Design Language (APDL) is used for the FE analysis, and evaluation of needed average strains and stresses and evaluation of the effective material properties are carried out. The material properties of constituents used for the analysis to evaluate the effective elastic modulus are, for the matrix material (Al 2618-T4) $E_m = 70$ GPa, $\nu_m = 0.3$ and for the fibres (SiC reinforcement) $E_f = 450$ GPa, $\nu_f = 0.17$ (Boehm

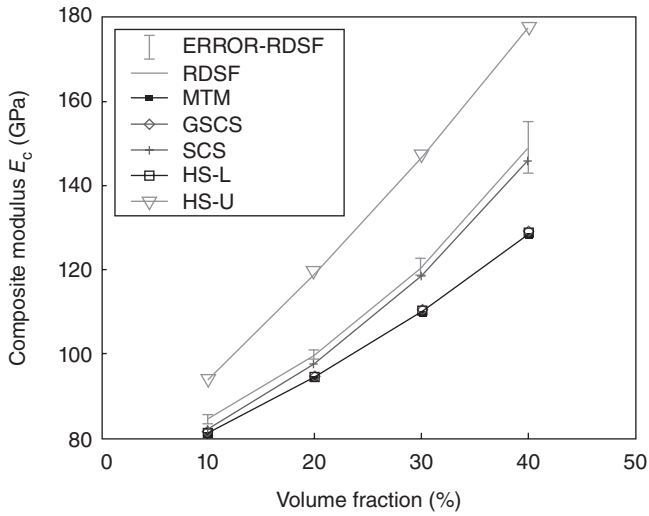

6.24 Comparison of the finite element results for the elastic modulus of randomly distributed short fibre (RDSF) composites with different analytical results. MTM: Mori–Tanaka estimates (1973), GSCS: generalised self-consistent method (Christensen and Lo, 1997), SCS: self-consistent method (Li and Wan, 2005), HS-L and HS-U: Hashin–Shtrikman lower and upper bounds (1963), respectively. Adapted from Kari *et al.* (2007).

et al., 2002). Though the evaluation is done for metal matrix composites with randomly distributed short fibres, the method is also applicable to prediction of the elastic modulus of SFRP composites. The FE results obtained are compared with different analytical models (Fig. 6.24). The numerical homogenisation technique provides results which are in between the Hashin–Shtrikman bounds (1963) and close to the results of the self-consistent approaches used by Li and Wan (2005).

6.8 Effect of interphase properties on the composite modulus

In the above sections, the effect of interphase properties has been ignored. Now the influence of an interphase on elastic modulus will be considered. Equation [6.19] which is equivalent to eqn [9.2] with the replacement of eqn [6.11] is used. Figure 6.25 shows a plot of stiffness ratio E_{ph}/E_c, where E_{ph} is the interphase modulus, against the shear modulus ratio G_{ph}/G_m (Lauke, 1992). It becomes clear that if $G_{ph} < G_m$ (G_{ph} is interphase shear modulus), the stiffness is reduced (and more pronounced for higher v_{ph} which is the interphase volume fraction). Yet it also becomes clear that the

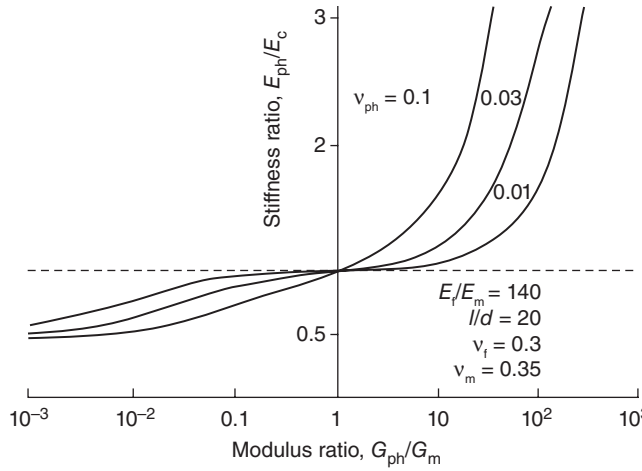

6.25 The plot of the stiffness ratio E_{ph}/E_c versus G_{ph}/G_m. Adapted from Lauke (1992).

interphase modulus has to be much smaller than G_m for the reduction to be important.

6.9 References

Bader M G and Hill A R (1993), 'Short fiber composites', *Materials and Technology, a comprehensive treatment*, ed. by R W Cahn, P Haasen and E J Kramer, VCH Publishers, Weinheim, 293–338.

Berger H, Kari S, Gabbert U, Rodriguez-Ramos R, Guinovart-Diaz R, Otero J A and Bravo-Castillero J (2005), 'An analytical and numerical approach for calculating effective material coefficients of piezoelectric fiber composites', *Int J Solids Struct*, 42 (21–22), 5692–5714.

Berger H, Kari S, Gabbert U, Rodriguez-Ramos R, Guinovart-Diaz R, Otero J A and Bravo-Castillero J (2006), 'Unit cell models of piezoelectric fiber composites for numerical and analytical calculation of effective properties', *Smart Mater Struct*, 15 (2), 451–458.

Berger H, Kari S, Gabbert U, Ramos R R, Castillero J B and Diaz R G (2007), 'Evaluation of effective material properties of randomly distributed short cylindrical fiber composites using a numerical homogenization technique', *J Mech Mater Struct*, 2 (8), 1561–1570.

Boehm H J, Eckschlager A and Han W (2002), 'Multi-inclusion unit cell models for metal matrix composites with randomly oriented discontinuous reinforcements', *Comput Mater Sci*, 25 (1–2), 42–53.

Callister Jr W D (1999), *Materials sciences and engineering: an introduction*. Wiley, New York.

Chin W K, Liu H T and Lee Y D (1988), 'Effects of fiber length and orientation distribution on the elastic modulus of short fiber reinforced thermoplastics', *Polym Composite*, 9 (1), 27–35.

Chou T W, Nomura S and Taya M (1980), 'A self-consistent approach to the elastic stiffness of short fibre composites', *J Compos Mater*, 14 (2), 178–188.

Chow T S (1977), 'Elastic moduli of filled polymers: the effect of particle shape', *J Appl Phys*, 48 (10), 4072–4075.

Choy C L, Leung W P, Kwok K W and Lau F P (1992), 'Elastic modulus and thermal conductivity of injection-molded short fibre-reinforced thermoplastics', *Polym Composite*, 13 (1), 69–80.

Christensen R M and Lo K H (1997), 'Solutions for effective shear properties of three phase sphere and cylinder models', *J Mech Phys Solids*, 27 (4), 315–330.

Cox H L (1952), 'The elasticity and strength of paper and other fibrous materials', *Brit J Appl Phys*, 3 (3), 72–79.

Eshelby J D (1957), 'The determination of the elastic field of an ellipsoidal inclusion and related problems', *Proc Roy Soc A*, 241, 376–396.

Eshelby J D (1961), 'Elastic inclusions and inhomogeneities', *Progress in Solid Mechanics, vol. 2*, ed. by Sneddon I N, Hill R, North-Holland, Amsterdam, pp. 89–140.

Fu S Y and Lauke B (1997a), 'Analysis of mechanical properties of injection molded short glass fibre/calcite/ABS composites', *J Mater Sci Technol*, 13 (5), 389–396.

Fu S Y and Lauke B (1997b), 'The fibre pull-out energy of misaligned short fibre composites', *J Mater Sci*, 32 (8), 1985–1993.

Fu S Y and Lauke B (1998a), 'Characterization of tensile behaviour of hybrid short glass fiber/calcite particle/ABS composites', *Compos Part A – Appl Sci Manu*, 29 (5–6), 575–583.

Fu S Y and Lauke B (1998b), 'Fracture resistance of unfilled and calcite-filled ABS composites reinforced by short glass fibers (SGF) under impact load', *Compos Part A – Appl Sci Manu*, 29 (5–6), 631–641.

Fu S Y and Lauke B (1998c), 'The elastic modulus of misaligned short fibre reinforced polymers', *Compos Sci Technol*, 58 (3–4), 389–400.

Fu SY and Lauke B (1998d), 'An analytical characterization of the anisotropy of the elastic modulus of misaligned short fibre reinforced polymers, *Compos Sci Technol*, 58 (12), 1961–1972.

Fu S Y, Hu X and Yue C Y (1998), 'A new model for the transverse modulus of unidirectional fiber composites', *J Mater Sci*, 33 (20), 4953–4960.

Fu S Y, Xu G and Mai Y-W (2002), 'On the elastic modulus of hybrid particle/short-fiber/polymer composites', *Compos Part B – Eng*, 33 (4), 291–299.

Gusev A A (1997), 'Representative volume element size for elastic composites: a numerical study', *J Mech Phys Solids*, 45 (9), 1449–1459.

Gusev A A, Lusti H R and Hine P J (2002), 'Stiffness and thermal expansion of short fiber composites with fully aligned fibers', *Adv Eng Mater*, 4 (12), 927–931.

Haddout A and Villoutreix G (1994), 'An experimental study of fiber orientation in injection moulded short glass fiber-reinforced polypropylene/polyarylamide composites', *Composites*, 25 (2), 147–153.

Halpin J C and Tsai S W (1967), 'Environmental factors in composite materials design', US Air Force Materials Lab. Rep. *AFML Tech Rep*, 67–423.

Hargarter N, Friedrich K and Cartsman P (1993), 'Mechanical properties of glass fiber/talc/polybutylene–terephthalate composites as processed by the radlite technique', *Compos Sci Technol*, 46 (3), 229–244.

Hashin Z and Rosen B W (1964), 'The elastic moduli of fiber-reinforced materials', *J Appl Mech*, 31 (2), 223–232.

Hashin Z and Shtrikman S (1963), 'A variational approach to the theory of the elastic behaviour of multiphase materials', *J Mech Phys Solids* 11 (2), 127–140.

Hermans J J (1967), 'The elastic properties of fibre reinforced materials when the fibers are aligned', *Proc K Ned Akad Wet Ser B* 70, 1–9.

Hill R (1963), 'Elastic properties of reinforced solids: some theoretical principles', *J Mech Phys Solids*, 11 (3), 357–372.

Hill R (1965a), 'Theory of mechanical properties of fibre-strengthened materials – III. Self-consistent model', *J Mech Phys Solids*, 13 (2), 189–198.

Hill R (1965b), 'A self-consistent mechanics of composite materials', *J Mech Phys Solids*, 13 (2), 213–225.

Hine P J, Lusti H R and Gusev A A (2002), 'Numerical simulation of the effects of volume fraction, aspect ratio and fibre length distribution on the elastic and thermoelastic properties of short fibre composites', *Compos Sci Technol*, 62 (10–11), 1445–1453.

Hine P J, Lusti H R and Gusev A (2004), 'On the possibility of reduced variable predictions for the thermoelastic properties of short fibre composites', *Compos Sci Technol*, 64 (7–8), 1081–1088.

Jayaraman K and Kortschot M T (1996), 'Correction to the Fukuda–Kawata Young's modulus and the Fukuda–Chou strength theory for short fibre-reinforced composite materials', *J Mater Sci*, 31 (8), 2059–2064.

Kardos L (1991), 'Short-fibre-reinforced polymeric composites, structure-property relations', in *International encyclopedia of composites, vol. 5*, ed. by S M Lee, VCH Publishers, New York, pp. 130–141.

Kari S, Berger H and Gabbert U (2007), 'Numerical evaluation of effective material properties of randomly distributed short cylindrical fibre composites', *Comput Mater Sci*, 39 (1), 198–204.

Kilchinskii A A (1965), 'On the model for determining thermoelastic characteristics of fibre reinforced materials', *Prikl Mekh*, 1, 1.

Kilchinskii A A (1966), 'Approximate method for determining the relation between the stresses and strains for reinforced materials of the fibre glass type', *Thermal Stresses in Elements of Construction*, Vol. 6, Naukova Dumka, Kiev, p. 123.

Lauke B (1992), 'Theoretical considerations on deformation and toughness of short fibre reinforced polymers', *Journal of Polymer Engineering*, 11 (1–2), 103–151.

Lavengood R E and Goettler L A (1971), 'Stiffness of non-aligned fiber reinforced composites', US Government R&D Reports, AD886372, National Technical Information Service, Springfield, VA.

Li L X and Wan T J (2005), 'A unified approach to predict overall properties of composite materials', *Mater Charact*, 54 (1), 49–62.

Lusti H R, Hine P J and Gusev A A (2002), 'Direct numerical predictions for the elastic and thermoelastic properties of short fibre composites', *Compos Sci Technol*, 62 (15), 1927–1934.

McGrath J J and Wille J M (1995), 'Determination of 3D fibre orientation distribution in thermoplastic injection molding', *Compos Sci Technol*, 53 (2), 33–143.

Mori T and Tanaka (1973), 'Average stress in matrix and average elastic energy of materials with misfitting inclusions', *Acta Metall et Mater*, 21 (5), 571–574.

Piggott M R (1980), *Load bearing fibre composites*, Pergamon Press, Oxford.

Price C D, Hine P J, Whiteside B, Cunha A M and Ward I M (2006), 'Modelling the elastic and thermoelastic properties of short fibre composites with anisotropic phases', *Compos Sci Technol,* 66 (1), 69–79.

Qiu Y P and Weng G J (1990), 'On the application of Mori–Tanaka's theory involving transversely isotropic spheroidal inclusions', *Int J Eng Sci*, 28 (11), 1121–1137.

Ramsteiner F and Theysohn R (1985), 'The influence of fibre diameter on the tensile behavior of short-glass-fibre reinforced polymers', *Compos Sci Technol*, 24 (3), 231–240.

Rueda L I, Anton C C and Rodriguez M C T (1988), 'Mechanics of short fibers in filled styrene–butadiene rubber (SBR) composites', *Polym Composite*, 9 (3), 198–203.

Sirkis J S, Cheng A, Dasgupta A and Pandelidis I (1994), 'Image processing based method of predicting stiffness characteristics of short fibre reinforced injection molded parts', *J Compos Mater*, 28 (9), 784–799.

Tandon G P and Weng G J (1984), 'The effect of aspect ratio of inclusions on the elastic properties of unidirectionally aligned composites', *Polym Composite*, 5 (4), 327–333.

Theocaris P S (1987), *The mesophase concept in composites*, Springer, Berlin.

Thomason J L (2008), 'The influence of fibre length, diameter and concentration on the modulus of glass fibre reinforced Polyamide 6,6', *Compos Part A – Appl Sci Manu*, 39 (11), 1732–1738.

Thomason J L and Vlug M A (1996), 'Influence of fibre length and concentration on the properties of glass fibre-reinforced polypropylene: 1. Tensile and flexural modulus', *Compos Part A – Appl Sci Manu*, 27 (6), 477–484.

Toll S and Andersson P O (1991), 'Microstructural characterization of injection moulded composites using image analysis', *Composites*, 22 (4), 298–306.

Tsai S W and Hahn H T (1980), *Introduction to composite materials*, Technomic, Lancaster, PA.

Tucker III C L and Liang E (1999), 'Stiffness predictions for unidirectional short-fibre composites: review and evaluation', *Compos Sci Technol*, 59 (5), 655–671.

Ward I M (1962), 'Optical and mechanical anisotropy in crystalline polymers', *Proc Phys Soc*, 80 (5), 1176–1188.

Warner T J and Stobbs W M (1989), 'Modulus and yield stress anisotropy of short fiber metal-matrix composites', *Acta Metall*, 37 (11), 2873–2881.

Xia M, Hamada H and Maekawa Z (1995), 'Flexural stiffness of injection molded glass fiber reinforced thermoplastics', *Int Polym Proc*, 10 (1), 74–81.

Yilmazer U (1992), 'Tensile, flexural and impact properties of a thermoplastic matrix reinforced by glass fibre and glass bead hybrids', *Compos Sci Technol*, 44 (2), 119–125.

Yu Z, Brisson J and Ait-Kadi A (1994), 'Prediction of mechanical properties of short Kevlar fibre-nylon-6,6 composites', *Polym Composite*, 15 (1), 64–73.

7

Flexural modulus of short fibre reinforced polymers

Abstract: Flexural stiffness of a SFRP composite plate with given fibre orientation and fibre length distribution is discussed. The flexural modulus of a unidirectional SFRP composite is first evaluated to provide a benchmark for comparison. Theoretical models for flexural modulus of SFRP composites with both uniform and continuous fibre orientation distributions and a layered structure are then discussed.

Key words: flexural modulus, unidirectional, uniform fibre orientation distribution, continuous fibre orientation distribution, layered structure.

7.1 Introduction

Short fibre reinforced polymer (SFRP) composites have many applications as engineering materials. Those composites based on thermoplastic matrices are often processed by extrusion compounding and injection moulding techniques (Fu and Lauke, 1997, 1998a,b; Ulrych *et al.*, 1993; Takahashi and Choi, 1991; Gupta *et al.*, 1989; Xia *et al.*, 1995; Chin *et al.*, 1988). Injection moulding grade thermoplastics are usually high viscosity materials which results in considerable shear-induced fibre breakage during compounding and moulding and finally causes a fibre length distribution (FLD). In addition, during the injection moulding process, progressive and continuous changes in fibre orientation throughout the moulded components take place. Cosequently, this leads to a fibre orientation distribution (FOD) in the final SFRP composite parts (Xia *et al.*, 1995; Chin *et al.*, 1988; Hine *et al.*, 1995; Fakirov and Fakirova, 1985; McGrath and Wille, 1995).

The mechanical properties of SFRP composites depend not only on the properties and volume fractions of the constituent materials but also on the FLD and FOD in the final injection moulded SFRP composite parts. In general, fibre content (volume fraction) and FLD are regarded explicitly or implicitly as uniform throughout the whole thickness of the product made of SFRP composites (Ulrych *et al.*, 1993; Gupta *et al.*, 1989; Xia *et al.*, 1995; Chin *et al.*, 1988; Baily *et al.*, 1989). However, unlike fibre content and FLD, the FOD is not only non-uniform but also varies through the thickness of the SFRP product. FOD can be divided into three major cases. The first case

is uniform fibre alignment whereby the fibres are distributed uniformly through the thickness. One limiting case is unidirectional fibre alignment. In injection moulded dumbbell-shaped specimens most fibres are aligned along the mould filling direction (Fu and Lauke, 1998b; Takahashi and Choi, 1991; Ramsteiner and Theysohn, 1979), thus the fibre alignment in these specimens can be regarded approximately as unidirectional. Another limiting case is random fibre alignment (O'Connell and Duckett, 1991) in which the fibres are distributed uniformly and randomly throughout the specimen.

The second case is continuous fibre alignment in which the fibre orientation changes continuously from the centre to the surface of the specimen. For example, the fibre orientation angle with respect to the mould filling direction is observed to increase from the surface to the centre of specimens of short glass fibre reinforced poly(ethylene terephthalate) (Fakirov and Fakirova, 1985); and in injection moulded plaques of short carbon fibre reinforced PEEK, the fibre orientation averages change continuously across the thickness of the plaque (O'Connell and Duckett, 1991). These can be roughly regarded as examples of the continuous case. The third case, namely, the skin-core layered structure in fibre orientation, is also often observed in injection moulded plaques or disc samples (Xia *et al.*, 1995; Karger-Kocsis, 1993; Spahr *et al.*, 1990; Harmia and Friedrich, 1995). In the core layer the fibres have a distinct FOD and are distributed uniformly; while in the skin layers the fibres have a different FOD and are also distributed uniformly.

The flexural stiffness of a SFRP composite plate with given fibre orientation and fibre length distribution is discussed in this chapter. The flexural modulus of a unidirectional SFRP composite will be first evaluated to provide a benchmark. Second, the flexural stiffness of the SFRP composite with a uniform fibre orientation distribution will be estimated. Third, SFRP composite with a continuous fibre orientation distribution will be studied. Fourth and last, the SFRP composite with a layered structure and fibre orientation will be considered. Planar fibre orientation distribution is considered for estimating the flexural modulus of SFRP composites. When there is a three-dimensional fibre orientation distribution, the out-of-plane fibres can be projected onto one plane so that all the fibres in the SFRP composite lie in the same plane and hence an approximate estimation of the flexural modulus can be similarly performed.

7.2 Flexural modulus of short fibre reinforced polymer (SFRP) composites

7.2.1 Unidirectional SFRP composites

Here, the unidirectional case is considered first as shown in Fig. 7.1, where the short fibres are aligned with an angle θ to the reference direction '1'.

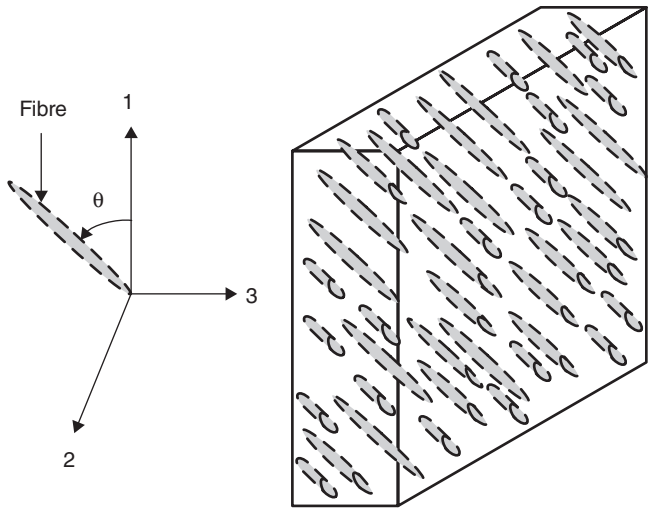

7.1 Schematic drawing of a unidirectional SFRP composite.

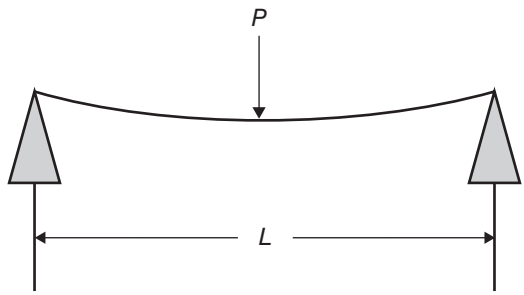

7.2 Schematic drawing of three-point bend testing for a SFRP composite beam with a span length of *L* under the applied load *P* at the mid-span.

The flexural modulus of such a SFRP composite plate containing aligned short fibres is analysed. The constitutive relations for the bending of a plate of thickness h as shown in Fig. 7.2 are given by:

$$\begin{bmatrix} M_1 \\ M_2 \\ M_6 \end{bmatrix} = \begin{bmatrix} D_{11} & D_{12} & D_{16} \\ D_{12} & D_{22} & D_{26} \\ D_{16} & D_{26} & D_{66} \end{bmatrix} \begin{bmatrix} k_1 \\ k_2 \\ k_6 \end{bmatrix}, \tag{7.1}$$

where M_1, M_2 and M_6 are resultant bending and twisting moments per unit width, k_1, k_2 and k_6 are bending and twisting curvatures of the plate, and D_{ij} are plate bending stiffnesses so that:

$$D_{ij} = \int_{-h/2}^{h/2} Q_{ij} z^2 \mathrm{d}z, \tag{7.2}$$

where z is the axis along the thickness direction and varies from $-h/2$ to $h/2$. Q_{ij} $(i, j = 1, 2, 6)$ are the tensile stiffness constants in the off-axis system (Tsai, 1980). Inverting the moment-curvature relation (eqn [7.1]) we obtain the following in terms of flexural compliances:

$$\begin{bmatrix} k_1 \\ k_2 \\ k_6 \end{bmatrix} = \begin{bmatrix} d_{11} & d_{12} & d_{16} \\ d_{12} & d_{22} & d_{26} \\ d_{16} & d_{26} & d_{66} \end{bmatrix} \begin{bmatrix} M_1 \\ M_2 \\ M_6 \end{bmatrix}, \tag{7.3}$$

where d_{ij} are flexural compliances which can be evaluated from D_{ij}. d_{11} is given by:

$$d_{11} = \left(D_{26}^2 - D_{22}D_{66}\right) \Big/ \left(D_{16}^2 D_{22} - 2D_{12}D_{16}D_{26} + D_{11}D_{26}^2 + D_{12}^2 D_{66} - D_{11}D_{22}D_{66}\right). \tag{7.4}$$

Under simple pure bending by M, for example, in a three-point bending test (Fig. 7.2), when a load is applied at mid-span, and the beam longitudinal direction is assumed in the reference direction '1' (see Fig. 7.1), for a beam with width b, we have:

$$M_1 = M/b \tag{7.5}$$

$$M_2 = M_6 = 0. \tag{7.6}$$

The resulting moment-curvature relation is:

$$k_1 = d_{11}M_1 = d_{11}\, M/b. \tag{7.7}$$

The rigidity of beam is given by:

$$E_{\text{flex}} I = M/k_1 = b/d_{11}, \tag{7.8}$$

where E_{flex} is the flexural modulus of the SFRP composite plate. I is the moment of inertia of the cross section of plate about the centroidal axis:

$$I = \frac{bh^3}{12}, \tag{7.9}$$

so that, we obtain:

$$E_{\text{flex}} = \frac{12}{h^3 d_{11}} = \frac{1}{I^* d_{11}}, \tag{7.10}$$

where $I^* = I/b$. Finally, the expression for the flexural modulus of the SFRP composite plate is obtained by:

$$E_{\text{flex}} = \left(D_{16}^2 D_{22} - 2D_{12}D_{16}D_{26} + D_{11}D_{26}^2 + D_{12}^2 D_{66} - D_{11}D_{22}D_{66}\right) \Big/ \left[I^*\left(D_{26}^2 - D_{22}D_{66}\right)\right], \tag{7.11}$$

where D_{ij} can be expressed as:

$$D_{11} = U_1 I^* + U_2 V_1 + U_3 V_2 \tag{7.12}$$

$$D_{22} = U_1 I^* - U_2 V_1 + U_3 V_2 \tag{7.13}$$

$$D_{12} = U_4 I^* - U_3 V_2 \tag{7.14}$$

$$D_{66} = U_5 I^* - U_3 V_2 \tag{7.15}$$

$$D_{16} = \frac{1}{2} U_2 V_3 + U_3 V_4 \tag{7.16}$$

$$D_{26} = \frac{1}{2} U_2 V_3 - U_3 V_4, \tag{7.17}$$

where V_i are:

$$V_1 = \int_{-h/2}^{h/2} \cos 2\theta z^2 \mathrm{d}z = I^* \cos 2\theta \tag{7.18}$$

$$V_2 = \int_{-h/2}^{h/2} \cos 4\theta z^2 \mathrm{d}z = I^* \cos 4\theta \tag{7.19}$$

$$V_3 = \int_{-\mathrm{h}/2}^{\mathrm{h}/2} \sin 2\theta z^2 \mathrm{d}z = I^* \sin 2\theta \tag{7.20}$$

$$V_4 = \int_{-h/2}^{h/2} \sin 4\theta z^2 \mathrm{d}z = I^* \sin 4\theta, \tag{7.21}$$

and U_i are functions of the tensile stiffness constants (Q_{xx}, Q_{yy}, Q_{xy} and Q_{ss}) in the on-axis system and can be expressed by (Tsai, 1980):

$$U_1 = \frac{1}{8}\left(3Q_{xx} + 3Q_{yy} + 2Q_{xy} + 4Q_{ss}\right) \tag{7.22}$$

$$U_2 = \frac{1}{2}\left(Q_{xx} - Q_{yy}\right) \tag{7.23}$$

$$U_3 = \frac{1}{8}\left(Q_{xx} + Q_{yy} - 2Q_{xy} - 4Q_{ss}\right) \tag{7.24}$$

$$U_4 = \frac{1}{8}\left(Q_{xx} + Q_{yy} + 6Q_{xy} - 4Q_{ss}\right) \tag{7.25}$$

$$U_5 = \frac{1}{8}\left(Q_{xx} + Q_{yy} - 2Q_{xy} + 4Q_{ss}\right), \tag{7.26}$$

and Q_{xx}, Q_{xy}, Q_{yy} and Q_{ss} are (Fu and Lauke, 1998c,d):

$$Q_{xx} = E_c / \left(1 - \nu_x \nu_y\right) \tag{7.27}$$

$$Q_{xy} = \nu_y Q_{xx} \tag{7.28}$$

$$Q_{yy} = E_{cy} / \left(1 - \nu_x \nu_y\right) \tag{7.29}$$

$$Q_{ss} = G_s, \tag{7.30}$$

where E_c, E_{cy}, G_s, ν_x and ν_y are longitudinal and transverse tensile modulus, shear modulus, longitudinal and transverse Poisson's ratio, respectively, of a unidirectional SFRP composite with fibres of length l. They can be expressed as functions of fibre modulus (E_f) and matrix modulus (E_m), matrix shear modulus (G_m), Poisson's ratio of fibre (ν_f) and matrix (ν_m), and fibre volume fraction (v) (Fu and Lauke, 1998c,d).

When a FLD exists in the unidirectional SFRP composite, D_{ij} in eqns [7.12]–[7.17] should be integrated to obtain the overall plate flexural stiffness matrix, A_{ij}, so that:

$$A_{ij} = \int_{l_{min}}^{l_{max}} D_{ij} f(l)\,\mathrm{d}l \quad i, j = 1, 2, 6; \tag{7.31}$$

where f has been defined in Chapter 3 (see eqn [3.9]) as the fibre length probability density function, in which a and b are size and shape parameters, respectively. Consequently, the effective flexural modulus of SFRP composites can be evaluated using eqn [7.11] by replacing D_{ij} with A_{ij}.

7.2.2 SFRP composite with a uniform fibre orientation distribution

When both FLD and FOD exist in a SFRP composite and the fibres are distributed uniformly through the composite thickness, D_{ij} must be integrated to obtain the flexural stiffness matrix:

$$A_{ij} = \int_{\theta_{min}}^{\theta_{max}} \int_{l_{min}}^{l_{max}} D_{ij} f(l) g(\theta)\,\mathrm{d}l\mathrm{d}\theta. \quad i, j = 1, 2, 6; \tag{7.32}$$

where $g(\theta)$ has been defined in Chapter 3 (see eqn [3.24]) as the fibre operation distribution function. The flexural modulus of the SFRP composite can be evaluated using eqn [7.11] by replacing D_{ij} with A_{ij}. It can be shown that when $\theta = \theta_{min} = \theta_{max}$, the uniform case becomes one limiting case of unidirectional fibre alignment; and when $g(\theta) = 2/\pi$, the uniform FOD becomes another limiting case of 2D random fibre alignment.

Comparison of theoretical results with available experimental data for a random, in-plane, short glass fibre reinforced polypropylene composite (Thomason and Vlug, 1996) is given in Fig. 7.3 for different fibre length and fibre weight fraction (Fu *et al.*, 1999), where $E_f = 75$ GPa, $\nu_f = 0.25$, $G_f = E_f/(2(1 + \nu_f)) = 30$ GPa, $E_m = 1.6$ GPa, $\nu_m = 0.35$, $G_m = E_m/(2(1 + \nu_m)) = 0.59$ GPa and $r_f = 6.5$ μm. For transformation between volume fraction and weight fraction, the following densities of fibre and matrix are used: density of glass fibres = 2.620 g cm^{-3}, density of polypropylene resin = 0.905 g cm^{-3}. It can be seen from Fig. 7.3 that the theoretical predictions by theory agree well with existing experimental data. These results show that the composite flexural modulus increases with fibre weight fraction (fibre volume fraction) (Fig. 7.3(a)). It also increases with the mean fibre length when it is small; but becomes insensitive to fibre length (or aspect ratio) when it is large enough (e.g. ≥~100) (Fig. 7.3(b)).

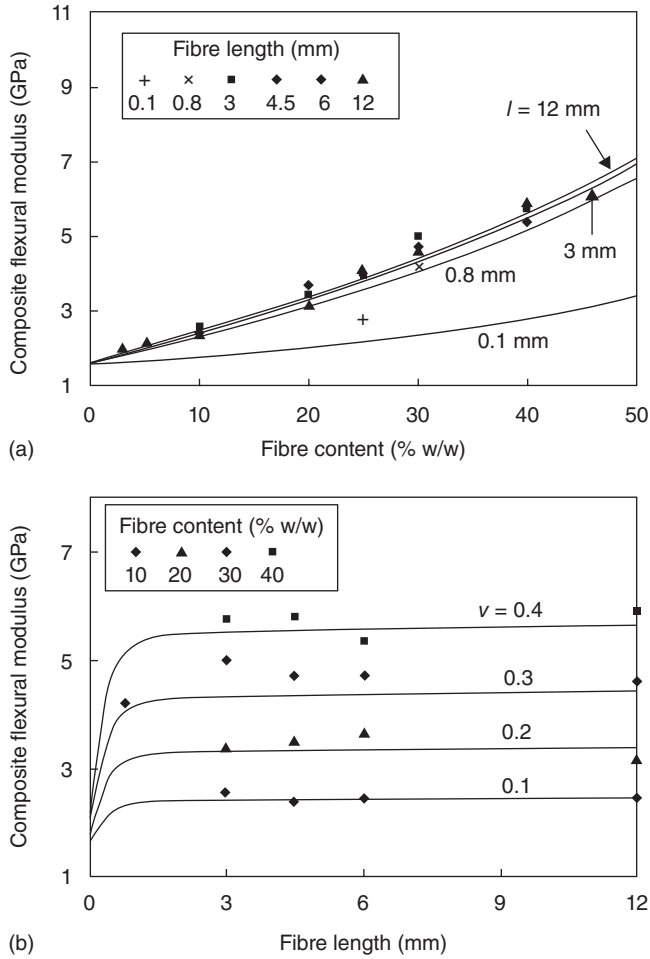

7.3 Comparison between predicted results and existing experimental data for a random, in-plane, short glass fibre reinforced polypropylene composite (Thomason and Vlug, 1996): (a) composite flexural modulus (E_{flex}) *vs* fibre weight fraction, (b) E_{flex} vs fibre length (Fu *et al.*, 1999).

The flexural modulus of composites based on acrylonitrile butadiene styrene (ABS) reinforced with short glass fibres (SGF) and glass beads (GB) as a function of filler content is shown in Fig. 7.4 (Hashemi, 2008), where it increases with increasing filler volume fraction. Further, SGF reinforced composites possess a higher flexural modulus than glass bead filled composites since SGF has an aspect ratio much larger than unity for glass beads (Hashemi, 2008), which is also why the SGF composite

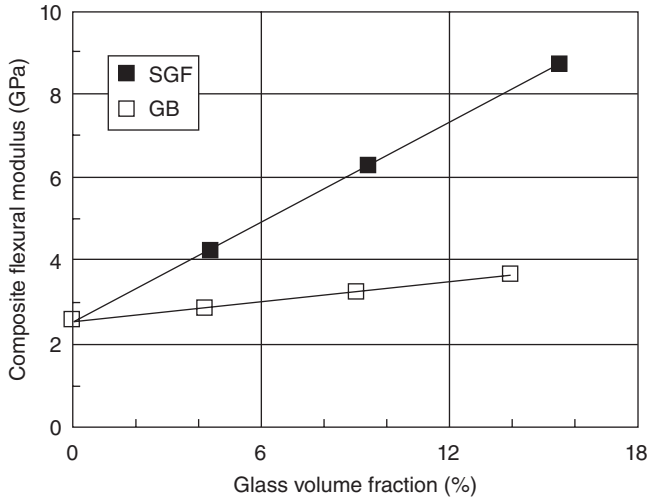

7.4 Composite flexural modulus based on acrylonitrile butadiene styrene (ABS) reinforced with short glass fibres and glass beads. Adapted from Hashemi (2008).

flexural modulus increases dramatically with increasing fibre volume fraction.

7.2.3 SFRP composite with a continuous fibre orientation distribution

Assume fibre orientation of a SFRP composite changes continuously from centre to surface. The fibre orientation angle is assumed minimum at the surface ($z = h/2$) and maximum at the centre ($z = 0$) of the specimen. The relationships of D_{ij} with V_i can be obtained and are the same as those (eqns [7.12]–[7.17]) for the unidirectional composite but V_i (i = 1–4) are different since Q_{ij} vary with θ. Thus, we evaluate V_i first and we have:

$$\frac{h/2 - z}{h/2} = \int_{\theta_{\min}}^{\theta} g(\theta)\,\mathrm{d}\theta. \tag{7.33}$$

So

$$z = \frac{h}{2} - \frac{h}{2}\int_{\theta_{\min}}^{\theta} g(\theta)\,\mathrm{d}\theta \tag{7.34}$$

and

$$dz = -(h/2)\,g(\theta)\,\mathrm{d}\theta. \tag{7.35}$$

Therefore, we obtain:

$$V_{[1,2,3,4]} = \frac{h^3}{4} \int_{\theta_{min}}^{\theta_{max}} [\cos 2\theta, \cos 4\theta, \sin 2\theta, \sin 4\theta] \left(1 - \int_{\theta_{min}}^{\theta} g(\theta) \mathrm{d}\theta \right)^2 g(\theta) \mathrm{d}\theta. \quad 7.36$$

D_{ij} can be obtained by inserting eqn [7.36] into eqns [7.12]–[7.17], and A_{ij} evaluated from eqn [7.32]. Finally, the flexural modulus of SFRP composites can be determined from eqn [7.11] by replacing D_{ij} with A_{ij}.

The following parametric data are used except otherwise given: E_f = 82.7 GPa, G_f = 27.6 GPa, ν_f = 0.22, E_m = 2.18 GPa, G_m = 1.03 GPa, ν_m = 0.35, d = 10 μm and ν = 0.30. The effect of mean fibre orientation angle, θ_{mean}, on composite flexural modulus is shown in Fig. 7.5 for the cases of uniform and continuous fibre orientation distributions (Fu *et al.*, 1999), where p = 0.5 and various q. In the continuous case, the fibre orientation angle changes continuously from the surface (minimum) to the core (maximum). Figure 7.5 shows that composite flexural modulus decreases with increasing mean fibre orientation angle for the two cases. This indicates that the unidirectional SFRP composite containing short fibres having an angle of zero degrees with the reference direction '1' corresponds to the maximum composite flexural modulus. The larger the deviation in the mean fibre orientation angle with the reference direction, the lower is the composite flexural modulus. Also, the flexural modulus for SFRP composite with a continuous fibre orientation distribution is larger than that with a

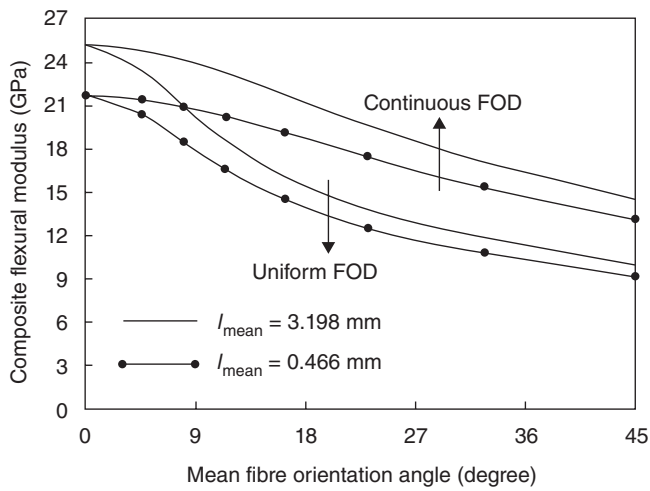

7.5 Effect of mean fibre orientation angle on flexural modulus of SFRP composites for cases of uniform and continuous fibre alignments for l_{mean} = 3.198 mm (a = 0.15, b = 1.5) and l_{mean} = 0.466 mm (a = 5, b = 2.5), for the meaning of a and b see eqn [3.9]. Adapted from Fu *et al.*, 1999.

uniform fibre orientation distribution. This is because, in the continuous case, the fibre orientation angle is assumed to change continuously from the sample surfaces (minimum: 0°) to the core (maximum: 90°) and, thus short fibres having a small fibre orientation angle near the surfaces for the continuous case would make a bigger contribution to the composite flexural strength than that by short fibres with a mean fibre orientation angle near the sample surfaces for the uniform case, leading to a higher composite flexural modulus for the continuous case than the uniform case. The continuous case is well known for bamboos that evolve for many years to withstand flexural forces from the wind.

The effect of mode fibre orientation angle on flexural modulus of SFRP composites is presented in Fig. 7.6 for the two cases of uniform and continuous fibre alignments (Fu *et al.*, 1999), where $l_{mean} = 3.198$ mm ($a = 0.15$, $b = 1.5$), and $\theta_{mean} = 12.95°$ (both p and q vary, see eqn [3.24]). It is clear that the composite flexural modulus decreases with increasing mode fibre orientation angle for these two cases. However, this effect is more remarkable for the continuous case than the uniform case. This is because the mean fibre orientation angle near the surface layers does not change for the uniform case but it increases with the mode fibre orientation angle for the continuous case (for example, within the one-quarter surface layers, $\theta_{mean} = 0.8133°$ for $\theta_{mod} = 6.59°$ ($p = 6$ and $q = 8$); and $\theta_{mean} = 2.761°$ for $\theta_{mod} = 12.866°$ ($p = 18$ and $q = 336.3$)), so that fibres near the surface layers play a more important part in controlling the composite flexural modulus.

Similar to the Young's modulus of SFRP composites via the paper physics approach (PPA), the modified rule-of-mixtures is also employed for estima-

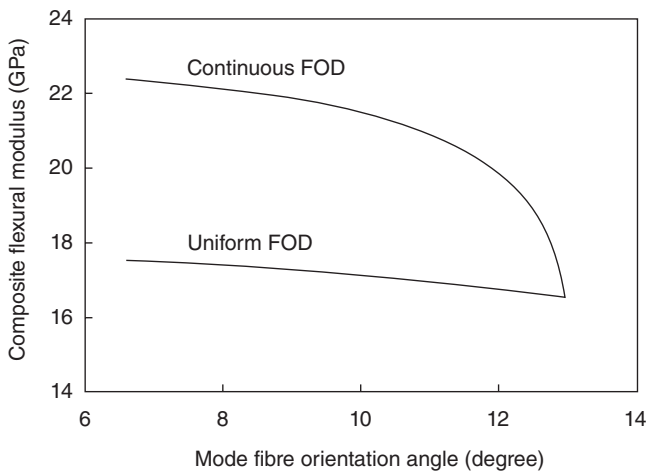

7.6 Effect of mode fibre orientation angle on the flexural modulus of SFRP composites for cases of uniform and continuous fibre alignments. Adapted from Fu *et al.,* 1999.

tion of the flexural modulus of short glass fibre reinforced polyoxymethylene composites by considering the fibre length and orientation factors (Hashemi *et al.*, 1997). Thus, we have:

$$E_{\text{flex}} = \eta_{\text{l}} \eta_{\theta} E_{\text{f}} v + E_{\text{m}} v_{\text{m}}, \tag{7.37}$$

where η_{l} and η_{θ} are, respectively, the fibre length and orientation factors for the composite flexural modulus and they are given by:

$$\eta_{\text{l}} = 1 - \frac{\tanh \eta l/2}{\eta l/2}, \quad \text{with} \quad \eta = \sqrt{\frac{2G_{\text{m}}}{E_{\text{f}} r_{\text{f}}^2 \ln\left(R/r_{\text{f}}\right)}}, \tag{7.38}$$

where G_{m} is matrix shear modulus, E_{f} is fibre Young's modulus, and R is mean separation of fibres normal to their length. The fibre orientation factor η_{θ} is determined from experiments. It is noted that eqn [7.38] is only an approximate expression to estimate the flexural modulus of SFRP composites, since strictly speaking, both η_{l} and η_{θ} are in general dependent on each other and cannot be separately evaluated.

7.2.4 SFRP composite with a layered structure

This case is shown in Fig. 7.7 (Friedrich, 1998) where the SFRP composite plate has two skin layers, h_{s}, and one core layer, h_{c}, across the thickness h. The fibre orientation distributions in the skin and core are different. In the skin layers, there is one fibre orientation distribution (FOD) and fibres are distributed uniformly; while in the core layer, there is another FOD and fibres are also distributed uniformly.

To derive the expression for the flexural modulus of the SFRP with a layered structure, we consider first the case of fibres in the core layer having one orientation angle θ_1 and those fibres in the skin layers having another orientation angle θ_2, then, we can obtain:

$$V_{\text{i}} = V_{\text{i}}^1 + V_{\text{i}}^2 \quad i = 1\text{–}4 \tag{7.39}$$

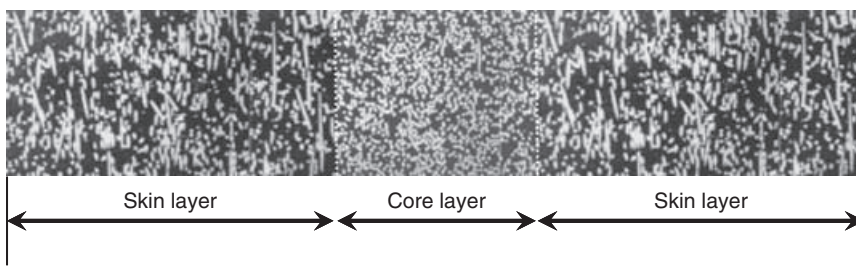

7.7 SEM micrograph of the layered structure of an injection moulded 45 wt% short glass fibre reinforced polyethyleneterephthalate (PET) composite. Adapted from Friedrich (1998).

and

$$V^1_{[1,2,3,4]} = I^*_c[\cos 2\theta_1, \cos 4\theta_1, \sin 2\theta_1, \sin 4\theta_1] \quad 7.40$$

$$V^2_{[1,2,3,4]} = (I^* - I^*_c)[\cos 2\theta_2, \cos 4\theta_2, \sin 2\theta_2, \sin 4\theta_2] \quad 7.41$$

where

$$I^*_c = \frac{h_c^3}{12}. \quad 7.42$$

Thus, we have:

$$D_{ij} = D^1_{ij} + D^2_{ij} \quad i, j = 1, 2, 6, \quad 7.43$$

where D^1_{ij} as a function of I^*_c and θ_1, and D^2_{ij} as a function of $(I^* - I^*_c)$ and θ_2 are the same as eqns [7.12]–[7.17]. The integration of D_{ij} should be carried out, respectively, for the core layer and the surface layers. Therefore, we obtain:

$$A_{ij} = \int_{\theta_{1\min}}^{\theta_{1\max}} \int_{l_{\min}}^{l_{\max}} D^1_{ij} f(l)\, g(\theta_1)\, \mathrm{d}l\mathrm{d}\theta_1 + \int_{\theta_{2\min}}^{\theta_{2\max}} \int_{l_{\min}}^{l_{\max}} D^2_{ij} f(l)\, g(\theta_2)\, \mathrm{d}l\mathrm{d}\theta_2. \quad 7.44$$

Finally, the flexural modulus of SFRP composites can be evaluated using eqn [7.11] by replacing D_{ij} with A_{ij}.

The effect of mean fibre orientation angle on composite flexural modulus for the case of layered structure is displayed in Fig. 7.8 (Fu *et al.*, 1999), where l_{mean} = 3.198 mm (a = 0.15, b = 1.5), p = 0.6 and various q except at $\theta_{mean} = 0°$ (p = 0.5 and $q = \infty$) and at $\theta_{mean} = 45°$ (p = 0.5 and q = 0.5) when θ_{mean} varies and (a) $\theta_{mean} = 12.95°$ (p = 0.6 and q = 8) in the skin layers and (b) $\theta_{mean} = 0°$ (p = 0.5 and $q = \infty$) in the core layer. The core thickness is assumed to be half the whole thickness of the composite plate. The composite flexural modulus is contributed from both the core layer and the skin layers. h vanishes finally, so the value of h_c/h is sufficient and their individual values are not needed for the calculations. Other parameters are the same as in Fig. 7.5 and this is also true for other figures unless otherwise stated. Figure 7.8 reveals again that the composite flexural modulus decreases with increasing mean fibre orientation angle. Moreover, when the fibre orientation distribution changes only in the skin layers (see curve b), the mean fibre orientation angle has a larger influence on the composite flexural modulus than when the fibre orientation distribution changes only in the core layer (see curve a). This result indicates that fibres in the skin layers play a more important role in determining the composite flexural modulus than those fibres in the core layer. This can be used to explain the above observation in Fig. 7.5 in which the composite flexural modulus for the continuous case is higher than that for the uniform case, since for the continuous case there are more fibres of small fibre orientation angle than those for the uniform case near their skin layers and the fibres near the skin layers are more important in governing the composite flexural modulus.

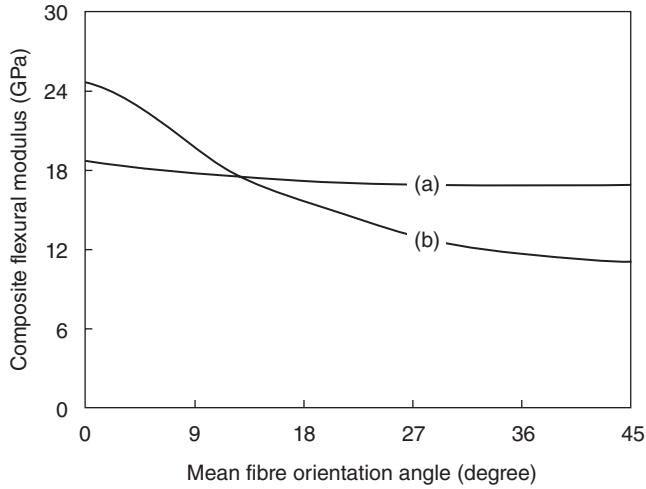

7.8 Effect of mean fibre orientation angle on the flexural modulus of SFRP composites for the case of layered structure: (a) θ_{mean} varies only in the core layer; (b) θ_{mean} varies only in the skin layers. Adapted from Fu *et al.*, 1999.

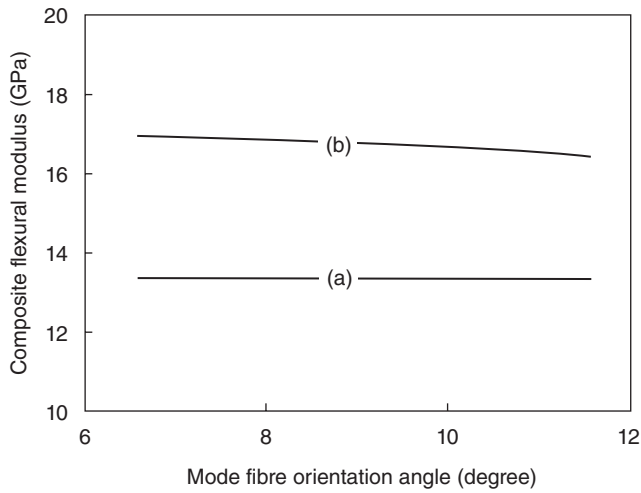

7.9 Effect of mode fibre orientation angle on the flexural modulus of SFRP for the case of layered structure: (a) θ_{mod} varies only in the core layer; and (b) θ_{mod} varies only in the skin layers. Adapted from Fu *et al.*, 1999.

Figure 7.9 shows the effect of mode fibre orientation angle on the flexural modulus of SFRP composites for the case with a layered structure (Fu *et al.*, 1999), where a, b, p and q are the same as in Fig. 7.5; and (a) $\theta_{mean} = 12.95°$ (p and q vary) in the core layer and $\theta_{mean} = 25.81°$ ($p = 0.6$ and $q = 2.0$) in the skin layers, and (b) $\theta_{mean} = 25.81°$ ($p = 0.6$ and $q = 2.0$) in the core

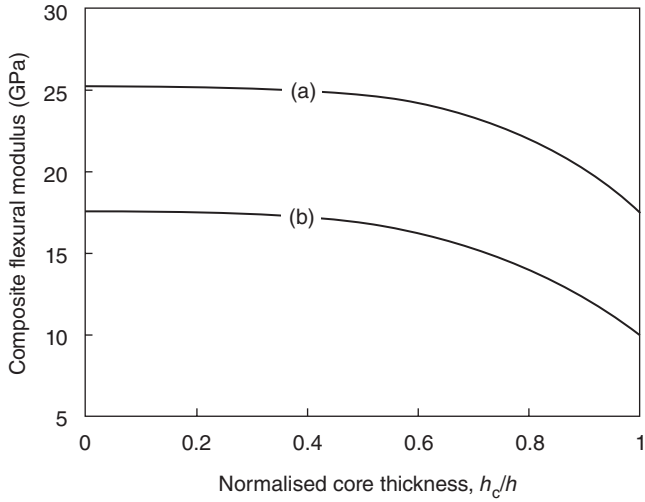

7.10 The flexural modulus of SFRP composites *vs* the core layer thickness for the case of layered structure: (a) $\theta_{mean} = 12.95°$ ($p = 0.6$ and $q = 8$) in the core layer and $\theta_{mean} = 0°$ ($p = 0.5$ and $q = \infty$) in the skin layers; and (b) $\theta_{mean} = 45°$ ($p = 0.5$ and $q = 0.5$) in the core layer and $\theta_{mean} = 12.95°$ ($p = 0.6$ and $q = 8$) in the skin layers. Adapted from Fu *et al.*, 1999.

layer and $\theta_{mean} = 12.95°$ (p and q vary) in the skin layers. It can be seen that the mode fibre orientation angle has a small influence on the composite flexural modulus. This is easily understood since the fibres in the core and skin layers are assumed to be distributed uniformly as for the uniform case.

The flexural modulus of SFRP composites *vs* core layer thickness for the case of a layered structure is shown in Fig. 7.10 (Fu *et al.*, 1999), where $l_{mean} = 3.198$ mm ($a = 0.15$, $b = 1.5$); and (a) $\theta_{mean} = 12.95°$ ($p = 0.6$ and $q = 8$) in the core layer and $\theta_{mean} = 0°$ ($p = 0.5$ and $q = \infty$) in the skin layers, and (b) $\theta_{mean} = 45°$ ($p = 0.5$ and $q = 0.5$) in the core layer and $\theta_{mean} = 12.95°$ ($p = 0.6$ and $q = 8$) in the skin layers (where a smaller mean fibre orientation angle in the skin layers than that in the core layer is assumed since this is consistent with experimental observations (Xia *et al.*, 1995; Friedrich, 1985, 1998)). Figure 7.10 reveals that the composite flexural modulus decreases slowly with increase of core thickness when the core is small (e.g. $<0.4\ h$), but it decreases markedly with increasing normalised core thickness when the core is large (e.g. $> 0.4\ h$). Moreover, the composite flexural modulus of (a) is higher than that of (b) because the mean fibre orientation angles of (a) are smaller than those of (b).

The effect of mean fibre length and, hence mean fibre aspect ratio, on the composite flexural modulus is shown in Fig. 7.11 (Fu *et al.*, 1999), where $\theta_{mean} = 12.95°$ ($p = 0.6$, $q = 8$), and $a = 0.15$ and different b for $l_{mean} \geq 1.0$ mm

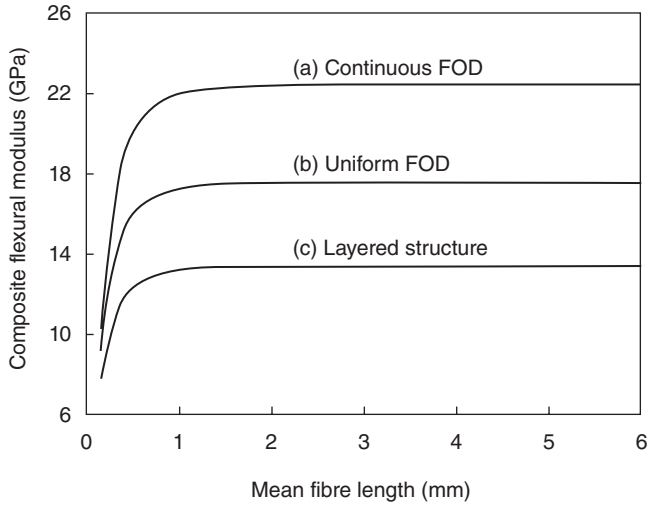

7.11 Effect of mean fibre length (or mean fibre aspect ratio) on the flexural modulus of SFRP for the cases of: (a) continuous FOD, (b) uniform FOD and (c) layered structure. Adapted from Fu *et al.*, 1999.

(or mean aspect ratio ≥ 100) and $a = 5$ and different b for $l_{mean} < 1.0$ mm (or mean aspect ratio < 100); and moreover, $\theta_{mean} = 25.81°$ ($p = 0.6$ and $q = 2.0$) in the skin layers for the case of a layered structure. Obviously, the flexural modulus of SFRP composites increases dramatically with increasing mean fibre length or mean aspect ratio when $l_{mean} \leq 1$ mm (or mean aspect ratio ≤ 100); but it is insensitive to mean fibre length (or mean fibre aspect ratio) when $l_{mean} > 1$ mm (or mean aspect ratio > 100). In addition, the composite flexural modulus for the case of continuous FOD is the highest since it has more fibres of small orientation angle in the skin layers than the other two cases while the flexural modulus for the layered structure case is the lowest as its mean fibre orientation angle (= 25.81°) in the skin layers is assumed less than that (=12.95°) of the uniform case.

The effect of mode fibre length and therefore mode fibre aspect ratio on the composite flexural modulus is shown in Fig. 7.12 for the two cases of a large and a small mean fibre length (or mean fibre aspect ratio) (Fu *et al.*, 1999), where the parameters are the same as in Fig. 7.11 except a and b. The composite flexural modulus increases slightly with the increase of mode fibre length or mode fibre aspect ratio when mean fibre length (or mean fibre aspect ratio) is large (see Fig. 7.12(a)). However, when l_{mean} (or l_{mean}/d) is small, the effect of mode fibre length (or mode fibre aspect ratio) on the composite flexural modulus is noticeable (see Fig. 7.12(b)) and the composite flexural modulus increases with increasing mode fibre length (or mode fibre aspect ratio).

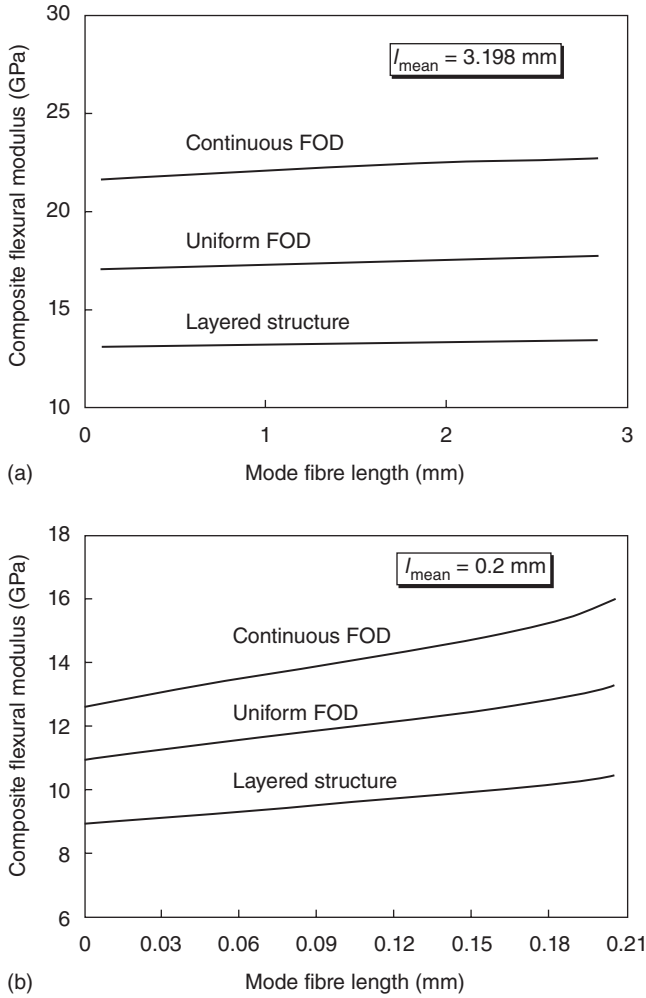

7.12 Effect of mode fibre length (or mode fibre aspect ratio) on the flexural modulus of SFRP for: (a) a large mean fibre length with a value of 3.198 mm (or a large mean fibre aspect ratio with a value of 319.8); and (b) a small mean fibre length with a value of 0.2 mm (or a small mean fibre aspect ratio with a value of 20). Adapted from Fu *et al.,* 1999.

Xia *et al.* (1995) proposed a model for prediction of the flexural modulus of SFRP composites in which the composite is treated as a sandwich beam. First, the elastic moduli for the skin and core layers are obtained. Then, the composite flexural modulus is obtained from the composite beam theory. Depending on the fibre orientation in the skin layer, its elastic modulus can be obtained from:

$$E_c^s = \int_{l_{min}}^{l_{max}} E_{11}(l) f(l) \mathrm{d}l. \tag{7.45}$$

Similarly, based on the fibre orientation in the core layer, the elastic modulus E_c^c of the core layer can be obtained using the modified Halpin–Tsai equation and eqn [7.45]. Finally, the flexural modulus of SFRP composites is determined from:

$$E_{Flex} = \left(E_c^s I_s + E_c^c I_c\right)/I, \tag{7.46}$$

where I_s, I_c and I are, respectively, the moments of inertia of the cross section of the skin layer, the core layer and the injection moulded composite part, and are given by:

$$I_s = b\left(h_s^3/6 + h_s\left(h_c + h_s\right)^2/2\right) \tag{7.47}$$

$$I_c = b\left(h_s^3/12\right) \tag{7.48}$$

$$I = b\left(h^3/12\right), \tag{7.49}$$

where h_s and h_c are, respectively, thickness of the skin and core layers, and b and h are the width and thickness of the injection moulded composite part.

Experimental results of flexural modulus in the 90° (flow direction) and 0° (transverse to resin flow direction) for long fibre reinforced polyamide (PAL) and short fibre reinforced polyamide (PAS) materials and the calculated results using eqn [7.46] are listed in Table 7.1 (Xia *et al.*, 1995). PAL shows about the same flexural modulus values as those of PAS. The theoretical results coincide with the experimental data. This is explained by the fibre orientation in the skin and core layers and fibre orientation is regarded as the most important factor influencing the flexural modulus of moulded composites. Moreover, since the fibres in the surface layers are well oriented along the flow direction, the anisotropy of the flexural modulus occurs in both the moulded PAL and PAS composites. Thus, the transverse composite

Table 7.1 Comparisons of experimental and theoretical results for flexural modulus of SFRP composites; all units in GPa. Adapted from Xia *et al.*, 1995

Material type	90° direction (main flow direction, MFD)		0° direction (transverse to MFD)	
	Experiment	Theory	Experiment	Theory
PAS	7.533	7.703	4.402	5.041
PAL	7.221	7.713	4.107	4.940

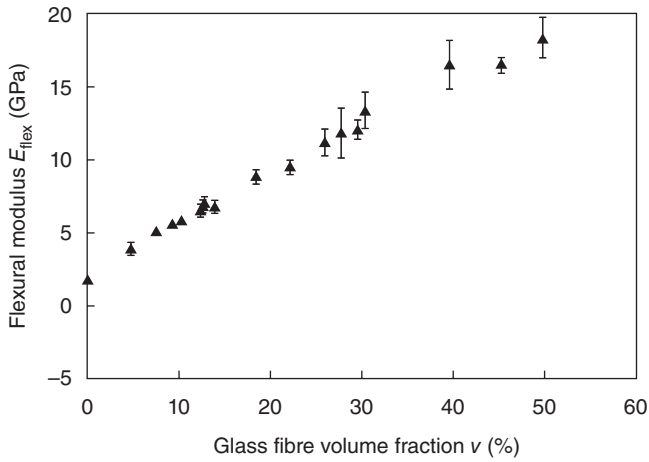

7.13 Composite flexural modulus *vs* fibre content. Adapted from Thomason (2005).

modulus is quite different from and much lower than the longitudinal composite flexural modulus.

Results for the flexural modulus of injection moulded discontinuous long glass fibre reinforced polypropylene composites are plotted in Fig. 7.13 (Thomason, 2005). It is seen that the composite flexural modulus increases almost linearly with increasing glass fibre content. In general, the composite flexural modulus increases with fibre content and fibre length but decreases with fibre orientation angle. It is shown that the mean fibre length decreases while the fibre orientation angle parallel to the flow direction increases with increasing fibre content (Thomason, 2005). Therefore, the effects of both fibre length and fibre orientation balance each other out as the fibre content increases. Consequently, the composite flexural modulus increases linearly with the increase of fibre content.

7.3 References

Baily R S, Davies M and Moore D R (1989), 'Processing property characteristics for long glass fiber reinforced polyamide', *Composites*, 20 (5), 453–460.

Chin W K, Liu H T and Lee Y D (1988), 'Effects of fiber length and orientation distribution on the elastic modulus of short fiber reinforced thermoplastic', *Polym Composite*, 9 (1), 27–35.

Fakirov S and Fakirova C (1985), 'Direct determination of the orientation of short glass fibers in an injection-molded poly(ethylene terephthalate) system', *Polym Composite*, 6 (1), 41–46.

Friedrich K (1985), 'Microstructural efficiency and fracture toughness of short fiber/thermo-plastic matrix composites', *Comp Sci Technol*, 22 (1), 43–74.

Friedrich K (1998), 'Mesoscopic aspects of polymer composites: processing, structure and properties', *J Mater Sci,* 33 (23), 5535–5556.
Fu S Y and Lauke B (1997), 'Analysis of mechanical properties of injection molded short glass fibre/calcite/ABS composites', *J Mater Sci Technol*, 13 (5), 389–396.
Fu S Y and Lauke B (1998a), 'Characterization of tensile behaviour of hybrid short glass fiber/calcite particle/ABS composites', *Compos Part A – Appl Sci Manu*, 29 (5–6), 575–583.
Fu S Y and Lauke B (1998b), 'Fracture resistance of unfilled and calcite-filled ABS composites reinforced by short glass fibers (SGF) under impact load', *Compos Part A – Appl Sci Manu*, 29 (5–6), 631–641.
Fu S Y and Lauke B (1998c), 'The elastic modulus of misaligned short fibre reinforced polymers', *Compos Sci Technol*, 58 (3–4), 389–400.
Fu S Y and Lauke B (1998d), 'An analytical characterization of the anisotropy of the elastic modulus of misaligned short fibre reinforced polymers', *Compos Sci Technol*, 58 (12), 1961–1972.
Fu S Y, Hu X and Yue C Y (1999), 'The flexural modulus of misaligned short-fiber-reinforced polymers', *Compos Sci Technol*, 59 (10), 1533–1542.
Gupta V B, Mittal R K and Sharma P K (1989), 'Some studies on glass fibre-reinforced polypropylene. Part I: reduction in fibre length during processing', *Polym Composite*, 10 (1), 8–15.
Harmia T and Friedrich K (1995), 'Fracture toughness and failure mechanisms in unreinforced and long-glass-fiber-reinforced PA6/PP blends', *Compos Sci Technol*, 53 (4), 423–430.
Hashemi S (2008), 'Tensile and flexural properties of injection-moulded short glass fibre and glass bead ABS composites in the presence of weldlines', *J Mater Sci*, 43 (2), 721–731.
Hashemi S, Elmes P and Sandford S (1997), 'Hybrid effects on mechanical properties of polyoxymethylene', *Polym Eng Sci*, 37 (1), 45–58.
Hine P J, Davidson N, Duckett R A and Ward I M (1995), 'Measuring the fibre orientation and modelling the elastic properties of injection-molded long-fibre-reinforced nylon', *Compos Sci Technol*, 53 (2), 125–131.
Karger-Kocsis J (1993), 'Instrumented impact fracture and related failure behavior in short- and long-glass-fiber-reinforced polypropylene', *Compos Sci Technol*, 48 (1–4), 273–283.
McGrath J J and Wille J M (1995), 'Determination of 3D fibre orientation distribution in thermoplastic injection molding', *Compos Sci Technol*, 53 (2), 133–143.
O'Connell PA and Duckett RA (1991), 'Measurement of fiber orientation in short-fiber-reinforced thermoplastics', *Compos Sci Technol*, 42 (4), 329–347.
Ramsteiner F and Theysohn R (1979), 'Tensile and impact strengths of unidirectional, short fiber-reinforced thermoplastics', *Composites*, 10 (2), 111–119.
Spahr D E, Friedrich K, Schultz J M and Bailey R S (1990), 'Microstructure and fracture behavior of short and long fiber-reinforced polypropylene', *J Mater Sci*, 25 (10), 4427–4439.
Takahashi K and Choi N S (1991), 'Influence of fibre weight fraction on the failure mechanisms of poly(ethylene terephthalate) reinforced by short-glass fibres', *J Mater Sci*, 26 (17), 4648–4656.
Thomason J L (2005), 'The influence of fibre length and concentration on the properties of glass fibre-reinforced polypropylene. 6. The properties of injection

moulded long fibre PP at high fibre content', *Compos Part A – Appl Sci Manu*, 36 (7), 995–1003.

Thomason J L and Vlug M A (1996), 'Influence of fibre length and concentration on the properties of glass fibre-reinforced polypropylene: 1. Tensile and flexural modulus', *Compos Part A – Appl Sci Manu*, 27 (6), 477–484.

Tsai S W (1980), *Introduction to composite materials*, Technomic Publishing Inc., Lancaster, PA.

Ulrych F, Sova M, Vokrouhlecky J and Turcic B (1993), 'Empirical relations of the mechanical properties of polyamide 6 reinforced with short glass fibers', *Polym Composite*, 14 (3), 229–237.

Xia M, Hamada H and Maekawa Z (1995), 'Flexural stiffness of injection molded glass fiber reinforced thermoplastics', *Int Polym Proc*, 10 (1), 74–81.

8

Thermal conductivity and expansion of short fibre reinforced polymer composites

Abstract: Polymers are added with inorganic short fibres such as short glass and short carbon fibres with relatively high thermal conductivity to fabricate composites that can meet high thermal conductivity requirements for applications where highly thermally conductive materials are required. Further, dimensional stability is also important for polymers that are used in areas where temperature changes often occur. In this chapter, theoretical models for the thermal conductivity and thermal expansion of SFRPs are presented and their thermal properties are discussed as a function of the component properties, fibre length distribution and fibre orientation distribution for the cases of unidirectional, misaligned and randomly distributed fibres.

Key words: thermal conductivity, thermal expansion, unidirectional, misaligned, random distribution.

8.1 Introduction

Polymer materials are often used as thermal insulators because of their low thermal conductivity. However, when they are used in electronic packaging applications, for example, where highly thermally conductive materials are required, polymers are added with inorganic fillers with high thermal conductivity to fabricate composites that can meet the high thermal conductivity requirement. In designing such filled polymers, the prediction of thermal conductivity of the final composite products is essential. Moreover, dimensional stability is important for polymers that are used in areas where temperature changes would occur. Polymers usually have a relatively high thermal expansion and therefore their thermal expansion should be decreased to increase dimensional stability for such applications in which temperature often changes. Hence, inorganic fillers such as short glass fibres and short carbon fibres are introduced to polymer matrices to significantly reduce thermal expansion. Thermal expansion of short fibre reinforced polymer (SFRP) composites is dependent on fibre length and orientation distributions and its prediction is addressed in this chapter.

8.2 Thermal conductivity

Many reports have been published on the improvement of thermal conductivity of polymers by filling with thermally conductive fillers. The thermal conductivity of composites is known to increase exponentially with increase of filler content. SFRP composites are attractive materials for electronic packaging applications where the combination of reinforcement with high thermal conductivity embedded in a resin matrix with low thermal conductivity is desirable to maintain a low temperature environment for thermally sensitive electronic packaging components. A number of analytical models have been proposed to predict thermal conductivity of short fibre reinforced polymer composites (Halpin, 1984; Nielsen, 1973; Willis, 1977; Normura and Chou, 1980; Chou and Nomura, 1981; Hatta and Taya, 1985; Chen and Wang, 1996). They are, however, focused on either aligned short fibre composites (Halpin, 1984; Normura and Chou, 1980) or completely random short fibre composites (Nielsen, 1973; Willis, 1977) or short fibre composites with fibres of a constant fibre length (Chou and Nomura, 1981; Hatta and Taya, 1985; Chen and Wang, 1996). Fibre length distribution (FLD) always exists in injection moulded SFRP composites. However, all the above models did not consider the effect of FLD on thermal conductivity of SFRP composites. It has been shown that FLD plays an important role in determining the thermal conductivity (Fu and Mai, 2003). Moreover, due to partial fibre alignment, the fibre orientation distribution (FOD) also has a significant effect on the thermal conductivity of SFRP composites.

In this chapter, the unidirectional SFRP case is first considered. The thermal conductivity of partially aligned SFRP composites with a FLD and a FOD is next discussed. Finally, the two-dimensional (2D) and three-dimensional (3D) random cases are considered.

8.2.1 Thermal conductivity of unidirectional SFRP composites

Thermal conductivity is a bulk property, analogous to elastic modulus. It is well accepted that a mathematical analogy exists between thermal conduction and elasticity of fibre composites. Similar to the predictions of the elastic modulus using the laminate analogy approach (LAA) (Fu and Lauke, 1998a) to evaluate the thermal conductivity of SFRP composite in the '1' direction as shown in Fig. 8.1, which depends on the orientation distribution of the angle (θ) that the fibres make with the '1' direction, we need to first evaluate the thermal conductivity of the corresponding unidirectional short fibre composites by assuming all the fibres lie in the 1–2 plane. It has been shown by Choy *et al.* (1992, 1994), Progelhof *et al.* (1976), Nielsen (1974), Bigg (1986) and Agari *et al.* (1991) that the Halpin–Tsai

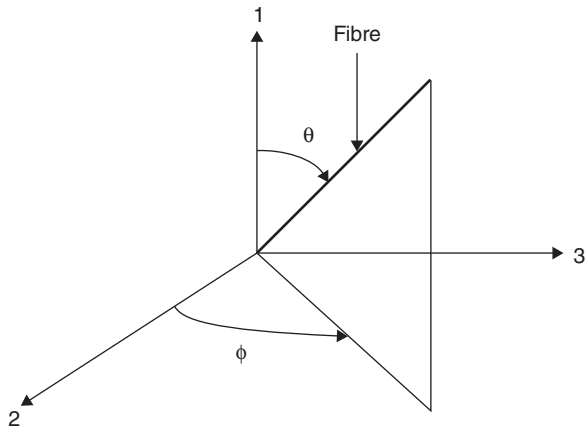

8.1 Definitions of spatial fibre orientation angles θ and ϕ.

equation can be used to describe the thermal conduction of unidirectional short fibre composites. For a unidirectional lamina, the thermal conductivities parallel (K_1) and perpendicular (K_2) to the fibre direction are given by (Halpin, 1984):

$$K_1 = \frac{1+2(l/d)\mu_1 v}{1-\mu_1 v} K_{\mathrm{m}} \tag{8.1}$$

$$K_2 = \frac{1+2\mu_2 v}{1-\mu_2 v} K_{\mathrm{m}}, \tag{8.2}$$

where l is fibre length and d is fibre diameter, and v is fibre volume fraction. K_{m} is the thermal conductivity of matrix, and μ_1 and μ_2 are obtained from:

$$\mu_1 = \frac{K_{\mathrm{f1}}/K_{\mathrm{m}} - 1}{K_{\mathrm{f1}}/K_{\mathrm{m}} + 2l/d} \tag{8.3}$$

$$\mu_2 = \frac{K_{\mathrm{f2}}/K_{\mathrm{m}} - 1}{K_{\mathrm{f2}}/K_{\mathrm{m}} + 2}, \tag{8.4}$$

where K_{f1} and K_{f2} are thermal conductivity of the fibre in the direction parallel and transverse to the fibre axis direction, respectively.

When the fibres in the lamina are oriented at an angle θ with respect to the 1-axis, the composite thermal conductivities along the 1-axis and 2-axis are given by Choy *et al.* (1994):

$$K_1' = K_1 \cos^2\theta + K_2 \sin^2\theta \tag{8.5}$$

$$K_2' = K_1 \sin^2\theta + K_2 \cos^2\theta. \tag{8.6}$$

The linear flux along a given direction through a lamina of a multidirectional laminate can be obtained by the temperature gradient. The total heat flux through the laminate can be obtained by integrating along it thickness. The thermal conductivity of a laminate can thus be integrated through its thickness since temperative gradient is continuous. By assuming the heat

flux through all the laminae, the composite thermal conductivities are determined by (Choy *et al.*, 1992, 1994):

$$K_1^c = \frac{1}{2}(K_1 + K_2) + \frac{1}{2}V(K_1 - K_2) \tag{8.7}$$

$$K_2^c = \frac{1}{2}(K_1 + K_2) - \frac{1}{2}V(K_1 - K_2), \tag{8.8}$$

where V is given by:

$$V = \frac{\lambda^2\left(1 + e^{-\lambda\pi/2}\right)}{\left(\lambda^2 + 4\right)\left(1 - e^{-\lambda\pi/2}\right)}, \tag{8.9}$$

and λ is a parameter characterising the degree of fibre orientation to be given later. On the contrary, it has been shown (Bigg, 1986) that the thermal conductivity of unidirectional SFRP composites can also be predicted accurately by Nielsen's model (1973):

$$K_1 = \frac{1 + 2(l/d)\xi_1 v}{1 - \xi_1 \psi v} K_m \tag{8.10}$$

$$K_2 = \frac{1 + 0.5\xi_2 v}{1 - \xi_2 \psi v} K_m, \tag{8.11}$$

in which

$$\xi_1 = \frac{K_{f1}/K_m - 1}{K_{f1}/K_m + 2l/d} \tag{8.12}$$

$$\xi_2 = \frac{K_{f2}/K_m - 1}{K_{f2}/K_m + 0.5} \tag{8.13}$$

$$\psi = 1 + \left(\frac{1 - v_{max}}{v_{max}^2}\right) v, \tag{8.14}$$

where v_{max} is the maximum fibre fraction possible while still maintaining a continuous matrix phase, and is referred to as the maximum packing fraction. The maximum filler packing volume fraction is dependent on the dispersion state and the filler shape as shown in Table 8.1 (Nielsen, 1974; Okamoto and Ishida, 1999).

It is easy to ascertain that the Halpin–Tsai and Nielsen equations give similar predictions. Comparison between these two models for the prediction of the thermal conductivities of SFRP composites is given in Fig. 8.2, where $v_{max} = 0.907$ for uniaxial hexagonal alignment ($v_{max} = 0.785$ for simple cubic alignment, similar results can be obtained), $d = 10\ \mu$m, $l = 0.5$ mm, $K_{f1} = K_{f2} = 10.4$ mW cm^{-1} K^{-1}, and $K_m = 2.0$ mW cm^{-1} K^{-1}. From Fig. 8.2, it can be seen that the two models give similar (very close) predictions, except there is a small difference in the transverse thermal conductivity. Thus, it is more convenient to use the Halpin–Tsai equation for prediction of thermal conductivity of unidirectional SFRP composites since it does not need the parameter, v_{max}, which depends on fibre alignment (or packing geometry).

Table 8.1 Maximum filler packing fractions (Nielsen, 1974; Okamoto and Ishida, 1999)

Shape of fillers	Type of packing	Maximum packing fraction
Spheres	Hexagonal close packed	0.741
Spheres	Face centered cubic	0.741
Spheres	Body centered cubic	0.600
Spheres	Simple cubic	0.524
Spheres	Random close packed	0.637
Spheres	Random loose packed	0.601
Rods or fibres	Uniaxial hexagonal close packed	0.907
Rods or fibres	Uniaxial simple cubic	0.785
Rods or fibres	Uniaxial random	0.820
Rods or fibres	Three-dimensional random	0.520

From Okamoto and Ishida (1999) (*Journal of Applied Polymer Science*, Vol. 72, No. 13, 1999, p. 1692. Copyright 1999 John Wiley & Sons Inc. Reprinted with permission of John Wiley & Sons Inc.).

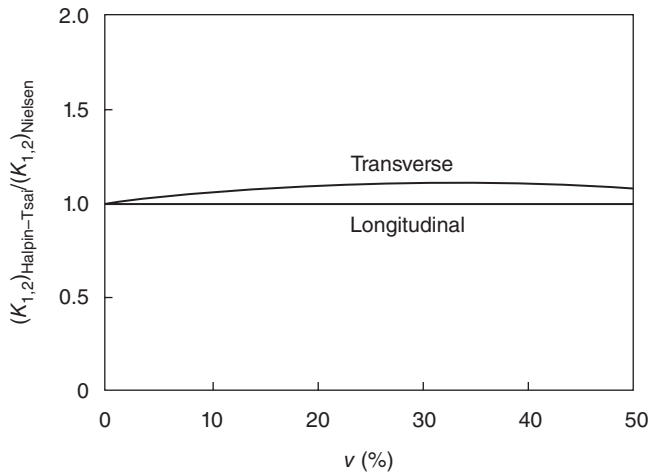

8.2 Predicted thermal conductivity of unidirectional short fibre composites by Halpin–Tsai equation (Halpin, 1984) and Nielsen equation (1974). Adapted from Fu and Mai (2003) (*Journal of Applied Polymer Science*, Vol. 88, No. 6, 2003, p. 1500. Copyright 2003, John Wiley & Sons Inc. Reprinted with permission of John Wiley & Sons Inc.).

Nomura and Chou (1980) presented bounds of the effective thermal conductivities for unidirectional short fibre composites based on an approach originally developed by them for the composite effective elastic modulus. For a binary system, the bounds of thermal conductivity are given by the following explicit forms:

$$\left\{\frac{v}{K_f}+\frac{v_m}{K_m}-\frac{vv_m\left(\frac{1}{K_f}-\frac{1}{K_m}\right)^2 h(t)}{(v_m-v)\left(\frac{1}{K_f}-\frac{1}{K_m}\right)h(t)+\frac{v}{K_f}+\frac{v_m}{K_m}}\right\}^{-1} \le K_1 \le vK_f +$$

$$v_m K_m - \frac{vv_m(K_f-K_m)^2(1-h(t))}{(v_m-v)(K_f-K_m)(1-h(t))+vK_f+v_mK_m}, \quad 8.15$$

where $h(t)$ is:

$$h(t)=\frac{t^2}{t^2-1}\left\{1-\frac{1}{2}\left[\left(\frac{t^2}{t^2-1}\right)^{1/2}-\left(\frac{t^2-1}{t^2}\right)^{1/2}\ln\left(\frac{t+(t^2-1)^{1/2}}{t-(t^2-1)^{1/2}}\right)\right]\right\}, \quad 8.16$$

and t is the fibre aspect ratio (l/d). In the case of spherical inclusion, $h(t)$ = 2/3 for $t = 1$. And for the special case of continuous fibres, $h(t) = 1$ for $t = \infty$, eqn [8.15] becomes:

$$K_1 = vK_f + v_mK_m. \quad 8.17$$

8.2.2 Thermal conductivity of misaligned SFRP composites

As mentioned above, thermal conductivity is a bulk property analogous to modulus. The elastic modulus of misaligned SFRP composites has been successfully predicted using the laminate analogy approach (LAA) (Fu and Lauke, 1998a). Therefore, here, the LAA is used to derive an expression for the thermal conductivity of SFRP composites including effects of fibre volume fraction, FLD and FOD.

In the LAA, the SFRP composites can be simulated as a sequence of a stack of various laminae with different fibre orientations and different fibre lengths. Successive development of the laminated plate model of a three-dimensionally (3D) misaligned SFRP composite is shown in Fig. 8.3. The SFRP composite with a 3D spatial FOD function $g(\theta,\phi) = g(\theta)g(\phi)/\sin\theta$ having fibre ends in the three visible planes (see Fig. 8.3(a)) is first replaced by a SFRP composite with the same $g(\theta)$ but $\phi = 0$, having no fibre ends in the 1–2 plane or no fibres in the out-of-plane direction (represented by the 3-axis) (see Fig. 8.3(b)). Then, according to the FLD, this composite is regarded as a combination of laminates, each comprising fibres having the same fibre length (see Fig. 8.3(c); 'L(l_i), i = 1, 2, . . . , n' denotes the ith laminate containing fibres of the same length l_i). Each laminate with the same fibre length is then treated as a stacked sequence of laminae; each lamina consists of fibres having the same fibre length and the same fibre orientation (see Fig. 8.3(d), 'L(l_i,θ_j), j = 1, 2, . . . , m'

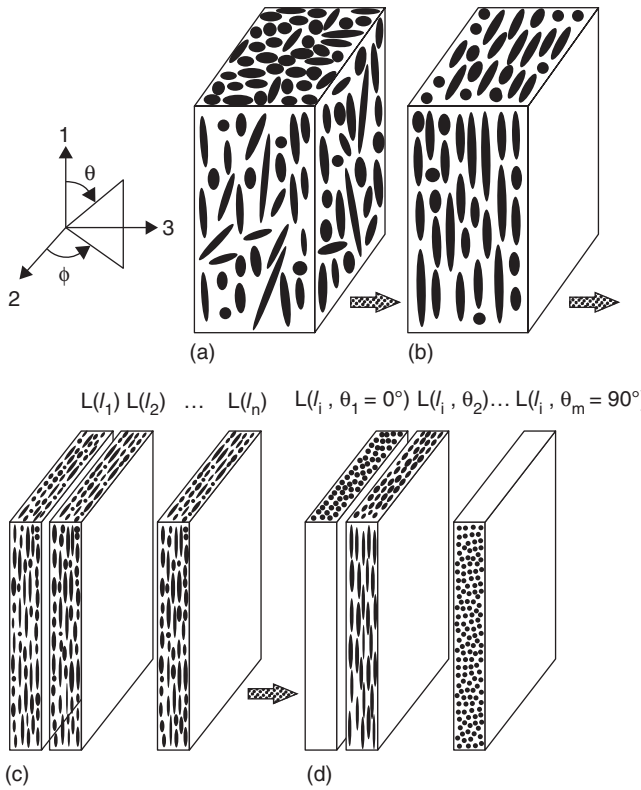

8.3 Simulations of the laminated plate model of a 3D misaligned SFRP composite: (a) real 3D SFRP; (b) supposed SFRP; (c) supposed SFRP is considered as combination of laminates – each laminate has the same fibre length; and (d) each laminate is treated as a stacked sequence of laminae – each lamina has the same fibre length and the same fibre orientation. Adapted from Fu and Mai (2003) (*Journal of Applied Polymer Science,* Vol. 88, No. 6, 2003, p. 1499. Copyright 2003, John Wiley & Sons Inc. Reprinted with permission of John Wiley & Sons Inc.).

denotes the jth lamina containing fibres having the same length l_i and the same angle θ_j).

In a unidirectional lamina, a linear relationship between heat flux and temperature gradient in the directions parallel and perpendicular to the fibre direction (namely, in the local coordinate system) is given by:

$$q_i = -K_i \nabla T_i, \quad i = 1, 2. \tag{8.18}$$

In the global coordinate system, the fibres of the lamina are oriented at an angle θ ($\theta \neq 0$) relative to the measured direction; the linear relationship between heat flux and temperature gradient is:

$$q_i' = -K_i' \nabla T_i', \quad i = 1, 2. \tag{8.19}$$

Let us introduce a transformation tensor X_{ij} defined by:

$$Y_i = X_{ij} Y_j', \tag{8.20}$$

where Y_i and Y_j' are the components of a vector Y in the local and global coordinate systems, respectively. Then, we have:

$$X_{ij}^{-1} q_i' = -K_i X_{ij} \nabla T_j'. \tag{8.21}$$

So,

$$K_i' = X_{ij}^{-1} K_i X_{ij}, \tag{8.22}$$

where the coordinate transformation tensor X_{ij} is given by:

$$X_{ij} = \begin{Bmatrix} \cos\theta & \sin\theta \\ -\sin\theta & \cos\theta \end{Bmatrix}. \tag{8.23}$$

Finally, we obtain:

$$K_1' = K_1 \cos^2\theta + K_2 \sin^2\theta. \tag{8.24}$$

The total heat flux along the 1′-axis in the global coordinate system for a multi-laminate then becomes:

$$Q_1' = \sum_{k=1}^{M} q_1' h_k = -\sum_{k=1}^{M} K_1' \nabla T_1' h_k, \tag{8.25}$$

where M represents the number of plies in the laminate, k is the serial index of the ply in the laminate, and h_k is the thickness fraction of the kth ply. Since the temperature gradient is continuous across the thickness, eqn [8.25] is reduced to:

$$Q_1' = -K_c \nabla T_1', \tag{8.26}$$

where the thermal conductivity of the composite laminae is:

$$K_c = \sum_{k=1}^{M} K_1' h_k = \int_{l=l_{min}}^{l_{max}} \int_{\theta=\theta_{min}}^{\theta_{max}} K_1' f(l) g(\theta) \mathrm{d}l \mathrm{d}\theta. \tag{8.27}$$

The thermal conductivity of the SFRP composite with a FLD and a FOD can be evaluated using eqn [8.27]. However, if it is used to predict the composite thermal conductivity, no interaction between short fibres with different orientation angles and different fibre lengths can be included. Thus, to consider the effect of fibre interaction on composite thermal conductivity, the fibres with a volume fraction v are divided into two equal halves having the same FLD and FOD. The first half of the fibres is incorporated into the pure polymer matrix. The thermal conductivity can then be evaluated using eqn [8.27]. The filled polymer matrix is considered as the

effective matrix for the second half of the fibres. It should be noted that the effective fibre volume fraction is $v/(2 - v)$ and the obtained thermal conductivity is taken as K_m for the second half of the fibres. Now, the second half of the fibres is incorporated into this effective matrix. The interaction between short fibres of different orientation angles and different lengths can then be incarnated in a manner such that the second half of the fibres is incorporated into the effective matrix containing the first half of the fibres. Finally, the overall composite thermal conductivity can be predicted using eqn [8.27] and the fibre volume fraction is equal to $v/2$ for the second half of the fibres.

Figure 8.4 shows the effect of mean aspect ratio on the thermal conductivity of short glass and short carbon fibre reinforced poly(phenylene sulfide) (PPS) composites (Choy *et al.*, 1992), where v is fixed at 0.3, θ_{mean} = 36° (p = 0.6 and q = 1 for fibre orientation distribution), for short carbon fibres (SCF), d = 7 μm, the thermal conductivities of carbon fibre are: K_{f1} = 94 mW cm^{-1} K^{-1}, K_{f2} = 6.7 mW cm^{-1} K^{-1} 27 and l_{mean}/d varies by changing a (b is fixed at 1.2) and other parameters are the same as in Fig. 8.2. It can be seen that the thermal conductivity of short glass fibre reinforced polymer composites increases very slightly with the increase of mean fibre aspect ratio when it is small (<~10) and becomes insensitive to fibre aspect ratio when the fibre aspect ratio is large (>~10). However, the thermal conductivity of short carbon fibre reinforced polymer composites increases dramati-

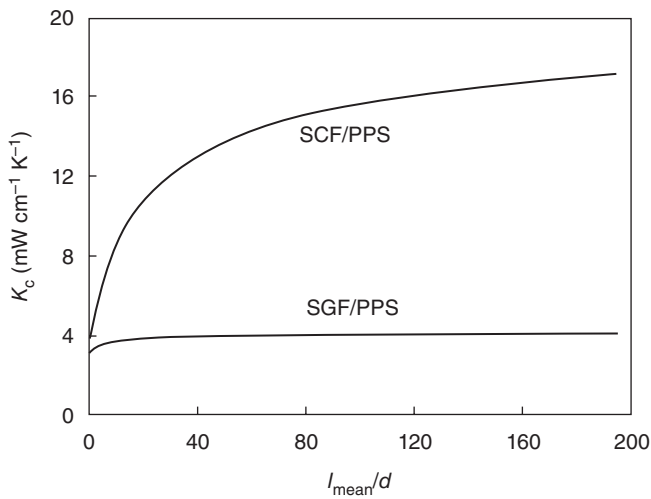

8.4 Effect of mean fibre aspect ratio on thermal conductivity of SFRP composites. Adapted from Fu and Mai (2003) (*Journal of Applied Polymer Science*, Vol. 88, No. 6, 2003, p. 1502. Copyright 2003, John Wiley & Sons Inc. Reprinted with permission of John Wiley & Sons Inc.).

cally with increase of mean fibre aspect ratio, especially when the fibre aspect ratio is less ~100. Moreover, the thermal conductivity of the glass fibre composite is much lower than the thermal conductivity of the carbon fibre composite. This is because the thermal conductivity of carbon fibre is much higher than that of glass fibre in the fibre axis direction ($K_{fl}/K_m = 5.2$ for glass fibre and $K_{fl}/K_m = 47$ for carbon fibre), and hence the thermal conductivity of the glass fibre composite will be much lower than that of the carbon fibre composite at a similar fibre content (e.g., by a factor of ~3.8 at $v = 0.3$ and fibre aspect ratio = 80). The thermal conductivity of the glass fibre composite is also much less sensitive to the fibre length than the thermal conductivity of the carbon fibre composite.

Figure 8.5 shows the effect of mean fibre orientation angle on the thermal conductivity of SFRP composites, where the parameters are the same as in Fig. 8.4 except $l_{mean} = 424\ \mu m$ ($a = 2.6$ and $b = 1.2$) and θ_{mean} varies by changing p (q is fixed at 1). It is observed that the thermal conductivity of short glass fibre reinforced polymer composites decreases slowly with increase of mean fibre orientation angle. But, the thermal conductivity of short carbon fibre reinforced polymer composites decreases significantly with increasing mean fibre orientation angle θ_{mean}. This indicates that the thermal conductivity of the carbon fibre composite is more sensitive to fibre orientation than the thermal conductivity of the glass fibre composite. This is because on one hand, glass fibres are isotropic, and on the other, the thermal

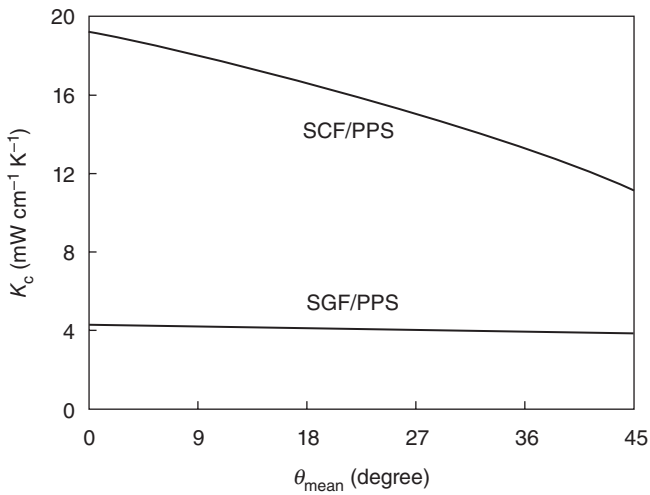

8.5 Effect of mean fibre orientation angle on thermal conductivity of SFRP composites. Adapted from Fu and Mai (2003) (*Journal of Applied Polymer Science*, Vol. 88, No. 6, 2003, p. 1502. Copyright 2003, John Wiley & Sons Inc. Reproduced with permission of John Wiley & Sons Inc.).

conductivity of carbon fibre is much higher than that of glass fibres in the fibre axis direction.

Also, eqn [8.27] can be used to evaluate the thermal conductivity of the SFRP composite in any given direction (Θ,Φ), but the angle θ must be replaced by the angle δ, where the angle δ is that between the fibre axial direction (θ,ϕ) and the direction (Θ,Φ), given by (Fu and Lauke, 1998b), see eqn [6.89]:

$$\cos\delta = \cos\Theta\cos\theta + \sin\Theta\sin\theta\cos(\phi - \Phi). \qquad 8.28$$

Combining eqns [8.27] with [8.28] gives predictions of the anisotropic thermal conductivity of SFRP composites.

The above theory is applied to published experimental results as shown in Table 8.2 for the thermal conductivity of short glass fibre and short carbon fibre reinforced poly(phenylene sulfide) (PPS) composites (Choy *et al.*, 1992) and poly(ether ether ketone) (PEEK) composites (Choy *et al.*, 1994). The thermal conductivities of the surface and skin layers were measured separately. The data for the parameters used are as follows: K_m = 2.43 mW cm^{-1} K^{-1} for PEEK, K_m = 2 mW cm^{-1} K^{-1} for PPS; K_{f1} = K_{f2} = 10.4 mW cm^{-1} K^{-1} for glass fibre; K_{f1} = 94 mW cm^{-1} K^{-1} for the carbon fibre used in PPS and K_{f1} = 80 mW cm^{-1} K^{-1} for the carbon fibre used in PEEK and K_{f2} = 6.7 mW cm^{-1} K^{-1}. An alternative expression for the FOD density function is given by Choy *et al.* (1992, 1994):

$$g(\theta) = -\lambda\cdot\exp(-\lambda\theta)/[1-\exp(-\lambda\pi/2)] \qquad 8.29$$

and values of λ are given in Table 8.2. The average fibre aspect ratios for the four composites of PEEK30cf, PPS30cf, PPS40cf and PPS40gf are, respectively, 17 (a = 55.4 and b = 2), 21 (a = 36.3 and b = 2), 16 (a = 62.7 and

Table 8.2 Comparison between theoretical predictions and experimental results (Choy *et al.*, 1992, 1994) for thermal conductivity K_c (mW cm^{-1} K^{-1}) of four composites

Composites	Volume fraction	λ		K_c					
				Surface layer			Middle layer		
		Surface layer	Middle layer	Exp.	Theo.[b1]	Theo.[b2]	Exp.	Theo.[b1]	Theo.[b2]
PEEK30cf[a]	0.214	3.3	2.4	11.6	9.96	11.87	10.8	9.45	11.16
PPS30cf[a]	0.243	4.1	1.9	15.2	12.50	14.96	12.4	10.97	12.88
PPS40cf[a]	0.335	4.7	2.1	17.2	15.89	19.76	15.6	13.92	16.96
PPS40gf[a]	0.264	5.3	2.9	4.08	3.93	3.96	3.99	3.84	3.89

Notes:
a: 30cf, 40cf, and 40gf denote 30 wt% carbon fibre, 40 wt% carbon fibre, and 40 wt% glass fibre, respectively. Theo.[b1] and Theo.[b2] denote the theoretical values before and after taking into account the effect of fibre interaction, respectively.

$b = 2$), and 17 ($a = 27$ and $b = 2$). Clearly, the theoretical results are in good agreement with experimental data when considering the effect of the fibre interaction. When the effect of fibre interaction is not included, the predicted results are lower than the experimental values.

Chen and Wang (1996) also studied the effective thermal conductivity of composites containing misoriented short fibres. The thermal conductivity of planar orientation distribution, namely, transversely isotropic distribution of fibres, was considered. A symmetrical angular fibre distribution function around the major alignment direction was assumed and a single parameter of an exponential function was used to describe the fibre orientation distribution in the SFRP composites. Fibre length distribution was not described and constant length was assumed implicitly in SFRP composites. A relatively complicated method based on the idea of Mori–Tanaka's mean field theory (1973) in conjunction with Eshelby's equivalent inclusion method (1957) for steady-state heat conduction in a composite including the effects of fibre length and orientation to predict the thermal conductivity of SFRP composites was presented. The theory was also used to examine the thermal conductivity of injection moulded tensile bars of poly(pheylene sulfide) reinforced with 30% and 40% by weight of carbon or glass fibres (Choy *et al.*, 1992). While their reported theoretical values are also close to the experimental data, their analytical expressions are quite complicated and difficult to use for the prediction of injection moulded SFRP composites.

8.2.3 Thermal conductivity of 2D and 3D random SFRP composites

For a two-dimensionally (2D) random short fibre composite, $g(\theta) = 2/\pi$, the expression for the composite thermal conductivity can be obtained from eqns [8.24] and [8.27] for $0 \le \theta \le \pi/2$ as follows:

$$K_c = \frac{1}{2}\left(\int_{l=l_{min}}^{l_{max}} K_1 f(l)\mathrm{d}l + \int_{l=l_{min}}^{l_{max}} K_2 f(l)\mathrm{d}l \right). \qquad 8.30$$

Similarly, for a 3D random short fibre composite, $g(\theta,\phi) = g(\theta)g(\phi)/\sin\theta = 1/2\pi$, and $g(\theta) = \sin\theta$. So, the expression for the composite thermal conductivity can be obtained from eqns [8.24] and [8.27] for $0 \le \theta \le \pi/2$, so that:

$$K_c = \frac{1}{3}\int_{l=l_{min}}^{l_{max}} K_1 f(l)\mathrm{d}l + \frac{2}{3}\int_{l=l_{min}}^{l_{max}} K_2 f(l)\mathrm{d}l. \qquad 8.31$$

When the fibre length has a constant value, eqns [8.30] and [8.31] can be simplified to:

$$K_c = \frac{1}{2}(K_1 + K_2) \quad \text{for} \quad \text{2D random case} \qquad 8.32$$

$$K_c = \frac{1}{3}K_1 + \frac{2}{3}K_2 \quad \text{for} \quad \text{3D random case.} \tag{8.33}$$

The above equations, [8.32] and [8.33], are employed to predict the thermal conductivity of 2D and 3D random short fibre composites, respectively. The predicted results are, respectively, shown in Figs 8.6(a) and 8.6(b), where the following values of the parameters are used: $l/\mathrm{d} = 100$, $K_{f1}/K_m =$

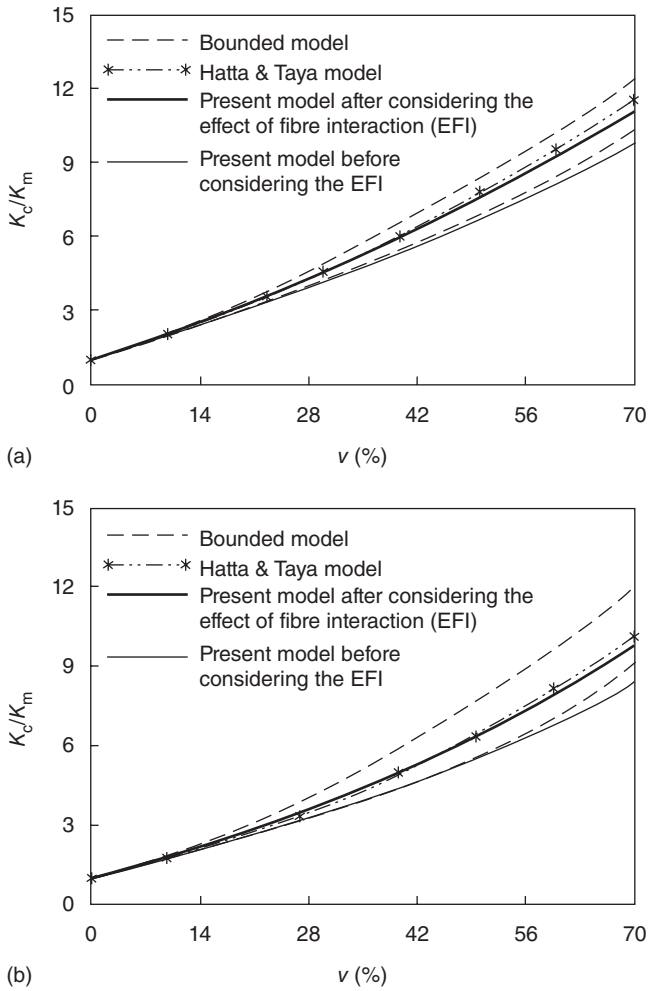

8.6 Thermal conductivity of (a) 2D and (b) 3D random SFRP composite as a function of v with $K_{f1}/K_m = K_{f2}/K_m = 20$ and $l/\mathrm{d} = 100$ (*Journal of Applied Polymer Science*, Vol. 88, No. 6, 2003, p. 1503. Copyright 2003, John Wiley & Sons Inc. Reproduced with permission of John Wiley & Sons Inc.).

$K_{f2}/K_m = 20$. The predicted results by other theories (Chou and Nomura, 1981; Hatta and Taya, 1985) are also displayed in these two figures. It is seen that when the fibre interaction is taken into account, the predicted values by the present theory, eqns [8.32] and [8.33], lie between those by the bounding model (Chou and Nomura, 1981) and are close to those by the Hatta and Taya model (1985) which also considers the effect of fibre interaction. Although the Hatta and Taya model can give accurate prediction of the thermal conductivity of short fibre composites having a constant fibre length, it is not suitable for the prediction of the thermal conductivity of injection moulded SFRP composites having a FLD. When the fibre interaction is not considered, the predicted values by the present model become lower and are close to the lower values predicted by the bounding model (Chou and Nomura, 1981). The composite thermal conductivity increases dramatically with increasing fibre volume fraction, indicating that the fibre content plays an important role in influencing the thermal conductivity of SFRP composites (see Fig. 8.6).

Comparison of the electrical and thermal conductivities of polyethylene composites filled with randomly dispersed and disoriented carbon fibres is made by Agari *et al.* (1991), in which the fibre aspect ratio changes from 1 to 21.8 (far less than 100). The composites show virtually the same level of electric conductivity as that of the polymer matrix until the filler fraction reaches the percolation threshold where a rapid increase in electric conductivity starts. After this critical volume fraction, the composite electric conductivity gradually approaches a plateau. It is noted that the critical volume fraction decreases dramatically with increasing fibre aspect ratio from 30.1% for powdery particles to 1.6% for short fibres with an aspect ratio of 21.8. Conversely, the thermal conductivity of short carbon fibre reinforced polyethylene composites consistently increases with increasing filler content. In the isotropic composite (namely, short carbon fibres are randomly dispersed and oriented), the longer the fibre length, the larger is the composite thermal conductivity. These observations are consistent with the theoretical results shown in Figs 8.4 and 8.6.

Dunn *et al.* (1991) presented a combined analytical and experimental study to study the effective thermal conductivity of hybrid Kerimid composite materials containing Al_2O_3 short fibres and Si_3N_4 whiskers. The analysis utilises the equivalent inclusion approach for steady-state heat conduction (Hatta and Taya, 1986) through which the interaction between various reinforcing phases at finite concentrations is approximately considered by Mori–Tanaka's (1973) mean field approach. The results show that the composite thermal conductivity increases markedly with increasing fibre volume fraction for 2D and 3D random cases. This observation is consistent with that shown in Fig. 8.6.

8.3 Thermal expansion

When a body undergoes a temperature change, there will be a change in its dimensions relative to its original dimensions proportional to the temperature change. The coefficient of thermal expansion is defined as the change in the linear dimension of the body per unit change of temperature. In this section, thermal expansions of SFRP composites are discussed, respectively, for the unidirectional case, the partially misaligned case, and the 2D and 3D random cases.

8.3.1 Thermal expansion of unidirectional SFRP composites

For a unidirectional lamina, the linear coefficients (α_1^0 and α_2^0) of thermal expansion parallel (1-direction) and transverse (2-direction) to the fibres are given by Schapery (1968):

$$\alpha_1^0 = \frac{E_f \alpha_f v + E_m \alpha_m v_m}{E_f v + E_m v_m} \tag{8.34}$$

$$\alpha_2^0 = (1+\nu_f)\alpha_f v + (1+\nu_m)\alpha_m v_m - \alpha_1^0 (\nu_f v + \nu_m v_m), \tag{8.35}$$

where α_f is the thermal expansion coefficient of the fibres, α_m the thermal expansion coefficient of the matrix. ν_f and ν_m are the Poisson's ratio of the fibres and the matrix, respectively.

Equations [8.34] and [8.35] for α_1^0 and α_2^0 are derived using the mechanics of materials approach. Assume only a temperature ΔT is applied, the unidirectional lamina has zero overall load in the unidirectional direction, then we have:

$$\sigma_F v + \sigma_M v_m = 0. \tag{8.36}$$

The stresses in the fibre and matrix (σ_F and σ_M) caused by the thermal expansion mismatch between fibre and matrix are:

$$\sigma_F = E_f (\varepsilon_F - \alpha_f \Delta T), \tag{8.37}$$

$$\sigma_M = E_m (\varepsilon_M - \alpha_m \Delta T). \tag{8.38}$$

Substitution of the above two equations in eqn [8.36] and realisation of iso-strains in the fibre and the matrix yield:

$$\varepsilon_F = \frac{\alpha_f E_f v + \alpha_m E_m v_m}{E_f v + E_m v_m} \Delta T. \tag{8.39}$$

For free expansion in the longitudinal direction in the composite, the longitudinal strain is:

$$\varepsilon_C = \alpha_1^0 \Delta T. \tag{8.40}$$

Since the composite strain is approximately equal to that in the fibre and matrix, combination of the above two equations gives α_1^0 (eqn [8.34]).

Moreover, the fibre stress in the longitudinal direction is:

$$(\sigma_F)_1 = E_f(\varepsilon_F)_1 = E_f\varepsilon_C^1 = E_f(\alpha_1^0 - \alpha_f)\Delta T. \quad 8.41$$

And the matrix stress in the longitudinal direction is:

$$(\sigma_M)_1 = E_m(\varepsilon_M)_1 = E_m\varepsilon_C^1 = E_m(\alpha_m - \alpha_1^0)\Delta T. \quad 8.42$$

The strains in the fibre and in the matrix in the transverse direction are, respectively, given by:

$$(\varepsilon_F)_2 = \alpha_f\Delta T - \frac{v_f(\sigma_F)_1}{E_f}, \quad 8.43$$

$$(\varepsilon_M)_2 = \alpha_m\Delta T - \frac{v_m(\sigma_M)_1}{E_m}. \quad 8.44$$

The transverse strain in the composite is given by the rule of mixtures as:

$$(\varepsilon_C)_2 = (\varepsilon_F)_2\, v + (\varepsilon_M)_2\, v_m. \quad 8.45$$

Substitution of eqns [8.43] and [8.44] in eqn [8.45] gives:

$$(\varepsilon_C)_2 = \left[\alpha_f\Delta T - \frac{v_f E_f(\alpha_1^0 - \alpha_f)\Delta T}{E_f}\right]v + \left[\alpha_m\Delta T + \frac{v_m E_m(\alpha_m - \alpha_1^0)\Delta T}{E_m}\right]v_m. \quad 8.46$$

Since $(\varepsilon_C)_2 = \alpha_2\Delta T$, then we obtain:

$$\alpha_2^0 = \left[\alpha_f - v_f(\alpha_1^0 - \alpha_f)\right]v + \left[\alpha_m + v_m(\alpha_m - \alpha_1^0)\right]v_m, \quad 8.47$$

and because $v_{12} = v_f v + v_m v_m$, in which $v + v_m = 1$, we have:

$$\alpha_2^0 = (1 + v_f)\alpha_f v + (1 + v_m)\alpha_m v_m - \alpha_1^0 v_{12}. \quad 8.48$$

When short fibres of length l are used in the SFRP composite, the effective fibre modulus E_f is reduced in the ratio (Cox, 1952):

$$\lambda = 1 - \frac{\tanh(\eta l/2)}{\eta l/2}, \quad 8.49$$

where η has been defined in Chapter 6. Thus, for SFRP composites, α_1^0 is given by:

$$\alpha_1^0 = \frac{\lambda E_f\alpha_f v + E_m\alpha_m(1-v)}{\lambda E_f v + E_m(1-v)}. \quad 8.50$$

Assumed that the packing of fibres is hexagonal as shown in Fig. 6.2(b) and the short fibres are uniformly distributed in the SFRP composite, the fibre volume fraction can be obtained as:

$$v = \frac{\pi r_f^2 l}{2\sqrt{3}R_0^2 (l+\delta)}, \tag{8.51}$$

where δ is the fibre end gap. If $\delta = 0$, eqn [8.51] becomes eqn [6.14].

If the fibres in the SFRP composite are oriented at an angle θ relative to the 1-direction as shown in Fig. 8.1, the thermal expansion coefficients in the 1-direction and in the 2-direction, respectively, become:

$$\alpha_1 = \alpha_1^0 \cos^2\theta + \alpha_2^0 \sin^2\theta \tag{8.52}$$

$$\alpha_2 = \alpha_1^0 \sin^2\theta + \alpha_2^0 \cos^2\theta \tag{8.53}$$

8.3.2 Thermal expansion of misaligned SFRP composites

Short fibre reinforced polymer (SFRP) composites are developed to fill the mechanical property gap between continuous fibre laminates and unreinforced polymers. SFRP composites are frequently fabricated using conventional techniques for making plastic materials such as extrusion compounding and injection moulding (Fu and Lauke, 1997a, 1998c,d; Fu *et al.*, 1999c; Ulrych *et al.*, 1993; Takahashi and Choi, 1991; Gupta *et al.*, 1989; Xia *et al.*, 1995; Chin *et al.*, 1988; Hine *et al.*, 1995). During processing, considerable shear-induced fibre breakage results in a fibre length distribution (FLD), and progressive and continuous changes in fibre orientation lead to a fibre orientation distribution (FOD) in final injection moulded composite parts. The FLD and the FOD affect both the mechanical and the thermal properties of SFRP composites. The mechanical properties of SFRP composites have been extensively studied by taking into account the effects of FLD and FOD (Fu and Lauke, 1996, 1997b, 1998a,b; Fu *et al.*, 1999a; Lauke and Fu, 1999) and discussed in other chapters of this book. In the following, the effects of FLD and FOD on the thermal expansion of misaligned SFRP composites are addressed.

The FLD and the FOD can be modelled by proper probability density functions (Fu and Lauke, 1996, 1997b, 1998a,b; Fu *et al.*, 1999b; Lauke and Fu, 1999); see also Chapter 3. The thermal expansion coefficients of a SFRP composite with an FLD and an FOD are derived as functions of FLD, FOD, fibre volume fraction and elastic properties of the fibres and the matrix based on Schapery's theory (1968). For the general case, i.e., when there are FLD, $f(l)$ and FOD, $g(\theta)$ in the composite, the thermal expansion coefficients are obtained from:

$$\alpha_1 = \int_{\theta=0}^{\pi/2} \int_{l=l_{\min}}^{l_{\max}} \left(\alpha_1^0 \cos^2\theta + \alpha_2^0 \sin^2\theta\right) f(l) g(\theta) \, \mathrm{d}l \mathrm{d}\theta \tag{8.54}$$

$$\alpha_2 = \int_{\theta=0}^{\pi/2} \int_{l_{\min}}^{l_{\max}} \left(\alpha_1^0 \sin^2\theta + \alpha_2^0 \cos^2\theta\right) f(l) g(\theta) \, \mathrm{d}l \mathrm{d}\theta. \tag{8.55}$$

The following values of the parameters, except otherwise specified, are used for all the figures in this section: $d = 10\ \mu$m, $\theta_{mean} = 12.95°$ ($p = 0.6$ and $q = 8$), $E_f = 72$ GPa, $E_m = 2$ GPa, $\nu_f = 0.25$, $\nu_m = 0.4$, $v = 30\%$, $\alpha_f = 0.54$ ppm/°C and $\alpha_m = 50$ ppm/°C. A hexagonal packing of fibres and a uniform fibre distribution are assumed in the SFRP composites. The effect of FLD on the thermal expansion coefficients of SFRP composites is shown in Figs 8.7 and 8.8, respectively, for the cases of fibre aspect ratio larger and less than 100. Figure 8.7 reveals that the thermal expansion coefficients are nearly independent of the mean fibre aspect ratio for the case of $l_{mean}/d > 100$. Figure 8.8 shows α_1 increases

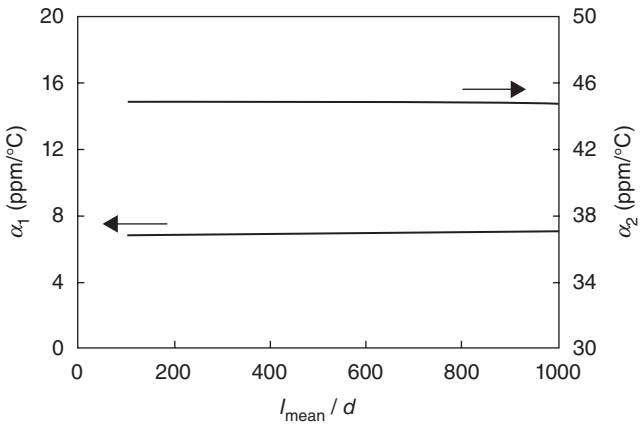

8.7 Effects of FLD on thermal expansion coefficients (α_1 and α_2) of SFRP composites, where $a = 5$ and various b.

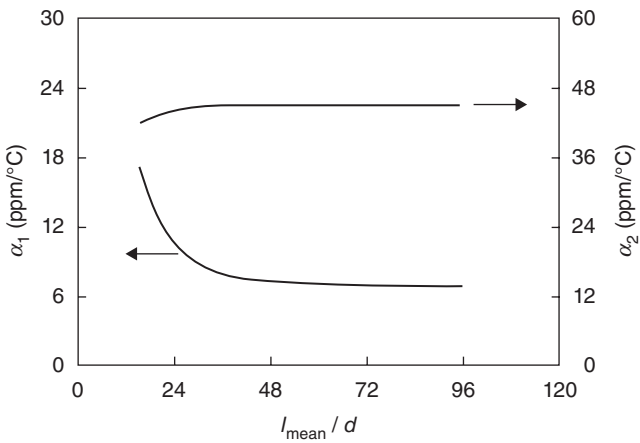

8.8 Effects of FLD on thermal expansion coefficients (α_1 and α_2) of SFRP composites, where $a = 0.15$ and various b.

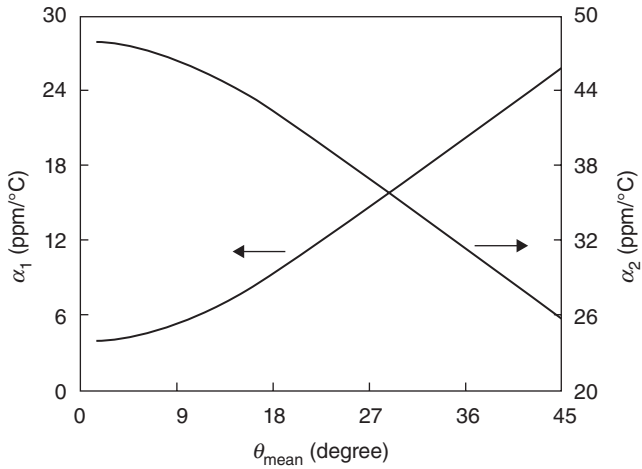

8.9 Effects of FOD on thermal expansion coefficients (α_1 and α_2) of SFRP composites, where $p = 0.6$ and various q.

with decreasing l_{mean}/d when l_{mean}/d is very small (<~40) while it is insensitive to l_{mean}/d when l_{mean}/d is > ~40. Further, α_2 is almost insensitive to mean fibre aspect ratio except when l_{mean}/d < ~25, α_2 increases slowly with the increase of l_{mean}/d. The insensitivity of the transverse expansion on mean fibre aspect ratio was also reported for oriented short fibre composites by Halpin (1969).

The effect of the FOD on the thermal expansion coefficients is shown in Fig. 8.9. It can be seen that the influence of the mean fibre orientation angle on the thermal expansion coefficients is significant. The thermal expansion α_1 increases dramatically while α_2 decreases significantly as the mean fibre orientation angle increases. That is, when the fibres in the composites are misaligned and deviate from the measuring direction, the fibres give less constraint to the thermal expansion of the SFRP composites in the '1' direction but they provide more constraint to the composite thermal expansion in the transverse direction '2'.

The effect of fibre volume fraction on the thermal expansion coefficients is shown in Fig. 8.10. It shows that fibre volume fraction has a significant influence on the thermal expansion coefficients. As the fibre volume fraction increases, both α_1 and α_2 decrease. This is because the fibres have a much lower thermal expansion coefficient than the matrix. Thus, it is an effective way to incorporate a sufficient amount of short fibres into a polymeric matrix to reduce thermal expansion.

In summary, the effects of FLD, FOD and fibre volume fraction on the thermal expansion coefficients of SFRP composites are discussed in detail. It is shown that FLD has a relatively small influence on the thermal expan-

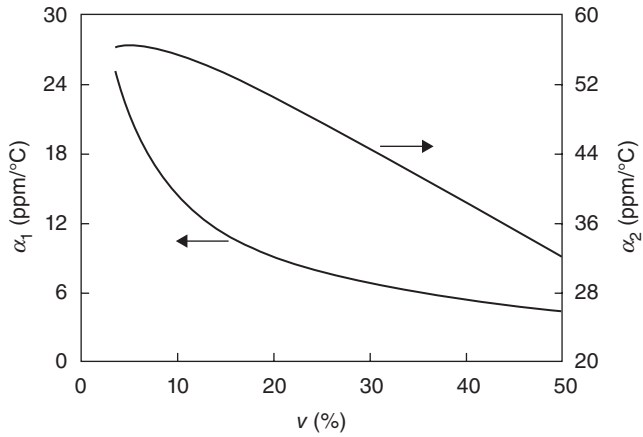

8.10 Effects of fibre volume fraction on thermal expansion coefficients (α_1 and α_2) of SFRP composites.

sion coefficients while FOD and fibre volume fraction have significant effects on the thermal expansion coefficients.

8.3.3 Thermal expansion of 2D and 3D random SFRP composites

The addition of short fibres to a polymer matrix will reduce the coefficient of thermal expansion (CTE). If the fibre orientation is truly random, the CTE will be the same in all directions in the 2D planar space or the 3D spatial space. Halpin and Pagano (1969) have proposed the following equation for the case of a 2D random fibre orientation:

$$\alpha_C = \frac{\alpha_1^0 + \alpha_2^0}{2} + \frac{(E_{11} - E_{22})(\alpha_1^0 - \alpha_2^0)}{2[E_{11} + (1 + 2\nu_{12})E_{22}]}, \quad 8.56$$

where α_1^0 and α_2^0 are longitudinal and transverse thermal expansion coefficients, respectively, of a unidirectional fibre composite and are given by eqns [8.34] and [8.35]. E_{11} and E_{22} are the longitudinal and transverse elastic modulus, respectively, of a unidirectional SFRP composite that was given in Chapter 6.

Further, for a 2D random short fibre composite, $g(\theta) = 2/\pi$, the composite thermal expansion coefficients can be obtained from eqns [8.54] and [8.55] by integration of θ for $0 \le \theta \le \pi/2$. Similarly, for a 3D random short fibre composite, $g(\theta,\phi) = g(\theta)g(\phi)/\sin\theta = 1/2\pi$, and $g(\theta) = \sin\theta$. So, the composite thermal coefficients can also be obtained from eqns [8.54] and [8.55] by integration of θ for $0 \le \theta \le \pi/2$.

8.4 References

Agari Y, Ueda A and Nagai S (1991), 'Thermal conductivity of a polyethylene filled with disoriented short-cut carbon fibres', *J Appl Polym Sci*, 43 (6), 1117–1124.

Bigg D M (1986), 'Thermally conductive polymer composites', *Polym Composite*, 7 (3), 125–140.

Chen C H and Wang Y C (1996), 'Effective thermal conductivity of misoriented short fibre reinforced thermoplastics', *Mech Mater*, 23 (3), 217–228.

Chin W K, Liu H T and Lee Y D (1988), 'Effects of fibre length and orientation distribution on the elastic modulus of short fibre reinforced thermoplastics', *Polym Composite*, 9 (1), 27–35.

Chou T W and Nomura S (1981), 'Fibre orientation effects on the thermoelastic properties of short-fibre composites', *Fibre Sci Technol*, 14 (4), 279–291.

Choy C L, Leung W P and Kwok K W (1992), 'Elastic moduli and thermal conductivity of injection-molded short-fiber-reinforced thermoplastics', *Polym Composite*, 13 (2), 69–80.

Choy C L, Kwok K W, Leung W P and Lau F P (1994), 'Thermal conductivity of poly(ether ether ketone) and its short-fiber composites', *J Polym Sci Part B Polym Phys*, 32 (8), 1389–1397.

Cox H L (1952), 'The elasticity and strength of paper and other fibrous materials', *Brit J Appl Phys*, 3 (3), 72–79.

Dunn M L, Taya M, Hatta H, Takei T and Nakajima Y (1991), 'Thermal conductivity of hybrid short fiber composites', *J Compos Mater*, 27 (15), 1493–1519.

Eshelby J D (1957), 'The determination of the elastic field of an ellipsoidal inclusion and related problems', *Proc Roy Soc London A*, 241 (4), 376–396.

Fu S Y and Lauke B (1996), 'Effects of fibre length and orientation distributions on the tensile strength of short-fibre-reinforced polymers', *Compos Sci Technol*, 56 (10), 1179–1190.

Fu S Y and Lauke B (1997a), 'Analysis of mechanical properties of injection moulded short glass fibre (SGF)/calcite/ABS composites', *J Mater Sci Technol*, 13 (5), 389–396.

Fu S Y and Lauke B (1997b), 'Fibre pull-out energy of misaligned short fibre composites', *J Mater Sci*, 32 (8), 1985–1993.

Fu S Y and Lauke B (1998a), 'The elastic modulus of misaligned short fibre reinforced polymers', *Compos Sci Technol*, 58 (3–4), 389–400.

Fu S Y and Lauke B (1998b), 'An analytical characterization of the anisotropy of the elastic modulus of misaligned short fibre reinforced polymers', *Compos Sci Technol*, 58 (12), 1961–1972.

Fu S Y and Lauke B (1998c), 'Characterization of tensile behaviour of hybrid short glass fibre/calcite particle/ABS composites', *Compos Part A – Appl Sci Manu,* 29 (5–6), 575–583.

Fu S Y and Lauke B (1998d), 'Fracture resistance of unfilled and calcite-particle-filled ABS composites reinforced by short glass fibers (SGF) under impact load', *Compos Part A – Appl Sci Manu*, 29 (5–6), 631–642.

Fu S Y and Mai Y-W (2003), 'Thermal conductivity of misaligned short-fiber- reinforced polymer composites', *J Appl Polym Sci*, 88 (6), 1495–1505.

Fu S Y, Hu X and Yue C Y (1999a), 'Effects of fiber length and orientation distributions on the mechanical properties of short-fiber-reinforced polymers – a review', *Mater Sci Res Intern*, 5 (1), 74–83.

Fu S Y, Hu X and Yue C Y (1999b), 'The flexural modulus of misaligned short-fiber-reinforced polymers', *Compos Sci Technol*, 59 (10), 1533–1542.

Fu S Y, Lauke B, Maeder E, Hu X and Yue C Y (1999c), 'Fracture resistance of short-glass-fiber-reinforced and short-carbon-fiber-reinforced polypropylene under Charpy impact load and its dependence on processing', *J Mater Process Tech*, 89–90 (5), 501–507.

Gupta V B, Mittal R K and Sharma P K (1989), 'Some studies on glass fibre-reinforced polypropylene. Part I: Reduction in fibre length during processing', *Polym Composite*, 10 (1), 8–15.

Halpin J C (1969), 'Stiffness and expansion estimates for oriented short fiber composites', *J Compos Mater*, 3 (10), 732–735.

Halpin, J C (1984), *Primer on composite materials analysis*, Technomic Publishing, Lancaster, PA.

Halpin J C and Pagano N J (1969), 'The laminate approximation for randomly oriented fibrous composites', *J Compos Mater*, 3 (10), 720–724.

Hatta H and Taya M (1985), 'Effective thermal conductivity of a misoriented short fiber composites', *J Appl Phys*, 58 (7), 2478–2486.

Hatta H and Taya M (1986), 'Equivalent inclusion method for steady-state heat conduction in composites', *Int J Engin Sci*, 24 (7), 1159–1172.

Hine P J, Davidson N, Duckett R A and Ward I M (1995), 'Measuring the fibre orientation and modelling the elastic properties of injection-molded long-fibre-reinforced nylon', *Compos Sci Technol*, 53 (2), 125–131.

Lauke B and Fu S Y (1999), 'The strength anisotropy of misaligned short-fiber-reinforced polymers', *Compos Sci Technol*, 59, 699–708.

Mori T and Tanaka (1973), 'Average stress in matrix and average elastic energy of materials with misfitting inclusions', *Acta Metall Mater*, 21 (5), 571–574.

Nielsen L E (1973), 'Thermal conductivity of particulate-filled polymers', *J Appl Polym Sci*, 17 (12), 3819–3820.

Nielsen L E (1974), 'The thermal and electrical conductivity of two-phase systems', *Ind Eng Chem Fund*, 13 (1), 17–20.

Normura S and Chou T W (1980), 'Bounds of effective thermal conductivity of short-fibre composites', *J Compos Mater*, 14 (4), 120–129.

Okamoto S and Ishida H (1999), 'A new theoretical equation for thermal conductivity of two-phase systems', *J Appl Polym Sci*, 72 (13), 1689–1697.

Progelhof R C, Throne J L and Ruetsch R R (1976), 'Methods for predicting the thermal conductivity of composite systems: a review', *Polym Eng Sci*, 16 (9), 615–625.

Schapery J (1968), 'Thermal expansion coefficients of composite materials based on energy principles', *J Compos Mater*, 2 (4), 380–404.

Takahashi K and Choi N S (1991), 'Influence of fibre weight fraction on failure mechanisms of poly(ethylene terephthalate) reinforced by short-glass fibres', *J Mater Sci*, 26 (17), 4648–4656.

Ulrych F, Sova M, Vokrouhlecky J and Turcic B (1993), 'Empirical relations of the mechanical properties of polyamide 6 reinforced with short glass fibers', *Polym Composite*, 14 (3), 229–237.

Willis J R (1977), 'Bounds and self-consistent estimates for the overall properties of anisotropic composites', *J Mech Phys Solids*, 25 (3), 185–202.

Xia M, Hamada H and Maekawa Z (1995), 'Flexural stiffness of injection moulded glass fibre reinforced thermoplastics', *Int Polym Proc*, 10 (1), 74–81.

9

Non-linear stress–strain behaviour

Abstract: Composites show deviations of the stress–strain curve from a straight line with increasing load. Localised failure mechanisms are responsible for the decrease of load-bearing capability leading to reductions of stiffness. In this chapter, fibre–matrix debonding and subsequent sliding as well as matrix plasticity are considered and their influence on composite stiffness is discussed. A viscoelastic, plastic or viscoplastic interface causes energy dissipation during cyclic loading. This energy loss is coupled with damping of the excited oscillations. Another remarkable effect is the strain rate dependence of the polymer matrix, which is described in this chapter. The behaviour is modelled and compared to published experimental results.

Key words: fibre–matrix debonding, sliding, viscoplastic interface, damping, energy loss, viscoelastic matrix.

9.1 Introduction

For calculation of the effective thermomechanical properties and the full macroscopic stress–strain relation of heterogeneous materials, a variety of techniques have been developed. Which kind of modelling should be used depends mainly on the objective target, that is, whether it is the effective macroscopic thermomechanical behaviour or internal stresses in the components which are of interest. Kreher and Pompe (1989) provided a comprehensive survey of the calculation of internal stresses in heterogeneous solids.

In the micromechanical approaches different length scales must be considered. On the macroscopic level, the composite shows effective properties. These properties are caused by the geometry, the interactions and the mechanical properties of the different components. In short fibre reinforced polymer (SFRP) composites only the fibres, interphases and matrix materials are distinct phases, where the matrix is the continuous phase which contains the others. On condition that the composite does not have large gradients of stresses, strains or structure, a so-called localisation can be performed for the local stresses $\sigma(\vec{x})$ and deformations $\varepsilon(\vec{x})$ by:

$$\sigma(x_i) = A(x_i)\langle\sigma\rangle \quad \text{and} \quad \varepsilon(x_i) = B(x_i)\langle\varepsilon\rangle$$

where $<\sigma>$ and $<\varepsilon>$ are the mean macroscopic composite stress and strain, respectively. The local fields within the components may depend on the location x_i.

Another relation is obtained by expressing the macroscopic behaviour by the local behaviour; this provides the so-called homogenisation relation, which is:

$$\langle\sigma\rangle = \int_V \sigma(x_i)\,\mathrm{d}V \quad \text{and} \quad \langle\varepsilon\rangle = \int_V \varepsilon(x_i)\,\mathrm{d}V.$$

It is an important task to find the local stresses so as to understand the composite behaviour. Especially, for interpretation of failure processes, it is necessary to know the local situation, since stress concentrates around the inclusions. However, considering the complex structure of most composite materials, it is hard to determine the functions, $A(x_i)$ and $B(x_i)$.

A basic survey of the different approaches that have been applied to fibre (and particle) reinforced composites was published by Böhm (1998). He discussed modelling of effective thermomechanical properties in the framework of the following techniques:

- mean field and related approaches,
- periodic micro-field approaches or unit cell methods,
- embedded cell approaches, and
- multi-scale models.

These techniques are capable of classifying a huge amount of publications concerning the general stress–strain response of composite materials. However, if plastic deformation of components also plays a role, other approaches have been developed that may not fit into this framework, such as empirical or semi-empirical models, see for example Dvorak and Bahei-el-Din (1987).

The mean field approach assumes the local stress and strain within the components are constants, i.e. $A(x_i) = A$ and $B(x_i) = B$. The often-used 'rules of mixtures' accounts for this type of approximation. They have been applied successfully to evaluate the thermomechanical properties of SFRP composites in the linear range, and the approach described in Chapter 6 is based on this kind of assumption.

Unit cell methods are especially appropriate for evaluation of local non-linearities, such as plasticity of one component or the interaction of a component with a crack. Embedded cell methods or self-consistent methods use the fictive knowledge of the macroscopic material law within which the cell is embedded; subsequent averaging about the embedded cell provides the boundary conditions (self-consistently) for the macroscopic law.

Multi-scale models use the hierarchical structure of some composites that consist of a special kind of sub-composite for which one of the above averaging techniques is applicable, i.e., a former component is now replaced, for example, by a unit cell or embedded cell.

For short fibre reinforced composites one of the first applied theories for elliptical inclusions was developed by Eshelby (1957), the so-called equivalent inclusion approach, which is one of the mean field approaches. This approach has the advantage that the geometry of the reinforcing component is taken into account.

In the elastic case, as for the calculation of modulus in Chapter 6, and in the following section we use the unit cell method, where a representative unit cell replaces the composite. The first aim is to describe the local variations of stress and strain within the fibres and matrix and the interphase. Then, with the subsequent application of the homogenisation equation, the macroscopic behaviour is calculated.

9.2 Macroscopic stress–strain relationship

In previous chapters composites with linear elastic components and ideal bonding at the fibre–matrix interface were considered. This necessarily provides linear relations between composite stress and strain. However, for higher loads the stress–strain curve will deviate more and more from a straight line due to the initiation of failure mechanisms (see Fig. 9.1). In the early stage damage may be restricted to local redistribution of stress concentrations. With increasing external load, the cracks cannot be stabi-

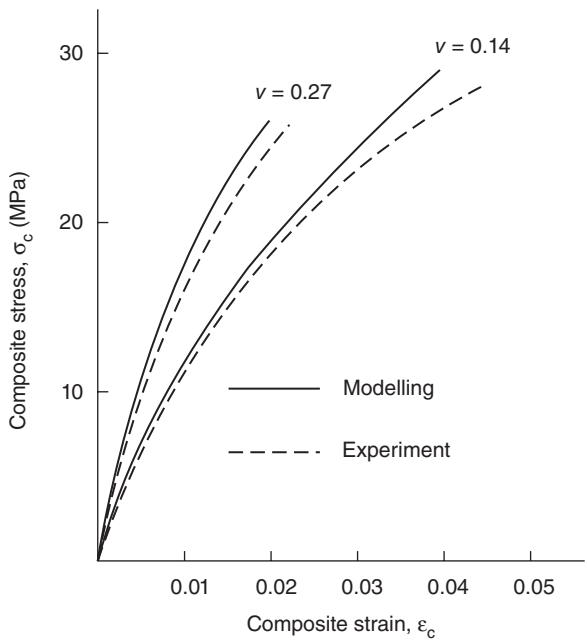

9.1 Stress–strain curves for short glass fibre reinforced polyethylene composites. Adapted from Lauke (1992).

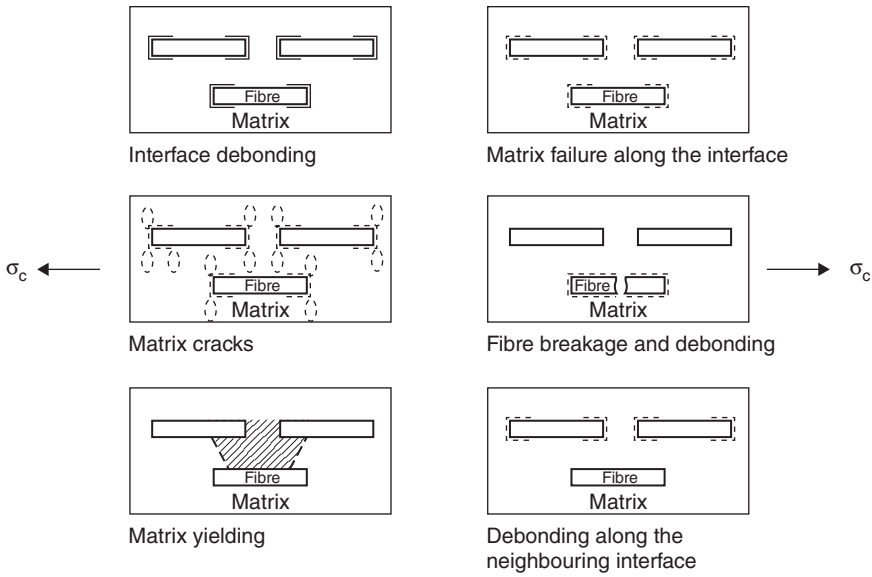

9.2 Failure mechanisms responsible for stiffness reduction.

lised and the accumulation of localised failure turns to macroscopic fracture (see Chapters 5 and 10).

In the present discussion of deformation behaviour we are interested only in the stage of stable structural weakening leading to a successively decreasing stiffness of the composite. Several failure mechanisms have been proposed in the literature, which are summarised in Fig. 9.2:

- interfacial debonding (Outwater and Murphy, 1969; Piggott, 1980; Lauke and Schultrich, 1983);
- interfacial cracking within the matrix (Sato *et al.*, 1982); crack growth into the matrix (Curtis *et al.*, 1978; Taya and Chou, 1982; Takao *et al.*, 1982);
- fibre breakage (Steif, 1984); and
- plastic instability of the matrix (Kelly and Tyson, 1965; Agarwal *et al.*, 1974; Pompe and Schultrich, 1974).

In general, these mechanisms may act in combination in a loaded composite. In this chapter, the fibre–matrix debonding and subsequent sliding and matrix plasticity are discussed in more detail. But at first the elastic case without damage is concisely given below.

9.2.1 Perfectly bonded fibre–matrix interface

Most studies on the macroscopic stress–strain relations of short fibre reinforced polymers are concerned with the deformation behaviour at small stresses, for example, stresses below critical values as debonding limits or stresses, which are able to cause matrix plasticity. This case of strictly linear

stress–strain relation corresponds to the problem of effective elastic modulus of SFRP composites (see Chapter 6). Therefore, the theory of heterogeneous elastic materials can be applied with success. General rules of the effective elastic constants can be derived, see for example Kreher and Pompe (1989), independent of the special composite structure. The existence of upper and lower bounds allows model evaluation.

The macroscopic deformation behaviour for such weakly loaded composites with elastic components and ideal bonding was considered in Chapter 6. Here, only the elastic stiffness along the fibre axis on the basis of the shear-lag model, described in Chapter 4, is given. In the subsequent section these considerations are extended to higher loadings where failure mechanisms or matrix plasticity is initiated.

Due to the load-carrying efficiency of short fibres, the effective modulus is reduced compared to those composites with continuous fibres. Within the framework of the single-fibre model discussed in Chapter 4, the macroscopic deformation can be derived by assuming that the elongation of the composite is equal to that of the matrix, averaged over the cross section and along the fibre:

$$\varepsilon_c = \bar{\varepsilon}_M = \frac{1}{l/2}\int_0^{l/2} \mathrm{d}z\,\varepsilon_M(z) = \frac{1}{E_m l/2}\int_0^{l/2} \mathrm{d}z\left(\frac{\sigma_c}{1-\nu} - \frac{\nu}{1-\nu}\sigma_F\right). \tag{9.1}$$

Inserting the rule of mixtures, eqn [4.4] together with relations [4.6], the stress–strain relation becomes linear as given below:

$$\varepsilon_c(\sigma_c) = \sigma_c / E_c^0 \quad \text{with} \quad E_c^0/E_m = \frac{1-\nu}{1-\nu\left(1-\dfrac{2}{\eta l}\tanh(l/2)\right)\dfrac{E_f}{\bar{E}}}, \tag{9.2}$$

where ε was given in eqn [4.10]. In the limiting case of $E_m \to 0$, the shear-lag model by Cox (1952), where fibres carry tensile stresses only, is obtained.

The influence of the surrounding region can be considered with self-consistent methods by embedding the components in an effective medium. Notwithstanding the higher complexity of such a calculation, a relative simple expression for E_c^0, was derived by Halpin and Tsai (1967):

$$E_c^0/E_m = \frac{1+2(l/d)\eta_1\nu}{1-\eta_1\nu} \quad \text{with} \quad \eta_1 = \left(\frac{E_f}{E_m}-1\right)\Big/\left(E_f/E_m + 2(l/d)\right). \tag{9.3}$$

Self-consistent methods of another kind were developed by Hill (1965), which have been adopted and applied, for example by Chou *et al.* (1980), to analyse the stiffness of short fibre reinforced composites. In this, the short fibres were treated as ellipsoidal inclusions. Bounds for elastic moduli were given by Nomura and Chou (1984) by using variational principles. With low fibre volume fractions the self-consistent model yields elastic moduli close to the lower bound, and the bounds narrow for increasing aspect ratio; for

example, the influence of the arrangement of the oriented fibres vanishes for long fibres. For more discussions of stiffness as a function of fibre volume fraction and geometry, and the elastic properties of the constituents under low applied strain, see Chapter 6.

9.2.2 Interface debonding and sliding

In this section, the implications of the failure processes on the deformation resistance are demonstrated in more detail for debonding at the fibre–matrix interface and the subsequent sliding of fibres against the matrix material.

When the applied load reaches the critical value, σ_c^d, debonding starts at the interface. At this critical stress the shear stress attains the adhesion shear strength, τ_d. It follows from the shear stress distribution, eqn [4.14]:

$$\sigma_c^d = \frac{2\tau_d \bar{E}}{r_f \eta E_f} \coth(\eta l/2) \approx \frac{2\tau_d \bar{E}}{r_f \eta E_f} \quad \eta l << 1. \tag{9.4}$$

Debonding is followed either by complete or by incomplete sliding depending on conditions for the relations between the material constants of the composite. Detailed equations have been derived by Lauke and Schultrich (1983) and Lauke *et al.* (1990).

Herein, only the expressions for the debonding and sliding lengths and the mean shear stress in the sliding region are given because they play a decisive role for the deformation and fracture (mechanical) behaviour.

After solving the differential equations for the elastic problem under consideration of all boundary and continuity conditions, the following formulae are obtained. The sliding length on one side of the fibre, l_s, and the mean shear stress are given by:

$$l_s = \frac{r_f}{2a} \ln \frac{1 - 2a/(r_f \eta)}{1 - a\dfrac{E_f}{\bar{E}} \dfrac{1}{b + \tau_s/\sigma_c}},$$

$$\bar{\tau}^{(s)} = \frac{1}{l_s\left(1 - \dfrac{4a}{d\eta}\right)} \left[\left(\frac{dE_f}{4\bar{E}} - \frac{b}{\eta} \right) (1-\nu)(1+\pi/2)\sigma_{M\cdot y} - \tau_s/\eta \right], \tag{9.5}$$

and the debonding length on one side of the fibre, l_d,

$$l_d = l_s + \frac{1}{\eta} \ln(\tau_g/\tau_d), \tag{9.6}$$

where the parameters as functions of the material constants become:

$$a = \mu(\nu\nu_1 + (1-\nu)\nu_2/(1-\nu), \quad b = \nu_1/(1-\nu), \quad \tau_s = \mu\sigma_n^T + \tau'$$

$$\nu_1 = \nu_m/(1+\nu_m) \quad \nu_2 = E_m\nu_f/(E_f(1+\nu_m)),$$

where σ_n^T is thermal stress, τ' is physical-chemical interaction stress at the interface, μ is fibre–matrix friction coefficient, and τ_g is shear stress at the transition point: $z = g = (l/2 - l_s)$ of the debonding to the sliding region:

$$\tau_g = \frac{\left(b - aE_f/\bar{E}\right)\sigma_c + \tau_s}{1 - 2a/(r_f\eta)}.$$

The macroscopic stress–strain relation can be determined by using the calculated stresses for the fibre σ_F in the debonded and sliding regions via integration along the fibre axis according to eqn [9.1]. For the case of complete sliding the following relation is obtained:

$$\varepsilon_c(\sigma_c) = \frac{\sigma_c}{\bar{E}} + \frac{r_f v}{l(1-v)E_m}\left[\sigma_c\left(\frac{E_f}{a\bar{E}}\right) + (\tau_d - \sigma_c)\frac{4}{(r_f\eta)^2}\left(1 - \frac{r_f\eta}{2a}\right) + \frac{2l_s}{ar_f}\left((aE_f/\bar{E} - b)\sigma_c - \tau_s\right)\right]. \quad 9.7$$

By means of the explicit stress dependence of the macroscopic deformation ε_c and the stress dependence of l_s (eqn [9.5]), the stress–strain relation becomes non-linear.

In Fig. 9.1, the theoretical results are compared to the experimental curves of short glass fibre reinforced polyethylene. The dependence of such curves on the variation of different material parameters such as aspect ratio, thermal stress, and frictional coefficient is discussed in detail by Piggott (1980) and Lauke and Schultrich (1983).

Figure 9.3 shows the variation of longitudinal stiffness, $E_c = \sigma_c/\varepsilon_c$ (normalised by the composite modulus for the undamaged system E_c^0) as a function of applied stress, revealing the two stages of the stress–strain relation. For small loads ($\sigma_c \le \sigma_c^s$) no sliding exists and the material behaves elastically. In the second stage, sliding starts and diminishes the modulus.

9.2.3 Matrix plasticity

A further possible cause of onset of non-linear deformation behaviour may be the plasticity of the matrix material (see Fig. 9.3). As already mentioned in Section 4.1, Kelly–Tyson's model (1965) was the first to consider matrix plasticity. Constant shear stresses at the interface due to matrix or interface plasticity are assumed. Force balance on the representative element (see Fig. 4.2) gives:

$$\sigma_F \pi r_f^2 = 2\pi r_f \int_{l/2-z}^{l/2} dz\,\tau_y = 2\tau_y \pi r_f z, \quad 9.8$$

where τ_y is matrix yield shear stress. Thus, force equilibrium of a fibre end yields the linear increase of fibre stress $\sigma_F = 2z\tau_y/r_f$ as shown in Fig. 4.1(b).

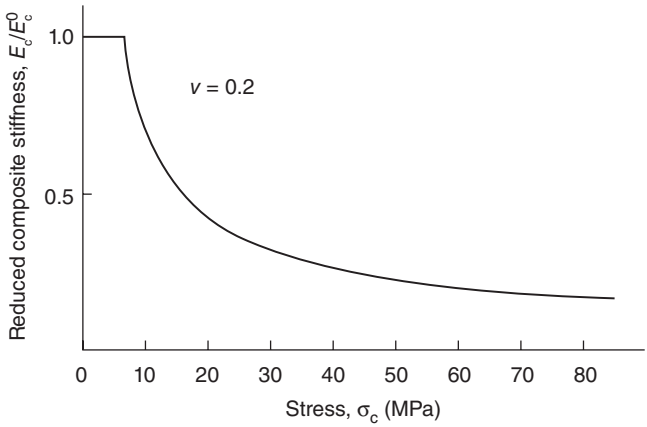

9.3 Stiffness reductions due to fibre–matrix debonding of short glass fibre reinforced polyethylene. Adapted from Lauke (1992).

With the additional assumption $\varepsilon_F \approx \varepsilon_c$, the fibre transfer length for this case of elastic fibre and plastic matrix is given by: $l_c/d = E_f\varepsilon_c/2\tau_y$. The fibre stress is limited by its tensile strength σ_F^u leading to the critical fibre length:

$$l_c/d = \sigma_F^u/2\tau_y. \qquad 9.9$$

However, in general, plastic yielding of the matrix will be restricted to the fibre end regions, whereas along the inner fibre region the matrix remains elastic. This situation is related to the sliding case discussed above for the single-fibre model.

Bowyer and Bader (1972) used this model to explain the stress–strain relation of short fibre reinforced polymers. The main assumption is a constant shear stress along the interface. Thus, it does not differentiate $\tau = \tau_y$ with τ_y as matrix yield shear stress and $\tau = \tau_f$ with τ_f as a frictional shear stress, which has already been discussed in the preceding section. They considered the dependence of the critical fibre length (eqn [9.9]) on composite deformation and on fibre length distribution. From eqn [9.8] the following average (over the fibre length) fibre stresses are obtained:

$$\bar{\sigma}_{F,i} = l_i\tau/d \qquad \text{for} \quad l_i \le l_c \qquad 9.10$$

$$\bar{\sigma}_{F,j} = \varepsilon_c E_f\left(1 - \frac{\varepsilon_c E_f}{4(l_j/d)\tau}\right) \qquad \text{for} \quad l_j \ge l_c. \qquad 9.11$$

With knowledge of the fibre length distribution it is possible to sum up separately over the fibres with lengths below or above the critical value. With the load-bearing contribution of the matrix, $\sigma_M = (1 - v)E_m\varepsilon_c$, they obtained:

$$\sigma_c = C_0\left(\sum_{l_i<l_c} v_i l_i \tau/d + \sum_{l_i>l_c} v_j \varepsilon_c E_f\left(1-\frac{\varepsilon_c E_f}{4(l_j/d)\tau}\right)\right)+(1-v)E_m\varepsilon_c. \qquad 9.12$$

The factor C_0 takes into account the fibre orientation distribution. The stress–strain curve becomes non-linear, similar to the variation shown in Fig. 9.1 where debonding and sliding are considered.

Jiang *et al.* (1998, 2004) have used a modified shear lag model to study the elastic-plastic stress transfer in short fibre reinforced metal composites. The basis is an extended expression for the shear stress distribution at the interface. The elastic-plastic deformation of the matrix is considered as in eqn [4.7] for the debonding mechanism. The misfit in displacements Δu caused by debonding is replaced by the plastic displacement. Also, the case of pure plastic stress transfer was considered. The basic ideas are very similar to the model published by Pompe and Schultrich (1974). Jiang *et al.* (2004), in addition, considered the influence of thermal residual stresses. The calculated non-linear stress–strain curves were compared for tensile and compressive loadings with experimental results for metal matrix composites.

Since the fibre ends and their mutual positions are of special importance for local plasticity, the multi-fibre model (see Section 4.3) with an elastic-plastic matrix provides a more realistic result.

For simplification, the case of low modulus ratio only is considered. Then, the decay length $1/\eta'$ (cf. eqn [4.19]) is nearly the size of the distance of fibres, $1/k$ being even smaller than $1/\eta'$. Further, it is assumed that the matrix axial tensile stress is predominant. Plastic flow will be initiated where the matrix tensile stress achieves the matrix flow stress. In these regions, the matrix tensile stress remains constant at $\sigma_{M,y}$ and the interface shear stress cannot exceed $\tau \le \tau_y = \sigma_{M,y}/2$. For simplicity, τ is equal to τ_y. In the elastic region, τ decreases rapidly along the fibre, and for this reason it is made equal to zero. The force redistribution between the components is expressed by:

$$\frac{\partial\sigma_{F1}}{\partial z} = -\frac{2}{d}\tau_1 \quad \frac{\partial\sigma_M}{\partial z} = \frac{\tau_1 - \tau_2}{D} \quad \sigma_F = E_f\varepsilon_F, \qquad 9.13$$

where D is the fibre to fibre spacing. In the elastic region:

$$\sigma_M = E_m\varepsilon_M \quad \tau = 0 \quad \varepsilon_M = \varepsilon_F, \qquad 9.14$$

and in the plastic matrix region:

$$\sigma_M = \sigma_{M,y} \quad \tau = \pm\tau_y = \sigma_{M,y}/2. \qquad 9.15$$

The index numbers (1,2) refer to individual fibres, as shown in Fig. 4.3. The equilibrium equations have to be completed by the boundary conditions [4.4] and [4.5]. σ_M, as before, denotes the cross-sectional average of matrix tensile stress and varies along the z-axis so that:

$$\sigma_M = \frac{\delta(z)}{D}\sigma_{M,y} + \frac{D-\delta(z)}{D}E_m\varepsilon_M, \qquad 9.16$$

$\delta(z)$ being the lateral extent of the plastic region at the site z. The balance of forces at an elastic cross section, say, at $z = l/4$ in Fig. 9.4, relates ε_M to the overall composite stress:

$$\varepsilon_M \bar{E} = \sigma_c. \qquad 9.17$$

Since $\sigma_{M,y}$ is constant, and ε_M and $(d/dz)\sigma_M$ are independent of z in the approximation (eqn [9.14]), differentiation of eqn [9.17] provides the result that $(d/dz)\ \delta(z)$ is independent of z. That is,

$$\frac{d}{dz}\delta(z) = \frac{\tau_y}{\sigma_{M,y} - \sigma_c E_m/\bar{E}}. \qquad 9.18$$

Thus, the boundaries between elastic and plastic regions are straight lines in this simple model (see Fig. 9.4). The process of plasticity passes through several stages: plastic zones originate at the fibre ends and spread in each direction, meeting neighbouring fibres. They grow along the fibres until the whole matrix is plastic. This can be described quantitatively as follows. The length λ_0 of Fig. 9.4, which determines the transfer of the load difference between elastic and plastic matrix cross sections, is derived from eqn [9.18], which is:

$$\lambda_0 = D\left(\sigma_{M,y} - \sigma_c E_m/\bar{E}\right)/\tau_y. \qquad 9.19$$

Load transfer between neighbouring fibres is affected by the length λ_0. Thus, in the middle of the fibre, at $z = 0$, the stress:

$$\sigma_{F,max} = 2\tau_y(\lambda_0 + 2\lambda)/d \qquad 9.20$$

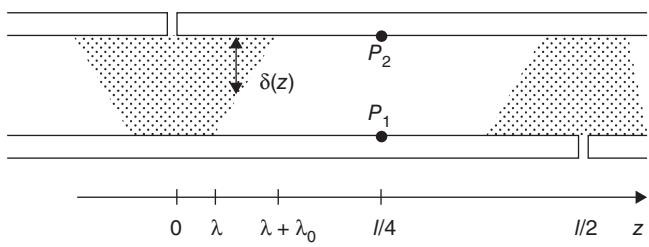

9.4 Plastic regions growing at fibre ends. Adapted from Lauke *et al.* (1990).

has been built up. (For simplicity, the reason is due to the special case of a maximum overlap, $a = l/2$.) The balance of forces at $z = 0$ relates to the effective composite stress, σ_c, where:

$$\sigma_c = \frac{(1-v)\sigma_{M,y} + v\tau_y\lambda/d}{1+(1-v)E_m/\bar{E}}. \qquad 9.21$$

Remember that $v = d/(d + D)$ in the multi-fibre model. To set up a stress–strain relation, the corresponding effective strain has to be calculated as the next step.

The composite strain ε_c is equal to the mean fibre strain between its mid-point at $z = 0$ and $z = l/4$:

$$\varepsilon_c = \bar{\varepsilon}_F = \frac{4}{l}\int_0^{l/4} dz\varepsilon_F(z). \qquad 9.22$$

The points P_1 and P_2 in Fig. 9.4 on the neighbouring fibres, being opposite to each other at $\sigma_c = 0$, stay exactly opposite if the composite is loaded. For $\lambda < z < l/2 - \lambda - \lambda_0$, ε_F is constant and equals the elastic matrix strain. From eqn [9.17] we obtain in this region, $\varepsilon_F = \sigma_c/\bar{E}$. At $z < \lambda$, the fibre strain varies linearly with z due to matrix shear stress so that:

$$\varepsilon_c = \sigma_c/\bar{E} + \frac{4\tau_y\lambda^2}{E_f l d}. \qquad 9.23$$

Elimination of λ from eqns [9.21] and [9.23] gives the following stress–strain relation:

$$\varepsilon_c = \sigma_c/\bar{E} + 4\frac{d}{l}\left(\frac{1-v}{v}\right)^2 \frac{\sigma_{M,y}}{\tau_y E_f}\left(\frac{\sigma_c}{\sigma_{c0}} - 1\right)^2. \qquad 9.24$$

Here, σ_{c0} stands for the combination of symbols in eqn [9.21] with $\lambda = 0$, which is that stress where the plastic region spreading from the fibre end has just reached the neighbouring fibre. At lower stress, $\sigma_c \le \sigma_{c0}$, the plastic regions are small areas embedded in the elastic material. Their influence on the mechanical behaviour is neglected in this simplified approach, which means that the material shows linear elasticity for smaller loads:

$$\varepsilon_c = \sigma_c/\bar{E} \quad \text{if} \quad \sigma_c \le \sigma_{c0}. \qquad 9.25$$

Figure 9.5 shows how composite stress at given strain is reduced if continuous reinforcement is replaced by shorter and shorter fibres, according to eqns [9.24] and [9.25]. The results show clearly the consequences of local matrix flow, which begins far below the proper matrix strain, $\varepsilon_{M,y}$.

There is still a lack in modelling of fibre–fibre interaction of polymer composites with plastic matrix behaviour. But much more research in this regard was done for metal matrix composites, and further research on SFRP

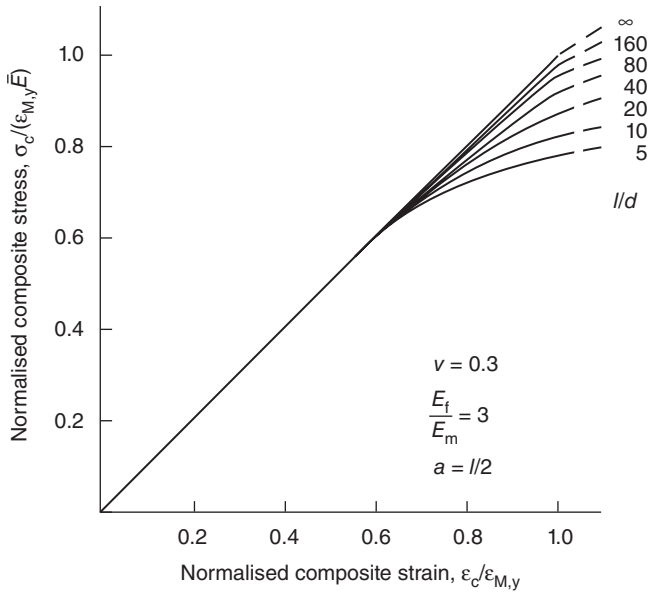

9.5 Stress–strain relationship according to eqns [9.23] and [9.24] and its dependence on fibre aspect ratio *l*/*d*. Adapted from Lauke *et al.* (1990).

should be focused on fibre–fibre interactions with non-linear polymer matrix behaviour.

Yang and Qin (2001) used the finite element method with a similar micromechanical model as described above to calculate the local stress state between neighbouring fibres and macroscopic stress–strain response of metal matrix composites. Calculations were conducted for boron fibres within aluminium matrix, with a ratio between the moduli of $E_f/E_m = 5.5$. In polymer matrix composites, this ratio is usually much higher; but the main mechanical mechanisms for stress transfer are very similar. Their result of interfacial shear stress at several overall strain levels is shown in Fig. 9.6. As a major difference to the elastic case, it becomes clear by comparison to the variations shown in Fig. 4.10 that the shear stresses remain finite for plastic matrix deformations. With increasing applied load, the efficiency of shear stress transfer to the fibre along the interfaces increases. The calculated macroscopic stress–strain curves for a boron fibre/aluminium matrix show the same trend as that given in Fig. 9.5.

Up to the present, cylindrical fibres have been well considered. However, if tapered fibres are applied as reinforcement in polymer matrices a different local stress distribution is obtained. Goh *et al.* (2000) used finite element analysis to calculate axial and radial stress distributions for fibres with different cross sections along the axial direction. For the tapered case with the thickness increase from the fibre end to the middle of the fibre they

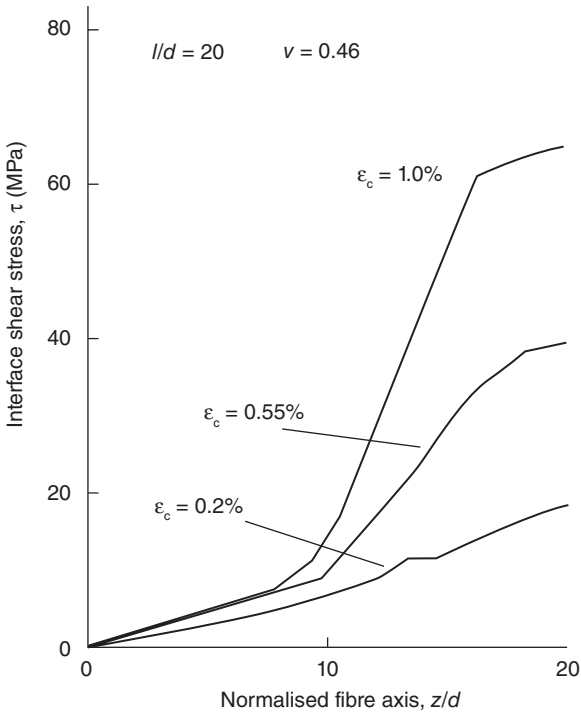

9.6 Shear stress at fibre–matrix interface for different strain levels of boron/aluminium composites. Adapted from Yang and Qin (2001).

calculated a uniform axial and radial stress within the fibre. Consequently, the tapered fibre shape leads to a reduction of maximum stresses in the fibre centre.

After these discussions we have to answer the following question: what should a materials engineer know, if he has to design a short fibre composite of this kind with certain stiffness? Initially, he must know the range of the applied load and the demands on the deformations. Then, he must decide, taking into account economic considerations, which materials can be applied. As a first evaluation of the stiffness that should be expected, he should use one of the simple formulae, for example, eqns [9.2] and [9.3] (more analytical equations of stiffness are given in Chapter 6). Afterwards, he must realise that at higher loads, failure mechanisms initiate and cause stiffness reduction. He can then use one of the previously summarised models to quantify these effects.

Thus, it is necessary to know the failure phenomena for the specified composite. For larger amounts of misoriented fibres with certain fibre length distribution, the orientation and length distributions must be taken into consideration (see Chapter 6).

9.3 Damping behaviour by interface non-elasticity

Non-elastic behaviour of the interface leads to deviations from the elastic stress–strain relation as discussed in Section 9.1. Besides these non-linear effects, certain irreversibility occurs. This is clearly revealed under cyclic loading, where the area surrounded by the path is proportional to the energy dissipation ΔU per cycle. This energy loss is coupled with damping of the excited oscillations, usually characterised by the quantity, Q^{-1}, the 'inverse quality factor' of the oscillating system, which is given by:

$$Q^{-1} = \frac{\Delta U}{2\pi \bar{U}} \quad \text{with} \quad \bar{U} = V\bar{\sigma}_c^2/E_c = V\sigma_0^2/(2E_c), \tag{9.26}$$

where $\bar{U}$ describes the mean energy of the sample, V is sample volume, and σ_0 amplitude of the external stress σ_c.

For oscillating loading with a frequency, ω, a stress $\sigma_c = \sigma_0 \exp(i\omega t)$ develops and lags behind the deformation, $\varepsilon_c = \varepsilon_0 \exp i(\omega t - \delta)$, where δ is the phase angle. The damping energy or the inverse quality factor is given in this case, by $Q^{-1} = \Delta U/(2\pi\bar{U}) = \tan\delta$. The value of $\tan\delta$ is related to the complex modulus $E^* = E' + iE'' = \sigma(t)/\varepsilon(t) = (\sigma_0/\varepsilon_0)\exp i\delta$ by the relation $\tan\delta = E''/E'$. This relation is the most important in the experimental determination of the damping energy during oscillating loading.

In this section the influence of a plastic, viscous and viscoplastic interface on damping behaviour is discussed for a cyclic stress (loading–unloading). For this, the basic model given in Section 4.2 is used. Consideration of energy loss follows the derivations shown in Pompe and Schultrich (1974) and Lauke *et al.* (1990).

The model allows consideration of a misfit in displacements at the fibre–matrix interface. That is,

$$\Delta u = u_p = u_m - u_f = u_i - u_f \approx u_i - u_F, \tag{9.27}$$

which covers all three above-mentioned interface properties. The time variation of this displacement misfit is dependent on the interface shear stress via a general function:

$$\frac{\partial}{\partial t} u_p = F[\tau]. \tag{9.28}$$

9.3.1 Ideal plastic interface

For the case of an 'ideal plastic interface', there is no interface sliding for interface shear stress τ below a certain critical value τ_y, which leads to:

$$\frac{\partial}{\partial t} u_p = 0 \quad \text{for} \quad \tau < \tau_y. \tag{9.29}$$

If this value is achieved, interface sliding proceeds in such a manner that $\tau = \tau_y$ always holds. Such interface behaviour may be realised by plastic processes within a thin boundary layer along the fibre–matrix interface or by friction effects at the debonded interface, as discussed in Section 9.1.2.

For the first loading, starting from the no sliding case, $u_p = 0$, the solutions for the stresses are given in eqn [4.14]. They hold in a slightly modified version for the present case of cyclic loading. For this, considering the linearity of the basic equations, the values at the foregoing maximum stress amplitude, σ_0, must be replaced by the corresponding differences; especially τ_y transforms to $\Delta\tau_y = \tau_y - (-\tau_y) = 2\tau_y$. Thus, interface sliding is directly obtained from the solution for non-cyclic load. It should also be considered that during cyclic loading all values must be interpreted as the difference values while τ_y must be replaced by $2\tau_y$ (Pompe and Schultrich, 1974).

The value of Δu_p for a closed hysteresis loop is consequently given by:

$$\Delta u_p = \left(\frac{\Delta\sigma_c}{E_m(1-\nu)} - \frac{2}{r_f} \frac{l\bar{E}\tau_y}{E_f E_m (1-\nu)} \right)(z-g) + \frac{2}{r_f} \frac{\bar{E}\tau_y}{E_f E_m (1-\nu)} \left(z^2 - g^2\right) \qquad 9.30$$

where g is defined as the point where sliding starts $z = g = l/2 - l_s$, with l_s given in eqn [9.5].

These relations describe closed hysteresis loops in the stress–strain diagram. From this follows the energy loss:

$$\Delta U = 2\pi r_f \tau_y N \int_0^{\lambda/2} dz \oint du_p, \qquad 9.31$$

where N is number of fibres in the sample. Hence, after integration and using eqn [9.26], the hysteresis damping is obtained as:

$$Q^{-1} = A \frac{4\bar{E}}{r_f l E_f} \left(l/2 - g(\sigma_0)\right)^2 \frac{\tau_y \left[\sigma_0 - \left(\frac{4\bar{E}}{3E_f} \right) \frac{\left(l/2 - g(\sigma_0)\right)}{r_f} \tau_y \right]}{\sigma_0^2}, \qquad 9.32$$

with $A = \dfrac{2r_f^2 l E_f}{(V/N)(1-\nu)E_m}$ and the sliding point, $g(\sigma_0) = l/2 + 1/\eta - r_f E_f \sigma_0/(2\bar{E}\tau_y)$.

By inserting g and considering that damping provides essential contributions only for higher stresses, the following approximate equations are obtained:

$$\begin{aligned} Q^{-1} &= (1/3) A (\sigma_0/\sigma^{**}) && \text{for} \quad \sigma_0 \le \sigma^{**} \\ &= A\sigma^{**}(\sigma_0 - 2\sigma^{**}/3)/\sigma_0^2 && \text{for} \quad \sigma_0 \ge \sigma^{**}. \end{aligned} \qquad 9.33$$

Herein, $\sigma^{**} = (1/r_f)(\bar{E}/E_f)\tau_y$ denotes the stress value for which interface sliding has nearly spread along the whole fibre length. According to the

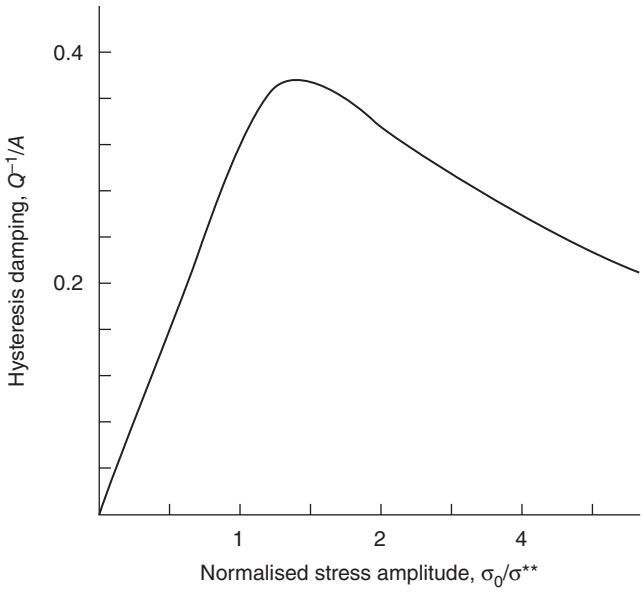

9.7 Dependence of hysteresis damping on stress amplitude at an ideal-plastic interface.

assumptions made about the interface behaviour, this kind of damping is independent of the stress rate but shows marked stress dependence (Fig. 9.7). For not too large amplitudes, it increases linearly where the slope is proportional to $1/\tau_y$. Damping becomes a maximum $Q^{-1}_{max} = \frac{3}{8}A$ at $\sigma_{0,max} = (4/3)\sigma^{**}$.

In this way, experimental investigation of the amplitude-dependent hysteresis damping offers several possibilities for determination of the critical interface stress τ_y:

- from the slope of the initial part of the damping curve,
- from the position of the damping peak, and
- from slope ($\sim\tau_y$) and intersection ($\sim(\tau_y)^2$) of the straight line in the plot of $\sigma_0^2 Q^{-1}$ *vs* σ_0 beyond the maximum.

9.3.2 Viscous interface

Time-dependent viscous effects at the interface can be described by a material law:

$$\frac{\partial}{\partial t}u_p = K_0\tau. \qquad 9.34$$

Because of the linearity of all equations for periodic external loading, $\sigma_c = \sigma_0 \exp(i\omega t)$, all quantities show the same time dependence. The material law [9.34] transforms to $u_p = \dfrac{\tau K_0}{i\omega}$. Hence the interface displacement, u_p, can be eliminated, leading to the solutions of a perfectly bonded composite (eqn [4.14]) where η is replaced by $\eta(t) = \eta/(1 - i\beta)^{1/2}$ and $\beta = (\bar{G}/h)(K_0/\omega)$. The energy loss ΔU is given by:

$$\Delta U = 2N\pi r_f \int_{-l/2}^{l/2} dz \int_0^T dt \, \mathrm{Re}\,\tau \frac{\partial \,\mathrm{Re}}{\partial t} u_p = 4\pi r_f K_0 \int_0^{l/2} dz |\tau|^2 T/2, \qquad 9.35$$

with $T = 2\pi/\omega$. By inserting the shear stress of eqn [4.14] and replacing $\eta \to \eta(t)$ from this relation, eqn [9.26] follows viscous damping as:

$$Q^{-1} = \frac{\Delta U \bar{E}}{\pi \sigma_0^2 V} = \frac{\pi}{8} A \frac{(1+\beta)^{1/2}}{\eta l} \frac{q \sinh(\eta l/2) - p \sin(q\eta l/2)}{\cosh(p\eta l/2) + \cos(ql/2)}, \qquad 9.36$$

with $p = \left(2\dfrac{(1+\beta^2)^{1/2} - 1}{1+\beta} \right)^{1/2}$ and $q = \left(2\dfrac{(1+\beta^2)^{1/2} + 1}{1+\beta} \right)^{1/2}$.

Damping is independent of stress amplitude but shows a characteristic frequency dependence with a damping maximum shown in Fig. 9.8 near $\omega_0 = 8K_0(1 - \nu) r_f E_f E_m/(l^2 \bar{E})$. An approximated evaluation yields the well-known expression of a simple relaxation process:

$$Q^{-1} = \Delta\omega\hat{\tau} \Big/ \left(1 + (\omega\hat{\tau})^2\right), \qquad 9.37$$

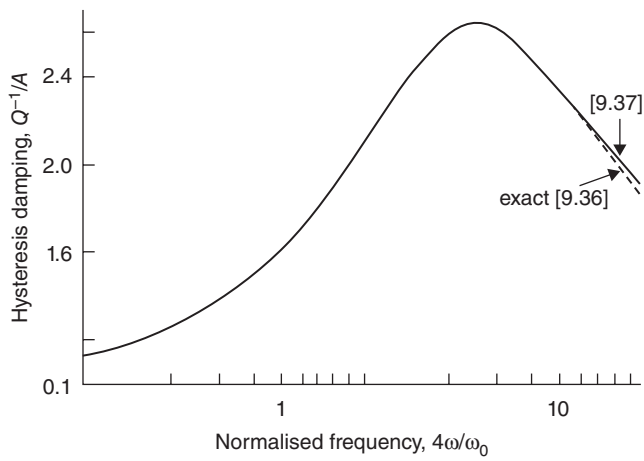

9.8 Dependence of damping on frequency for a viscous interface.

with the relaxation strength $\Delta = 6.64A$ and relaxation time $\hat{\tau} = 1.63/\omega_0$. The height of the damping peak $Q^{-1}_{\max}$ is (within approximation) independent of interface parameters (the same was stated for the ideal plastic interface); its position $\omega_{\max} = 1/\hat{\tau} \sim K_0/l^2$ is proportional to the relaxation constant K_0. With $K_0 = K_0' \exp(-\Delta H/k\mathrm{T})$, the activation enthalpy ΔH of the underlying process can be determined from the frequency or the temperature dependence of the position of the damping maximum.

9.3.3 Viscoplastic interface

In general, non-linear stress effects and rate dependence act simultaneously and superpose to more complex interface behaviour. It may be characterised by a material law:

$$\begin{aligned} \frac{\partial}{\partial t} u_\mathrm{p} &= 0 && \text{for} \quad \tau \le \tau_\mathrm{y} \\ &= K(\tau - \tau_\mathrm{y}) && \text{for} \quad \tau \ge \tau_\mathrm{y} \end{aligned} \qquad 9.38$$

The resulting damping depends on both factors: stress amplitude and frequency.

In principle, the dependence of damping on each of these quantities agrees with that observed in the limiting cases of hysteresis damping and viscous damping, respectively. In both cases, a maximum occurs in the damping curve, but position and height of this maximum are modified (see Fig. 9.9).

The maximum dependence on stress amplitude for a given frequency shifts towards smaller stresses with increasing frequency. It rises with

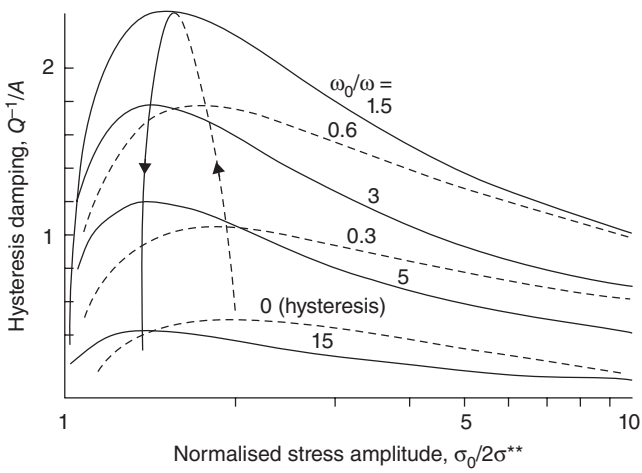

9.9 Dependence of damping on stress amplitude for a viscous interface at different frequencies.

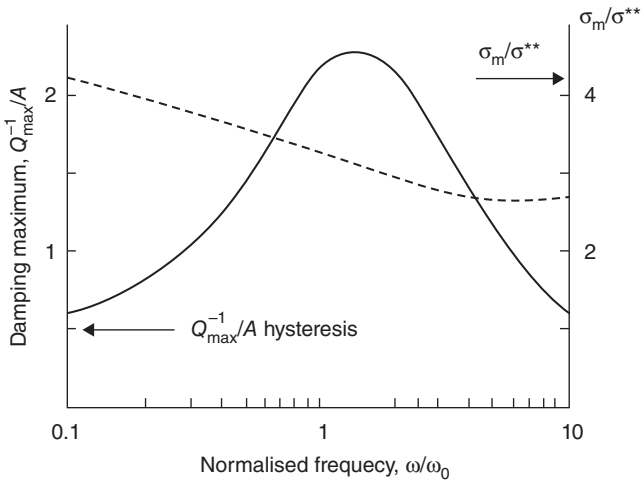

9.10 Dependence of location and value of damping maximum on frequency according to the stress given in Fig. 9.9.

increasing frequency and achieves a four-fold value at about $\omega \approx 1.5\omega_0$ compared with the static hysteresis damping. For larger frequencies, damping diminishes since the interface cannot follow the fast stress oscillations as shown in Fig. 9.10. The limiting case for viscous behaviour corresponds to large stress amplitudes when sliding occurs over the whole fibre length.

9.4 Relaxation effects caused by viscoelastic matrix behaviour

9.4.1 Viscoelastic behaviour of bulk matrix

In the foregoing section the thermoplastic matrix was considered as an elastic or elasto-plastic material and all time dependencies are neglected. In reality, there is a remarkable effect of strain rate and the matrix material should be described by viscoelastic deformation behaviour. This means that the strain $\varepsilon_M(t)$ depends on the loading history apart from the instantaneous stress. According to Boltzmann's superposition principle (see, for example, Findley *et al.* (1976)) this yields:

$$\varepsilon_M(t) = M_m^u \left(\sigma_M(t) + \Delta \int_{-\infty}^{t} dt' g(t-t') \sigma_M(t') \right), \qquad 9.39$$

with M_m^u as the unrelaxed compliance of the matrix and Δ the relaxation strength.

For simplicity, the problem is treated as a unidirectional one without considering any tensorial complications. The function $g(t)$, normalised

according to $\int_{-\infty}^{+\infty} dtg(t) = 1$, describes the decaying influence of the former stress states and has therefore been called the 'memory function'. The relevant timescale can be estimated from the 'relaxation time':

$$\hat{\tau} = \int_{-\infty}^{+\infty} dtg(t)t.$$

The importance of the after-effects is expressed by the 'relaxation strength' Δ.

To elucidate its physical meaning, a sudden loading with constant stress: $\sigma_M(t) = 0$ for $t < 0$; and $\sigma_M(t) = \sigma_M$ for $t \geq 0$ is assumed. Then from eqn [9.39] it follows that:

$$\varepsilon_M(t) = M_m^u \left(1 + \Delta \int_{-\infty}^{t} dt' g(t') \right) \sigma_M = M_m(t)\sigma_M. \qquad 9.40$$

The function $M_m(t)$ is called the creep compliance, and its reciprocal corresponds to the time-dependent Young's modulus, $E_m(t) = 1/M_m(t)$. As shown in Fig. 9.11, the strain relaxes by restricted viscous processes from a lower initial value, $\varepsilon_M(0) = M_m^u \sigma_M$, to a final value, $\varepsilon_M(\infty) = M_m^r \sigma_M$. Thus, the modulus decreases from its unrelaxed value, $E_m^u = 1/M_m^u$ to the relaxed value, $E_m^r = 1/M_m^r = 1/(M_m^u(1 + \Delta))$. So, the relaxation strength is simply the relative difference of these quantities:

$$\Delta = \left(M_m^r - M_m^u\right)/M_m^u = \left(E_m^u - E_m^r\right)/E_m^r . \qquad 9.41$$

The usual integral formulation of eqn [9.39] for linear viscoelastic material behaviour is equivalent to the description as differential equations. In many cases the viscoelastic effects can be described by springs and dashpots,

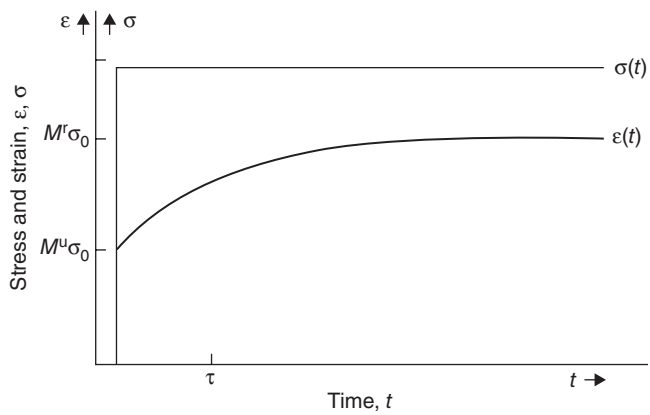

9.11 Retarded deformation of a polymer at sudden stress changes due to viscoelastic effects.

connected in series and parallel. One example is the so-called linear standard solid with a spring in series with an element consisting of another spring and a dashpot. This leads to the generalisation of Hooke's law by adding terms with time derivatives:

$$\hat{\tau}_\mathrm{m}\frac{\partial\sigma_\mathrm{M}}{\partial t}+\sigma_\mathrm{M}=\hat{\tau}_\mathrm{m}M_\mathrm{m}^\mathrm{u}\frac{\partial\varepsilon_\mathrm{M}}{\partial t}+M_\mathrm{m}^\mathrm{r}\varepsilon_\mathrm{M}.$$

A survey about possible superpositions of such elements and their characteristic differential equations is given by Findley *et al.* (1976) and Backhaus (1983).

9.4.2 Composites with viscoelastic matrix

The extension of the single-fibre model with elastic matrix properties, as given in Section 4.2, to a fibre embedded within a viscoelastic material is presented herein. The derivation follows considerations in Lauke and Schultrich (1983) and Schultrich (1990).

Similar to the bulk matrix material, for the case of sudden loading, the resulting relaxation strength of the composite is:

$$\Delta_\mathrm{c}=\left(M_\mathrm{c}^\mathrm{r}-M_\mathrm{c}^\mathrm{u}\right)\Big/M_\mathrm{m}^\mathrm{u}=\left(E_\mathrm{c}^\mathrm{u}-E_\mathrm{c}^\mathrm{r}\right)\Big/E_\mathrm{c}^\mathrm{r} \tag{9.42}$$

following the deformation behaviour at very short and very long times, respectively.

In these limiting cases the matrix modulus can be considered as constant in time. Hence, eqn [9.2] for the composite modulus in the purely elastic case can be used where $1/E_\mathrm{m}$ must be replaced by the unrelaxed (u) and relaxed (r) matrix compliance, respectively:

$$M_\mathrm{c}^\mathrm{s}=\frac{1}{\bar{E}^\mathrm{s}}\left(1+\frac{v}{1-v}E_\mathrm{f}M_\mathrm{m}^\mathrm{s}\frac{2}{\eta_\mathrm{s}l}\right)\quad(s=u,r), \tag{9.43}$$

with $\bar{E}^\mathrm{s}=(1-v)/M_\mathrm{m}^\mathrm{s}+vE_\mathrm{f}$ and η_s is according to eqn [4.10] where $\bar{E}$ is replaced by $\bar{E}^\mathrm{s}$.

Inserting [9.43] into [9.42] provides the relaxation strength of the composite for the sudden loading:

$$\Delta_\mathrm{c}=\frac{1}{1+\lambda/m}\left[\frac{m\Delta}{1+\Delta+m}+\frac{\lambda}{m}\left(1+\Delta\left(\frac{(1+m)(1+\Delta)}{1+\Delta+m}\right)^{3/2}-1\right)\right], \tag{9.44}$$

where $m=(1-v)/(vM_\mathrm{m}^\mathrm{u}E_\mathrm{f})$, $\lambda=2/(\eta_\mathrm{u}l)$ and Δ is according to eqn [9.41]. As seen from Fig. 9.12, the relaxation strength increases markedly with decreasing fibre length especially for weaker matrices ($m \ll 1$).

To investigate the dependency of fibre and matrix stresses on time and coordinate along the fibre axis under these loading conditions, the matrix

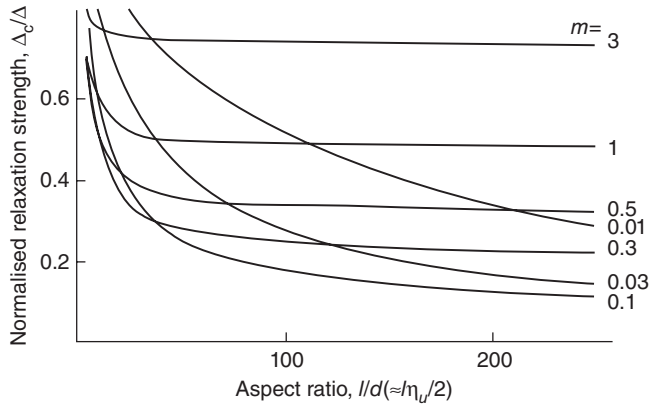

9.12 Dependence of relaxation strength of composite on aspect ratio (proportional to $l\eta_u/2$) and modulus ratio (proportional to m) for $\Delta = 0.1$.

material law [9.40] is inserted in the basic equations of the fibre reinforced composite, yielding a modified version of eqn [4.9] in the form of an integral differential equation. Details about an approximate solution were provided by Lauke *et al.* (1990).

The large effect of the finite fibre length points to an interesting application field of short fibre reinforced composites as structural components with improved damping behaviour in comparison to continuous fibre strengthening. This possibility was first elaborated by McLean and Read (1975), who proved experimentally, for a special polymer composite with 10% volume fraction carbon fibres, the increase of the damping part (i.e., the imaginary part) of the composite modulus from ~33 MPa for continuous reinforcement to ~8 GPa for finite fibres with an aspect ratio of ~100. Their damping calculations are based on the relation $E''_c/E'_c = (E''_m/E'_m)(U_m/U_c)$, which assumes that the energy loss ΔU can be likewise expressed by $\Delta U/U = E''/E'$ for the composite and matrix. Herein, the energies U_m and U_c elastically stored in the matrix and the composite were calculated by the usual elastic stress fields. This energy approach was improved by Gibson *et al.* (1982), Suarez *et al.* (1986) and Gibson (1992) by taking into account the strain energy in the matrix. In an alternative approach, these authors used the fact that for oscillatory loading, it is sufficient to consider the moduli, which depend on frequency. According to the elastic-viscoelastic correspondence principle they are formally identical with the effective moduli in the purely elastic case where the matrix modulus is complex. The essential result is the striking increase of the extensional loss modulus E''_c with decreasing fibre aspect ratio l/d below ~100, thus achieving a maximum at low aspect ratios between 3 and 10. Typical experimental results from Suarez *et al.* (1986) and model

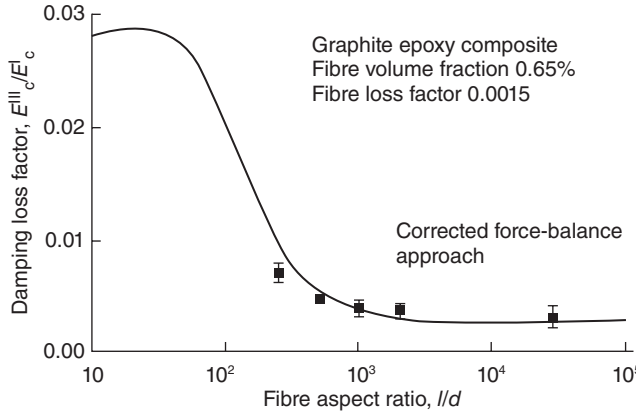

9.13 Damping loss factor as a function of fibre aspect ratio. Adapted from Finegan and Gibson (1999).

predictions by Finegan and Gibson (1999) are shown in Fig. 9.13. These results are also confirmed by numerical calculations using the finite element (FE) method of Sun *et al.* (1985a,b).

On the basis of FE analysis, Brinson and Knauss (1992) calculated the loss modulus of viscoelastic filler and viscoelastic matrix composites with difference in behaviour of softer or stiffer components. They found that the composite behaviour is more affected by stiff inclusions in a soft matrix compared to the case of a stiff matrix and a soft inclusion.

Experimental investigation with dynamic mechanical thermo-analysis (DMTA) on fibre reinforced polypropylene composites was carried out by Amash and Zugenmaier (1997). They observed a decrease of damping with increasing fibre volume fraction. The influences of other parameters of short fibre composites, such as fibre–matrix interface quality or coating effects and fibre interactions, were discussed by Finegan and Gibson (1999, 2000).

Recent developments of nano-fibre materials lay the basis to produce composites with short fibre reinforcements of very low aspect ratios. Finegan *et al.* (2003) reported damping behaviour of carbon nano-fibre (aspect ratio $l/d = 19$) reinforced polypropylene. DMTA was used to analyse the damping and stiffness of the composite. The analytical prediction of the dynamic loss factor ($\tan\delta = E''_c/E'_c$) shows a decrease as the fibre aspect ratio increases.

Most of the simple phenomenological models, such as superposition of springs and dashpots, do not allow adequate description of the loading and unloading characteristics of polymers and their composites. To overcome this, Reymond (2005) proposed the introduction of additional dissipation potentials to take into account the recovery behaviour more exactly.

9.5 References

Agarwal B D, Lifshitz J M and Broutman L J (1974), 'Elastic-plastic finite element analysis of short fibre composites', *Fibre Sci Technol*, 7 (1), 45–62.

Amash A and Zugenmaier P (1997), 'Thermal and dynamic mechanical investigations of fiber-reinforced polypropylene composites', *J Appl Polym Sci*, 63 (9), 1143–1154.

Backhaus G (1983), *Deformationsgesetze*, Akademieverlag, Berlin.

Böhm H J (1998), 'A short introduction to basic aspects of continuum micromechanics', European Advanced Summer School, National University of Ireland, Galway, July 6–10.

Bowyer W H and Bader M G (1972), 'On the reinforcement of thermoplastics by imperfectly aligned discontinuous fibres', *J Mater Sci*, 7 (11), 1315–1321.

Brinson L C and Knauss W G (1992), 'Finite element analysis of multiphase viscoelastic solids', *Trans of the ASME*, 4 (59), 730–737.

Chou T W, Nomura S and Taya M (1980), 'A self-consistent approach to the elastic stiffness of short-fiber composites', *J Compos Mater*, 14 (3), 178–188.

Cox H L (1952), 'The elasticity and strength of paper and other fibrous materials', *Brit J Appl Phys*, 3 (3), 72–79.

Curtis P T, Bader M G and Baily J E (1978), 'The stiffness and strength of a polyamide thermoplastic reinforced with glass and carbon fibres', *J Mater Sci*, 13 (2), 377–390.

Dvorak G J and Bahei-el-Din Y A (1987), 'A bimodal plasticity theory of fibrous composite materials', *Acta Mech*, 69 (1–4), 219–241.

Eshelby J D (1957), 'The determination of the elastic field of an ellipsoidal inclusion and related problems', *Proc Roy Soc London A*, 241 (4), 376–396.

Findley W, Lai J and Onaran K (1976), *Creep and relaxation of nonlinear viscoelastic materials*, North-Holland, Amsterdam.

Finegan I and Gibson R F (1999), 'Recent research on enhancement of damping in polymer composites', *Compos Struct*, 44 (2–3), 89–98.

Finegan I and Gibson R F (2000), 'Analytical modeling of damping at micromechanical level in polymer composites reinforced with coated fibers', *Compos Sci Technol*, 60 (7), 1077–1084.

Finegan I, Gray T and Gibson R F (2003), 'Modeling and characterization of damping in carbon nanofiber/polypropylene composites', *Compos Sci Technol*, 63 (11), 1629–1635.

Gibson R F, Chaturvedi S K and Sun C T (1982), 'Complex moduli of aligned discontinuous fibre-reinforced polymer composites', *J Mater Sci*, 17 (12), 3499–3509.

Gibson R F (1992), 'Damping characteristics of composite materials and structures', *Journal of Materials Engineering and Performance*, 1 (1), 11–20.

Goh K L, Mathias K J, Aspen R M and Hukins D W L (2000), 'Finite-element analysis of the effect of fibre shape on stresses in an elastic fibre surrounded by a plastic matrix', *J Mater Sci*, 35 (10), 2493–2497.

Halpin J C and Tsai S W (1967), 'Environmental factors in composite materials design', *AFML TR*, 67–423.

Hill R (1965), 'A self-consistent mechanics of composite materials', *J Mech Phys Solids*, 13 (4), 213–222.

Jiang Z H, Lian J, Yang D and Dong S (1998), 'An analytical study of the influence of thermal residual stresses on the elastic and yield behaviors of short fiber-reinforced metal matrix composites', *Mat Sci Eng A – Struct*, 248 (1–2), 256–275.

Jiang Z H, Li G, Lian J S, Ding X D and Sun J (2004), 'Elastic-plastic stress transfer in short fibre-reinforced metal-matrix composites', *Compos Sci Technol*, 64 (10–11), 1661–1670.

Kelly A and Tyson W R (1965), 'Tensile properties of fibre-reinforced metals: copper-tungsten and copper-molybdenum', *J Mech Phys Solids*, 13 (6), 329–338.

Kreher W and Pompe W (1989), *Internal stresses in heterogeneous solids*, Akademie-verlag, Berlin.

Lauke B (1992), 'Theoretical considerations on deformation and toughness of short-fibre reinforced polymers', *J Polym Engng*, 11 (1–2).

Lauke B and Schultrich B (1983), 'Deformation behaviour of short-fibre reinforced materials with debonding interfaces', *Fibre Sci Technol*, 19 (2), 111–126.

Lauke B, Schultrich B and Pompe W (1990), 'Theoretical considerations of toughness of short-fibre reinforced thermoplastics', *Polymer–Plastics Technol Enging*, 29 (7–8), 607–832.

McLean D and Read B E (1975), 'Storage and loss moduli in discontinuous composites', *J Mater Sci*, 10 (3), 481–492.

Nomura S and Chou T W (1984), 'Bounds for elastic moduli of multiphase short fibre composites', *J Appl Mech*, 51 (3), 540–545.

Outwater J and Murphy M C (1969), 'On the fracture energy of uni-directional laminates', 24th Annual Tech. Conf. Reinforced Plastics/Composites Div. of SPI, Paper IIc, Section 11-C, pp. 1–8.

Piggott M R (1980), *Load bearing composites*, Pergamon Press, Oxford.

Pompe W and Schultrich B (1974), 'Zur Grenzschichtdämpfung von Verbundwerkstoffen mit kurzfasrigen Einlagerungen', *Annalen der Physik*, 486 (2), 101–119.

Reymond F (2005), 'Constitutive modelling of viscoelastic unloading of short glass fibre-reinforced polyethylene', *Compos Sci Technol*, 65 (3–4), 421–428.

Sato N, Sato S and Kurauchi T (1982), 'Fracture mechanism of short glass fibre reinforced polyamide thermoplastics', *Proceedings of ICCM IV*, Tokyo, p. 1061.

Schultrich B (1990), Private communication in preparation of Lauke, Schultrich and Pompe (1990).

Steif P S (1984), 'Stiffness reduction due to fibre breakage', *J Compos Mat*, 18 (2), 153–172.

Suarez S A, Gibson R F, Sun C T and Chaturvedi S K (1986), 'The influence of fiber length and fiber orientation of damping and stiffness of polymer composite materials', *Exp Mech*, 26 (2), 175–184.

Sun C T, Chaturvedi S K and Gibson R F (1985a), 'Internal damping of short fibre reinforced polymer matrix composites', *Comput Struct*, 20 (1–3), 391–400.

Sun C T, Gibson R F and Chaturvedi S K (1985b), 'Internal material damping of polymer matrix composites under off-axis loading', *J Mater Sci*, 20 (7), 2575–2585.

Takao Y, Taya M and Chou T W (1982), 'Effects of fiber-end cracks on the stiffness of aligned short-fibre composites', *Int J Solids Struct*, 18 (8), 723–728.

Taya M and Chou T W (1982), 'Prediction of the stress–strain curve of a short fibre reinforced thermoplastic', *J Mater Sci*, 17 (10), 2801–2808.

Yang Q S and Qin Q H (2001), 'Fiber interactions and effective elasto-plastic properties of short-fiber composites', *Compos Struct*, 54 (4), 523–528.

10
Fracture mechanics

Abstract: The crack resistance of composites is characterised. Composite materials show extended damage zones in front of the crack tip comparable to plastic zones of homogeneous materials. The energy dissipation processes within these damage zones are qualitatively and quantitatively described. These include fibre breakage, interface debonding and sliding, local matrix plasticity and matrix fracture. On the basis of this knowledge, different fracture mechanics parameters are discussed, including critical stress intensity factor, critical energy release rate, work of fracture and essential work of fracture. All these quantities are given as functions of the fibre, interface and matrix properties, and structural parameters such as volume fraction and/or fibre orientation.

Key words: stress intensity factor, energy release rate, essential work of fracture (EWF), energy dissipation, dissipation zone, process zone.

10.1 Introduction

Over recent decades toughness parameters in addition to the conventional strength have become more and more important in the characterisation of the mechanical behaviours of homogeneous and heterogeneous materials. What are the special advantages of these quantities?

The strength of composite materials depends on the flaw size distribution and, consequently, on sample shape and size; and hence it is not really a property of the material. But given the sample shape and flaw size, we can proceed from strength to a critical stress intensity factor, K_c, or to a critical energy release rate, G_c, which represents an inherent material property. For this purpose, samples with notches of definite length instead of natural flaws are used. All the different definitions of fracture toughness have in common that they characterise the crack resistance of the material. They can be divided corresponding to the different stages of crack growth:

- crack initiation,
- slow crack growth,
- transition to unstable crack growth,
- unstable crack growth, and
- crack arrest.

It is the main purpose of fracture mechanics to characterise the physical situation near the crack tip in an adequate way, thus providing means for

predicting the progress of damage depending on the properties of the material and on the external load. According to fracture mechanics, strength is governed by two things, namely, the properties of a flawless (assumed) sample and presence of pre-existing flaws. The origin of the latter is beyond the scope of fracture mechanics, and therefore this chapter deals with the crack stages listed above.

For general references about fracture and particularly fracture mechanics see, for example, Liebowitz (1968), Broek (1974), Cherepanov (1979), Blumenauer and Pusch (1987), Pompe *et al.* (1985), Atkins and Mai (1985) and Anderson (1995). Special attention to fracture behaviour of polymers is given by Kausch (1978), Kinloch and Young (1983), Williams (1984) and Grellmann and Seidler (1998). Fracture characterisation and fracture mechanics of composite interfaces are given by Kim and Mai (1998). There is also a research monograph on fracture mechanics of cementitious matrices and their fibre composites written by Cotterell and Mai (1996).

Elaborate linear elastic fracture mechanics (LEFM) deals with unstable propagation of sharp cracks under brittle fracture behaviour; that is, the surrounding material deforms purely elastically except for a small plastic region around the crack tip. In this case, the transition to unstable crack growth is described by critical toughness parameters such as the critical stress intensity factor (K_c) and critical energy release rate (G_c). For simplicity, we use the shorter denotation 'fracture toughness' for K_c and G_c bearing in mind their different characteristics.

Composite materials, however, show extended damage zones in front of crack tips comparable to plastic zones of homogeneous materials. These zones change the elastic stress fields around the crack, necessitating the transition from LEFM to extended concepts such as J-integral, crack-opening displacement (COD) or essential work of fracture (EWF) concepts.

The great majority of works concerning fracture toughness of fibre-reinforced materials use the concepts of LEFM. However, in the last few years, more and more publications have appeared which consider the non-linearity of stress-crack opening displacement behaviour. Major efforts in developing the fracture mechanics of composites have been summarised, for example, in the books edited by Friedrich (1989), Williams and Pavan (1995, 2000), Moore *et al.* (2001), Moore (2004) and Blackman (2006).

The determination of fracture toughness parameters happens on two levels, macroscopic and microscopic:

1. The heterogeneous, anisotropic material is approximated by a homogeneous, anisotropic material with effective elastic properties. This method allows the application of the concepts developed for homogeneous materials, which are modified according to the anisotropy.
2. The microscopic processes within the heterogeneous materials are considered. This allows insight into the special failure processes and into

the role of characteristic material parameters such as structural properties (e.g., fibre length, orientation, volume fraction) and mechanical properties of the components, and interface between fibre and matrix.

The above two concepts require both experimental and theoretical research, which will be described in the following sections for short fibre reinforced polymers.

10.2 Basic concepts for homogeneous materials

10.2.1 Stress field near the crack tip

Consider a sample under uniaxial tensile stress σ_A due to an external applied load. Local stresses near notches or pores or crack tips present within the solid may be much higher than the nominal stress σ_A. In linear elastic materials the local stress fields at a point (r, θ) in a plane of the material are proportional to σ_A, which is:

$$\sigma_{ij}(r,\theta) = k_{ij}(r,\theta)\sigma_A . \qquad 10.1$$

The stress enhancement factors k_{ij} depend on all relevant details such as size, shape, and orientation of crack and sample. Near the tip of a sharp crack, that is, at distances much smaller than the crack length c, this function of position can be factorised, with one factor depending only on the distance from the crack tip r, and another factor describing an angular dependence:

$$\sigma_{ij}(r) = Kg_{ij}(\theta)/(2\pi r)^{1/2} \quad \text{for} \quad (\sigma_A/E)^2 << r/c << 1. \qquad 10.2$$

K may depend weakly on a third coordinate which runs along the crack front. For larger distances r away from the crack tip, additional terms must be considered and this approximation is no longer valid. The stress field at the crack tip of an elastic isotropic material can be expressed as a power series, such as that shown by Williams (1957). The region, as shown in Fig. 10.1, where the first term is the dominating one is usually called the 'singularity dominating region'.

A crack tip can be conceived as a singularity of the continuum. This becomes apparent when extrapolating eqn [10.2] to $r \rightarrow 0$. It should be mentioned that the exclusion of very small r in [10.2] reflects the fact that this result is derived from the mechanics of small deformation, that is, under the condition: $\varepsilon^2 \approx (\sigma_A/E)^2 c/r << 1$.

There are three essentially different ways of propagating a crack by displacing the two crack surfaces relative to each other: pulling them apart (mode I) or shearing them along the crack (mode II) or perpendicular to it (mode III). Corresponding to these three modes of crack propagation there are three (and only three) sets of functions g_{ij}. In general, cracks are

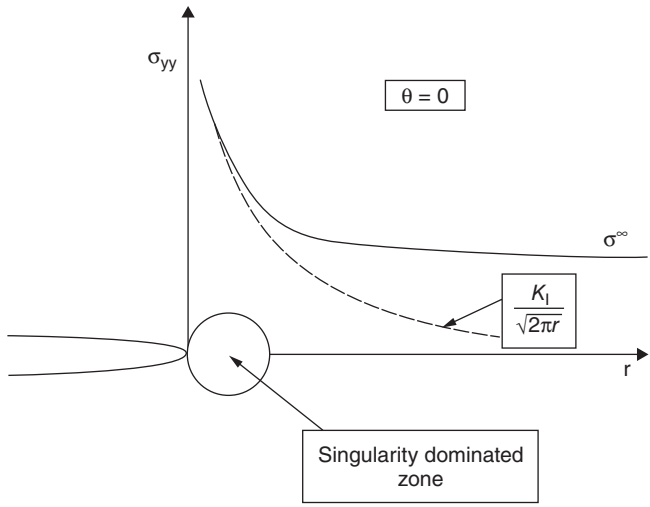

10.1 Stress perpendicular to the crack plane for mode I loading, $\theta = 0$. Adapted from Anderson (1995).

of the mixed type. Those of mainly mode I type, however, are considered to be the most important in materials without macroscopic plasticity. So here considerations are restricted to pure mode I type cracks. Curved cracks do not represent a different type since small sections of them appear approximately straight. Thus, the stress field near the tip of any elastic crack is known. Its spatial structure is given by the universal expression, $g_{ij}(\theta)/r^{1/2}$, whereas K represents its 'intensity'.

Various crack configurations and sample shapes differ only by their stress intensity K whereas the type of the stress field near the crack tip is the same in all cases. According to eqn [10.2] the stress intensity factor K has the dimension of stress times square root of length. The only length by which K can be determined is the crack length itself, provided the boundaries of the sample are so far away that they do not interfere. The only stress that can enter a formula for K is the applied stress σ_A. So, we have:

$$K_I = Y\sigma_A c^{1/2}. \qquad 10.3$$

The dimensionless factor Y depends on specimen configurations and loading mode. We have restricted our considerations to the simple case of uniaxial tension because in more complex situations of cracks within tri-axial or localised stress fields, the basic relation eqn [10.1] is still valid while [10.2] is not universal.

Transforming stresses into strains via Hooke's tensor, the displacements are obtained. The latter, taken at the position of the crack plane, can be regarded as representing the shape of the crack tip, with the above restric-

tion that a tiny region at the very tip has to be excluded. Strictly speaking, only mode I crack tips have a shape. It is described by the one displacement component s, which is perpendicular to the crack plane:

$$s \approx (K_I/E)(r/2\pi)^{1/2} \quad \text{for} \quad (\sigma_A/E)^2 << r/c << 1. \tag{10.4}$$

There is no exact solution very close to the crack tip in linear elastic material, but then no real material remains linearly elastic up to large deformations. So, often some corrections are made to adjust the result to the properties of real materials. According to eqn [10.2] it becomes clear that at the crack tip very high stresses would be produced. In reality, stress does not increase with strain *ad infinitum* but drops after passing a maximum. It was shown by Barenblatt (1962) that this behaviour of the elastic forces created a pointed crack tip with stresses remaining finite.

Clearly plastic flow will occur at the crack tip, reducing the infinite stress of the elastic solution [10.2] to the level of yield stress σ_y. The size r_p of the plastic zone may be estimated by inserting σ_y into [10.2]:

$$r_p = K_I^2 \Big/ \left[2\pi (\sigma_y)^2 \right]. \tag{10.5}$$

The shape of the plastic zone under plane strain, which is realised in the bulk of the sample, is shown in Fig. 10.2. This small-scale yielding affects

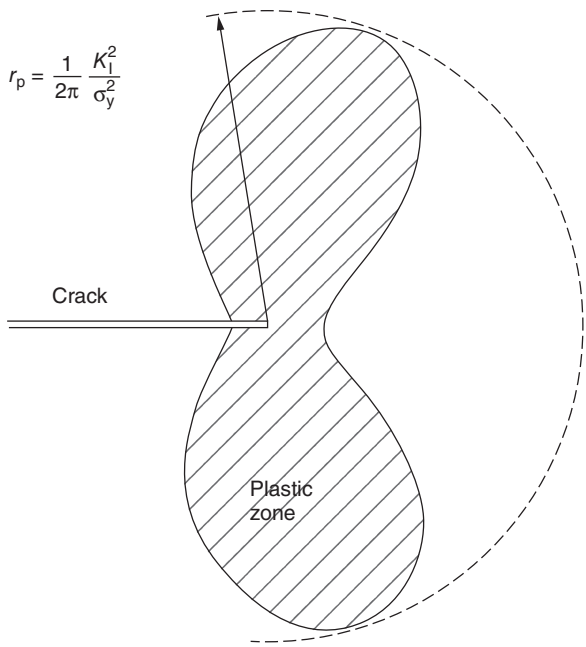

10.2 Shape of plastic zone in the vicinity of crack tip under plane strain conditions, σ_y is yield stress.

the proximate elastic field only slightly so that stress in medium distances, $r_p << r << c$, may still be described by the stress intensity factor, K, according to eqn [10.2]. Though the situation in the vicinity of the crack tip is not much altered by the presence of a small plastic zone, the structure of the very tip is essentially changed.

The crack opening displacement (COD) of the crack at its tip: $s_c = 2s$ now becomes:

$$s_c \approx \sigma_y r_p / E \approx K_I^2 / (\sigma_y E). \qquad 10.6$$

Within polymeric materials we see not only spherical plastic zones but linear structures called 'crazes'. For this special geometry the extension r_p of that zone was calculated by Williams (1973) on the basis of the Dugdale (1960) model, to be:

$$r_p = \frac{\pi}{8} K_I^2 / (\sigma_y)^2. \qquad 10.7$$

10.2.2 Energetics of cracks

As is well known from other fields of physics, much of a phenomenon can be understood already by analysing the redistribution of energy connected with it. For this reason, we shall discuss the redistribution of energy within a stressed body along with crack growth. First, an infinite body loaded by a tensile stress σ_A is considered. Its strain energy per volume is: $\sigma_A^2/(2E)$. Now a plane cut is introduced into the body, which is allowed to open quasi-statically until a new equilibrium has established itself. This relaxed cut is what is called a sharp crack. Obviously, mechanical work is done in the relaxation process against the forces applied to the cut to prevent it from snapping open suddenly. That is, a certain amount of energy is released at the site of the crack.

The applied tensile loading may contribute work in addition to the change of elastic energy within the body. In either case we obtain for the decrease $-\Delta U_{pot}$ of the total potential energy (which is the sum of strain energy U_e and potential energy U_p of the loading system):

$$-\Delta U_{pot} = -(\Delta U_e + \Delta U_p) = W. \qquad 10.8$$

This means the energy W released on the crack surfaces after making the cut is equal to the loss of total potential energy of the sample including the loading system. Two extreme forms of the problem are commonly considered: (a) fixed grip and (b) fixed load.

In (a) no work is done at the remote boundary, and the released energy W is completely supplied by a decrease $-\Delta U_e$ of the elastic strain energy:

$$-\Delta U_e = W(\text{fixed grip}). \qquad 10.9$$

In case (b) it can be shown that an amount equal to $2W$ is supplied by the external forces. Usually this amount is described as loss of potential energy of the loading force $-\Delta U_p$ so the above statement can be written as:

$$-\Delta U_p = 2W(\text{fixed load}). \tag{10.10}$$

However, contrary to case (a), the total elastic strain energy increases by an amount W:

$$\Delta U_e = W(\text{fixed load}). \tag{10.11}$$

It is concentrated near the crack tip whereas the elastic energy stored far away is not changed. In connection with the analysis of crack growth, the rate of change of potential energy with crack size is of special interest, since it has to be equal, according to eqn [10.8], to the rate of change of the energy W released at the site of the crack. This quantity is called 'energy release rate' and is usually denoted by G:

$$G = -\mathrm{d}U_{\text{pot}}/\mathrm{d}A = \mathrm{d}W/\mathrm{d}A. \tag{10.12}$$

Here, $\mathrm{d}A$ stands for incremental crack area. In simple cases, such as the one discussed above, the incremental area may be replaced by an incremental length dc: $\mathrm{d}A = Bdc$, with B as the sample thickness.

Instead of comparing energies of two cracks of sizes A and $A + \mathrm{d}A$ which were cut independently and left to relax, as was considered so far, we could relate $\mathrm{d}W = G\mathrm{d}A$ to the energy released during quasistatic crack growth, $A \rightarrow A + \mathrm{d}A$.

By using the stress and strain fields around the crack tip, we obtain for plane stress the relation:

$$G = K_I^2/E. \tag{10.13}$$

This result relates the energy release rate as a global parameter to the stress intensities at the crack tip, which is a local parameter; and in the elastic case they are equivalent.

There is another possibility for relating the energy release rate to the stress and strain fields around the crack. It is the J-integral provided by Eshelby (1951), Cherepanov (1968) and Rice (1968). That is,

$$G = J = \int_\Gamma \left(\eta_e \mathrm{d}x_2 - \frac{\partial u_i}{\partial x_i} \sigma_{ij} n_k \mathrm{d}s \right) \quad \text{with} \quad \eta_e = \int \sigma_{ij} \mathrm{d}\varepsilon_{ij}. \tag{10.14}$$

Integration has to be performed along an arbitrary path Γ around the crack tip (Fig. 10.3). The J-integral describes the flux of that part of energy through the closed (by Γ) area around the crack tip, which is not absorbed but dissipated during crack growth.

J does not depend on the path of integration, which is a major advantage since the path may be chosen in a convenient way. As another advantage J

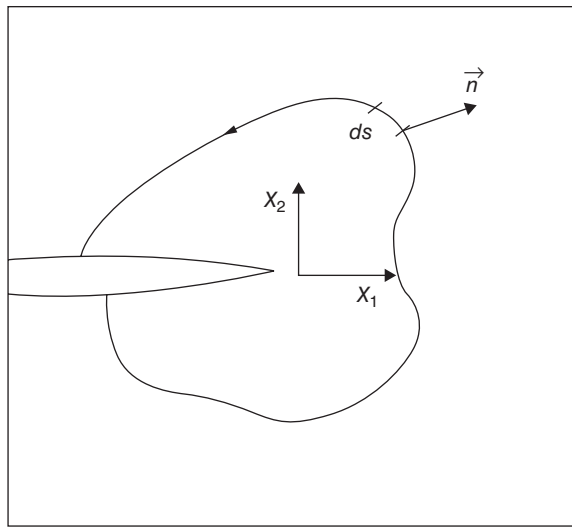

10.3 Integration path of J-integral.

applies to any elastic material, whether linear or non-linear, while eqn [10.13] is restricted to linear elasticity.

The J-integral and results derived from it apply to general elastic behaviour. It is worth noting that the results obtained for non-linear elastic materials provide useful approximations for non-elastic materials.

The calculation of K or G for special configurations of cracks within samples of given shape and loading is the crucial problem of theoretical fracture mechanics. It requires sophisticated analysis in every single case. We can approach the problem experimentally to avoid the trouble, at least in principle, by carefully measuring the compliance of the specimen considered for different crack size. The compliance is defined by: $C = \delta/F$, where F is external load and δ is the load-point displacement. The elastic energy stored in the material is then, $U_e = F\delta/2 = \delta^2/2C$. For fixed boundaries of the specimen according to [10.9], all released energy is drawn from elastic energy: $G\mathrm{d}A = -\mathrm{d}U_e = -\frac{1}{2}\delta^2\mathrm{d}(1/C)$. This leads to:

$$G = \frac{1}{2}F^2\frac{\mathrm{d}C}{\mathrm{d}A}. \qquad 10.15$$

Thus, the energy release rate and corresponding stress intensity may be derived from the change of compliance with crack size. The condition of fixed grip is not relevant for this result since it is valid for all other cases of load and displacement variations.

Many polymers show large plastic deformations during loading, especially ahead of notches or cracks where large plastic zones are developing. There have been many efforts to take this into account for the determination of fracture toughness. In recent years the essential work of fracture (EWF) concept has been developed to evaluate the toughness of polymers. For details readers may refer to the European Structural Integrity Society (ESIS) *Test Protocol on Essential Work of Fracture*, Version 5 (October 1997).

Broberg (1975) proposed a specific essential work of fracture, w_e, for cases where the fracture of a polymer specimen is preceded by extensive yielding. The basic idea behind this approach is that the failure mechanisms in front of a crack are contained within a process zone which is subdivided, respectively, into a process plane where the crack propagates and a surrounding dissipation zone where the plastic deformations are concentrated.

Introducing the specific fracture energy, w_e, the specific volume energy, η_p, and the surface and volume quantities (cf. Mai and Cotterell, 1986), the work of fracture, W_f, is given by:

$$W_f = w_e LB + \eta_p V_p, \tag{10.16}$$

where L is ligament length, B specimen thickness and V_p volume of plastic zone. With the assumption that V_p is proportional to BL^2 with the shape factor β: $V_p = \beta BL^2$, the specific total work of fracture becomes:

$$w_f = \frac{W_f}{LB} = w_e + \beta \eta_p L. \tag{10.17}$$

This provides the basis for the determination of the specific essential work of fracture, w_e, from the intercept of the linear regression curve of experimentally determined w_f *vs* L-curve, where L is given by notching and W_f by the integral under the load (F)-displacement (u)-curve.

While examining the deformation rate and thickness dependence of the work of fracture, Karger-Kocsis *et al.* (1997, 1998) have discovered from the shape of the load-displacement curve that it is possible to distinguish between fracture energies for yielding and necking with subsequent fracture. It is noted that recently the EWF has been used to analyse the toughness behaviour of polymer nanocomposites containing clay (Yoo *et al.*, 2007), multi-walled carbon nanotubes (Satapathy *et al.*, 2007) and Mg-Al layered double hydroxide (Costa *et al.*, 2006). Interested readers may refer to these papers. More relevant to this book and most recently, the EWF method has been applied to SFRP composites and particulate reinforced polymers; this topic will be discussed in detail in Section 10.6.7.

10.2.3 Crack propagation criteria

The question whether a crack will remain at rest or will start propagating in a given situation can be decided by crack propagation criteria. There are several of these, based on different notions. Since they all describe the same phenomenon, they are equivalent to a certain extent. Their differences lie mainly in being adapted to special problems or materials. Below, we will discuss only a criterion based on energy variation since it proves most useful in linear elastic fracture mechanics. (It should be noted that the energy criterion is equally applicable to non-linear elastic and plastic fracture mechanics. See, for example, Atkins and Mai (1985). But these specialised topics will not be covered in this book.)

The phenomenon of crack propagation may be separated, in thought, into two simpler phenomena occurring simultaneously: first, energy release as discussed in the preceding subsection; second, energy consumption in creating the cut which enlarges the crack. The former reflects geometrical properties such as crack length, sample shape, and mode of stressing, whereas the latter is considered to be a property of the material. This is a kind of separation generally aimed at in materials science.

As usual, we denote the specific fracture surface energy by γ (energy per unit area of crack surface). Then, the total energy of the loaded sample may be written as potential energy of the sample including the loading system, cf. eqn [10.8], plus the energy consumed by the two crack surfaces of area A. That is,

$$U_t = U_{pot} + 2\int \gamma \mathrm{d}A. \qquad 10.18$$

With the previous definition of energy release rate in eqn [10.12] its derivative provides:

$$\mathrm{d}U_t/\mathrm{d}A = -G + 2\gamma. \qquad 10.19$$

Crack propagation (i.e. $\mathrm{d}A > 0$) is only possible if the total energy U_t decreases:

$$\mathrm{d}U_t/\mathrm{d}A \leq 0. \qquad 10.20$$

Combining [10.19] and [10.20] provides the following crack propagation criterion:

$$G \geq G_c \equiv R \equiv 2\gamma. \qquad 10.21$$

This means that the crack can propagate only if the release of energy surpasses its consumption, that is, if G is larger than a critical value G_c specific to the material. This is a necessary condition for crack extension. The left and right side of the above equation are quite different: G is a function of geometry, mechanical properties and applied load; and R or G_c,

respectively, is a material property. However, the crack may propagate in a stable or unstable manner, as will be discussed below.

The consumption of energy, or the energy necessary for crack growth, is also called the crack resistance R of a material. The critical energy release rate G_c is usually called 'fracture toughness'. In nearly all real materials, phenomena other than pure surface energy contribute to G_c (or R), among which energy consumed in plastic flow (and thereby mostly transformed into heat) is most important. Despite this complication G_c justifies its existence by proving itself a material constant, which it is intended to be, with tolerable accuracy in the majority of cases. By means of eqn [10.13] a critical stress intensity factor K_c is related to G_c.

For polymeric materials where a craze-like plastic zone is developed in front of a notch, Williams (1972) showed that the following relation between the critical energy release rate and the crack opening displacement (COD), s_c, exists:

$$G_{Ic} = s_c \sigma_y, \tag{10.22}$$

where σ_y is yield stress.

This relation makes it clear that the critical crack opening displacement s_c is appropriate for estimation of unstable crack propagation of polymers. The advantage of this method in comparison to the fracture toughness, K_c, is the same as that of the J-integral, namely that these values can be determined without any requirements of the sample geometry.

Consideration of crack growth in terms of variable $G(c)$ and constant G_c provides useful results to many crack problems. However, if we need to follow the cracks in heterogeneous materials from microscopic to macroscopic size, we also have to allow for changing G_c. The crack starts inside one component and moves finally through the effective material. This change in G_c or γ is usually called the 'crack growth resistance' $R(c)$. R often does not depend on c but rather Δc, the increase in crack length with respect to a given initial length. This indicates that the structure of the moving crack tip differs in some way from that of the initial crack tip, and the initial crack needs some distance of growth to obtain the stationary structure of its tip.

The average value of R for the whole crack growth process is called the 'work of fracture' and the specific work of fracture is given by:

$$w = \frac{1}{\Delta c_{max}} \int_0^{\Delta c_{max}} R(\Delta c) d\Delta c, \tag{10.23}$$

where Δc_{max} is defined as the maximal crack path through the sample.

For large crack increments, the work of fracture approaches the stationary value of R, if there is any.

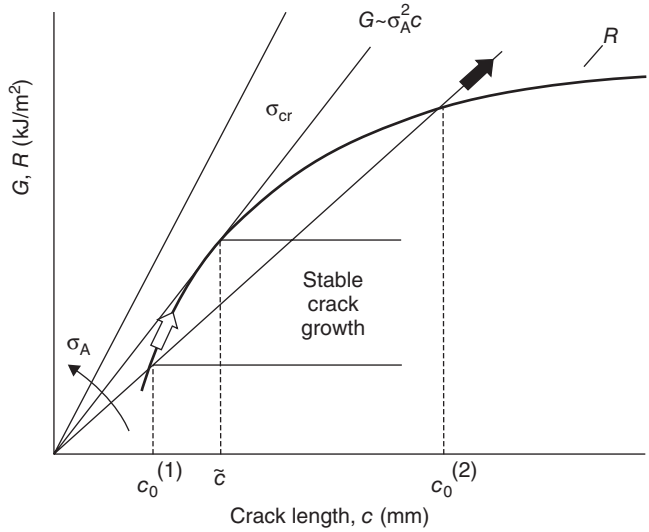

10.4 Schematic showing crack propagation in the presence of curved $R(c)$ under increasing load σ_A. Loading below σ_{cr}: stable growth if $c_0 < \tilde{c}$; unstable propagation if $c_0 \geq \tilde{c}$. Unstable propagation above a certain load σ_{cr} regardless of initial flaw size c_0.

The work of fracture approach, similar to J-integral, has an advantage compared to the critical stress intensity factor in that it allows the change of energy; that is, it contains stress and strain. If $R(c)$ is curved downward (see Fig. 10.4), initial cracks grow stably at first until they become unstable at $\tilde{c}$. Initial cracks larger than $\tilde{c}$ grow unstably from the start and they cannot be stabilised again. The critical length, $\tilde{c}$, which is decisive for the behaviour of the initial cracks after the start, is determined by the condition of equal tangents of $G(c)$ and $R(c)$, as becomes evident in Fig. 10.4:

$$G = R \quad \text{and} \quad \mathrm{d}G/\mathrm{d}c = \mathrm{d}R/\mathrm{d}c \quad \text{for} \quad c = \tilde{c}. \tag{10.24}$$

10.2.4 Dynamic fracture toughness

Methods to determine the dynamic fracture toughness are mainly extensions of the previously described methods for static loading conditions. Reviews on the theoretical concepts and test methods were given, for example, by Kanninen (1978), Blumenauer and Pusch (1987) and Grellmann (1985).

For interpretation of the dynamic fracture toughness it becomes necessary to distinguish between the resistance of the material against crack initiation (critical point) and against crack propagation with crack speed, $\mathrm{d}c/\mathrm{d}t = \dot{c}$. Analogous to static methods the energy and stress concepts are

applicable. The equivalence of both methods was proposed by Kanninen (1978). The critical conditions are now changed to:

$$K(c, \sigma_A, t) = K_{c,d}(\dot{c}) \qquad 10.25a$$

and

$$G(c, \sigma_A, t) = G_{c,d}(\dot{c}), \qquad 10.25b$$

where t is time.

Again, the values on the left-hand side represent the stress and energy available for crack propagation with crack speed, $\dot{c}$; and the values on the right-hand side, the crack resistance of the material. The dynamic toughness parameters are mainly determined by such test methods as impact bending (Charpy and Izod), drop weight, and impact tension. If these methods are applied without instrumented equipment, the direct determination of fracture toughness is impossible since the force-displacement curves are not known.

Marshall *et al.* (1973) and Brown (1973) showed that under the supposition of elastic deformations, it is possible to calculate the fracture toughness directly from the elastic energy, U_e, stored in the material. This is achieved by rearranging the relations [10.15] in the form:

$$G = U_e \frac{1}{C} \mathrm{d}C/\mathrm{d}A. \qquad 10.26$$

With the critical condition [10.21], this provides:

$$U_e = G_c B \Phi T, \qquad 10.27$$

with $\Phi = \dfrac{1}{T} \dfrac{C}{\mathrm{d}C/\mathrm{d}c}$ and T as the width of the specimen.

After measuring the elastic energy, U_e, as the deformation energy until fracture of the sample, and the function Φ, G_c can be calculated. Φ is determined under static loading conditions. Yet, this is somewhat questionable because it is not proven if the result is applicable to impact loads.

For many relatively brittle thermoplastics, relation [10.27] is linear with G_c as the slope. However, if tougher polymers are tested, non-linearities may occur because of the plastic deformations of the material. This difficulty was overcome by Birch and Williams (1978) by the incorporation of a plastic zone correction of the crack length.

Further problems associated with this method arise from the measurement of U_e. This energy also involves kinematic energies of the sample and the test device. These effects were considered, for example, by Plati and Williams (1975) and by Newmann and Williams (1980). Nezbedova and Turcic (1984) considered these corrections to determine the condition

under which this method can be used to determine the fracture toughness of brittle PMMA and tough PP and ABS thermoplastics.

10.3 Application of fracture mechanics to fibre reinforced composites

10.3.1 Theoretical and experimental bases

The crack resistance of fibre reinforced composites can be characterised by the concepts described above, which were developed for homogeneous materials. Thus, we must realise the assumptions and hence limitations in transferring the concepts to heterogeneous, anisotropic materials.

The main assumptions to apply LEFM in the macroscopic approach to heterogeneous, anisotropic materials are:

- The crack growth is self-similar (no change of crack direction under mode I loading). This is sometimes not the case for fibre composites. When a crack meets fibres with orientation away from the crack direction it may grow along the fibres so that the composite structure has to be considered.
- Stress distribution around a crack in anisotropic materials is similar to that of homogeneous, isotropic material. This means the prevailing singular term has the same power of singularity but may have an intensity that depends on the anisotropy.
- The inhomogeneity, i.e., structural parameters, for example fibre diameter or fibre length, must be small compared to the K-dominance zone and continuum mechanics is applicable. Otherwise, local structure affects the stress field and the macroscopic relation for stress intensity is modified. For example, when the crack moves along the fibre–matrix interface, the fracture mechanics of a bi-material crack is necessary.

Consequently, when fracture mechanical concepts are applied it is important to include details of structural heterogeneity. The problem lies in the resolution of even small structures by the steep stress gradients ahead of the crack tip (this thus violates the second assumption above). The condition for infinitesimal crack growth, and the basic process for testing the crack stability in homogeneous materials, varies with the local structure. Hence, crack growth, which appears stable on average, may be composed of stable growth in one phase and sudden cracking in another. Therefore, part of the released energy appears as kinetic energy, whose existence is usually ignored in the energy balance involving a finite increment of crack length, as is required for describing heterogeneous materials. This means the tacit assumption that the energy carried away by elastic waves is in some

way re-absorbed by the crack tip moving slowly into the other component and becomes the crack surface energy again.

This redistribution of energy (and also the non-linear redistribution of stresses) is mostly promoting fracture so that the fracture toughness calculated under this assumption has the meaning of a lower bound, K_c^-, respectively, G_c^-. In the other extreme, it is assumed that the energy released excessively at some place on the crack front is not fed into areas of deficient energy release but is completely dissipated. Obviously this situation favours crack propagation the least. Thus, it represents an upper bound, K_c^+, G_c^+, for the macroscopic stress intensity and energy release rate, respectively. In reality, K_c is somewhere between these two bounds, depending on the material and on specimen geometry:

$$K_c^- \le K_c \le K_c^+ \quad \text{or} \quad G_c^- \le G_c \le G_c^+ . \tag{10.28}$$

The basic equations for the stress intensity factor and energy release rate of a homogeneous, isotropic material are given by eqns [10.3], [10.15] and [10.27] with relation [10.13]. These equations are now applied to the inhomogeneous, anisotropic materials:

$$K_I = Y_a \sigma_c c^{1/2}, G_I = \frac{1}{2} F^2 \frac{dC_a}{dA} \quad \text{or} \quad G_I = \frac{U_e}{BT\Phi} \quad \text{with} \quad G_I = K_I^2 / E_a \tag{10.29}$$

and are also used for their critical values, the fracture toughness.

Evidently, this expression for critical stress intensity factor involves difficulties in the interpretation of the right-hand side quantities of composites, viz. the calibration factor, Y_a, critical applied load σ_c, and crack length, c. Y_a now becomes a function of stiffness in different material directions E_{ij}: $Y_a = Y_a(E_{ij}, c)$. In the relation between the energy release rate and the stress intensity factor, the effective stiffness E_a of the anisotropic material must be considered.

The critical stress for crack initiation in fibre composites is difficult to identify. Further, it must be taken into account that the crack resistance of a heterogeneous material depends on the direction of crack propagation.

For continuous-fibre reinforced polymers the problem of critical load and effective crack length was considered by Guess and Hoover (1973) and by Gaggar and Broutman (1975). The anisotropic calibration factor was dealt with by Barnby and Spencer (1976), Sweeney (1986) and Hine *et al.* (1988). The last paper also provides for three-point bending and double-cantilever-beam tests a compliance C, which is dependent on the stiffness E_{11}, necessary for the application of the second of eqn [10.29]. A third possibility to determine the fracture toughness of fibre reinforced composites is to use the last of eqn [10.29]. Instead of the elastic modulus of the homogeneous material, E, now an 'anisotropic modulus', E_a, must be used. For orthotropic properties of the composite the relation was derived by Sih *et al.* (1965).

For short fibre reinforced polymers (SFRP), this problem was tackled by the ESIS group and resulted in the protocol by Moore (2001), where a calibration function Y_a that depends only on the specimen geometry is used. More details are given in the next section.

In addition to these stress-field concepts, the energy concept, based on the determination of the critical energy release rate, G_c, by compliance calibration has been used. Application of eqn [10.15] to composites was studied, for example, by Guess and Hoover (1973). Also, different J-integral measurements according to eqn [10.14] were performed by Grellmann (1985), Hoffmam *et al.* (1985), and Grellmann *et al.* (1991) for SFRP.

However, the measurement of work of fracture-like quantities as the impact toughness in un-instrumented dynamic tests incorporates some major disadvantages. Since the stress–strain curve is not known it cannot be concluded whether a change is caused by the change of maximal load or by a change in the deformation ability of the material. This drawback leads to the necessity of instrumented impact loading apparatus. A comprehensive survey about devices and methods was given by Grellmann (1985), who evaluated the applicability of different fracture mechanic concepts for homogeneous polymers and for fibre reinforced thermoplastics. Using the instrumented impact device, Karger-Kocsis (1993) could distinguish between crack initiation and crack propagation stages.

In the micromechanical approach, which is used in theoretical considerations of crack resistance, the heterogeneities of composite materials can be better taken into account. In this approach, a straightforward idea is to sum up all contributions of parts and components to an effective fracture energy. It corresponds to the global energy approach where the elastic energy released during finite crack growth over a structural element is equated to the different kinds of energy consumption, R_i, as fibre break, matrix fracture, interface sliding, etc. Consequently, the crack resistance is given by:

$$R = \sum_i \alpha_i R_i, \qquad 10.30$$

with α_i as a weighting fraction of the mechanism (i) of the crack area.

It is not an assumption that single mechanisms must not interact, however, the calculation of the single contributions under consideration of the other ones is mostly a very complex task and that is why the dissipation energies are simply superimposed in most theoretical studies.

If eqn [10.30] is interpreted in the sense of work of fracture (i.e., as the sum of individual energy contributions of different mechanisms to the total energy for driving the crack through the specimen) and not in the framework of fracture mechanics (as the change of energy for an infinitesimal crack growth, G), then such equation can be traced back to the works of Cottrell (1964) and Cooper and Kelly (1967). This concept was subse-

quently further developed by Beaumont and Harris (1972) and Harris (1972). This approach will be used for the derivation of the work of fracture in Section 10.5.

In SFRPs there appears to be a substantial amount of slow crack growth prior to unstable fracture under increasing load/increasing displacement conditions. It is therefore necessary to distinguish between crack initiation, crack propagation and complete failure. Crack initiation is characterised by the balance of available energy dW with the energy dQ that is necessary for crack tip propagation. That is,

$$\mathrm{d}W \geq \mathrm{d}Q = R\mathrm{d}c. \tag{10.31}$$

The calculation of crack resistance and critical energy release rate will be shown in detail in Section 10.10.

A corresponding expression for the effective fracture toughness, K_c, in terms of the single values K_{ic} for the different phases (i) and their volume fractions (v_i) of multiphase materials was derived by Kameswara Rao (1983). For the special case of a two component composite, this is given by:

$$K_c = (K_{1c} - K_{2c})(1 - v_1)^{1/2} + K_{2c}. \tag{10.32}$$

The above equation is based on the superposition principle of stresses which is valid in linear elastic theory, i.e., the total force in a cross section is equal to the sum of its parts. If this is expressed in terms of the stress intensity factor definition (eqn [10.2]) the above equation is obtained.

A similar approach was applied by Becher *et al.* (1988) and Song *et al.* (2002). They also used the stress superposition principle, for example, for mode I loading, all stress components in one direction of different components (such as σ_{yy}) can be added. If the components are generalised to different dissipative mechanisms, the stress intensities can be summed up and this provides:

$$K_{\text{composite}} = \sum_i K_i, \tag{10.33}$$

where K_i is the stress intensity factor of the i-mechanism. This simple superposition is only allowed if the stresses contributing to the single mechanism in one direction are not disturbed by the other mechanisms. Bearing in mind the complex structure of a composite material it is questionable whether the local stress field can be considered, as for example only a mode I loading situation. It is expected that a multi-axial loading situation exists in front of a crack leading locally to superposition of different modes (modes I, II and III). But the different modes are not allowed to add (because adding loads in different directions as σ_{xx} and σ_{yy} is not permitted). Hence, it seems more appropriate to use the formulation in terms of energy, as in eqn [10.30] than in terms of stresses as in eqn [10.33].

In the work by Friedrich (1984) fracture toughness of the composite, K_c, was calculated by relating it to that of the matrix, $K_{c,m}$:

$$K_c = MK_{c,m}, \tag{10.34}$$

where M is a microstructural efficiency factor that takes into account the fibre–matrix interaction energies.

Short fibre reinforced polymers generally show a substantial amount of slow crack growth before crack instability, so that a single parameter like K_c or G_c is not appropriate to characterise the total fracture behaviour. For this reason the R-curve concept was used by Gaggar and Broutman (1975) and by Agarwal and Giare (1981). They used it for short-fibre reinforced epoxy and found that the results are useful for comparing different composite variants but they fail to predict the toughness as a material parameter because it depends on the initial crack length. Thus, the R-curve concept will be described in more detail in Section 10.10.5.

Another fruitful approach for considering structural aspects in fracture mechanics is the so-called laminate analogy. This method is based upon the combination of micro- and macro-mechanical considerations. A composite material is subdivided into different layers with varying structural parameters (such as fibre orientation). After calculation of the effective elastic constants for each layer, LEFM is applied. Thus, subsequent superposition provides the fracture toughness of the composite. This approach was used mainly for continuous fibre reinforced polymers (Harris, 1986). However, it has also been successfully applied to short fibre reinforced composites by Tsanas and Kardos (1985) and Fu *et al.* (2002c).

The fracture toughness K_c of composites can be evaluated by a bimodal equation:

$$K_c = \frac{2S}{B} K_{c,skin} + \frac{C_0}{B} K_{c,core}, \tag{10.35}$$

where $K_{c,skin}$ is fracture toughness of the skin layers; $K_{c,core}$ is fracture toughness of the core layer. Since the size ($2S$) of the skin layers is much larger than the size (C_0) of the core layer (see Chapter 3), the fracture toughness of the skin layers will play a dominant role in determining the total composite toughness.

For ductile polymers the methods of LEFM as described above and their extension to non-linear elastic materials, as J-integral, which also has limited validity for small-scale yielding, are inappropriate. For these materials the concept of essential work of fracture (EWF) was applied to find reliable fracture mechanics parameters. This concept was extended to short fibre reinforced polymers by Wong and Mai (1999) and Tjong *et al.* (2002a, 2002b). A detailed description of the EWF method and results will be given in Section 10.12.

This short review suggests clearly that the experimental determination of a real fracture toughness value for a heterogeneous material is a very complex problem.

Conversely, materials science has to answer the questions as to the nature of the main processes of energy dissipation during failure and how the material parameters must be changed to improve the crack resistance.

10.3.2 Experimental findings of fracture toughness

In the following some typical experimental results are used to illustrate the complex variation of fracture toughness and work of fracture with material parameters. At first, quasi-static loading with crosshead speed of ~0.2 mm/min is considered. Over the years, a number of different fracture mechanics tests have been established; overviews are given by Broek (1974), Mai and Atkins (1980), and Anderson (1995).

Most often, the compact tension (CT) specimen (Fig. 10.5) is used for SFRP. For this geometry the general equation [10.29] takes the form:

$$K_c = Y_a \sigma_c \sqrt{c} = Y_a \left(\frac{c}{T} \right) \cdot \frac{F_c}{B \cdot T} \cdot \sqrt{c}, \qquad 10.36$$

where c is crack length, B specimen thickness, T specimen width and F_c the critical force. For calibration factor Y_a different functions are used. Broek (1974) and Friedrich (1985) used:

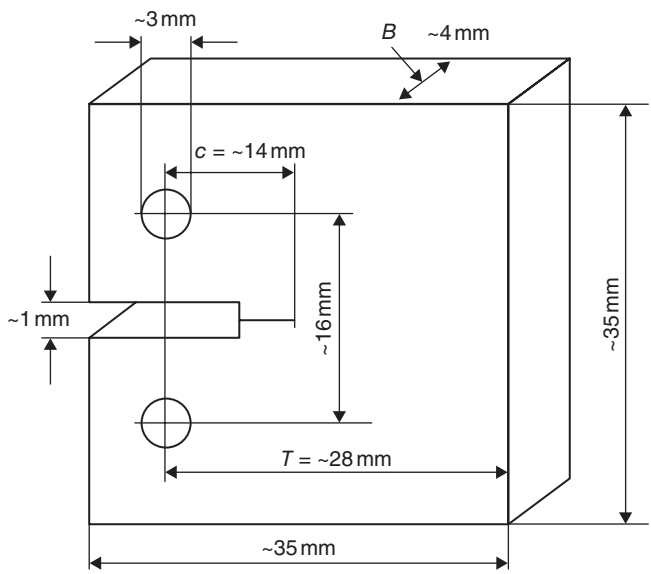

10.5 Geometry and dimensions of a compact tension specimen.

$$Y_1\left(\frac{c}{T}\right) = 29.6 - 185.5\left(\frac{c}{T}\right) + 655.7\left(\frac{c}{T}\right)^2 - 1017\left(\frac{c}{T}\right)^3 + 639\left(\frac{c}{T}\right)^4, \qquad 10.37$$

but Williams (2001) in the ESIS protocol and Anderson (1995) used the following relation, which corresponds to the ASTM E399 (1983) standard:

$$Y_2\left(\frac{c}{T}\right) = \left(\frac{T}{c}\right)^{1/2}\left(\frac{2 + c/T}{(1 - c/T)^{3/2}}\right)$$
$$\left[0.886 + 4.64\left(\frac{c}{T}\right) - 13.32\left(\frac{c}{T}\right)^2 + 14.72\left(\frac{c}{T}\right)^3 - 5.6\left(\frac{c}{T}\right)^4\right]$$
$$\text{for} \quad 0.2 \le c/T \le 0.8. \qquad 10.38$$

These two functions provide very similar values in the range $0.3 \le c/T \le 0.7$. Outside of this range they are slightly different; however, in view of the uncertainties in determination of critical crack length and/or critical force F_c it may be neglected. For the critical load, it can be taken as the maximum load or the so-called 5% offset load, F_Q. This K_Q method was first introduced in engineering fracture mechanics to consider small non-linearities in the stress-deflection curves, see Broek (1974), i.e., the maximum load F_{max} as the critical value is replaced by a modified load F_Q. Usually, that load is defined by a 5% reduced slope of the load-deflection curve. More details and discussions about K_c testing of SFRP are found in Moore (2001). In particular, the condition for the application of LEFM according to specimen size to realise a plane strain stress state and the measurement of yield stress σ_y are given. The sample thickness (B), crack length (c) and ligament (T-c) shall be larger than the minimum values:

$$B_{min}, c_{min}, (T - c)_{min} = 2.5\left(\frac{K_c}{\sigma_y}\right)^2. \qquad 10.39$$

Similar standards exist for other specimen geometries, for example, three-point bending specimen whose geometry is very often used in impact testing, e.g., Charpy impact test.

The stress concept to determine fracture toughness K_c for SFRP was used by Friedrich (1982, 1984, 1985). Compact tension testing geometry was applied and cracks were propagated both parallel and perpendicular to the mould flow direction (MFD) as shown in Fig. 10.6.

Figures 10.7 and 10.8 show the dependence of K_c on the two perpendicular crack propagation directions (T-perpendicular and L-parallel to the mould-fill direction) for the relatively brittle polyethylene-terepthalate (PET) and the tough polycarbonate, respectively. Comparing both curves, it is clear that the tendency of toughness variation with increasing fibre volume fraction depends strongly on the deformation behaviour of the matrix material. The initially more brittle material (PET) shows an increase of fracture toughness

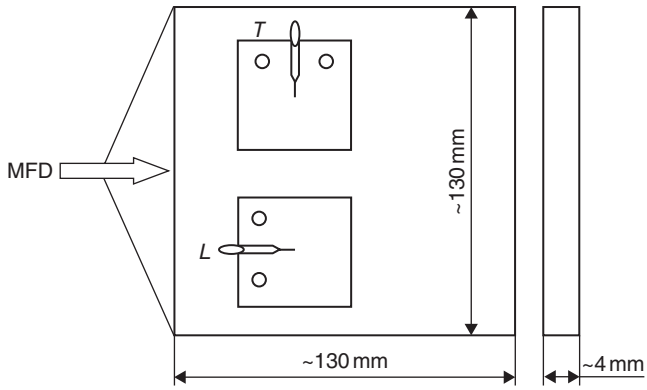

10.6 Macrostructure of injection-moulded plaques and orientation of compact tension test specimen, *T*: crack direction transverse to the mould flow direction (MFD), *L*: crack direction in the MFD.

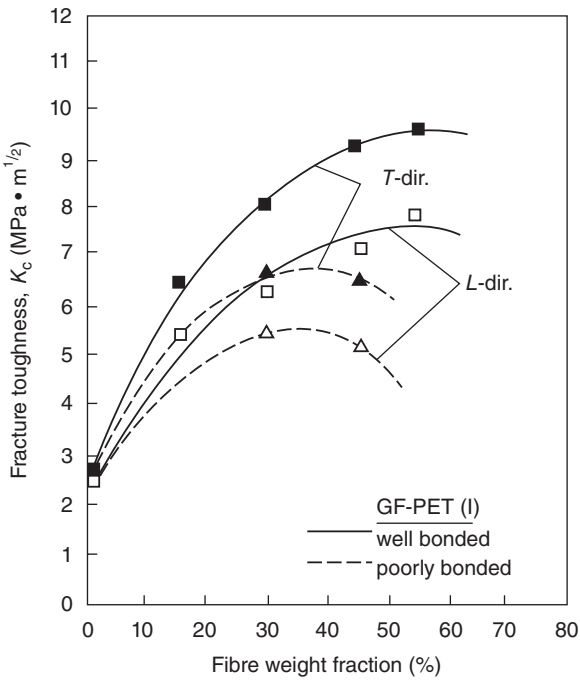

10.7 Fracture toughness K_c *vs* fibre weight fraction as a function of crack direction for GF-PET (I) composites with different fibre–matrix bond qualities. Adapted from Friedrich (1985).

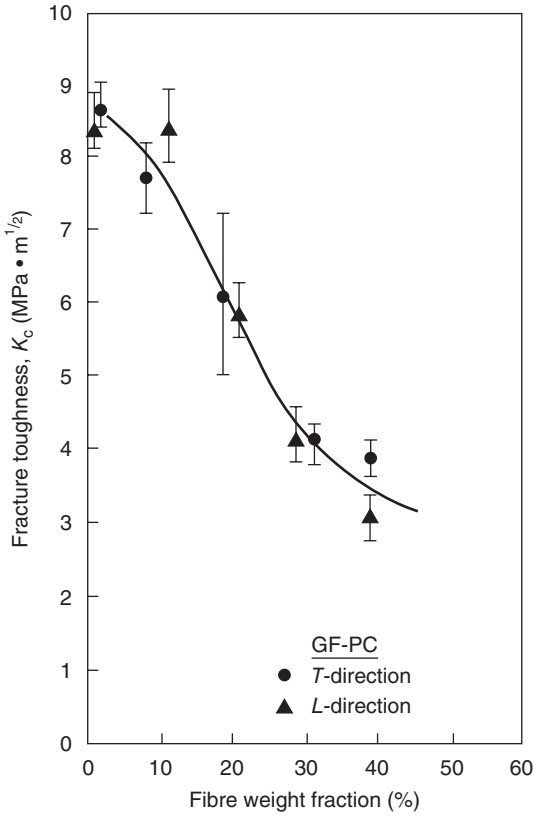

10.8 Fracture toughness, K_c, *vs* fibre weight fraction as a function of crack direction for GF-PC composites. Adapted from Friedrich (1985).

with increasing glass fibre content, whereas the initially more ductile polycarbonate (PC) shows a decrease. An improved bonding quality between the polymer matrix and the fibres results in an increase of fracture toughness tested in both directions, as Fig. 10.7 shows. The decrease of K_c for the PC composite is not so sensitive to the crack propagation direction, indicating that the change in matrix behaviour is prevailing. The reasons for this behaviour will be discussed in detail in Section 10.10.

The influence of crack orientation relative to the mould-fill direction (MFD) for polypropylene reinforced with short glass and short carbon fibres was examined by Fu *et al.* (2002a). For both composites, the fracture toughness for cracks parallel to the MFD remains unchanged while it decreases for the *L*-cracks with the increase of fibre volume fraction, see Fig. 10.9.

In a comprehensive study of fracture of SFRP by Karger-Kocsis (1989) a huge amount of data were collected for different polymer materials and

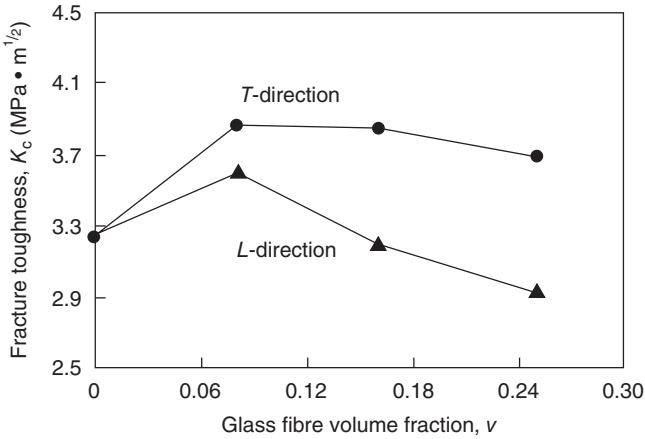

10.9 Fracture toughness, K_c, *vs* fibre volume fraction: (a) short glass fibre reinforced polypropylene, and (b) short carbon fibre reinforced polypropylene. Adapted from Fu *et al.* (2002a).

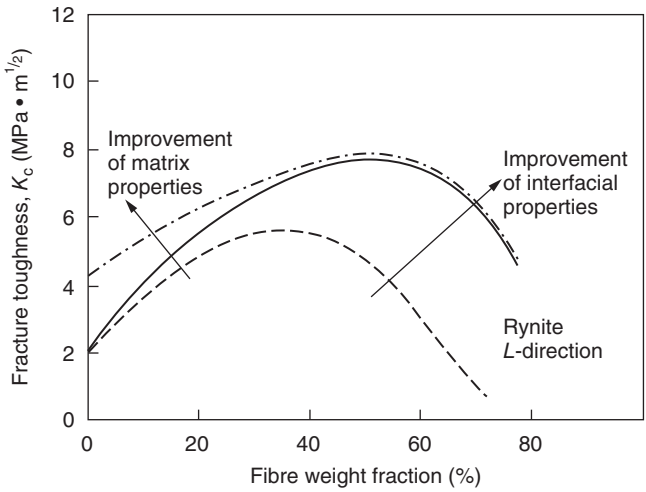

10.10 Effect of matrix and interface properties on fracture toughness K_c as a function of fibre weight fraction for glass fibre reinforced poly(ethyleneterepthalate) (GF-PET). Adapted from Karger-Kocsis (1989).

their composites. As an example, Fig. 10.10 shows the variation of K_c with fibre weight fraction where the matrix material was modified and the fibre–matrix interface properties are improved to enhance fracture toughness.

Another important structural parameter is the aspect ratio (l/d) of the fibres. The increase of K_c with increasing l/d is shown in Fig. 10.11.

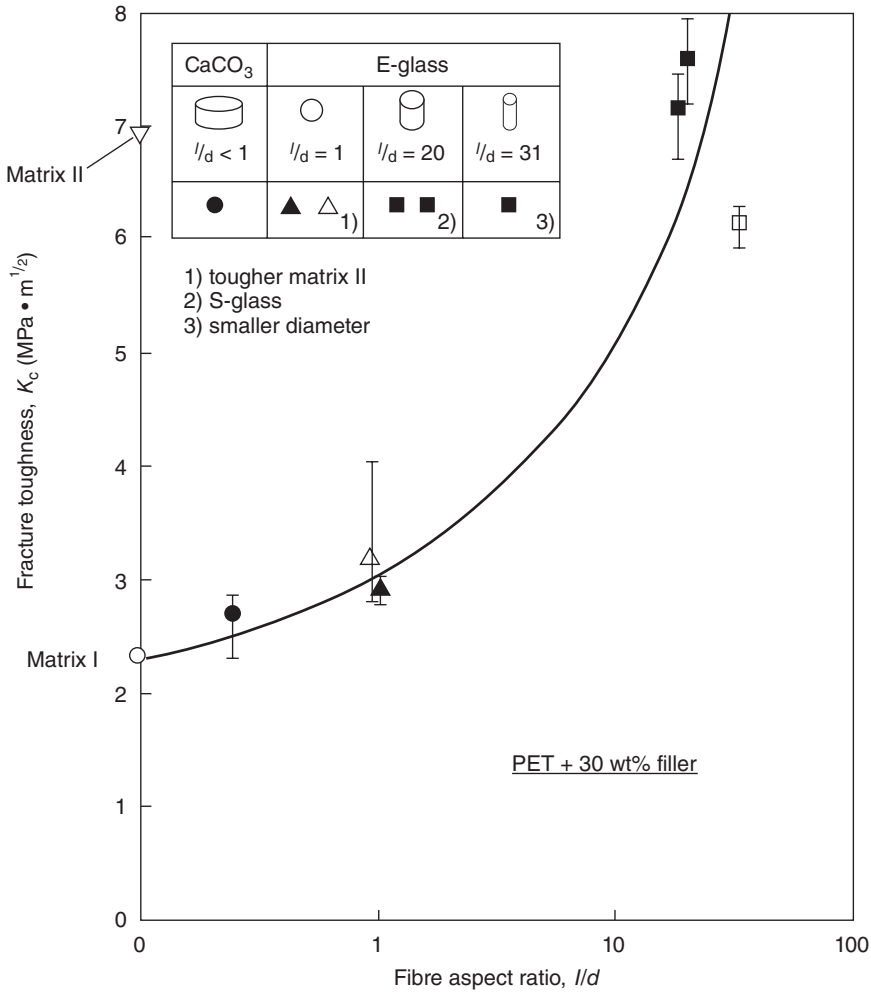

10.11 Fracture toughness, K_c, in dependence on aspect ratio. Adapted from Friedrich (1984).

The determination of the crack initiation point in composites is very often quite difficult; rapid photography is helpful to identify this important point. It improves the determination of the critical load. Using this technique, Akay and O'Regan (1995) found that the 5% offset force F_Q is lower than the load at crack initiation, hence leading to an underestimation of the fracture toughness.

There are also external parameters that need to be considered for the evaluation of toughness, such as the loading rate, environmental conditions and mode of testing.

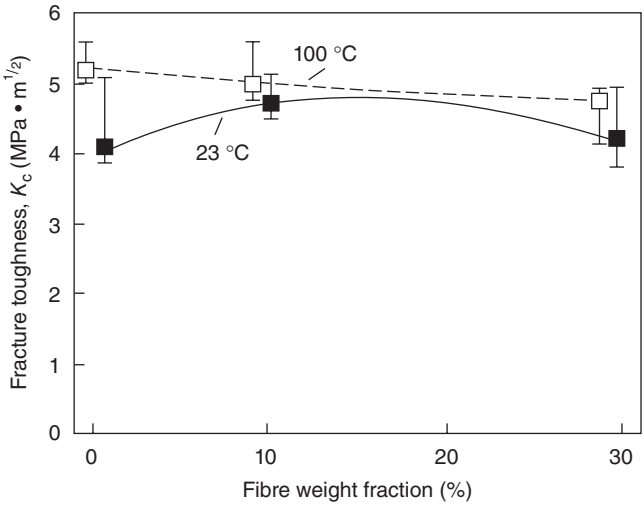

10.12 Fracture toughness, K_c, of glass fibre reinforced PCAE as a function of fibre weight fraction for two different temperatures: 23 °C and 100 °C. Adapted from Choi and Takahashi (1996).

The effect of temperature on fracture toughness was considered by Choi and Takahashi (1996). The variation of K_c with glass fibre weight fraction in thermoplastic poly(cyano aryl-ether) (PCAE) is shown in Fig. 10.12 for two temperatures. The unreinforced matrix material exhibits a higher toughness at 100 °C than at room temperature (23 °C) because of its higher ductility. But it remains almost unchanged at room temperature with increasing fibre weight fraction and decreases slightly at 100 °C.

The influence of moisture on K_c was examined by Ishiaku *et al.* (2005). For glass and carbon fibre reinforced polyamide they observed much higher values for the samples that were exposed to humidity compared to dry material. The influence of water uptake, strain rate and temperature of glass and carbon fibre reinforced polyarylamide owing to hygrothermal ageing was studied by Ishak *et al.* (1998).

The fracture behaviour of polypropylene (PP) composites reinforced with hybrid short glass fibres (GF) and short carbon fibres (SCF) was studied by Fu *et al.* (2002b). An interesting result was that the composite showed a positive hybrid (synergistic) effect. The results of K_c *vs* relative carbon fibre volume fraction ratio, shown in Fig. 10.13, demonstrate the synergism.

New technology of co-injection moulding, which is working with two injection moulding units, was applied by Solomon *et al.* (2005). However, they found that the fracture toughness of such sandwich skin-core hybrids (short glass and carbon fibre reinforced polyamide 6) could not be improved compared to traditional carbon fibre composites.

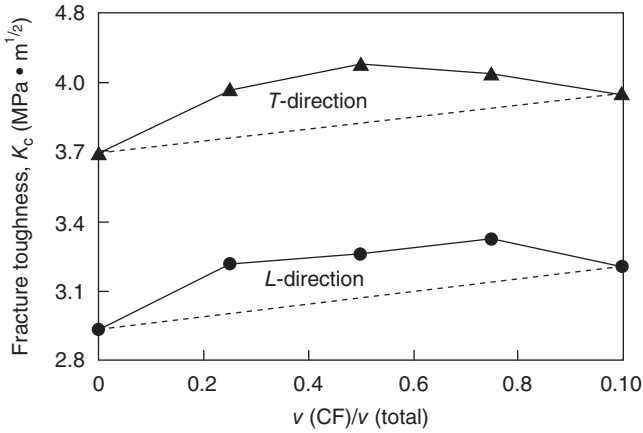

10.13 Fracture toughness, K_c, of PP composites reinforced with glass and carbon fibres *vs* relative carbon fibre volume fraction. Adapted from Fu *et al.* (2002b).

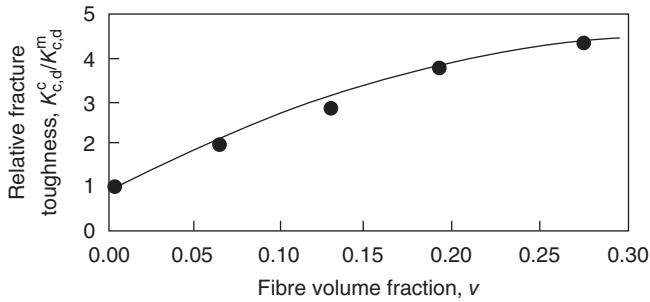

10.14 Fracture toughness, $K_{c.d}$, of short carbon fibre reinforced nylon 6.6 under impact load *vs* fibre volume fraction. Adapted from Ishak and Berry (1993).

Most of the published work on impact fracture properties of reinforced polymers is determined on the basis of the work of fracture, as given in eqn [10.23]. For impact loading it is understandable to use this property as it is difficult to measure the load-displacement curve. A major drawback, however, is that it is not truly a material constant but depends on the specimen geometry. Thus, for certain defined geometry given in the standards for the determination of impact toughness, for example, DIN 53453 and ISO 179-92, it provides a basis to compare materials. The work of fracture calculation and discussion of the results will be given in Section 10.5.

However, with instrumented impact tests, the application of fracture mechanics concepts is possible. For short carbon fibre reinforced nylon 6.6, Ishak and Berry (1993) measured the load-time curve for a falling weight impact tester. One of their results, which were determined on the basis of eqn [10.29], is shown in Fig. 10.14. It reveals an increase of the

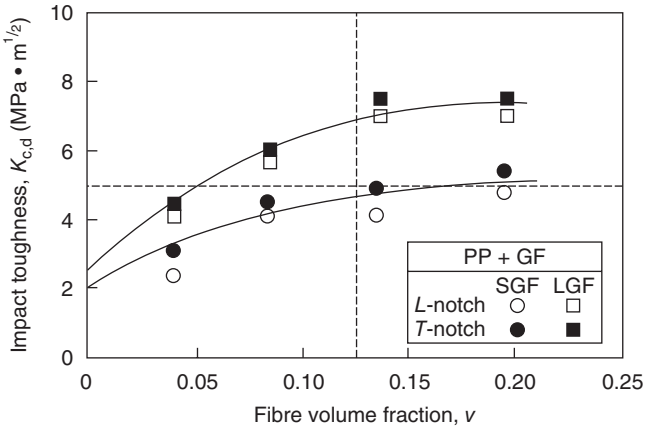

10.15 Variation of impact toughness, $K_{c,d}$, with fibre volume fraction for short glass fibre (SGF) and long glass fibre (LGF) reinforced polypropylene (PP), tested at room temperature. Adapted from Karger-Kocsis (1993).

critical stress intensity factor with increasing carbon fibre content. The same equation was used by Karger-Kocsis (1993) to determine the stress intensity factor, K_d, of Charpy experiments on short fibre reinforced polypropylene. The increase of this property with fibre volume fraction is shown in Fig. 10.15.

The correlation between the total absorbed energy during Charpy impact loading $G_{c,d}$ determined by the instrumented testing equipment to the notched Charpy impact toughness, w, was shown by Karger-Kocsis (1993). Both quantities agree very well with each other, as shown in Fig. 10.16. However, the initiation fracture toughness $G_{c,d}$ (initiation), which was calculated with the energy absorbed until the peak load, is much smaller than this value. However, care must be taken in the interpretation of the measured values.

Since bulk polymers, and their fibre composites, show plastic deformations around the crack tip, this may require the use of non-linear fracture mechanics. The extension of non-linear elastic J-integral, as given in eqn [10.14], to elastic-plastic materials is the most commonly used approximation. For the non-linear elastic case, combination of eqns [10.12] and [10.14] provides:

$$G = -\frac{\mathrm{d}U_{\mathrm{pot}}}{\mathrm{d}A} = -\frac{\mathrm{d}U_{\mathrm{pot}}}{B\mathrm{d}c} = J. \qquad 10.40$$

This relation was extended to the elastic-plastic case by Sumpter and Turner (1976). The total energy is subdivided into an elastic and plastic part:

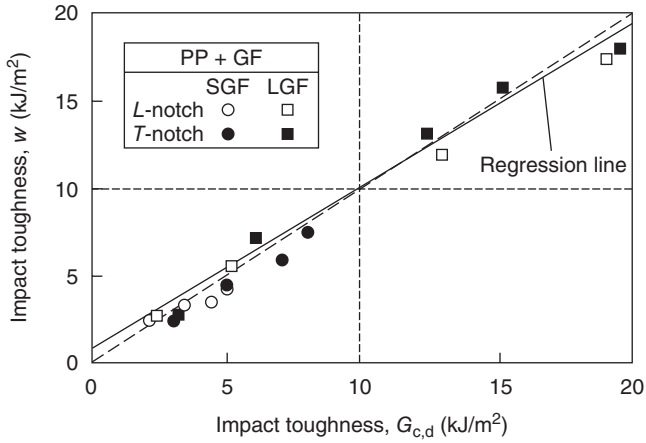

10.16 Correlation between notched Charpy impact toughness and fracture toughness, $G_{c,d}$, for short glass fibre (SGF) and long glass fibre (LGF) reinforced polypropylene (PP), tested at room temperature. Adapted from Karger-Kocsis (1993).

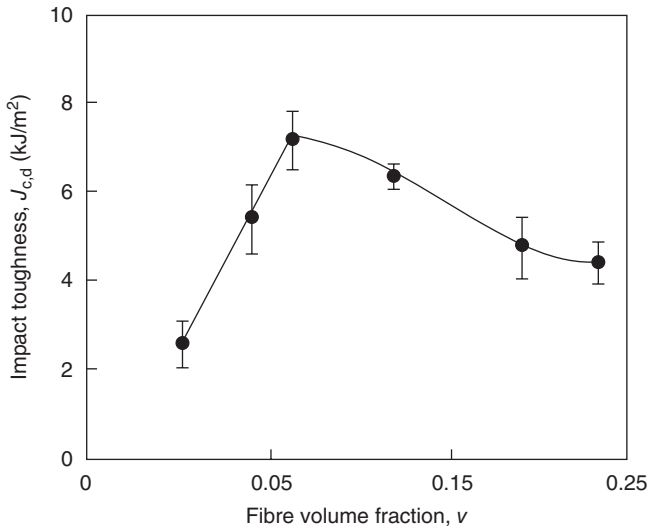

10.17 Impact toughness, $J_{c,d}$, of short carbon fibre reinforced polyamide *vs* fibre volume fraction. Adapted from Langer *et al.* (1996).

$$J = \tilde{\eta}_{el} U_e + \tilde{\eta}_{pl} U_{pl}, \qquad 10.41$$

where the coefficients $\tilde{\eta}_{el}$ and $\tilde{\eta}_{pl}$ depend on specimen and loading geometry, U_e and U_{pl} are elastic and plastic energies under the measured load-displacement curve.

This method was applied by Langer *et al.* (1996) to determine the impact J-integral (instrumented Charpy test) for short carbon fibre reinforced polyamide. The J-integral, characteristic of unstable crack growth, passes a maximum with increasing fibre content, as shown in Fig. 10.17.

The characterisation of fracture toughness of composites is not a simple 'one-number property' but a complex crack growth process characterised by different stages. Hence, the attributes of fracture toughness, such as initiation, propagation, total crack growth and crack arrest, must be specified during testing. The *R*-curve concept that provides the crack resistance for considered crack length can characterise all the above stages of crack propagation. Some explanations of the *R*-curve concept are given in Section 10.10.5.

10.4 Mechanisms of fracture toughness and energy dissipation

The fracture process of fibre reinforced composites is characterised above all by the formation of different kinds of fracture surfaces across the fibres and matrix, and along the interfaces. According to a model developed by Outwater and Murphy (1969) crack growth starts from the fibre ends and spreads along the fibre interface. However, it is also possible that the developing crack grows from the fibre into the matrix (see Curtis *et al.*, 1978; Gurney and Hunt, 1967). This behaviour is characterised by different modes of crack propagation; either the crack causes fracture of the neighbouring fibres, or it surrounds them, or it releases debonding processes far from the main crack.

In any particular composite, the fracture mode is determined above all by the ductility of the matrix and whether the matrix material reacts to the high stress enhancement in front of the crack by brittle fracture or by plastic flow. During crack propagation energy is absorbed by the fractures of fibres and matrix. But a number of other energy dissipation mechanisms have also been proposed, which may act in the composite other than those of the components, viz.

- pull-out of the fibres (Beaumont, 1971; Piggott, 1974);
- mode I debonding remote from the crack tip (Marston *et al.*, 1974);
- mode II debonding after matrix fracture (Gurney and Hunt, 1967; Outwater and Murphy, 1969);
- stress relaxation (Piggott, 1980); and
- friction after debonding (Kelly, 1970; Harris *et al.*, 1975).

For early literature surveys, see, for example, Phillips and Tetelman (1972), Cooper and Piggott (1977), Pompe (1978), Harris (1980), Wells and Beaumont (1985a) and Kim and Mai (1991).

All these failure mechanisms may not operate simultaneously for a given fibre–matrix system, and in some composites one of these toughness contributions may dominate the total fracture toughness of short fibre

composites. Which energy dissipation mechanisms are working for a certain fibre composite depends mainly on the fracture mode of the matrix and fibre length. Some of these contributions do not work for short fibres if the fibres are shorter than a certain critical length, where the necessary fracture stresses cannot be developed.

Harris (1980) and Wells and Beaumont (1985a) gave a survey about failure mechanisms for continuous fibre reinforced composites. They clarified the complex mechanisms of the last three points above, which resulted in the statement that these mechanisms quantify the same energy change, where the differences arise from the assumptions made and the methods of derivation. They summarise the energy dissipation process for fibres of super-critical length (i.e., fibres are long enough to build up a tension stress which can reach the fibre strength, σ_F^u) in three mechanisms: pull-out, surface energy, and one involving changes in the elastic strain energy of fibres. In the above papers and in Wells and Beaumont (1985b), the dissipation energies are determined in a comprehensive manner.

In this section we focus on the theoretical and experimental considerations of toughness of SFRP with fibres of sub-critical lengths; composites with fibres of super-critical lengths are only briefly discussed.

Whether the matrix breaks in a brittle or ductile mode depends essentially on the crack speed and thus also on the loading rate and temperature, respectively. For high loading rates a predominantly brittle matrix fracture mode is observed for short glass fibre reinforced thermoplastics. For static (monotonic) tests, however, most polymer matrices show extensive plastic deformation.

A composite with predominant brittle matrix behaviour is polyamide reinforced by glass fibres (GF/PA). Bader and Collins (1982) observed intense debonding in this material (polyamide-6, containing 10 and 25 vol% glass fibres), whereas the matrix failed in an obvious brittle manner.

Some interesting insight into the initiation and propagation of cracks in a similar material (polyamide-6.6, containing 15 vol% E-glass fibres) was obtained by Sato *et al.* (1983, 1985) by *in-situ* scanning electron microscopic observations of the tensile side of a sample in a bending test. The failure proceeded in three characteristic stages. In the first, separation of the fibre ends from the matrix occurred. The second fracture mechanism was characterised by the appearance of interfacial cracks; in the last stage, bands of microcracks developed within the matrix, joining debonded regions of the neighbouring fibres. This corresponds to the predominantly brittle behaviour of the polyamide matrix (only some limited regions show ductile fracture). Similar results were obtained by Mandell *et al.* (1982), Lhymn and Schultz (1983) and Friedrich (1985, 1989). The failure development in short glass fibre reinforced polyethylene terephthalate (PET) is shown in Fig. 10.18. Typical mechanisms are recognised.

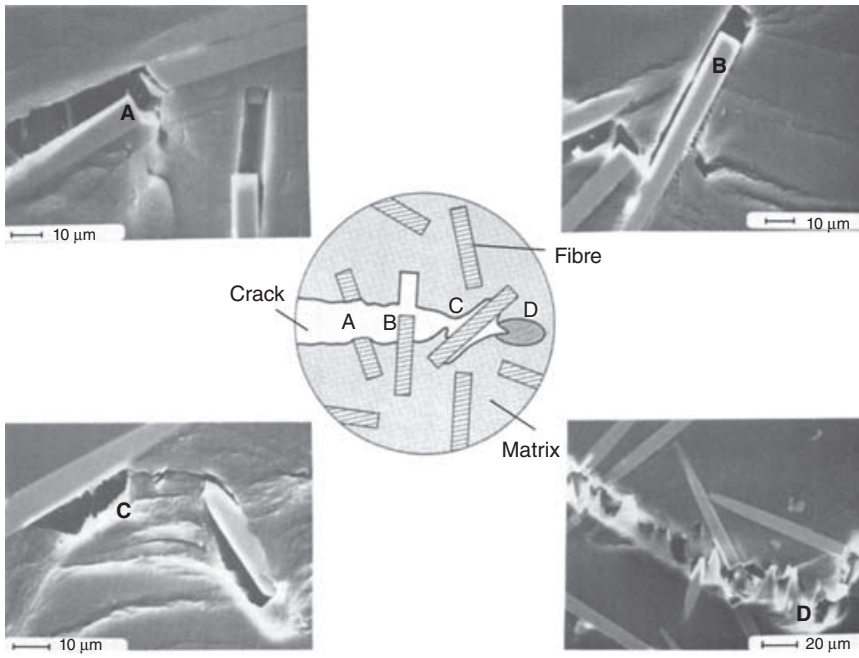

10.18 Typical failure modes in short fibre reinforced polymer, A: fibre fracture, B: fibre pull-out, C: fibre–matrix debonding, D: plastic deformation and fracture of the polymer matrix. Adapted from Friedrich (1989).

Inspection of the cracked surfaces and examinations under *in-situ* conditions reveal that the fracture process is not limited to a crack plane but fracture happens within an extended dissipation zone around the crack tip. For instance, the matrix in glass fibre reinforced (high density) polyethylene shows clear plastic deformation. On the fracture surface (Fig. 10.19) extended matrix tongues (flow regions) can be seen with lengths of the order of the fibre separation, together with clean fibres from which the matrix is completely debonded.

From these observations, we may conclude that the matrix plastic deformation provides a substantial contribution to the fracture work, whereas matrix plasticity and limited interfacial strength restrict the role of fibre pull-out, if it occurs at all. Due to the complex microstructure of the composite, a crack may propagate with different speeds through the cross section, resulting in zones with prevailing brittle or ductile matrix fracture.

Another helpful method to evaluate the failure mechanism of composites is acoustic emission (AE). This method enables the determination of critical stresses responsible for micro fracture initiation via measurements of acoustic signals. Different failure processes release different amounts of

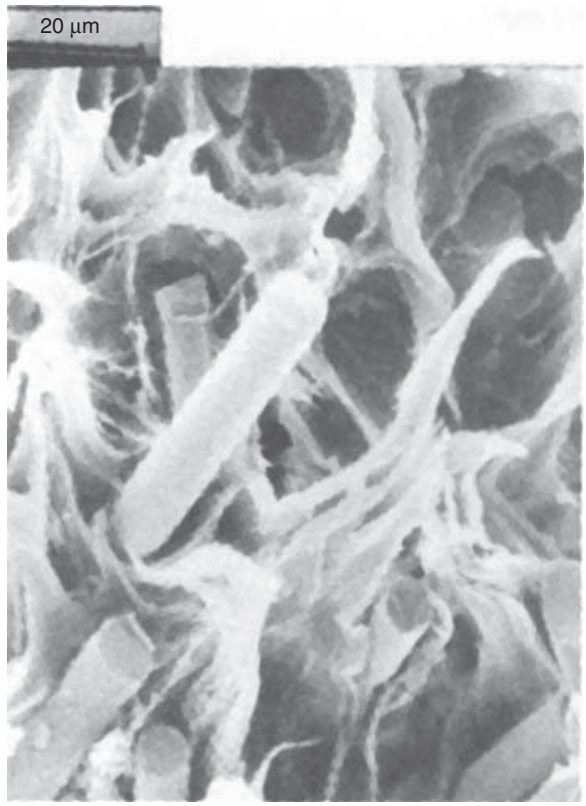

10.19 Fracture surface of high-density polyethylene reinforced with 20 vol% glass fibres; SEM observation. Adapted from Lauke *et al.* (1990).

energy as stress waves, and therefore conclusions concerning such processes are possible. The advantage of this technique to characterise the failure processes of fibre reinforced thermoplastics was proven, for example, by Sato *et al.* (1984) and Leps and Bohse (1985).

On the basis of the above-summarised experimental observations, it is concluded that the relevant failure mechanisms are:

- debonding (mode I and mode II);
- sliding of fibres against matrix within the debonded region;
- pull-out of fibres;
- brittle matrix fracture;
- ductile matrix fracture; and
- brittle or ductile fibre fracture.

As already mentioned, the failure processes will not be limited to the fracture surface but will take place within a certain damage zone in front

of the notch. This has led to an extension of the work of fracture and fracture toughness concepts (see Lauke *et al.*, 1985, 1986a,b, 1990).

To assess the effects of different structural changes on the crack resistance it is necessary to analyse the failure processes near the crack tip in further detail. Thus, it is useful to divide the deformation mechanisms into two groups. The first comprises those mechanisms that are acting directly on the crack surfaces. This zone of material situated immediately near the crack surfaces is called the '*process zone*'. The second is made up of more extended structural damage around the crack path that can also increase the crack resistance. Hence, it is convenient to introduce a second characteristic region, the '*dissipation zone*', whereby any additional components of energy dissipation can be included. The ideas of such an enlarged interaction zone have been introduced in other models by means of a 'damage parameter'.

In the following subsections, the energy dissipation processes are separately discussed for predominantly brittle and ductile matrix fractures.

10.4.1 Brittle matrix fracture

Even if the polymer is not intrinsically brittle, still brittle matrix fracture may be initiated by high loading rates (e.g., impact loading) or at low temperatures.

Dissipation zone

Based on previous examinations, the initial stage of failure is characterised by debonding of the fibre–matrix interface (W_d = debonding energy of one fibre) along the debonding length, l_d, and sliding (W_s = sliding energy of one fibre) along the sliding length, l_s at the fibre end regions.

Process zone

As a consequence of high crack speed, no matrix yielding may be initiated, and hence brittle matrix fracture dominates the failure mode just ahead of the notch tip providing a contribution to the specific process zone energy, q_{pz}. However, there is a second important mechanism, namely, the pull-out of fibres with pull-out energy of one fibre, W_{po}, or the restricted pull-out of one fibre, W_{po}^{Δ}. This restriction means that the fibre is not completely pulled out of the matrix but only over a distance, Δ. In papers concerning the work of fracture, this contribution is related to the crack propagation energy (cf. Miwa *et al.*, 1979). In contrast, however, it is also assumed characteristic for crack initiation and is thus used for fracture toughness calculations (Lhymn and Schultz, 1983). These different approaches are discussed in more detail in Section 10.10.

In agreement with experiments, the energy of totally pulled out fibres describes the main part of the crack propagation energy. This means that when the work of fracture is considered, the energy for a totally pulled out fibre, W_{po}, has to be used. However, when considering the point of crack instability it must be realised that the pull-out length will be restricted to a certain length, Δ, since the crack opening displacement limits the pull-out process; that is, W_{po}^{Δ} should be used.

The energy dissipation processes are shown in Fig. 10.20 for brittle fibre composites. If ductile fibres are used in the composite, their plastic deformation potential must also be considered.

10.4.2 Ductile matrix fracture

If a composite with a ductile polymer matrix at low loading rates is examined we have to distinguish between failure processes for low and high fibre concentrations. As stated above, application of LEFM to composites works

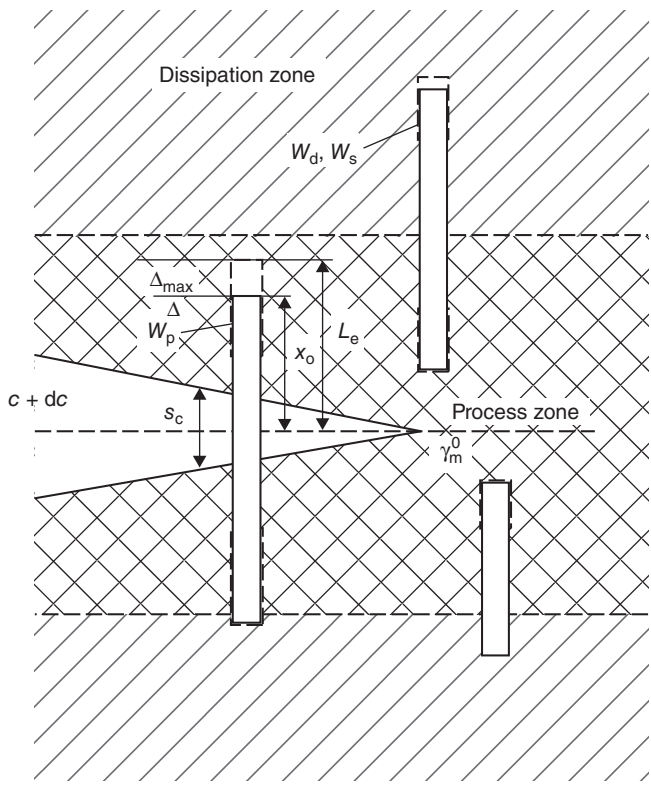

10.20 Failure modes for brittle matrix fracture; dissipation zone: debonding, W_d, sliding, W_s; process zone: brittle matrix fracture, γ_m^0, and pull-out, W_{po}, or restricted pull-out, W_{po}^{Δ}.

only for small-scale damage; however, this condition will be fulfilled only at higher fibre volume fractions because these prevent the macroscopic yielding of the reinforced matrix.

Dissipation zone

The first stages of failure for weak interfaces are the debonding and sliding processes. It is assumed that the critical stresses for initiation of these mechanisms are smaller than the matrix yield stress, the stress distribution is still elastic. A major contribution to the total energy is provided by the subsequent yielding of matrix bridges between the fibres, W_m.

Process zone

Final failure will occur only just ahead of the main crack tip destroying the already yielded matrix bridges. The fracture energy, $\gamma_{m,y}$, of this deformed material is in general smaller than that of the bulk matrix. Although the matrix shows necking, a certain pull-out contribution, pW_{po}, or, pW_{po}^{Δ}, respectively, with ($p < 1$), is expected. The factor p is used to account for a reduced fraction of fibres being pulled out. These processes are shown in Fig. 10.21.

The energy dissipation mechanisms operating in the dissipation and process zones are summarised in Table 10.1 for brittle and ductile matrix fracture conditions.

Another group of short fibre reinforced composites are those materials with discontinuous long fibres, which can be processed by the pultrusion technique. Such composites range between the two extremes of short fibre and continuous fibre composites. A possible fracture mode of such composites is given in Fig. 10.22(a). A major difference to the failure mode of short fibre reinforced composites is that not all the fibres are pulled out, but only those whose ends are lying at a distance relative to the crack plane which is shorter than the critical fibre length, l_c. The debonding (mode II) and sliding processes are initiated in all fibres within the dissipation zone.

As already mentioned, the mechanisms acting in continuous fibre reinforced materials are summarised by Wells and Beaumont (1985a). They are only typical for such fibres whose ends are far enough away from the crack surface, as may be the case for discontinuous long fibres. That is, only for such fibres can mode I debonding in front of the notch and fibre fracture be initiated.

If relatively ductile thermoplastics are considered under static loading, the toughness contribution by plastic deformation of the matrix bridges must be included (see Fig. 10.22(b)). The pull-out contribution is reduced in analogy to the short fibre case because of the necking of matrix bridges.

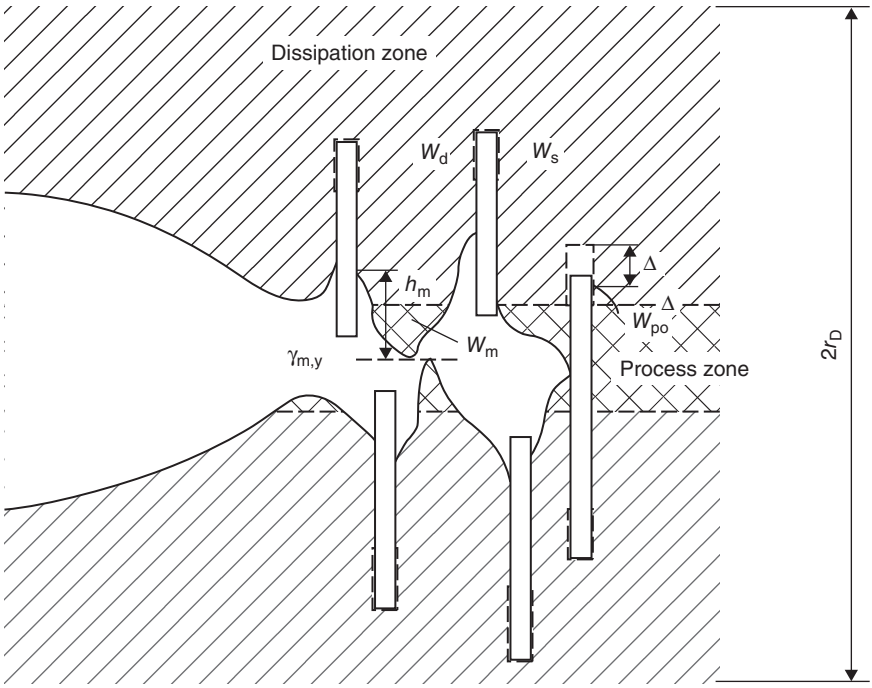

10.21 Failure modes for ductile matrix fracture; dissipation zone: debonding, W_d, sliding, W_s, plastic deformation of matrix bridges, W_m; process zone: pull-out, W_{po}, restricted pull-out, W_{po}^{Δ}; fracture of deformed matrix, $\gamma_{m,y}$.

Table 10.1 Energy absorption mechanisms in process zone and dissipation zone for brittle and ductile matrices

	Energy absorption mechanisms for	
	Brittle matrix fracture	Ductile matrix fracture
Dissipation zone	Debonding, W_d; Sliding, W_s	Debonding, W_d; Sliding, W_s; Plastic deformation of matrix bridges, W_m
Process zone	Pull-out, W_{po} and restricted pull-out, W_{po}^{Δ}; Brittle fracture of matrix bridges, γ_m^0	Reduced pull-out energy, pW_{po} or pW_{po}^{Δ} respectively, $p < 1$; Fracture of ductile matrix bridges, $\gamma_{m,y}$

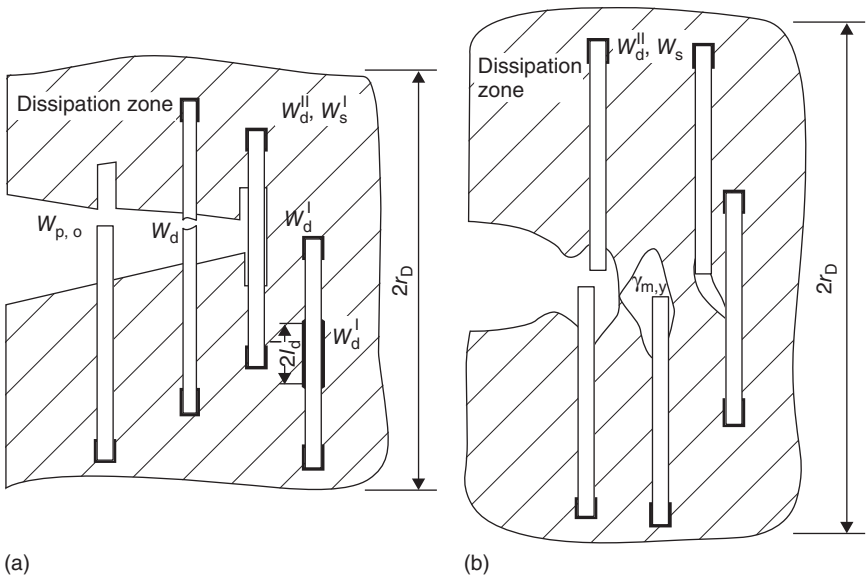

10.22 Failure modes for discontinuous long fibre reinforced composites: (a) brittle matrix; and (b) ductile matrix. Adapted from Lauke *et al.* (1990).

10.5 Work of fracture of notched specimens

The characterisation of fracture toughness of composite materials is of importance for many applications. A common and approved measure is the work of fracture, the work required for driving the crack through the whole sample. It averages the various contributions from the separate components, thus considering the finite process of crack propagation, necessary for characterisation of heterogeneous materials, instead of infinitesimal steps.

The measured work of fracture differs for impact and static loading conditions, not only quantitatively but often also in its qualitative behaviour.

The impact toughness increases at first with fibre volume fraction and then becomes stationary or even decreases (see Fig. 10.23). This refers to additional energy dissipation by fibre–matrix interactions (e.g., debonding and sliding of interfaces), which are very effective at low fibre contents but become successively restricted by increasing constraints at higher concentrations of reinforcing fibres.

In contrast to these general trends observed under impact testing, the work of fracture measured under static conditions depends strongly on the intrinsic ductility of the matrix material.

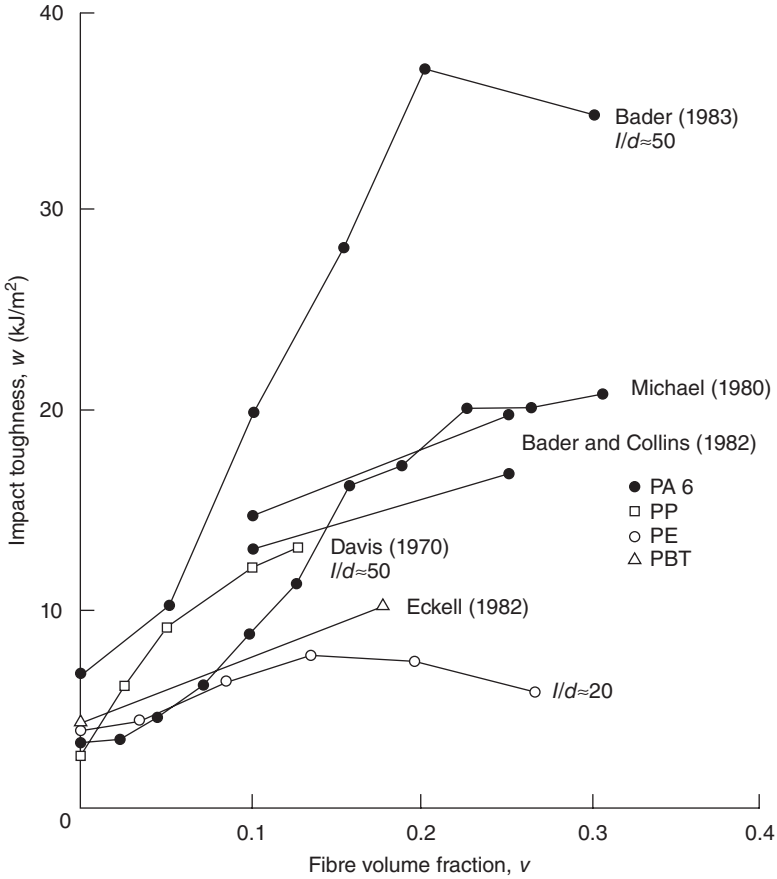

10.23 Impact toughness of different reinforced thermoplastics as a function of fibre volume fraction.

For relatively brittle materials, such as epoxy resins, ceramics and concretes, the static work of fracture increases with fibre fraction (see for example, Gershon and Marom, 1975; Mai, 1979) as in the impact case. However, in composites with tougher matrices the fracture work is decreased by the addition of short fibres. This is caused by the high deformability of the ductile matrix at low loading rates, which is restricted by the stiffer fibres.

The different behaviour is also reflected by the fracture toughness (cf. Figs 10.7 and 10.8). Thus, differences in static and impact fracture work behaviour correspond to the tough–brittle transition of the matrix with increasing loading rates. Hence, by neglecting inertial effects, the impact case can be approximated by static calculations by using modified matrix properties.

For this purpose the energy dissipation mechanisms must be checked due to the changing nature of the fracture process, considering the varying matrix deformability. A number of such mechanisms have been proposed in Chapter 9. But the usual methods of calculating these effects and summarising various relevant contributions into a total work of fracture are lacking in that they do not account for the fact that the dependence on fibre fraction may change in a complex manner as discussed above. The energies dissipated by the fibre–matrix interactions are proportional to the number of fibres involved and the length over which the energy dissipation proceeds, that is, pull-out length, debonding length, or sliding length. In many models, it is assumed that only those fibres, which cross the crack plane, contribute to energy consumption. Hence, the specific number, n_0, of active fibres is linear to the fibre volume fraction, v. For composites with fibres longer than the critical fibre length, l_c, which is the case most frequently assumed, the characteristic lengths for intense interfacial processes are proportional to the critical length, l_c. Thus, they become independent of fibre content, and the respective energy expressions increase linearly with volume fraction. These interaction terms are superimposed on the contributions of fibres and matrix. The energy dissipation due to fibre breaks can often be neglected by virtue of their brittleness. That of the matrix is usually assumed proportional to the matrix volume fraction, $v_m = (1 - v)$, thus again leading to a linear variation with fibre content, but now in the reverse direction.

In the following, it is intended to overcome this unsatisfactory situation by using a modified model. The proposed corrections concern the number of active fibres (not only fibres crossing the main crack plane are considered) and their dissipation lengths are considered as functions of structural parameters and applied load.

Starting from scanning electron microscope (SEM) observations of the fracture surface it is assumed that all fibres lying within a certain damage zone around the crack tip contribute to energy dissipation, with the dimensions of this zone depending on fibre spacing. Furthermore, experimental determinations of debonding and sliding lengths show an essential variation instead of a constant value. By inserting these experimental lengths into the respective energy expressions results in a non-linear dependence on fibre content (see Beaumont and Anstice, 1980).

In Section 9.2.2, different dissipation lengths (for debonding and sliding) are calculated as functions of composite material parameters. They represent a rational base for calculating the energy dissipation of a characteristic structural element consisting of a fibre end and the surrounding matrix bridge.

Additionally, an attempt is made below to explain theoretically the impact toughness of un-notched short fibre reinforced thermoplastics.

Although this fracture energy does not describe the toughness in the sense of fracture mechanics it is very often used to characterise the fracture behaviour of composites under impact loading.

The unnotched impact toughness of several short glass fibre reinforced thermoplastics shows a wide spectrum of variations (see Fig. 10.24). Reasons for these variations may be found in the diverging ductility of matrix materials, different fibre length and properties of the fibre/matrix interface.

The low unnotched impact toughness of brittle thermoplastics, for example, polymethyl-methacrylate (PMMA) is not affected by addition of reinforcing fibres (cf. Ramsteiner and Theysohn, 1979). However, that value of relatively ductile thermoplastics such as PE or PA is much more complex. Measurements of impact toughness of the bulk material show no fracture but the incorporation of only a few fibres leads to a drastic embrittlement. These changes are much stronger compared to the notched case. The main reason is because the impact toughness of un-notched materials is a superposition of energy to

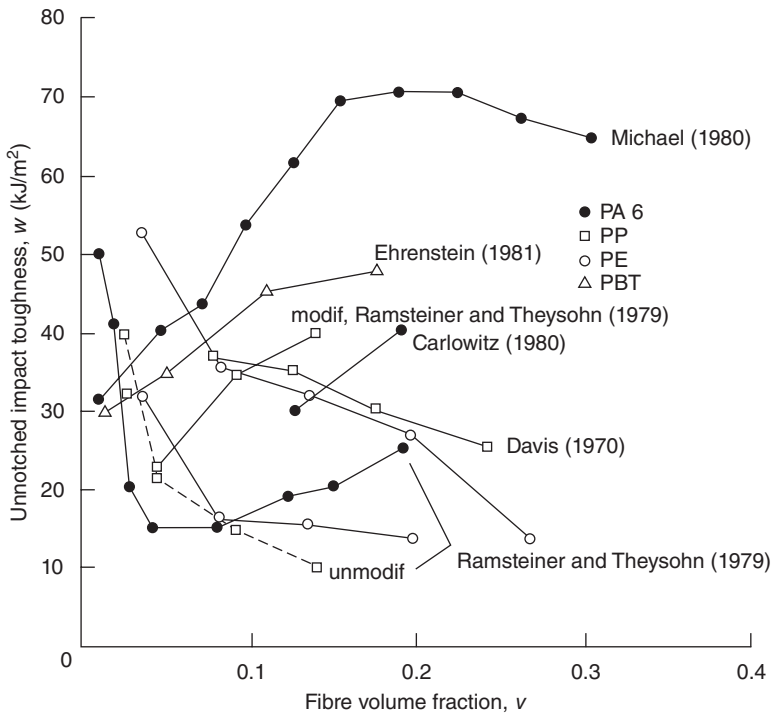

10.24 Un-notched impact toughness of different reinforced thermoplastics as a function of fibre volume fraction.

crack formation and crack propagation (that is, the work of fracture as discussed above).

10.5.1 General concept

Due to the heterogeneous nature of composite materials, several fracture modes are activated during crack propagation, which contribute to the fracture energy in their own particular way. These are contributions, w_j, of different components, $j = fi$ (fibre), m (matrix), and interaction terms, w_{fm}^{i}, corresponding to mechanism i of interface failure between fibre (f) and matrix (m). Therefore, for the transverse rupture of a unidirectionally reinforced fibre composite, the specific work of fracture, w, of the composite is given by:

$$w = w_{fi} + w_m + \sum_i w_{fm}^{(i)} = w_{fi} + w_m + \sum_i w_i . \tag{10.42}$$

Herein, the values are normalised to the fracture plane, that is, the specimen cross-sectional area in front of the pre-notch – the ligament. For simplicity, we omit the subscript (f, m) and replace $w_{fm}^{(i)}$ by w_i with the index i describing the different active dissipation mechanisms.

The terms of the specific work of fracture can be calculated by multiplying the number of active fibres n per unit area of crack plane N_A by the corresponding energy W_i:

$$w_i = nW_i \text{ and } w_{fi} = nW_{fi}. \tag{10.43}$$

There are two approaches to calculate the specific number n. If it is assumed that only such fibres crossing the crack plane are contributing to all energy dissipation processes, then it is given by:

$$n = \frac{N_A}{A} = \frac{v}{\pi r_f^2} = n_0, \tag{10.44}$$

where the definition of the fibre volume fraction in a cross section of the specimen has been used.

However, as already discussed above, this simple approach is inadequate for short fibre composites. Because of the high density of potential flaw centres, namely the fibre ends, some energy-dissipating processes such as interface failure and localised matrix necking may occur in a region around the crack tip. It is clear that a concept of a sharp boundary is a crude simplification for the continuously diminishing damage distribution, but it may serve as a first approximation. It corresponds to a critical distance r_D from the main crack, where the stresses are just sufficient to activate essential interface failure, as shown in Figs 10.20 to 10.22.

The number n of active fibres in that volume per unit fracture area is given by:

$$n = \frac{N_V}{A} = 2r_D \cdot \frac{v}{\pi r_f^2 l} = 2r_D \cdot \tilde{n}, \tag{10.45}$$

where the definition of the fibre volume fraction in a volume of the specimen has been used. Consequently, the specific energies of [10.43] can be written as:

$$w_i = nW_i = 2r_D \tilde{n} W_i = 2r_D \eta_i, \tag{10.46}$$

where η_i is the volume specific dissipation energy of the i-th process. The width, $2r_D$, of the dissipation zone depends on specimen and notch geometry and on the special load conditions. A reduction of notch depth delocalises the damage and thus increases the dissipated energy.

For composites with a small macroscopic damage region in comparison to the crack length and the sample dimensions, the width of the dissipation zone can be estimated by consideration of the stress field in front of the notch (crack). The local stress perpendicular to the crack plane is given by eqn [10.2] as $\sigma \sim K \cdot r^{-1/2}$, that is, in a maximum distance r_D, the debonding stress, σ_c^d, is just reached: $\sigma_c^d \sim K \cdot r_D^{-1/2}$. Conversely, at the neighbour fibre, a distance $D = d\sqrt{(1-v)/v}$ away, the fibre strength, σ_F^u, is reached: $\sigma_F^u \sim K \cdot D^{-1/2}$. Combining these two expressions results in the following approximate value for r_D given by:

$$r_D = d\left[(1-r)/r\right]^{1/2} \left(\frac{\sigma_F^u}{\sigma_c^d}\right)^2.$$

Now, it is emphasised that fibre fracture and fibre pull-out processes are only possible for fibres that cross the crack plane and consequently the specific number of contributing fibres is $n = n_0$. Also, the matrix may show brittle behaviour, w_m^0, in one part of the whole crack growth process and ductile fracture in another part (maybe caused by a reduction of crack speed), $w_{m,y} = 2r_D\eta_m$. The fraction of the brittle part of the crack plane is designated by α. Thus, the matrix contribution becomes:

$$w_m = \alpha w_m^0 \quad \text{for brittle matrix fracture} \tag{10.47a}$$

$$= (1-\alpha) w_{m,y} = (1-\alpha) n W_m = (1-\alpha) 2r_D \eta_m \quad \text{for ductile matrix frature.} \tag{10.47b}$$

Hence, finally, by inserting all these expressions in eqn [10.42], the work of fracture in a fibre reinforced composite is obtained. That is,

$$w = n_0 W_{fi} + n_0 W_{po} + \alpha w_m^0 + 2r_D \left((1-\alpha)\eta_m + \sum_i \eta_i \right) \quad \text{with} \quad i = d, s. \tag{10.48}$$

The different models discussed in the literature can be incorporated into this scheme by definition of the parameters and energies, respectively, by reduction of this equation that considers the energy consumption within a dissipation zone to energy dissipated only on the crack plane.

10.5.2 Dissipation energies for unidirectional short fibre reinforced composites

An important parameter that determines what kind of energy values must be used is the fibre length relative to the critical fibre length. The first term in eqn [10.48] only contributes to the fracture work if the fibres are long enough to break, i.e., the fibres must be longer than the critical fibre length, l_c. However, if the fibres are brittle (e.g., glass fibres), this contribution is orders of magnitude lower than other contributions. And if the fibres of super-critical lengths ($l > l_c$) do not break in a brittle manner, only a fraction $(1 - l_c/l)$ of the fibres crossing the crack plane can break (Piggott, 1980). If so, the energy of fibre fracture, W_{fi}, is given by:

$$W_{fi} = \pi r_f^2 \cdot 2\gamma_{fi}, \tag{10.49}$$

where the factor two considers the fact that there are two surfaces after fracture with γ_f as the specific fracture surface energy of the fibre material. This leads to:

$$w_f = 0 \qquad \text{for} \quad l \le l_c, \tag{10.50a}$$

$$= 2\gamma_{fi} v(1 - l_c/l) \qquad \text{for} \quad l \ge l_c. \tag{10.50b}$$

For ductile fibres their surface energy, γ_{fi}, may be replaced by the plastic deformation energy per volume ($\omega_{fi} = \int \sigma_{fi} d\varepsilon_{fi}$) multiplied by the length of the plastic flow region, as will be discussed below for the matrix.

In the following we focus on short fibre composites with fibre lengths, $l \le l_c$. Then, no fibre fails, the lengths being too small to build up a sufficiently high tensile stress, σ_F^u, within the fibres via the interface shear stress, τ, which is restricted by matrix yielding and boundary sliding. This means that $W_{fi} = 0$. The cases of composites with continuous and long discontinuous fibres ($l \ge l_c$) were discussed comprehensively by Beaumont and Harris (1972) and Wells and Beaumont (1985a,b) and have been reviewed by Lauke *et al.* (1990) and Kim and Mai (1991).

According to experimental findings summarised in Chapter 9, the following scheme of the dominating fracture process would be expected. For a small applied stress, σ_c, below a critical value, σ_c^d, ideal bonding exists along the fibre–matrix interface. With increasing load the shear stress, τ, at the interface is also increased until debonding starts at $\tau = \tau_d$. Here, debonding means rupture of atomic bonds and displacements of atomic order, but it

must not result in macroscopic displacements at the interface. Thus, debonding provides a contribution to the fracture energy but does not necessarily change the stress field.

As a result of friction and adhesion, sliding at the broken interface may be inhibited until a higher stress, σ_c^s, is achieved. Then, by initiation of the sliding processes, that part of the external load which is transmitted to the fibres is diminished, and the load sharing between matrix and fibre will be changed. In the slipped regions the matrix is not restrained by the stiff fibres; it is thus carrying a larger part of the load and is capable of larger deformations.

In accordance with this scheme, several energy dissipation mechanisms are activated progressing from the first flaw at the interface to the fully developed crack surface, viz., debonding energy, w_d, and sliding energy, w_s, at the interface and plastic work, w_m, in the matrix. A schematic illustration of this fracture process is given in Fig. 10.25. The debonding and sliding processes were theoretically investigated in detail in Section 9.2.2.

The quantities necessary for the work of fracture calculations are given by: debonding stress in eqn [9.4], debonding and sliding lengths in eqns [9.5] and [9.6], respectively. The debonding and sliding stresses are restricted by the condition that no extended matrix flow occurs at the crack tip such that:

$$\sigma_c < \sigma_c^{max} \quad \text{with} \quad \sigma_c^{max} = (1-\nu)(1+\pi/2)\sigma_{M,y}. \qquad 10.51$$

At larger composite stresses, $\sigma_c > \sigma_c^{max}$, interface debonding and sliding cannot continue because of the plastic relaxation of the matrix.

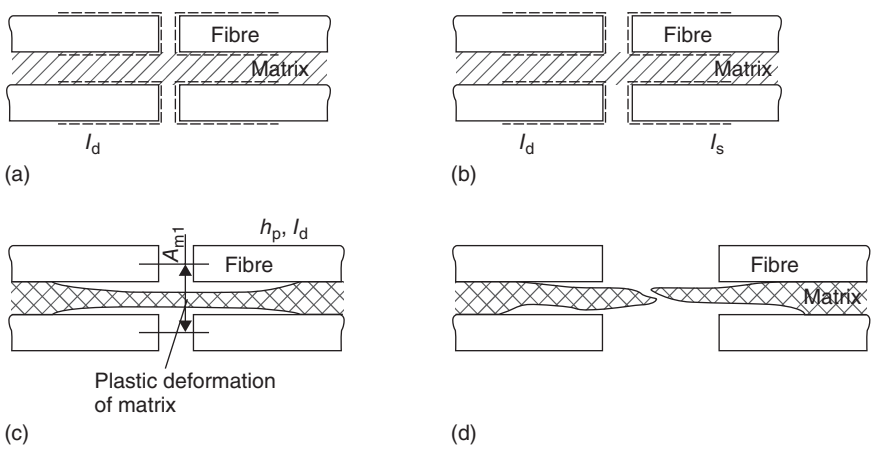

10.25 Fracture modes: (a) debonding; (b) sliding; (c) stable plastic flow of matrix, and (d) fractured matrix.

For brittle matrix fracture the surface energy of the matrix is the characteristic parameter that determines the contribution to the total work of fracture:

$$w_{\mathrm{m}}^{0} = (1-v)2\gamma_{\mathrm{m}}^{0}. \qquad 10.52$$

In case of ductile matrix fracture the following expressions are true, as derived in Lauke *et al.* (1985). At sufficiently high fibre volume fractions, $v > v_{\mathrm{c}}$, macroscopic plasticity is suppressed and intense plastic flow occurs at the debonded and slipped fibre ends within the damage zone only. However, for lower fibre volume fractions, $v < v_{\mathrm{c}}$, an extended plastic zone develops, depending on testing conditions. For small notch depths, it approaches the order of specimen width according to the final failure, by macroscopic necking in this case.

The critical fibre volume fraction can be determined approximately by the condition that extended plastic flow starts when the distance, $D = d((1 - v)/v)^{1/2}$, between the neighbouring fibres is equal to the fibre length:

$$v_{\mathrm{c}} = \left(1+(l/d)^{2}\right)^{1/2}. \qquad 10.53$$

One plastically deformed volume, see Fig. 10.25(c), is given by: $V_{\mathrm{p1}} = 2h_{\mathrm{p}}A_{\mathrm{m1}}$. With the fibre volume fraction definition, the cross section of one element is: $A_{\mathrm{m1}} = \pi r_{\mathrm{f}}^{2}(1 - v)/v$, thus leading to:

$$W_{\mathrm{m}} = \omega_{\mathrm{m}} \cdot 2h_{\mathrm{p}} \cdot A_{\mathrm{m1}} = \omega_{\mathrm{m}} \cdot 2h_{\mathrm{p}} \cdot \pi r_{\mathrm{f}}^{2}(1-v)/v, \qquad 10.54$$

where ω_{m} is plastic fracture work per unit volume which can be expressed by the true matrix stress, σ_{M} (force normalised by the actual cross section), and strain, ε_{M} (for example, Hencky strain), below:

$$\omega_{\mathrm{m}} = \int_{0}^{\varepsilon_{\mathrm{M}}^{\mathrm{u}}} \sigma_{\mathrm{M}}\,\mathrm{d}\varepsilon_{\mathrm{M}}. \qquad 10.55$$

Assuming the length of the plastically deformed region is equal to the debonding lengths: $h_{\mathrm{p}} = l_{\mathrm{d}}$ and definition of volume specific matrix energy, η_{m} within the dissipation zone, we obtain:

$$\eta_{\mathrm{m}} = \tilde{n} W_{\mathrm{m}} = \omega_{\mathrm{m}} 2l_{\mathrm{d}}(1-v)/l \quad \text{for} \quad v > v_{\mathrm{c}}. \qquad 10.56$$

For fibre volume fractions lower than the critical value, the matrix shows large-scale yielding that is hindered only by the fibres in the neighbourhood. Thus, their fracture energy should be lower than that of the bulk matrix material and is designated as: $\gamma_{\mathrm{m,y}}$. Consequently, the matrix contribution to the total fracture energy can be expressed by:

$$w_{\mathrm{m,y}} = 2(1-v)\gamma_{\mathrm{m,y}} \quad \text{for} \quad v \le v_{\mathrm{c}} \qquad 10.57a$$

$$= 2r_{\mathrm{D}} \cdot \omega_{\mathrm{m}} \cdot 2l_{\mathrm{d}}(1-v)/l \quad \text{for} \quad v \ge v_{\mathrm{c}}. \qquad 10.57b$$

The critical fibre volume fraction v_c corresponds to spreading of the zone $2r_D$ of intensive plastic flow over the order of the necking length, $2h_p \approx 2l_d$. With $l_d = l/2$ in this case and $\gamma_{m,y} = \omega_m l_d$, the two energy expressions become identical.

For a brittle matrix the fracture surface propagates perpendicular to the macroscopic tensile stress, thus leading to pull-out of fibres which cross the fracture plane. The energy contribution of the pull-out of fibres of length l crossing the crack plane can be calculated by the integration of the product of force $\pi d\tau_p$ and distance x for an embedded length L_e and subsequent consideration that the embedded length lies between $0 \le L_e \le l/2$. Thus,

$$W_{po} = \pi d l^2 \tau_p / 24, \tag{10.58}$$

where τ_p is shear stress during pull-out of the fibre from matrix. Multiplying by the specific number n_0 of eqn [10.44] provides the well-known expression:

$$w_{po} = \frac{v l^2 \tau_p}{6d} \quad \text{for} \quad l \le l_c. \tag{10.59}$$

For fibres with $l \ge l_c$ a modified expression is obtained. If homogeneous fibre strength is assumed, the pull-out energy is obtained by the above equation where we have to treat the pull-out length as varying between zero and half the critical fibre length $l_c/2$. Further, the number of contributing fibres will be reduced by the fraction l_c/l because fibres with embedded length greater than $l_c/2$ will break at the matrix fracture surface. Thus, eqn [10.59] yields:

$$w_{po} = \frac{v l_c^2 \tau_p}{6d} \cdot \frac{l_c}{l} = \frac{v l_c^3 \tau_p}{6dl} \quad \text{for} \quad l \ge l_c. \tag{10.60}$$

The debonding energy of a single fibre, as shown in Fig. 10.25(a), can be easily obtained by:

$$W_d = \pi d \cdot 2 l_d \cdot 2\gamma_d^{II}, \tag{10.61}$$

where the first '2' is for both fibre ends and the second '2' for two newly created surfaces after debonding between fibre and matrix. Multiplying this energy of one fibre with number n, eqn [10.45], of debonded fibres within the dissipation zone provides:

$$w_d = 2r_D \cdot \frac{4v\gamma_d^{II} l_d}{dl}. \tag{10.62}$$

This is a lower bound for debonding energy dissipation because there may be an additional mode I debonding process directly in front of the notch, as sketched in Fig. 10.22(a), which is especially pronounced for discontinuous long fibres. This energy is given analogously to eqn [10.61]

replacing the mode II debonding length and energy by the mode I values:

$$W_{\mathrm{d}} = \pi d \cdot 2 l_{\mathrm{d}}^{\mathrm{I}} \cdot 2 \gamma_{\mathrm{d}}^{\mathrm{I}}. \tag{10.63}$$

Different to the mode II debonding process, mode I debonding is only caused by high stresses normal to the interface that act mainly in the process zone, which is why this energy must be multiplied by n_0:

$$w_{\mathrm{d}}^{\mathrm{I}} = \frac{v}{\pi r_{\mathrm{f}}^2} \cdot \pi d \cdot 2 l_{\mathrm{d}}^{\mathrm{I}} \cdot 2 \gamma_{\mathrm{d}}^{\mathrm{I}} = 16 v l_{\mathrm{d}}^{\mathrm{I}} \gamma_{\mathrm{d}}^{\mathrm{I}} / d. \tag{10.64}$$

Whether or not this is an important contribution to the total work of fracture depends on the debonding energy in mode I loading and on the debonding length. An upper bound for the debonding length $l_{\mathrm{d}}^{\mathrm{I}}$ would be achieved by assuming that the fibres crossing the crack plane debond over their length l. But this has never been observed experimentally; this would mean that there is no debonding process of fibres afterwards. More realistic is to consider the lower bound, which is given by debonding length of about a fibre diameter providing: $w_{\mathrm{d}}^{\mathrm{I}} = 16 v \gamma_{\mathrm{d}}^{\mathrm{I}}$. For usually low values of the fracture surface energy in the range of about 10 to 100 J/m^2 this energy contribution can be neglected.

For mode II debonding given by eqn [10.62], this contribution, however, should not be neglected because for most material combinations the mode II debonding energy $\gamma_{\mathrm{d}}^{\mathrm{II}}$ is much higher than the mode I value and this process takes place within the whole dissipation zone and is not limited to the process zone around the crack tip.

As the last contribution that enters in the general eqn [10.48], the sliding energy within the dissipation process must be considered. The work W_{s} dissipated during sliding in the region $l_{\mathrm{s}} = l/2 - g_{\mathrm{s}}$ (see eqn [9.5]) on both ends of a fibre is given by:

$$W_{\mathrm{s}} = 2\pi d \int_{\sigma_{\mathrm{c}}^{\mathrm{s}}}^{\sigma_{\mathrm{c}}^{\max}} \mathrm{d}\sigma_c \int_{g_{\mathrm{s}}}^{l/2} \mathrm{d}z \tau \frac{\mathrm{d}\Delta u}{\mathrm{d}\sigma_{\mathrm{c}}}. \tag{10.65}$$

Herein the maximum composite stress, $\sigma_{\mathrm{c}}^{\max}$ is given in eqn [10.51] and the difference of the displacement, Δu, at the interface is obtained by inserting the stress field in the debonded region into differential eqn [4.9] and subsequent integration. The derivation and dependence of Δu and W_{s} on material parameters are given by Lauke *et al.* (1985). This extended expression can be replaced by an approximation as proposed in Lauke and Pompe (1986).

It is assumed that the sliding force, F_{s}, is constant along the sliding length, l_{s}, thus: $F_{\mathrm{s}} = \pi d \overline{\tau}^{(\mathrm{s})} l_{\mathrm{s}}$ with $\overline{\tau}^{(\mathrm{s})}$ as the mean sliding stress according to eqn [9.5] in the sliding zone l_{s}. Furthermore, it was assumed that the discontinuity of fibre matrix displacement, Δu, is given by: $\Delta u \approx \Delta \varepsilon \cdot l_{\mathrm{s}}$ with $\Delta \varepsilon$ as the

difference in the ultimate deformation of the matrix, ε_M^u, and the fibres, ε_F^u ($\Delta\varepsilon = \varepsilon_M^u - \varepsilon_F^u$). Thus, the sliding work is obtained as:

$$W_s = 2\pi d\bar{\tau}^{(s)} l_s^2 \Delta\varepsilon. \qquad 10.66$$

For certain material combinations or loading conditions, the approximation $|\Delta\varepsilon| \approx \varepsilon_F^u$ or $|\Delta\varepsilon| \approx \varepsilon_M^u$ is true.

Inserting all the single energy contributions and the approximation for the radius of the dissipation zone into eqn [10.48] provides the work of fracture of unidirectional reinforced short fibre composites. Experimental information about the kind of fracture are also essential to estimate the share α of brittle and ductile regions and to decide which equation for the matrix fracture energy, i.e., brittle fracture (eqn [10.52]) or ductile fracture (eqn [10.57]) must be used.

In practice, as discussed comprehensively in Chapter 3, SFRP composites show fibre length and orientation distributions. Some aspects of this dependence will be concisely discussed in Section 10.9.

10.6 Work of fracture of un-notched specimens

To calculate the fracture energy of un-notched composites it is necessary to consider this quantity as involving two kinds of energy: the energy to create a moving crack and the energy of crack propagation. The total specific fracture energy thus becomes:

$$w_{un} = w_{init} + w. \qquad 10.67$$

These values are normalised to the sample cross section. It is assumed that the mechanisms described in the previous section are responsible for crack creation and crack propagation. The main difference lies in the fact that the energy dissipation processes during crack creation are spread over a much larger volume than that of crack propagation. Crack creation occurs within the sample volume. With Ω denoting the specific volume of crack creation normalised by the fracture plane (A), and ω_c the energy necessary for crack creation per volume of the composite, the crack initiation energy is given by:

$$w_{init} = \Omega\omega_c. \qquad 10.68$$

The subsequent crack propagation process is characterised by energy dissipation, w, given by eqn [10.48].

Now the crack initiation energy w_{init} must be derived. For this purpose, it is assumed that the deformation energy released during debonding and sliding at the fibre ends is completely available to meet the energy necessary for the fracture processes. The deformation energy of the composite until the moment of crack propagation is given by:

$$\eta_c = \int_0^{\varepsilon'_c} \sigma_c \mathrm{d}\varepsilon_c = \sigma'_c \varepsilon'_c - \int_0^{\sigma'_c} \varepsilon_c \mathrm{d}\sigma_c. \qquad 10.69$$

The local micro defects combine with each other to create a macrocrack when the remaining matrix bridges reach their fracture strength, σ_M^u, where $\sigma'_c = (1 - v)\sigma_M^u$. The corresponding critical strain ε'_c is given by inserting the above stress σ'_c into the stress–strain relation of eqn [4.7].

The deformation energy η_c of the composite consists of two contributions, the elastically stored energy:

$$\eta_e = \frac{(\sigma'_c)^2}{(2E_c)},$$

where E_c denotes the modulus of the damaged material, and the energy of crack creation, ω_c, which is given therefore by:

$$\omega_c = \eta_c - \eta_e = \sigma'_c \varepsilon'_c - \int_0^{\sigma'_c} \varepsilon_c \mathrm{d}\sigma_c - \frac{(\sigma'_c)^2}{(2E_c)}. \qquad 10.70$$

This derivation is illustrated in Fig. 10.26 for loading until σ'_c, where the damage process of microcrack coalescence reaches the level of a macrocrack, and upon subsequent unloading, where the elastic energy η_e is released. During unloading the deformation does not fall to zero because of the sliding process; therefore the slope is characterised by the linear stress–strain relation, that is, $E_c = E_c^0$.

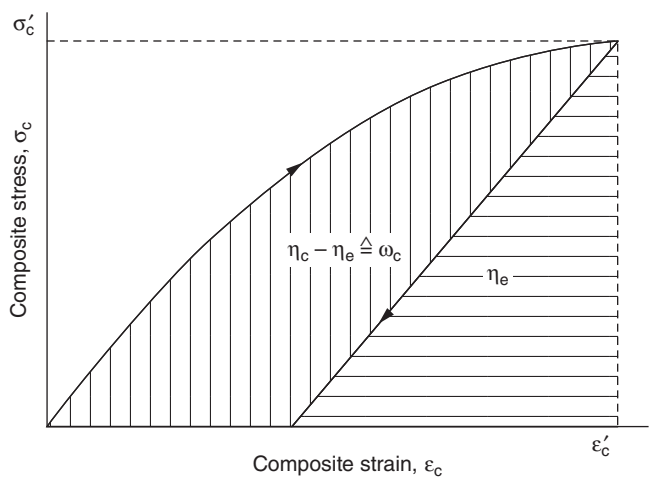

10.26 Deformation energy of un-notched specimen, η_e: elastically stored energy, ω_c: energy for crack creation.

10.7 Discussion on the work of fracture and its dependence on loading rate, volume fraction and interface quality

The general behaviour of the energy contributions to the work of fracture with increasing fibre volume fraction can be discussed without inserting the specific material parameters. The work, w_m, dissipated by plastic deformation in the matrix decreases monotonically with v because of the factor $(1 - v)$, and for $v < v_c$ also because of the decreasing length, l_d of the slipped region. Conversely, the interface contributions w_d and w_s show a maximum.

At smaller fibre volume fractions, the increasing number of activated fibre ends prevails, and with larger volume fractions this trend is overcompensated by the decreasing length of debonded and slipped regions. The characteristic of the total work of fracture of the composite depends on the relative contribution of the different parts. With ductile matrix materials such as polyethylene, and under static loading conditions, intense plastic flow occurs locally in the matrix. Thus, the composite work of fracture for static loading is mainly represented by w_m decreasing monotonically with the fibre volume fraction, as shown in Fig. 10.27(a). Under impact loading, the matrix should respond in a more brittle manner, yet with plastic necking sufficient to prevent fibre pull-out. Thus, the interface contribution (w_d + w_s) dominates, and w passes through a maximum, as shown in Fig. 10.27(b). If the matrix fails completely as a brittle material no necking occurs and pull-out must now be considered. Depending on the absolute value of the pull-out energy, in comparison to (w_d + w_s + w_m), the impact toughness

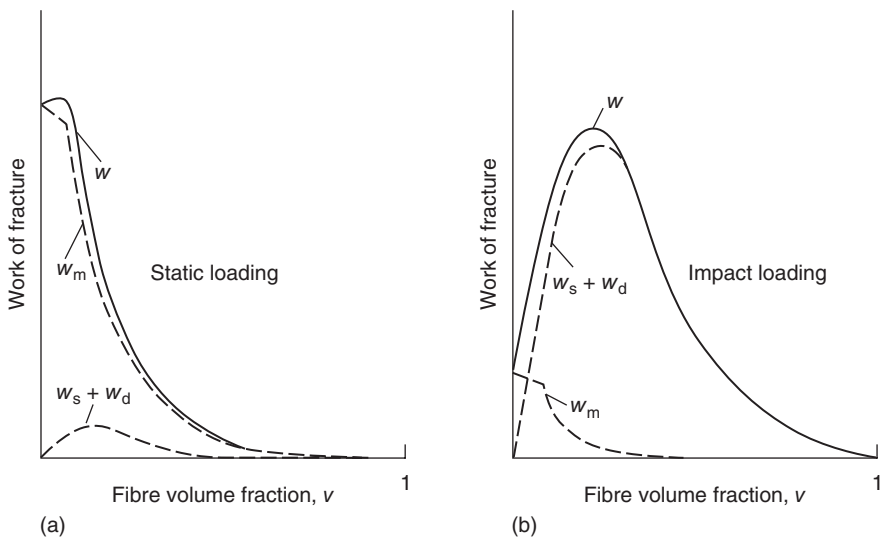

10.27 Work of fracture dependence on volume fraction for different loading rates: (a) static loading; and (b) impact loading.

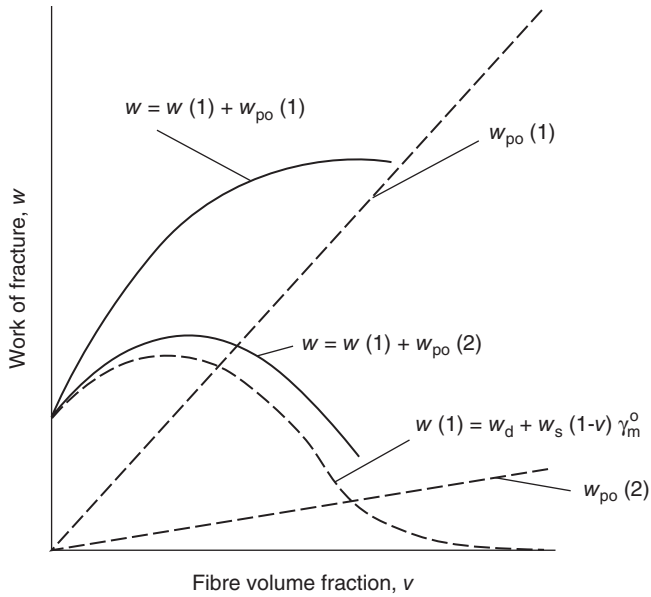

10.28 Work of fracture dependence on differing pull-out energy contributions; $w_{po}(1) > w_{po}(2)$.

shows a maximum, a saturation region, or even a steady increase, as sketched in Fig. 10.28.

Evaluation of the adhesion parameters is even more complex. At first several parameters concerning this matter must be distinguished. The work of fracture depends on parameters which control the initiation of interface debonding, such as τ_d and γ_d^{II}, and other parameters which are important for the sliding process after debonding, such as μ, τ_p and $\hat{\tau}^{(s)}$.

From the general eqn [10.48] with $\alpha = 1$ or $\alpha = 0$ for complete brittle or ductile matrix behaviour, respectively, the total work of fracture as a function of the interface parameters is given for impact loading by:

$$w = w_m + c_p\tau_p + c_d\gamma_d^{II} l_d(\mu, \tau_d) + c_s\hat{\tau}^{(s)}(\mu, \tau_d) l_s^2(\mu, \tau_d) \qquad 10.71$$

and for static loading by:

$$w^{(st)} = c_m^{(st)} l_s(\mu, \tau_d) + c_p\tau_p + c_d\gamma_d^{II} l_d(\mu, \tau_d) + c_s\hat{\tau}^{(s)}(\mu, \tau_d) l_s^2(\mu, \tau_d), \quad 10.72$$

where c_i (i = m, p, s, d) denotes the multiplying factor which does not contain any interface parameters for i^{th} interfacial failure mechanism between fibre and matrix. For example, the second term on the right-hand side of eqn [10.71] is fibre pull-out toughness contribution given by eqn [10.59] so that c_i is $vl^2/6d$ with no interfacial properties. The dissipation zone width, $2r_D$, is assumed independent of shear strength τ_d because $\sigma_c^u \sim \tau$ (with $\tau \sim \tau_d$) and $\sigma_c^d \sim \tau_d$. The characteristic lengths l_d and l_s depend on the friction coefficient μ and on the debonding shear strength τ_d according to eqns [9.4] and [9.5]. These lengths decrease when μ or τ_d is increased.

The sliding energy and plastic matrix energy contributions can decrease with increasing shear strength at the interface, τ_d. The behaviour of the debonding contribution depends on the variation of the product of γ_d^{II}, which increases, and the debonding length, l_d, which decreases with improving adhesion. The pull-out contribution is proportional to τ_p. Its value depends not only on the structure at the interface (and hence on the friction coefficient) but also on the normal stresses acting on the fibre surface. Increasing interface adhesion strength might not necessarily lead to an increased friction coefficient μ. However, it is quite certain that a correlation exists. One argument may be the fact that the chemical structure and bonding mechanisms which determine the adhesive bond strength do not completely vanish after the bond has failed. Consequently, it can happen that the work of fracture under ductile matrix fracture conditions decreases with increasing adhesion strength, while the same material shows an increase under brittle matrix fracture conditions.

It is not possible, therefore, to give a general rule on how to change adhesion to improve the toughness of short fibre reinforced thermoplastics.

At this point, we must remember that we have considered until now composites with aligned fibres only. In reality the fibres show an orientation distribution and thus debonding processes under mode I may also occur and become important. To evaluate the interface properties it will be necessary to extend the theoretical model in this regard (cf. eqn [10.64]). Since the mode I debonding energy is proportional to the fracture surface energy, γ_d^I, this contribution should cause the work of fracture to increase with improved adhesion strength.

We suspect that for short fibre composites with fibres of sub-critical length, where no fibre fracture appears, the pull-out process plays an important role also for the case of high interface toughness values. As long as the matrix shows brittle fracture the fibres are being pulled out during crack propagation. This process will also take place even if the interface strength is higher than the cohesion of the matrix. Then the fibres at the fractured surface may be coated with matrix material. Naturally in this case, the pull-out energy does not necessarily increase with increasing adhesion strength for it is not controlled by the debonding strength but predominately by the sliding behaviour, and then the other mechanisms such as debonding and sliding within the dissipation zone are responsible for the work of fracture increase. On the contrary, experimental examination of post mortem morphology of fractured surfaces by Fu *et al.* (2005) have shown that matrix coated fibres do not simply give a hint to a good adhesion between matrix and fibres. Strictly speaking, the amount of matrix material on the fibre surface does not provide a measure of the adhesion quality as is commonly assumed. Additionally, it could be shown (Fu and Lauke, 1998) that when investigating the influence of the fibre–matrix interface on the work of

fracture, the fibre length distribution must be taken into consideration. This becomes obvious when the pull-out contributions given in eqns [10.59] for $l \le l_c : w_{po} = v l^2 \tau_p/(6d)$ and [10.60] for $l \ge l_c : w_{po} = v l_c^3 \tau_p/(6dl)$ are considered in more detail.

For composites with fibres of sub-critical length, the pull-out contribution increases with increasing fibre length and/or decreasing fibre diameter until the maximum at the critical fibre length is reached.

If in eqn [10.60] the critical fibre length (given by eqn [9.9] as $l_c/d = \sigma_F^u/2\tau$) is inserted, the following relationship is obtained:

$$w_{po} = v\left(\sigma_F^u\right)^3 d^2 \Big/ \left(96 l \tau_p^2\right) \quad l \ge l_c. \tag{10.73}$$

Thus, the pull-out energy of composites with fibres of super-critical length increases when shorter and/or thicker fibres are being used. The maximum is reached at the fibre length $l = l_c$. If the friction stress, τ_p, at the interface is increased (for example, by sizing at the interface or by change of the annealing system to induce higher normal stresses), the pull-out contribution decreases as long as the fibres remain longer than the new (τ_p dependent) l_c. This is the opposite behaviour when compared to composites with fibres of sub-critical length where w_{po} increases with l and τ_p.

The influence of increasing frictional stress τ_p on the pull-out energy is illustrated in Fig. 10.29. With fibres of length $l^{(1)}$ the increase from $\tau_p^{(1)}$ to $\tau_p^{(2)}$ provides a w_{po} increase as demonstrated by the arrow. Fibres of length $l^{(2)}$ now become super-critical, but their energy contribution still increases. Fibres of length $l^{(3)}$, however, also become super-critical but provide a

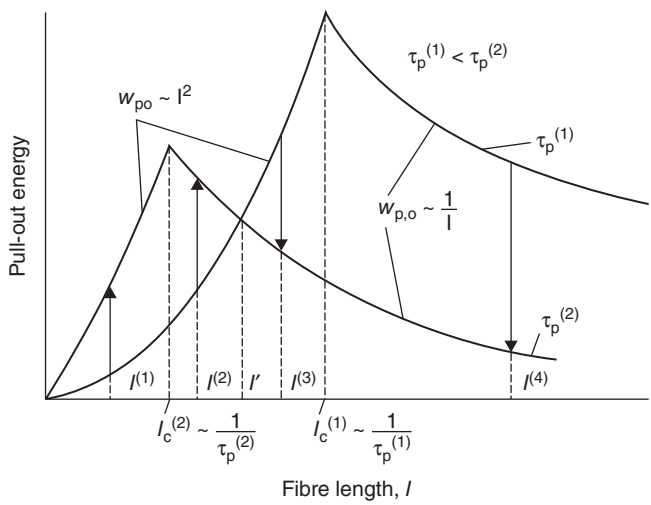

10.29 Pull-out energy as a function of fibre length for two pull-out shear strength values, $\tau_p^{(1)} < \tau_p^{(2)}$.

lower energy. The fibres with $l^{(4)}$ remain super-critical and their energy contribution decreases. Thus, we conclude that a modification which leads to an increase in pull-out shear stress, τ_p, provides an increase of the corresponding energy as long as the fibre length is smaller than the limiting value l', where

$$l' = \frac{d\sigma_F^u}{2\tau_p^{(2)}} \cdot \left(\frac{\tau_p^{(2)}}{\tau_p^{(1)}} \right)^{1/3}. \qquad 10.74$$

For composites with reinforcing fibres $l > l'$, increase of τ_p results in a loss of pull-out energy. (For discussions on optimisation and experimental verification of pull-out toughness of short fibre polymer composites due to pull-out shear stress and fibre diameter, see Wagner and Lustiger (2009)). The pull-out contribution is, in most composites, an important one and therefore modifications of the interface quality with the aim to improve the interfacial shear stress may lead to a reduction of work of fracture; while at the same time it will improve the strength of the composite. But if the pull-out energy is marginal compared to mode I debonding or to the plastic matrix work, modification of the fibre–matrix interface may cause an improvement of toughness. A review of existing methodologies to achieve both high strength and high fracture toughness by interface control was given by Kim and Mai (1991). One of the most effective methods for this is to use an appropriate coating material of the fibres, i.e., not only a sizing that improves the chemical and physical bonding but an extended material with its own mechanical properties. The quantification of the interfacial properties between fibre and matrix is a very complex problem. A number of micromechanical tests, such as for example, the single fibre pull-out and micro droplet tests and the fragmentation test, and their theoretical evaluations have been dealt with during the last 30 years in a large number of publications. The fracture mechanical approach on the basis of analytical modelling was discussed by Nairn (2004) and finite element calculations are summarised by Lauke *et al.* (2004).

An intermittent bonding quality was proposed for reaching the aim of high strength and toughness by Mullin *et al.* (1968) and applied by Atkins (1975). It combines areas of high bonding quality, which ensure the required strength, and areas of low adhesion for crack bifurcation along the fibre length to increase toughness of fibre composites. For more details, refer to the review by Kim and Mai (1991).

10.8 Discussion of experimental and modelling results for short glass fibre reinforced polyethylene

The theoretical model will be applied to calculate the work of fracture and to compare it with experimental data. To demonstrate the rate effect on the work of fracture, specimens of the same material were tested under impact and static loading conditions. The experimental composites consist of a polyethylene (PE) matrix reinforced with short glass fibres. Compounding

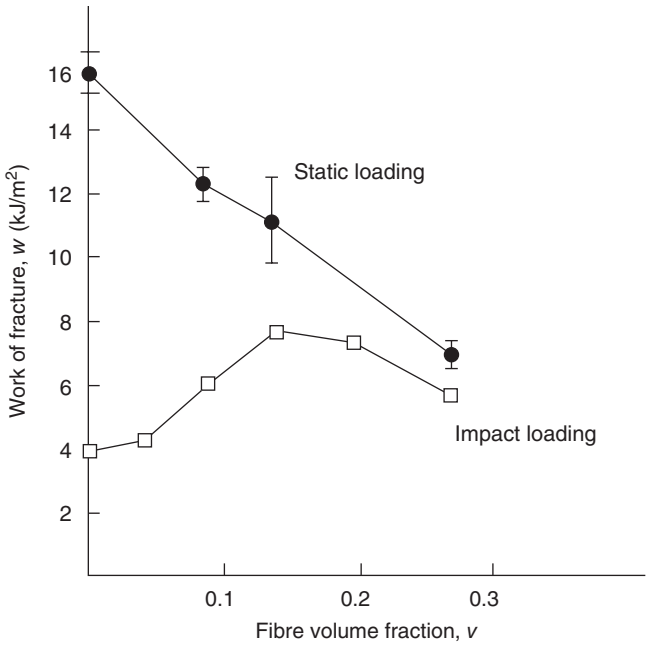

10.30 Work of fracture for impact and static loadings as a function of fibre volume fraction for short glass fibre (*l*/d = 20) reinforced polyethylene composites.

was carried out on a twin-screw extruder and the test specimens were prepared by injection moulding. Thus, a high degree of preferential fibre orientation was achieved.

The impact work of fracture or notched impact toughness was determined by means of Charpy impact tests; and the static work of fracture, w, by three-point bending. The fracture surfaces were studied by SEM. The dependence of the work of fracture on volume fraction, v, follows from the general trends outlined above and are given for glass fibre PE composite in Fig. 10.30. The impact toughness shows a maximum at $v = \sim 0.15$, whereas the static fracture work continuously decreases with increasing v. Hence, the difference between these two values diminishes for higher fibre contents. This behaviour is caused by the fact that different energy dissipation mechanisms are acting for low and high loading rates, which may show opposite dependence on fibre volume fraction. This conclusion is confirmed by the inspection of the fracture surfaces. Large plastic deformations of matrix bridges between the fibres (which were uncoated) are typical for the whole cross section. In contrast, the fracture surface of an impact-tested sample, taken from near the notch, reveals brittle matrix fracture and holes that indicate extensive fibre pull-out.

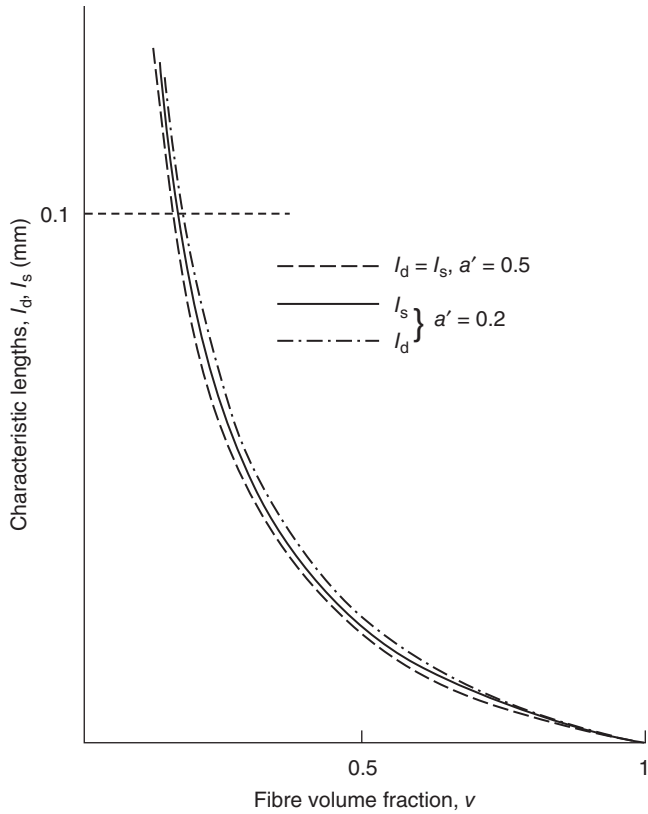

10.31 Debonding and sliding lengths as a function of fibre volume fraction with $\tau_d = a'\tau_{m,y}$.

The general expressions given earlier for the work of fracture of unidirectionally reinforced composites were applied to polyethylene with short glass fibres (cf. Lauke and Schultrich, 1986a). The following mechanical properties were used for the calculation: $E_f = 70$ GPa; $E_m = 0.5$ GPa; $v = 0.3$; $l/d = 20$; $v_f = 0.3$; $v_m = 0.4$; $\omega_m = 5.6$ MPa; $\sigma_{M,y} = 55$ MPa; $\sigma_n^T = 30$ MPa; $\mu = 0.3$; $\gamma_d^{II} = 40$ J/m^2; $\tau_d = a'\sigma_{M,y}$ ($a' = 0.5$); impact loading: $E_m = 0.9$ GPa.

The composite strength, σ_c^u, is obtained from tensile tests. Figures 10.31–10.33 summarise the results for the impact case, and Figs 10.34 and 10.35 for static conditions. The debonding and sliding lengths increase with decreasing fibre fraction (Fig. 10.31). Finally, for low concentrations the fibres are completely debonded and l_d and l_s achieve their limiting value of half the fibre length $l/2$. In the expressions for debonding and sliding energies, w_d and w_s, these lengths and the number of active fibre ends compete, leading to a maximum value at a critical fibre fraction (Fig. 10.32). Under

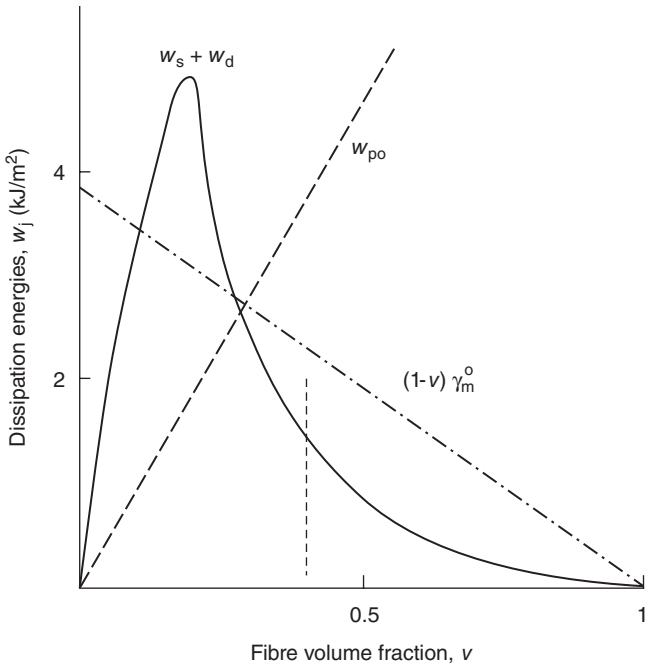

10.32 Dissipation energies as functions of fibre concentration for the impact test.

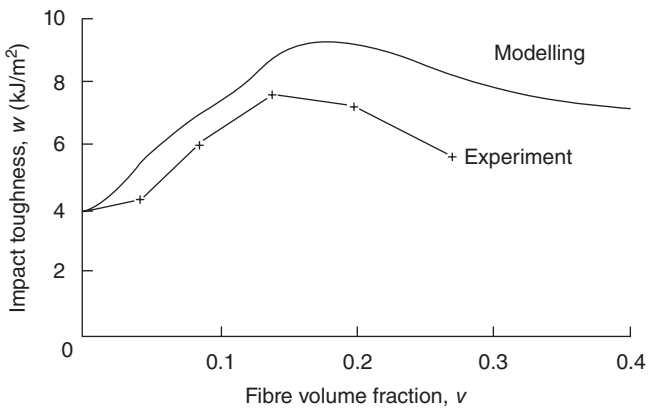

10.33 Comparison of experimentally determined work of fracture for impact loading and modelling result for short glass fibre ($l/d = 20$) reinforced polyethylene composites.

impact loading, they compete with the pull-out and the matrix terms, linearly increasing and decreasing, respectively, with fibre volume fraction. The energies, w_d and w_s, are only exact for $v < 0.4$ because of the lack of composite strength values for calculating the dissipation zone width, $2r_D$, in the case of higher fibre concentrations. The superposition of all these

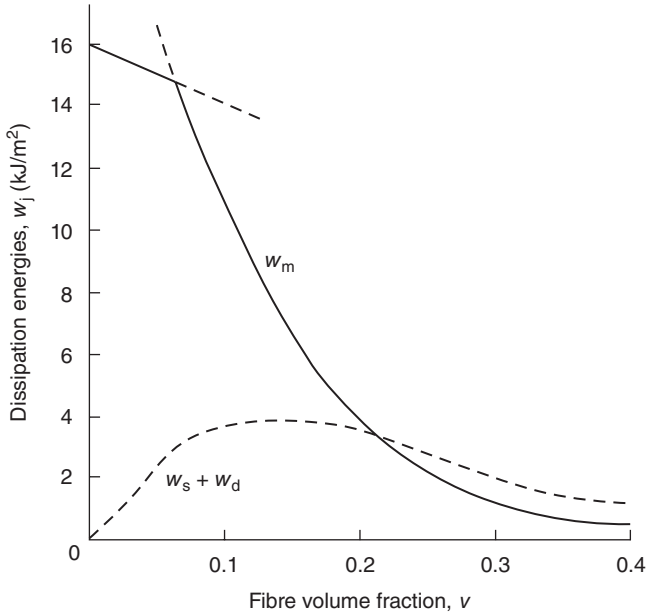

10.34 General variation of dissipation energies for the static test with fibre concentration.

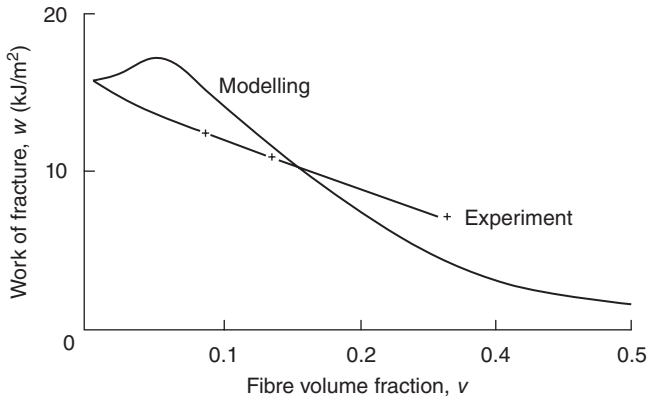

10.35 Comparison of experimentally determined work of fracture for static loading and modelling result for short glass fibre ($l/d = 20$) reinforced polyethylene composites.

contributions to the composite work of fracture results in the anticipated non-linear variation with v (Fig. 10.33).

In the static case, w_d, w_s and w_m show the same qualitative trends. However, whereas $(w_d + w_s)$ is only slightly changed, the matrix contribution rises by a factor of about 4 at smaller fibre concentration (Fig. 10.34). Here, the two

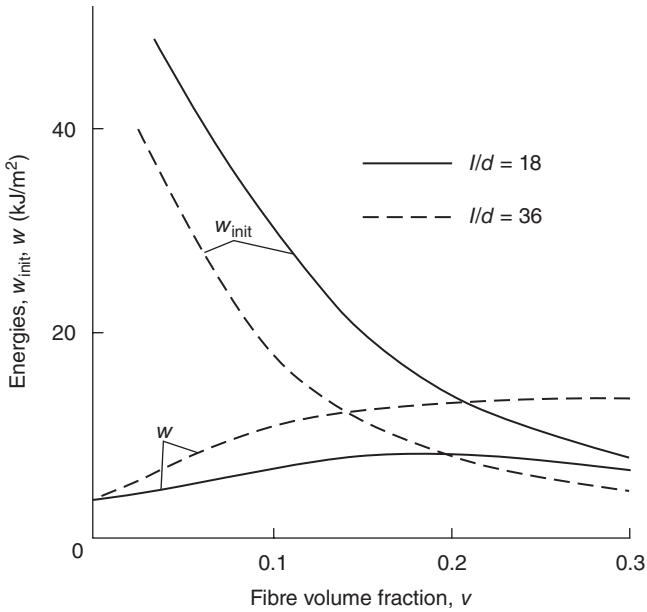

10.36 Initiation, w_{in}, and propagation, w, energies of un-notched specimen as a function of fibre volume fraction.

regions mentioned above for macroscopic plastic flow ($v \leq v_c$) and localised plastic deformation ($v \geq v_c$), are reflected in a different slope of w_m *vs* v. In the total work of fracture (Fig. 10.35) this leads to a weak maximum at a very small fibre content followed by a general descending trend. More experimental work is necessary to explore the functional dependence at small fibre fractions.

In another study (Lauke and Schultrich, 1986b) the un-notched impact toughness of the same material was examined. For the calculation, the material constants given above have been used. The relative dissipation volume (normalised by the crack plane) was estimated to be $\Omega = 44$ mm. After the calculation of the stress–strain curves with relation [4.7], eqn [10.68] with crack initiation [10.69] and propagation energies [10.48] have been used. The results showing the dependence on the fibre volume fraction are illustrated in Fig. 10.36. The crack propagation energy, w, increases while the crack initiation energy decreases steadily; that is, the presence of fibres tends to reduce the crack initiation energy. The dependence on the aspect ratio also shows opposite tendency of crack initiation and crack propagation energy. To obtain higher impact toughness values it is necessary to focus attention on the energy part with the greatest share. At lower fibre volume fractions initiation energy prevails and at higher v crack propagation energy is more important. Comparison of experiments and theory is

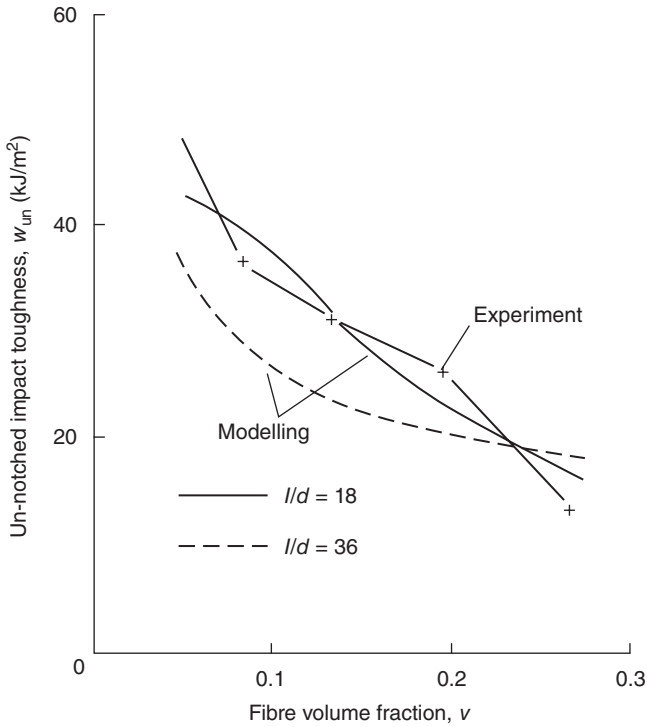

10.37 Un-notched impact toughness *vs* fibre volume fraction for glass fibre reinforced polyethylene composites showing comparison of experiments and modelling results.

shown in Fig. 10.37. Especially important is the result that the crack initiation energy, w_{init}, is responsible for the different fibre volume dependences compared to the notched samples.

Altogether, comparison of experimental and theoretical curves shows the proposed model reproducing the contrasting behaviours of composites with matrices of different ductility in an appropriate manner. However, for quantitative predictions much work is needed with regard to experimental determination of the input parameters used, and to further verification of the theoretical model. This concerns the effects of fibre misalignment, length distribution, and especially the changing nature of the fracture process during crack propagation.

10.9 The influence of fibre orientation, length and shape on the work of fracture

The great majority of theoretical investigations of fracture toughness or work of fracture deals with crack propagation perpendicular to aligned

fibres. The consideration of fibre orientation effects was done mainly to improve understanding of stiffness and strength behaviour (see Chapters 5 and 6). But such research has been extended to clarify the crack propagation behaviour and thus the fracture toughness. Because of the strong anisotropy of composites, the fracture toughness and work of fracture depend on the crack direction relative to the fibre angle. The change of the energy dissipation mechanisms with the angle was first considered in the works of Miwa *et al.* (1979), Piggott (1980), Friedrich (1984, 1985), Brandt (1985) and Wells and Beaumont (1987).

The applicability of Piggott's model is restricted to the case where the fibres are long enough to break. For fibres in an angle θ to the crack front he has obtained a reduced fibre fracture stress σ_F^u and consequently also a reduced critical fibre length. Application of this concept together with the mean fibre orientation angle to the unidirectional case led Friedrich (1984) to calculate the fracture toughness of composites with fibres of super-critical length.

Brandt (1985) calculated the energy due to the fibres passing the crack plane at a certain angle on the basis of three main phenomena, namely, plastic deformation of the fibres, matrix compression, and friction between matrix and fibre due to local compression. Furthermore, the pull-out and debonding mechanisms are considered, where the energies are determined by measuring the area under the load-displacement curves of the pull-out tests. Brandt has obtained optimum fibre angles as a function of aspect ratio and debonding and frictional shear stresses. For composites with randomly oriented fibres, Miwa *et al.* (1979) proposed a simple modification of the equations used in the aligned case. They have calculated the breaking probability of fibres as $P = (1 - l_c/l)$ and thus the pull-out probability is given by $P_{po} = (1 - P)$. The contribution due to fibre fracture was obtained by the superposition of fibre debonding and fracture energy. Based on the discussion of Wells and Beaumont (1987), it seems favourable to use only the contribution resulting from the change in the elastic energy of the deformed fibres, which includes both dissipation mechanisms.

As reported above, the fibre length spectrum of reinforced thermoplastics shows a certain number of fibres of sub- and super-critical length. Consequently, failure modes associated with these two fibre types will be activated during the dissipation processes. A main question in the solution of this complex problem is whether these modes can be approximated as being independent. If this were the case, then linear superposition (as has already been done for the deformation and strength behaviour) would provide first results. (However, the distribution of fibres with different orientations and lengths may yield stress concentrations and promote interactions, which lead to failure modes that cannot be described by this simple

superposition method.) Doing so, it would lead to a general work of fracture expression below:

$$w = w_{\mathrm{fi}} + w_{\mathrm{m}} + \sum_{l \le l_{\mathrm{c}}} w_{\mathrm{i}} + \sum_{l \ge l_{\mathrm{c}}} w_{\mathrm{j}} \qquad 10.75\mathrm{a}$$

with

$$w_{\mathrm{i}} = \int_0^{\theta_{\max}} \int_0^{l_{\mathrm{c}}} n_{\mathrm{i}}(\theta, l) W_{\mathrm{i}}(\theta, l) g(\theta) f(l) \mathrm{d}l \mathrm{d}\theta \qquad 10.75\mathrm{b}$$

and

$$w_{\mathrm{j}} = \int_0^{\theta_{\max}} \int_{l_{\mathrm{c}}}^{l_{\max}} n_{\mathrm{j}}(\theta, l) W_{\mathrm{j}}(\theta, l) g(\theta) f(l) \mathrm{d}l \mathrm{d}\theta, \qquad 10.75\mathrm{c}$$

where $l_{\max}$ is maximum fibre length and $\theta_{\max}$ maximum fibre angle, as well as the fibre length distribution and fibre orientation distribution functions as discussed in Chapter 3.

Based on only geometrical consideration, the maximum angle may be $\theta_{\max} = \pi/2$ for the corresponding definition of distribution density. But from physical consideration, as proposed by Piggott (1980), the strength of an oblique fibre in an angle θ to the crack plane, is lower (because of bending) than the strength of a fibre perpendicular to the crack plane and is called the inclined strength of fibres. This leads to reduction of the maximum angle: $\theta_{\max} \le \pi/2$. The number of contributing fibres $n_{\mathrm{i}}(l, \theta)$ and the corresponding energies $W_{\mathrm{i}}(l, \theta)$ must be specified for the different energy dissipation mechanisms.

In the following, the effect of fibre length and fibre orientation distribution is considered first for the fibre pull-out process in more detail, because it is in most cases the most important energy dissipation process. The brief derivation is adopted from Fu and Lauke (1997) where more details can be found.

When there is a distribution of fibre lengths, the fibre pull-out energy of unidirectional composites can be expressed as the superposition of energy contributions of the sub- and super-critical fibre length as given in eqns [10.59] and [10.60] and provided by Gupta *et al.* (1990) as follows:

$$w_{\mathrm{po}} = \frac{\tau_{\mathrm{p}}}{6d} \sum_{l_{\mathrm{i}} \le l_{\mathrm{c}}} v_{\mathrm{i}} l_{\mathrm{i}}^2 + \frac{\tau_{\mathrm{p}} l_{\mathrm{c}}^3}{6d} \sum_{l_{\mathrm{j}} \ge l_{\mathrm{c}}} \frac{v_{\mathrm{j}}}{l_{\mathrm{j}}}, \qquad 10.76$$

where l_{i} and l_{j} are fibre lengths of sub-critical and super-critical fibres, respectively; v_{i} and v_{j} denote the sub-fractions of sub- and super-critical fibres, respectively.

For non-unidirectional composites with short fibres of a constant length, the fibre pull-out energy was studied by Wetherhold and Jain (1992, 1993) and Jain and Wetherhold (1992). The effect of snubbing friction between

fibres and matrix at the fibre exit point was taken into account when the fibres cross obliquely the fracture plane. Figure 10.38 shows the pull-out of a single fibre with shorter embedded segment of length L_e and orientation angle θ in respect to the loading direction. The pull-out energy as a function of fibre orientation angle is given in Fig. 10.39, where

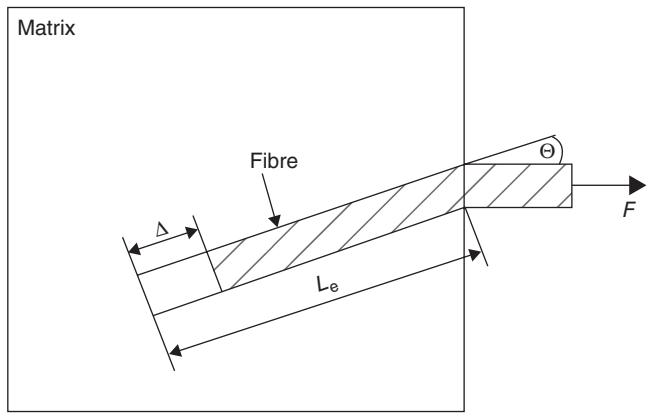

10.38 Oblique fibre crossing the crack plane. Adapted from Jain and Wetherhold (1992).

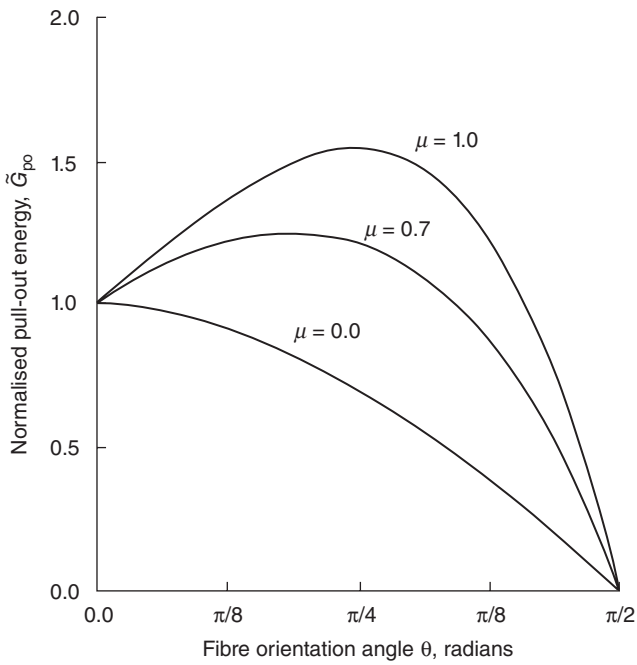

10.39 Pull-out energy for aligned fibres as a function of the fibre orientation angle for different snubbing friction coefficients. Adapted from Wetherhold and Jain (1993).

the results are normalised to the pull-out energy for sub-critical fibres, given in eqn [10.59]. The variation depends on the so-called snubbing friction coefficient μ introduced by Li *et al.* (1990), that is, for higher snubbing friction an increase of pull-out energy for lower orientation angles can be expected.

Two probability density functions are introduced by Fu and Lauke (1997) for modelling the fibre length and fibre orientation distributions, which have already been used to determine the strength and stiffness in Chapters 5 and 6, respectively.

The fibre pull-out energy is derived as a function of fibre length and orientation distributions and the interfacial properties by considering the snubbing friction effect and the inclined fibre strength effect, where the consideration of the fibre orientation effect is based on the derivations provided by Wetherhold and Jain (1992, 1993) and Jain and Wetherhold (1992). All the factors that influence the fibre pull-out energy are discussed in detail, so that the necessary information is provided to achieve a high fibre pull-out energy and hence a high fracture toughness of composites for a given fibre–matrix system.

The general equation for a constant interfacial shear stress τ_p during pull-out is derived below:

$$w_{po} = \frac{8v\tau_p}{dl_{mean}}\left[\int_{\theta=0}^{\theta_{max}}\int_{l=l_{min}}^{l_{c\theta}}\int_{L_e=0}^{l/2}\frac{L_e^2}{2}f(l)g(\theta)\cos(\theta)\exp(\mu_S\theta)\,dL_e\,dl\,d\theta + \int_{\theta=0}^{\theta_{max}}\int_{l=l_{c\theta}}^{l_{max}}\int_{L_e=0}^{l_{c\theta}/2}\frac{L_e^2}{2}f(l)g(\theta)\cos(\theta)\exp(\mu_S\theta)\,dL_e\,dl\,d\theta\right], \qquad 10.77$$

where $l_{c\theta}$ is the critical fibre length for an oblique fibre pulled out at an angle, θ, with the loading direction: $l_{c\theta} = l_c(1 - k\tan\theta)/\exp(\mu_s\theta)$. The constant k determines the fibre inclined strength (Piggott, 1980). The lengths l_{min} and l_{max} are, respectively, the minimum and maximum fibre lengths within the specimen and L_e is the embedded length of the fibre.

For the unidirectional short fibre composite this expression is reduced to:

$$w_{po} = \frac{8v\tau_p}{dl_{mean}}\left[\int_{l=l_{min}}^{l_{c\theta}}\int_{L_e=0}^{l/2}\frac{L_e^2}{2}f(l)dL_e\,dl + \int_{l=l_{c\theta}}^{l_{max}}\int_{L_e=0}^{l_{c\theta}/2}\frac{L_e^2}{2}f(l)\,dL_e\,dl\right]. \qquad 10.78$$

Based on general eqn [10.78], the fibre pull-out energy can be predicted. The effects of mean fibre length and critical fibre transfer length on the fibre pull-out energy are shown in Fig. 10.40. For a given critical fibre length, the fibre pull-out energy increases with the mean fibre length until a certain value slightly less than the critical transfer length l_c, at which the maximum of fibre pull-out energy is reached (see Points A, B and C in the curves). This is because the pull-out energy is contributed by sub-critical fibres of lengths less than $l_{c\theta}$ and super-critical fibres of lengths greater than $l_{c\theta}$, the

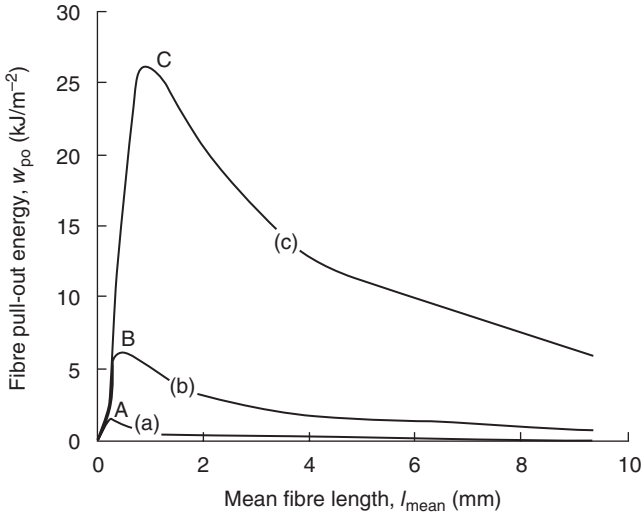

10.40 Fibre pull-out energy as a function of mean fibre length for different critical fibre lengths: (a) l_c = 0.376 mm, (b) l_c = 0.837 mm, and (c) l_c = 1.71 mm.

sum of the two parts reaches the maximum at a certain mean fibre length slightly less than $l_{c\theta}$. Afterwards, the fibre pull-out energy decreases with the mean fibre length since more fibres will rupture and will not contribute to the fibre pull-out energy. For different critical fibre length cases, the fibre pull-out energy increases with critical fibre length. So, a large critical fibre length is very efficient to achieve high fibre pull-out energy. Another way to increase the pull-out energy contribution is to change the end structure of the fibres. According to reports by Phan-Thien (1980, 1981), enlarged end fibres can increase the strength and fracture toughness over those of composites with straight structures. This idea was also used by Zhu *et al.* (1998, 1999) and Beyerlein *et al.* (2001) who considered the mechanical properties of bone-shaped short fibre reinforced composites; Fig. 10.41 shows such a kind of glass fibre. Zhu and Beyerlein (2002) gave a survey about the mechanics of bone-shaped short fibre composites and recommendations about future research necessary to understand the micromechanics involved.

Fracture toughness tests have shown that these fibres can bridge the crack surfaces much more effectively than conventional straight fibres leading to improved toughness. Thus, with the modification of the fibre structure the very complex problem of interface bonding quality modification may be avoided. Very often, there exists a trade-off between strength and toughness. A strong interface can transfer higher load to the fibres but cause at the same time higher stress concentrations, which may lead to fibre or matrix failure instead of the more effective fibre pull-out. Typical load-

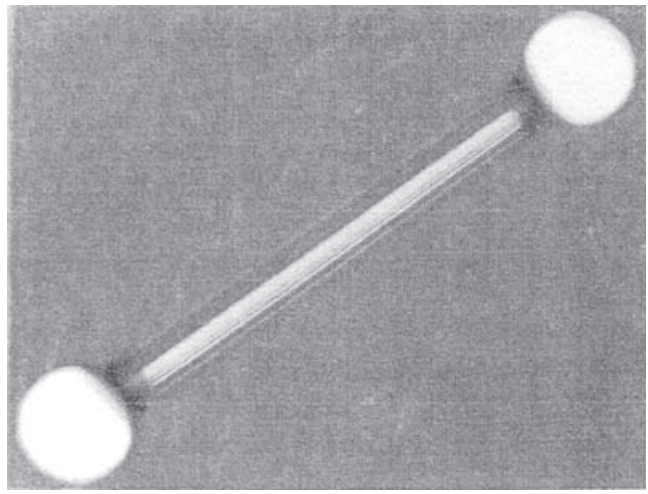

10.41 Sketch of a bone-shaped short fibre (length 1.5 mm) made by melting the ends of a glass fibre. Adapted from Beyerlein *et al.* (2001).

displacement curves for the single fibre pull-out for straight (CSS) and bone-shaped (BSS) fibres are compared in Fig. 10.42. The peak loads and energy consumptions for bone-shaped fibres are much higher than those of straight fibres.

Shaped fibres for improving the pull-out energy where considered experimentally by Wetherhold and Lee (2001) and theoretically by Tsai *et al.* (2003), where the shape of the ductile fibres is optimised. Simulation of the experimental load-displacement curve was improved by the application of a combined cohesive/friction zone interface model by Tsai *et al.* (2005).

Used end-impacted copper fibres, whose shape depends on the strength of the impact that causes the shape variation, are shown in Fig. 10.43. The pull-out work *vs* embedded length for straight and end-impacted fibres is shown in Fig. 10.44. For shorter embedded lengths the shaped fibres provide higher energies; but depending on the friction coefficient between fibre and matrix for higher embedded lengths, there may or may not exist a break-even point. More experimental results concerning fracture toughening with copper fibres in an epoxy matrix are reported by Bagwell and Wetherhold (2005).

Especially for ductile-fibre reinforced composites it is important to use the potential of plastic deformation of the fibres to increase fracture toughness, i.e., the volume of fibres that yield should be large. Possibilities to reach this aim are discussed by Wetherhold *et al.* (2007). Additional to anchoring fibres in matrix with a shape variation of the fibre ends, mechanical and

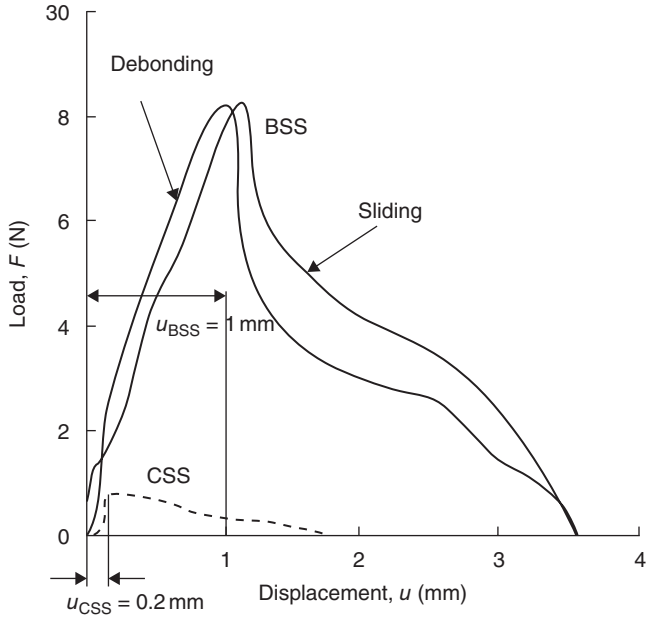

10.42 Load-displacement curve of a pull-out experiment with a single bone-shaped short polyethylene fibre (BSS) and a straight fibre (CSS) in polyester matrix, embedded length L_e = 3.5 mm. Adapted from Zhu *et al.* (1999).

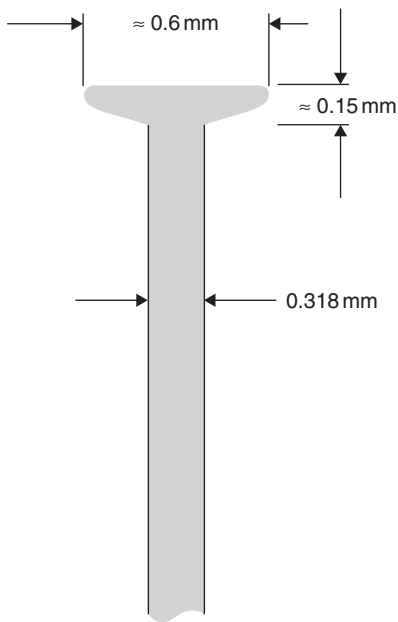

10.43 End-shaped copper or nickel fibres made by impact. Adapted from Wetherhold and Lee (2001).

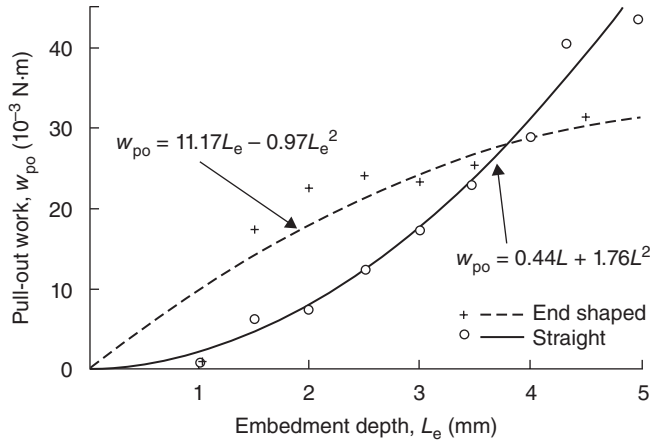

10.44 Comparison of pull-out work for straight and end-shaped copper fibres *vs* embedded length L_e. Adapted from Wetherhold and Lee (2001).

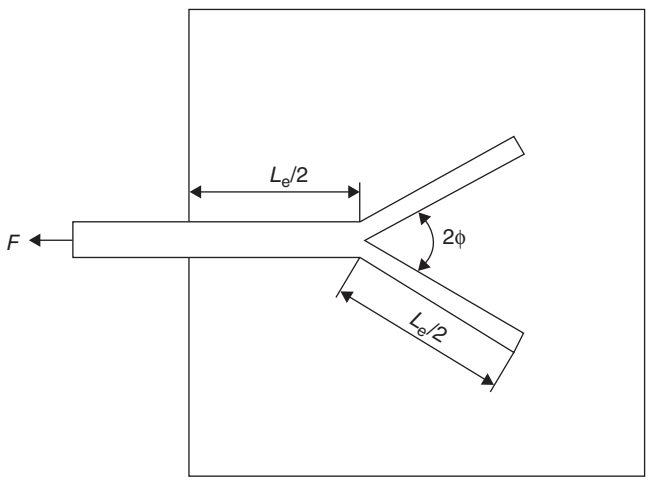

10.45 Model of fibre pull-out work calculation for a one-step branched fibre. Adapted from Fu *et al.* (1992).

chemical modifications of the fibre surface to improve the pull-out energy are discussed.

Another idea to improve the toughness was on the fractal tree structure of the fibres. Fu *et al.* (1992) used this idea for the calculation of the pull-out work. The model for this kind of fibres is shown in Fig. 10.45. The force (F) *vs* embedded length (L_e) plot for the one-step branched fibre is obtained by the superposition of the contributions of the straight and oblique parts

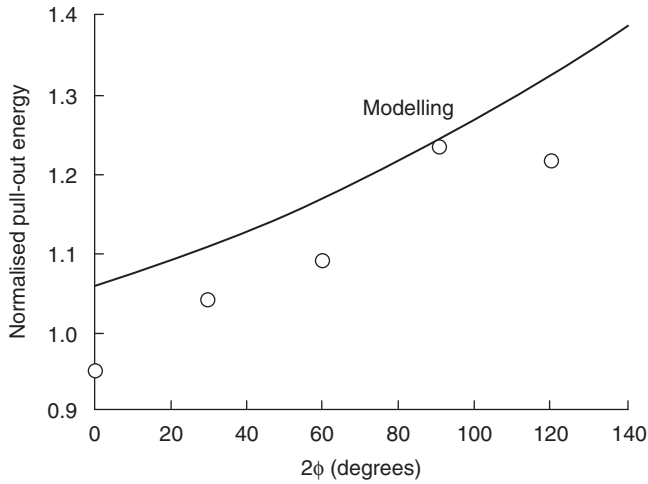

10.46 Normalised pull-out energy with branching angle; comparison of experiment and model as given in eqn [10.79].

of the fibre using the models developed above for these cases. Thus, the corresponding pull-out energy is derived as:

$$\frac{W_{\mathrm{po1}}}{W_{\mathrm{po}}} = 3/4 + S_2 \exp(\mu_{\mathrm{s}}\varphi)/(2S_1), \qquad 10.79$$

where W_{po} is pull-out energy for a straight fibre from eqn [10.58], and S_1 and S_2 perimeters of the stem and branch of the fibre, respectively.

The experimental and theoretical results for a special case (steel fibres) are compared in Fig. 10.46. Both theoretical and experimental pull-out energy values of the branched fibres increase with branching angle and are greater than those of the straight fibres.

Until now only one energy dissipation mechanism, fibre pull-out that enters the general expression [10.75], has been considered for its dependence on fibre length and fibre orientation distributions. However, other contributions also depend on these parameters. A first approach to include fibre orientation for the debonding and sliding processes for a constant mean sub-critical fibre length was described in Lauke and Freitag (1987) and later summarised in Lauke *et al.* (1990).

The basic idea consists in subdividing the whole crack growth process into propagation perpendicular and parallel to the fibres, taking into account the specific failure processes and the fraction of fibres which are involved in these two main states.

The terms w_{i} of general eqn [10.42] can be calculated by multiplying the corresponding energy, $W_{\mathrm{i}}(\theta)$, dissipated at one fibre with the angle θ by the

specific number, $n_i(\theta)$, of fibres involved and by subsequent integration over all possible fibre angles:

$$w_i = \int_0^{\pi/2} n_i(\theta) W_i(\theta) g(\theta) \mathrm{d}\theta \quad \text{with} \quad \int_0^{\pi/2} g(\theta) \mathrm{d}\theta = 1. \tag{10.80}$$

Distinct from eqn [10.45] where the specific number of fibres is given for the aligned fibre case, now this number $n_i(\theta)$ is different for different processes since the dissipation zone width $2r_D$ is different.

For calculation of the dissipation energies, two approximations are used: (a) the complex loading of a fibre under a certain angle to the applied load is separated into independent superposition of longitudinal and transverse loading; and (b) dissipation energies are assumed to be independent of the fibre angle within the two main fibre regions $\theta \leq \theta_c$ and $\theta \geq \theta_c$. The critical angle θ_c is defined as that angle where the applied load causes local tension at the fibre–matrix interface high enough for mode I failure. With these assumptions in mind the interaction energy (eqn [10.80]) can be expressed for transversal (to the MFD) cracks (T) and longitudinal cracks (L) (see Fig. 10.6), as:

T-crack:

$$w_i = w_{i(p)} F_T + w_{i(l)} (1 - F_T) \quad \text{with} \quad F_T = \int_0^{\theta_c} g(\theta) \mathrm{d}\theta \tag{10.81}$$

L-crack:

$$w_i = w_{i(p)} F_L + w_{i(l)} (1 - F_L) \quad \text{with} \quad F_L = \int_{\theta_c}^{\pi/2} g(\theta) \mathrm{d}\theta, \tag{10.82}$$

with $w_{i(p)} = n_{i(p)} W_{i(p)}$ for cracks perpendicular (p) to the fibres and $w_{i(1)} = n_{i(1)} W_{i(1)}$ for cracks longitudinal (l) to the fibres. The energy dissipation mechanisms and the corresponding expressions for crack propagation perpendicular to the fibre were discussed, considering that $w_{i(p)} = n_{i(p)} W_{i(p)} = w_i = nW_i$.

The energy dissipation for crack propagation parallel to the fibres is determined mainly by debonding at the fibre–matrix interface in mode I, $W_{d(l)} = W_d^I$, and brittle or ductile matrix fracture. This is sketched in Fig. 10.47. On the basis of these assumptions the works of fracture for transversal and longitudinal cracks were calculated (see Lauke *et al.*, 1990) and they are shown in Fig. 10.48.

It can be concluded that consideration of fibre orientation in the proposed way provides more realistic work of fracture values for short-fibre reinforced composites than the approximation based on a composite with parallel fibre alignment. The comparison reveals that the fracture work of a parallel fibre composite overestimates the real value for T-cracks and provides a lower bound for L-cracks.

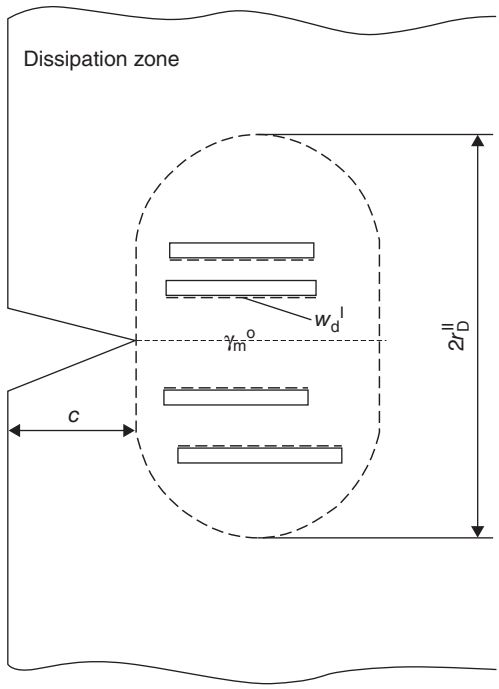

10.47 Failure modes for crack propagation along the fibre axis, W_d^I: mode I debonding energy, γ_m^0: matrix fracture energy, $2r_D^{II}$-dissipation zone width.

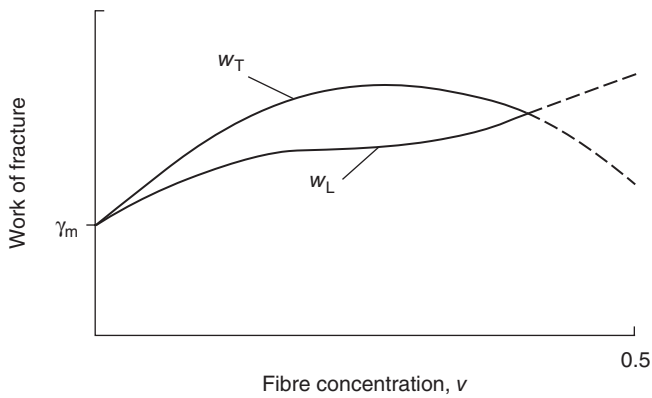

10.48 Comparison of fracture work for transverse (to the MFD) and longitudinal crack propagation.

10.10 Fracture toughness

10.10.1 General remarks

Fracture toughness is a well-established parameter to characterise the resistance of crack initiation of a material. Its calculation requires full knowledge of the failure initiation processes. The failure process of short fibre reinforced thermoplastics is characterised by different energy dissipation mechanisms, as discussed in Section 10.4. These mechanisms are assumed to act within a certain zone ahead of the notch tip – the dissipation zone. The modes of energy dissipation are affected mainly by the matrix fracture mode (whether brittle or ductile), which is decisively determined by the loading rate or temperature conditions. On the basis of an energy principle and relationships regarding the different energy dissipation mechanisms, in the following, theoretical expressions for both static and impact fracture toughness will be proposed and compared with experimental results.

In the basic studies by Beaumont and Harris (1972) and Harris (1972) they worked out the differences between different toughness values, pointing out particularly that the critical energy release rate describes the stage of crack initiation, and the work of fracture mainly concerns that of crack propagation. It is plausible that in general these two stages are governed by different fracture modes, which depend on the composite structure and loading conditions.

Fractographic or *in-situ* observations of crack propagation in a given composite material show macroscopic crack initiation preceded by a certain extent of microscopic structural instability. Thus, such a parameter as the macroscopic critical energy release rate, G_c, *includes* elements of sub-critical crack growth. This sub-critical crack growth can be modelled by a continuum theoretical approach considering the formation of a zone of energy dissipation near the crack tip for a given amount of crack growth, *dc*. Hence, a conceptual connection exists with the macroscopic work of fracture, which means that G_c can be understood as a 'restricted work of fracture' for a limited crack growth which is large with respect to the characteristic microstructural dimensions (e.g., fibre diameter or fibre separation) but small compared with crack length and sample dimensions. To calculate the critical energy release rate, the energy dissipation zone concept is used and it was qualitatively discussed already in Section 10.5.2. In contrast to other models, where this damage parameter is an experimentally determined value, the following treatment is founded on a fracture mechanical determination of the damage zone size. With this concept, it is possible to evaluate the influence of different microscopic energy dissipation mechanisms in short fibre reinforced polymers on the fracture

toughness that depends on structure and loading conditions. For simplicity, the case of crack growth perpendicular to unidirectional short fibres is considered.

As a first approximation, a uniform and homogeneous fibre distribution is assumed, although such distributions are rarely achieved in injection moulded composites. In particular, the influence of different loading rates is discussed. High loading rate (or low temperature) and high fibre contents imply a predominantly brittle matrix fracture and hence the condition of small-scale damage is satisfied. For a ductile matrix (or static loading and high temperature) the model applies only if the damage zone remains sufficiently small.

10.10.2 Energy criterion of fracture toughness

In the following, a connection is established between the macroscopic critical energy release rate, G_c, and different microscopic failure processes. To derive G_c the model developed for energy dissipation of ceramics and transformation toughened materials (Kreher and Pompe, 1981) is used. The fracture toughness is obtained by comparing the available energy of crack extension, $-\mathrm{d}U_{\mathrm{pot}}$, with that of the energy dissipation in creating the cut which enlarges the crack, $\mathrm{d}Q$:

$$-\mathrm{d}U_{\mathrm{pot}} = \mathrm{d}Q \equiv R\,dc \qquad 10.83$$

assuming throughout the following unit thickness of the considered specimen with a crack. This equation defines the so-called crack resistance R of the material already introduced in Section 10.2.3, which is generally a function of crack growth, $\Delta c = (c - c_0)$.

If we assume small-scale damage (dissipation zone width, $2r_D$, is very small compared to the crack length and sample size) the available energy for an infinitesimal crack extension, dc, is given by the elastic energy release rate, G, according to eqn [10.12]:

$$-\mathrm{d}U_{\mathrm{pot}} = G\,dc. \qquad 10.84$$

Combining eqns [10.83] and [10.84] provides the left-hand side of the crack propagation criterion of eqn [10.24]. As already discussed in Section 10.2.3 it is a necessary condition for crack initiation. The crack becomes unstable if also the second condition of the criterion [10.24] is fulfilled at the critical crack length $c = \tilde{c}$. This will be discussed in Section 10.10.5 in more detail.

The above concept is applicable to reinforced polymers if at high loading rates the matrix fails macroscopically in a predominantly brittle manner and thus limits the development of large plastic deformation or large damage zones. In the case of quasi-static loading, the extension of large

plastic zones will be restricted for higher fibre concentration. For low fibre volume fractions, the matrix behaves like an unreinforced material and shows large-scale plastic deformation, while at intermediate concentrations the fibres affect the plastic matrix flow. The influence of fibre concentration on the general behaviour depends mainly on the fibre–matrix interface conditions. For application of the model, we have to decide whether or not the condition of small-scale damage is fulfilled.

The energy consumed during crack propagation must be considered; and for this, as was already done for the calculation of the work of fracture (cf. Sections 10.5 and 10.6), the dissipation and process zone concept is used.

For brittle materials it is generally known that a small damage zone may be developed in front of the notch. We assume that for points beyond $2r_D$ the material behaves elastically. By analogy with this zone, the stress concentration ahead of a notch in a composite material causes localised instabilities. These instabilities act only within the damage or dissipation zone of dimension $2r_D$. Immediately in front of the notch we have to consider an additional process zone caused by the interaction of the main crack and the dissipation zone, e.g., microcrack coalescence or fibre pull-out. Within this zone the crack propagates by creation of a new macroscopic fracture surface, dc, consuming the specific energy q_{pz} (see Fig. 10.49). If the total energy dissipated within $2r_D$ is designated by dQ_D and the specific fracture energy of the process zone by q_{pz}, the dissipated energy is given by:

$$dQ = q_{pz}dc + dQ_D. \tag{10.85}$$

From this equation together with the definitions of [10.21] and the criterion [10.24] it follows that the fracture toughness for crack initiation is given by:

$$G_c = R = q_{pz} + \frac{dQ_D}{dc}. \tag{10.86}$$

Generally, the energy dissipation process will be affected by different local instabilities that are initiated at different critical local stress levels, σ_c^i. This means, however, that there will also exist different extensions, r_D^i, of the corresponding sub-zones (see Fig. 10.49).

If again the definition of a volume specific dissipation energy of the mechanism (i), η_i, is used, the increment dQ_D can be generalized as:

$$dQ_D = \sum_i 2r_D^i \eta_i dc. \tag{10.87}$$

Inserting this expression into [10.86] provides the fracture toughness:

$$G_c = R = q_{pz} + 2\sum_i r_D^i \eta_i. \tag{10.88}$$

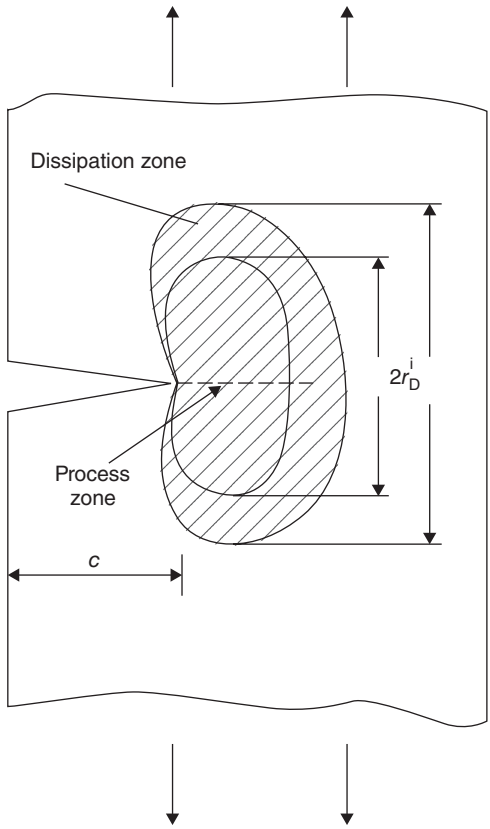

10.49 Damage zone near the tip of the macrocrack: *c*, crack length; $2r_D^i$, width of the dissipation zone for the mode (i); process zone of direct interaction of the propagating crack with the damaged material.

For calculation of the dissipation radii, r_D^i, several approximations are possible. In Section 10.5 a stress criterion was proposed and it provided the relation after eqn [10.46]. Now the basic relation of fracture mechanics is applied to estimate the radius of the dissipation zone.

With the small-scale damage approximation, the radius can be calculated similar to the plastic zone from eqn [10.5] together with the relationship between fracture toughness and stress intensity factor [10.13]:

$$r_D^i = \beta_i E_c G_c / \left(\sigma_c^i\right)^2, \qquad 10.89$$

where E_c is Young's modulus of composite, and σ_c^i is critical stress for the material instability (i). As shown by Kreher and Pompe (1981), the factor β_i (which depends on the local deformation and the ratio of Young's moduli of different components) can be approximated for a single microcrack dissipation mechanism in brittle materials by $\beta \approx 1/3$, using the elastic

stress-field approach. If different energy dissipation processes are considered, an interaction of various zones is possible and unloading of the internal zones may occur. More extended numerical calculations by Budiansky *et al.* (1983) have shown that β_i is not constant but depends sensitively on the characteristics of the dissipation process. The micro instabilities induce local unloading near the crack tip. Thus, $\beta_i \approx 1/3$ corresponds to an upper limit for the damage zone calculation. With increasing η_i a diminishing β_i can be expected, particularly in the case of interacting zones when β_i of the internal zone will decrease significantly. Keeping in mind all these problems, we use in our approach $\beta_i = \beta \geq 1/3$ as a free parameter fitted by experimental data.

As a result of difficulties in determining β_i and σ_c^i, another approach becomes plausible, viz., the introduction of r_D as a material parameter. This approach was used in the 'inherent flaw model' by Waddoups *et al.* (1971), the point stress and average stress criteria by Whitney and Nuismer (1974) and the damage parameter theory by Zhen (1983). Within the framework of these approaches, the radius, r_D, is determined by comparison of the connection between the local stress field and K_c on the one hand, and the applied load and K_c on the other. Then, it is obtained that:

$$r_D^i = r_D^0 \tag{10.90}$$

as a material parameter which depends on the fracture toughness of the material and the local strength distribution, as well as the redistribution of stresses under loading of the region near the crack tip.

By inserting eqn [10.89] or [10.90] into eqn [10.88], the two expressions for the critical energy release rate are obtained:

$$G_c = R = \frac{q_{pz}}{1 - 2\beta E_c \sum_i \eta_i \Big/ \left(\sigma_c^i\right)^2}, \tag{10.91}$$

or

$$G_c = R = q_{pz} + 2r_D^0 \sum_i \eta_i. \tag{10.92}$$

Equation [10.91] is used to account approximately for the dependence of r_D^i on the critical energy release rate, G_c, as given in eqn [10.89].

10.10.3 Micromechanical approximation of toughening mechanisms

In Section 9.2.2 a deformation model of short fibre reinforced composites with debonding interfaces was derived. As a characteristic composite element, a single fibre embedded within a matrix cylinder was considered

(without local fibre–fibre interaction) and where the load is applied in the fibre direction.

This model provides us with the critical stresses, σ_c^i, and the debonding (l_d) and sliding (l_s) lengths, which are necessary for the calculation of dissipation energies within the dissipation zone. With this knowledge we are able to determine the debonding (W_d) and sliding (W_s) energies of one fibre. The volume specific energies, η_i, are obtained by multiplying these energies by the number, $\tilde{n}$, of activated fibres per unit volume, as defined in eqns [10.4] and [10.5], such that:

$$\eta_i = \tilde{n} W_i = \frac{v}{\pi r_f^2 l} W_i. \tag{10.93}$$

The debonding and sliding energies are given by eqns [10.63] and [10.66], respectively. Inserting these into [10.93] yields:

$$\eta_d = 16 v l_d \gamma_d^{II} / (ld) \tag{10.94}$$

$$\eta_s = 8 v \bar{\tau}^{(s)} l_s^2 \Delta\varepsilon / (ld), \tag{10.95}$$

where γ_d^{II} is specific debonding energy for mode II debonding of the fibre–matrix interface, $\bar{\tau}^{(s)}$ is mean sliding stress and $\Delta\varepsilon$ is difference of the ultimate deformations of fibre and matrix. Detailed expressions for these values are given in Section 9.2.2.

In the case of ductile matrix fracture, matrix deformation is expected between the neighbouring fibres within the whole dissipation zone. The following expression was derived in eqn [10.56]:

$$\eta_m = \omega_m 2 l_d (1 - v) / l. \tag{10.96}$$

(η_d, η_s,η_m) describe the energies within the dissipation zone for increasing load. The final stage of failure is characterised by the interaction of the main crack and the already damaged zone. Analysis of the corresponding interactions (see Table 10.1 on page 266) provides the process zone energy, q_{pz}.

Immediately in front of a crack the matrix will fracture, contributing to the energy dissipation. In the case of brittle matrix fracture in the crack plane, its contribution is, according to eqn [10.52], given by: $w_m^0 = 2(1 - v)\gamma_m^0$.

However, when the matrix fails in a ductile fashion the crack meets already stretched matrix areas. Due to that stretching, the matrix microstructure may have been changed (e.g., by orientation of macromolecules). This in general results in an embrittlement of the material.

During matrix yielding the volume of the matrix remains nearly constant and hence the cross section of the matrix strip becomes smaller: $A \rightarrow A/(1 + \tilde{\varepsilon}_M)$, where $\tilde{\varepsilon}_M$ corresponds to that level of deformation in the true stress–strain relation at which the necking process is stabilised. The matrix volume fraction in the process zone is therefore reduced to: $v_m = (1 - v)/(1$

$+\tilde{\varepsilon}_M$). Consequently, the process zone energy for ductile matrix fracture, as may be the case for a static test, is given by:

$$w_{m,y} = \frac{2(1-\nu)\gamma_{m,y}}{1+\tilde{\varepsilon}_M}, \tag{10.97}$$

with $\gamma_{m,y}$ as the fracture surface energy of the plastically deformed matrix, which might be different from that of the bulk matrix material that may even fail in a brittle manner, with the fracture surface energy γ_m^0.

One other important mechanism acting within the process zone is fibre pull-out. But other than the calculation of this contribution to the work of fracture, where crack propagation over the whole cross section is considered, it is limited in case of crack initiation.

With the assumption of a constant shear stress during pull-out, τ_p, the energy to pull out a fibre with embedded length L_e over a distance Δ is given (see Fig. 10.20) by:

$$W_{po} = \pi d\tau_p \int_{L_e-\Delta}^{L_e} x\,dx = \frac{\pi d\tau_p}{2}\left(2L_e\Delta - \Delta^2\right). \tag{10.98}$$

A stationary distribution of Δ is assumed for a certain distance in front of the notch during an infinitesimal increment of crack growth *dc*. If the embedded length of a fibre is smaller than Δ, this fibre will be pulled out completely. Thus, we obtain the pull-out energy from:

$$\begin{aligned} W_{po} &= \pi d\tau_p\left(2L_e\Delta - \Delta^2\right)/2 \quad \text{for} \quad L_e \geq \Delta \\ W_{po} &= \pi d\tau_p L_e^2/2 \qquad\qquad\quad \text{for} \quad L_e \leq \Delta. \end{aligned} \tag{10.99}$$

The mean energy of one fibre becomes:

$$\bar{W}_{po} = \frac{2}{l}\int_0^{l/2} W_{po}\,dL_e = \frac{\pi d\tau_p}{l}\left(\frac{\Delta^3}{3} - \frac{\Delta^2 l}{2} + \frac{\Delta l^2}{4}\right). \tag{10.100}$$

When the crack opening starts, the fibres at the crack tip are pulled out. The crack opening displacement s_c corresponds approximately to the fibre pull-out length Δ. After a certain amount of crack opening, these fibres have suffered a pull-out length of Δ while the fibres immediately at the crack tip show a pull-out length of $\Delta = 0$. Thus, we obtain the mean energy of one fibre within the process zone as:

$$W_{po}^{\Delta} = \frac{1}{\Delta}\int_0^{\Delta} \bar{W}_{po}(\Delta)\,d\Delta = \frac{\pi d\tau_p}{2l}\left(\frac{\Delta^3}{6} - \frac{\Delta^2 l}{3} + \frac{\Delta l^2}{4}\right). \tag{10.101}$$

By assuming homogeneous fibre distribution, the specific fracture energy (i.e., energy per unit area of crack growth) is given by multiplying this equation with the specific number, n_0, of active fibres, which is (i.e., eqn [10.44]):

$$w_{\mathrm{po}}^{\Delta} = n_0 W_{\mathrm{po}}^{\Delta} = \frac{2v\tau_{\mathrm{p}}}{ld}\left(\frac{\Delta^3}{6} - \frac{\Delta^2 l}{3} + \frac{\Delta l^2}{4}\right). \qquad 10.102$$

To evaluate the maximum possible pull-out length $\Delta = \Delta_{\max}$, knowledge of crack opening at crack instability is used. According to this concept, the crack instability of ductile materials is controlled not by a critical stress intensity factor (as in elastic materials) but by a critical plastic deformation in front of the notch, that is the critical crack tip opening displacement, s_{c}. We assume that the pull-out length, Δ, is approximately equal to u_{c}. If the crack edges show a displacement, s_{c}, then the fibres suffer a movement (cf. Fig. 10.20) of

$$\Delta_{\max} = s_{\mathrm{c}} \quad \text{for} \quad \Delta_{\max} \le l/2. \qquad 10.103$$

With the relationship between s_{c} and critical energy release rate G_{c} (cf. equation [10.6] and [10.13]),

$$s_{\mathrm{c}} = G_{\mathrm{c}}/\sigma_{\mathrm{c}}^{\mathrm{d}}. \qquad 10.104$$

(Here, we use the critical stress for the start of debonding, $\sigma_{\mathrm{c}}^{\mathrm{d}}$, instead of the yield stress.) Thus, it is obtained that:

$$\Delta_{\max} = G_{\mathrm{c}}/\sigma_{\mathrm{c}}^{\mathrm{d}} \le l/2. \qquad 10.105$$

Finally, the pull-out contribution is given by the following relation:

$$w_{\mathrm{po}}^{\Delta} = \frac{v\tau_{\mathrm{p}} l}{2d\sigma_{\mathrm{c}}^{\mathrm{d}}} G_{\mathrm{c}}\alpha \quad \text{for} \quad \Delta_{\max} = G_{\mathrm{c}}/\sigma_{\mathrm{c}}^{\mathrm{d}} \le l/2 \qquad 10.106$$

and $\alpha = 1 - \frac{4}{3l}\left(G_{\mathrm{c}}/\sigma_{\mathrm{c}}^{\mathrm{d}}\right) + \frac{2}{3l^2}\left(G_{\mathrm{c}}/\sigma_{\mathrm{c}}^{\mathrm{d}}\right)^2.$

According to eqn [10.105] the pull-out length, Δ, is obviously restricted to half the fibre length; thus for a critical crack opening displacement $s_{\mathrm{c}} > l/2$ the pull-out contribution also remains restricted. Inserting $\Delta = l/2$ into eqn [10.102] provides in this case:

$$w_{\mathrm{po}}^{\Delta} = \frac{v\tau_{\mathrm{p}} l^2}{8d} \quad \text{for} \quad \Delta_{\max} = G_{\mathrm{c}}/\sigma_{\mathrm{c}}^{\mathrm{d}} > l/2. \qquad 10.107$$

It is slightly different from eqn [10.59] for the case of completely pulled-out fibres during crack propagation over the total cross section.

10.10.4 Results and discussion of fracture toughness for crack initiation

The fracture toughness can now be calculated by inserting the above derived energy contributions into the general equation [10.91], which fulfils the necessary condition for crack initiation [10.24] which is: $G_{\mathrm{c}} = R$.

Doing so, it must be distinguished between predominately brittle matrix fracture, caused intrinsically by the matrix or by impact loading and ductile matrix behaviour throughout the testing. The process zone energies for both of these cases are given for brittle matrix fracture by:

$$q_{\mathrm{pz}} = w_{\mathrm{m}}^{0} + w_{\mathrm{po}}^{\Delta}, \tag{10.108}$$

where w_{m}^{0} is given by eqn [10.52] and for ductile matrix fracture, this becomes:

$$q_{\mathrm{pz}} = w_{\mathrm{m,y}} + w_{\mathrm{po}}^{\Delta} \tag{10.109}$$

and $w_{\mathrm{m,y}}$ is given by eqn [10.97].

Inserting the corresponding energies provides the following equations for the fracture toughness of crack initiation:

For brittle matrix fracture:

$$G_{\mathrm{c}} = \frac{2\gamma_{\mathrm{m}}^{0}(1-\nu)}{1-2\beta E_{\mathrm{c}}\left(\eta_{\mathrm{d}}/(\sigma_{\mathrm{c}}^{\mathrm{d}})^{2} + \eta_{\mathrm{s}}/(\sigma_{\mathrm{c}}^{\mathrm{s}})^{2}\right) - \dfrac{v\tau_{\mathrm{p}}l}{2d\sigma_{\mathrm{c}}^{\mathrm{d}}}\alpha(G_{\mathrm{c}})} \quad \text{for} \quad G_{\mathrm{c}}/\sigma_{\mathrm{c}}^{\mathrm{d}} \le l/2, \tag{10.110a}$$

$$G_{\mathrm{c}} = \frac{2\gamma_{\mathrm{m}}^{0}(1-\nu) + \dfrac{v\tau_{\mathrm{p}}l^{2}}{8d}}{1-2\beta E_{\mathrm{c}}\left(\eta_{\mathrm{d}}/(\sigma_{\mathrm{c}}^{\mathrm{d}})^{2} + \eta_{\mathrm{s}}/(\sigma_{\mathrm{c}}^{\mathrm{s}})^{2}\right)} \quad \text{for} \quad G_{\mathrm{c}}/\sigma_{\mathrm{c}}^{\mathrm{d}} > l/2, \tag{10.110b}$$

For ductile matrix fracture:

$$G_{\mathrm{c}} = \frac{2\gamma_{\mathrm{m,y}}^{0}(1-\nu)/(1+\tilde{\varepsilon}_{\mathrm{M}})}{1-2\beta E_{\mathrm{c}}\left(\eta_{\mathrm{d}}/\left(\sigma_{\mathrm{c}}^{\mathrm{d}}\right)^{2} + \eta_{\mathrm{s}}/\left(\sigma_{\mathrm{c}}^{\mathrm{s}}\right)^{2} + \eta_{\mathrm{m}}/\left(\sigma_{\mathrm{M,y}}\right)^{2}\right) - \dfrac{v\tau_{\mathrm{p}}l}{2d\sigma_{\mathrm{c}}^{\mathrm{d}}}\alpha(G_{\mathrm{c}})} \tag{10.111a}$$

for $G_{\mathrm{c}}/\sigma_{\mathrm{c}}^{\mathrm{d}} \le l/2$,

$$G_{\mathrm{c}} = \frac{2\gamma_{\mathrm{m,y}}(1-\nu)/(1+\tilde{\varepsilon}_{\mathrm{M}}) + \dfrac{v\tau_{\mathrm{p}}l^{2}}{8d}}{1-2\beta E_{\mathrm{c}}\left(\eta_{\mathrm{d}}/(\sigma_{\mathrm{c}}^{\mathrm{d}})^{2} + \eta_{\mathrm{s}}/(\sigma_{\mathrm{c}}^{\mathrm{s}})^{2} + \eta_{\mathrm{m}}/(\sigma_{\mathrm{M,y}})^{2}\right)} \tag{10.111b}$$

for $G_{\mathrm{c}}/\sigma_{\mathrm{c}}^{\mathrm{d}} > l/2$.

For the case $G_{\mathrm{c}}/\sigma_{\mathrm{c}}^{\mathrm{d}} \le l/2$ these equations are transcendental.

To substantiate this general model the theoretical result is compared with experimental data for a particular case. Experimental studies were conducted on a short glass fibre filled polyethylene compounded in a twin-screw extruder and test specimens were then prepared by injection moulding. Impact fracture toughness was determined by an instrumented Charpy-impact device by Grellmann (1985), which provides the load-deflection curve during impact loading necessary to obtain fracture toughness values. The critical energy release rate based on the J-integral (J^{BL})

proposed by Begley and Landes (1972) was used for characterisation of the material. The following material parameters are employed for the calculations: $E_f = 70$ GPa, $\nu_f = 0.3$, $l/d = 20$, $\varepsilon_F^u = 0.01$, $\mu = 0.3$, $\sigma_n^T = 30$ MPa, $\tau' = 0$; $E_m = 500$ MPa, $\nu_m = 0.4$, $\sigma_{m,y} = 55$ MPa, $\tau_d = a'\sigma_{m,y}/2$ ($a' = 0.4$); $\tau_p = 0.8\tau_d$. The debonding energy γ_d^{II} is approximated by the fracture mechanics relation for mode II loading, according to eqn [10.13]:

$$2\gamma_d^{II} = K_{II}^2/E_c \cong \left(\tau_d l_d^{1/2}\right)^2/E_c \qquad 10.112$$

and this provides for the debonding energy:

$$\gamma_d^{II} \approx \frac{\tau_d^2 l_d}{2E_c}. \qquad 10.113$$

The composite modulus, E_c is taken from experimental results. For β two values were used: $\beta = 1/18$ and $\beta = 1/24$.

The experimental and theoretical results are compared in Fig. 10.50. It becomes clear that the model is indeed suitable for predicting the energy release rate of this kind of materials. The maximum in G_c is mainly connected with the influence of the energies and critical stresses in the denominator of eqn [10.110] and especially with the dependence of the characteristic lengths (l_d, l_s) on fibre concentration.

The debonding and sliding lengths decrease with increasing fibre volume fraction at certain applied load because the local stresses in the matrix are decreasing. Thus, debonding and sliding will be shifted to the fibre end

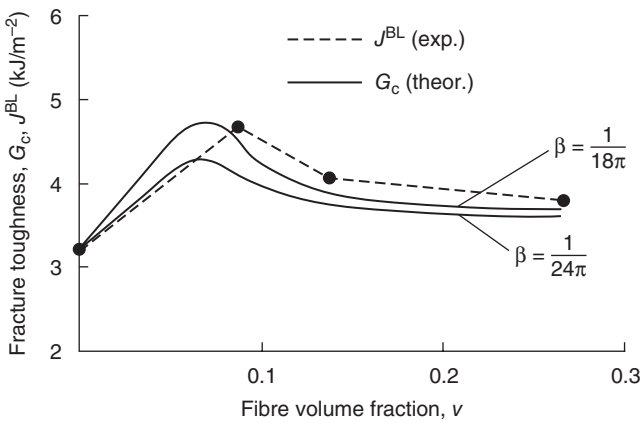

10.50 Experimental and theoretical results of dynamic fracture toughness as a function of fibre volume fraction (short glass fibre reinforced polyethylene).

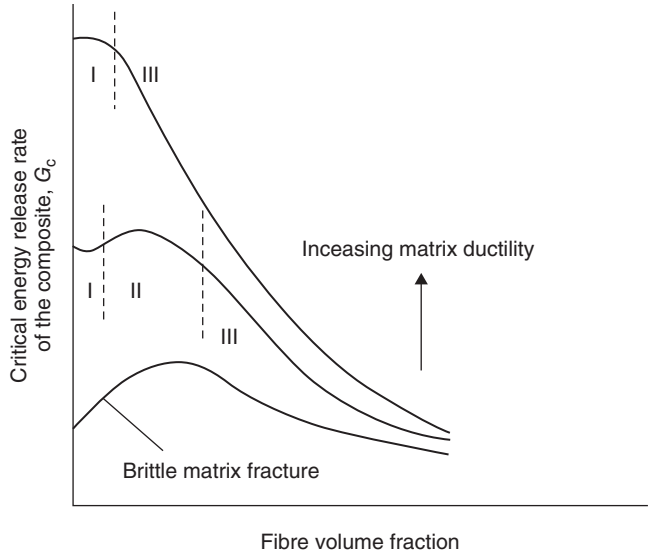

10.51 Qualitative behaviour of energy release rate for ductile matrix fracture conditions: I, undisturbed macroscopic yielding of the matrix; II, fibres restrict the macroscopic yielding, energy dissipation by fibre–matrix interaction; III, small-scale damage, plastic deformation energy dominates the energy dissipation process.

region. An increase in G_c for higher v can be achieved by increasing the pull-out stress, τ_p, by introducing residual stresses, for example.

The qualitative behaviour of G_c for a static test with a plastic matrix is proposed in Fig. 10.51. It is assumed that there are different regions of crack resistance which depend on v and matrix ductility. For very low fibre concentrations in the range (I), a damage zone near the crack tip cannot be formed because of the stress relaxation in the ductile matrix. Therefore, G_c for low fibre volume fractions is determined by the crack resistance of the matrix, $(1 - v)2\gamma_{m,y}$ (according to eqn [10.57]) and the interaction of the crack with single fibres that may break, $w_{fi} = v2\gamma_{fi}$:

$$G_c = (1-v)2\gamma_{m,y} + v2\gamma_{fi} \quad \text{for lower fibre volume fractions.} \quad 10.114$$

Because the first term prevails over the second term for brittle fibre fracture, the fracture toughness decreases with increasing v.

For high fibre volume fractions, however, the dense packing of the structural elements in connection with restricted matrix ductility causes the formation of a damage zone as discussed above. Thus, in this region (III) our model (eqn [10.111]) becomes applicable. Also, in this region the plastic deformation of the matrix is expected to be dominant. Thus, G_c decreases with v, because the matrix energy contribution, w_m, decreases with increasing v.

For a matrix with intermediate ductility, it is assumed that there exists a region (II) where the increase of fibre–matrix interaction by debonding and sliding prevails over the decrease in w_m with increasing fibre concentrations.

10.10.5 Calculation of crack-resistance (*R*) curve

To characterise the crack resistance of fibre reinforced composites, in particular short fibre reinforced thermoplastics, different concepts have been used in the above sections – the work of fracture, the critical stress intensity factor (K_c), and the critical energy release rate (G_c). The first parameter describes the energy necessary for driving the crack through the whole sample while the last two parameters characterise the stage of crack initiation. Experimental studies of crack growth kinetics in these materials have, however, shown that a substantial amount of slow crack growth occurs before crack instability. Therefore, a single parameter such as K_c or G_c is not fully appropriate to characterise the total fracture behaviour.

For this reason the *R*-curve concept is used to describe the failure process. Experimental studies by Karger-Kocsis (1989), Friedrich *et al.* (1988, 1991), and Grellmann and Seidler (1992) on crack growth kinetics in SFRPs showed that a so-called *R*-curve (crack-resistance curve) characterises the crack propagation behaviour. A typical crack-resistance curve is shown in Fig. 10.52 for bulk PET and a glass fibre reinforced PET. It reveals that the matrix absorbs a much higher amount of energy necessary for stable crack growth than the composite.

Assuming the existence of such an *R*-curve, a model is proposed to calculate this function on a micromechanical basis.

In Section 10.4 the micromechanical failure mechanisms of SFRPs were studied. As has already been pointed out for calculation of the fracture toughness due to crack initiation, two dominating processes in the crack tip vicinity have to be distinguished. Immediately in front of the notch the creation of a new fracture surface is connected with the consumption of specific energy, q_{pz}, in the process zone. A substantial part of the elastic energy is dissipated in a larger dissipative zone near the crack tip. Failure is spread over a certain region and is not limited to the crack path. Microstructural changes induced by the propagating crack yield an additional crack resistance. These processes are concentrated in the so-called dissipation zone. Starting with an initial crack of length c_0, both of these zones are formed when the crack propagates a certain length, Δc (see Fig. 10.49).

The corresponding energy dissipation mechanisms have been derived in Section 10.10.3. Considering all the equations, it becomes clear that only the pull-out energy of eqn [10.101] is still dependent on the pull-out length

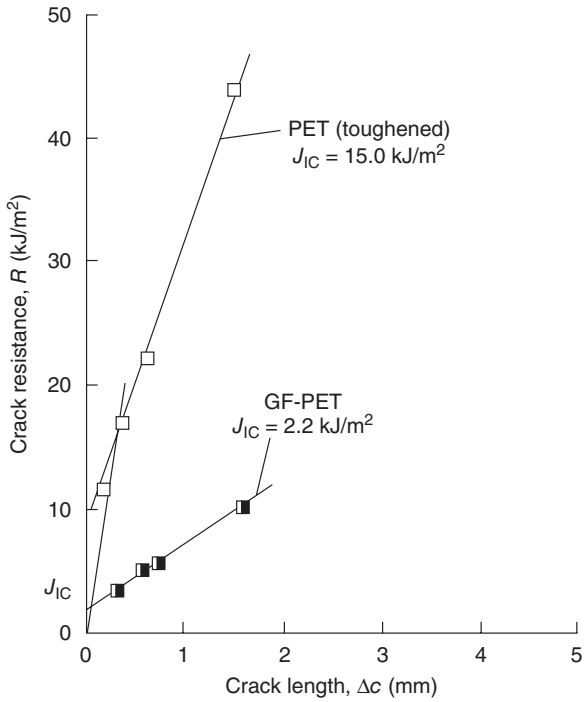

10.52 Crack resistance curve of toughened and fibre reinforced PET composites. Adapted from Lauke and Friedrich (1992).

and this geometrical value is connected to the crack growth value, Δc. This fact provides the basis for calculation of the R-curve as the change of crack resistance with increasing crack length.

For this evaluation the restricted pull-out energy of eqn [10.101] is used; that is:

$$w_{\mathrm{po}}^{\Delta} = n_0 W_{\mathrm{po}}^{\Delta} = \frac{2v\tau_{\mathrm{p}} l^2}{d}\left(\frac{\Delta^3}{6} - \frac{\Delta^2}{3} + \frac{\Delta^2}{4}\right) \quad \text{with} \quad \Delta \leq 1/2, \qquad 10.115$$

where Δ is now normalised by the fibre length l.

In this section and in the following all characteristic lengths, such as initial crack length, c_0, crack growth, Δc, critical crack growth, $\Delta \tilde{c}$, fibre pull-out length, Δ and sample width T, are normalised by fibre length l. The restriction $\Delta \leq 1/2$ relates to the fact that the maximum possible pull-out length is given by half the fibre length. For a pull-out length $\Delta \geq 1/2$, the mean pull-out energy in the crack region remains limited to the constant value given in eqn [10.107].

The pull-out length Δ during loading of a specimen is given by the corresponding crack opening displacement s_{c}. In Section 10.5, the relation

between crack opening displacement and energy release rate was used, now the relation between crack opening displacement and crack growth is required. It is provided by the basic relations of fracture mechanics given in eqns [10.3] and [10.6]. Combining these yields:

$$\Delta = s_c = \frac{K_c^2}{\sigma_c^d E_c} \cong \frac{\left(\sigma_c^d\right)^2 \Delta c}{\sigma_c^d E_c} = \frac{\sigma_c^d \Delta c}{E_c} = \varepsilon_d \Delta c, \qquad 10.116$$

where ε_d can be considered a failure strain needed for debonding at the fibre–matrix interface and where instead of the plastic yield strength of a material, the critical stress for debonding initiation σ_c^d is used and the crack length is replaced by the change of crack length $\Delta = c - c_0$, because all fracture mechanics parameters of eqn [10.116] are also valid for their changes.

Consequently, the pull-out energy for a moving crack is given by:

$$w_{po}^{\Delta} = n_0 W_{po}^{\Delta} = \frac{2v\tau_p l^2}{d}\left(\frac{(\varepsilon_d \Delta c)^3}{6} - \frac{(\varepsilon_d \Delta c)^2}{3} + \frac{(\varepsilon_d \Delta c)}{4}\right) \quad \text{for} \quad \Delta \le 1/2 \qquad 10.117a$$

and

$$w_{po}^{\Delta} = \frac{v\tau_p l^2}{8d} \quad \text{for} \quad \Delta \ge 1/2. \qquad 10.117b$$

Inserting this energy term and the matrix contributions (given in eqs [10.52] and [10.97]) into the general eqn [10.91] under consideration of eqn [10.108] provides finally the crack-resistance curve for brittle matrix fracture (R-curve) as:

$$R(\Delta c) = \frac{w_m^0}{1 - 2\beta E_c \sum_i \eta_i / \left(\sigma_c^i\right)^2}\left[1 + \Gamma\left(\frac{(\varepsilon_d \Delta c)^3}{6} - \frac{(\varepsilon_d \Delta c)^2}{3} + \frac{(\varepsilon_d \Delta c)}{4}\right)\right] \qquad 10.118$$

for $\Delta c \le \Delta c^*$,

with $\Gamma = \dfrac{2v\tau_p l^2}{d w_m^0}$, $i = s$ means sliding, $i = d$ means debonding. Because the maximum possible normalised pull-out length is limited to $\Delta = 1/2$, the corresponding limit for crack growth follows from eqn [10.115] as $\Delta c^* = 1/(2\varepsilon_d)$. For crack growth higher than this value, the crack resistance becomes constant so that:

$$R(\Delta c) = R^0 = \frac{w_m^0}{1 - 2\beta E_c \sum_i \eta_i / (\sigma_c^i)^2}[1 + \Gamma/16] \quad \text{for} \quad \Delta c \ge \Delta c^*. \qquad 10.119$$

Figure 10.53 shows the general variation of crack resistance as a function of crack growth. If the considerations are extended to the problem of fracture toughness, the model provides also the critical crack growth at the

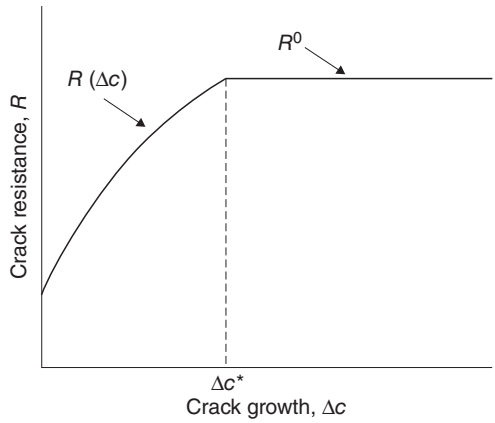

10.53 General behaviour of crack resistance (R) as a function of crack growth (Δc), where Δc^* indicates the point where the pull-out energy has reached the maximum and constant value.

instability point and the critical energy release rate. Considerations concerning this matter will be presented in the next section.

For the case where the matrix fails predominately in a ductile manner, this can be discussed in a similar way and was shown by Lauke and Friedrich (1992); readers are referred to this paper for details.

A similar approach to calculate the R-curve was published by Qiao and Kong (2004); however, they considered energy dissipations only within the process zone, which are caused mainly by matrix fracture and fibre pull-out. Rigorous fracture mechanics modelling of R-curves for cement-based fibre composites in which fibre pull-out in the crack-wake zone is the predominant mechanism has been given by Cotterell and Mai (1996) in their research monograph. Based on the fibre bridging (pull-out) law, the effects of specimen size, geometry and loading configuration on R-curves are obtained. The same methods of analysis apply to SFRP composites with brittle matrices and mainly fibre debond and pull-out mechanisms.

10.11 Relation between fracture toughness and the work of fracture

As in the previous section, in all equations herein, all the characteristic lengths such as initial crack length, c_0, characteristic crack length, c_0', crack growth, Δc, critical crack growth, $\Delta\tilde{c}$, fibre pull-out length, Δ, and sample width, T, are normalised by fibre length l.

In the previous two sections, the fracture toughness for crack initiation and the crack-resistance curve where calculated, respectively. To determine the fracture toughness, G_c, the criterion of critical crack opening displacement at the point of instability was used (eqn [10.104]). And for the calcula-

tion of the R-curve the relation between the pull-out length Δ and the changed crack length Δc is crucial (see eqn [10.116]).

Now the consideration shall be extended to explain the development of a critical crack from sub-critical crack growth. Since G_c can be understood as a restricted work of fracture for limited crack growth, we show below the conceptual connection and the difference of G_c compared to the work of fracture, w.

Further, the fracture toughness at crack instability is derived distinct from the fracture toughness for crack initiation as provided by eqns [10.110] and [10.111], which fulfils only the necessary condition: $G_c = R$. But to decide if the crack becomes unstable, the second condition of eqn [10.24] must be considered.

The crack propagation resistance is generally a function of the crack growth, $\Delta c = c - c_0$. Increasing loading brings about an increase in Δc which finally reaches the critical value, $\Delta\tilde{c}$, necessary for crack instability. The point of crack instability is characterised by the two conditions [10.24]. In terms of crack growth, Δc, they can be written as:

$$G(\Delta c) = R(\Delta c) \quad \text{and} \quad \frac{\mathrm{d}G}{\mathrm{d}\Delta c} = \frac{\mathrm{d}R}{\mathrm{d}\Delta c} \quad \text{for} \quad \Delta c = \Delta\tilde{c}. \tag{10.120}$$

The $\Delta\tilde{c}$ value is determined by the point of tangency of $G(\Delta c)$ to $R(\Delta c)$ as shown in Fig. 10.4. It follows that the critical energy release rate for crack instability is given by:

$$G(\Delta\tilde{c}) = G_c = R(\Delta\tilde{c}) \tag{10.121}$$

together with the above derived relations $R(\Delta c)$, eqns [10.118] and [10.119].

From eqns [10.120] and [10.121], we also obtain the relation:

$$\frac{\mathrm{d}G}{\mathrm{d}\Delta c} \cong \frac{R(\Delta\tilde{c})}{c_0 + \Delta\tilde{c}} = \frac{\mathrm{d}R}{\mathrm{d}\Delta c} \quad \text{at} \quad \Delta c = \Delta\tilde{c}. \tag{10.122}$$

Solving this equation provides $\Delta\tilde{c}$.

To simplify the numerical calculation, the cubic term in $R(\Delta c)$ is neglected because ε_d represents a small value. The approximation is especially good for small Δc. By doing so, $\Delta\tilde{c}$ can be obtained by:

$$\Delta\tilde{c} = \left[c_0^2 - \frac{3}{\Gamma\varepsilon_d^2} + \frac{3c_0}{4\varepsilon_d}\right] - c_0 \quad \text{for} \quad c_0 \geq c_0' \tag{10.123a}$$

$$= 0 \quad \text{for} \quad c_0 \leq c_0', \tag{10.123b}$$

which is a function of initial crack length, c_0. The characteristic crack length, c_0', is obtained from eqn [10.122] for $\Delta\tilde{c} = 0$ to be: $c_0' = 4/\Gamma\varepsilon_d$ and it considers the fact that composites with $c_0 \leq c_0'$ show no stable crack growth prior to unstable crack growth when the load is increased to $\sigma_c^2 = R(\Delta\tilde{c} = 0)E_c/c_0$. Γ is already defined in eqn [10.118].

Inserting $\Delta\tilde{c}$ into eqn [10.117] provides the fracture toughness G_c for unstable crack growth. Unlike this, the G_c derived in the foregoing section and given in eqns [10.110] and [10.111] characterises the initiation of crack growth. The main differences between the two approaches lie in the assumptions concerning the restricted pull-out length Δ as given in eqns [10.105] and [10.116], respectively; and the criterion of crack growth [10.24]: on the one hand, only the left equation and, on the other hand, both relations have been used, respectively.

A major difference between G_c results for crack initiation and unstable crack propagation is that the latter depends on the initial crack length, c_0. To calculate the relation between fracture toughness and the work of fracture only large propagated crack lengths are considered, that is, $\Delta c_{max} >> \Delta c^* = 1/2\varepsilon_d$. This has the advantage of simplifying the integration of eqn [10.23], but is not a loss of basic understanding.

Under this condition the work of fracture, given in [10.23], can be approximated by:

$$w \cong R^0, \tag{10.124}$$

where R^0 is from eqn [10.119].

Finally, the relation between fracture toughness and the work of fracture is obtained by combining [10.118] and [10.124] to give:

$$\frac{G_c}{w} = \frac{1+\Gamma\left(\frac{(\varepsilon_d\Delta\tilde{c})^3}{6} - \frac{(\varepsilon_d\Delta\tilde{c})^2}{3} + \frac{(\varepsilon_d\Delta\tilde{c})}{4}\right)}{1+\Gamma/16} \quad \text{for} \quad \Delta\tilde{c} \le \Delta c^* = 1/2\varepsilon_d \tag{10.125a}$$

and

$$\frac{G_c}{w} = 1 \quad \text{for} \quad \Delta\tilde{c} \ge \Delta c^* = 1/2\varepsilon_d. \tag{10.125b}$$

We now discuss the dependence of this ratio on the material parameters involved in Γ and ε_d. The ratio of G_c/w as a function of Γ for constant ε_d at different initial crack lengths is shown in Fig. 10.54. Two regions of different crack propagation modes can be distinguished. For low Γ values the characteristic crack length, $c_0' = 4/\Gamma\varepsilon_d$, may result in $c_0 < c_0'$. In this case G_c is equal to R at $\Delta\tilde{c} = 0$ for the first time, but with a slope $dG/dc > dR/d\Delta c$ that results in immediate unstable crack propagation. With increasing Γ the point $c_0 = c_0'$ is reached where stable crack growth starts. The curves reveal, especially for small c_0 that two parameters are necessary to characterise the failure behaviour, namely the fracture toughness, G_c, for crack instability or strength and the work of fracture, w, as the energy necessary to drive the crack through the whole sample.

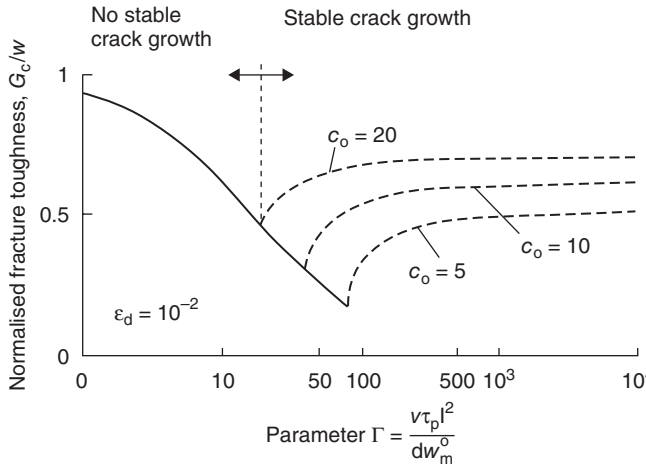

10.54 Ratio between fracture toughness for unstable crack propagation $G_c(\Delta\bar{c})$ and work of fracture, w, as a function of the parameter $\Gamma = \frac{2v\tau_p l^2}{dw_m^0}$, which is proportional to the ratio of pull-out energy and matrix fracture energy for different initial crack lengths c_0 (c_0 is normalised by the fibre length l) and $\varepsilon_d = 0.01$.

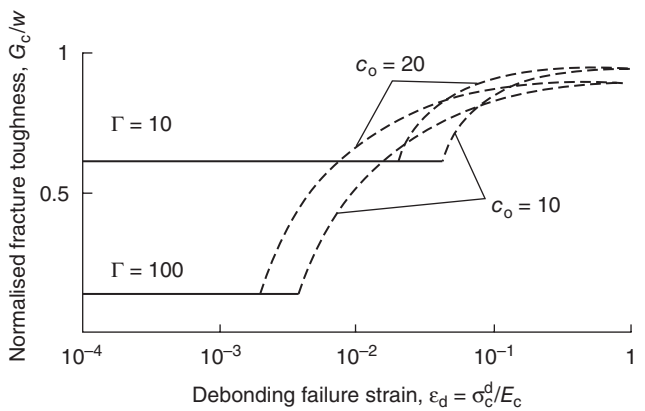

10.55 Ratio between fracture toughness for unstable crack propagation $G_c(\Delta\bar{c})$ and work of fracture, w, as a function of ε_d, the failure strain for debonding at the fibre–matrix interface, for different initial crack lengths c_0 (c_0 is normalised by the fibre length l) and Γ = 10,100.

Figure 10.55 shows the variation of G_c/w with ε_d. It becomes clear that for high ε_d the work of fracture becomes nearly equal to the fracture toughness, independent of c_0 and Γ.

Summarising the results, it can be concluded that for the interpretation of toughness of short fibre reinforced composites the conditions for the

applicability of the work of fracture concept instead of fracture toughness must be clearly distinguished. For a wide range of the characteristic parameters c_0, $\Gamma = 2v\tau_p l^2/dw_m^0$, and $\varepsilon_d = \sigma_c^d/E_c$, the work of fracture value is much higher than the fracture toughness counterpart.

10.12 Essential work of fracture criterion

The essential work of fracture (EWF) concept was introduced in Section 10.2.2. A simple experimental method was developed using a deep-edge-notched tension (DENT) geometry in which separation of the total work of fracture (W_f) into two components: (a) specific essential work (w_e) in the inner process zone, and (b) non-specific essential work ($\beta\eta_p$) in the outer plastic zone is relatively simple. Details of the methodology, required testing conditions and data analysis are given by Wu and Mai (1996); and a European Structural Integrity Society (ESIS) *Test Protocol on Essential Work of Fracture*, Version 5 (October 1997) has since been established.

In short fibre reinforced polymers, the basic EWF concept can still be applied. But in this case, the essential work of a SFRP, as shown in Fig. 10.56, is that required to debond, slide and pull out the fibres, and subsequently to break any matrix bridges on the crack plane inside the process zone. All other dissipative processes are involved outside the process zone. When all the essential (W_e) and non-essential (W_p) works of fracture are contained in the ligament L of the DENT specimen, as shown in Fig. 10.57, eqn [10.17]

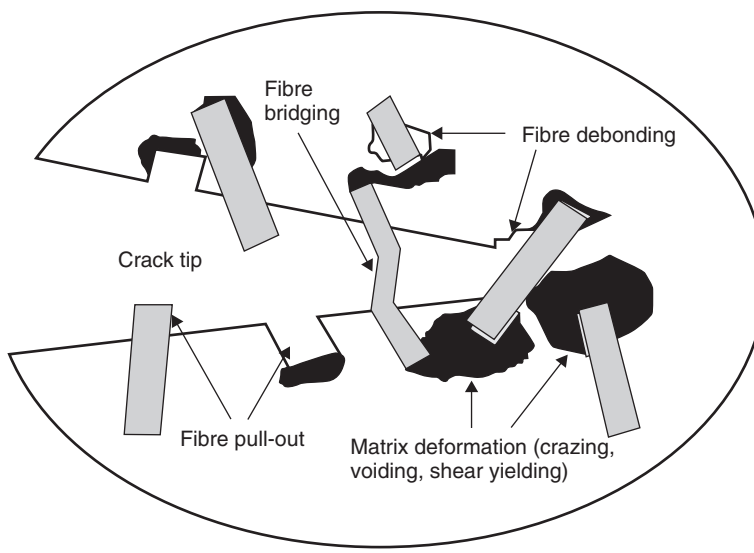

10.56 Schematic of typical failure mechanisms in SFRP and process zone near crack tip. Adapted from Wong and Mai (1999).

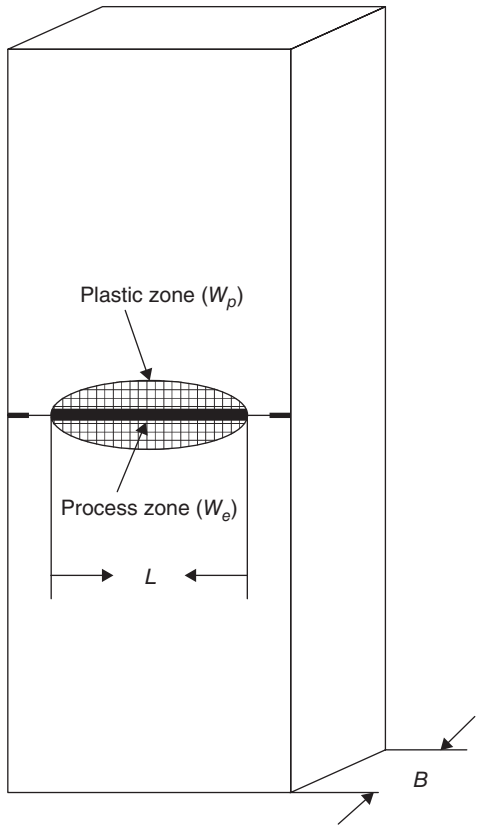

10.57 DENT specimen geometry for EWF test.

holds. By performing a series of fracture experiments with different L, the total fracture work (W_f) can be measured under the load-deflection curve. Plotting the specific total fracture work, $W_f/(LB)$, against the ligament length L, a least squares straight line can be obtained with the intercept on the y-axis as the specific essential fracture work w_e.

Mouzakis *et al.* (1998) and Wong and Mai (1999) were among the first investigators to apply the EWF technique to characterise the fracture behaviour of SFRPs. Experiments were carried out on polypropylene/glass bead/elastomer hybrids by Mouzakis *et al.* and they found the specific essential work to increase with elastomer content. EWF was particularly useful as crack growth was difficult to identify. The system studied by Wong and Mai was a PA6,6/PP (75/25 weight ratio) blend containing SEBS (20 wt%) grafted with different amounts of maleated anhydride (MA). Two major results are observed. First, the skin-core structure of the injection moulded samples is reflected by the W/BL *vs* L plots at very short liga-

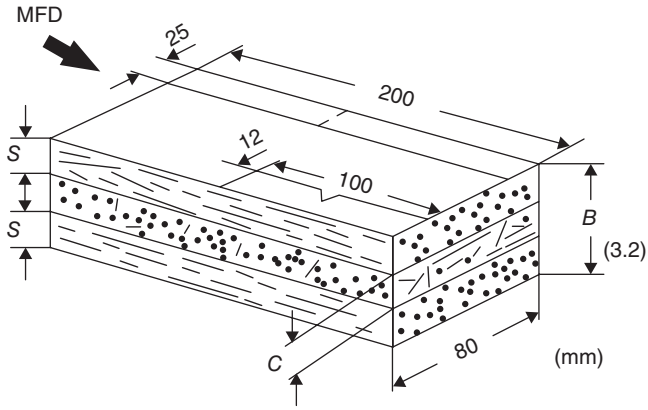

10.58 Schematic showing fibre orientation in DENT and Izod impact specimens. Adapted from Tjong *et al.* (2002b).

ments, particularly for those hybrids with severe skin-core effect induced fibre distribution. Second, there is a good straight line correlation between w_e and J_{Ic} for crack initiation for all the hybrids.

Later, Tjong *et al.* (2002a,b) conducted more intensive EWF studies on short glass fibre reinforced (a) polyamide (PA)6,6/SEBS-*g*-MA, and (b) PP/SEBS using DENT specimens machined from injection moulded plaques, as shown in Fig. 10.58. Izod impact fracture experiments were also done. In the PA6,6/SEBS-*g*-MA (80/20) blends, it is shown that adding short glass fibres of different amounts (5–30 wt%) improves the specific essential fracture work w_e (see Fig. 10.59) but the failure mechanisms are different. Matrix yielding, especially near fibre ends, fibre debonding and pull-out predominate in hybrids with 5, 10 and 15 wt% fibres. Only fibre debonding and pull-out are seen in hybrids with 20 and 30 wt% glass fibres since matrix plasticity is constrained. Unlike the EWF tests at relatively low rates, under impact loading, however, the Izod notched strength of these hybrids is not sensitive to glass fibre content.

In the short glass fibre/PP/SEBS hybrids, MA was either grafted to PP and/or to SEBS. It is shown that, either way, the resultant hybrids exhibit much lower essential fracture work w_e (~7.8 kJ/m^2) compared to the w_e (~29 kJ/m^2) of short glass fibre/PP/SEBS hybrids with no compatibiliser of MA. These results confirm that too strong an interfacial bond between glass fibre and PP can impair the fracture toughness of the SFRP blends.

To date, theoretical studies on the EWF of SFRP composites are few and far between. For example, issues on skin and core effects, fibre length and orientation distributions, etc., must be studied in depth. In the last few years, the application of the EWF concept to a range of polymer nanocomposites with layered and particulate nano-sized fillers has been critically examined

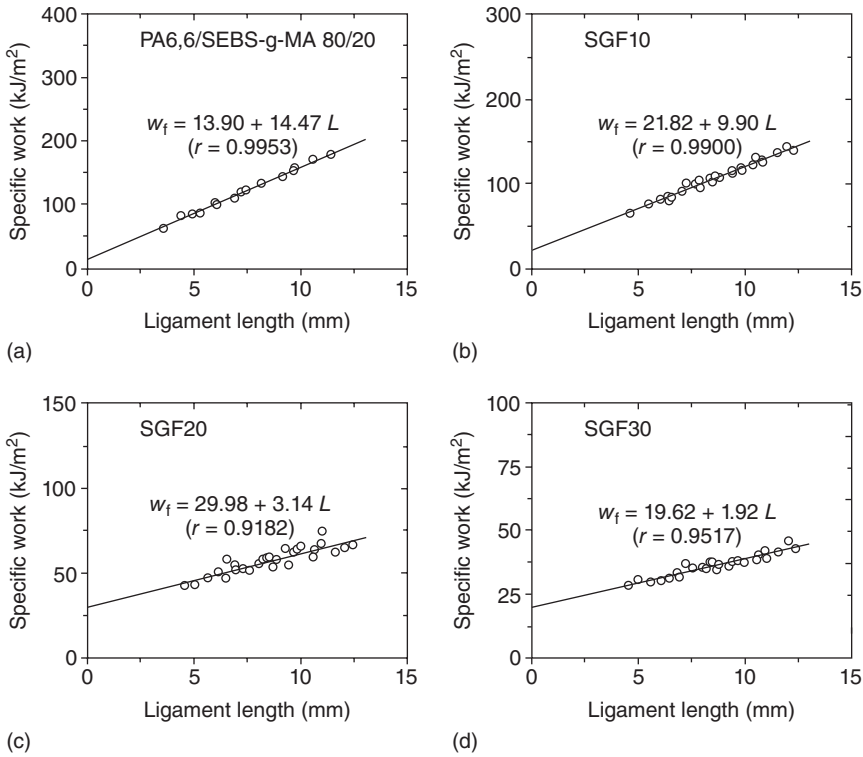

10.59 Specific total fracture work (w_f) *vs* ligament length L for (a) PA6,6/SEBS-g-MA (80/20) blend, (b) SGF10, (c) SGF20 and (d) SGF30 hybrid composites. In SGF10, SGF20 and SGF30, matrix is PA/SEBS-g-MA blend, SGF stands for short glass fibres and 10, 20 and 30 represent wt% of fibre. Adapted from Tjong *et al.* (2002b).

by several groups of researchers (Costa *et al.*, 2006; Satapathy *et al.*, 2007; Yoo *et al.* 2007; Vu *et al.*, 2008; Tjong and Ruan, 2008; Ganss *et al.*, 2008; Bureau *et al.*, 2006). There is much room for further rigorous research with EWF applied to this emerging class of nanomaterials.

10.13 References

Agarwal B D and Giare G S (1981), 'Crack growth resistance of short fibre composites', *Fibre Sci. Technol.*, 15 (4), 283–298.

Akay M and O'Regan D F (1995), 'Fracture behaviour of glass fibre reinforced polyamide mouldings', *Polym Test*, 14 (2), 149–162.

Anderson T L (1995), *Fracture mechanics, fundamentals and applications*, CRC Press, Boca Raton, FL.

ASTM E399 (1983), *Standard Test Method for Plane-Strain Fracture Toughness of Metallic Materials*.

Atkins A G (1975), 'Intermittent bonding for high toughness/high strength composites', *J Mater Sci*, 10 (5), 819–832.

Atkins A G and Mai Y-W (1985), *Elastic and Plastic Fracture: metals, polymers, ceramics, composites, biological materials*, Ellis Horwood, Chichester.

Bader M G and Collins I F (1982), 'The strength, ductility and failure of thermoplastics reinforced with short-glass fibres', *Proc Fourth International Conference on Composite Materials*, ICCM4, Tokyo, Japan.

Bader M G (1983), 'Reinforced thermoplastics', in *Handbook of Composites, Fabrication of Composites*, Vol. 4, Elsevier Science, New York.

Bagwell R M and Wetherhold R C (2005), 'End-shaped copper fibers in an epoxy matrix-predicted versus actual fracture toughnening', *Theor Applied Fract Mech*, 43 (2), 181–188.

Barenblatt G I (1962), 'The mathematical theory of equilibrium cracks brittle fracture', *Adv Appl Mech*, 7, 55–129.

Barnby J T and Spencer B (1976), 'Crack propagation and compliance calibration in fibre-reinforced polymers', *J Mater Sci*, 11 (1), 78–82.

Beaumont P W R (1971), 'Fracture and fatique of carbon fibre reinforced plastics', PhD Dissertation, University of Sussex.

Beaumont P W R and Anstice P D (1980), 'A failure analysis of the micromechanisms of fracture of carbon fibre and glass fibre composites in montonic loading', *J Mater Sci*, 15 (10), 2619–2635.

Beaumont P W R and Harris B (1972), 'The energy of crack propagation in carbon fibre-reinforced resin systems', *J Mater Sci*, 7 (11), 1265.

Becher P F, Hsueh C H, Angelini P and Tiegs T (1988), 'Toughening behavior in whisker-reinforced ceramic matrix composites', *J Am Ceram Soc*, 71 (12), 1050–1061.

Begley J A and Landes J D (1972), ASTM STP 5 14, p. 1.

Beyerlein J, Zhu Y T and Mahesh S (2001), 'On the influence of fibre shape in bone-shaped short-fibre composites', *Compos Sci Technol*, 61 (10), 1341–1357.

Birch M W and Williams J G (1978), 'The effect of rate on the impact fracture toughness of polymers', *Int J Fract*, 14 (1), 69–84.

Blackman B R K (2006), 'Fracture of polymers, composites and adhesives', *Enging Fract Mech*, 73 (16), 2251–2587.

Blumenauer H and Pusch G (1987), *Technische Bruchmechanik*, VEB Deutscher Verl. für Grundstoffindustrie, Leipzig.

Brandt A M (1985), 'On the optimal direction of short metal fibres in brittle matrix composites', *J Mater Sci*, 20 (11), 3831–3841.

Broberg K B (1975), 'Stable crack growth', *J Mech Phys Solids*, 23 (3), 215–237.

Broek D (1974), *Elementary engineering fracture mechanics*, Noordhoff, Leyden, The Netherlands.

Brown H R (1973), 'A critical examination of the impact test for glassy polymers', *J Mater Sci*, 8, 941–948.

Budiansky B, Hutchinson J and Lambropoulos J C (1983), Continuum theory of dilatant transformation toughening in ceramics', *Int. J. Solids Structures,* 19 (4), 337–355.

Bureau M N, Ton-That M T and Perrin-Sarazin F (2006), 'Essential work of fracture and failure mechanisms of polypropylene-clay nanocomposites', *Enging Fract Mech*, 73 (16), 2360–2374.

Carlowitz B (1980), 'Thermoplastische Kunststoffe', Zechner & Hüthing Verlag GmbH, Speyer, 143.

Cherepanov G P (1968), 'Cracks in solids', *Int J Solids Struct*, 4 (8), 811–831.
Cherepanov G P (1979), *Mechanics of brittle fracture*, McGraw-Hill, New York.
Choi N S and Takahashi K (1996), 'Toughness and microscopic fracture mechanisms of unfilled and short-glass-fibre-filled poly(cyano arylether)', *J Mater Sci,* 31 (3), 731–740.
Cooper G A and Kelly A (1967), 'Tensile properties of fibre reinforced metals: fracture mechanics', *J Mech Phys Solids*, 15 (4), 279–297.
Cooper G A and Piggott M R (1977), 'Cracking and fracture in composites', *Proc. International Conference on Fracture*, ICF 4, Waterloo, Canada.
Costa F R, Satapathy B K, Wagenknecht U, Weidisch R and Heinrich G (2006), 'Morphology and fracture behaviour of polyethylene/Mg-Al layered double hydroxide (LDH) nanocomposites', *Eur Polym J*, 42 (9), 2140–2152.
Cotterell B and Mai Y-W (1996), *Fracture Mechanics of Cementitious Materials*, Blackie A & P/Chapman & Hall, Glasgow/London.
Cottrell A H (1964), 'Strong solids', *Proc Roy Soc*, A282 (1388), 2–9.
Curtis P T, Bader M G and Baily J E (1978), 'The stiffness and strength of a polyamide thermoplastic reinforced with glass and carbon fibres', *J Mater Sci*, 13 (2), 377–390.
Davis J H (1970), 'Fundamentals of fibre-filled thermoplastics', *Plast Polym,* 38 (4), 137–143.
Dugdale D S (1960), 'Yielding of steel sheets containing slits', *J Mech Phys Solids*, 8 (2), 100–104.
Eckell A (1982), 'Die Chemie und Physik von Verbundwerkstoffen mit Polymermatrix', Verbundwerkstoffe und Werkstoflerbunde in der Kunststoflechnik, VDI Verlag, Duesseldorf.
Ehrenstein, G (1981), 'Glasfaserverstarkte Kunststoffe', *Expert Verlag*, Vol. 62, 189.
Eshelby J D (1951), 'The force on an elastic singularity', *Phil Trans Roy Soc London A*, 244 (877), 87–112.
European Structural Integrity Society (ESIS) (1997), *Test Protocol on Essential Work of Fracture*, Version 5 (October).
Friedrich K (1982), *Microstructure and fracture of fibre reinforced thermoplastic polyethylene terephthalate*, VDI-Verlag, Düsseldorf.
Friedrich K (1984), *Fracture mechanical behaviour of short fibre reinforced thermoplastics*, VDI-Verlag, Düsseldorf.
Friedrich K (1985), 'Microstructural efficiency and fracture toughness of short fibre/thermoplastic matrix composites', *Compos Sci Technol*, 22 (1), 43–47.
Friedrich K (1989), 'Fractographic analysis of polymer composites', in Friedrich K, *Application of fracture mechanics to composite material*, Composite Materials Series, Elsevier, Oxford.
Friedrich K, Walter R and Voigt J (1988), 'Fracture toughness of short fibre thermoplastic matrix composites, compared on the basis of different test methods', *Thermoplastic Compos Mater*, 1 (1), 68–93.
Friedrich K, Carlsson L A, Gillespie J W and Karger-Kocsis J (1991), 'Fracture of thermoplastic composites', in Carlsson L A (ed), *Thermoplastic Composite Materials*, Composite Materials Series, 7, Elsevier Science Amsterdam.
Fu S Y and Lauke B (1997), 'The fibre pull-out energy of misaligned short fibre composites', *J Mater Sci*, 32 (8), 1985–1993.

Fu S Y and Lauke B (1998), 'Fracture resistance of unfilled and calcite-particle-filled ABS composites reinforced by short glass fibre (SGF) under impact load', *Composites Part A*, 29A (5–6), 631–641.

Fu S Y, Zhou B and Lung C (1992), 'On the pull-out on fibres with fractal-tree structure and the inference of strength and fracture toughness of composites', *Smart Mater Struct*, 1, 180–185.

Fu S Y, Mai Y-W, Lauke B, Xu G and Yue C Y (2002a), 'Fracture behaviour of short glass fibre and short carbon fibre reinforced polypropylene composites', *Int J Mater Product Technol*, 17 (1–2), 108–120.

Fu S Y, Mai Y-W, Lauke B and Yue C Y (2002b), 'Synergistic effect on the fracture toughness of hybrid short glass fibre and short carbon fibre reinforced polypropylene composites', *Mater Sci Eng A: Struct*, 323 (1–2), 326–335.

Fu S Y, Mai Y-W, Lauke B, Xu G and Yue C Y (2002c), 'Combined effect of fiber content and microstructure on the fracture toughness of SGF and SCF reinforced polypropylene composites', *J Mat Sci*, 37 (14), 3067–3074.

Fu S Y, Lauke B, Zhang Y H and Mai Y-W (2005), 'On the post-mortem fracture surface morphology of short fibre reinforced thermoplastics', *Compos Part A – Appl Sci Manu*, 36 (7), 987–994.

Gaggar S and Broutman L J (1975), 'Crack growth resistance of random fibre composites', *J Compos Mater*, 9 (Jul), 216–227.

Ganss M, Satapathy B K, Thunga M, Weidisch R, Potschke P and Jehnichen D (2008), 'Structural interpretations of deformation and fracture behavior of polypropylene/multi-walled carbon nanotube composites', *Acta Materia*, 51 (10), 2247–2261.

Gershon B and Marom G (1975), 'Fracture toughness and mechanical properties of glass fibre-epoxy composites', *J Mater Sci*, 10 (9), 1549–1556.

Grellmann W (1985), 'Beurteilung der Zähigkeitseigenschaften von Polymerwerkstoffen durch bruchmechanische Kennwerte', Thesis (B), TH Merseburg.

Grellmann W and Seidler S (1992), 'J-integral analysis of fibre-reinforced injection-moulded thermoplastics', *J Polym Eng*, 11 (1–2), 71–102.

Grellmann W and Seidler S (1998), *Deformation und Bruchverhalten von Kunststoffen*, Springer, Berlin.

Grellmann W, Seidler S and Lauke B (1991), 'Application of the J-integral concept for the description of toughness properties of fibre reinforced polyethylene composites', *Polymer Composites*, 12 (5), 320–326.

Guess T R and Hoover W R (1973), 'Fracture toughness of carbon-carbon composites', *J Mater Sci*, 7 (Jan), 2–20.

Gupta V P, Mittal R K and Goel M (1990), 'Energy absorbing mechanisms in short-glass-fibre-reinforced polypropylene', *Compos Sci Technol*, 37 (4), 353–369.

Gurney C and Hunt J (1967), 'Quasi-static crack propagation', *Proc R Soc Lond*, A 299, 508–524.

Harris B (1972), 'The strength of composites', *Composites*, 3 (4), 152–167.

Harris B (1980), 'Micromechanisms of crack extension in composites', *Metall Sci,* 14 (8–9), 351–362.

Harris B (1986), *Engineering Composite Materials*, The Institute of Metals, London.

Harris B, Morley J and Phillips D C (1975), 'Fracture mechanisms in glass-reinforced plastics', *J Mater Sci*, 10 (12), 2050–2061.

Hine P J, Brew B, Duckett R A and Ward I M (1988), 'The fracture behaviour of carbon fibre reinforced poly(ether etherketone)', *Compos Sci Technol*, 33 (1), 35–71.

Hoffmann H, Grellmann W and Martin H (1985), 'Untersuchungen zum Einfluss von Füllstoffen auf die Zähigkeitseigenschaften von PE-HD', *Plaste und Kautschuk*, 32 (3), 107–110.

Ishak Z A M and Berry J B (1993), 'Impact properties of short carbon fibre reinforced nylon 6.6', *Polym Eng Sci*, 33 (22) 1483–1488.

Ishak Z A M, Ishiaku U S and Karger-Kocsis J (1998), 'Microstructure-related fracture behaviour of injection moulded short fibre reinforced polyarylamide in dry and wet states', *J Mater Sci,* 33 (13), 3377–3389.

Ishiaku U S, Hamada H, Mizoguchi M, Chow W S and Ishak Z A M (2005), 'The effect of ambient moisture and temperature conditions on the mechanical properties of glass fiber/carbon fibre/nylon 6 sandwich hybrid composites consisting of skin-core morphologies', *Polym Composite*, 26 (1), 52–59.

Jain L K and Wetherhold R C (1992), 'Effect of fibre orientation on the fracture toughness of brittle matrix composites', *Acta Metall Mater*, 40 (6), 1135–1143.

Kameswara Rao C V S (1983), 'A note on fracture toughness of multiphase materials', *Eng Fract Mech*, 18 (1), 35–38.

Kanninen M F (1978), 'A critical appraisal of solution techniques in dynamic fracture mechanics', *Proceedings Numerical Methods in Fracture Mechanics*, University College of Swansea.

Karger-Kocsis J (1989), 'Microstructure and fracture mechanical performance on short-fibre reinforced thermoplastics', in Friedrich K, *Application of fracture mechanics to composite material*, Composite Materials Series, Elsevier, Oxford.

Karger-Kocsis J (1993), 'Instrumented impact fracture and related failure behaviour in short- and long-glass-fibre-reinforced polypropylene', *Compos Sci Technol*, 48 (1–4), 273–283.

Karger-Kocsis J, Czigany T and Moskala E J (1997), 'Thickness dependence of work of fracture parameters of an amorphous copolyester', *Polymer*, 38 (18), 4587–4593.

Karger-Kocsis J, Czigany T and Moskala E J (1998), 'Deformation rate dependence of the essential and non-essential work of fracture parameters in an amorphous copolyester', *Polymer*, 39 (17), 3939–3944.

Kausch H J (1978), *Polymer Fracture*, Springer, Berlin.

Kelly A (1970), 'Interface effects and the work of fracture of a fibrous composite', *Proc. Roy. Soc. (London)*, A319 (1536), 95–116.

Kim J K and Mai Y-W (1991), 'High strength, high fracture toughness fibre composites with interface control – a review', *Compos Sci Technol*, 41 (4), 333–378.

Kim J K and Mai Y-W (1998), *Engineered Interfaces in Fibre Reinforced Composites*, Oxford, Elsevier.

Kinloch A J and Young R J (1983), *Fracture behaviour of polymers*, Barking, Elsevier.

Kreher W and Pompe W (1981), 'Increased fracture toughness of ceramics by energy dissipation mechanisms', *J Mater Sci*, 16 (3), 694–706.

Langer B, Seidler S and Grellmann W (1996), 'Charakterisierung stabiler Bruchvorgänge in kurzfaser-Verbundwerkstoffen', *Mat-wiss u Werkstofftech*, 27 (2), 96–104.

Lauke B and Friedrich K (1992), 'Fracture toughness modelling of fibre reinforced composites by crack resistance curves', *Adv Compos Mater*, 2 (4), 261–275.

Lauke B and Pompe W (1986), 'Fracture toughness of short-fibre reinforced thermoplastics', *Compos Sci Technol*, 26 (1), 37–57.

Lauke B and Schultrich B (1986a), 'Calculation of fracture work of short-glass-fibre reinforced polypropylene for static and dynamic loading rates', *Compos Sci Technol*, 26 (1), 1–16.

Lauke B and Schultrich B (1986b), 'Zur Berechnung der Schlagzähigkeit von kurzglas-faserverstärkten Polyethylen', *Plaste und Kautschuk*, 33 (5), 184–186.

Lauke B, Schultrich B and Barthel R (1985), 'Contribution to the micromechanical interpretation of fracture work of short-fibre-reinforced thermoplastics', *Compos Sci Technol*, 23 (1), 21–35.

Lauke B and Freitag K-H (1987), 'Zum Einfluss der Faserorientierung und der Rißrichtung auf die Brucharbeit von kurzfaserverstärkten Thermoplasten', *Plaste und Kautschuk,* 34 (4), 137–139.

Lauke B, Schultrich B and Pompe W (1990), 'Theoretical considerations of toughness of short-fibre reinforced thermoplastics', *Polymer – Plastics Techno Engng*, 29 (7–8), 607–832.

Lauke B, Schüller T and Beckert W (2004), 'Determination of interface adhesion in single-fibre pull-out and microbond experiments', in Moore D R, *The application of fracture mechanics to polymers, Adhesives and Composites*, ESIS Publication 33, Elsevier, Amsterdam.

Leps G and Bohse J (1985), 'Schallemissionsuntersuchungen an gefüllten und verstärkten Thermoplasten', *Wiss. Beitr. der IH für Seefahrt*, 57 (4), 57–60.

Li V C, Wang Y and Backer S (1990), 'Effect of inclining angle, bundling, and surface treatments on synthetic fibre pull-out from a cement matrix', *Composites*, 21 (2), 132–139.

Liebowitz H (ed.) (1968), *Fracture-An Advanced Treatise, Vol. 2*, Academic Press, New York and London.

Lhymn C and Schultz J M (1983), 'Fracture behaviour of collimated thermoplastic poly(ethylene terephthalate) reinforced with short E-glass fibres', *J Mater Sci*, 18 (7), 2029–2046.

Mai Y-W (1979), 'Strength and fracture properties of asbestos–cement mortar composites', *J Mater Sci*, 14 (9), 2091–2102.

Mai Y-W and Atkins A G (1980), 'Crack stability in fracture toughness testing', *J Strain Anal*, 15(2), 63–74.

Mai Y-W and Cotterell B (1986), 'On the essential work of ductile fracture in polymers', *Int J Fract*, 32 (2), 105–125.

Mandell F, Huang D D and McGarry F J (1982), 'Crack propagation modes in injection molded fibre reinforced thermoplastics', *Short Fibre Reinforced Composite Materials*, ASTM STP, 772, 3–72.

Marshall G P, Coutts L H and Williams J G (1973), 'Fracture toughness and absorbed energy measurements in impact tests on brittle materials', *J Mater Sci*, 8 (7), 949–956.

Marston T U, Atkins A G and Felbeck D K (1974), 'Interfacial fracture energy and the toughness of composites', *J Mater Sci*, 9 (3), 447–455.

Michael G (1980), 'Polyamide', *Kunststoffe*, 70 (10), 629–636.

Miwa M, Ohsawa T and Tsuji N (1979), 'Temperature dependence of impact fracture energies of short glass fibre-epoxy and unsaturated polyester composites', *J Appl Polym Sci*, 23 (6), 1679.

Moore D R (2001), 'The measurement of K_c and G_c at slow speeds for discontinuous fibre composites', in Moore D R, Pavan A and Williams J G, *Fracture mechanics*

testing methods for polymers, adhesives and composites, ESIS Publication 28, Elsevier, Amsterdam, 59–71.

Moore D R (2004), *The application of fracture mechanics to polymers, adhesives and composites*, ESIS Publication 33, Elsevier, Amsterdam.

Moore D R, Pavan A and Williams J G (2001), *Fracture mechanics testing methods for polymers, adhesives and composites*, ESIS Publication 28, Elsevier, Amsterdam.

Mouzakis D E, Stricker F, Mulhaupt R and Karger-Kocsis J (1998), 'Fracture behaviour of polypropylene/glass bead elastomer composites by using the essential work of fracture method', *J Mater Sci*, 33(10), 2251–2562.

Mullin J, Berry J M and Gatti A (1968), 'Some fundamental fracture mechanisms applicable to advanced filament reinforced composites', *J Compos Mater*, 2 (1), 82–103.

Nairn J A (2004), 'Fracture mechnaics of the microbond and pull-out tests', in Moore D R, *The application of fracture mechanics to polymers, Adhesives and Composites*, ESIS Publication 33, Elsevier, Amsterdam.

Newmann L V and Williams J G (1980), 'A comparative study of the tensile and Charpy impact tests from a fracture mechanics viewpoint', *Polym Eng Sci*, 20 (8), 572–578.

Nezbedova E and Turcic B (1984), 'Zähigkeit von Polymerwerkstoffen bei schlagartiger Beanspruchung', *Plaste und Kautschuk*, 31 (7), 264–267.

Outwater J and Murphy M C (1969), 'On the fracture energy of uni-directional laminates', *24th Annual Tech. Conf. Reinforced Plastics/Composites Div. of SPI*, Paper 11C, Section 11-C, pp. 1–8.

Phan-Thien N (1980), 'On the pull-out of fibres with enlarged ends', *Fibre Sci Tech*, 15 (2), 111–116.

Phan-Thien N (1981), 'Effective elastic moduli of enlarged-end-reinforced solids', *Fibre Sci Techol*, 14 (4), 241–250.

Phillips D C and Tetelman A S (1972), 'The fracture toughness of fibre composites', *Composites*, (9), 216–223.

Piggott M R (1974), 'The effect of aspect ratio on toughness in composites', *J Mater Sci*, 9 (3), 494–502.

Piggott M R (1980), *Load bearing composites*, Pergamon Press, Oxford.

Plati E and Williams J G (1975), 'The determination of the fracture parameters for polymers in impact', *Polym Eng Sci*, 15 (6), 470–477.

Pompe W (1978), Rissausbreitung und Bruchzähigkeit bei Sinter- und Verbundwerkstoffen', *Neue Hütte*, 23 (9), 321–326.

Pompe W, Bahr H-A, Gille G, Kreher W, Schultrich B and Weiss H-J (1985), 'Mechanical properties of brittle materials, modem theories and experimental evidence', *Current Topics in Material Science*, Vol. 12 (E. Kaldis, ed.), Elsevier, p. 262.

Qiao Y and Kong X (2004), 'Unstable crack advance across a regular array of short fibres in brittle matrix', *Compos Sci Technol*, 64 (5), 711–717.

Ramsteiner F and Theysohn R (1979), 'Tensile and impact strengths of unidirectional, short fibre-reinforced thermoplastics', *Composites*, 10 (2), 111–119.

Rice J R (1968), 'A path-independent integral and the approximate analysis of strain concentration by notches and cracks', *ASME Trans J Appl Mech*, 33, 379–385.

Satapathy B K, Weidisch R, Potschke P and Janke A (2007), 'Tough to brittle transition in multi-walled carbon nanotube (MWNT)/polycarbonate nanocomposites', *Compos Sci Technol*, 67(5), 867–879.

Sato N, Kurauchi T, Sato S and Kamigaito O (1983), 'SEM observations on the initiation and propagation of cracks on a short-fibre reinforced thermoplastic composite under stress', *J Mater Sci* Lett, 2 (5), 188–190.

Sato N, Kurauchi T, Sato S and Kamigaito O (1984), 'Mechanism of fracture of short glass fibre-reinforced polyamide thermoplastic', *J Mater Sci*, 19 (4), 1145–1152.

Sato N, Kurauchi T, Sato S and Kamigaito O (1985), '*In situ* SEM observation of fracture processes in short glass fibre reinforced thermoplastic composite', ASTM STP 868, 493–502.

Sih G C, Paris P C and Irwin G P (1965), 'On cracks in rectilinearly anisotropic bodies', *Int J Fract Mech*, 1 (3), 189–203.

Solomon S, Bakar A A, Ishak Z A M, Ishiaku U S and Hamada H (2005), 'Microstructure and fracture behaviour of (co)injection-molded polyamide 6 composites with short glass/carbon fibre hybrid reinforcement', *J Appl Polym Sci*, 97 (3), 957–967.

Song G M, Li Q, Wen G W and Zhou Y (2002), 'Mechanical properties of short carbon fibre-reinforced TiC composites produced by hot pressing', *Mat Sci Eng A: Struct*, 326 (2), 240–248.

Sumpter J D G and Turner C E (1976), 'Method for laboratory determination of J_c' *ASTM STP* 601, 3–18.

Sweeney J (1986), 'Finite width correction factors for SEN testing of orthotropic materials in opening mode', *J Strain Analysis*, 21 (2), 99–107.

Tjong S C and Ruan Y H (2008), 'Fracture behaviour of thermoplastic polyolefin/clay nanocomposites', *J Appl Polym Sci*, 110 (2), 864–871.

Tjong S C, Xu S A, Li R K Y and Mai Y-W (2002a), 'Mechanical behaviour and fracture toughness evaluation of maleic anhydride compatibilized short glass fibre/SEBS/ polypropylene composites', *Compos Sci Technol*, 62 (6), 831–840.

Tjong S C, Xu S A, Li R K Y and Mai Y-W (2002b), 'Short glass fibre-reinforced polyamide 6,6 composites toughened with maleated SEBS', *Compos Sci Technol*, 62 (15), 2017–2027.

Tsai J, Patra A K and Wetherhold R C (2003), 'Numerical simulations of fracture-toughness improvement using short shaped head ductile fibres', *Compos Part A – Appl Sci Manu*, 34 (11), 1255–1264.

Tsai J, Patra A K and Wetherhold R C (2005), 'Finite element simulation of shaped ductile fiber pullout using a mixed cohesive zone/friction zone interface model', *Composites Part A,* 36 (6), 827–838.

Tsanas A and Kardos J L (1985), 'Fracture toughness of short fibre reinforced composites', *ANTEC*, 377.

Vu H N, Vermogen A, Gauthier C, Masenelli-Varlot K and Cavaille J Y (2008), 'Microstructure and fracture behaviour of semicrystalline polymer-clay nanocomposites', *J Polym Sci B: Polym Phys*, 46(17), 1820–1836.

Waddoups M E, Eisenmann J R and Kaminski B E (1971), 'Macroscopic fracture mechanics of advanced composite materials', *J Compos Mater*, 5 (4), 446–454.

Wagner H D and Lustiger A (2009), 'Optimized toughness of short fibre-based composites: The effect of fibre diameter', *Comps Sci Technol*, 69 (7–8), 1323–1325.

Wells J K and Beaumont P W R (1985a), 'Crack-tip energy absorption processes in fibre composites', *J Mater Sci*, 20 (8), 2735–2749.

Wells J K and Beaumont P W R (1985b), 'Debonding and pull-out processes in fibrous composites', *J Mater Sci*, 20 (4), 1275–1284.
Wells J K and Beaumont P W R (1987), 'The prediction of R-curves and notched tensile strength for composite laminates', *J Mater Sci*, 22 (4), 1457–1468.
Wetherhold R C and Jain L K (1992), 'The toughness of brittle matrix composites reinforced with discontinuous fibres', *Mater Sci Eng A: Struct*, 151 (2), 169–177.
Wetherhold R C and Jain L K (1993), 'The effect of crack orientation on the fracture properties of composite materials', *Mater Sci Eng A: Struct*, 165 (2), 91–97.
Wetherhold R C and Lee F K (2001), 'Shaped ductile fibres to improve the toughness of epoxy-matrix composites', *Compos Sci Technol*, 61 (4), 517–530.
Wetherhold R C, Corjan M and Das K P (2007), 'Multiscale considerations for interface engineering to improve fracture toughness of ductile fiber/thermoset matrix composites', *Compos Sci Technol*, 67 (11–12), 2428–2437.
Whitney J M and Nuismer R J (1974), 'Stress fracture criteria for laminated composites containing stress concentrations', *J Compos Mater*, 8 (3), 253–265.
Williams J G (1972), 'Visco-elastic and thermal effects on crack growth in PMMA', *Int J Fact Mech*, 8 (4), 393–401.
Williams J G (1973), *Stress Analysis of Polymers*, Longman, London.
Williams J G (1984), *Fracture Mechanics of Polymers*, Ellis Horwood, Chichester.
Williams J G (2001), 'K_c and G_c at slow speeds for polymers', in Moore D R, Pavan A and Williams J G, 'Fracture Mechanics Testing Methods for Polymers', *Adhesives and Composites*, ESIS Publication 28, Elsevier, Amsterdam, pp. 11–26.
Williams J G and Pavan A (1995), *Impact and Dynamic Fracture of Polymers and Composites*, ESIS Publication 19, Mechanical Engineering Publ Ltd, London.
Williams J G and Pavan A (2000), *Fracture of Polymers, Composites and Adhesives*, ESIS Publication 27, Elsevier, Amsterdam.
Williams M L (1957), 'On the stress distribution at the base of a stationary crack', *J Appl Mech*, 24, 109–114.
Wong S C and Mai Y-W (1999), 'Essential fracture work of short fibre reinforced polymer blends', *Polym Eng Sci*, 39 (10), 356–364.
Wu J S and Mai Y-W (1996), 'The essential fracture work concept for toughness measurement of ductile polymers', *Polym Eng Sci*, 36 (18), 2275–2288.
Yoo J Y, Shah R K and Paul D R (2007), 'Fracture behaviour of nanocomposites based on poly(ethylene-co-methacrylic acid) ionomers', *Polymer*, 48 (16), 4867–4873.
Zhen S (1983), 'The D criterion theory in notched composite materials', *J. Reinf Plast Compos*, 2 (2), 98–110.
Zhu Y T and Beyerlein J (2002), 'Bone shaped short fiber composites – an overview', *Mater Sci Eng A: Struct*, 326 (2), 208–227.
Zhu Y T, Valdez J A, Shi N, Lovato M L, Stout M G, Zhou S and Blumenthal B R (1998), 'A composite reinforced with bone-shaped short fibers', *Acta Mater,* 38 (9), 1321–1325.
Zhu Y T, Valdez J A, Beyerlein I J, Zhou SJ, Liu C, Stout M G, Butt D P and Lowe T C (1999), 'Mechanical properties of bone-shaped short-fibre reinforced composites', *Acta Mater*, 47 (6), 1767–1781.

Index